Interacties tussen de reologische eigenschappen en het verpompen van zelfverdichtend beton

Interactions between Rheological Properties and Pumping of Self-Compacting Concrete

Dimitri Feys

Promotoren: prof. dr. ir. G. De Schutter, prof. dr. ir. R. Verhoeven
Proefschrift ingediend tot het behalen van de graad van
Doctor in de Ingenieurswetenschappen: Bouwkunde

Vakgroep Bouwkundige Constructies
Voorzitter: prof. dr. ir. L. Taerwe

Vakgroep Civiele Techniek
Voorzitter: prof. dr. ir. J. De Rouck

Faculteit Ingenieurswetenschappen
Academiejaar 2008 - 2009

UNIVERSITEIT
GENT

ISBN 978-90-8578-277-3
NUR 955, 956
Wettelijk depot: D/2009/10.500/33

DANKWOORD

Voila, het is er. De proeven zijn afgelopen, de conclusies zijn getrokken en het boekje is klaar. En hoewel ik volledig heb ingestaan voor iedere letter, ben ik toch niet de enige die dit werk heeft mogelijk gemaakt.
Vooreerst zou ik twee mensen willen bedanken, die er enerzijds voor gezorgd hebben dat ik aan dit werk kon beginnen, en die er ook altijd tijdens dit werk waren wanneer het nodig was. Prof. De Schutter en Prof. Verhoeven (Geert en Ronny voor de vrienden), bedankt voor de vele momenten dat ik jullie heb kunnen en mogen verhinderen om ander werk te doen. De vele discussies van 5 minuutjes, vergaderingen en minder wetenschappelijke (maar meer sociale) activiteiten werden opgefleurd door jullie wetenschappelijke input, enthousiasme en humoristische opmerkingen. Bedankt om mij de mogelijkheid te geven om mijn geest te verruimen en mijn capaciteiten te kunnen ontwikkelen en om mij nu en dan eens bij te sturen waar nodig. Bedankt voor het vele leeswerk, niet alleen voor dit boekje, maar ook de vele papers.
Verder grote dank aan onze "techniekers". Zonder jullie mateloze inzet en input was de inhoud van dit werk veel magerder (en 'k ben nu geen honing aan 't smeren). Dieter, Jan, Marc, Marcel, Martin, Nathan, Nicolas, Peter, Peter, Stefaan, Stefan en Tom. Dank u. Tommy, bedankt om enkele collega's af te schepen als ze op hetzelfde moment als mij proeven wilden uitvoeren, en Sandra, bedankt voor de hulp bij het aanleren en interpreteren van voor mij nieuwe meettechnieken.
Een woordje van dank gaat ook uit naar enkele "wijze" mensen (de keuze ligt aan de lezer zelf of dit in het Oost-Vlaams wordt geïnterpreteerd): de professoren Luc Taerwe, Pascal Verdonck, Nele De Belie, Peter Troch, Stijn Matthys en Patrick Segers. Gedurende vele jaren heb ik jullie kunnen observeren en van jullie kunnen leren.
Ook de andere collega's mogen niet vergeten worden. Anibal, Aniello, Anne-Mieke, Arnold, Bart, Bart, Binod, Brenda, Ceren, Christel, Davy, Dorleta, Edawi, Elke, Emmanuel, Frederik, Geoffrey, Gert, Jan, Kathelijn, Katrien, Kevin, Kim, Lander, Liesbet, Lin, Liu, Liu, Manuella, Mariette, Marijke, Nicolas, Pepa, Peter, Philip, Pieter, Qiang, Robby, Robert, Sieglien, Veerle, Viviane, Wang, Willem, Ye en Yin. Jullie hebben allemaal, elk op zijn/haar eigen manier, de onderzoekssfeer aangenaam beïnvloed. De aprilvisactiviteiten op Magnel, de kookmomenten op Hydraulica, de verschillende recepties, discussies in de keuken, grappen van en met collega's en de sportnamiddagen en after-sport avonden zullen niet snel vergeten worden.

In dit project heb ik ook de hulp gehad van twee zeer gemotiveerde thesisstudenten. Joris Rooseleer en Bart Calie, bedankt voor jullie inzet, het vroeg opstaan, de hulp in de productie en het beproeven van het beton en voor de wetenschappelijke input in dit onderzoek.
Verder ook een woordje van dank aan diegenen die niet aan deze universiteit zijn verbonden: Gert Heirman (KUL) en Niki Cauberg (WTCB) voor de uitvoering van gezamenlijke proeven. Betoncentrale OBC-Ottevaere uit Oudenaarde voor het leveren van zelfverdichtend beton op maat. Pompfirma Dejonghe uit Zonnebeke, en in het bijzonder Chris en Frederik voor hun expertise, werkijver en anekdotes. De firma's Denys en Socea voor de samenwerking en het gebruik van de buizen. Holcim voor de levering van veel cement, BASF voor het delen van zeer nuttige informatie, betoncentrale Tanghe en in het bijzonder Yvan, voor de toelichting van de praktische kanten van zelfverdichtend beton en het bedrijf De Cock uit Harelbeke voor het ter beschikking stellen van het afzuigsysteem voor de uitlaatgassen.
A word of thanks to all international people I have met during several meetings. Thanks for your comments, informations and discussions. Especially Dr. Nicolas Roussel, for the discussions and exchanges of ideas all over the world (Québec-City, Copenhagen, Ghent, Paris, Monterey and Chicago) and for the time you have spent. Also a special word of thanks to Prof. K.H. Khayat and Prof. R. Haldenwang for offering me very unique opportunities abroad.
Bedankt aan de voetballers voor de wekelijkse in- en ontspanning. De Freggles, voor de vele jaren voetbalplezier, de 641 tegengoals en ook de nevenactiviteiten. Een revanche voor de ontvoering volgt nog. Wacht maar tot jullie naar Canada komen …
De shotters van de personeelscompetitie, voor de deugddoende overwinningen, de soms zware verliezen en de pintjes achteraf.
Bedankt aan nog vier mensen die als heel goede vrienden overblijven uit de studententijd: Jean, Belle, Koen en Karen. Dat we nog veel gezellige momenten mogen beleven.
Bedankt aan ma en pa, om mij de mogelijkheid te geven om te kunnen studeren, om mij niks in de weg te leggen om mezelf te ontplooien en voor de vele steun in de moeilijkere momenten. Claude en Nancy, ook aan jullie een grote dank u wel voor de toffe, gezellige maar ook serieuze momenten samen. Verder ook bedankt aan de grootouders, broer en schoonzussen om een hechte, steunende familieband te smeden.
Verder denk ik dat ik stilletjes aan rond ben, maar ik ben nog één iemand vergeten. Het is een vrouw, klein van gestalte, maar groot van hart. Een schatje voor het leven. Een rots waarop je kan steunen in de moeilijkere momenten en een zonnetje in huis. Jij bent diegene die deze presentatie al het meest heeft gehoord. Bedankt om daarbij te proberen begrijpen wat voor mij evident lijkt, bedankt om er voor mij te zijn als ik irritant, ambetant, gestresseerd en zelfs als ik niet thuis was. Wendy, bedankt…

Dimitri

Gent, 15 mei 2009.

TABLE OF CONTENTS

PART I: RHEOLOGY

CHAPTER 2: SUSPENSION RHEOLOGY

CHAPTER 3: RHEOMETRY

CHAPTER 5: CONCRETE RHEOLOGY: TIME DEPENDENT BEHAVIOUR

PART II: PRESSURE DRIVEN CONCRETE FLOW

CHAPTER 6: THE POISEUILLE FORMULA FOR LAMINAR FLOW

CHAPTER 7: GRAVITATIONAL FLOW TESTS

CHAPTER 8: PUMPING TESTS: TEST SETUP AND PROCEDURES

APPENDICES

APPENDIX A: CALIBRATION OF THE TATTERSALL MK-II RHEOMETER

APPENDIX B: TEST RESULTS OF RHEOLOGICAL MEASUREMENTS

APPENDIX C: GRAVITATIONAL FLOW TESTS

APPENDIX D: PUMPING TESTS

LIST OF SYMBOLS

1 Symbols

a	=	particle radius (m)
A_b	=	breakdown area (thixotropy – loop curve) (Pa/s)
A_{SF}	=	parameter for the evolution of slump flow (loss of workability) (-)
A_{thix}	=	characteristic time for structuration of cement paste of concrete (Pa/s)
A_{VF}	=	parameter for the evolution of V-funnel flow time (loss of workability)(-)
A_{visc}	=	parameter for the evolution of viscosity (loss of workability) (-)
A_{YS}	=	parameter for the evolution of yield stress (loss of workability) (-)
B	=	structural breakdown parameter (s^{-1})
c	=	second order parameter in modified Bingham equation (Pa s^2)
Ca	=	capillary number (-)
d_{max}	=	maximal aggregate/bubble size (m)
d_{50}	=	average aggregate/bubble size (m)
D	=	diameter (m)
F	=	force (N)
g	=	gravitational acceleration (m/s^2)
G	=	"yield torque" parameter in Reiner-Riwlin equation (Nm)
h	=	height (m)
H	=	"viscosity" parameter in Reiner-Riwlin equation (Nm s)
H	=	coagulation rate constant (Hattori-Izumi) (s^{-1})
J_t	=	number of reversible junctions per unit of volume (Hattori-Izumi) (m^{-3})
L	=	length (m)
K	=	consistency factor (Herschel-Bulkley) (Pa s^n)
m	=	consistency factor (power-law model) (Pa s^n)
n	=	consistency index (power-law model – Herschel-Bulkley) (-)
n_t	=	total number of particles per unit of volume (Hattori-Izumi) (m^{-3})
n_3	=	number of primary particles per unit of volume (Hattori-Izumi) (m^{-3})
N	=	rotational velocity (revolutions/s)
p	=	pressure (Pa)
Δp	=	pressure loss per unit of length (Pa/m)
Δp_{sp}	=	special pressure loss (Pa)
Δp_{tot}	=	total pressure loss (Pa)
Pe	=	Peclet number
Q	=	discharge (m^3/s)
r	=	distance from the centre of the pipe (m)

r_{plug} = plug radius (m)
R = radius of the pipe (m)
R = radius of plate (parallel rotating plate rheometer) (m)
R_i = radius of the inner cylinder (concentric cylinder rheometer) (m)
R_o = radius of the outer cylinder (concentric cylinder rheometer) (m)
Re = Reynolds number (-)
Re_p = particle Reynolds number (-)
t = time (s)
T = torque (Nm)
T = temperature (°C or K)
U_0 = initial coagulation state (Hattori-Izumi) (-)
U_3 = coagulation state (Hattori-Izumi) (-)
v = velocity (m/s)
V = volume (m^3)
x = distance (m)
α = cone angle (cone and plate rheometer) (rad)
α = characteristic parameter for destructuration (thixotropy) (-)
γ = angle of deformation (-)
$d\gamma/dt$ = shear rate (s^{-1})
$\dot{\gamma}$ = shear rate (s^{-1})
Γ = surface tension (N/m)
Γ = memory module for shear (mod. Hattori-Izumi) (-)
η = (apparent) viscosity (Pa s)
η_r = relative viscosity (-)
η_s = viscosity of the suspending medium (Pa s)
θ = characteristic parameter for structuration (thixotropy) (s)
Θ = memory module for coagulation (mod. Hattori-Izumi) (-)
λ = friction factor (hydraulics) (-)
λ = structure parameter (thixotropy) (-)
λ_0 = initial structural state (thixotropy) (-)
μ = viscosity (Pa s)
μ" = thixotropic counterpart of viscosity (Pa s)
μ_p = plastic viscosity (Bingham) (Pa s)
ρ = density (kg/m^3)
τ = shear stress (Pa)
τ_w = wall shear stress (Pa)
τ_0 = yield stress (Pa)
τ_0" = thixotropic counterpart of yield stress (Pa)
$\tau_{0,r}$ = relative yield stress (Pa)
$\tau_{0,s}$ = yield stress of the suspending medium (Pa)
φ = volume fraction (-)
φ_{max} = maximum volume fraction (-)
Ω = rotational velocity (rad/s)
Ω_i = rotational velocity of inner cylinder (rad/s)
Ω_o = rotational velocity of outer cylinder (rad/s)

2 Abbreviations

C	=	cement
FA	=	fly ash
LS	=	limestone filler
MRI	=	Magnetic Resonance Imaging
P	=	powder (= cement + filler)
SCC	=	self-compacting concrete
SF	=	slump flow (mm)
SiF	=	silica fume
SP	=	superplasticizer
TC	=	traditional concrete
VF	=	V-funnel flow time (s)
W	=	water

SUMMARY

This thesis describes the interactions between rheological properties and pumping of self-compacting concrete. In the first chapter, after the introduction of self-compacting concrete, the research goals have been set. As a first goal, the rheological properties of self-compacting concrete, including the time dependent behaviour need to be studied in detail. As a second goal, the influence of these rheological properties on the parameters during pumping, which are mainly the pressure and the discharge, must be investigated. On the other hand, the influence of the pumping process on the rheological properties must not be forgotten, as this will serve as an input for future research projects dealing with the filling of formworks.
Due to these two different goals, this thesis has been divided into two main parts: part 1 deals with the rheology (chapters 2-5), while part 2 deals with pressure driven concrete flow (chapters 6-9). Chapter 10 concludes this thesis and opens perspectives for future research.
Rheology is defined as the study of deformation of materials. When focussing on liquid materials, the relationship between shear stress and shear rate must be found. For concrete in general, two rheological parameters must be defined: the yield stress, which must be exceeded in order to initiate flow, and the (plastic) viscosity, which is the resistance to an increase in flow velocity. By means of several rheometers, a third parameter has been found for the steady state rheological properties of self-compacting concrete, namely shear thickening.
An extensive study on this shear thickening behaviour has been performed, showing that it is not a measurement artefact due to thixotropy, particle migration and plug flow. As it has been measured with three different devices, it is not a rheometer artefact neither. In case of concrete, shear thickening can have two main causes: grain inertia and cluster formation. Grain inertia is the result of the inertia forces working on solid particles, which are not negligible compared to the viscous forces. Consequently, the importance of grain inertia increases with increasing (relative) grain size. Cluster formation on the other hand only works on the smaller particles. The high hydrodynamic forces become larger than the inter-particle repulsive forces, and the particles are assembled in temporary clusters, increasing the flow resistance.
Shear thickening has two parameters: the intensity of shear thickening, indicating how fast the shear stress or viscosity increases with increasing shear rate (or shear stress) and the critical shear stress, which indicates at what magnitude of the shear stress shear thickening is being observed. From the experimental results on several self-compacting concretes, it has been observed that decreasing the w/p-ratio

increases the intensity of shear thickening, but it does not significantly affect the critical shear stress. Increasing slump flow (possibly by increasing superplasticizer content) increases the intensity and decreases the critical shear stress. The shear thickening is dependent on the type of filler applied, as SCC with silica fume did not show shear thickening behaviour. Tests with a parallel plate rheometer on cement pastes have shown that shear thickening is already present in the self-compacting cement paste. Somewhat surprisingly, shear thickening decreases with increasing amount of coarse aggregates. Adding demoulding oil decreases shear thickening due to a currently unknown reason.

From the experiments, it can be concluded that cluster formation is the more likely cause for shear thickening, although grain inertia cannot be fully eliminated.

The time dependent rheological behaviour of concrete can be divided, theoretically, into three main parts: thixotropy, structural breakdown and loss of workability. Thixotropy is caused by the reversible breaking and rebuilding of physical connections between cement particles. Structural breakdown is in theory the result of the breaking of chemical linkages while loss of workability is induced by connections or linkages which can no longer be broken. The research on these phenomena is continuing in different institutes and an overview of the results has been given. It should be kept in mind that this time dependent behaviour complicates the rheological measurements significantly.

Based on the available models in order to describe the (steady state) rheological properties of self-compacting concrete, which are the Bingham model, the Herschel-Bulkley equation and the modified Bingham model, an attempt has been made to extend the Poiseuille formula for laminar flow in circular pipes. For the Bingham and modified Bingham models, the extended equation is analytically perfect, and the comparison between the flow of SCC in pipes, by means of gravitational flow tests and the rheometer has indicated quite good agreements, in a first stage. As a result, the flow of SCC in pipes occurs in laminar conditions and no significant wall slip has been observed.

As a main disadvantage of the gravitational flow tests, the very small discharges of maximal 1 l/s can be mentioned. As in practice the discharges are much higher, full scale pumping tests have been executed. The results of these tests indicate that for SCC, the pressure losses per unit of length relate very well with the viscosity and the possible shear thickening of the concrete. Calculations have also revealed that the plug radius, which is determined by the part of the concrete flowing at uniform velocity, is very small in case of SCC, which is in large contrast with traditional concrete.

Theoretical predictions by means of the extended Poiseuille formula indicate that a kind of slippage or a lubrication layer must be formed. As SCC is a rather sticky material, slippage is assumed not to occur. The lubrication layer is thought to be caused by three phenomena: the geometrical wall effect, structural breakdown and dynamic segregation. All effects cause a decrease of the viscosity of the material in the vicinity of the wall, increasing the velocity gradient and the discharge at equal pressure loss. Unfortunately, the sampling, rheometer, testing procedures and mathematical models are not sufficiently accurate in order to confirm or decline the occurrence of one of the phenomena. As a result, the specific behaviour of concrete

at the wall is currently unknown. This can be solved by directly measuring the velocity profile, but this is nowadays not evident at a reasonable price.
Based on the extended Poiseuille equation with the incorporation of the geometrical wall effect, which certainly occurs, shear thickening has been observed during pumping. However it is not as intense as predicted by the extrapolated rheometer data.
During pumping of SCC, the rheological properties are modified due to two main causes: structural breakdown and an increase in air content. Both effects cause a decrease in viscosity of the concrete, but they act in an opposite way on the yield stress. Structural breakdown decreases the yield stress while an increase in air content causes an increase in yield stress. Depending on which phenomenon dominates, SCC can evolve in two different directions. If structural breakdown is more important, segregation can be provoked. If the increase in air content dominates, the filling ability of the SCC can be lost. Performing a slump flow and sieve stability test before and after pumping are advised in order to monitor the changes during pumping.
This research has also revealed that during pumping operations, some hazardous situations can occur. Blocking causes a sudden and significant increase in pressure, which can lead to the rupture of some parts of the conveying line or excessive swings in the placing boom. During cleaning with air pressure, the cleaning sponge can become a dangerous projectile. When these phenomena are handled inappropriately, injuries or even death can occur.

SAMENVATTING

Deze doctoraatsthesis beschrijft de interacties tussen de reologische eigenschappen en het verpompen van zelfverdichtend beton. In het eerste hoofdstuk worden de onderzoeksdoelstellingen gedefinieerd, na de introductie van zelfverdichtend beton. De eerste doelstelling is de fundamentele studie van de reologische eigenschappen van zelfverdichtend beton, inclusief het tijdsafhankelijk gedrag. De tweede doelstelling bestaat uit het onderzoeken van de invloed van deze reologische eigenschappen op de belangrijkste parameters tijdens het pompen: druk en debiet. Hierbij mag echter de invloed van het pompproces op de reologische eigenschappen niet uit het oog verloren worden, gezien dit als beginvoorwaarde geldt voor toekomstige onderzoeksprojecten omtrent het vullen van bekistingen.
Omwille van deze twee doelstellingen, werd dit werk onderverdeeld in twee grote delen. Deel 1 bevat de studie van reologie op zich (hoofdstukken 2-5), terwijl in deel 2 de stroming van beton onder druk wordt beschreven (hoofdstukken 6-9). Hoofdstuk 10 besluit dit doctoraat en opent perspectieven voor verder onderzoek.
Reologie is gedefinieerd als de studie van de vervorming van materialen. Specifiek voor vloeistoffen dient het verband tussen de afschuifspanning (shear stress) en afschuifsnelheid (shear rate) gevonden te worden. Voor beton in het algemeen dienen twee parameters bepaald te worden: de vloeigrens, die overschreden moet worden om de stroming te starten, en de (plastische) viscositeit, de weerstand tegen een toename in stromingssnelheid. Met behulp van verschillende reometers werd een derde parameter gevonden die de reologische eigenschappen van zelfverdichtend beton beschrijft: namelijk shear thickening (dilatantie).
Diepgaand onderzoek aangaande dit shear thickening gedrag heeft aangetoond dat dit geen meetfout is ten gevolge van thixotropie, migratie van de korrels of plugstroming. Gezien dit verschijnsel werd waargenomen in drie verschillende toestellen is het ook geen fout geïnduceerd door de reometer zelf. Voor beton worden twee oorzaken voor shear thickening weerhouden: inertie van vaste deeltjes (grain inertia) en de vorming van clusters. Inertie van vaste deeltjes is het gevolg van de hoeveelheid traagheidskracht inwerkend op een vaste korrel die niet meer verwaarloosbaar is ten opzichte van de viskeuze krachten. Logischerwijze wordt inertie belangrijker bij een toename van de grootte van de deeltjes. De vorming van clusters werkt aan de andere zijde in op de kleinere deeltjes aanwezig in beton. Door de hoge hydrodynamische krachten worden de afstotingskrachten tussen de deeltjes overwonnen en worden verschillende, tijdelijke clusters gevormd die de stromingsweerstand doen toenemen.

Shear thickening wordt beschreven door twee parameters: de intensiteit, die aanduidt hoe snel de afschuifspanning of viscositeit stijgt bij toenemende afschuifsnelheid (of afschuifspanning), en de kritieke waarde voor de afschuifspanning, vanaf dewelke shear thickening wordt waargenomen. De experimenten op verschillende zelfverdichtende betonsamenstellingen hebben aangetoond dat de intensiteit toeneemt met dalende w/p-verhouding, maar dat de kritieke waarde voor de afschuifspanning niet noemenswaardig wijzigt. Bij toenemende slump flow (mogelijk door een toename in hoeveelheid superplastificeerder) neemt de intensiteit toe en daalt de kritieke afschuifspanning. Shear thickening is afhankelijk van het aangewende type vulstof. Voor zelfverdichtend beton met silica fume werd geen shear thickening waargenomen. Proeven op cement pasta's hebben aangetoond dat de shear thickening intrinsiek in de zelfverdichtende pasta aanwezig is, en dat, toch verrassend, shear thickening daalt met een toename in hoeveelheid grof granulaat. Toevoegingen van ontkistingsolie doen de shear thickening dalen omwille van een tot nog toe onbekende oorzaak.
Uit deze experimenten kan besloten worden dat de vorming van clusters een meer waarschijnlijke oorzaak van shear thickening is dan de inertie van vaste deeltjes.
De tijdsafhankelijke reologische eigenschappen kunnen, theoretisch althans, opgedeeld worden in drie verschillende verschijnselen: thixotropie, structural breakdown en verlies aan verwerkbaarheid. Thixotropie wordt veroorzaakt door het omkeerbaar breken en terug opbouwen van fysische verbindingen tussen cementdeeltjes. Structural breakdown is in theorie de afbraak van chemisch gevormde verbindingen, terwijl verlies aan verwerkbaarheid veroorzaakt wordt door fysische en/of chemische verbindingen die niet meer verbroken kunnen worden. Verschillende onderzoeksinstellingen verdiepen zich momenteel in deze verschijnselen en een overzicht van de resultaten werd opgenomen in deze thesis. Als belangrijkste besluit geldt dat het tijdsafhankelijk gedrag de metingen heel wat complexer maakt.
Op basis van de reologische modellen die gebruikt worden om de eigenschappen van zelfverdichtend beton (in evenwicht) te beschrijven (Bingham, Herschel-Bulkley en modified Bingham), werd de formule van Poiseuille voor de laminaire stroming in cilindervormige buizen herwerkt. Deze herwerking was succesvol voor het Bingham en modified Bingham model. Dit werd geverifieerd door middel van gravitaire stromingsproeven, waarvan de resultaten een goede overeenkomst aangeven tussen de reometer en de stromingsproeven. De stroming gebeurt bijgevolg in laminair regime zonder noemenswaardige slip aan de wand van de leiding.
Het grootste nadeel aan deze gravitaire stromingsproeven is het lage debiet van maximaal 1 l/s. In de praktijk zijn de debieten heel wat hoger en om aan die eis te voldoen werden grootschalige pompproeven uitgevoerd. De resultaten van deze proeven hebben aangetoond dat voor zelfverdichtend beton de drukverliezen hoofdzakelijk worden beïnvloed door de viscositeit en het shear thickening gedrag. Uit berekeningen blijkt dat de hoeveelheid beton dat met uniforme snelheid stroomt, de zogenaamde plug, relatief klein is. Dit is in groot contrast met traditioneel beton.
De voorspellingen met behulp van de herwerkte formule van Poiseuille tonen echter aan dat er zeker een slip- of smeringslaag aanwezig moet zijn. Gezien

zelfverdichtend beton een vrij plakkerige substantie is, wordt slip uitgesloten. De smeringslaag wordt toegeschreven aan drie effecten: het geometrisch wandeffect, structural breakdown en dynamische segregatie. Elk van deze effecten veroorzaakt een daling van de viscositeit van het materiaal in de nabijheid van de wand, wat op zich een stijging in snelheidsgradiënt en een stijging in debiet met zich meebrengt. Helaas zijn de monstername, de reometer, de testprocedure en de wiskundige berekeningen niet nauwkeurig genoeg om één van deze effecten te bewijzen of uit te sluiten. Bijgevolg is het gedrag van beton nabij de wand momenteel nog altijd ongekend. Een directe opmeting van het snelheidsprofiel zou dit probleem kunnen oplossen, maar tot op vandaag is dit niet evident tegen een redelijke prijs.
Op basis van de herwerkte formule van Poiseuille, met inbegrip van het geometrisch wandeffect (dit treedt zeker op), werd aangetoond dat shear thickening effectief optreedt tijdens de pompproeven, maar dat de intensiteit lager is dan deze voorspeld op basis van de geëxtrapoleerde reometer gegevens.
Tijdens het verpompen wijzigen de reologische eigenschappen van zelfverdichtend beton omwille van twee oorzaken: structural breakdown en een toename in luchtgehalte. Beide effecten zorgen voor een daling in de viscositeit, maar wat betreft de vloeigrens hebben deze effecten een tegengestelde invloed. Structural breakdown doet de vloeigrens afnemen, terwijl een toename in luchtgehalte een stijging in de vloeigrens veroorzaakt. Afhankelijk van het belang van het ene effect ten opzichte van het andere kan het beton in twee richtingen evolueren. In geval structural breakdown belangrijker is, kan de segregatieweerstand van het zelfverdichtend beton afnemen, terwijl in het andere geval, indien de toename in lucht de belangrijkste parameter is, een verlies aan vulcapaciteit (filling ability) van het beton kan optreden. Door middel van een slump flow en een zeefstabiliteitstest voor en na het verpompen kan de evolutie van de eigenschappen nagegaan worden.
Dit onderzoeksproject heeft ook aangetoond dat gevaarlijke situaties kunnen ontstaan tijdens het verpompen. Door blokkeringen kan de druk plots heel snel stijgen, wat op zijn beurt kan leiden tot breuk in een deel van de pijpleiding of tot het ver uitzwaaien van de pomparm. Bij het reinigen van de leidingen met luchtdruk kan de gebruikte spons een gevaarlijk projectiel worden. Enige nalatigheid tijdens deze verschijnselen kan leiden tot ernstige kwetsuren en zelfs de dood.

CHAPTER 1:

INTRODUCTION

1 Self-Compacting Concrete

1.1 Historical evolution and general research overview

Self-Compacting Concrete (SCC) has been developed in Japan during the 1980's [1.1]. At that time, the Japanese construction industry suffered from a lack of skilled and qualified workmen, which slowed down the construction pace and impaired the durability of new concrete structures. In the following decade, SCC made its entry into Europe through the Netherlands and the Scandinavian countries [1.2-1.4]. Gradually, the amount of SCC applied in construction is increasing, together with the number of countries where it is being used [1.5].

During the last two decades, researchers all over the world have focussed on several topics (note that the list of references is not complete but only gives some examples):

- Composition of the concrete, including constituent materials, with special attention to the plasticizing and stabilizing of the concrete [1.6-1.10].
- Rheological properties of the concrete in fresh state, including numerical modelling [1.11-1.16].
- Casting of SCC, including the reduction of formwork pressures [1.17-1.20].
- Hydration, creep and shrinkage of SCC [1.21-1.25].
- Compressive and flexural strength of the concrete, with or without incorporation of fibres [1.26-1.30].
- Bonding between SCC and steel rebars [1.31-1.33].
- Microstructure of SCC, in relation to the durability in aggressive environments [1.34-1.39].
- Spalling and fire resistance [1.40-1.43].
- Architectural design [1.44-1.46].
- Special applications.

1.2 Definition

Self-compacting concrete is defined by De Schutter and Poppe as [1.5][1.47-1.48]: "a kind of concrete which needs to possess sufficient fluidity in order to be able to fill a formwork completely (filling ability) without the aid of other forces than gravity, even when having to flow through narrow gaps (passing ability), but also showing a sufficient resistance to segregation, during flow and in stationary conditions (stability)."
This definition may seem contradictory: the filling and passing ability require a very fluid (water-like) material, but the stability condition on its turn requires almost the opposite. As a consequence, producing SCC is finding a compromise between the fluidity and the stability, forming a challenge for every SCC-manufacturer each day.

1.3 Composition of self-compacting concrete

In order to achieve sufficient fluidity in self-compacting concrete, of course without increasing the water content, superplasticizers must be applied. Laboratories and companies are investigating the working principle of superplasticizers and improving their characteristics and efficiency continuously [1.9][1.49-1.52]. The superplasticizers of the so-called "third generation", poly-carboxyl-ethers (PCE), have a double working principle. First, they provide the cement-particles with equal charges, creating electrostatic repulsion. Secondly, they have side-chains creating a spatial barrier which other particles cannot cross easily. This is called steric hindrance. More details on the inter-particle forces will be given in chapter 2, when dealing with colloidal suspensions.
Only adding superplasticizers to traditional concrete is not sufficient to create self-compacting concrete, due to the large amount of coarse aggregates in traditional concrete (TC). These coarse particles can create particle bridges when flowing through a narrow gap, causing blocking [1.6], which must be avoided in SCC. In order to fulfil the passing ability condition, the amount of coarse aggregates is reduced. In [1.6], it is postulated that the amount of coarse aggregates is 50% of the volume the aggregates would take in closest packing. The remaining part of the concrete is mortar, of which 40% consists of sand (fig. 1.1).
When applying these rules, and taking a low w/c-ratio into account in order to create a high-quality product, a high amount of cement should be added. Of course, this is not advantageous, not only from an economical point of view, but also for technical reasons. A high amount of cement causes high hydration heat which can lead to thermal cracking. Instead, a part of the cement is replaced by other fine materials, like limestone filler, fly ash, silica fume, …
By adding this extra amount of fine materials, the stability of the SCC-mix is increased. During the last decade, other products have been developed to enhance the stability of SCC, like viscosity-modifying agents or thixotropy-modifying agents [1.53-1.55]. These products have not been applied during this research and as a result, the stability has only been obtained by a sufficiently large amount of fine materials and a sufficiently low amount of superplasticizer.
Finding the proper amount of superplasticizer is still a very challenging task, even for a known and extensively tested SCC mix. The fresh properties of SCC are very

sensitive to any changes in each of the composing elements, making it (almost) impossible to duplicate a SCC mixture.
The proposed compositions for the reference mixes (see chapter 4), are based on standard compositions of SCC in Belgium, in which a large amount of powder (= cement + filler) of at least 550 kg/m³ is applied. The w/c-ratio, equal to 0.45, is chosen in order to comply with the most severe durability class in the NBN EN 206-1. In practice, further changes to the compositions can be applied when considering strength, possibly at early ages, other durability classes, creep, shrinkage, … No specific strength measurements have been performed on the produced concretes, but based on previous Ph-D researches on similar concrete compositions, the compressive strength at 28 days is around 60 to 70 MPa [1.21][1.35].

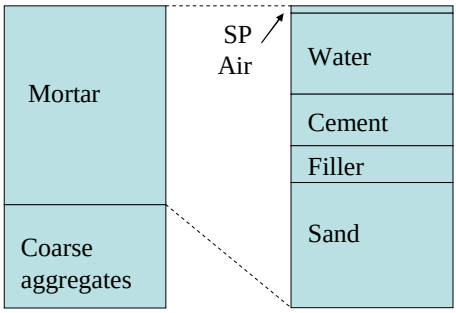

Figure 1.1: Principle of self-compacting concrete composition.

1.4 Standard tests to evaluate SCC

In this section, the standard tests to evaluate the fresh properties of SCC are briefly discussed. The main focus is on the tests applied in this research. In [1.5] and [1.48], a detailed description of all standard tests on SCC can be found.

1.4.1 Slump flow

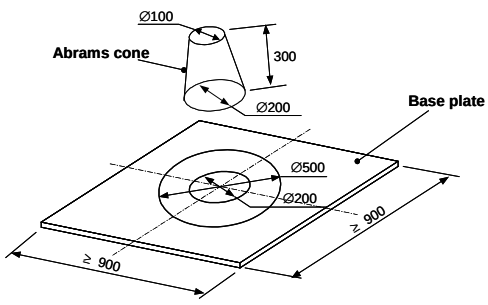

Figure 1.2: Slump flow. Dimensions in mm.

The slump flow test (fig. 1.2) is the easiest and the most widely applied test method for fresh self-compacting concrete. It is very similar to the slump test performed on traditional concrete. An Abrams-cone (diameter 200 mm at the bottom and 100 mm at the top, and a height of 300 mm), is filled with SCC, without compaction. The cone is lifted vertically and the SCC spreads out. In case of traditional concrete, the decrease in height is measured, but for SCC, this would be a very inaccurate measurement. Instead, the average diameter of the resulting SCC-cake is taken as slump flow value. Due to the low velocities during the flow, it can be stated that the slump flow value is quite well related to the yield stress of the material [1.56]. A value larger than 625 mm is required for SCC, while at a value of 900 mm, the risk on segregation is significant.

1.4.2 V-funnel

The V-funnel flow time is measured as the time SCC needs to empty the V-funnel through the narrow opening at the bottom. The dimensions of the V-funnel are given in figure 1.3. High V-funnel flow times indicate that the SCC is quite stiff and is not easily deformable. Low V-funnel times are the result of a very fluid SCC, with an increasing risk for segregation. A V-funnel time between 4 and 12 seconds is considered to be ideal.

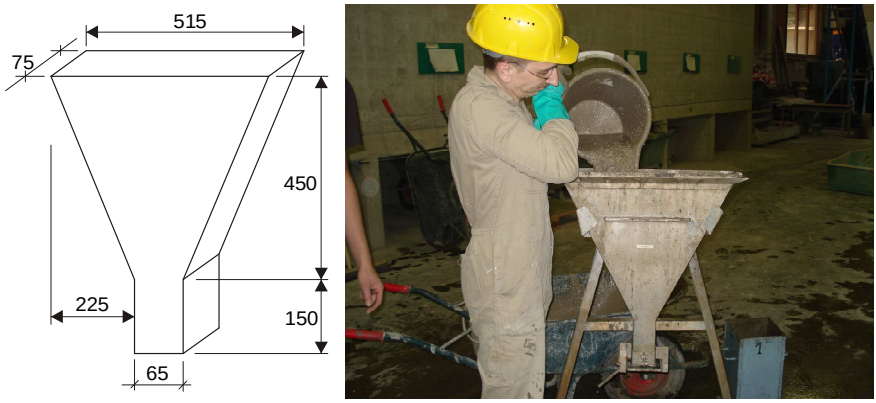

Figure 1.3: V-funnel. Dimensions in mm.

1.4.3 L-box

The L-box (fig. 1.4) consists of a vertical rectangular reservoir connected to a horizontal part. These parts are separated from each other by means of a valve. In the transition zone between the vertical and horizontal part, reinforcement bars (mostly 3) are installed. In this way, the passing ability of the SCC can be evaluated. After 2 minutes of rest, the valve is opened and the SCC flows into the horizontal part, trying to level. The ratio of the concrete height at the end of the horizontal part to the concrete height in the vertical reservoir is calculated. If this ratio ≥ 0.8, the

SCC is supposed to be sufficiently self-compacting. If the SCC segregates or blocking occurs near the reinforcement bars, a lower L-box ratio will be obtained.
In case of SCC with very low viscosity, inertia can become important when doing an L-box test. As a result, a kind of wave of SCC flows further than predicted by the viscous forces only and can possibly create an L-box ratio larger than 1.

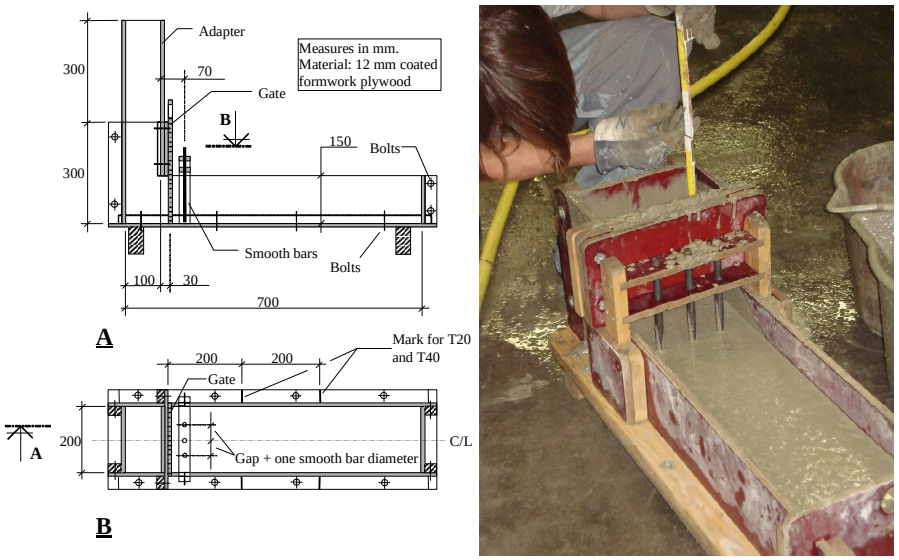

Figure 1.4: L-box. Note that on the right picture the upper part of the vertical reservoir has been removed in order to facilitate the measurements. Dimensions in mm.

1.4.4 Sieve stability test

The sieve stability test consists of pouring 5 ± 0.2 kg of SCC on a sieve with a mesh size of 5 mm. After a rest period of 2 minutes on the sieve, the amount of cement paste/mortar which has fallen through the sieve is weighted. The ratio of this percolated material to the total amount of concrete is called the sieve stability value. The lower this value, the more stable the SCC. In [1.48], SCC is defined as segregating at a sieve stability value larger than 20%, although a value of 15% is more recommended [1.57].
The testing procedure prescribes that the concrete must have rested 15 minutes (in a bucket) before pouring it onto the sieve. I, personally, do not agree with this waiting time, because the concrete has the time to develop an internal structure due to thixotropy, which is not sufficiently broken down when performing the sieve stability test. As a result, segregation is underestimated. In this research project, no waiting time of 15 minutes has been introduced and consequently, the sieve stability tests have been performed as soon as possible.

1.4.5 Density and air content

Density is easily measured by determining the net weight of a reservoir with a fixed, known volume filled with SCC, and dividing the net weight by this volume. The air content has been determined by means of the pressure method, according to NBN – EN 12350-7 (2000).

1.5 Some advantages and disadvantages of SCC

1.5.1 Advantages

Due to the high fluidity of SCC, the air can escape without the aid of any compaction energy. This results in a less noisy and vibration free environment, especially for the workmen on site [1.3] and a substantial reduction of energy needed. As a consequence, the properties of the final structural element constructed with SCC are less dependent on the skills of the workmen on site. However, total independency cannot be achieved, as will be illustrated in chapter 9, dealing with the results of the full scale pumping tests.

During casting of an element with normal/traditional concrete, the process is interrupted each time a layer needs to be compacted. In case of self-compacting concrete, the casting can practically occur in one layer, as long as the formwork can withstand the occurring pressures. Examples of high wall castings on site in Belgium can be found in Bredene (Staf Versluys-centre), where a wall of 12 m high has been cast, and the new cultural centre in Avelgem, where the height was 8.25 m.

In addition, as SCC is able to flow through almost all complex geometries, architects can increase their creativity when designing concrete structures, with lower risks of obtaining a “njet” from the engineer or the contractor. In case of normal concrete, the presence of a window opening causes problems because the concrete cannot be vibrated in an efficient way. Self-compacting concrete flows under the window opening and completely fills the formwork, although special attention has to be paid to air inclusions at the bottom of the window opening.

As SCC does not need any form of compaction, it can be pumped in the formwork from the bottom, instead of from the top. As a consequence, the height of structural elements in the precast industry can be increased and large air inclusions or segregation can be avoided because the concrete does not have to fall from a certain height.

SCC has also successfully been applied in concrete structures with a very dense reinforcement grid, due to its passing ability. Furthermore, examples can be found in literature where the filling ability has proven to be very useful when the element to cast was not easily achievable, for example when reinforcing bridges by adding a layer of SCC at the bottom.

1.5.2 Disadvantages

As a disadvantage, the higher cost of the material can be mentioned, which currently slows down the pace of transition from applying TC to SCC. Although the application of SCC induces a more efficient use of the working staff and probably

causes construction times to decrease, a full cost-benefit analysis (including all factors) should be made in order to justify the application of SCC. Especially in countries with high labour costs, the application of SCC will easily be justified.
Self-compacting concrete is in its fresh state much more sensitive to fluctuations in one of its constituent materials, as mentioned before, making it more difficult to make the same mix twice, even in laboratory conditions. Especially the moisture content of the sand is an important factor, which can cause a total failure of the SCC mix design if not controlled in a proper way. A severe quality control of all constituent materials is necessary, which is currently one of the toughest issues to comply with in concrete industry.
As the fluidity of SCC is higher than that of TC, the applied formworks must be completely tight. In case this is not fulfilled, the cement paste can locally escape, creating voids between the aggregates in the final structural elements. In the worst case, the formwork cannot withstand the occurring pressures and SCC turns into SEC (Self-Escaping Concrete). As anyone knows, SEC is not really useful from a practical point of view.

2 Goals and significance of this research project

2.1 General research planning

This research project forms the basis of the current and future part of the research on fresh self-compacting concrete, performed and to be performed at Ghent University. As main goals, this research field focuses on the fundamental understanding of the flow of self-compacting concrete in pipes and in the formwork, aiming on supporting the industry in order to develop new production methods or to solve occurring problems.
The research can be divided into three main blocks: rheology, flow of SCC in pipes and flow of SCC in the formwork.
A detailed study of the rheological properties of self-compacting concrete, including thixotropy, loss of workability, structural breakdown, … must form the background for the following parts in the project. At the start of this project, research on the rheological properties of SCC composed with Belgian materials, has been executed at the Belgian Building Research Institute (BBRI) and the KULeuven, each institute having a different final goal. As a result, as the aims of the research were different, the research methods, boundary conditions and important parameters have been chosen differently. As a final goal of this part, the rheological behaviour of SCC must be at least understood, and possibly controlled.
In the second step of this research field, the study of the flow of SCC in pipes must be very well understood. This part can be regarded in two different ways: it is necessary to understand the phenomena occurring during pumping of SCC, and to distinguish the most influencing factors. In this way, a possible prediction of pumping pressures or maximal length of the conveying pipes can be calculated, based on the concrete properties, geometrical restrictions and desired construction speed. On the other hand, it is also necessary to know whether the concrete properties after pumping are still the same as before pumping, and in case there is a difference, what is the cause and how do the properties evolve?
Based on the output of the previous part, the flow of SCC in formworks can be studied, both experimentally and numerically. In this way, several formwork filling procedures can be studied, including pumping SCC from the bottom of the formwork. Based on the (pumped) concrete properties, the geometry of the formwork and the reinforcement grid, the optimal filling procedure can be determined. This is the main topic of a second Ph-D research project dealing with the flow of fresh self-compacting concrete.
As a final goal, we want to design a fully automated production plant, in which only a few workers control the mixing of the SCC, the transport through the pipes and the filling of the formworks, based on the obtained knowledge, experience and computer models.

2.2 Original goals of this research project

This project is the initial stage of the current research in the field of the flow of fresh self-compacting concrete. The goals of this project have been defined, based on the desired research strategy and output.
As a first goal, the fundamental study of the rheological properties of self-compacting concrete, including time dependent behaviour, has been set. During the execution of this part of the research, it has been kept in mind that this study must serve as an input for both the flow of SCC in pipes, which occurs quite fast, and the flow in the formwork, which is rather slow. As a result, these conditions have had their repercussions on certain choices which had to be made.
A second goal was the study of the flow of SCC in pipes. Based on literature, and the results of the rheological investigation, the most influencing factors on the pressure must be determined. In this way, the possible problems occurring during pumping of SCC can be better understood. But, as mentioned in the previous section, the influence of pumping on the properties of SCC must not be forgotten, as this serves as an input for the next Ph-D project.
As will be shown in the next section, the final goals deviated somewhat from the original ones, leading to the incompletion of some aspects of the stated goals.

2.3 Contents of this Ph-D-thesis

In part 1 of this thesis, only rheology is described, containing a short introduction into general rheology, a more detailed study on suspension rheology (chapter 2) and the measurement systems and procedures (chapter 3). Chapters 4 and 5 focus on the rheological properties of self-compacting concrete, including shear thickening behaviour and thixotropy. Part 2 of this thesis focuses more on the pressure driven flow of SCC. In chapter 6, the Poiseuille formula for laminar flow has been "re-derived" for shear thickening materials as SCC, whereas in chapter 7, this formula has been applied to gravity-driven concrete flow in pipes. Chapters 8 and 9 describe the seven full scale pumping tests which have been performed at the Magnel Laboratory for Concrete Research. Chapter 10 concludes this Ph-D, giving an overview of the most important results and conclusions. During the study of the rheological properties, after elimination of the time dependent behaviour, a significant complexity, being shear thickening, has been observed and investigated in great detail, as this specific behaviour can have a large influence on the pumping process. As a result of lack of time and the complexity of thixotropy, the experimental characterisation of thixotropy has been cancelled and the results are based on the literature available (see section 2 in chapter 5).

2.4 Research significance

As can be seen in the list of section 1.1, showing the research topics on SCC, one specific point is still missing in the list. Between the rheological characterisation and the flow in the formwork, the concrete must get in some way inside the formwork. Currently, there are two possible ways; by means of a concrete scip or by means of pumping. Especially in small, on-site building sites, where no construction crane is

available, pumping of concrete is the most applied solution. The research performed on the pumping of concrete is quite restricted, focussing on traditional concrete [1.58-1.62] and light-weight-self-compacting concrete [1.63]. Some research institutes provide guidelines for the pumping equipment (pump, pipes, …) and the needed concrete properties (but not the rheological properties) [1.64-1.65].
As a result, the pumping of self-compacting concrete has not been studied extensively and in practice, the rules derived for traditional concrete are applied and people trust on the experience of the pumping operator.
Hopefully, this Ph-D-thesis can put a basis to the fundamental understanding of the pumping process, giving concrete manufacturers the possibility to apply the results to improve their construction procedures. One of the ultimate goals which can be reached by this Ph-D and the "follow-up"-projects dealing with the filling of formworks, is the creation of fully automated precast factories where a line of formworks will be filled with SCC by pumping.
This research can also have a great significance for the fundamental study of the rheological properties of SCC, especially the shear thickening behaviour. Researchers should get more and more convinced that there is more shear thickening in SCC than has been reported in the world. Hopefully, this research can provide at least some insights into the fundamental behaviour and the parameters influencing shear thickening. As will be mentioned in chapters 2 and 4, shear thickening only starts to occur from a certain shear stress on. As a result, in practical situations where higher shear stresses are applied, like pumping, rheological measurements performed at only the lowest shear stresses will underestimate the viscosity. Of course, concrete rheometry is not an easy task. Concrete is described by rheologists as one of the most difficult materials to measure. Precautions need to be taken when performing measurements and a very critical mind must analyse the results.

References

[1.1] Ozawa K., Maekawa K., Kunishima M., Okamura H., "High-Performance Concrete Based on the Durability Design of Concrete Structures," Proc. of the 2nd East Asia – Pacific Conference on Structural Engineering and Construction, Chiang Mae (1989), Vol. 1, 445-456.

[1.2] Skarendahl A., "Self-Compacting Concrete in Sweden. Research and Application.", Proc. of the Int. Workshop on SCC, Kochi (1998), 60-71.

[1.3] Skarendahl A., "Market acceptance of self-compacting concrete, the swedish experience", Proc. of the 2nd Int. RILEM Symp. on SCC, Tokyo (2001), 1-12.

[1.4] Walraven J., "State of the art on self compacting concrete in the Netherlands," Proc. of the 2nd Int. RILEM Symp. on SCC, Tokyo (2001), 13-24.

[1.5] De Schutter G., Bartos P., Domone P., Gibbs J., "Self-Compacting Concrete," Whittles Publishing, Caithness (2008), 296pp.

[1.6] Okamura H., Ozawa K., "Mix design for Self-Compacting Concrete," Concrete library of JSCE **25** (1995), 107-120.

[1.7] Sedran T., de Larrard F., "Optimizing of self-compacting concrete thanks to packing model," Proc. of the 1st Int. RILEM Symp. on SCC, Stockholm (1999), 321-332.

[1.8] Khayat K.H., Ghezal A., Hadriche M.S., "Utility of statistical models in proportioning self-consolidating concrete," Proc. of the 1st Int. RILEM Symp. on SCC, Stockholm (1999), 345-360.

[1.9] Flatt R.J., "Towards a prediction of super-plasticized concrete rheology," Mat. Struct. **37** (2004), 289-300.

[1.10] Bonen D., Deshpande Y., Olek J., Shen L., Struble L., Lange D., Khayat K.H., "Robustness of Self-Consolidating Concrete," Proc. of the 5th Int. RILEM Symp. on SCC, Ghent (2007), 33-42.

[1.11] Wallevik O.H., "Rheology – a scientific approach to develop self-compacting concrete," Proc. of the 3rd Int. RILEM Symp. on SCC, Reykjavik (2003), 23-31.

[1.12] De Larrard F., Ferraris C.F., Sedran T., "Fresh Concrete: A Herschel-Bulkley material?" Mat. Struct. **31** (1998), 494-498.

[1.13] Wallevik J.E., "Rheology of particle suspensions, Fresh concrete, mortar and cement paste with various types of lignosulphonates," Ph-D dissertation, The Norwegian University of Science and Technology, Trondheim (2003).

[1.14] Roussel N., "A thixotropy model for fresh fluid concretes: theory, validation and applications," Cem. Conc. Res. **36** (2006), 1797-1806.

[1.15] Roussel N., Geiker M.R., Dufour F., Thrane L.N., Szabo P., "Computational modeling of concrete flow: a general overview," Cem. Conc. Res. **37** (2007), 1298-1307.

[1.16] Gram A., Farhang A., Silfwerbrand J., "Computer-aided modelling of self-compacting concrete flow," Proc. of the 5th Int. RILEM Symp. on SCC, Ghent (2007), 455-460.

[1.17] Billberg P., "Form pressure generated by self-compacting concrete – Influence of thixotropy and structural behaviour at rest," Ph-D dissertation, School of Architecture and Built Environment, Stockholm (2006).

[1.18] Assaad J., Khayat K.H., "Formwork pressure of self-consolidating concrete made with various binder types and contents," ACI Mat. J. **102:4** (2005), 215-223.

[1.19] Thrane L.N., Stang H., Geiker M.R., "Flow induced segregation in full scale castings with SCC," Proc. of the 5th Int. RILEM Symp. on SCC, Ghent (2007), 449-454.

[1.20] Roussel N., Cussigh F., "Distinct-layer casting of SCC: The mechanical consequences of thixotropy." Cem. Conc. Res. **38** (2008), 624-632.

[1.21] Poppe A.-M., "Influence of fillers on hydration and properties of self-compacting concrete," Ph-D dissertation (in Dutch), Ghent University, Ghent (2004).

[1.22] Poppe A.-M., De Schutter G., "Cement hydration in the presence of high filler contents," Cem. Conc. Res. **35** (2005), 2290-2299.

[1.23] Kadri E.H., Duval R., "Effect of ultrafine particles on heat of hydration of cement mortars," ACI Mat. J. **99:2** (2002), 138-142.

[1.24] Pons G., Proust E., Assie S., "Creep and shrinkage of self-compacting concrete: A different behaviour compared with vibrated concrete?" Proc. of the 3rd Int. RILEM Symp. on SCC, Reykjavik (2003), 645-654.

[1.25] Vieira M., Bettencourt A., "Deformability of hardened SCC," Proc. of the 3rd Int. RILEM Symp. on SCC, Reykjavik (2003), 637-644.

[1.26] Gibbs J.C., Zhu W., "Strength of hardened self-compacting concrete," Proc. of the 1st Int. RILEM Symp. on SCC, Stockholm (1999), 199-209.
[1.27] Domone P.L., "A review of mechanical properties of hardened self-compacting concrete," Cem. Conc. Comp. **29:1** (2007), 1-12.
[1.28] Khayat K.H., Roussel Y., "Testing and performance of fibre-reinforced, self-consolidating concrete, " Proc. of the 1st Int. RILEM Symp. on SCC, Stockholm (1999), 509-521.
[1.29] Grünewald S., Walraven J.C., "Maximum content of steel fibres in self compacting concrete," Proc. of the 2nd Int. RILEM Symp. on SCC, Tokyo (2001), 137-146.
[1.30] Uebachs S., Brameshuber W., "Self-compacting concrete with carbon fibre reinforcement for industrial floor slabs," Proc. of the 2nd North-American Conf. on the design and use of SCC and the 4th Int. RILEM Symp. on SCC, Chicago (2005).
[1.31] de Almeida Filho F.M., El Debs M.K., El Debs A.L.H.C., "Bond-slip behavior of self-compacting concrete and vibrated concrete using pull-out and beam tests," Mat. Struct. **41** (2008), 1073-1089.
[1.32] Desnerck P., De Schutter G., Taerwe L., "Experimental determination of Bond Strength of Reinforcing Bars in Self-Compacting Concrete," Proc. of the 5th Int. RILEM Symp. on SCC, Ghent (2007), 659-664.
[1.33] Domone P.L., "A review of the hardened mechanical properties of self-compacting concrete," Cem. Conc. Comp. **29** (2007), 1-12.
[1.34] Audenaert K., "Transport mechanisms in self-compacting concrete in relation to carbonation and chloride penetration," Ph-D dissertation (in Dutch), Ghent University, Ghent (2006).
[1.35] Boel V., "Microstructure of self-compacting concrete in relation to gas permeability and durability aspects," Ph-D dissertation (in Dutch), Ghent University, Ghent (2006).
[1.36] Boel V., De Schutter G., "Porosity of superplasticised cement paste containing limestone filler," Adv. Cem. Res. **18** (2006), 97-102.
[1.37] Qiang Y., Caijun S., Fuqiang H., De Schutter G., Audenaert K., Keren Z., "Effect of hydroxyl ions on chloride penetration depth measurement using the colorimetric method," Cem. Conc. Res. **38** (2008), 1177-1180.
[1.38] Persson B., "Sulphate resistance of self-compacting concrete," Cem. Conc. Res. **33** (2003), 1933-1938.
[1.39] Neville A., "The confused world of sulfate attack on concrete," Cem. Conc. Res. **34** (2004), 1275-1296.
[1.40] Ye G., De Schutter G., Taerwe L., " Spalling behaviour of small self-compacting concrete slabs under standard fire conditions," Proc. of the 5th Int. RILEM Symp. on SCC, Ghent (2007), 799-804.
[1.41] Bostrom L., Jansson R., "Spalling of self-compacting concrete," in "structures in fire", Proc. of the 4th Int. Workshop, Aveiro (2006), 757-776.
[1.42] Annerel E., Taerwe L., Vandevelde P., "Assessment of temperature increase and residual strength of SCC after fire exposure," Proc. of the 5th Int. RILEM Symp. on SCC, Ghent (2007), 715-720.
[1.43] Liu X., "Microstructural Investigation of Self-Compacting Concrete and High-Performance Concrete during Hydration and after Exposure to High Temperatures," Ph-D dissertation, Ghent University – Tongji University, Ghent (2006).
[1.44] Annerel E., De Schutter G., "Microstructure and aesthetic appearance of SCC," Proc. of the 5th Int. RILEM Symp. on SCC, Ghent (2007), 381-386.
[1.45] Dursin F., Moyaert J., "The influence of formwork release agents at the surface appearance and texture of self-compacting concrete," Master thesis, KHBO, Ostend (2003).
[1.46] Gram H.E., "Oberflächenschäden bei Selbstverdichtendem Beton, Diskussion möglicher Ursachen," BFT **8** (2004), 28-33.
[1.47] Poppe A.-M., De Schutter G., Audenaert K., Boel V., "Kennismaking met zelfverdichtend beton (1): samenstelling en reologie", Bouwkroniek (feb. 2002), 30-34 (in Dutch).
[1.48] EFNARC European Project, "The European Guidelines for Self-Compacting Concrete: Specification, Production and Use," EFNARC (2005).
[1.49] Ferraris C.F., Obla K.H., Hill R., "The influence of mineral admixtures on the rheology of cement paste and concrete," Cem. Conc. Res. **31** (2001), 245-255.
[1.50] Vickers T.M.Jr., Farrington S.A., Bury J.R., Brower L.E., "Influence of dispersant structure and mixing speed on concrete slump retention," Cem. Conc. Res. **35** (2005), 1882-1890.
[1.51] Flatt R.J., "Dispersion forces in cement suspensions," Cem. Conc. Res. **34** (2004), 399-408.

[1.52] Kjeldsen A., Geiker M., "Modelling inter-particle forces and resulting agglomerate sizes in cement-based materials," Proc. of the 2nd North-American Conf. on the design and use of SCC and the 4th Int. RILEM Symp. on SCC, Chicago (2005).
[1.53] Assaad J.J., Khayat K.H., "Effect of Viscosity-Enhancing Admixtures on Formwork Pressure and Thixotropy of Self-Consolidating Concrete," ACI Mat. J. **103:4** (2006), 280-287.
[1.54] Khayat K.H., Assaad J.J., "Use of Thixotropy-Enhancing Agent to Reduce Formwork Pressure Exerted by Self-Consolidating Concrete," ACI Mat. J. **105:1** (2008), 88-96.
[1.55] Terpstra J., "Thixotropy-enhancing agents for stabilization of SCC and earth moist concrete," Proc. of the 5th Int. RILEM Symp. on SCC, Ghent (2007), 869-874.
[1.56] Roussel N., "Correlation between yield stress and slump: Comparison between numerical simulations and concrete rheometers results," Mat. Struct. **39** (2006), 501-509.
[1.57] "European guidelines for self-compacting concrete", Joint Research Group, EFNARC, Brussels (2005).
[1.58] Kaplan D., "Pumping of concretes," Ph-D dissertation (in French), Laboratoire Central des Ponts et Chausées, Paris (2001).
[1.59] Kaplan D., de Larrard F., Sedran T., "Design of Concrete Pumping Circuit," ACI Mat. J. **102:2** (2005), 110-117.
[1.60] Tattersall G.H., Banfill P.F.G., "The rheology of fresh concrete," Pitman, London (1983).
[1.61] Ede A.N., "The resistance of concrete pumped through pipelines," Mag. Conc. Res. **9** (1957), 129-140.
[1.62] Browne R.D., Bamforth P.B., "Tests to establish concrete pumpability," Proc. of the American Concrete Institute **74** (1977), 193-207.
[1.63] Haist M., Müller H.S., "Optimization of the pumpability of self-compacting lightweight concrete," Proc. of the 2nd North-American Conf. on the design and use of SCC and the 4th Int. RILEM Symp. on SCC, Chicago (2005).
[1.64] Guptill N.R. et al., "Placing Concrete by Pumping Methods," Report of ACI Committee 304, American Concrete Institute (1996).
[1.65] Crepas R.A., "Pumping Concrete, techniques and applications, 3rd edition," Crepas and Associates Inc., Elmhurst (Ill.) (1997).

PART I:

RHEOLOGY

CHAPTER 2:

SUSPENSION RHEOLOGY

This chapter contains an introduction into suspension rheology, without details of specific measurements and procedures, which will be covered by chapter 3. Before going into the fundamentals of suspension rheology, the term "rheology" will be defined in the first section. In the second section a distinction will be made between solid and liquid materials, focusing mainly on the liquid materials. Sections 3 and 4 deal with non-colloidal and colloidal suspensions respectively, giving an overview of literature results relevant for concrete rheology. In section 5, foam rheology will be briefly introduced.

1 Definition of rheology

Rheology is generally defined as "the study of deformation of matter [2.1-2.2]." Strictly speaking, when referring to the Greek roots of the word, it should be defined as "the study of flow," but this definition is too strict to cover all subjects studied in rheology [2.1-2.2].

With this definition, people do not get much wiser about what rheology really is. In fact, in many cases, scientists do not know they are dealing with rheology. Structural engineers for example, dealing with the theory of strength, calculating the deflection or distortion angle of their steel girder, concrete beam or complete bridge: this is rheology. In hydraulics: pipe flow, open channel flow, sediment transport, blood flow: this is rheology. Steel production: casting molten iron in a mould, or rolling a steel slab into a thin plate: this is (maybe only partly) rheology. The mayonnaise on your fries (in order to give a typical Belgian example): why it stays there, why it partly sticks on your fries, and why you do not have to chew on it: rheology. As one can see, rheology is everywhere, only it is not recognised as rheology each time.

In order to be theoretically correct, rheology should be described by means of 3-D tensors, with variability in time [2.1]. In this thesis, 3-D phenomena are not taken into account, and instead of using the complex 3-D notations, every equation will be simplified to its 1-D equivalent.

2 Solid versus liquid materials

2.1 Hooke's law

Robert Hooke stated in 1678 that "the power of any spring is in the same proportion with the tension thereof [2.3]." As can be seen, the statement is focussed on the behaviour of springs, but the defined relationship between stress and strain can be generalised for any perfectly elastic material. Hooke's law is better known under the form of equations (2.1) and (2.2) [2.4].

$$\sigma = E \cdot \varepsilon \tag{2.1}$$

$$\tau = G \cdot \gamma \tag{2.2}$$

where: σ = *axial stress (Pa)*
E = *Young's modulus (Pa)*
ε = *strain (-)*
τ = *shear stress (Pa)*
G = *shear modulus (Pa)*
γ = *angle of deformation (-)*

Equation (2.1) applies on axial deformation, for example when determining the stress – strain relationship of a steel bar in the elastic region. In this case, the deformation occurs in the direction of the applied stress. For equation (2.2), the deformation occurs in a different way, which is illustrated in figure 2.1. The strain differences are expressed by the angle of deformation γ.
In order to be fully correct, a third equation should be added to the two former equations, describing torsion. In addition, Hooke's law in equations (2.1) and (2.2) describes a linear relationship between stress and deformation, but for very large strains, for example for rubber materials, the stress – strain relationship is no longer linear, which is described by the neo-Hookean model [2.5].

2.2 Newton's law

2.2.1 Newtonian behaviour

For perfectly viscous materials, Isaac Newton (1687) proposed the following relationship: "The resistance which arises from the lack of slipperiness originating in a fluid, other things being equal, is proportional to the velocity by which the parts of the fluids are being separated from each other [2.6]." This sounds quite complicated, but translated into an equation, it is much easier:

$$\tau_{yx} = \eta \cdot \frac{dv_x}{dy} = \eta \cdot \dot{\gamma} \tag{2.3}$$

where: τ_{yx} = *shear stress (Pa)*
η = *viscosity (Pa s)*
dv_x/dy = *velocity gradient (1/s) or shear rate* ($d\gamma/dt$)

Equation (2.3) states that applying a shear stress in the x-direction on a plane with the normal vector in the y-direction is proportional to the (x-)velocity gradient in the y-direction. The proportionality constant (η) is defined as the viscosity, which is the "lack of slipperiness" in Newton's definition. The velocity gradient can also be expressed as the time variation of the angle of deformation, which is called the shear rate.

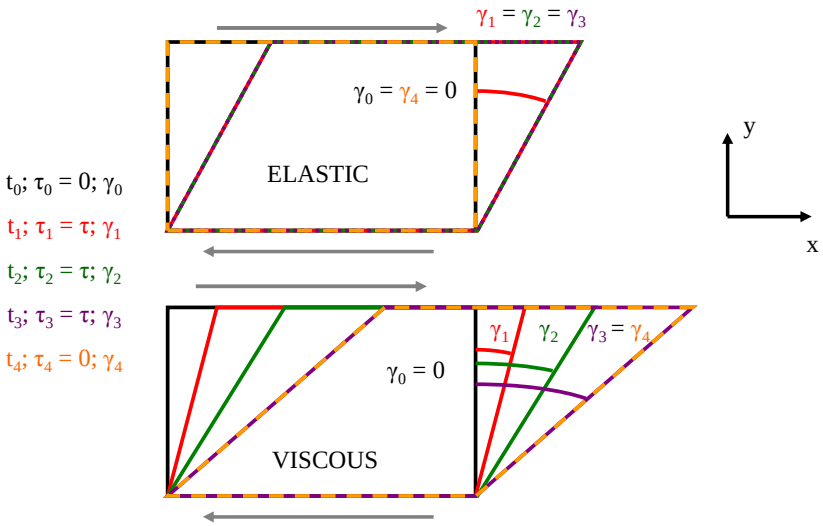

Figure 2.1: Representation of the response of the angle of deformation for an elastic (top) and viscous material (bottom), to a stepwise stress function. Stress is increased from 0 to τ just after t_0 and is released just after t_3.

The difference between a perfectly elastic and a perfectly viscous material is shown in figure 2.1, where for a constant stress, the angle of deformation is constant for the elastic material, while the angle of deformation changes at a constant rate for the viscous material. Once the stress is removed, the elastic material returns to its original condition, but a viscous material stays in its finally achieved shape. The elastic material is said to have a perfect memory, while the viscous material does not have any memory [2.1][2.7].
Analogous to the relation between equations (2.2) and (2.3) for shear stresses, equation (2.4) describes the proportionality between stress and rate of deformation in the axial direction, based on equation (2.1). In this Ph-D thesis, no further attention will be paid to extensional/axial flow of liquids.

$$\sigma_{xx} = \eta_u \cdot \dot{\varepsilon} \tag{2.4}$$

where: σ_{xx} = *axial stress (Pa)*
η_u = *extensional viscosity (Pa s)*
$d\varepsilon/dt$ = *rate of axial deformation (1/s)*

In equation (2.3), a linear relationship between shear stress and shear rate is described if the viscosity remains constant in time and for all shear rates. In this case, the material is defined as a Newtonian material, of which water and oil are the best known examples. In most cases, the rheological behaviour of liquids is non-Newtonian, which means that the rheological law deviates from the Newtonian law.

2.2.2 Non-linear behaviour

One of the possibilities for non-Newtonian behaviour is a non-linear relationship between shear stress and shear rate. As a result, the viscosity is no longer constant for all shear rates. When viscosity decreases with increasing shear rate, the fluid is called shear thinning and the flow curve (= curve in shear stress – shear rate diagram) bends downward. In the opposite case, when viscosity is increasing with increasing shear rate, the material is shear thickening and the flow curve bends upward. Equation (2.5), which is called the power-law model, is able to describe shear thinning and shear thickening behaviour, and is one of the most applied models in rheology.

$$\tau = m \cdot \dot{\gamma}^n \tag{2.5}$$

where: m = *consistency factor (Pa* s^n*)*
n = *consistency index (-)*

The distinction between shear thinning and shear thickening is made by the consistency index "n". For $n < 1$, the material is shear thinning, for $n > 1$, it is shear thickening. If $n = 1$, the linear, Newtonian behaviour is obtained again.

2.2.3 Yield stress

Some materials need a certain stress to be applied before flow initiates, which means that they have a yield stress. The best known yield stress materials are paint, toothpaste and ketchup. For toothpaste for example, pressing on the tube causes a high shear stress and the paste is squeezed out through the nozzle. When the paste is on the toothbrush, it keeps its shape and does not flow between the brushes, due to the low shear stress (gravity) applied. When brushing the teeth, the paste is again subjected to high stresses and deforms easily. From this example, it can be seen that a certain stress must be applied before the material flows. This can be expressed by adding an extra term to the Newtonian or the power-law model. In case the relationship between shear stress and shear rate remains linear once the yield stress is exceeded, the material can be described by the Bingham model [2.8] (eq. 2.6):

$$\tau = \tau_0 + \mu_p \cdot \dot{\gamma} \tag{2.6}$$

$$\tau = \tau_0 + K \cdot \dot{\gamma}^n \tag{2.7}$$

where: τ_0 = *yield stress (Pa)*
μ_p = *plastic viscosity (Pa s)*
K = *consistency factor (Pa s^n)*

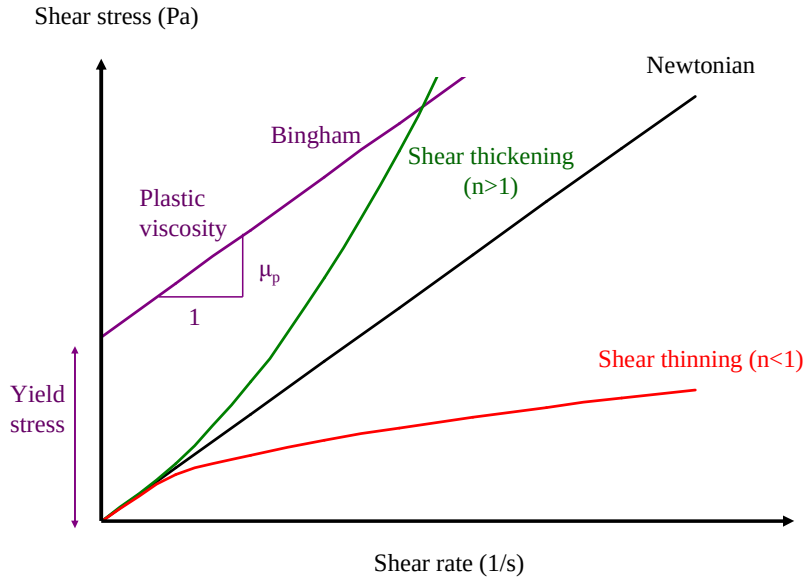

Figure 2.2: Flow curves for a Newtonian (black), shear thinning (red), shear thickening (green) and Bingham material (purple).

As can be seen in equations (2.6) and (2.7), the shear rate can only be non-zero when the shear stress (τ) exceeds the yield stress (τ_0). Equation (2.7) includes a yield stress into the power-law model, resulting in the Herschel-Bulkley model [2.9]. A material, obeying Herschel-Bulkley is shear thinning or shear thickening for the same conditions as mentioned for the power-law model.
Figure 2.2 shows the flow curves for a Newtonian, shear thinning, shear thickening and yield stress material (Bingham).

2.2.4 Time dependency

For some materials, the viscosity can change with time, caused by physical or chemical phenomena. Thixotropy and anti-thixotropy are well known time dependent effects. A detailed description of the time effects on concrete, being thixotropy, structural breakdown and loss of workability, will be given in chapter 5.

2.2.5 Three kinds of viscosity

Several definitions of viscosity are found in literature and will also be used in this thesis. For the sake of clarity, a clear distinction between three types of viscosities will be made in this section: the apparent viscosity, the tangential viscosity and the plastic viscosity.

The apparent viscosity at a certain shear rate is the inclination of a line connecting the flow curve at that specific shear rate with the origin. It can be very simply calculated by dividing the shear stress by the shear rate. The apparent viscosity is mostly applied in literature dealing with non-concrete rheology.

The tangential viscosity at a certain shear rate is the inclination of the flow curve at that specific shear rate. It can be calculated as the first derivative of the flow curve to the shear rate, at that specific shear rate.

The plastic viscosity only has a meaning when the Bingham model is applied, and consequently, the flow curve is a straight line. It represents the inclination of this line, which equals, in fact, the tangential viscosity for shear rates larger than 0.

The difference between apparent and tangential viscosity is shown in figure 2.3, while the plastic viscosity is shown in figure 2.2. For a Newtonian liquid, these three different types of viscosity are all equal.

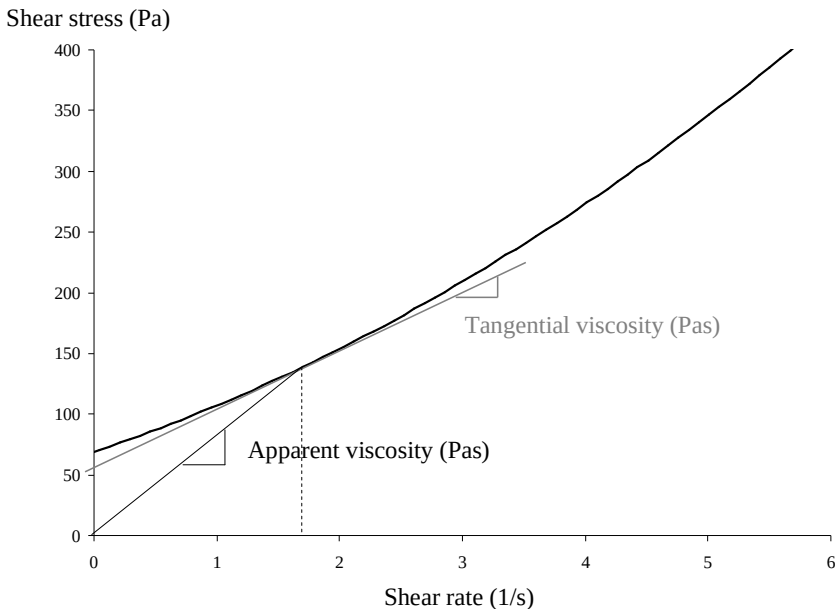

Figure 2.3: Difference between apparent viscosity (black) and tangential viscosity (grey).

2.3 Visco-elasticity

Some materials act both as an elastic and a viscous material, depending on the time scale of the stress applied. At constant stress, the material undergoes immediately an instantaneous strain, which corresponds to elastic behaviour, and during time, strain can increase, due to the viscous properties [2.1]. The best way to investigate visco-elastic behaviour is by applying a sinusoidal stress or strain to the material and see what the respective strain or stress response is. If, for example, a sinusoidal stress is applied with a certain frequency, the strain response will also be sinusoidal, but with a fase-shift between 0 and $\pi/2$. In case the fase shift is 0, which means that the strain scales linearly with the stress (eq. 2.2), the material behaves perfectly elastic at that frequency. If the fase shift equals $\pi/2$, it means that the strain scales with the time-derivative of the stress (eq. 2.3), indicating perfectly viscous behaviour. Any fase-shift in between indicates a combination of elastic and viscous deformation [2.1].
One particular example of a visco-elastic behaviour is the response of hardened concrete under a constant load [2.10-2.12]. In a so-called creep test, the compressive strain at constant stress as a function of time is measured. A typical result of a creep test in figure 2.4 shows an immediate increase in strain when the load is applied, indicating elastic deformation, followed by a further increase in strain at a constant load, indicating creep, which is viscous flowing of the hardened concrete (with a very high viscosity).
In fact, to be fully correct, all materials are visco-elastic [2.1]. For example, glass has a viscosity of around 10^{40} Pa s, which means it flows really slowly and the deformation is only noticeable after many years. Water, which is best known as a liquid, can behave as an elastic material if the stress is applied very suddenly. From a practical point of view, the time scale determines whether the elastic or viscous properties (or both) of the material are dominant.

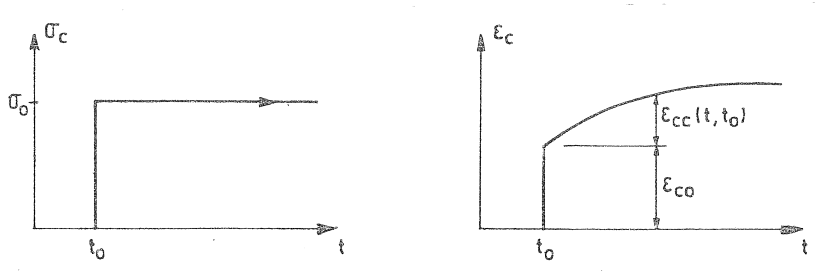

Figure 2.4: Creep test on hardened concrete indicating visco-elastic behaviour. It shows the instantaneous deformation due to elasticity (ε_{c0}) and the time dependent strain due to viscous flowing (ε_{cc}). Figure from [2.13].

3 Non-colloidal suspensions

Suspensions are mixtures of solid particles in a liquid medium. The liquid medium is called the suspending material, the solid particles form the suspended phase. Liquid-in-liquid mixtures and gas-in-liquid mixtures are called emulsions and foams respectively.

3.1 Distinction between colloidal and non-colloidal particles

Colloidal particles have a typical particle size smaller than 1 μm [2.1][2.14]. For these particles, the influence of the inter-particle forces, which will be described in section 4.2 of this chapter, is no longer negligible, and will influence the behaviour of the suspension. For non-colloidal particles, logically, the opposite applies, which means that particle interactions are caused by direct contact or by increasing the hydrodynamic forces between and around particles. This section will focus on the non-colloidal suspensions, while the next section incorporates the inter-particle forces and the behaviour of colloidal suspensions. As concrete contains both colloidal and non-colloidal particles, both sections will have reflections on concrete rheology.

3.2 Influence of suspended non-colloidal particles on the viscosity

3.2.1 Maximum volume fraction

In a suspension of particles, unless the particles are all cubic and perfectly organized, the volume fraction of particles, which is the ratio of the volume the particles include to the total suspension volume, is always lower than 1. In case of monodisperse (all particles have same size), spherical particles, the theoretical, maximum, 3-D volume fraction is 0.74 [2.15-2.16]. This is the maximum possible volume fraction, when the spheres are all put in the best possible organization one by one. In a normal system, the random maximum volume fraction is even lower [2.17-2.18].
Mixing two monodisperse batches of particles can in most cases, when the finer particles fit (even only partly) in the voids between the coarser particles, increase the maximum volume fraction for a certain replacement ratio (fig. 2.5). Adding a third particle batch increases the maximum volume fraction even more.
In case of particles in concrete, which is a nice example of a very broad polydisperse system with particle sizes varying between 0.1 μm (or even lower) and 1 cm, relationships have been determined in order to obtain an optimal packing. Very familiar are the experimental curves of Fuller and Bolomey in concrete technology [2.13][2.19].
More recently, several theoretical approaches have been developed in order to determine the maximum volume fraction as a function of particle size, particle distribution and particle shape. The best known theory for concrete is the compressible packing model of F. de Larrard [2.18]. Recent calculations have shown that self-compacting concrete has a maximum volume fraction of around 84 to 86 %

[2.20], which is much larger than the maximum, random, volume fraction for monodisperse hard spheres (≈ 64 %) [2.21].

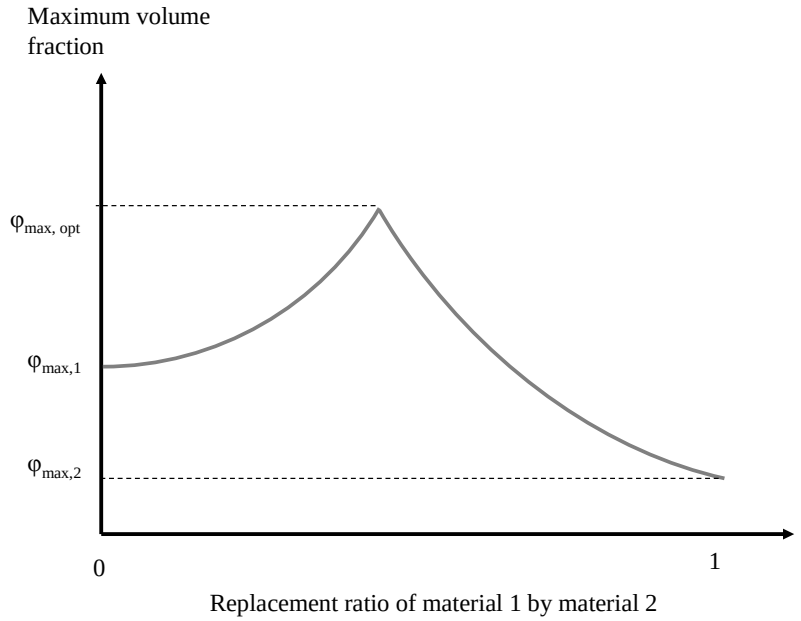

Figure 2.5: Maximum volume fraction as a function of the replacement ratio of material 1 (with $\varphi_{max,1}$) by material 2 (with $\varphi_{max,2}$), shows in this case a larger volume fraction for a combination of material 1 and 2 ($\varphi_{max,opt}$). Figure from F. de Larrard [2.18].

This maximum volume fraction is a very important physical parameter, because, at this specific value, the interstitial fluid does not have the space to move between the particles and any shearing flow is prevented.

3.2.2 Dilute suspensions

Dilute suspensions are suspensions with very low volume fractions (lower than 5 %). In this case, the solid particles cause a change in streamlines which results in a local increase in flow resistance. In dilute suspensions, the flow field influenced by a particle is not additionally influenced by another particle. In this case, Einstein's equation applies (eq. 2.8) [2.22-2.23]:

$$\eta_r = \frac{\eta}{\eta_s} = 1 + 2.5 \cdot \varphi \tag{2.8}$$

where: η_r *= apparent relative viscosity (-)*

η = apparent viscosity of the suspension (Pa s)
η_s = apparent viscosity of the suspending medium (Pa s)
φ = volume fraction (-)

In equation 2.8, the relative viscosity is described, which is the ratio of the suspension viscosity to the viscosity of the suspending medium. As a result, for example, doubling the (suspending) medium viscosity will cause the suspension viscosity to double. The relative viscosity increases linearly with increasing volume fraction. The factor 2.5, obtained by Einstein is only valid for a specific series of conditions: spherical particles, no interaction between particles, no slip at the particle surface, … [2.14][2.22]

3.2.3 Semi-dilute suspensions

In case of semi-dilute suspensions, up to a volume fraction of 10 to 12 %, there are some interactions between the particles. When particles are flowing on two streamlines which are located at a distance less than a particle diameter from each other, the faster particle needs to move around the slower one, causing squeezing of the fluid between the particles when approaching, and suction of the fluid when being removed from each other again. The case of direct collision is not mentioned here, but will be covered by section 3.3.3. The larger the particle displacement, the larger influence the particles have on the flow field and the resulting squeezing and suction cause an additional energy loss to the one caused by the presence of the particles without interactions, described by Einstein's equation (eq. 2.8). In order to solve the problem, Batchelor and Green extended Einstein's equation with a second order term in the volume fraction (eq. 2.9) [2.24-2.25]:

$$\eta_r = 1 + 2.5 \cdot \varphi + c_2 \cdot \varphi^2 \tag{2.9}$$

where: c_2 = factor depending on the type of flow and particle shape. c_2 equals 5 in case of monodisperse spherical particles in a shearing flow.

3.2.4 Concentrated suspensions

Equation (2.9) is not valid anymore when the suspension has a higher concentration of solid particles. Theoretical models are not available, and as a result, the relative viscosity is described by means of semi-empirical equations or it has been determined by means of simulations. The most famous equation for the relative viscosity in concentrated suspensions is the Krieger-Dougherty equation (eq. 2.10) [2.26]. It has been derived by increasing the number of particles one by one and calculating the resulting viscosity. Finally, when the volume fraction approaches the maximum volume fraction, no more particles can be added and the viscosity becomes infinite.

$$\eta_r = \left(1 - \frac{\varphi}{\varphi_{\max}}\right)^{-[\eta]\cdot\varphi_{\max}} \qquad (2.10)$$

$$[\eta] = \lim_{\varphi \to 0}\left(\frac{\eta/\eta_s - 1}{\varphi}\right)$$

where: φ_{max} *= maximum volume fraction (-)*
$[\eta]$ *= intrinsic viscosity (Pa s), equal to 2.5 for spheres, higher for other particle shapes.*

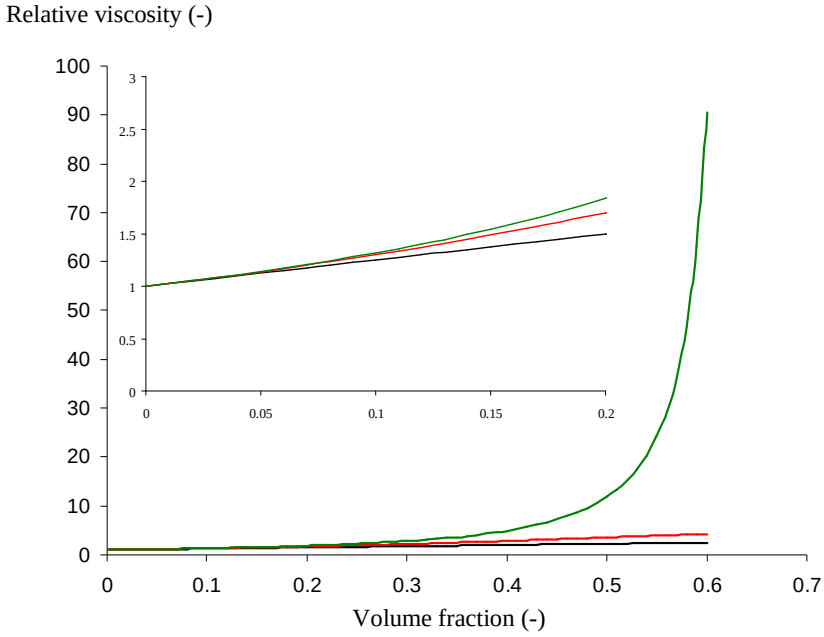

Figure 2.6: Relative viscosity as a function of the volume fraction according to the Einstein equation (black), the Batchelor-Green equation (red) and the Krieger-Dougherty model (green) with a maximum volume fraction of 0.64. The inset shows a detail of the three models for small volume fractions.

Figure 2.6 shows the relative viscosity as a function of volume fraction for the Einstein equation (eq. 2.8), the Batchelor-Green equation (eq. 2.9) and the Krieger-Dougherty equation (eq. 2.10). It can be seen that Einstein's equation underestimates the relative viscosity starting from a volume fraction of 5%. The Batchelor-Green equations gives an underestimation from a volume fraction of 12% on.

The advantage of the Krieger-Dougherty equation is that, no matter what the particle size, shape or distribution is, the equation scales all data on a master curve, when the relative viscosity is plotted to the ratio of the volume fraction to the maximum volume fraction [2.26-2.27]. As a result, increasing maximum volume fraction decreases the relative viscosity at a certain volume fraction, justifying the research and development of models which can determine and control the maximum volume fraction. This decrease in relative viscosity can be very significant if the volume fraction is very close to the maximum volume fraction. This can be the reason why the fresh properties of concrete are quite sensitive to changes in one of the constituting elements.

3.3 Shear thinning and shear thickening

Shear thinning and shear thickening of a suspension can be the result of shear thinning and shear thickening of the suspending medium. As has been shown in the previous section, increasing volume fraction increases the viscosity with a certain factor, but it does not change the fundamental rheological behaviour. The next sections will show this is not completely the truth. Shear thinning and shear thickening can also be introduced by the suspended phase itself, while the suspending medium does not show the corresponding behaviour.

3.3.1 Particle migration

At high shear rates, some surprising measurements can be obtained. Gadala-Maria and Acrivos [2.28] discovered in 1980 that shearing a concentrated suspension in a Couette rheometer (see chapter 3) leads to a decrease in relative viscosity with time. Ovarlez et al. [2.29] discovered that when a shear rate distribution is applied to a concentrated suspension, for example in a wide gap Couette rheometer, the particles have a tendency to move to regions with lower shear rates, resulting in a flow-induced concentration profile (fig. 2.7), and also resulting in more particles at the bottom of the rheometer. They have also observed that the phenomenon was independent on the magnitude of the shear rate applied.

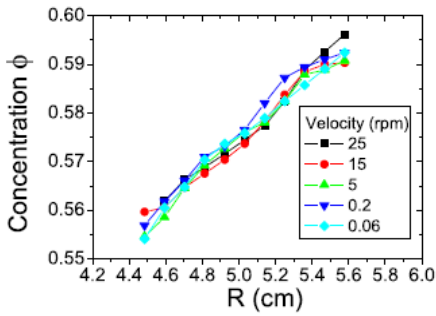

Figure 2.7: Concentration of particles in a large-gap Couette rheometer increases with increasing radius, indicating particle migration into zones with lower shear rates. Figure from G. Ovarlez et al. [2.29]

This migration of particles into zones of smaller shear rates is a phenomenon concrete rheologists have to deal with. It can happen in a rheometer, and it has been experienced during the pumping of traditional concrete. Appropriate actions need to be taken if the real rheological characteristics of the material need to be determined.

3.3.2 Shear-induced ordering and disordering

Shear-induced ordering and disordering has been mostly observed in Brownian suspensions (see section 4.1), but it has also been reported for small, monodisperse non-colloidal particles [2.30]. At low shear rates, the particles organize themselves in different layers, having interstitial layers containing only the suspending fluid. Due to the absence of particles in the interstitial layer, shearing requires less energy and consequently, the viscosity decreases with increasing shear rate. Contrary to Brownian suspensions, this shear thinning is not a reversible effect. If no energy is added to the suspension to reorganize into a random packing, the layers continue to exist, even at very low or zero shear rate.
From a certain shear rate (or shear stress) on, the particles quit their layered positions and start forming a random packing again. As a result, viscosity drastically increases with increasing shear rate, and shear thickening is observed. During a long time, the ordering-disordering theory (ODT) has been believed to be the cause of shear thickening. As will be shown later, this is not needed to obtain shear thickening in Brownian suspensions. ODT only applies for narrow monodisperse suspensions. In case polydispersity increases, the layers are not formed easily and the resulting shear thinning and shear thickening are not observed [2.31-2.32].
Shear-induced ordering can also occur for non-spherical particles. When starting from a random situation, the particles align in the flow direction at a certain shear rate, causing shear thinning behaviour. On the other hand, particles do not loose significantly the flow alignment at high shear rates, and as a result, shear thickening is not necessarily observed. Similarly to the spherical particles, this shear thinning is non-reversible, because when no energy source is applied to randomise the particle orientation, the flow alignment remains, even at zero shear rate.

3.3.3 Grain inertia

Shear thickening in non-colloidal suspensions is not always the consequence of an order-disorder transition. It can also be caused by the particles having some non-negligible amount of inertia which causes particle collisions. This has been observed by Bagnold when suspending 1 mm wax spheres in a glycerine-water-alcohol mixture. The mixture was adapted in order to make the particle neutrally buoyant, so gravity did not have any influence on the experiments [2.33]. Bagnold found that the viscosity of the mixture increased linearly with the shear rate, resulting in a quadratic relationship between shear stress and shear rate. Consequently, shear thickening has been observed, which Bagnold dedicated to the collision between the particles and direct momentum transfer, which scales with the velocity squared.
Grain inertia is significant when it has at least an equal magnitude as the viscous forces. In order to quantify the effect of the inertia forces relative to the viscous forces, the particle Reynolds number, Re_p, (eq. 2.11) can be calculated [2.1][2.34-

2.35]. For Re_p much smaller than 0.1, it is stated that the inertia forces can be neglected.

$$\mathrm{Re}_p = \frac{\rho_s \cdot \dot{\gamma} \cdot a^2}{\eta_s} \tag{2.11}$$

where: Re_p = *Particle Reynolds number (-)*
ρ_s = *density of suspending medium (kg/m³)*
$d\gamma/dt$ = *applied shear rate (1/s)*
a = *particle radius (m)*
η_s = *apparent viscosity of the suspending medium (Pa s)*

For example, spherical particles with a radius of 1 mm, suspended in pure water have a particle Reynolds number which equals the shear rate. As a result, even at a low shear rate of 1 s^{-1}, inertia forces are important during the flow of this suspension and increasing particle size will increase the importance of inertia forces.
On the other hand, even at high particle Reynolds numbers, the viscous forces still contribute to the shear stress at a certain shear rate. As a result, the shear stress can be written as the superposition of a viscous part, which scales linearly with the shear rate, and a part due to inertia, which scales with the shear rate squared [2.36-2.37]. In [2.38], this method has not been applied, but the shear stress – shear rate relationship has been modelled with the power-law model. Chen and Ling [2.38] showed that, even for the experiments of Bagnold which occurred at quite high particle Reynolds numbers up to 500, the power-law index did not exceed the value of 1.58. This indicates that the stress transfer is not purely due to direct momentum transfer between the particles, but the stress still has a non-negligible contribution of viscous forces. According to a very careful prediction of Chen and Ling, the viscous forces should be negligible in case of Bagnold's experiments from a particle Reynolds number of 10^4 on.
Tests with a gas as suspending medium show that, at low solid concentrations and at rather low shear rates, the shear stress scales with the shear rate squared [2.37]. On the other hand, increasing the concentration and increasing the shear rate causes the magnitude of this relationship to decrease, most probably due to the large difficulties arising from the type of experiments, the materials (dry solid particles) and the test setup.

3.4 Yield stress

3.4.1 Yield stress caused by friction

When the volume fraction of a non-colloidal suspension is approaching the maximum volume fraction, direct contact between the particles is likely to occur. At high shear rates, these direct contacts can transfer momentum and result in shear thickening behaviour. At very low shear rates, the direct contacts can cause an extra resistance to flow, due to the friction between the particles. In this case, the

hydrodynamic interactions acting in the interstitial fluid between the particles can be neglected. A transition has been made between hydrodynamic and frictional flow [2.39].
This occurs when comparing self-compacting and traditional concrete with low w/c-ratios. As mentioned in chapter 1, the amount of coarse aggregates in SCC has been reduced in order to enhance the fluidity of the concrete. When regarding concrete as a suspension of aggregates in cement paste, the amount of suspended particles is much higher for traditional concrete. In case of a low w/c-ratio, the amount of interstitial fluid between the particles is very low and the particles can have very close contacts. When flow stops or starts, the friction between the aggregates dominates the flow and determines the magnitude of the yield stress. Due to the low amount of coarse particles in SCC, the frictional contacts are less likely to occur and the frictional yield stress is of no significant importance.

3.4.2 Yield stress caused by other phenomena

In case the suspending medium has a yield stress, the further addition of particles amplifies the magnitude of the yield stress. Measurements have been performed on different yield stress materials, with different concentrations of monodisperse spherical particles. Results indicate that the relative yield stress (similar to the relative viscosity), shows a Krieger-Dougherty-like relationship with the relative volume fraction. The maximum volume fraction (φ_m) applied in equation 2.12 does not refer to the maximum possible volume fraction (φ_{max}, from eq. 2.10), but to the volume fraction at which friction is assumed to dominate the flow process [2.40-2.41].

$$\tau_{0,r} = \frac{\tau_0}{\tau_{0,s}} = \sqrt{(1-\varphi)\cdot\left(1-\varphi/\varphi_m\right)^{-2.5\cdot\varphi_m}} \qquad (2.12)$$

where: $\tau_{0,r}$ *= relative yield stress, which is the ratio of the yield stress of the suspension* (τ_0) *to the yield stress of the suspending medium* ($\tau_{0,s}$) *(-)*

As a result, the addition of non-colloidal particles to a yield stress material does not change the origin of the yield stress, it only amplifies the yield stress value. This has also been confirmed by measuring the static yield stress for thixotropic materials. The static yield stress of a suspension after a certain resting time scales with the static yield stress of the suspending medium according to equation 2.12 [2.41].

4 Colloidal suspensions

4.1 Brownian motion

Every material is subjected to thermal agitation when temperature is higher than 0 K. The thermal energy equals kT, where k is the Boltzmann constant and T is the temperature in Kelvin [2.14]. For larger particles suspended in a certain medium, for example, the energy exerted by temperature is too low, compared to gravity and viscous drag forces. The thermal activation does not influence the behaviour of the suspension. When particles are getting smaller than 1 μm, the Brownian force (kT/a, which equals Brownian/thermal energy, divided by the particle radius a) has a similar or higher order of magnitude as gravity, meaning that it can no longer be neglected.
Brownian force causes colloidal particles (also called Brownian particles) to move permanently in a random pattern [2.42]. This Brownian motion can be slowed down by a high viscosity of the suspending medium, by a high diffusive flux, … As particle size decreases, Brownian motion gains importance relative to the other forces. A lower limit of Brownian particles is set at 1 nm, below which the size of molecules becomes significant and the homogeneity of the suspending medium can no longer be assumed.
The next sections will discuss the forces acting on Brownian particles when they approach each other. Finally, the consequences of these inter-particle forces on rheology will be given.

4.2 Inter-particle forces

4.2.1 Van der Waals attraction forces

The van der Waals forces have three components [2.14][2.17][2.43-2.45], of which the London-dispersion force is the most important one. This force induces always an attraction between particles, caused by the interaction between induced dipoles in the neighbouring molecules. The van der Waals potential is the product of the Hamaker constant, which depends on the dielectric properties of the particles and the suspending medium, and a geometrical factor, which depends on size and shape of the particles and the separation distance between the particles.
For cement, due to the large complexity of the material, no values for the Hamaker constant have been measured [2.46]. Published results are based on assumptions and measurements on other minerals.

4.2.2 Electrostatic Forces

If only the van der Waals forces would be present in a suspension, all particles would be attracted to each other and a large agglomeration of particles would be formed. Particles in suspensions are electrically charged on their surface. In the suspending medium, counter-ions, which are ions with opposite charge, are attracted to the particles, resulting in a decreasing concentration of these counter-ions with

increasing distance from the particle, creating the diffuse double layer [2.14][2.17][2.45].
When two particles approach, their diffuse double layers will start to overlap, creating a higher concentration of counter-ions. As a result, an osmotic pressure is created in order to neutralize this overconcentration of counter-ions and the particles are repelled from each other.

4.2.3 Steric hindrance

Adding a polymer layer to a particle surface can create a geometrical barrier for other particles. As a result, two particles cannot approach closer than the separation distance created by the polymers. In contrast to the van der Waals forces and the electrostatic repulsion forces, the absolute value of the potential caused by the polymers is not a monotone decreasing function of the inter-particle distance. Instead, it shows a more abrupt change from its characteristic value near the particle surface, to zero at a particle distance equal to the effective length of the polymers [2.14][2.17][2.45]. This repulsion mechanism is called steric hindrance and is a purely geometrical phenomenon.

4.2.4 DLVO-theory

Derjaguin and Landau, and Verwey and Overbeek discovered, at almost the same time, that the inter-particle potentials may be added in order to calculate the total potential (DLVO-theory) [2.47-2.48]. A qualitative example is given in figure 2.8, showing the large attraction when the particle separation distance is very low, but also showing the repulsion “mountain”, which the particles must conquer in order to be attracted. In order to modify this potential, one can easily change the electrostatic repulsion forces and the steric hindrance. In this way, more attraction or more repulsion can be created, depending on the expected outcome. Note that figure 2.8 is a simplified representation. In real circumstances, a 3-D pattern of potential mountains (repulsion) and wells (attraction) is continuously varying.

4.2.5 The working principle of superplasticizers in cement based systems

Based on the above mentioned inter-particle forces, the working principle of superplasticizers will be explained very briefly. Much more detailed information can be found in literature [2.44][2.46][2.49-2.56].
In a non-plasticized system, the electrostatic repulsive forces of cement particles in water are not very large. As a result, the particles coagulate (or flocculate) quite easily. Depending on the type of superplasticizer, the polymers can create an additional electrostatic repulsion or a steric hindrance, or both. During mixing, particles are separated, the polymer chains attach to the cement particles and the repulsive forces are increased. As a result, fewer particles coagulate, creating more individual particles. Shear stresses are no longer transferred through the agglomerates, but through the suspension and the mixture becomes more fluid.
In time, as hydration continues, superplasticizers can loose their efficiency, which will be discussed in chapter 5, when dealing with loss of workability.

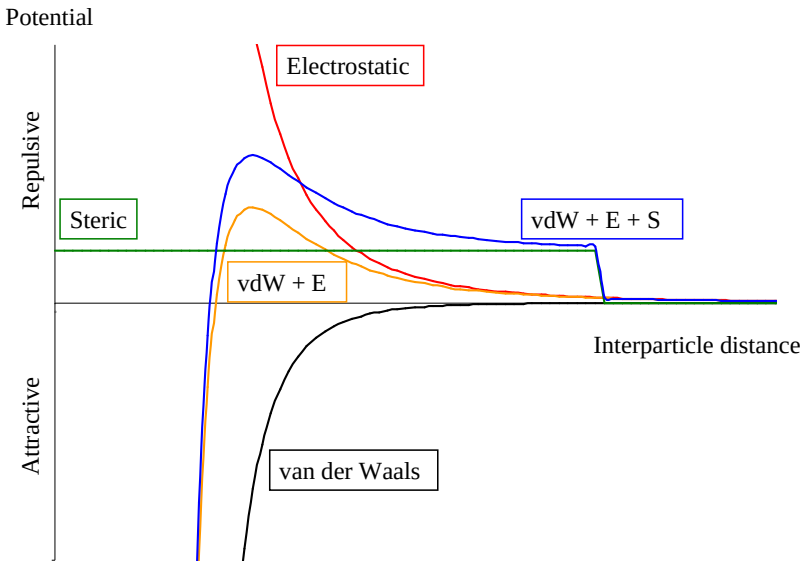

Figure 2.8: Simplified approach of inter-particle forces: van der Waals attraction (black), Electrostatic repulsion (red), steric hindrance (green). The combination of van der Waals and the electrostatic forces (orange) shows a large attraction at small interparticle distances, but also a repulsion barrier which the particles can only pass when having sufficient energy. Incorporating the steric hindrance (blue) increases the repulsive effect.

4.3 Influence of suspended colloidal particles on viscosity

The results described in section 3.2 have been obtained for non-colloidal particles, for which Brownian motion was not important. For colloidal particles and at low shear rates, a non-negligible amount of Brownian stress (=kT/a^3, which is the stress executed by Brownian motion on the particle) is present in the suspension. Brownian motion tends to keep the particles apart and creates a kind of microstructure, which must be broken or disturbed during shearing. As a result, the relative viscosity of a suspension can be divided into a hydrodynamic part, to which the findings of section 3.2 apply, and a thermodynamic part, due to Brownian stresses [2.57-2.59]. When defining the Brownian relaxation time as the time needed for Brownian motion to re-arrange a certain suspension into random order, after a disturbing action has been applied, the Brownian relaxation time is too large at high shear rates, and as a result, re-organisation of the suspension due to Brownian motion is not possible. Figure 2.9 shows the division of relative viscosity into the hydrodynamic and thermodynamic (Brownian) part, as a function of the Péclet number [2.60], which is a dimensionless shear rate, given in equation 2.13. The Péclet number indicates the relative importance of shear (hydrodynamic) forces to

Brownian (thermodynamic) forces. The larger the Pe-number, the more important the hydrodynamic part.

$$Pe = \frac{\eta_s \cdot \dot{\gamma} \cdot a^3}{k \cdot T} \tag{2.13}$$

where: η_s = *apparent viscosity of suspending medium (Pa s)*
$d\gamma/dt$ = *shear rate (1/s)*
a = *particle radius (m)*
k = *Boltzmann's constant = 1.38* 10^{-23} *(J/K)*
T = *temperature (K)*

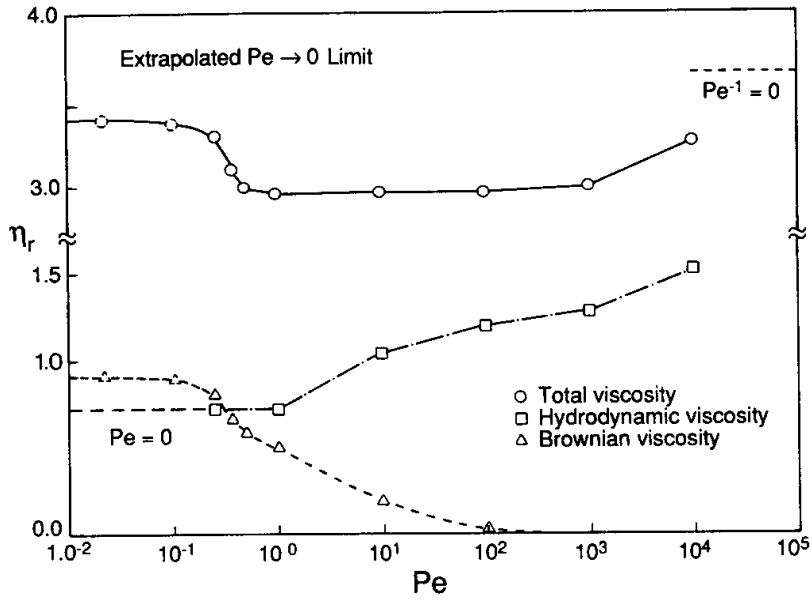

Figure 2.9: The Brownian contribution to viscosity decreases with increasing Pe-number, while the hydrodynamic contribution increases. Shear thickening due to hydrocluster formation (see 4.5.1) is consequently a purely hydrodynamic effect. Figure from G. Bossis and J.F. Brady [2.60].

In figure 2.9, it can be seen that the importance of the thermodynamic forces decreases when the Pe-number is larger than 1.
The same scaling as mentioned at the end of section 3.2.4 applies for Brownian particles. Plotting relative viscosity as a function of the relative volume fraction (volume fraction relative to the maximum volume fraction), leads to a master curve, but the curves are different for low and high shear rates, due to the thermodynamic contribution to the relative viscosity. This thermodynamic contribution is also partly the cause for the presence of a yield stress in a material.

4.4 Shear thinning in colloidal suspensions

Apart from particle migration in a measurement device, shear thinning in colloidal suspensions has the same origin as mentioned for non-colloidal suspensions: shear-induced ordering [2.31-2.32]. The same principle applies as described in section 3.3.2, only, for Brownian suspensions, this effect is reversible. If the shear rate is sufficiently small in order to let Brownian motion reorganise the distribution of the particles, the suspension can transform from its shear-induced ordered state into a random state again. The transition from disordered to ordered state, or vice versa, occurs at Pe ~ 1.
For non-spherical particles, the same principle applies. Brownian motion keeps the particles in a random state, while shearing forces induce flow alignment and a decrease in viscosity.

4.5 Shear thickening in colloidal suspensions

4.5.1 Cluster formation

Figure 2.10 [2.61] shows the apparent viscosity as a function of the shear stress for monodisperse latex particles suspensions, with a particles diameter of 250 nm. At low volume fractions, viscosity does not significantly change with increasing shear stress. When increasing the volume fraction, a clear change in viscosity can be seen, and viscosity becomes dependent on the shear stress. At low shear stresses, viscosity decreases with increasing shear stress, indicating shear thinning. At higher shear stresses, viscosity increases with increasing shear stress, which is defined as shear thickening behaviour.
The mechanism behind the shear thinning behaviour has been explained in the previous sections. According to the authors [2.61], shear thickening occurs due to the loss of the ordered state. Due to the high shear stresses, an order-disorder transition has occurred and consequently, viscosity must increase [2.61-2.65]. Recently, several authors have observed that the order-disorder transition, as described above is not a necessary phenomenon to describe shear thickening behaviour of Brownian suspensions [2.60][2.66-2.68].
Shear thickening occurs due to large hydrodynamic forces, which are the result of the high shear stresses, acting between the particles in the suspension. These hydrodynamic forces can become larger than the repulsive forces between the particles (electrostatic, steric or due to Brownian motion), and a temporary assembly of particles is formed. In fact, it is better to say that the relaxation time of the repulsive forces becomes too large compared to the characteristic time of the hydrodynamic forces [2.60][2.66-2.68]. Shear thickening occurs from a certain value of the applied shear stress on, named the critical shear stress, at which the hydrodynamic forces equal the repulsive forces. When increasing the shear stress above the critical shear stress, clusters are formed. When decreasing the shear stress under the critical shear stress, the relaxation time of the repulsive forces is sufficiently small compared to the characteristic time of the hydrodynamic forces and the clusters disappear. This shear thickening behaviour is consequently a fully

reversible phenomenon, which has been confirmed in the measurements executed by different authors [2.66][2.69-2.70].
A single equation for the critical shear stress is not available due to the differences in repulsive forces. Depending on the kind of repulsive force, the critical shear stress can scale with the particle radius to the power -1 to -3 [2.67-2.69][2.71].

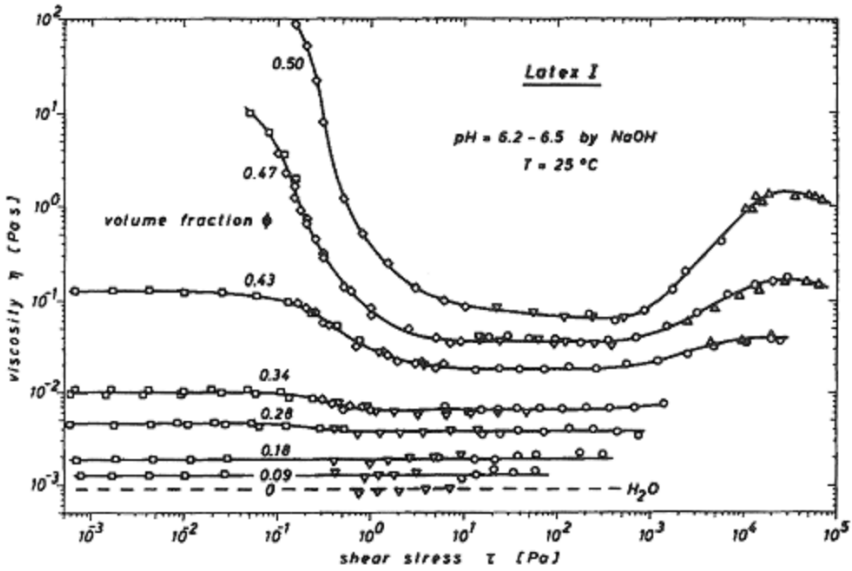

Figure 2.10: Apparent viscosity as a function of shear stress for monodisperse latex suspensions. Shear thinning and shear thickening effects increase with increasing volume fraction. Figure from H.M. Laun [2.61].

When clusters are formed through the entire shearing zone, jamming will occur and the flow will be stopped. In some suspensions, at very high volume fractions, jamming can cause a sudden increase in viscosity with a few orders of magnitude, possibly destroying the measurement system. As a result, observing, understanding and controlling shear thickening behaviour is extremely important in situations where jamming is likely to occur [2.72-2.73].
When referring back to figure 2.9 [2.60], showing the relative importance of thermodynamic contribution to viscosity compared to hydrodynamic contribution, one can see that the suspension in figure 2.9 shows shear thickening behaviour from a Pe-number of 10^3 on. At these high Pe-numbers, the thermodynamic contribution to the total viscosity is quasi nihil, confirming that shear thickening behaviour is a purely hydrodynamic phenomenon. Still, Bossis and Brady [2.60] mention that at these high Péclet numbers, Brownian stresses are still somewhat important to cause the clusters to be transient in time.
Clusters can only form in the compressive direction of the flow field (fig. 2.11) [2.73]. Any deviation from this compressive axis causes the cluster to dissolve. Non-

spherical particles and particle softness can increase the lifetime of clusters, due to larger possible deviations in orientation relative to the compressive axis.
The coming sections will discuss the influence of several parameters on the shear thickening behaviour of Brownian suspensions. Most of the results reported deal with monodisperse suspensions of spherical particles, unless mentioned otherwise. Two parameters will be investigated: the critical shear stress, which is a measure for the onset of shear thickening, and the intensity of shear thickening, which can be seen by the inclination of the viscosity as a function of shear stress or shear rate.

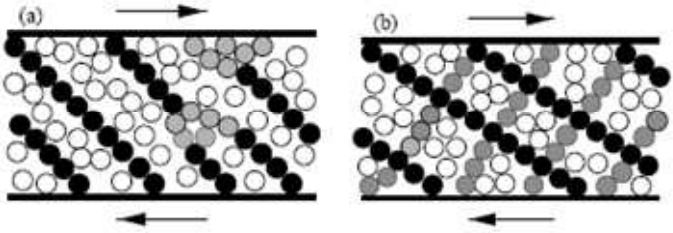

Figure 2.11: Right: ideal situation of the presence of a compressive axis in a shearing flow, formed by the black particles. Left: A more realistic approach, where some particle clusters can transfer the force from one to another chain, which all have the direction of the compressive axis. Figure from M.E. Cates et al. [2.73].

4.5.2 Influence of particle size

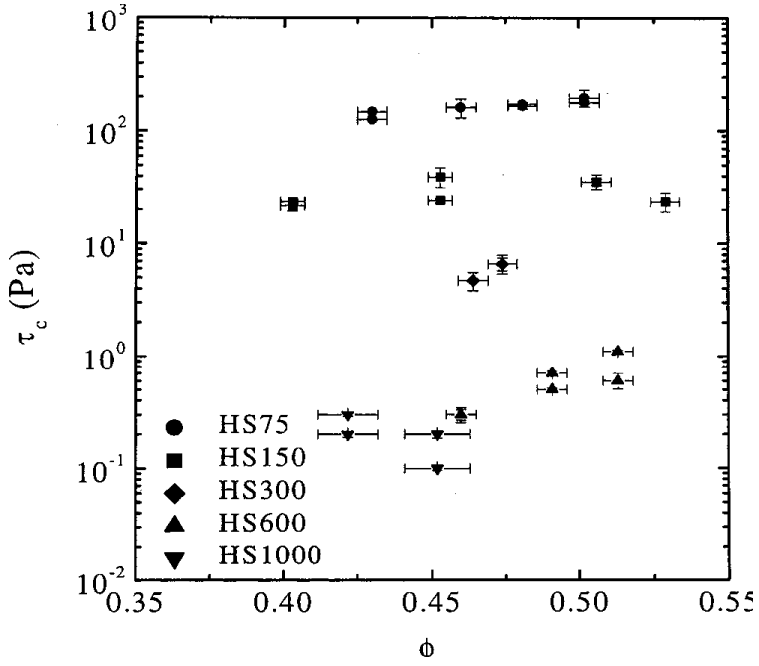

Figure 2.12: The critical shear stress is rather independent on the volume fraction, but decreases with increasing particle size. The symbols represent hard spheres (HS) with the dimensions of the particles in nm (number after HS). Figure from B.J. Maranzano and N.J. Wagner [2.67].

Taking the ratio of the hydrodynamic stresses to the repulsive stresses, the critical shear stress scales with the particle radius to the power -1 to -3 [2.67-2.69][2.71], depending on the kind of repulsive force. On the other hand, no matter what the origin of the repulsive forces is, it can be noticed that increasing particle size decreases the critical shear stress. This can be seen in figure 2.12 [2.67], which shows the critical shear stress as a function of volume fraction for different particle sizes. The larger the particle size, the lower the critical shear stress.
On the other hand, as can be seen in figure 2.13 [2.68], increasing particle size does not influence significantly the intensity of shear thickening behaviour.

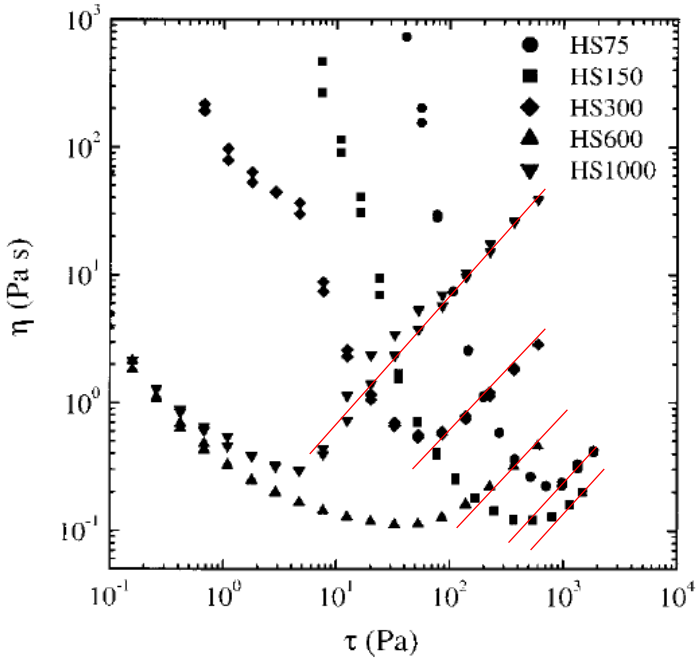

Figure 2.13: Increasing particle size does not influence the intensity of shear thickening, which is visualized by the full lines. The symbols represent hard spheres (HS) with the dimensions of the particles in nm (number after HS). Figure from B.J. Maranzano and N.J. Wagner [2.68].

4.5.3 Influence of volume fraction

Increasing volume fraction does not influence the critical shear stress, as demonstrated in figure 2.12 [2.67], for different particle sizes. On the other hand, as already shown in figure 2.10 [2.61], the volume fraction must have a certain value in order to observe shear thickening. The intensity of shear thickening increases with increasing volume fraction [2.61][2.67-2.68][2.71], which is also shown in figure 2.14 [2.68].

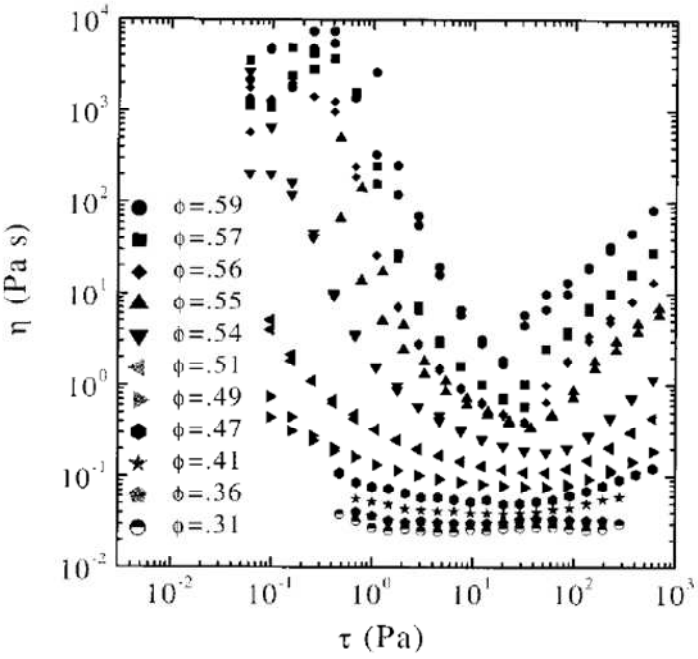

Figure 2.14: Increasing volume fraction increases the intensity of shear thickening behaviour. Figure from B.J. Maranzano and N.J. Wagner [2.68].

4.5.4 Influence of polymer coatings

Polymer coatings are mostly added to stabilize a certain suspension, in order to prevent flocculation. This stabilization is caused by influencing the repulsive forces. As a result, adding polymer coatings will also influence the critical shear stress for shear thickening behaviour [2.74]. Polymer coatings do not only influence the repulsive forces, but they can decrease the hydrodynamic forces if the coatings are partly permeable [2.74]. Figure 2.15 [2.74] shows the results of poly-methyl-methacrylate (PMMA)-particle suspensions with three different particle sizes and coated with a 9 nm polymer layer. The solid lines in figure 2.15 [2.74] represent the calculation of the critical shear stress, based on a hard-sphere (non-permeable polymer coating) assumption. As can be seen, the experimental critical shear stresses are larger than the calculated critical shear stresses, indicating that polymer coatings can "postpone" shear thickening behaviour.

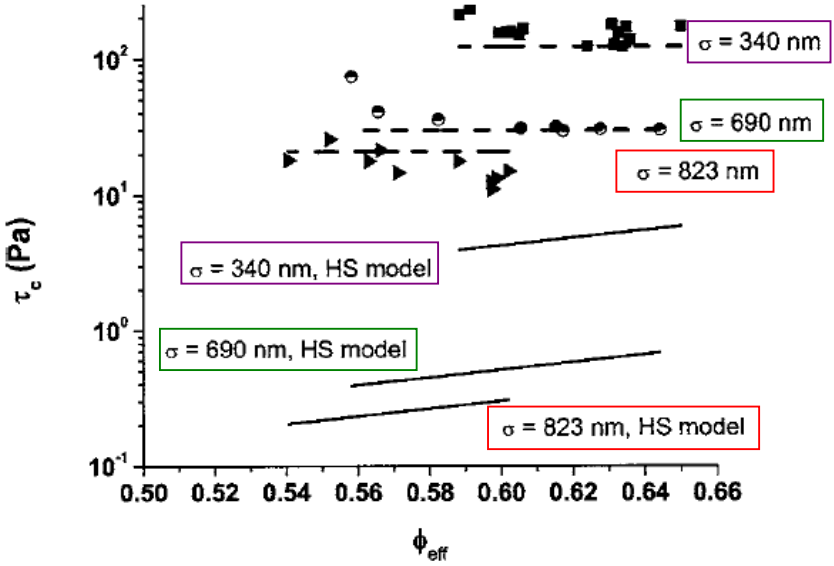

Figure 2.15: Adding polymer coatings to Brownian particles increases the critical shear stress. The obtained results for particles with different diameters with a polymer coating (upper results in the figure) show a higher critical shear stress than the calculated results according to the hard sphere model (lower results). Figure from L.-N. Krishnamurthy et al. [2.74].

4.5.5 Influence of polydispersity

Polydispersity increases the maximum volume fraction, and as a result, at equal volume fraction, a monodisperse system will show a higher relative viscosity than a polydisperse system. As a result, the intensity of shear thickening decreases for polydisperse systems due to the lower hydrodynamic forces between the particles [2.71]. It has also been mentioned that polydispersity increases the critical shear rate, but no evidence has been found that it significantly increases the critical shear stress. Bender and Wagner have found that the critical shear stress for a bi-disperse system is between the critical shear stresses of the two monodisperse suspensions [2.66].

4.5.6 Influence of particle shape

At zero, or very low shear rates, Brownian motion causes the alignment of non-spherical particles to be isotropic, except for highly concentrated suspensions. Increasing shear stress causes flow alignment and as a result, shear thinning is observed. Egres and Wagner [2.75-2.76] have studied the shear thickening behaviour of suspensions with ellipsoidal particles, having an aspect ratio of 1/2, 1/4 and 1/7. They observed particle alignment in their rheometer which causes shear thinning behaviour. When further increasing the shear stress, beyond the critical shear stress, no significant change in particle alignment has been found. Apparently,

shear thickening of non-spherical particles suspensions is not caused by changes in alignment of particles or particles tumbling in the flow. Instead, it is the result of the same phenomenon for shear thickening in spherical particle suspensions: cluster formation.
The critical shear stress in a suspension of non-spherical particles is determined by the small radius of the particles, which is, due to the particle alignment, perpendicular to the flow direction. As a result, substituting spheres by ellipsoids with a small radius equal to the radius of the spheres will not affect the critical shear stress.
The intensity of shear thickening on the other hand increases with increasing ratio between large and small radius. This is due to the lower maximum volume fraction in case of long ellipsoidal particles. As a result, hydrodynamic forces increase between the particles and intensity of shear thickening increases at equal absolute volume fraction.

4.5.7 Flocculated particles

In case particles are flocculated (or coagulated), less particles are available for the formation of clusters, and shear thickening decreases and even disappears [2.71]. This will have consequences in case of cement-based systems, where the cement particles have large tendency to coagulate or flocculate when no superplasticizer is added to the mixture.

4.6 Yield stress

At very low shear rates, as mentioned in section 4.3, there is a thermodynamic contribution to the viscosity, which corresponds to particle arrangement due to the inter-particle forces. In some systems, a large stress must be added in order to disturb the arrangement and apparently, a yield stress is observed. Consequently, a yield stress is, at least partly, the result of a colloidal particle structure, significantly depending on the inter-particle forces. Buscall et al. [2.77] mention that the yield stress depends on the volume fraction by means of a power-law and that it increases with decreasing particle size.
When suspending non-colloidal particles in a colloidal suspension, having a yield stress, the principle of section 3.4.2 applies, indicating an increase in yield stress, relative to the increase in volume fraction, as long as a certain critical volume fraction for friction is not exceeded. This principle applies on self-compacting concrete.
In addition, adding superplasticizers in a cement paste increases the repulsive forces, leading to smaller attraction forces and a lower yield stress.

4.7 Flocculation and thixotropy

Flocculation of Brownian particles occurs when the particles are “trapped” in a potential minimum and do not have sufficient energy, due to Brownian motion or shearing, to leave this well. As a result, these particles stick together, increasing the viscosity of the suspension. When sufficient particles are connected together, gravity

can act on the particle assembly and sink it to the bottom of the reservoir, in case the density of the particles is larger than the density of the suspending medium. This procedure is often applied in water treatment plants in order to remove small particles from the water [2.78-2.80].
Coagulation of particles has a similar effect with equal consequences. As a result, flocculation or coagulation can lead to solid-like behaviour of the suspension, but when a sufficient amount of energy is added, the particles loose their connection and the suspension can become fluid again, resulting in thixotropic behaviour. In literature, the definitions of thixotropy are numerous [2.81], but the one most applicable to concrete rheology is as follows: "Thixotropy is defined as a decrease in time of viscosity under constant shear stress or shear rate, followed by a gradual recovery when the stress or shear rate is removed [2.82]."
Describing thixotropy by means of a microstructural approach is very challenging, and as a result, thixotropy is mainly described macroscopically in literature, introducing a structure parameter λ, which influences the apparent rheological properties of the material. Thixotropy is described by one constitutive equation as a function of λ (eq. 2.14), and a second one describing the rate of change of the internal structure (eq. 2.15) [2.83].

$$\tau = \eta(\gamma, \lambda) \cdot \gamma \tag{2.14}$$

$$\frac{d\lambda}{dt} = f(\gamma, \lambda) \tag{2.15}$$

where: τ = *shear stress (Pa)*
$\eta(d\gamma/dt, \lambda)$ = *viscosity, which is a function of the shear rate and the structure parameter (Pa s)*
$d\gamma/dt$ = *shear rate (1/s)*
λ = *structure parameter, varying between 0 (no structure) and 1 or* ∞ *(full structure) (-)*
$f(d\gamma/dt, \lambda)$ = *function describing the rate of change of the structure parameter, as a function of shear rate and the structure parameter itself.*

Equations 2.14 and 2.15 define the principle idea behind thixotropy, while equations 2.16 and 2.17 show a more detailed model in order to describe thixotropy [2.84].

$$\tau(\gamma, t) = \lambda \cdot \tau_0 + \lambda \cdot K_{st} \cdot \gamma^n + K_\infty \cdot \gamma^n \tag{2.16}$$

$$\frac{d\lambda}{dt} = -k_1 \cdot \gamma \cdot \lambda + k_2 \cdot \gamma^m \cdot (1-\lambda) + k_3 \cdot (1-\lambda) \tag{2.17}$$

where: τ_0 = *yield stress (Pa)*
K_{st} = *consistency factor due to the structure (Pa* s^n*)*
K_∞ = *consistency factor at* $\lambda = 0$ *(Pa* s^n*)*
k_1, k_2, k_3, m = *factors describing change of structure in time*

Equation 2.16 is an extension of the Herschel-Bulkley model, in which the first term represents the yield stress influenced by the structure and the last term is the power-law function of stress as a function of shear rate in case the structure has been broken down completely. The second term is the increase in stress caused by the structure during flow. Equation 2.17 describes the changes of the structure with time, indicating breakdown, which is a decrease in structure (first term), build-up due to Brownian motion (last term) and shear-induced build-up (second term). As can be seen, at low shear rates, shear-induced build-up can be larger than the shear-induced breakdown, leading to a faster increase in structure compared to the situation of zero shear, where only Brownian motion causes build-up of structure.
Other models, describing the thixotropic behaviour of concrete and cement paste will be discussed in chapter 5.

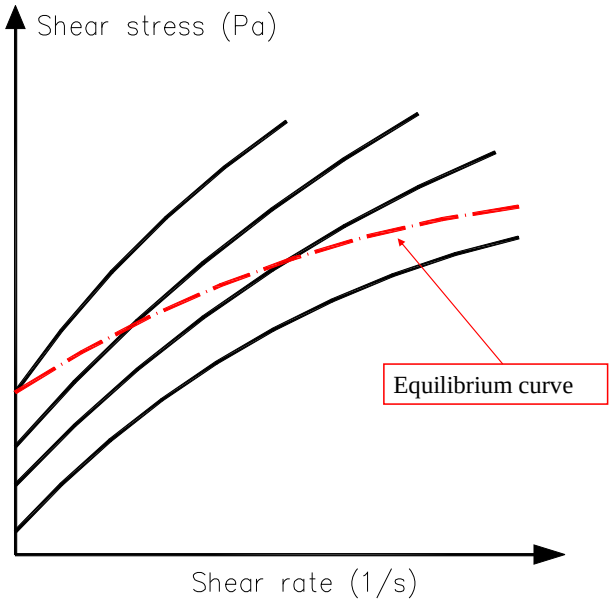

Figure 2.16: Rheological properties of a thixotropic materials. The solid black lines represent flow curves at constant structure (constant λ), the dash-dotted line is the equilibrium curve. Figure after D.C.-H. Cheng [2.83].

Depending on the magnitude of attraction between two flocculated particles, a certain amount of energy can be sufficient to overcome the attraction in one case, but not sufficient in another case. As a result, for each shear rate, an equilibrium structure exists [2.83]. Connecting all equilibrium points at all shear rates delivers the equilibrium curve, which is represented in figure 2.16 by the dash-dotted line [2.83]. The solid lines in figure 2.16 [2.83], are the lines of constant structure, which represent the constitutive equation (eq. 2.14 or 2.16). As can be seen, large

difficulties arise when determining the rheological properties of a thixotropic material. Some researchers state that the real rheological properties of the thixotropic material from figure 2.16 are represented by the equilibrium curve [2.83]. Others argue that the real rheological properties need to be determined at the lowest structure (λ_{ref}) achieved [2.85]. These two different definitions will have consequences on the measurement procedure, as discussed in chapters 3 and 5.
Assuming that structure can be described by a single parameter is in fact not completely correct [2.86]. When the structure rebuilds after a higher shear rate, it is most probable that the newly formed connections between the particles need other amounts of energy to be disrupted. As a result, not only a parameter to describe the amount of structure, like λ, is needed, but also a parameter describing the kind or the quality of structure is needed [2.86]. Unfortunately, due to the extreme complexity of this problem, not many results have been reported.

5 Foam

Concrete is not only a suspension, it is in fact a three-phase system, containing air, water and a lot of solid particles. As air content will influence the rheological properties of concrete, a very small introduction into foam rheology is given. Note that the review given in this section only deals with dilute foams, with low amounts of gas, and that no surfactant is applied in order to keep the foam stable.
The particles in a suspension are solid and assumed to be undistorted, or at least only small distortions occur. As a result, the influence of the flow field on particle deformation must not be taken into account. Air bubbles in a liquid are deformable, and hence, these bubbles will influence the rheological properties of the foam. Two different forces (or stresses) are working on an air bubble in a foam subjected to flow. The shear stresses try to deform the air bubble into a flat rod aligned with the flow direction in order to minimize the disturbance in the flow field. The surface tension on the other hand tries to keep the air bubble in its spherical shape. The capillary-number, defined in equation 2.18, indicates the relative importance of the shear stresses to the surface tension stresses [2.87]:

$$Ca = \frac{a \cdot \dot{\gamma} \cdot \eta_s}{\Gamma} \tag{2.18}$$

where: Ca = *capillary-number (-)*
a = *undeformed particle radius (m)*
$d\gamma/dt$ = *shear rate (1/s)*
η_s = *apparent viscosity of the suspending medium (Pa s)*
Γ = *surface tension (N/m)*

For high capillary-numbers, say much larger than 1, the shear stresses dominate the surface tension, causing the air bubble to deform in the flow. As a result, the resistance in the flow caused by the deformed bubble is decreased and the apparent viscosity at this specific shear rate is reduced [2.87]. For low Ca-numbers, much lower than 1, the air bubbles remain spherical due to the dominance of the surface tension forces. In this case, an extra energy loss is caused and the apparent viscosity of the foam will increase, which can be treated in a similar way (at least in cases of dilute foams) as for dilute suspensions [2.87]. The factor 2.5 in Einstein's equation (eq. 2.8) is not valid, due to slip on the surface of the air bubble, but roughly speaking, in case of low Ca-numbers, the air bubbles can be treated as solid particles in a flow field.
In case the Ca-number is close to 1, both effects have similar importance and not much is known in this specific case [2.87].

6 Summary

Liquid materials are described by a relationship between shear stress and shear rate. This relationship can incorporate non-linear behaviour (shear thinning and shear thickening), a yield stress and time dependency.

For all particle suspensions, viscosity increases with increasing volume fraction. For volume fractions near the maximum volume fraction, the viscosity increases significantly and can become infinite at the maximum volume fraction. Shear thickening in non-colloidal particle suspensions is most likely due to grain inertia, which causes a direct momentum transfer between large particles. In order to investigate the importance of inertia, the particle Reynolds number should be calculated. Large Re_p indicate a relatively large influence of inertia, while for low Re_p (< 0.1), grain inertia can be neglected. Yield stress can be caused by friction between particles at very high volume fractions. At lower volume fractions, the suspended particles cause an amplification of the yield stress of the suspending medium.

Colloidal particles are subjected to thermally activated Brownian motion, which is able to reorganise any colloidal suspension into a random system. Combining the van der Waals attractive forces, the electrostatic repulsion forces and the steric hindrance (DLVO-theory) leads to an attraction-repulsion diagram as a function of particle separation distance. Shear thinning in colloidal suspensions is caused by shear-induced ordering and/or shear-induced flow alignment of non-spherical particles. Shear thickening is caused by the formation of clusters, which are due to the larger hydrodynamic stresses relative to the repulsive stresses between particles.

Decreasing particle size, increasing polydispersity and adding polymer coatings cause the critical shear stress to increase. Increasing relative volume fraction and decreasing polydispersity result in an increase in intensity of shear thickening. Particle shape does not influence the critical shear stress, nor the intensity. Suspensions containing flocculated particles are less prone to shear thickening.

Thixotropy has been defined as the decrease in time of viscosity during shear and the rebuild of structure at rest. Thixotropy seriously complicates rheological measurements.

Air bubbles in a liquid will deform if the capillary-number, which is the ratio between shear stress and surface tension, is high, causing viscosity to decrease. For low Ca-numbers, the bubbles remain spherical, resulting in an increase in viscosity.

7 References

[2.1] Macosko C.W., "Rheology Principles, measurements and applications," Wiley-VCH, New-York (1994).

[2.2] Ferguson J., Kemblowski Z., "Applied fluid rheology," Elsevier Applied Science, London (1991).

[2.3] Hooke R., "Lectures de Potentia Restitution," John Martin, London (1678); reprinted by R.T. Gunter, "Early Science in Oxford, Vol.8," Oxford University Press, London, (1931), 331-388.

[2.4] Rivlin R.S., "Large Elastic Deformations of Isotropic Materials. IV. Further Developments of the General Theory," Phil. Trans. R. Soc. **241A** (1948), 379-397.

[2.5] Treloar L.R.G., "The physics of rubber elasticity, 3rd ed." Oxford University Press, London (1975).

[2.6] Newton I.S., "Principia Mathematica," (1687).

[2.7] European Society of Rheology, "Short course on Rheological Measurements," 10th European School of Rheology, Leuven (2006).

[2.8] Bingham E.C., "An investigation of the laws of plastic flow," U.S. Bur. Stand. Bull. **13** (1916), 309-353.

[2.9] Herschel W.H., Bulkley R., "Konsistenzmessungen von Gummi-Benzol-Lösungen," Kolloid Z. **39** (1926), 291-300.

[2.10] Poppe A.-M., "Influence of fillers on hydration and properties of self-compacting concrete," Ph-D dissertation (in Dutch), Ghent University, Ghent (2004).

[2.11] Pons G., Proust E., Assie S., "Creep and shrinkage of self-compacting concrete: A different behaviour compared with vibrated concrete?" Proc. of the 3rd Int. RILEM Symp. on SCC, Reykjavik (2003), 645-654.

[2.12] Neville A.M., "Creep of concrete: plain, reinforced and prestressed," North-Holland, Amsterdam (1970).

[2.13] Taerwe L., De Schutter G., "Betontechnologie," bachelor course Ghent University, Ghent (2007).

[2.14] Mewis J., Wagner N.J., "Suspension Rheology," Short course from the society of rheology, Monterey (2008).

[2.15] Steinhaus H., "Mathematical Snapshots," 3rd ed., Dover, New-York, (1999).

[2.16] Wells D., "The Penguin Dictionary of Curious and Interesting Numbers," Penguin Books, Middlesex, (1986).

[2.17] Geiker M.R., Wallevik O.H., "Rheology of cement based materials," DTU-RILEM Doctoral course, Lyngby (2007).

[2.18] de Larrard F., "Concrete Mixture-Proportioning – A scientific approach," E&FN SPON, London (1991), 421 pp.

[2.19] Magnel G., "Pratique du calcul du béton armé, 1re partie, 5me édition," Editions Fecheyr, Ghent (1949).

[2.20] Fennis S.A.A.M., internal communication.

[2.21] Jaeger H. M., and Nagel S. R., "Physics of Granular States," *Science* **255** (1992), 1524.

[2.22] Einstein A., "Eine neue Bestimmung der Moleküldimensionen," Annalen der Physik, **19** (1906), 289-306.

[2.23] Einstein A., "Berichtigung zu meiner Arbeit: „Eine neue Bestimmung der Moleküldimensionen"," Annalen der Physik, **34** (1911), 591-592.

[2.24] Batchelor G.K., Green J.T., "The hydrodynamic interaction of two small freely-moving spheres in a linear flow field," J. Fluid Mech. **56:2** (1972), 375-400.

[2.25] Batchelor G.K., Green J.T., "The determination of the bulk stress in a suspension of spherical particles to order c^2," J. Fluid Mech. **56:3** (1972), 401-427.

[2.26] Krieger I.M., "Rheology of monodisperse lattices," Adv. Coll. Interface Sc. **3:2** (1972), 111-136.

[2.27] Sierou A., Brady J.F., "Accelerated Stokesian Dynamics simulations," J. Fluid Mech. **448** (2001), 115-146.

[2.28] Gadala-Maria F., Acrivos A., "Shear-Induced Structure in a Concentrated Suspension of Solid Spheres," J. Rheol. **24** (1980), 799-814.

[2.29] Ovarlez G., Bertrand F., Rodts S., "Local determination of the constitutive law of a dense suspension of non-colloidal particles through MRI," J. Rheol. **50** (2006), 259-292.

[2.30] Bertrand E., Bibette J., Schmitt V., "From shear thickening to shear-induced jamming," Phys. Rev. E. **66** (2002), 060401.
[2.31] Rastogi S.R., Wagner N.J., Lustig S.R., "Rheology, self-diffusion, and microstructure of charged colloids under simple shear by massively parallel nonequilibrium Brownian dynamics," J. Chem. Phys. **104:22** (1996), 9234-9248.
[2.32] Rastogi S.R., Wagner N.J., Lustig S.R., "Microstructure and rheology of polydisperse, charged suspensions," J. Chem. Phys. **104:22** (1996), 9249-9258.
[2.33] Bagnold R.A., "Experiments on a gravity-free dispersion of large solid spheres in a Newtonian fluid under shear," Proc. Roy. Soc. **225A** (1954), 49-63.
[2.34] Batchelor G.K., "The stress system in a suspension of force-free particles," J. Fluid Mech. **41:3** (1970), 545-570.
[2.35] Coussot P., "Mudflow rheology and dynamics," Balkema, Rotterdam (1997), 252 pp.
[2.36] Savage S.B., Jeffrey D.J., "The stress tensor in a granular flow at high shear rates," J. Fluid Mech. **110** (1981), 255-272.
[2.37] Savage S.B., Sayed M. "Stresses developed by dry cohesionless granular materials sheared in an annular shear cell," J. Fluid Mech. **142** (1984), 391-430.
[2.38] Chen C.-I., Ling C.-H., "Granular-flow Rheology: Role of shear-rate number in transition regime," J. Eng. Mech. **122:5** (1996), 469-480.
[2.39] Yammine J., Chaouche M., Guerinet M., Moranville M., Roussel N., "From ordinary rheology concrete to self compacting concrete : A transition between frictional and hydrodynamic interactions," Cem. Conc. Res. **38** (2008), 890-896.
[2.40] Mahaut F., Chateau X., Coussot P., Ovarlez G., "Yield stress and elastic modulus of suspensions of noncolloidal particles in yield stress fluids, " J. Rheol. **52** (2008), 287-313.
[2.41] Mahaut F., Mokéddem S., Chateau X., Roussel N., Ovarlez G., "Effect of coarse particle volume fraction on the yield stress and thixotropy of cementitious materials," Cem. Conc. Res. **38** (2008), 1276-1285.
[2.42] Perrin J., "Atoms," translated by Hammick D.L., Van Nostrand, New York (1916).
[2.43] Shaw D.J., "Colloid and surface Chemistry," 4th edition, Butterworth Heinemann (1992).
[2.44] Wallevik J.E., "Rheology of particle suspensions, Fresh concrete, mortar and cement paste with various types of lignosulphonates," Ph-D dissertation, The Norwegian University of Science and Technology, Trondheim (2003).
[2.45] Hiemenz P.C., Rajagopalan R., "Principles of Colloid and Surface Chemistry 3rd ed.," Marcel Dekker, New York (1997).
[2.46] Flatt R.J., "Dispersion forces in cement suspensions," Cem. Conc. Res **34** (2004), 399-408.
[2.47] Derjaguin B., Landau L., "Theory of the stability of strongly charged lyophobic sols and the adhesion of strongly charged particles in solution of electrolytes," Acta Physicochim. URSS **14** (1941), 633-662.
[2.48] Verwey E.J.W., Overbeek J.T.G., "Theory of the Stability of Lyophobic Colloids," Elsevier, Amsterdam (1948).
[2.49] Yamada K., Hanehara S., "Interaction Mechanism of Cement and Superplasticizers – The role of Polymer Adsorption and Ionic Conditions of Aqueous Phase," Conc. Science and Engineering **3** (2001), 135-145.
[2.50] Flatt R.J., Houst Y.F., "A simplified view on chemical effects perturbing the action of superplasticizers," Cem. Conc. Res. **31** (2001), 1169-1176.
[2.51] Kjeldsen A., Flatt R.J., Bergström L., "Relating the molecular structure of comb-type superplasticizers to the compression rheology of MgO suspensions," Cem. Conc. Res. **36** (2006), 1231-1239.
[2.52] Sugamata T., Edamatsu Y., Ouchi M., "Distinction between particle-dispersion and particle-repulsion effects of superplasticizers on the viscosity of fresh mortar," Proc. of the 2nd Int. RILEM Symp. on SCC, Tokyo (2001), 213-220.
[2.53] Sugamata T., Edamatsu Y., Ouchi M., "A study of particle dispersing retention effect of polycarboxylate-based superplasticizers," Proc. of the 3rd Int. RILEM Symp. on SCC, Reykjavik (2003), 420-431.
[2.54] Kauppi A., Anderson K.M., Bergström L., "Probing the effect of superplasticizer adsorption on the surface forces using the colloidal probe AFM technique, Cem. Conc. Res. **35** (2005), 133-140.
[2.55] Flatt R.J., "Towards a prediction of superplasticized concrete rheology," Mat. Struct. **37** (2004), 289-300.

[2.56] Vickers T.M.Jr., Farrington S.A., Bury J.R., Brower L.E., "Influence of dispersant structure and mixing speed on concrete slump retention," Cem. Conc. Res. **35** (2005), 1882-1890.
[2.57] Wagner N.J., Woutersen A.T.J.M., "The viscosity of bimodal and polydisperse suspensions of hard spheres in the dilute limit," J. Fluid Mech. **278** (1994), 267-287.
[2.58] Brady J.F., "The rheological behavior of concentrated colloidal dispersions," J. Chem. Phys. **99** (1993), 567.
[2.59] Brady J.F., "Brownian motion, hydrodynamics, and the osmotic pressure," J. Chem. Phys. **98** (1993), 3335.
[2.60] Bossis G., Brady J.F., "The rheology of Brownian suspensions," J. Chem. Phys. **91:3** (1989), 1866-1874.
[2.61] Laun H.M., "Rheological properties of aqueous polymer dispersion," Angew. Makromol. Chem. **123** (1984), 335-359.
[2.62] Hoffman R.L., "Discontinuous and dilatant viscosity behavior in concentrated suspensions i. observation of a flow instability," Trans. Soc. Rheol. **16** (1972), 155-173.
[2.63] Hoffman R.L., "Discontinuous and dilatant viscosity behavior in concentrated suspensions ii. theory and experimental tests," J. Chem. Phys. **46** (1974), 491-506.
[2.64] Laun H.M., Bung R., Hess S., Loose W., Hahn K., Hadicke E., Hingmann R., Schmidt F., Lindner P., "Rheological and small angle neutron scattering investigation of shear induced particle structures of concentrated polymer dispersions," J. Rheol. **36** (1992), 743-787.
[2.65] Boersma W.H., Laven J., Stein H.N., "Shear thickening (dilatancy) in concentrated suspensions," AIChE J. **36** (1990), 321-332.
[2.66] Bender J., Wagner N.J., "Reversible shear thickening in monodisperse and bidisperse colloidal suspensions," J. Rheol. **40:5** (1996), 899-916.
[2.67] Maranzano B.J., Wagner N.J., "The effects of interparticle interactions and particle size on reversible shear thickening: Hard-sphere colloidal dispersions" J.Rheol. **45:5** (2001), 1205-1222.
[2.68] Maranzano B.J., Wagner N.J., "The effect of particle size on reversible shear thickening of concentrated colloidal dispersions," J. Chem. Phys. **114** (2001), 10514-10527.
[2.69] Melrose J.R., Ball R.C., "Continuous shear thickening transitions in model concentrated colloids – The role of interparticle forces," J. Rheol. **48:5** (2004), 937-960.
[2.70] Melrose J.R., Ball R.C., ""Contact networks" in continuously shear thickening colloids," J. Rheol. **48:5** (2004), 961-978.
[2.71] Barnes H.A., "Shear-thickening ("Dilatancy") in Suspensions of Nonaggregating Solid Particles Dispersed in Newtonian Liquids," J. Rheol. **33:2** (1989), 329-366.
[2.72] Liu A.J., Nagel S.R., "Jamming is not just cool any more," Nature **396** (1998), 21-22.
[2.73] Cates M.E., Wittmer J.P., Bouchaud J.-P., Claudin P., "Jamming, Force Chains and Fragile Matter," Phys. Rev. Lett. **81:9** (1998), 1841-1844.
[2.74] Krishnamurthy L.-N., Wagner N.J., Mewis J., "Shear thickening in polymer stabilized colloidal dispersions," J. Rheol. **49:6** (2005), 1347-1360.
[2.75] Egres R.G., Wagner N.J., "The rheology and microstructure of acicular precipitated calcium carbonate colloidal suspensions through the shear thickening transition," J. Rheol. **49:3** (2005), 719-746.
[2.76] Egres R.G., Nettesheim F., Wagner N.J., "Rheo-SANS investigation of acicular-precipitated calcium carbonate colloidal suspensions through the shear thickening transition," J. Rheol. **50:5** (2006), 685-709.
[2.77] Buscall R., Mills P.D.A., Goodwin J.W., Lawson D.W., "Scaling behaviour of the rheology of aggregate networks formed from colloidal particles," J. Chem. Soc.: Farad. Disc. **84** (1988), 4249-4260.
[2.78] Hammer M.J., Hammer M.J.Jr., "Water and Wastewater Technology, 6th edition," Pearson education, Inc., Upper Saddle River, New Jersey (2008).
[2.79] Fair G.M., Geyer J.C., Okun D.A., "Water and Wastewater Engineering, Volume 2: Water purification and wastewater treatment and disposal," John Wiley and Sons, Inc., New York (1968).
[2.80] Wagner E.G., Pinheiro R.G., "Upgrading water treatment plants," Spon Press, New York (2001).
[2.81] Barnes H.A., "Thixotropy - a review," J. Non-Newt. Fluid Mech. **70** (1997), 1-33.
[2.82] Barnes H.A., Hutton J.F., Walters K., "An introduction to Rheology," Elsevier, Amsterdam (1989).

[2.83] Cheng D.C.-H., “Hysteresis Loop Experiments and the Determination of Thixotropic Properties,” Nature **216** (1967), 1099-1100.
[2.84] Mewis J., Wagner N.J., “Thixotropy,” Adv. Colloidal Interface Sci., **147-148** (2009), 214-227.
[2.85] Roussel N., “A thixotropy model for fresh fluid concretes: Theory, validation and applications,” Cem. Conc. Res. **36** (2006), 1797-1806.
[2.86] Mewis J., Spaull A.J.B., Helsen J., “Structural hysteresis,” Nature **253** (1975), 618-619.
[2.87] Rust A.C., Manga M., “Effect of bubble deformation on the viscosity of dilute suspensions,” J. Non-Newt. Fluid Mech. **104** (2002), 53-63.

CHAPTER 3:

RHEOMETRY

This chapter contains the basic information about how the rheological properties of a certain material subjected to shear are measured. It is not in my intention to give a detailed description of each apparatus and their latest most sophisticated features. The aim is to describe in general terms the available equipment (first section), and how this equipment can be applied to measure some rheological characteristics like viscosity, visco-elasticity, yield stress and thixotropy (second section). The final section of this chapter will focus on concrete rheometry, and will specifically describe in detail the two rheometers used in this research project: the ConTec-Viscometer 5 and the Tattersall Mk-II rheometer.

1 Rheometers

The rheometers used to determine the properties of a material subjected to shear can be divided into two different classes, depending on their working principle. If one part of the rheometer is moving, and the sample is subjected to shear due to a difference in motion between its boundaries, the material is said to undergo drag flow (fig. 3.1). If the apparatus has no moving parts, but the applied stress is caused by a pressure difference, the material is said to be subjected to a pressure driven flow (fig. 3.3, see section 1.2). In the following sections, drag flow and pressure driven flow will be discussed separately [3.1-3.2].
For all geometries, a stress transfer between the equipment and the material, and vice versa, is established. During measurements, there can be a difference between the velocity of the boundary and the velocity of the material near the boundary, which is called wall slip [3.1-3.3]. Wall slip should be carefully investigated in order to eliminate its disturbing effect on the measurements.

DRAG FLOWS:

Parallel sliding plates

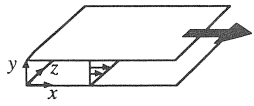

Concentric cylinders

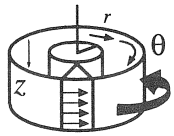

Cone and plate

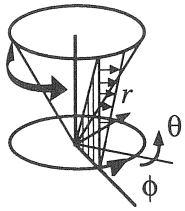

Plate and plate (rotating)

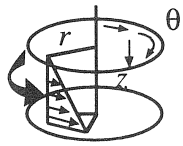

Figure 3.1: Rheometer designs based on drag flows. The arrows visualize the velocity field. Note that the angle of the cone in the cone and plate rheometer is much larger in this figure, compared to reality. Figure from C.W. Macosko [3.1].

1.1.1 Parallel sliding plates

This test geometry consists of two parallel plates, between which a relative motion in one direction is applied. In case the plates are infinitely long and wide, the transformation equations between the measured force, velocity and separation distance on the one hand, and the fundamental rheological properties shear stress and shear rate on the other hand are very easy (eq. 3.1 and 3.2) [3.1]:

$$\tau = \frac{F}{b \cdot d} \tag{3.1}$$

$$\dot{\gamma} = \frac{v_0}{h} \tag{3.2}$$

where: τ *= shear stress (Pa)*
F *= total force applied (N)*
$b\ d$ *= unit area (m²)*

$d\gamma/dt$ = shear rate (1/s)
v_0 = relative velocity between the plates (m/s)
h = separation distance between the plates (m)

Although the equations are very easy, the application of this geometry as a rheometer is very tough. The larger the plates, the larger the risk of non-parallelism [3.1]. On the other hand, the shorter the plates, the larger the risk for erroneous measurements due to the end effects [3.1][3.4]. As a result, in spite of the theoretical advantages, this geometry has not been applied very frequently. Instead, several scientists have tried to develop similar geometries approaching this most favourable theoretical situation.

1.1.2 Concentric cylinder rheometer

The concentric cylinder rheometer has been originally developed by Maurice Couette in 1890 [3.5], and this type of rheometer is also named to its inventor: the Couette-rheometer. It consists of two concentric cylinders, having a difference in rotational velocity relative to each other. When fulfilling the following assumptions [3.1]

- Steady, laminar and isothermal flow
- No flow in the radial and vertical direction
- Negligible gravity and end effects
- Symmetry in the tangential direction,

equation 3.3 may be applied to determine the shear stress, and equation 3.4 [3.1][3.6-3.7] for determining the shear rate, when the gap is small, saying when $R_i/R_o > 0.99$. In this case, the shear rate is considered to be constant in the gap [3.1-3.3].

$$\tau = \frac{T_i}{2 \cdot \pi \cdot R_i^2 \cdot h} \tag{3.3}$$

$$\dot{\gamma} = \frac{\Omega_{i\cdot} \cdot \left(R_o + R_i\right)}{2 \cdot \left(R_o - R_i\right)} \tag{3.4}$$

where: *T_i = torque measured at the inner cylinder (Nm)*
R_i = radius of inner cylinder (m)
R_o = radius of outer cylinder (m)
h = height of the cylinder submerged in the material (m)
Ω_i = rotational velocity at the inner cylinder (rad/s)

If the gap is not small, the shear rate varies with the radius in the gap, depending on the rheological properties of the material, and equation 3.5 needs to be applied [3.1][3.6-3.7]. As the shear stress is in most cases determined at the inner cylinder, the shear rate must be calculated in the same location, even in case the outer cylinder is rotating. In this case, equation 3.5 is slightly modified, but the principle for the calculation of the shear rate does not change.

$$\dot{\gamma}_i = \frac{2 \cdot \Omega_i}{n \cdot \left(1 - \left(R_i / R_0\right)^{2/n}\right)} \tag{3.5}$$

with $n = \frac{d\ln(T_i)}{d\ln(\Omega_i)}$

Consequently, for large gaps, the transformation into fundamental rheological parameters (shear stress and shear rate) is not straightforward. In case the small gap assumption is applied in a large gap rheometer, large errors can be obtained.
One of the assumptions which is not really obvious to achieve is the negligibility of the end effects. At the bottom of the material reservoir, the shearing is no longer one dimensional, as assumed, but a very complex 3-D flow pattern is established, disturbing the torque measurement. Several solutions have been proposed to minimize or eliminate this 3-D flow pattern. Different bottom geometries have been worked out [3.1], calculations and simulations have been performed in order to correct the end effect [3.8], but the most effective one, at least in my opinion, is to divide the inner cylinder into two parts: an upper part, at which torque is measured, and a lower part, which does not participate in the measurements. This system has been applied in the ConTec viscometer 5 (see section 3.2) [3.8-3.10].

1.1.3 Parallel (rotating) plates

This parallel plate geometry [3.11] should not be confused with the parallel plate geometry of section 1.1.1 of this chapter. In the previous case, the plates were sliding relative to each other, while in this case, a relative rotation is imposed, resulting in a much smaller sample and a better control over the disturbing factors. In contrast to the concentric cylinder rheometer, the equation for the shear rate is quite simple, but the calculation of the shear stress is more complicated. This is due to the variation of the shear rate from 0 in the centre of the plate to its maximal value at the outer edge. The transformations are given in equations 3.6 and 3.7 [3.1]:

$$\dot{\gamma}_R = \frac{R \cdot \Omega}{h} \tag{3.6}$$

$$\tau = \frac{T}{2 \cdot \pi \cdot R^3}\left(3 + \frac{d\ln T}{d\ln \dot{\gamma}_R}\right) \tag{3.7}$$

where: *R = radius of the plate (m)*
Ω = rotational velocity of the plate, relative to the other (rad/s)
h = gap = separation distance between the plates (m)
T = measured torque (Nm)

In this geometry, special attention must be paid to the edges of the sample [3.12]. If the sample is too large, for example when the two plates have different sizes, the material at a distance larger than the outer radius of the smallest plate must be removed. On the other hand, it can be that before or during measurements, some material escapes from in between the plates, causing an underestimation of the real rheological properties. In this case, a smaller gap can improve the performance, but this is not always guaranteed.

Figure 3.2: Paar Physica MCR-501 rheometer (Anton Paar), equipped with parallel plates (right) and concentric cylinders (left).

1.1.4 Cone and plate rheometer

The cone and plate rheometer is the favourite rotational rheometer, because of its ease of working with and the simplicity of transformation of data. It consists of a bottom stationary plate and a cone with small angle as "top plate" [3.11]. This geometry creates a uniform shear rate over the sample, avoiding shear-induced segregation during the test. The transformation into fundamental rheological units is very simple (eq. 3.8 and 3.9):

$$\tau = \frac{3 \cdot T}{2 \cdot \pi \cdot R^3} \tag{3.8}$$

$$\dot{\gamma} = \frac{\Omega}{\alpha} \tag{3.9}$$

where: α *= angle between the plates, which must remain smaller than 0.1 (rad)*

In principle, the top of the cone should touch the bottom plate, but as this is a very sensitive part of the equipment, the top of the cone is flattened, and a very small gap is created in the centre, inducing a very small, mostly negligible, error in the measurements. As it is the case for the parallel plates, the cone and plate rheometer also demands special attention at its outer edge.

1.2 Pressure driven flow

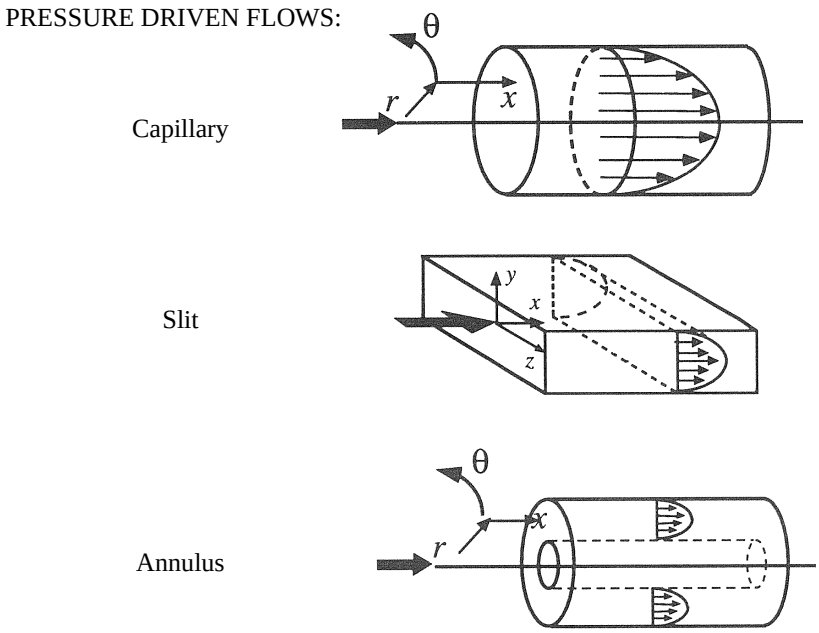

Figure 3.3: Rheometers in which the flow is driven by pressure. The arrows visualize the velocity field. Figure from C.W. Macosko [3.1].

1.2.1 Capillary rheometer

This type of rheometer exists of a circular tube, with radius R and length L, which forms the capillary [3.14-3.15]. Upstream of the capillary, there is a reservoir filled with the material, on which a certain range of pressures can be applied. Downstream of the capillary, there is mostly a free exit, where the material leaves the apparatus.

During measurements, the pressure and the flow rate (discharge) are measured and are transformed into shear stress and shear rate by equations 3.10 and 3.11.

$$\tau_w = \frac{R}{2} \cdot \frac{p}{L} \tag{3.10}$$

$$\gamma_w = \frac{Q}{\pi \cdot R^3} \cdot \left(3 + \frac{d \ln Q}{d \ln p} \right) \tag{3.11}$$

where: *subscript "w" = value taken at the wall*
R = radius of the capillary (m)
p = pressure applied (Pa)
L = length of the capillary (m)
Q = flow rate through the capillary (m^3/s)

The shear stress in a capillary rheometer varies linearly between 0 in the centre of the capillary to its maximal value at the wall, expressed by equation 3.10. This relationship is universal, meaning that it is valid for any material, no matter what the rheological properties are [3.1-3.3]. The calculation of the shear rate is more complicated and depends on the rheological properties of the material. In some cases, the last term in equation 3.11, which is defined as the Weissenberg-Rabinowitch correction [3.1], is difficult to solve, and approximations need to be made.
Equations 3.10 and 3.11 are only valid in case the following assumptions are fulfilled [3.1]:

- The flow must be fully developed, steady, isothermal and laminar
- There is no velocity component in the radial and tangential direction
- There is no slip at the wall, meaning that the velocity equals 0 at the wall
- The fluid is incompressible and the viscosity is independent on the pressure

The no slip assumption is in some cases not complied with, but it can be observed and eliminated from the measurements by applying capillaries with different radii, but a constant L/R ratio [3.16-3.18].
Some inaccuracies in the measurements can arise due to additional pressure drops in the system. There are additional pressure losses in the reservoir, at the entrance in the capillary, and at the exit. The pressure loss in the reservoir can be neglected in case of large (or wide) reservoirs. The entrance and exit losses can be calculated, or can be more easily eliminated by installing two pressure sensors in the capillary. If properly installed, the pressure p in equations 3.10 and 3.11 should be replaced by the pressure loss Δp over the sensors and the length of the capillary must be reduced to the length between the two pressure sensors.
The capillary rheometer is also very well known in hydraulics, but instead of determining the rheological properties from the pressure loss and flow rate, the

pressure loss at a certain flow rate is determined by means of the rheological properties and the geometry of the test equipment [3.19]. In case of a Newtonian liquid in laminar conditions, this can be achieved by means of the Poiseuille equation. The derivation of the Poiseuille equation, for Newtonian and non-Newtonian materials will be presented in chapter 6, with an application on self-compacting concrete in chapter 7.

1.2.2 Slit and annulus

The capillary rheometer is the most easy pressure driven rheometer to use (and also to manufacture), but other geometries are available. The slit geometry is very similar to the capillary, but instead of a circular tube, a tube with rectangular cross section is used. In case of the annulus, the material flows between two concentric (stationary!) cylinders. The principle of executing measurements is analogue to the capillary rheometers. More details on these geometries, including transformation formulae can be found in [3.1].

2 Measurement procedures

This section will describe briefly how rheological properties can be measured and what the standard procedures are. Four different kinds of properties will be discussed: flow curve, visco-elasticity, yield stress and thixotropy.

2.1 Flow curve

The flow curve of a certain liquid material is the plot of shear stress as a function of shear rate [3.1]. From these data, the apparent viscosity (= shear stress/shear rate) can be very easily calculated as a function of shear stress or shear rate, and can be plotted in a viscosity curve. Several examples of these viscosity curves are shown in chapter 2: figures 2.9, 2.10, 2.13 and 2.14. Figure 2.2 shows typical flow curves.
The flow curve or viscosity curve can be easily determined by increasing or decreasing the shear rate and measuring the corresponding stress, or vice versa. The second option, namely imposing the stress, is a safer procedure to determine very intense shear thickening behaviour. The flow curve is defined to be reversible if the ascending and descending curves are equal. Non-reversibility can be due to particle alignment without randomising effect to create anisotropy (section 3.3.2 of chapter 2), or it can be due to time dependent phenomena in the material, like thixotropy, which will be discussed later.
Continuously increasing or decreasing shear stress or shear rate delivers a very accurate measurement, but it is not always practical. For a capillary rheometer, for example, it can be that the pressure in the reservoir is not easy to adjust. In these cases, some discrete points of the flow curve can be measured, possibly by averaging a number of data points at equal shear rate (and shear stress), and the best fitting model can be determined.
When performing measurements in a rheometer, one should be aware of the range of shear rates (or shear stresses) the material will undergo in practice [3.9]. It is of no use to apply a shear rate range from 10^{-6} to 10^{6} s^{-1}, if only the data between 0.1 and 1 s^{-1} are needed. Furthermore, a rheological model will only be valid for a certain range of shear rates, and it can change in another range. This can be clearly seen in figure 2.10, where for low shear rates (and high volume fractions), shear thinning is observed. At high shear rates, shear thickening occurs and in between, one can see a Newtonian plateau.

2.2 Visco-elasticity

Visco-elasticity has been briefly described in section 2.3 of chapter 2. These materials show a combination of viscous and elastic behaviour. Figure 2.4 shows the strain response of hardened concrete to an instantaneous increase in stress, indicating it is a visco-elastic material. With sudden increases and decreases in stress, visco-elasticity can be determined [3.1]. Remark that the response to a stress is expressed in strain for a visco-elastic material, and not in shear rate. As a result, pressure driven rheometers do not seem very useful to determine visco-elastic behaviour.

Apart from instantaneous increases and decreases in stress, visco-elasticity can also be determined by means of oscillatory tests [3.1]. When applying for example a sinusoidal shear stress with a certain frequency to the material, one can measure the strain response. If the strain response is in fase with the stress, the material behaves perfectly elastic at that frequency. When the response occurs with a fase difference of $\pi/2$, the material behaves as a perfectly viscous material. Any fase shift in between 0 and $\pi/2$ indicates a combination of elastic and viscous behaviour. The response can be decomposed into an elastic and a viscous part, of which the magnitude depends on the fase shift, and the corresponding moduli, G' and G" can be determined. G' stands for the elastic part, G" corresponds to the viscous part. Plotting G' and G" as a function of the angular velocity (which is related to the applied frequency and the amplitude of the oscillation) shows the relative importance of the elastic or the viscous part. At low angular velocities, G" is mostly larger than G', indicating that viscous flowing is the most important behaviour. At high angular velocities, G' is generally larger than G", revealing the larger importance of the elastic response.
This method is quite easy to work with in case the material has a linear response to the applied stress. In case the response is non-linear, things get much more complicated, but this is beyond the scope of this thesis.

2.3 Yield stress

Yield stress is a very difficult property to determine accurately. In literature, even a debate is still going on whether the yield stress really exists [3.20-3.24][3.1][3.3]. Some authors suggest that the yield stress is in fact a Newtonian plateau, with a very high viscosity at very low shear rates. In fact, the material still flows at these shear rates, but during the observation time, no flow is measured. Therefore, as the debate is still going on, yield stress is only defined from a practical point of view as "the maximal stress at which no flow is observed during a reasonable time frame [3.22]."
Measuring yield stress can be done in two different ways, namely measuring the stress that needs to be applied in order to start flow, or by extrapolating the flow curve to zero shear rate. With the first method, the static yield stress is obtained, while the second method gives the dynamic yield stress.
Static yield stress is, especially in case of suspensions, mostly measured by means of a vane test [3.25-3.28]. The vane equipment is based on the principle of the concentric cylinders, but the inner cylinder is imaginary, formed by the four or six blades which rotate in the material. The vane test seems not suitable in order to determine flow curves, but it is an accurate instrument to investigate the static yield stress. During a test, the stress is increased gradually and the strain is measured. When the stress – strain curve shows a plateau or an overshoot (fig. 3.4), the material starts flowing and the static yield stress has been determined. This test setup has been applied by some authors in concrete literature [3.26-3.28], in order to investigate the influence of thixotropy on the static yield stress.

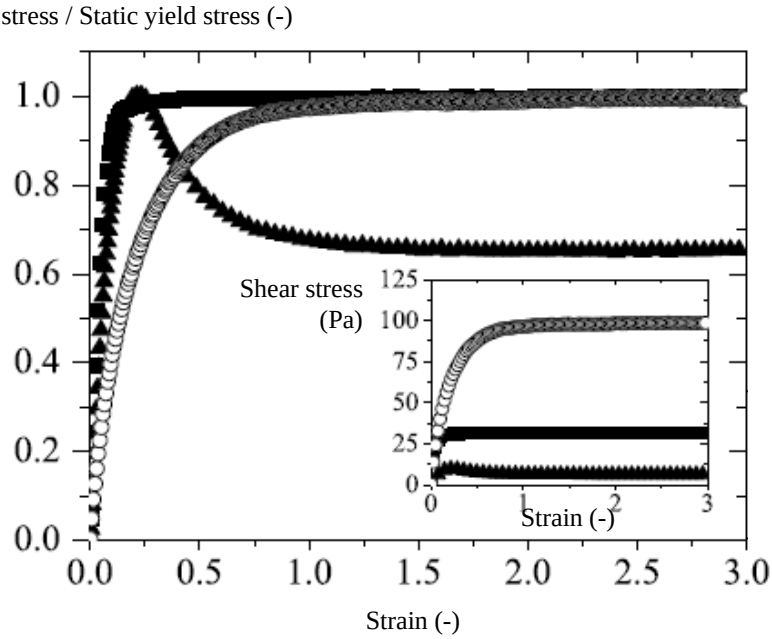

Figure 3.4: Determination of static yield stress of three different materials. The inset shows the stress – strain curves. The larger figure shows the dimensionless stress to strain curve. The triangles represent a thixotropic bentonite suspension. Figure after F. Mahaut et al. [3.25].

The test method in order to determine the dynamic yield stress is much easier to perform, but it is much more sensitive to variations and errors [3.1][3.22]. Figure 3.5 shows a flow curve of traditional cement paste, measured in a plate – plate rheometer, by decreasing the shear rate linearly from 100 to 1 s^{-1}, after a pre-shearing period at 100 s^{-1} in order to eliminate thixotropy (see next section and chapter 5). Three different values of the dynamic yield stress have been determined, depending on the choice of the minimal shear rate (data at lower shear rates are ignored in order to determine the dynamic yield stress). In case the minimal shear rate is 40 s^{-1}, the yield stress is 17.1 Pa, for 20 s^{-1}, it is 15.1 Pa and for 1 s^{-1}, it is 10.6 Pa. As can be seen, the choice of the minimal shear rate influences the value of the dynamic yield stress significantly, even when each time the same model (here the Bingham model) is applied. Changing the rheological model also influences the value of the obtained yield stress. Applying the Herschel-Bulkley model on the full data set delivers a yield stress of -2.7 Pa (which is physically impossible). Only incorporating the data points between 1 and 40 s^{-1} changes the yield stress to -4.3 Pa (also physically impossible). In case only the data between 1 and 5 s^{-1} are used, then a dynamic (Bingham) yield stress of 1.0 Pa is obtained. As can be seen, many different values of the yield stress, even illogical values, can be obtained with one measurement. Consequently, when determining the dynamic yield stress, one should

be consistent in the applied model and data points used and care should be taken when interpreting the results.

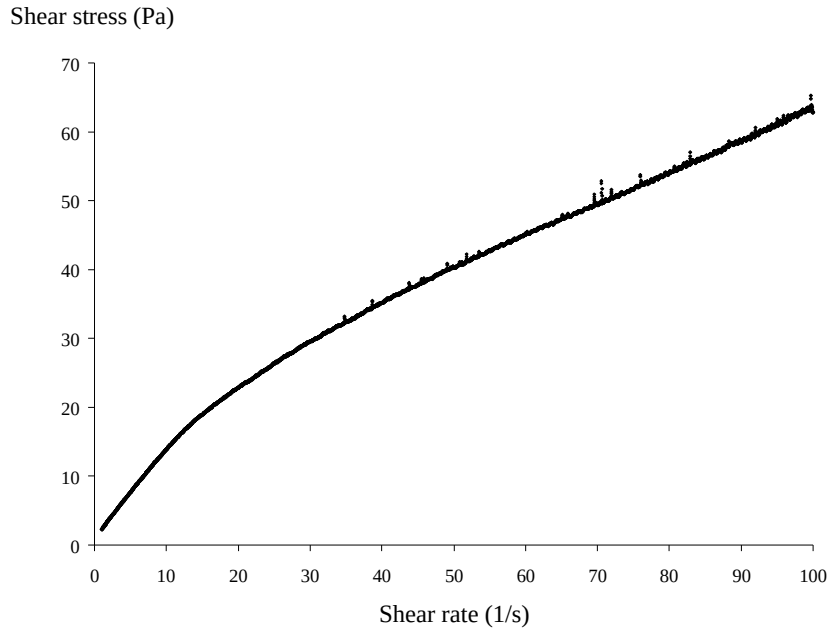

Figure 3.5: Flow curve of traditional cement paste in a parallel plate rheometer. Difficulties arise when determining the dynamic yield stress.

In this thesis, no static yield stress measurements have been performed. Consequently, anytime the term "yield stress" is mentioned, it represents the dynamic yield stress. If the static yield stress is meant, it will be mentioned explicitly.
A last method to determine the yield stress is by means of simple slump tests [3.29-3.32]. Although these tests do not provide a direct result for the yield stress, due to the very complex stress distribution in the material, it is known that when the material achieves its final shape, no stress anywhere in the material is larger than the (real) yield stress. Different authors have tried to establish a relationship between different "slump methods" and the "yield stress" of the material.

2.4 Thixotropy

Thixotropy has been described in section 4.7 of chapter 2. Although the equations describing thixotropy seem very logic, it is not evident to determine the different parameters in the equations. The major difficulty in determining thixotropic properties consists of the influence of the shear history of the material, which influences the behaviour of the material at the moment the measurements are

performed [3.33-3.35]. Therefore, some authors have suggested, in order to investigate thixotropy accurately, to start from a certain reference state (the most de-structured state) and examine the changes after the reference state has been obtained [3.36-3.37].
Different test methods are available in literature. A more detailed description on thixotropy of concrete will be given in chapter 5.

2.4.1 Sudden change in shear rate

The most easy and straightforward way to investigate thixotropy is to determine the stress response to a certain, sudden change in shear rate [3.2][3.38]. This is illustrated in figure 3.6, where the shear rate is increased suddenly and later decreased again to the original value. The shear stress response of a non-thixotropic material is shown by the dashed line, showing also a sudden increase and decrease, but as long as the shear rate is constant, the shear stress remains also constant.

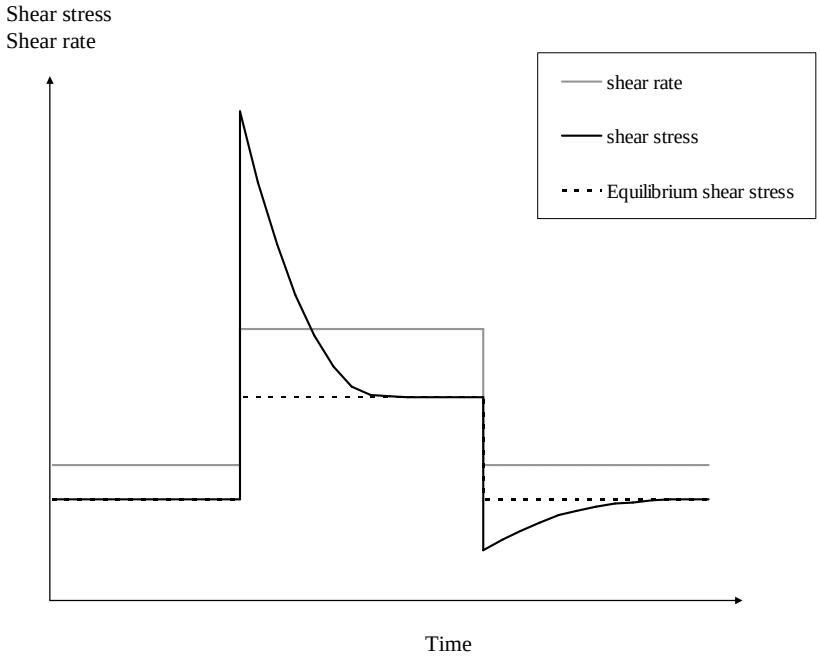

Figure 3.6: Response of a non-thixotropic (dashed line) and a thixotropic (full black line) material to a sudden increase and decrease in shear rate (full grey line).

For a thixotropic material, the behaviour is different. Normally, when increasing shear rate, an overshoot of the shear stress is observed, followed by a breakdown period. Decreasing the shear rate leads to an instantaneously lower value of the shear stress, followed by a build-up period. Generally, build-up takes longer than breakdown. From the differences between the thixotropic stress response and the

equilibrium values, and the time needed to obtain the equilibrium, one should be able to obtain values for the parameters in the thixotropic equations of chapter 2 (eq. 2.16-2.17). However, as the results are dependent on shear history, intermediate time, testing time, …, this is not straightforward.
The stress response shown in figure 3.6 is only valid when the shear rates applied are sufficiently large. In case of low shear rates, shear-induced agglomeration can be more significant than breakdown due to shearing, making this figure invalid (see eq. 2.17) [3.38].

2.4.2 Hysteresis loops

A second method to determine thixotropic properties of a material is to execute a hysteresis loop [3.8-3.9][3.33-3.35][3.39-3.40]. This loop consists of increasing shear rate to a maximal value, followed by a decrease in shear rate. As the material is thixotropic, the up and down curves do not coincide. Depending on the speed of breakdown and build-up, and on the shear history, one can obtain many different curves. In figure 3.7 a, a material which breaks down fast and builds up slowly is shown. Figure 3.7 b shows the opposite: slow breakdown and fast build-up. Figure 3.7 c is the response of a material which has previously been subjected to a higher shear rate than the maximal shear rate obtained in the loop test, and which did not have time to build up. As can be seen in this case, the up curve is lower than the down curve, indicating permanent build-up of the material. The thixotropic properties of the material are determined by the breakdown area between the up and down curve. This parameter is very dependent on the applied maximal shear rate, the rate of increase and decrease in shear rate, the shear history of the material and even the rheometer. Comparison of data between different laboratories is consequently almost impossible. Even a comparison of data within one laboratory is doubtful. As a result, the loop test is not my favourite test to determine thixotropy, and although some attempts have been made in this research project, the results are not reported due to the large inaccuracies and uncertainties.

2.4.3 Static yield stress measurements

The influence of thixotropy on the increase in static yield stress due to build-up can be determined very easily by performing static yield stress measurements on a material, which has been resting in the rheometer for a certain amount of time [3.25-3.28]. Comparing the results obtained at different resting times can give some information on thixotropic build-up. More details will be given in chapter 5.

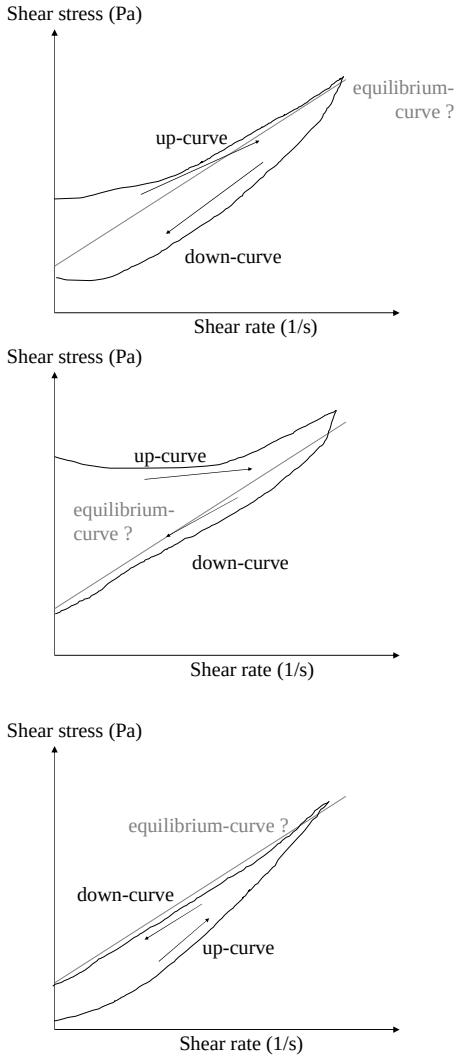

Figure 3.7: a (top): thixotropic loop with fast breakdown and slow build-up.
b (middle): thixotropic loop with slow breakdown and fast build-up.
c (bottom): thixotropic loop of a highly de-structured, rebuilding material.

2.4.4 Oscillatory testing

Although it has not been reported on concrete or cement paste yet, oscillatory testing, similar to the determination of visco-elasticity, is very promising in determining thixotropy, especially when investigating the thixotropic recovery after shearing. When performing the tests, small amplitudes must be applied in order not to interfere with the build-up process [3.2].

2.4.5 Influence of thixotropy on the determination of the flow curve

The different up and down curves from figure 3.7 indicate that determining the real rheological properties of a thixotropic material is a challenging job. A discussion on the influence of thixotropy on rheological measurements will be given in chapter 5. Only one specific measurement procedure will be highlighted, because it is important to understand the results presented in chapter 4.
As thixotropy is an error-inducing factor when determining steady state rheological properties (see chapter 4), it has been "eliminated" by following the same procedure during the full research project. Before determining the "real" flow curve, the material is pre-sheared in the rheometer at the maximal shear rate it will undergo, until equilibrium is reached [3.9][3.39]. This is the chosen reference state of the material [3.36]. Once equilibrium is obtained, the shear rate is decreased stepwise. In this way, the down curve is described by the averages of shear stress and shear rate at each step, giving us the opportunity to check whether each point is determined in equilibrium conditions. When the shear stress still decreases at constant shear rate, no equilibrium is obtained and the data point is rejected for further analysis.

3 Concrete rheometry

3.1 Difficulties in concrete rheometry

Cement-paste, mortar and concrete contain solid particles. As a result, the free space to make the material flow must be sufficiently large. Rheologists claim that the gap size must be at least 10 times larger than the size of the coarsest particle [3.41], but in concrete rheology, a factor 5 is considered to be sufficient [3.9]. If a smaller gap is applied, the homogeneity of the material in the instrument can be questioned and perhaps, some illogical results can be obtained due to the individual influence of the largest particles. The large gap size imposes some restrictions on possible geometries. The cone and plate geometry is of no use and in case of parallel plates, one must prevent the material to escape from between the plates.

As mentioned in section 3.3.1 of chapter 2, particles can migrate to regions with lower shear rates [3.8][3.42]. As the cone and plate geometry is already excluded, and small gap concentric cylinder rheometers are not really of practical use because of their extreme sizes, no rheometer imposing a constant shear rate in the sample is available. As a result, particle migration is an important phenomenon in concrete rheology [3.9].

Due the (large) differences in density between the suspended phase and the suspending medium, not only shear-induced segregation will occur, but also vertical segregation, due to gravity, must be studied [3.8-3.9]. Some mixer-type concrete rheometers have been developed in order to overcome the gravitational segregation by remixing the concrete in the rheometer during the test.

The choice of the shear rate range is another critical point in concrete rheometry. It should be chosen in accordance to the expected application of the concrete. Mixing occurs at very high shear rates, estimated to be in the order of 100 s^{-1} to even 1000 s^{-1} [3.9][3.43], while for casting on site, the shear rate is estimated to be in the order of 1 s^{-1} to 10 s^{-1} [3.9][3.43]. For pumping, as will be shown in chapter 9, the shear rate for concrete will vary between 10 s^{-1} and 50 s^{-1} [3.9][3.43], but it can be much higher in the lubrication layer near the wall. As a result, for the regular casting without a pump, shear rates do not exceed 10 s^{-1} and consequently, low shear rates must be applied in the rheometer. In the case of pumping, higher shear rates should be applied, but this will induce measurement artefacts, like particle migration. As a result, the shear rate in a concrete rheometer cannot be increased infinitely.

A last point of attention in concrete rheometry is the time dependent nature of the material. From mixing to hardening, the rheological properties of the concrete change permanently, due to thixotropy, structural breakdown and loss of workability. Some of the consequences of thixotropy on the measurement procedure have been described in section 2.4.5, and should be considered when performing tests on any cement-based material.

3.2 ConTec - BML viscometers

3.2.1 Geometry

The geometry of the ConTec – BML viscometers [3.8-3.10] (which will be named as ConTec viscometers from this point on) is based on the principle of the concentric cylinders. The concrete is placed in a reservoir, of which its outer boundary forms the outer cylinder. The inner cylinder consists of two parts. The upper part is the part which measures the torque, the lower part does not participate in the measurements, in order to eliminate the influence of the complex 3-D flow pattern at the bottom of the rheometer. Both cylinders are equipped with vertical ribs in order to prevent wall slip. Several inner and outer cylinders with different heights and diameters are available. The rheometer used in this research project, being the ConTec Viscometer 5 (fig. 3.8), has an outer cylinder with a radius of 14.5 cm, an inner cylinder with R_i = 10 cm and the height of the inner cylinder, submerged in the concrete measures 12.5 cm. The total volume of concrete needed in this rheometer is around 12-15 liter.

Figure 3.8: ConTec Viscometer 5.

3.2.2 Measurement systems and procedure

Shear is induced in the rheometer due to the rotation of the outer cylinder at a fixed set of rotational velocities. The upper part of the inner cylinder is connected to a

torque transducer, registering torque response. A full software program enables easy working with the device, with as standard options the measurement of the flow curve or a thixotropic loop. These curves are determined by a stepwise change in rotational velocity. In the software, the maximal and minimal rotational velocity, the time for pre-shearing and the time each step must take, can be easily set. The data are registered in a file at a rate of 25 Hz, and at each time step, the software calculates the average of the five lowest torque values.
Measurements are performed by decreasing the rotational velocity profile stepwise, after a pre-shearing period. The duration of the pre-shearing period, the duration of each velocity step and the number of steps need to be predefined in the software. At the end of each measurement, the rotational velocity is increased up to 2/3 of the maximal rotational velocity. This point is called the segregation point and if it deviates significantly from the obtained flow curve, it indicates that some changes may have occurred in the material during the test.

3.2.3 Data treatment and transformation

As the software calculates averages of torque and rotational velocity at each time step, a set of discrete points in a torque – rotational velocity diagram is obtained. These points need to be transformed into a flow curve, expressing the relationship between shear stress and shear rate. This can be done with analogue transformation equations as 3.3 and 3.5, or it can be achieved by applying the Reiner-Riwlin equation [3.8-3.9][3.44]. The Reiner-Riwlin equation has the advantage that the transformed values are perfectly correct, independent of the geometry, as long as it is a concentric cylinder geometry. On the other hand, the transformation by Reiner-Riwlin needs a preliminary choice of the rheological model. Changing the rheological model will change the transformation equations. When applying equations 3.3 and 3.5, no choice of rheological model must be made, but the solution is not perfect, only approximate, due to the discrete number of data points.
The developers of the ConTec viscometers have chosen to impose the Bingham model on all results in order to be able to transform the data into fundamental rheological units. The transformation of the torque versus rotational velocity is as follows. In a first step: the linear relationship of torque as a function of rotational velocity is determined according to equation 3.12.

$$T = G + H \cdot N \tag{3.12}$$

where: T = *torque (Nm)*
G = *intercept of the relationship with the T-axis, for N = 0 (Nm)*
H = *inclination of relationship between T and N (Nm s)*
N = *rotational velocity (revolutions/s)*

By means of equations 3.13 and 3.14, the values of G and H are transformed into yield stress (τ_0) and plastic viscosity (μ_p), which are the two parameters of the Bingham model. The derivation of the Reiner-Riwlin equation is not given in this thesis, but can be found in [3.8].

$$\tau_0 = \frac{G \cdot \left(1/R_i^2 - 1/R_o^2 \right)}{4 \cdot \pi \cdot h \cdot \ln\left(R_i / R_o \right)} \tag{3.13}$$

$$\mu_p = \frac{H \cdot \left(1/R_i^2 - 1/R_o^2 \right)}{8 \cdot \pi^2 \cdot h} \tag{3.14}$$

where: τ_0 = *yield stress (Pa)*
G = *G from equation 3.12 (Nm)*
R_i = *radius of inner cylinder (m)*
R_o = *radius of outer cylinder (m)*
h = *height of inner cylinder submerged into the material (m)*
μ_p = *plastic viscosity (Pa s)*
H = *H from equation 3.12 (Nm s)*

Equations 3.13 and 3.14 are only valid if the material between the two cylinders is fully sheared. If the shear stress at a certain radius in the rheometer is lower than the instantaneous, local yield stress, the material is not sheared and plug flow is observed. In case plug flow occurs, the equations need slight modifications as described in [3.8]. Note that the Reiner-Riwlin equation does not transform data points from the T – N graph to a shear stress – shear rate diagram, but a pre-defined relationship between T and N is transformed into shear stress – shear rate relationship.
In case the Bingham model is not valid, equations 3.13 and 3.14 need to be changed. A new "Reiner-Riwlin" equation has been derived in [3.45-3.46], based on a Herschel-Bulkley relationship. This relationship incorporates a third parameter which needs to be determined and transformed. With equations 3.16 to 3.18, the relationship between T and N (eq. 3.15) is transformed to a Herschel-Bulkley relationship.

$$T = G_{HB} + K_{HB} \cdot N^m \tag{3.15}$$

$$\tau_0 = \frac{G_{HB}}{4 \cdot \pi \cdot h} \cdot \left(\frac{1}{R_i^2} - \frac{1}{R_o^2} \right) \cdot \frac{1}{\ln\left(R_o / R_i \right)} \tag{3.16}$$

$$K = \frac{K_{HB}}{2^{2n+1} \cdot \pi^{n+1} \cdot h} \cdot n^n \cdot \left(\frac{1}{R_i^{2/n}} - \frac{1}{R_o^{2/n}} \right)^n \tag{3.17}$$

$$n = m \tag{3.18}$$

where: G_{HB}, K_{HB}, m = *Herschel-Bulkley parameters of the T-N relationship.*

τ_0, *K, n = Herschel-Bulkley parameters of the shear stress – shear rate relationship.*

For other rheological models, other transformation formulae may be found, although obtaining an analytical solution is not straightforward [3.45].
After each test in the ConTec rheometer, the raw data are temporarily available for separate analysis. This can be useful in order to investigate whether each data point has been obtained in equilibrium conditions or whether no large fluctuations in the torque measurements occur. One can use this raw data file in order to omit the averaging procedure of the software, or in order to apply equations 3.15 to 3.18, which are not (yet) incorporated in the software.

3.2.4 Remarks

The ConTec viscometers have been developed with a lot of care and are considered as one of the most useful and practical rheometers for cement paste and concrete. The flow in the measurement section approaches the 1-D flow as well as possible, which is only achieved in this type of concrete rheometers. The software makes the rheometer an easy tool to work with, and creates very stable measurements. By means of the segregation point, a utility is provided to observe particle migration (or material changes in general) during testing and analysis.
As disadvantages, the danger for particle migration, both horizontal and vertical, can be mentioned. Further, due to the developments to keep measurements as easy as possible for the user, this rheometer has turned into a kind of black box and people working with it should be critical when investigating the data.
The gap between the inner and outer cylinder equals 4.5 cm in this configuration, resulting in a maximal aggregate size of 16 mm in order to avoid a significant influence of the coarse particles on the measurement results.

3.3 BTRHEOM

3.3.1 Geometry

The BTRHEOM has been developed in France and is based on the parallel (rotating) plates geometry (fig. 3.9) [3.47-3.49]. It consists of a stationary reservoir, with an outer radius of 120 mm, forming the bottom plate. The top plate is connected to the motor and the torque transducer through the sample and the connection shaft has a radius of 20 mm. The height of the sample is usually around 100 mm. The sideway outflow of concrete is prevented by a seal between the edge of the reservoir and the vertical wall rotating with the upper plate. A calibration has been performed to determine the resistance of the seal itself. Due to this partly rotating, partly stationary vertical wall, the velocity profile near the edges is disturbed. Both the upper and lower plates are equipped with a rib-like structure in order to prevent slippage between the material and the plates. The vertical walls are smooth, in order to prevent as much as possible the disturbing effect.

3.3.2 Measurement systems and procedures

The shear is induced by the rotation of the upper plate relative to the lower plate. Similar to the ConTec viscometer, a stepwise increase or decrease in shear rate can be imposed and the resulting torque response is measured. The BTRHEOM also provides the possibility to impose the stress (or torque). Apart from the geometry, the BTRHEOM works quite similarly as the ConTec viscometers.

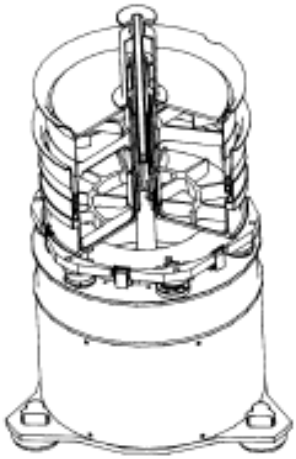

(a) 3-D diagram of the apparatus (Body dimensions: H 30 x φ 30 cm container dimensions: H 24 x φ 27 cm

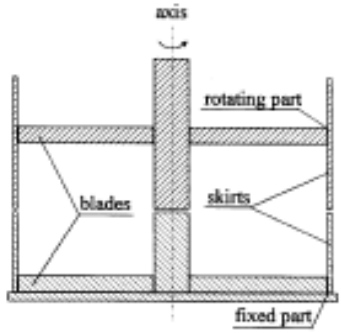

(b) 2-D diagram of the container

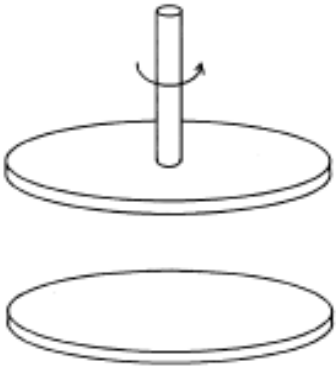

(c) Schematic diagram of the principle

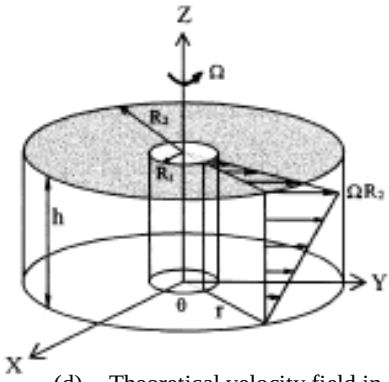

(d) Theoretical velocity field in the test sample

Figure 3.9: BTRHEOM. Figure from C. Hu et al. [3.47].

3.3.3 Data treatment and transformation

As the torque or rotational velocity is changed stepwise, the averages are calculated at each step. Similarly to the ConTec viscometers, a set of discrete points is created and need to be transformed into fundamental rheological units. The principle is similar to the Reiner-Riwlin equation for concentric cylinders. The data in the T – N diagram are fitted by means of equation 3.19. The transformation formulae are given in equations 3.20 and 3.21.

$$T = T_0 + A \cdot N^n \tag{3.19}$$

$$\tau_0 = \frac{3 \cdot T_0}{2 \cdot \pi \cdot \left(R_2^3 - R_1^3\right)} \tag{3.20}$$

$$K = 0.9 \frac{n+3}{\left(2 \cdot \pi\right)^{n+1}} \frac{h^n \cdot A}{\left(R_2^{n+3} - R_1^{n+3}\right)} \tag{3.21}$$

where: *T_0, A, n = Herschel-Bulkley parameters of T – N relationship*
τ_0, K, n = Herschel-Bulkley parameters of shear stress – shear rate relationship
R_2 = outer radius (m)
R_1 = radius of the shaft (m)
h = height of the sample (m)

As can be seen in equation 3.19, a Herschel-Bulkley model is imposed on the resulting data, with a consistency index (n) varying between 1 and 3.

3.3.4 Remarks

The BTRHEOM is a very compact and light rheometer, which can be used on site to perform measurements. In spite of the practical use of the instrument, and the small size of the sample needed, it did not conquer the rheometer market. Currently, not many results obtained with the BTRHEOM are reported.

3.4 Tattersall Mk-II

3.4.1 Geometry

The Tattersall Mk-II rheometer (fig. 3.10) [3.50-3.54] has been developed by Tattersall in order to measure the rheological properties of concrete with medium to high workability. The design is based on the principle of the concentric cylinders, but in order to avoid gravity-induced segregation of the concrete in the rheometer, the inner cylinder is equipped with an interrupted helical screw, which mixes the concrete, but it also gives the concrete the possibility to fall back between the blades. The outer cylinder is formed by the concrete reservoir and it is equipped with ribs, in order to prevent wall slip.

In the Magnel Laboratory for Concrete Research, a copy of this rheometer has been made in the 1980's. Preliminary results with this device did not give the expected Bingham relationship, but more complicated and illogical results have been obtained [3.55]. The machine was put on early retirement and has been forgotten for one and a half decade. Lately, in 2005, the rheometer has been rediscovered. The strain gauges and alternator, which served for measuring torque and rotational velocity respectively, have been replaced by a modern torque transducer (fig. 3.10), also capable of measuring rotational velocity. The steering of the rheometer has been simplified with some basic electrics, but a fully automated procedure by means of software is not installed.
The outer cylinder of this rheometer measures 12.5 cm. The distance between the outer edges (of the blades) of the inner cylinder measures 16 cm in horizontal direction and 14 cm in vertical direction.

Figure 3.10: Modernised Tattersall Mk-II rheometer.

3.4.2 Measurement systems and procedures

The shearing in the Tattersall Mk-II rheometer is caused by the rotation of the inner cylinder, while the outer cylinder remains stationary during the test. The torque response is also measured at the inner cylinder. The data of torque and rotational velocity are registered at a rate of 5000 Hz by the torque transducer, and the average of 2000 measurements is saved into a data file. As a result, five measuring points are obtained in two seconds.

The rotational velocity is imposed by controlling the electrical current sent to the electromotor. The maximal rotational velocity is around 90 rotations per minute when the rheometer is empty or between 75 and 85 rot/min when filled with concrete, depending on the flow resistance of the concrete. The rotational velocity can be reduced in 11 steps, each time by reducing the electrical current sent to the electromotor. The rotation of the electromotor is transmitted to the inner cylinder by means of a reduction system. The losses over the reduction system are irrelevant, because the torque transducer is placed between the inner cylinder and the reduction system.
Similarly to the ConTec viscometers, a stepwise decrease in rotational velocity is imposed and the resulting torque is measured. Before the start of each test, the concrete sample is pre-sheared at the maximal rotational velocity, until equilibrium in the resulting torque is achieved. This is controlled manually, based on the results shown on the computer screen. As a result, the definition of equilibrium also depends on the operator.

3.4.3 Data treatment and transformation

The results of a rheometer test are expressed in torque and rotational velocity. For each step in the test, the data at constant rotational velocity ànd constant torque are averaged and represent one data point in a T – N diagram. Originally, this apparatus has been used to determine two points of the flow curve and the corresponding Bingham parameters. In this procedure, 11 data points are available, and in some cases, the Bingham relationship is not valid (see chapter 4).
Due to the complex geometry of the inner cylinder, no formulae are available to transform torque and rotational velocity into fundamental rheological units. As a result, a calibration has been performed with oil and honey, and a transformation procedure has been worked out [3.56]. A detailed description of the calibration and transformation procedure is given in Appendix A.

3.4.4 Remarks

The transformation procedure does not deliver the exact rheological properties of the concrete, but it appears to be very useful for comparing different results. Due to the interrupted screw, concrete is less sensitive to segregation, although no prevention of particle migration to the outer radius is present. Software is only applied for the registration and visualisation of the data. The tests are executed manually, giving the opportunity to the operator to adjust some items in the procedure depending on the obtained results. For example, a longer pre-shearing period can be necessary in case of very thixotropic mixtures.

3.5 Other rheometers

Other rheometers are also available for concrete rheometry, but for most of them, a similar calibration procedure must be applied in order to obtain the fundamental rheological properties. In some cases, authors prefer to express data in torque versus rotational velocity instead of shear stress versus shear rate to avoid the

transformation. Some of the other rheometers are the Cemagref-IMG rheometer [3.57-3.58] (very large concentric cylinders), the IBB-rheometer [3.57-3.58] and Tattersall Mk-III [3.50] (H-shape inner device making a planetary motion), the Rheomixer [3.9] (rheometer which remixes the sample), the vane rheometer [3.26-3.28] (good for yield stress, not so good for viscosity), falling ball viscometers [3.59], rotating ball viscometers [3.60], the BT2-viscometer [3.61] (similar to the rotating ball viscometer), a capillary rheometer for concrete [3.62-3.63] and even a mixing truck [3.64]. Even a number of workability tests can be interpreted as rheometer tests, but mostly only one parameter is determined (e.g. slump flow related to yield stress).
As can be seen, the number of different devices is large. Each rheometer has its advantages and disadvantages, its possibilities and limitations. In this research project, most results have been obtained with the Tattersall Mk-II rheometer. Some measurements have been performed on the ConTec viscometer 5 of the BBRI or the KULeuven.

3.6 Comparison of rheometers

There is a saying mentioning that when someone has one watch, he knows the time, but when he has two, time is not known anymore. The same principle is applicable for rheometers: each rheometer delivers different values for the same material and as a result, the real values are not known.
Two international campaigns have been performed in order to compare the most standard rheometers for different concrete mixtures [3.57-3.58]. The results indicate indeed that all rheometers deliver different results, but they can be divided in some groups delivering similar values for the same concrete. These campaigns reveal that the Tattersall Mk-II rheometer and the BML-viscometer deliver similar values, which can be seen in figure 3.11, showing yield stress and plastic viscosity obtained with different rheometers for different concrete mixtures, assuming Bingham behaviour.
As will be shown in chapter 4, self-compacting concrete is not always a Bingham material, as it can show shear thickening behaviour. In order to be certain this behaviour is not dependent on the type of rheometer, the Tattersall Mk-II rheometer has been moved to the KULeuven, next to their ConTec Viscometer 5 and measurements on different concrete mixes have been executed simultaneously [3.65]. Very similar values for the consistency factor (K) and consistency index (n) have been obtained, when applying the Herschel-Bulkley model, indicating rheometer-independence of the shear thickening behaviour. Some differences in the yield stress have been observed. In cases of extremely fluid SCC, the Tattersall Mk-II rheometer overestimates the shear thickening significantly, and difficulties arise when applying the transformation procedure. As a result, the Tattersall Mk-II rheometer cannot be used in case of extremely fluid self-compacting concretes.

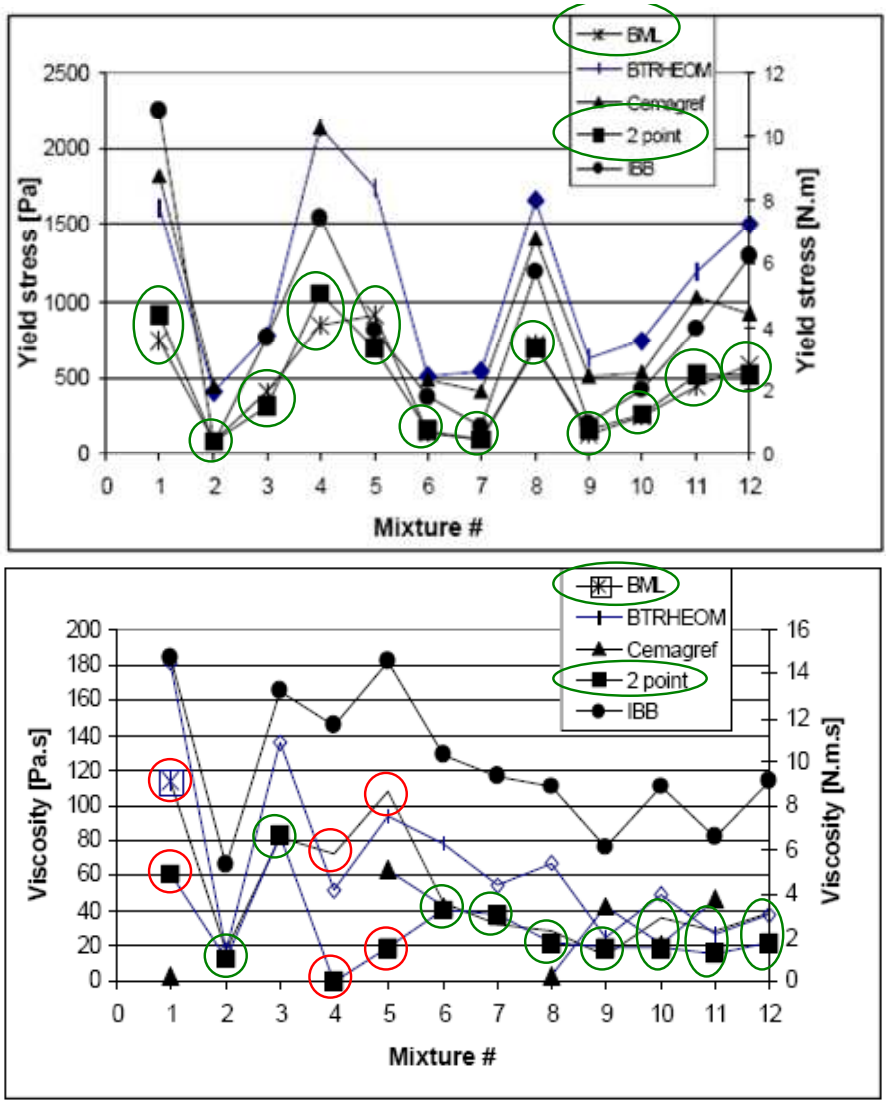

Figure 3.11: Comparison of 5 different concrete rheometers. The Tattersall Mk-II (2-point) and ConTec viscometer (BML) deliver, apart from some exceptions, mostly similar values for yield stress and plastic viscosity. Note that the values for the IBB-rheometer are expressed in Nm and Nms. Figure from C.F. Ferraris et al. [3.57].

4 Summary

In this chapter, the science (or art) of obtaining rheological properties of liquid materials is described. In a first part, different kinds of rheometers are mentioned. A division is made between the drag flow rheometers and the pressure driven rheometers. In case of a drag flow rheometer, one part of the device moves (mostly rotating) relative to the other part and shear is induced in the sample between the moving and stationary part. The geometry, working principle and transformation formulae are discussed for the parallel sliding plates, the concentric cylinder rheometer, the parallel rotating plates rheometer and the cone and plate rheometer.
The capillary rheometer is the best known pressure driven rheometer. During the flow of a material through a tube, the pressure loss and flow rate are measured. By means of transformation formulae, the occurring shear stress and shear rate can be calculated. Recall that the shear stress distribution in a capillary rheometer is a universal law, meaning it is independent of the kind of material used. In addition, the slit and annulus geometries are mentioned.
In the second section, the procedures to determine the flow curve, visco-elasticity, yield stress and thixotropic properties are described. Note that there is a difference between the static and the dynamic yield stress and that thixotropy complicates rheological measurements significantly.
Finally, as an introduction to the next chapter, concrete rheometry is described. Special attention is paid to the ConTec Viscometer 5 and the Tattersall Mk-II rheometer, which have been used extensively in this research project. For both rheometers, the geometry, testing procedure, data treatment and transformation of data are discussed. Finally, some results of comparative tests with different rheometers are mentioned, indicating differences in the measured values for the same concrete mix.

5 References

[3.1] Macosko C.W., "Rheology Principles, measurements and applications," Wiley-VCH, New-York (1994).

[3.2] European Society of Rheology, "Short course on Rheological Measurements," 10th European School of Rheology, Leuven (2006).

[3.3] Ferguson J., Kemblowski Z., "Applied fluid rheology," Elsevier Applied Science, London (1991).

[3.4] Reiner M., "Deformation and flow," Wiley-Interscience, New York (1960).

[3.5] Couette M.M., "Etudes sur le frottement des liquides, " Ann. Chim. Phys. **21** (1890), 433-510.

[3.6] Krieger I.M., Elrod H., "Direct Determination of the Flow Curves of Non-Newtonian Fluids. II. Shearing Rate in the Concentric Cylinder Viscometer," J. Appl. Phys. **24** (1953), 134.

[3.7] Yang T.M.T., Krieger I.M., "Comparison of Methods for Calculating Shear Rates in Coaxial Viscometers," J. Rheol. **22** (1978), 413-421.

[3.8] Wallevik J.E., "Rheology of particle suspensions, Fresh concrete, mortar and cement paste with various types of lignosulphonates," Ph-D dissertation, The Norwegian University of Science and Technology, Trondheim (2003).

[3.9] Geiker M.R., Wallevik O.H., "Rheology of cement based materials," DTU-RILEM Doctoral course, Lyngby (2007).

[3.10] Wallevik J.E., Wallevik O.H., "Effect of eccentricity and tilting in coaxial cylinder viscometers when testing cement paste," Nordic Concrete Research, Oslo (1998), 144-152.

[3.11] Mooney M., Ewart R.H., "The Conicylindrical Viscometer," Physics **5** (1934), 350.

[3.12] Broyer E., Macosko C.W., "Comparison of cone and plate, bicone and parallel plates geometries for melt rheological measurements," Soc. Plast. Eng. Tech. Papers **21** (1975), 343.

[3.13] Hagen G., "Ueber die Bewegung des Wassers in engen cylindrischen Rohren," Poggendorfs Ann. Phys. Chem. **46** (1839), 423-442.

[3.14] Poiseuille J.L.M., "Recherches expérimentales sur le mouvement des liquides dans les tubes de très-petits diamètres," CR Acad. Sci. Paris. **11** (1840), 961-967, 1041-1049.

[3.15] Poiseuille J.L.M., "Recherches expérimentales sur le mouvement des liquides dans les tubes de très-petits diamètres," CR Acad. Sci. Paris. **12** (1841), 112-115.

[3.16] Mooney M., "Explicit Formulas for Slip and Fluidity," Trans. Soc. Rheol. **2** (1931), 210-222.

[3.17] Laun H.M., Hirsch G., "New laboratory tests to measure rheological properties of paper coatings in transient and steady-state flows," Rheol. Acta **28** (1989), 267-280.

[3.18] Bagley E.B., "End Corrections in the Capillary Flow of Polyethylene," J. Appl. Phys. **28** (1957), 624.

[3.19] Fox J.A., "An Introduction to Engineering Fluid Mechanics," The MacMillan Press Ltd, London (1974).

[3.20] Boger D.V., Walters K., Webster M.F., Williams R.P., "Yield stress," Proc. of the XVth Int. Cong. On Rheology, Monterey (2008).

[3.21] Barnes H.A., Walters K., "The yield stress myth?" Rheol. Acta **24** (1985), 323-326.

[3.22] Barnes H.A., "The yield stress – a review or 'παντα ρει' – everything flows?" J. non-Newt. Fluid Mech. **81** (1999), 133-178.

[3.23] Hartnett J.P., Hu R.Y.Z., "Technical note: The yield stress – An engineering reality," J. Rheol. **33** (1989), 671-679.

[3.24] Evans I.D., "Letter to the editor: On the nature of the yield stress," J. Rheol. **36** (1992), 1313-1318.

[3.25] Mahaut F., Chateau X., Coussot P., Ovarlez G., "Yield stress and elastic modulus of suspensions of noncolloidal particles in yield stress fluids," J. Rheol. **52** (2008), 287-313.

[3.26] Mahaut F., Mokéddem S., Chateau X., Roussel N., Ovarlez G., "Effect of coarse particle volume fraction on the yield stress and thixotropy of cementitious materials," Cem. Conc. Res. **38** (2008), 1276-1285.

[3.27] Billberg P., Österberg T., "Thixotropy of self-compacting concrete," Proc. of the 2nd Int. RILEM Symp. on SCC, Tokyo (2001), 99-108.

[3.28] Ovarlez G., Roussel N., "Structuration rate of fresh SCC: Influence of the state of shear during rest," Proc. of the 5th Int. RILEM Symp. on SCC, Ghent (2007), 285-290.

[3.29] Wallevik J.E., "Relationship between the Bingham parameters and slump," Cem. Conc. Res. **36** (2006), 1214-1221.

[3.30] Roussel N., Stefani C., Leroy R., "From mini-cone test to Abrams cone test: measurement of cement-based materials yield stress using slump tests," Cem. Conc. Res. **35** (2005), 817-822.
[3.31] Roussel N., "Correlation between yield stress and slump: Comparison between numerical simulations and concrete rheometers results," Mat. Struct. **39** (2006), 501-509.
[3.32] Roussel N., Coussot P., ""Fifty-cent rheometer" for yield stress measurements: From slump to spreading flow," J. Rheol. **49** (2005), 705-718.
[3.33] Cheng D.C.-H., "Hysteresis Loop Experiments and the Determination of Thixotropic Properties," Nature **216** (1967), 1099-1100.
[3.34] Mewis J., Spaull A.J.B., Helsen J., "Structural hysteresis," Nature **253** (1975), 618-619.
[3.35] Barnes H.A., "Thixotropy - a review," J. Non-Newt. Fluid Mech. **70** (1997), 1-33.
[3.36] Roussel N., "A thixotropy model for fresh fluid concretes: Theory, validation and applications," Cem. Conc. Res. **36** (2006), 1797-1806.
[3.37] Roussel N., "Steady and transient flow behaviour of fresh cement pastes," Cem. Conc. Res. **35** (2005), 1656-1664.
[3.38] Mewis J., Wagner N.J., "Thixotropy," Adv. Colloidal Interface Sci., **147-148** (2009), 214-227.
[3.39] Geiker M.R., Brandl M., Thrane L.N., Bager D.H., Wallevik O., "The effect of measuring procedure on the apparent rheological properties of self-compacting concrete," Cem. Conc. Res. **32** (2002), 1791-1795.
[3.40] Billberg P., "Form Pressure generated by Self-Compacting Concrete – Influence of thixotropy and Structural Behaviour at Rest," Ph-D-dissertation, School of Architecture and Built Environment, Stockholm (2006).
[3.41] Mewis J., Wagner N.J., "Suspension Rheology," Short course from the society of rheology, Monterey (2008).
[3.42] Ovarlez G., Bertrand F., Rodts S., "Local determination of the constitutive law of a dense suspension of non-colloidal particles through MRI," J. Rheol. **50** (2006), 259-292.
[3.43] Helmuth R., Hills L.M., Whiting D.A., Bhattacharja S., "Abnormal Concrete Performance in the Presence of Admixtures," Report of the Portland Cement Association, Skokie (1995).
[3.44] Reiner M., "Deformation and flow; An elementary Introduction to Theoretical Rheology," H.K. Lewis & Co. Limited, Great Britain (1949).
[3.45] Heirman G., Vandewalle L., Van Gemert D., Wallevik O., Cauberg N., "Contribution to the solution of the Couette inverse problem for Herschel-Bulkley fluids by means of the integration method," Proc. of the 2nd Int. Symp. on Advances in Concrete through Science and Engineering, Québec-City (2006).
[3.46] Heirman G., Vandewalle L., Van Gemert D., "An analytical solution of the Couette inverse problem for shear thickening SCC in a wide-gap concentric cylinder rheometer," J. non-Newt. Fluid Mech. **150** (2008), 93-103.
[3.47] Hu C., de Larrard F., Sedran T., Boulay C., Bosc F., Deflorenne F., "Validation of BTRHEOM, the new rheometer for soft-to-fluid concrete," Mat. Struct. **29** (1996), 620-631.
[3.48] Hu C., de Larrard F., "The rheology of fresh high-performance concrete," Cem. Conc. Res. **26** (1996), 283-294.
[3.49] Kaplan D., "Pumping of concretes," Ph-D dissertation (in French), Laboratoire Central des Ponts et Chaussées, Paris (2001).
[3.50] Tattersall G.H., Banfill P.F.G., "The rheology of fresh concrete," Pitman, London (1983).
[3.51] Tattersall G.H., "The rationale of a two-point workability test," Mag. Conc. Res. **25** (1973) 169-172.
[3.52] Tattersall G.H., Bloomer S.J., "Futher development of the two-point test for workability and extension of its range," Mag. Conc. Res. **31** (1979), 202-210.
[3.53] Wallevik O.H., Gjørv O.E., "Modification of the two-point workability apparatus," Mag. Conc. Res. **42** (1990), 135-142.
[3.54] Domone P.L.J., Yongmo X., Banfill P.F.G., "Developments of the two-point workability test for high-performance concrete," Mag. Conc. Res. **51** (1999), 171-179.
[3.55] Degroote G., "Evaluation of the Tattersall viscometer for concrete," Master-thesis (in Dutch), Ghent University, Ghent (1988).
[3.56] Feys D., Verhoeven R., De Schutter G., "Evaluation of time-independent rheological models applicable to fresh Self Compacting Concrete," Appl. Rheol. **17:5** (2007), 56244.
[3.57] Ferraris C.F., Brower L.E., Banfill P., Beaupré D., Chapdelaine F., de Larrard F., Domone P., Nachbaur L., Sedran T., Wallevik O., Wallevik J.E., "Comparison of concrete rheometers:

International tests at LCPC (Nantes, France) in October, 2000," NIST report 6819, Gaithersburg (2001).

[3.58] Ferraris C.F., Brower L.E., Beaupré D., Chapdelaine F., Domone P., Koehler E., Shen L., Sonebi M., Struble L., Tepke D., Wallevik O., Wallevik J.E., "Comparison of concrete rheometers: International tests at MB (Cleveland OH, USA) in May, 2003," NIST report 7154, Gaithersburg (2004).

[3.59] Gregori A., Sun Z.S., Douglas R.P., Shah S.P., Bonen D., "The evaluation of viscosity using a novel viscometer for SCC," Proc. of the 4th Int. RILEM Symp. on SCC and the 2nd North-American Conf. on the design and use of Self-Consolidating Concrete, Chicago (2005), 775-782.

[3.60] Läuger J., Müller M., Tyrach J., "A new ball measuring system for large particle suspensions," Appl. Rheol. **9** (1999), 145-147.

[3.61] Golaszewski J., "Influence of mortar volume on the rheological properties of fresh high-performance concrete," Proc. of the 3rd Int. Symp. on non-traditional cement and concrete, Brno (2008), 282-291.

[3.62] Roshavelov T., "Prediction of fresh concrete flow behavior based on analytical model for mixture proportioning," Cem. Conc. Res. **35** (2005), 831-835.

[3.63] Roshavelov T., "New viscometer for Measuring flow properties of fluid concrete," ACI Mat. J. **102:6** (2005), 397-404.

[3.64] Amziane S., Ferraris C.F., Koehler E.P., "Rheology measurements of fresh concrete with a Mixing Truck," Proc. of the 4th Int. RILEM Symp. on SCC and the 2nd North-American Conf. on the design and use of Self-Consolidating Concrete, Chicago (2005), 539-544.

[3.65] Feys D., Heirman G., De Schutter G., Verhoeven R., Vandewalle L., Van Gemert D., "Comparison of two concrete rheometers for shear thickening behaviour of SCC," Proc. of the 5th Int. RILEM Symp. on SCC, Ghent (2007), 365-370.

CHAPTER 4:

CONCRETE RHEOLOGY: STEADY STATE

This chapter contains the first of two parts dealing with concrete rheology, namely the steady state properties, determined after elimination of the time dependency. In the next chapter, this time dependency (being thixotropy, structural breakdown and loss of workability) will be discussed. The first section of this chapter gives a discussion of some of the applicable models in steady state (self-compacting) concrete rheology. The second section explains briefly the difference between traditional and self-compacting concrete, but purely from a rheological point of view. The third section contains the details on the rheological testing, including concrete compositions, mixing and testing procedure. The fourth section studies the influence of the constituent elements of concrete on yield stress and viscosity while the fifth section focuses entirely on shear thickening behaviour, its influencing factors and the possible cause(s) of it.

1 Material models

1.1 Linear model

It has been reported extensively in literature that, when measuring the rheological properties of fresh concrete in general, at least two parameters need to be determined [3.1-3.5]. This is due to the yield stress of the concrete. The most applied model to determine the rheological properties in steady state conditions is the Bingham model, which describes a linear relationship between shear stress and shear rate, once the yield stress is exceeded (eq. 4.1) [4.6].

$$\tau = \tau_0 + \mu_p \cdot \dot{\gamma} \tag{4.1}$$

where: τ = *shear stress (Pa)*
τ_0 = *yield stress (Pa)*
μ_p = *plastic viscosity (Pa s)*

dγ/dt = shear rate (1/s)

Equation 4.1 is, in order to be theoretically correct, only valid for shear stresses ≥ yield stress. In case the shear stress is lower than the yield stress, the equation should express that the shear rate equals 0.

1.2 Non-linear models

1.2.1 Mathematical models

In cases non-linear steady state rheological behaviour has been measured, the favourite model applied is the Herschel-Bulkley model (eq. 4.2) [4.7], especially in cases of shear thickening behaviour [4.8-4.11]. In case of shear thinning (or pseudoplasticity), Yahia and Khayat have investigated several models and the influence of the choice of the model on the determination of (dynamic) yield stress [4.12]. From Yahia and Khayat, we have retained the modified Bingham model (eq. 4.3) [4.12] in order to describe non-linear steady state (shear thickening) behaviour.

$$\tau = \tau_0 + K \cdot \dot{\gamma}^n \tag{4.2}$$

$$\tau = \tau_0 + \mu \cdot \dot{\gamma} + c \cdot \dot{\gamma}^2 \tag{4.3}$$

where: *K = consistency factor (Pa s^n)*
n = consistency index (-)
c = second order parameter (Pa s^2)

1.2.2 Discussion

Although the Herschel-Bulkley model is most frequently applied in non-linear concrete rheology, it has several disadvantages. When investigating the dimensions of the parameters in the Herschel-Bulkley equation, one can see that large problems will arise when determining the physical meaning of the consistency factor K. The dimension of K is Pa s^n, meaning it is dependent on the material properties. For the modified Bingham equation, no physical meaning of the second order term has been found yet, but still, a possibility remains, due to the fixed dimension of c.
When deriving the Herschel-Bulkley equation to the shear rate (eq. 4.4) and consequently investigating the inclination of the curve, difficulties arise when the shear rate approaches 0.

$$\frac{d\tau}{d\dot{\gamma}} = n \cdot K \cdot \dot{\gamma}^{n-1} \tag{4.4}$$

For n < 1 (shear thinning), equation 4.4 becomes infinite. For n > 1, equation 4.4 approaches 0. As a result, the Herschel-Bulkley curve at zero shear rate is vertical for shear thinning materials and horizontal for shear thickening materials. When

determining the (dynamic) yield stress, the Herschel-Bulkley equation always gives the lowest prediction of the yield stress for shear thinning [4.12] and the highest prediction in case of shear thickening, compared to any other applicable model. In order to overcome this problem, a linear term in the shear rate must be incorporated in any rheological model, making the modified Bingham more advantageous.
A third advantage of the modified Bingham model will be discussed in chapter 6, when deriving the Poiseuille equation for non-Newtonian materials.
The Herschel-Bulkley and modified Bingham model are not completely independent from each other. In fact, the modified Bingham model can be regarded as a Taylor-expansion series of Herschel-Bulkley of the order 2. As the exponent n in Herschel-Bulkley rarely exceeds the value of 2 (at least for the concretes tested in this research project), this approximation is justified and the intensity of shear thickening can be described by n of Herschel-Bulkley or c/μ of the modified Bingham model. In this thesis, the modified Bingham equation will be applied, except in cases where the Herschel-Bulkley model is imposed, for example, when measuring with the ConTec Viscometer 5 [4.11].

2 Difference between traditional and self-compacting concrete

Without going into the concrete compositions of traditional concrete (TC) and self-compacting concrete (SCC), the difference between these two types of concrete can be easily explained by means of their steady state rheological behaviour. When assuming Bingham behaviour for both types of concrete – this is not always the case, as will be shown in section 5 of this chapter – the differences between TC and SCC must be due to different values in yield stress and plastic viscosity. Recalling the basic properties of SCC, mentioned in chapter 1, the filling ability can only be achieved when the yield stress of SCC is sufficiently low [4.13-4.14], due to a good dispersion of the cement particles (see section 4.2.5 of chapter 2). In this way, without the need of any other force than gravity, SCC is able to spread out much further than TC. The low yield stress also causes the self-compaction, as large air bubbles are not prevented to escape.

On the other hand, the (coarse) aggregates can sink in the cement paste if the yield stress of the paste cannot withstand the stress induced by gravity on the aggregates. The art of producing SCC is to create a yield stress which is sufficiently low to let the air bubbles escape, but sufficiently high to prevent segregation of the aggregates. As a kind of safety, the viscosity of SCC is increased by addition of an extra amount of fine materials (powder type SCC) [4.15-4.16], or by adding a viscosity modifying admixture (VMA) [4.15][4.17]. In Western-Europe, the increase in powder amount in order to increase the viscosity (and hence the stability) is mostly applied. By increasing the viscosity, the sedimentation process of the aggregates is slowed down, until it is completely stopped due to an increase in yield stress, caused by thixotropy or loss of workability, or both. For traditional concrete, the yield stress is sufficiently high (at least in normal cases), and as a result, it is not necessary to modify the viscosity.

Figure 4.1 shows the flow curve of two traditional and one self-compacting concrete. The w/c-ratios are 0.45 and 0.55 for the TC (TC 1 and TC 2, respectively) and 0.45 for the SCC (SCC 48-4). Note that, even at lower w/c-ratio, the yield stress of the SCC is lower than for the TC, but the “viscosity” is higher for the SCC. The SCC presented in figure 4.1 also shows shear thickening behaviour.

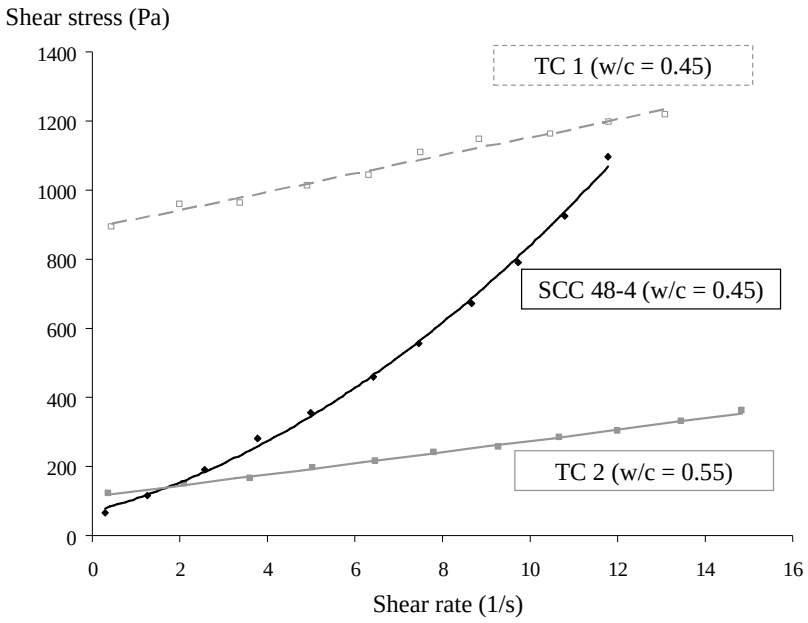

Figure 4.1: Flow curves of TC 1 (w/c = 0.45, grey dashed line), TC 2 (w/c = 0.55, grey full line) and SCC 48-4 (w/c = 0.45, black line), indicate the lower yield stress and higher viscosity of SCC. Note that this SCC shows shear thickening behaviour.

3 Rheological testing

3.1 Concrete compositions

During this research project, 62 concrete mixes have been produced explicitly for rheometer testing, of which 59 were (supposed to be) self-compacting and 3 mixes were traditional concretes. These mixes have been produced at the Magnel Laboratory and have been tested with the Tattersall Mk-II rheometer (Appendix B, section 2). 8 additional mixes have been produced in order to test the influence of demoulding oil (see section 5.4.6 and Appendix B, section 6), also with the Tattersall Mk-II rheometer. 14 mixes have been produced at the KULeuven for comparative testing with the Tattersall Mk-II rheometer and the ConTec viscometer 5 (see section 3.6 of chapter 3 and Appendix B, section 4) [4.18] and 3 mixes have also been produced in the KULeuven in order to investigate the influence of the coarse aggregates on the rheological properties (Appendix B, section 5). As a preliminary investigation, 35 mixes have been produced at the BBRI of which the rheological properties have been determined with the ConTec viscometer 5 (Appendix B, section 3). Most of these mixes have been repeated in the 62 mixes for the rheometer testing in the Magnel Laboratory. The results of this preliminary testing are very similar to the results obtained with the Tattersall Mk-II rheometer. Two traditional cement pastes and four self-compacting cement pastes have been tested with a plate-plate rheometer.
The concrete compositions of all these mixes can be found in Appendix B. All mixes have retained their original numbers. The reference mixes are chosen to be mix 36-3 and mix 48-4. The composition of these two reference mixes is given in table 4.1. As a reference, the total powder amount, which is the sum of the amount of cement and filler is chosen to be 600 kg/m³ and the w/p-ratio is 0.275.

	SCC 36-3	SCC 48-4
Gravel 8/16	434	434
Gravel 2/8	263	263
Sand 0/4	853	853
CEM I 52.5 N	360	360
Limestone filler 1	240	240
Water	165	165
SP (l/m³)	3 (SP 1)	14.55 (SP 2)

Table 4.1: Composition of the reference mixes SCC 36-3, with SP 1 and SCC 48-4, with SP 2. All units are in kg/m³ of concrete, unless expressed otherwise.

Table 4.2 shows the minimal and maximal values of the different parameters which have been changed in the concrete compositions, dependent on the type of SP used. Three different kinds of superplasticizers (SP) have been used in this research project. SP 1 and 2 are both from the same manufacturer, while SP 3 (only applied in SCC 57-59) originated from a different supplier. All SP are poly-carboxyl-ethers,

which have a double working principle: electrostatic repulsion and steric hindrance (see section 4.2.5 of chapter 2). SP 1 is very efficient (low amounts are needed), but it has a short workability retention, while SP 2 is less efficient, but keeps the workability of the SCC sufficiently well during a longer time.

		Mixes with SP 1		Mixes with SP 2	
		Min	Max	Min	Max
Cement (C)	(kg/m³)	250	450	300	400
Powder (P)	(kg/m³)	400	700	500	700
C/P	(-)	0.417	0.75	0.5	0.67
Water (W)	(kg/m³)	165	192.5	133.3	186.5
W/C	(-)	0.37	0.66	0.4	0.55
W/P	(-)	0.24	0.41	0.23	0.32
SP	(l/m³)	1.8	4.7	7	18
SP/C	(-)	0.0063	0.0131	0.0192	0.0547

Table 4.2: Minimal and maximal values of the constituent elements for the entire range of mixes, tested with the Tattersall Mk-II rheometer, per type of superplasticizer.

The reference mixes have been made with rounded aggregates with a maximum size of 16 mm, sand, CEM I 52.5 N, limestone filler 1, water and SP 1 and 2. A few mixes have been made with crushed aggregates, other cement (CEM I 52.5 R and CEM I 52.5 HSR) and different fillers (limestone filler 2 (from a different supplier), fly ash, silica fume, quartzite filler and even kaolinite clay). The mixtures with quartzite filler (SCC 32 and 33) and with the clay (SCC 67) will not be incorporated in the analysis, due to their low self-compactability and their enormous SP-demands.

3.2 Mixing procedure

3.2.1 Standard rheological investigations

The 62 concrete mixes tested in the Tattersall Mk-II rheometer and the 8 concrete mixes in order to investigate the influence of the demoulding oil have been produced in a planetary concrete mixer according to the scheme presented in figure 4.2 [4.19]. The time the water is added to the concrete is defined as the reference time. As can be seen in the procedure, no SP has been added to the mixing water, resulting in a more efficient use of the SP [4.13][4.20]. On the other hand, when the total amount of SP has been added in different steps, due to insufficient workability at previous interruptions, a reduced efficiency of the SP has been observed in this case.

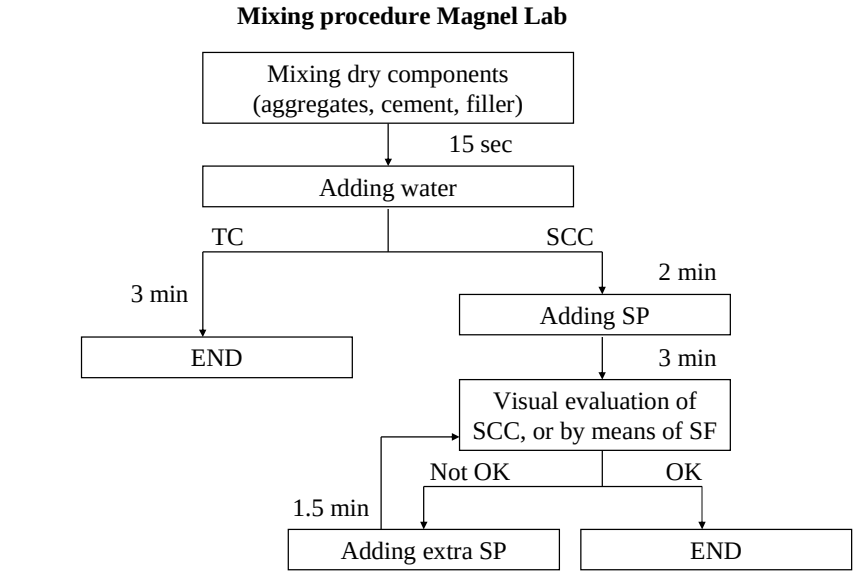

Figure 4.2: Mixing procedure for the concretes tested in the Magnel Laboratory.

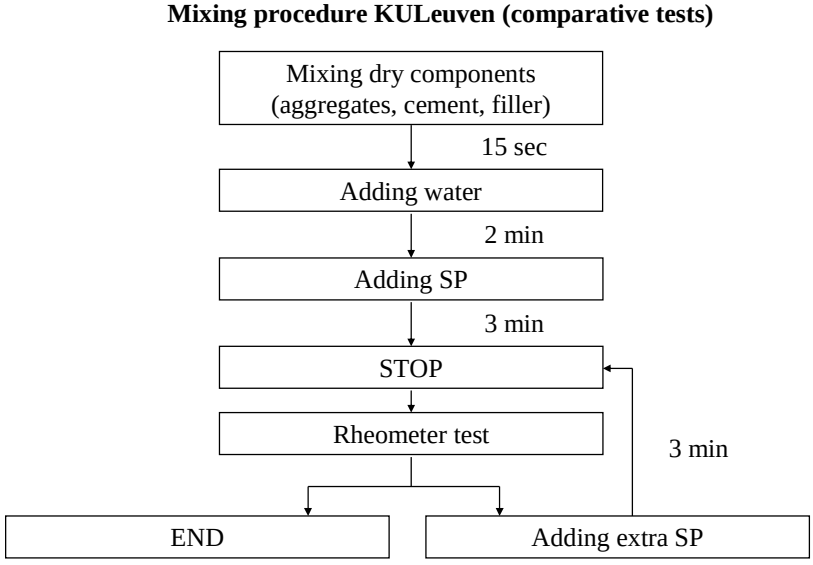

Figure 4.3: Mixing procedure for the concretes used for the comparative tests with both the Tattersall Mk-II rheometer and ConTec viscometer 5.

Each batch of concrete has a total volume of 55 l. As a result, differences in rheological properties can only be induced by differences in the composition, or maybe by the delayed extra additions of SP [4.13][4.21-4.23].
For the comparative testing with both the Tattersall Mk-II rheometer and the ConTec viscometer 5 at KULeuven, the procedure of figure 4.3 applies. The mixes for the preliminary testing at BBRI have been produced according to figure 4.4, keeping in mind that the total volume of concrete was 60 l in this case, and that the mixer was not a planetary concrete mixer.

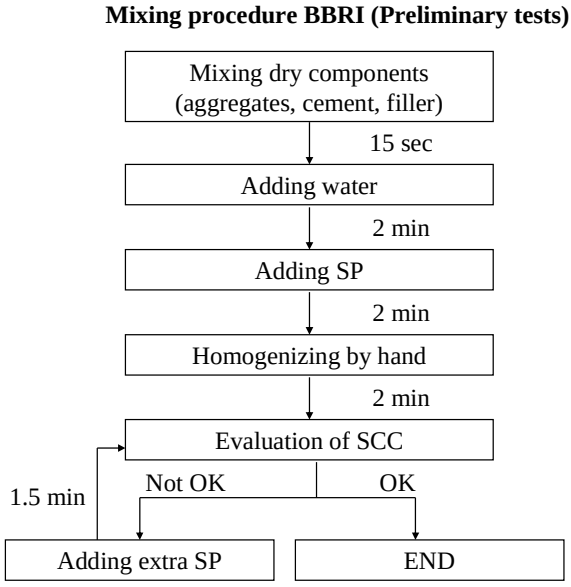

Figure 4.4: Mixing procedure for the SCC used for the preliminary testing at BBRI.

3.2.2 Cement pastes

The cement pastes have been produced in a mortar mixer, according to the scheme of figure 4.5. All mixing was performed at the lowest velocity of 140 rpm, in order to avoid splashing.

3.2.3 Special mortar – concrete tests

One special test series on 3 different SCC mixes has been executed at the KULeuven. Self-compacting mortars have been made, based on SCC compositions, without any coarse aggregates. The mixing procedure is depicted in figure 4.6. The total amount of coarse aggregates has been added in three steps: first the 2/8 mm fraction, later the 8/12 mm fraction and finally the 12/16 mm fraction.

Mixing procedure Magnel Lab: cement paste

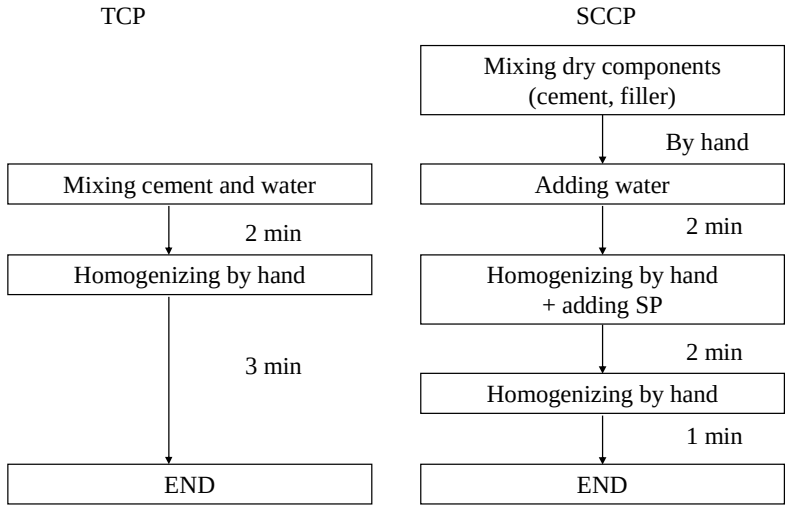

Figure 4.5: Mixing procedure for traditional cement paste (left) and self-compacting cement paste (right).

Mixing procedure KULeuven (mortar - concrete tests)

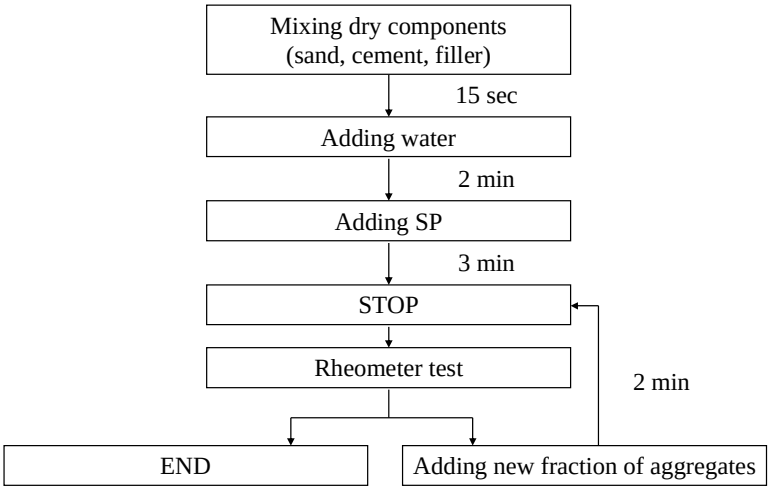

Figure 4.6: Mixing procedure of mortar and concrete in order to study the influence of the coarse aggregates on the rheological properties with the ConTec viscometer 5.

3.3 Testing procedure

3.3.1 Standard rheological investigations

The standard rheological investigations have been executed in the Magnel Laboratory on 59 SCC and 3 TC, produced according to figure 4.2. After mixing, the concrete was placed inside the reservoir of the rheometer and in several buckets. At an age of 15 minutes, four different tests have been executed: slump flow, V-funnel, L-box and a rheometer test with the Tattersall Mk-II rheometer. The slump flow, V-funnel and L-box tests have been performed in this exact order, and for each test, a different sample (bucket) of concrete has been taken. The rheometer test occurs simultaneously with the three other tests. During the execution of all tests, segregation has been determined by visual examination, but no specific test has been executed, except for the SCC numbered SCC 60 (1-4), 61 (1-4), 62 (1-4) and 63, where the sieve stability has been determined. For the traditional concretes, a similar procedure has been followed, but only a slump test has been performed.
The results of all tests, including the results of the rheometer tests can be found in Appendix B, section 2.
For the preliminary tests at BBRI, with the ConTec viscometer 5, the same procedure has been followed and the same tests have been performed.
For the comparative tests with the two rheometers at the KULeuven, after each addition of SP, the slump flow of the SCC has been determined, followed by the rheometer tests which have been executed simultaneously with both rheometers. Both the results of the ConTec viscometer 5 at the BBRI and the comparative tests at the KULeuven are not incorporated in the analyses of the next sections. On the other hand, similar results have been obtained in these cases, proving the validity of the obtained results.
The testing procedure with the rheometers has been described in chapter 3. It consists of a pre-shearing period in order to achieve equilibrium and a stepwise decrease in rotational velocity. Data which have not been obtained in equilibrium are omitted in the analysis. Almost all concretes tested at 15 min of age show a decrease of torque at constant rotational velocity during the pre-shearing period. As a result, the reference state of the concrete is defined by the maximal rotational velocity of the rheometer.
In case the production of the SCC took longer than 15 minutes, due to several extra additions of SP, the first tests have been executed later, at an age of 20, 25 or even 30 minutes, but these results are not incorporated in the analyses. Also segregating concretes have not been included, and the concretes with a different filler type have been analysed separately, but are not included in the main analysis, which is based on the results for SCC with limestone filler 1.

3.3.2 Cement pastes

After the production of the cement pastes, the samples were transported in sealed reservoirs to the location of the plate-plate rheometer, which is not in the Magnel laboratory. As a result, the tests have not been executed at an age of 15 minutes, and any quantitative comparison with the concrete results is not possible, due to ageing

effects. On the other hand, the reference state of the cement pastes is defined by the maximal shear rate in the rheometer and the testing procedure is similar as for the concretes: first a pre-shearing period, followed by a stepwise or continuous decrease in shear rate. The main purpose of the rheometer tests with cement pastes was to investigate the differences in shear thickening behaviour, which are rather independent on the loss of workability (see chapter 5). No other tests than rheometer tests have been executed on the cement pastes. The composition of the cement pastes can be found in Appendix B, section 7.

3.3.3 Special mortar – concrete tests

For the 3 SCC-mixes where the coarse aggregates have been gradually added, the rheometer tests have been performed as soon as possible after mixing. The time between 2 rheometer tests was between 9 and 15 minutes. As a result, the time difference between the first and last rheometer tests was not longer than 45 minutes, which should be sufficient in order to have no significant influence of loss of workability. Each rheometer test (with the ConTec viscometer 5) has been executed in the same way as the tests with the Tattersall Mk-II rheometer.
Simultaneously with the last rheometer test, the slump flow, V-funnel flow time, sieve stability, air content and density have been determined (see Appendix B for the results).

3.3.4 Tests with oil

In order to investigate the influence of oil on the rheological properties of SCC, a 55 l concrete batch has been produced according to the scheme of figure 4.2. After mixing, the slump flow has been determined. The concrete has been divided in four parts (4 buckets). Parts 1 and 4 have been poured in the rheometer and the rheological properties have been determined, following the procedure of section 3.3.1. After the rheometer test, the V-funnel flow time and sieve stability of this part of the concrete have been determined. Simultaneously to the rheometer test on parts 1 and 4, parts 2 and 3 have been placed inside the (empty) mixer, the oil has been added and the concrete has been mixed for 2 minutes. After mixing, this part of the concrete has been tested according to the same procedure as the concrete without oil. For 2 SCC-mixes, an extra batch of concrete has been produced and divided into two parts, to which 2 different amounts of oil have been added. The testing procedure is similar, with the only difference that also parts 1 and 4 have been remixed with oil.
During this investigation, all tests have been performed within 1 hour after the water addition. Loss of workability is suspected not to have a significant influence on the obtained values, because the rheometer tests even occurred within a time span of 10 minutes.

4 Influence of constituent elements on yield stress and viscosity

In literature, authors have tried to establish relationships between the concrete compositions and the rheological properties. This is a very challenging task, due to the large sensitivity of SCC to a change in any of its constituent elements. Furthermore, as SCC is different from country to country, from region to region, a relationship established by one institute could be invalid for an other [4.13][4.24-4.25]. As a result, a general model to determine the relationship between rheological properties and the concrete composition has not been found yet.

In this section, a brief overview of the results in literature will be given, with some personal reflections, based on the obtained results in this research project. Note that most authors apply the Bingham relationship. In order to be able to compare our data with the results in literature, the viscosity has been defined as the tangential viscosity at a shear rate of 5/s. In case of Bingham materials, this tangential viscosity equals the plastic viscosity. A discussion on the parameters influencing shear thickening behaviour will be given in the next section.

The graph in the middle of figure 4.7 is called a "rheo-graph" [4.13][4.25], showing the variation in plastic viscosity (horizontal axis) and yield stress (vertical axis) due to a variation in air, water, SP or silica content. The side graphs in figure 4.7 show the flow curves.

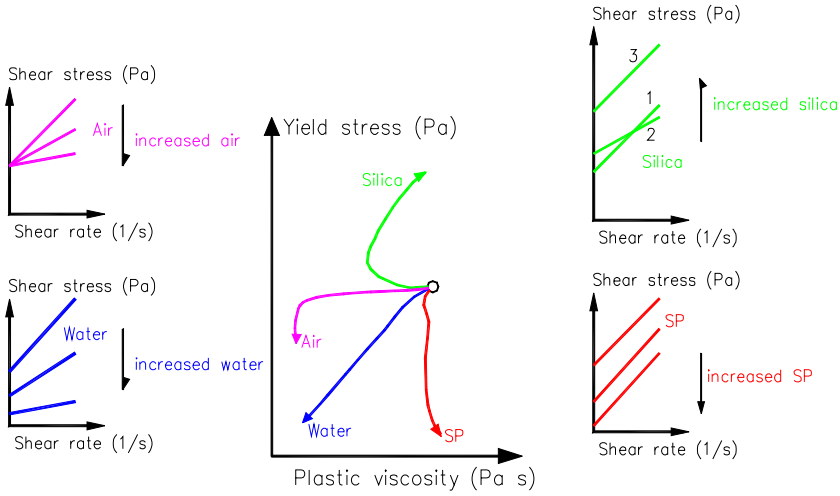

Figure 4.7: Middle figure: Rheograph, showing the influence of air, water, silica and SP on yield stress and plastic viscosity, based on the flow curves shown in the side figures. Figure after O.H. Wallevik [4.25].

The influence of these and other constituent elements on the rheological properties, obtained by the group of O.H. Wallevik, has been summarised in table 4.3. A "+" in this table indicates that increasing that element in the composition causes an increase in yield stress or plastic viscosity. A "-" means the opposite. The advantage of the

rheograph is that, to a certain extent, the effects of the different constituent elements may be superposed to each other.

	Yield stress (Pa)	Plastic Viscosity (Pa s)
Air Content	1: / 2: -	-
Water	-	-
Superplasticizer	-	/
Silica	1: / 2: +	1: - 2: +
Cement	1: / 2: +	1: + 2: /
Rounded - Crushed aggr.	+	+
Sand	+	-

Table 4.3: Influence of an increase in different elements of the composition on yield stress and plastic viscosity. A "+" stands for an increase, a "-" for a decrease, and "/" stands for no significant influence. In case a "1" and "2" are mentioned, 1 stands for small increases, 2 stands for large increases of the constituent element. Table after O.H. Wallevik [4.25].

Other authors confirm the information of the rheograph or provide some additional information. Wallevik and Nielsson [4.26] have found that increasing the content of the SP 1, which is used in this research project, decreases significantly the yield stress, but also the plastic viscosity. At larger dosages, the plastic viscosity remains constant. Carlswärd et al. [4.27] have found a very similar reograph. Vikan and Justnes [4.28] confirm the increase of yield stress with increasing silica content, but they state that the influence of silica content on plastic viscosity depends on the type of SP. Struble and Jiang [4.29] mention that increasing air entraining agent increases yield stress and decreases viscosity if no SP is applied, but that both yield stress and viscosity increase in case a SP is applied. Yahia et al. [4.30] and Billberg [4.31] have investigated the influence of (limestone) fillers on the rheological properties. In [4.30], it can be found that under a certain critical content of limestone filler, the plastic viscosity is not affected, but increasing the amount of filler above the critical value causes the viscosity to increase. Billberg [4.31] states that increasing the fineness of the filler causes a decrease in yield stress and an increase in plastic viscosity. Sheinn et al. [4.32] have shown that the shape of the fine particles (in pastes) does not significantly affect the rheological properties when SP are applied. Brameshuber and Uebachs [4.33] state that temperature can have a very different influence, depending on the type of SP.

As mentioned before, generalizing the above mentioned conclusions is not advised. These trends have been obtained in specific (laboratory) conditions, but can be invalid in case, for example, other materials are applied. As a result, these trends can be a kind of guideline, but testing must confirm their validity.

From the results obtained with the Tattersall Mk-II rheometer, some of the above mentioned trends, like the influence of water, SP and cement content are confirmed. In case of SP 2, it has been observed that the viscosity also decreases significantly with increasing SP content, which is less obvious for SP 1. This is most probably caused by the lower concentration of active elements in SP 2, and consequently, a larger amount of water added. In chapter 9, some results on the influence of air

content will be presented. These results are quite unique, because the air is not entrained by means of air entraining agents containing surfactants, which influence the rheological behaviour themselves.

5 Shear thickening

5.1 Importance of shear thickening

Shear thickening has been defined as an increase in (apparent) viscosity with increasing shear rate. As a result, the shear stress response will increase more than linearly with increasing shear rate. At low shear rates, shear thickening will not have a significant influence, but when the shear rate increases (possibly exceeding a certain critical value), the shear thickening effect can increase the apparent (or tangential) viscosity significantly.
The flow of concrete mostly occurs at low shear rates, for example when emptying the concrete mixer, when casting by means of a concrete scip, and the flowing of concrete inside a formwork. In these cases, shear thickening should not be considered. On the other hand, a few operations in construction occur at relatively high shear rates, of which mixing and pumping are best known. In these cases, shear thickening should be considered, especially when the apparatus is regulated by controlling a parameter related to shear rate (rot/min in the mixer and discharge in case of a pump). If shear thickening is not considered in these cases, the work the apparatus must deliver can be much higher than predicted. Breaking of a certain part of the apparatus, occasionally resulting in injuries or death of people nearby, can be a very nasty consequence.
As this thesis is dealing with the pumping of self-compacting concrete, it would be a huge mistake to neglect shear thickening behaviour. A detailed investigation on shear thickening has been performed and the results will be shown in this section.

5.2 Elimination of measurement artefacts

When shear thickening is observed, it is not always certain whether it is a real material property. Several errors during the rheological measurements, called measurement artefacts, can be the cause of apparent shear thickening behaviour [4.34-4.35]. On the other hand, when observing apparent shear thickening behaviour, one should not hide behind the principle of measurement artefacts, but really investigate whether an artefact has occurred. Before discussing any shear thickening results, proof will be given that the observed shear thickening in the self-compacting concretes, made with Belgian materials, is not a measurement artefact.

5.2.1 Thixotropy

Measuring the rheological properties of concrete which is not in equilibrium conditions for the highest shear rates applied, will result in an overestimation of shear thickening behaviour. In case the concrete is a real Bingham material, non-linearity can result as a false conclusion [4.13][4.34-4.36]. The only way to investigate whether all data points, and especially the data points at the highest shear rates, are in equilibrium, is to keep the shear rate (or rotational velocity) constant during a certain time. This procedure has been executed during the measuring of all

concretes tested. Figure 4.8 shows the time plot of rotational velocity and torque for reference mix 1 (SCC 36-3) in the Tattersall Mk-II rheometer.

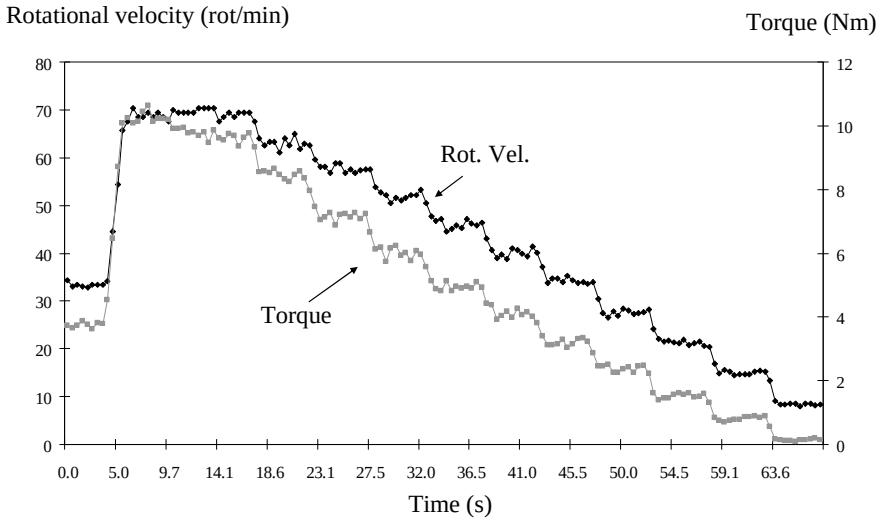

Figure 4.8: Torque (grey) and rotational velocity (black) as a function of time for SCC 36-3 (ref. mix with SP 1), tested in the Tattersall Mk-II rheometer. Note that one step of constant rotational velocity takes around 5 seconds.

Figures 4.9 and 4.10 also show the rotational velocity and torque related to time for a mix, similar to reference mix 1 (SCC 2-2, BBRI) and an extremely shear thickening mix (SCC 14, BBRI) respectively. As can be seen in these figures, maybe apart from the first measuring point, all data have been obtained in equilibrium conditions. As a result, thixotropy does not influence the shear thickening behaviour observed.

5.2.2 Particle migration

During rheometer testing, the coarse particles can migrate horizontally to the region with lower shear rates, and vertically due to segregation [4.36-4.37]. If this occurs during the measurements, the viscosity of the material in the zone with higher shear rates will decrease, and as the shear rate is decreased stepwise, apparent shear thickening behaviour can be observed. As a first control, it can be checked whether at each time step the measured torque is in equilibrium. On the other hand, if the migration is occurring slowly, and due to some fluctuations in torque measurements, it is not straightforward to investigate particle migration in this way. For the Tattersall Mk-II, no direct tool has been developed in order to investigate particle migration, but it is known that the interpretation of the results of extremely fluid SCC is very difficult and can be questioned. In the ConTec viscometer 5, the segregation point is a good indicator for changes in the material during the measurement. Figure 4.11 shows the torque as a function of rotational velocity for

the reference mix at BBRI (SCC 2-2, BBRI) and the extremely shear thickening mix (SCC 14, BBRI). As can be seen, the segregation point does not significantly deviate from the obtained flow curve, indicating that, at least for the 10 data points obtained at the lowest rotational velocities, no segregation has occurred. If the data points at rotational velocities higher than the segregation point are omitted, shear thickening is still observed, indicating it is a real material parameter.

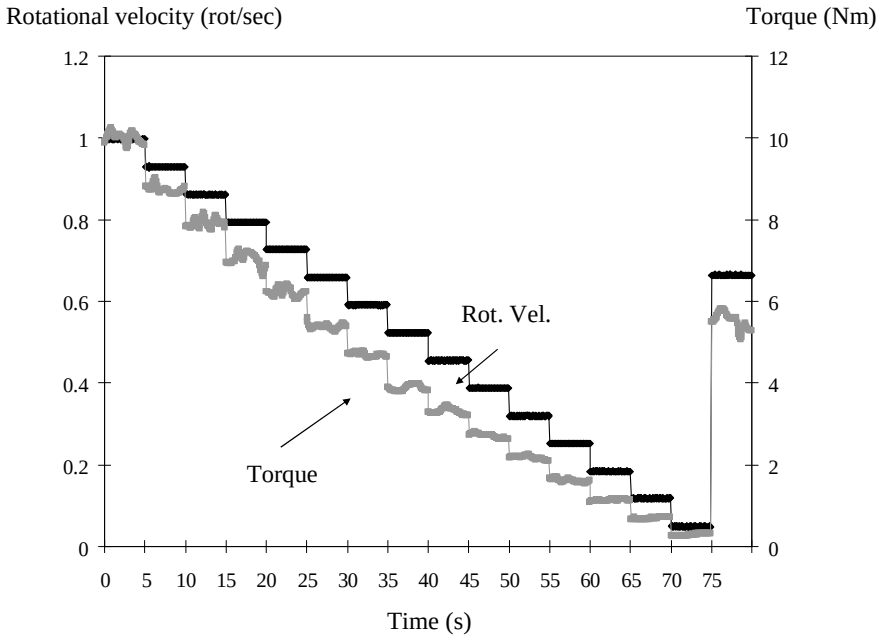

Figure 4.9: Torque (grey) and rotational velocity (black) as a function of time for SCC 2-2, tested in the ConTec viscometer 5 at BBRI.

5.2.3 Plug flow

Plug flow occurs when the instantaneous, local yield stress of the material is higher than the applied shear stress. As a result, the concrete is not completely sheared in the rheometer and the Reiner-Riwlin equation is no longer valid in its form presented in chapter 3 [4.36]. For the results obtained with the Contec Viscometer 5, the shear stress at the outer cylinder has been calculated and compared with the extrapolated yield stress by means of Herschel-Bulkley. In most cases, the data point at lowest rotational velocity needed to be eliminated from the measurements. For the Tattersall Mk-II, due to the complex flow pattern in the rheometer, no calculations have been made. When plug flow is present in the rheometer, it is incorporated in the transformation procedure, because the honey, used for the calibration, showed a high yield stress (around 700 Pa) at the lowest temperature. In this way, it is suspected that plug flow does not influence the obtained results.

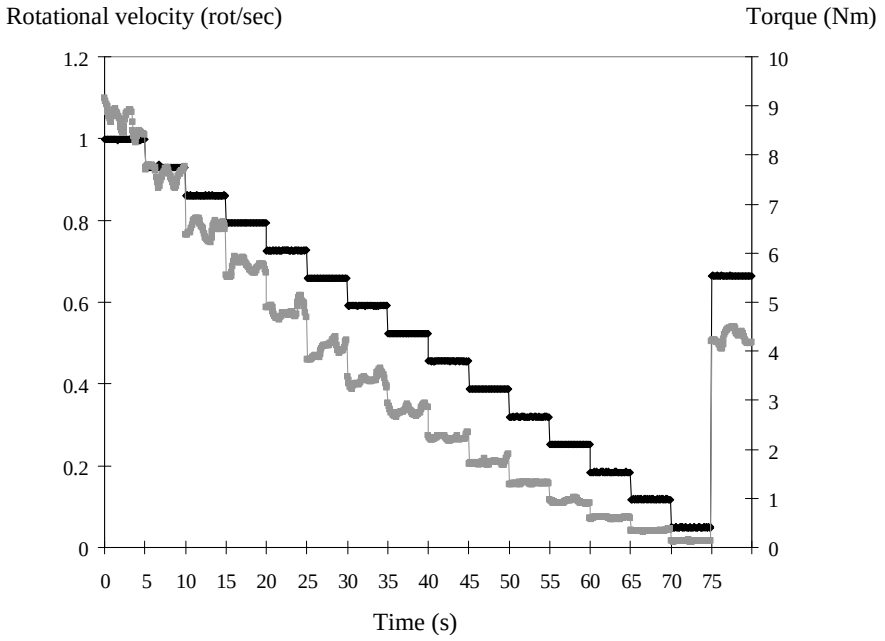

Figure 4.10: Torque (grey) and rotational velocity (black) as a function of time for SCC 14, tested in the ConTec viscometer 5 at BBRI.

5.2.4 Rheometer dependence

As has been shown in chapter 3, different rheometers deliver different values for the rheological properties. One can argue that shear thickening can be a rheometer-induced artefact. By means of measurements on two different concrete rheometers, and the measurements on cement pastes with a plate-plate rheometer (see section 5.4.1), it has been shown that shear thickening occurs independent of the rheometer. Furthermore, the comparative testing with the Tattersall Mk-II and the ConTec viscometer 5 have shown that the obtained intensity of shear thickening, expressed by the consistency index n of Herschel-Bulkley, is similar for both rheometers [4.18].

5.2.5 Inertia

Inertia does not show a significant influence in the results, as it is counteracted by the viscous forces in less than one second after the transition between two different rotational velocities. In the transformation of the data, as mentioned in chapter 3, as only the results obtained at constant rotational velocity and constant torque have been taken into account, inertia is eliminated from the measured data points.

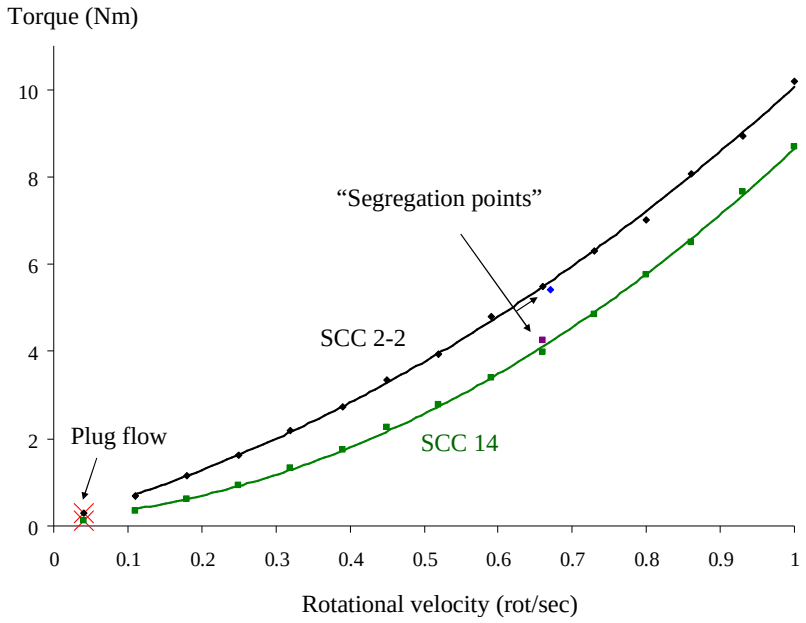

Figure 4.11: Torque as a function of rotational velocity for SCC 2-2 (black) and SCC 14 (green), both tested with the ConTec viscometer 5 at BBRI. The segregation points of each curve indicate no significant material change (and no particle migration) during the test. On the other hand, the data points at the lowest rotational velocity have not been incorporated due to plug flow.

5.3 Applicable theories

In chapter 2, some theories for shear thickening behaviour have been described. Two of these theories will be retained for further investigation. The order-disorder transition theory is expected to fail due to the large poly-dispersity in concrete. Another theory has been mentioned by J. Mewis [4.38] in which he states that the desorption of the SP due to high shear rates and the re-adsorption at low shear rates is a possible cause of shear thickening. On the other hand, this would mean that the connection between the SP and the cement particle should be broken during mixing, which occurs at much higher shear rates. Furthermore, when the desorption of the SP occurs, the cement particles are not longer prevented to coagulate, and as the shear rate is not as high as in the mixer to break the connections, this would mean that the concrete would be stiffer after than before the rheometer test, resulting in a kind of anti-thixotropy. Also the SP-manufacturer states that this effect is very unlikely to occur [4.39].

The two theories remaining are the cluster formation theory [4.40] and the grain inertia theory [4.41]. Cluster formation applies on the small particles, intensifying shear thickening due to a higher volume fraction and less poly-dispersity. Recall the definition of the critical shear stress, which is the stress at which shear thickening

starts to be observed. The critical shear stress increases with decreasing particle size, increasing poly-dispersity and the addition of polymers. Connected particles show less tendency to shear thicken.
The grain inertia theory applies more on the large particles in the suspension, which transfer a part of their momentum by direct collisions. The shear stress due to the collisions scales with the square of the shear rate. In fact, the total shear stress can be divided into three contributing parts: yield stress, viscous stress, which scales linearly with the shear rate, and the inertia stresses. If this theory applies, a nice physical meaning to the modified Bingham model could be defined.

5.4 Parameters influencing shear thickening

5.4.1 Cement paste

In order to eliminate any possible influence on the rheology caused by the aggregates, rheometer tests with a parallel plate rheometer have been executed on cement pastes. As the testing procedure is different for the cement pastes compared to the testing of concrete, a quantitative comparison between the results is impossible. The composition of the cement pastes is based on the concrete compositions and is shown in Appendix B, section 7. Two traditional pastes and four self-compacting pastes have been produced.

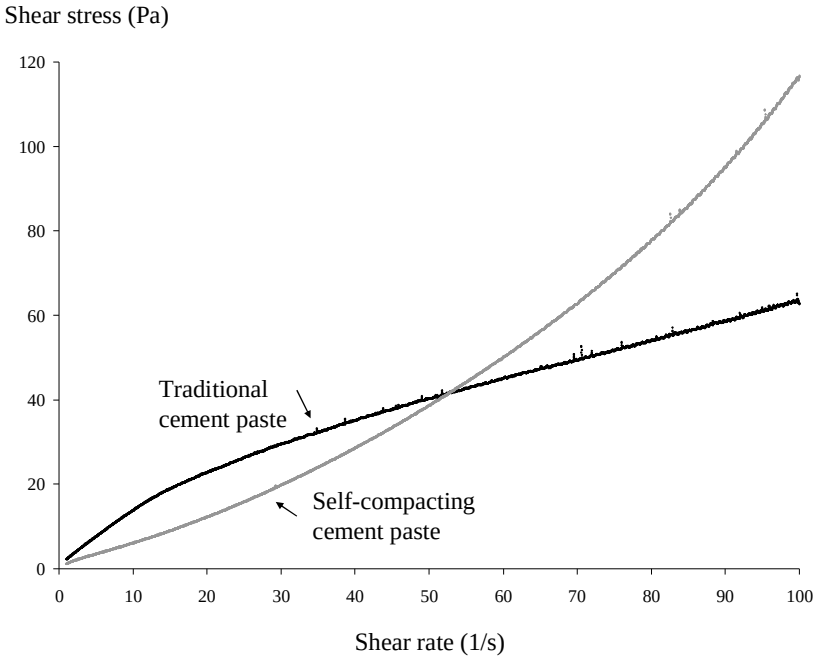

Figure 4.12: Flow curve for traditional cement paste (black) and self-compacting cement paste (grey), indicating shear thickening only in case of the self-compacting cement paste.

Figure 4.12 shows the flow curve for a traditional (TCP 2) and a self-compacting paste (SCCP 4), obtained by decreasing the shear rate continuously from 100 s^{-1} to 1 s^{-1} during 90 s, after a pre-shearing period of 60 s at a shear rate of 100 s^{-1}. It can be seen that the traditional cement paste can be classified as a Bingham material at high shear rates and shear thinning is observed at low shear rates. For the self-compacting paste, shear thickening is clearly visible. Only at low shear rates, some shear thinning can be seen. Figure 4.13 even gives a better view on the shear thickening behaviour, as apparent viscosity is plotted as a function of shear rate. The apparent viscosity of the traditional paste is continuously decreasing, while the apparent viscosity of the self-compacting paste starts to increase from a shear rate of 12 s^{-1} on. The other results reveal similar behaviour: shear thickening for the self-compacting pastes, while not for the traditional paste. This is also in accordance with [4.42], where similar results have been obtained.

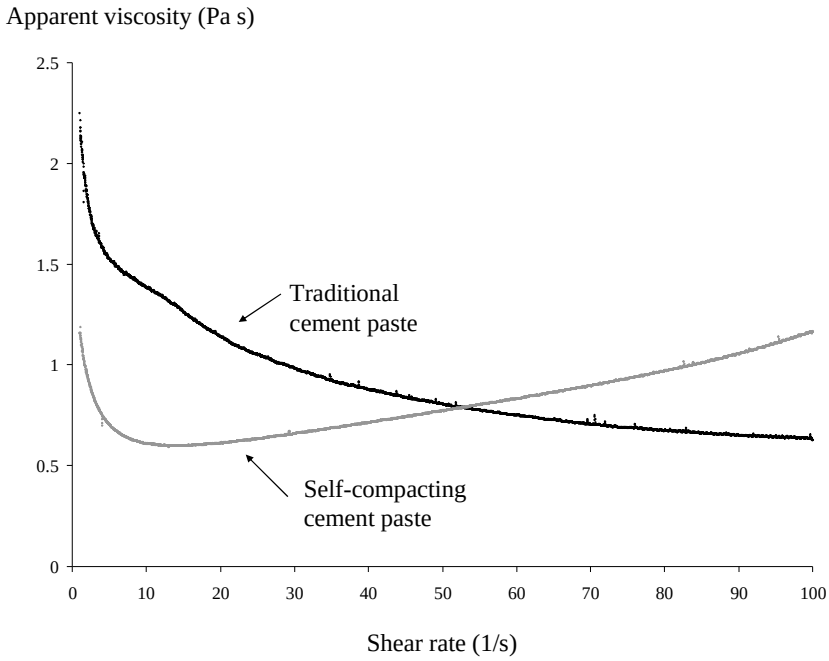

Figure 4.13: Apparent viscosity as a function of shear rate indicates that shear thickening starts around 12 s^{-1} for the self-compacting paste, and that no shear thickening can be observed for the traditional cement paste.

From these results, it is clear that, at least a part of shear thickening behaviour is caused by the ingredients of the self-compacting cement paste: cement, water, limestone filler (both 1 and 2) and SP. In order to find out which theory is applicable, the particle Reynolds number [4.43], defined in section 3.3.3 of chapter 2 can be calculated for the self-compacting cement paste of figure 4.13. The value of the density of the cement paste is assumed to be 2200 kg/m³, which is an

overestimation. The shear rate chosen is the maximal shear rate in the rheometer: 100 s^{-1} and the viscosity is the minimal apparent viscosity measured, namely at the onset of shear thickening: 0.5 Pa s. As can be seen, the values of the viscosity and the shear rate do not match, but this is a safe assumption. The cement paste itself is chosen as the suspending medium, because isolating two particles from the cement paste will not fundamentally change its properties. As particle size, 1 μm and 300 μm is chosen, which corresponds to a small and a very large particle in the cement paste. The particle Reynolds numbers are 10^{-7} and 10^{-2} for the 1 μm and 300 μm particle respectively, indicating no significant influence of grain inertia for the small particles. Depending on the definition of "much lower than 0.1" (see chapter 2), it can be argued whether grain inertia is not important for the large particles. As a result, shear thickening in self-compacting cement paste is probably, at least in this case, not due to grain inertia, although when increasing the shear rate, grain inertia can become important. As a result, at least in this case, shear thickening in concrete is consequently not caused by grain inertia only.
As the presence of large (non-Brownian) particles generally only amplifies the rheological behaviour of the suspending medium, shear thickening should also be observed in mortar and concrete, even when its only cause is due to the cement paste. On the other hand, several effects caused by the aggregates can increase or decrease the shear thickening behaviour (see section 5.4.5).

5.4.2 Water/powder

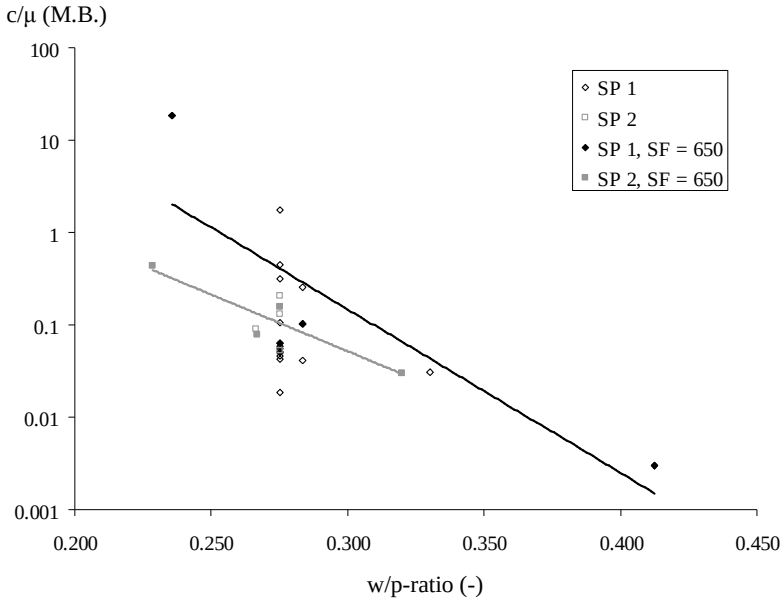

Figure 4.14: Intensity of shear thickening (c/μ from the modified Bingham model) increases with decreasing w/p-ratio, depending on the type of SP (SP 1 = black, SP 2 = grey). Only the data points with equal slump flow have been connected (full data points).

The intensity of shear thickening, which is characterized by c/μ in the modified Bingham model, increases with decreasing w/p-ratio, as can be seen in figure 4.14. In this figure, all results of SCC with limestone filler 1 (LS 1), obtained at 15 minutes of age are represented. Per type of SP, and per w/p-ratio, the data points with equal slump flow are chosen to define the trend (see next section). Figure 4.15 shows the critical shear stress for the onset of shear thickening, which is defined as the shear stress with the lowest apparent viscosity. As can be seen, the w/p-ratio does not influence the critical shear stress significantly.
When reducing the w/p-ratio, the volume fraction of solid materials is increased. As mentioned in chapter 2, according to the theory of cluster formation, increasing volume fraction increases the intensity of shear thickening, but it does not significantly influence the critical shear stress [4.44-4.45]. This is exactly what is shown in figures 4.14 and 4.15.
When considering the most extreme shear thickening concrete (SCC 42), the decrease in w/p-ratio has been established by increasing the powder content of the SCC, while reducing the aggregate content. In this case, as the intensity of shear thickening increases, it can be concluded that the aggregates do not cause an increase in shear thickening behaviour.

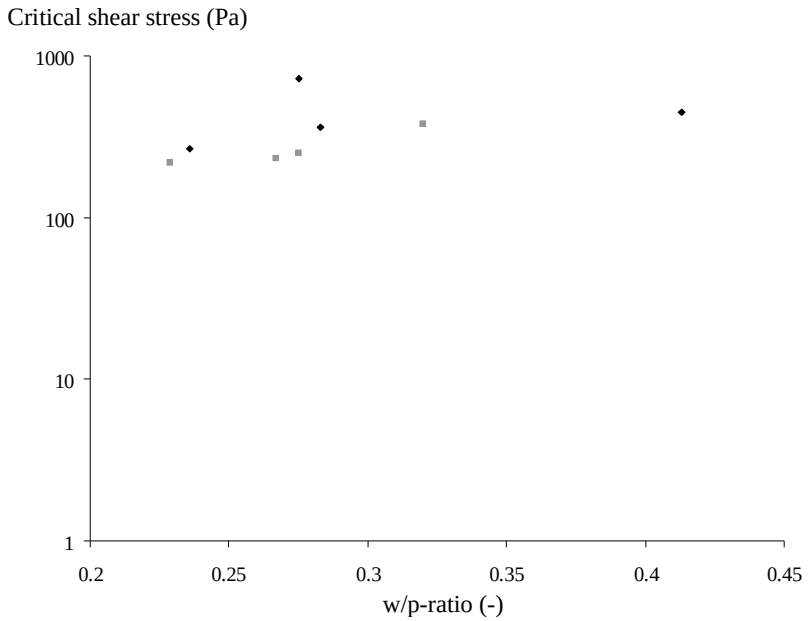

Figure 4.15: The critical shear stress does not show a significant dependency on the w/p-ratio. The data points represent the full data points from figure 4.14.

5.4.3 Slump flow and superplasticizer content

Figure 4.16 shows the intensity of shear thickening for all concretes with a w/p-ratio of 0.275 and with LS 1. As slump flow increases, the intensity of shear thickening increases. In figure 4.17, it is shown that the critical shear stress decreases with increasing slump flow. The SCC numbered SCC 60 (1 to 4), SCC 61 (1 to 4) and SCC 62 (1 to 4) have been produced with limestone filler 1, limestone filler 2 and fly ash respectively. Each "sub-number" 1 to 4 indicates a different amount of SP added. A plot of the apparent viscosity as a function of shear stress for SCC 61 (1 to 4) is shown in figure 4.18. It can be seen that, with increasing SP-content and consequently increasing slump flow, the critical shear stress decreases and the intensity of shear thickening increases. For SCC 61-4, which has a very low SP-content and a slump flow of only 300 mm, no shear thickening has been observed.

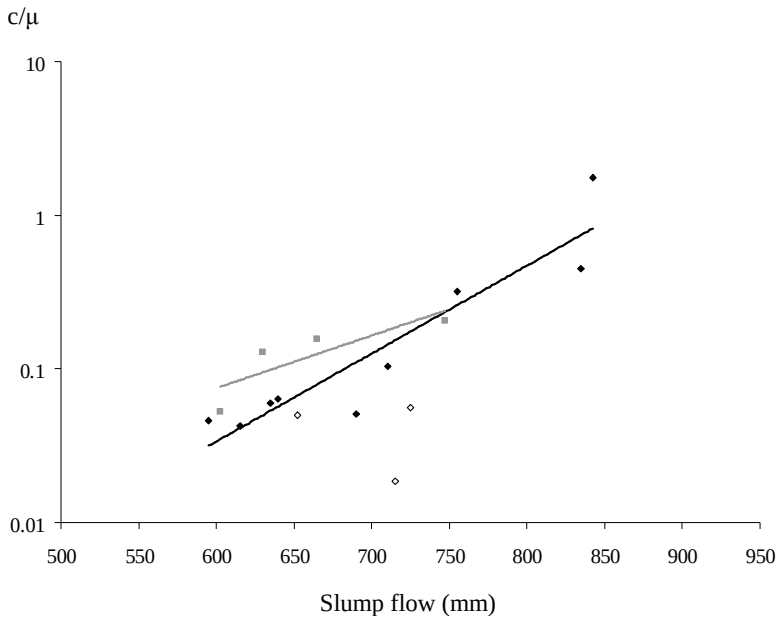

Figure 4.16: The intensity of shear thickening (c/μ from the modified Bingham model) increases with increasing slump flow at equal w/p-ratio (= 0.275), depending on the type of SP (SP 1 = black, SP 2 = grey). The open dots, showing a lower intensity of shear thickening, represent SCC with a larger fraction of very coarse aggregates, which is discussed in section 5.4.5.

The results shown in figures 4.16 to 4.18 are contradictory to the results obtained in [4.42]. Artelt and Garcia have observed an increase in critical shear rate with increasing SP-dosage for cement pastes made with a fine fly ash. On the other hand, for the shear rate range studied, they did not observe shear thickening in self-compacting cement pastes made with limestone filler.

Although these results appear contradictory, they can be explained by means of the cluster theory. In case of cement paste or concrete made with limestone filler, a large number of particles have a size in the order of 10 μm. Adding more superplasticizer causes more particles to be dispersed and less particles to be connected. As mentioned in the cluster theory, connected particles show less tendency to shear thicken. As a result, increasing SP-content increases the number of particles susceptible to shear thickening, increasing its intensity and decreasing the critical shear stress. Why did Artelt and Garcia observe the opposite? The fly ash used in their cement paste contained a "significant fraction of particles of the order of 1 μm and below." This means that already a lot of particles susceptible for shear thickening are available, and that the influence of the polymers is more significant [4.46]. Furthermore, as they used a loop curve as rheological experiment, they based their reports on the up-curve, in which a full elimination of thixotropy is not guaranteed.

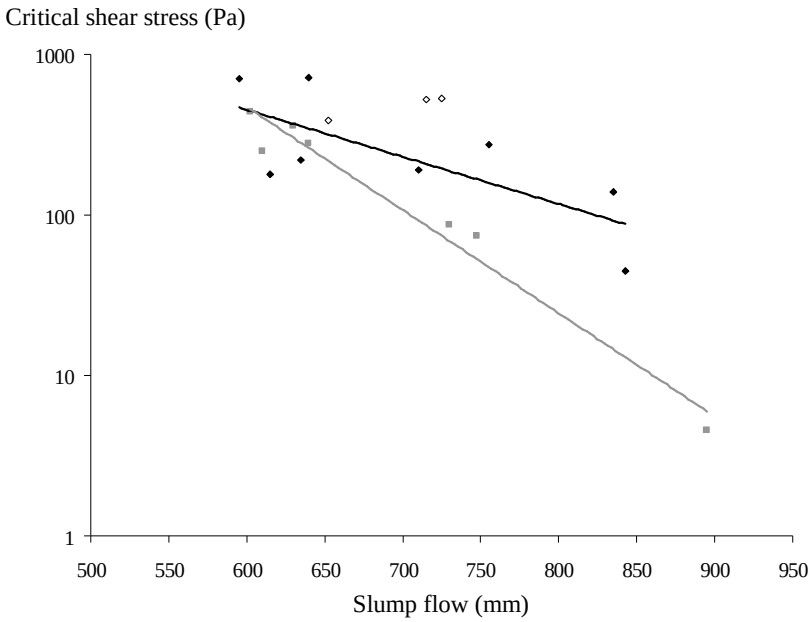

Figure 4.17: The critical shear stress decreases with increasing slump flow, depending on the type of SP (SP 1 = black, SP 2 = grey). The open dots, showing a higher critical shear stress, represent SCC with a larger fraction of very coarse aggregates, which is discussed in section 5.4.5.

As also can be seen in figures 4.14, 4.16 and 4.17, the type of SP has an influence on the shear thickening behaviour. This is most probably due to differences in the dispersion action of the polymers, leading to different repulsive forces, influencing the formation of the clusters.

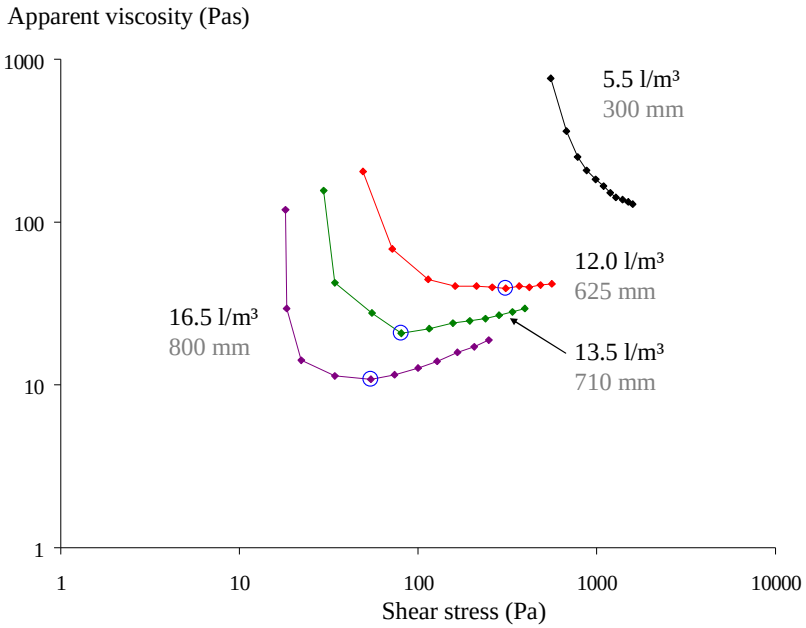

Figure 4.18: Apparent viscosity as a function of shear stress for 4 mixes SCC 61 with different amounts of SP (black numbers) and different slump flows (grey numbers). With increasing SP-content, the critical shear stress (data point with blue circle) decreases and the intensity of shear thickening (inclination of the curve at stresses > critical shear stress) increases. Note that the SCC 61-4, with 5.5 l/m³ SP 2 does not show shear thickening in the stress range measured.

5.4.4 Fillers

Although it has not been the main purpose of this research project, some SCC mixes have been produced in order to investigate the influence of the filler type on the shear thickening behaviour. SCC 61, 62 and 63 have been produced, based on the composition of SCC 60. The limestone filler 1 of SCC 60 has been replaced by limestone filler 2 (SCC 61), fly ash (SCC 62) and silica fume (SCC 63). The replacement ratio is based on the absolute volume the filler takes. Due to differences in density, the mass of filler added was different, but the volume was equal. By adapting the SP-dosage, a slump flow of 660 mm was targeted. The results of the rheological tests on the four mixes is shown in figure 4.19. The first conclusion from figure 4.19 is that the SCC with silica fume does not show shear thickening behaviour in the range of shear stresses measured. This can be due to two reasons: As silica fume contains much smaller particles, the critical shear stress for shear thickening is increased [4.44-4.45]. Furthermore, the critical shear stress of the three other mixes in figure 4.19 is around 300 Pa, while the maximal stress applied on the silica fume-mix is only 160 Pa. From this measurement, it is unclear when or whether this mix will show shear thickening behaviour. The other mixes show

similar behaviour, although a difference between the two mixes with limestone filler can be seen. The mix with LS 2 shows less shear thickening behaviour than the mix with LS 1. This can be attributed to a small difference in grain size distribution of the limestone fillers. Although these fillers have approximately the same d_{50}, a larger amount of coarse particles (between 100 and 300 μm) has been observed for the LS 2 filler. As a result, the specific surface of LS 2 is somewhat lower, creating more free water and increasing the effective w/p-ratio.

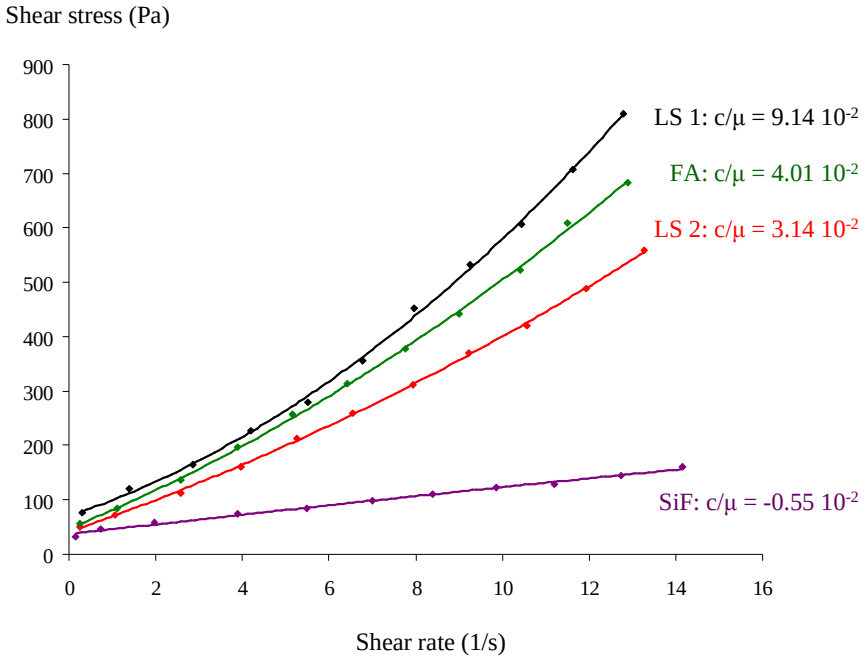

Figure 4.19: The flow curves for SCC with limestone filler 1 (LS 1, black), limestone filler 2 (LS 2, red), fly ash (FA, green) and silica fume (SiF, purple) indicate no shear thickening for the SCC with silica fume and a slight difference between the SCC with LS 1 and the SCC with LS 2.

5.4.5 Coarse aggregates

The influence of the coarse aggregate content has been tested with the ConTec viscometer 5 at the KULeuven. Three different SCC mixes have been prepared and tested according to the procedures described in sections 3.2.3 and 3.3.3 of this chapter. The results, of which the details can be found in Appendix B, have been analysed by means of the Herschel-Bulkley equation, imposed by the transformation procedure (see chapter 3), meaning that the intensity of shear thickening is described by the parameter n. The value of n is plotted as a function of the maximum grain size added in the mix in figure 4.20. While the yield stress and the tangential

viscosity at 5/s increase as a function of maximum grain size (or with increasing amount of coarse aggregates), it can be seen that the intensity of shear thickening decreases with increasing grain size, from a value of 8 mm on.
In order to explain this phenomenon, the particle Reynolds numbers of the coarse aggregates must be calculated. The values of the suspending medium are chosen to be those of the mortar, as the principle of making SCC states that the amount of coarse aggregates must be reduced. In this way, the presence of other coarse aggregates will not influence the properties of the surrounding liquid nearby a certain aggregate. The values of density and apparent viscosity are chosen to be 2400 kg/m³ and 10 Pa s respectively. The shear rate is chosen to be close to the maximal shear rate in the rheometer, namely 20 s^{-1}. The values of the particle Reynolds number for particles with a maximum diameter of 2, 8, 12 and 16 mm are reported in table 4.4. As can be seen, from a diameter of 8 mm on, the influence of grain inertia is no longer negligible. But instead of making collisions with other coarse aggregates, the coarse aggregates do not adapt to a sudden change in flow velocity as easily as the fine aggregates or the paste. As a result, due to inertia, the coarse aggregates are suspected to destroy the clusters formed nearby and thus reducing shear thickening behaviour. The larger the amount of coarse aggregates, the larger the reduction.

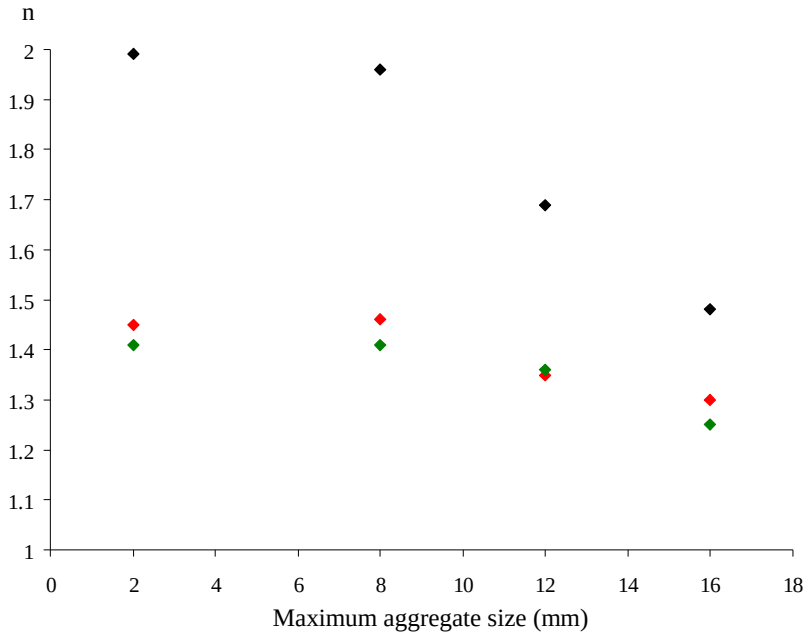

Figure 4.20: The intensity of shear thickening (described by n from Herschel-Bulkley) decreases with increasing maximum aggregate size, larger than 8 mm. (SCC 1 = red; SCC 2 = green; SCC 3 = black).

In figure 4.16, three open black dots can be seen. These data points correspond to SCC mixes where the fraction 2/8 has been entirely replaced by coarse aggregates from the fraction 8/16. As a result, these SCC mixes contained 698 kg/m³ gravel 8/16. As can be seen in figure 4.16, these mixes show less intense shear thickening behaviour, which is most probably due to two effects: the above described destruction of clusters due to inertia and the lower specific surface of the coarser aggregates, increasing the effective w/p-ratio.

Maximal aggregate size (mm)	Re_p (-)
2	$5.0\ 10^{-3}$
8	$7.7\ 10^{-2}$
12	$1.7\ 10^{-1}$
16	$3.0\ 10^{-1}$

Table 4.4: Particle Reynolds numbers, indicating the relative importance of inertia to the viscous forces, for aggregates with different sizes, suspended in a mortar with a density of 2400 kg/m³ and an apparent viscosity of 10 Pa s, subjected to a shear rate of 20 s^{-1}.

5.4.6 Oil in SCC

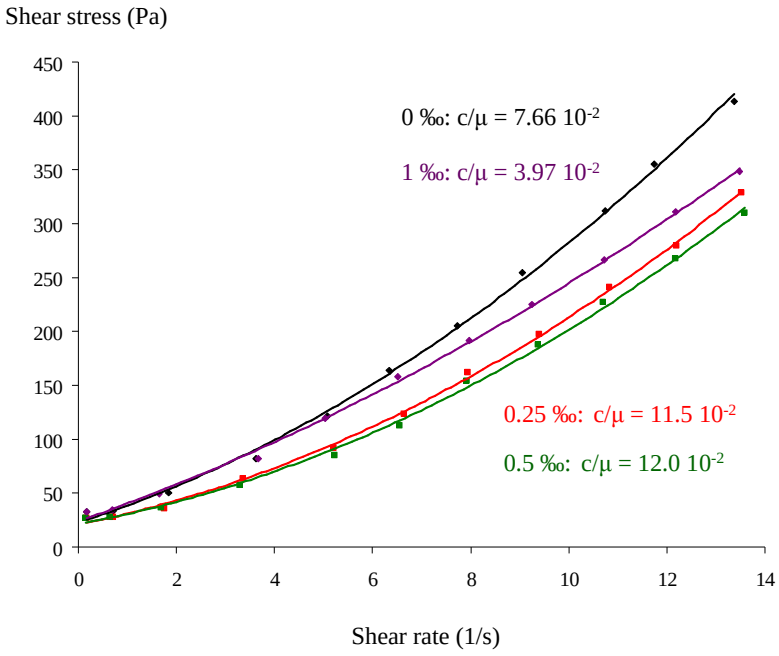

Figure 4.21: Small additions of oil (smaller than 1 ‰, by volume) do not affect the rheological properties significantly. Results of SCC 48-8 and SCC 48-8a.

The influence of demoulding oil on the rheological properties of self-compacting concrete has been discovered accidently. Once during preparation, the reservoir of the rheometer was not pre-wetted with water, but sprayed with demoulding oil. The resulting rheological properties were almost perfectly Bingham (SCC 35). Reproducing the same mix on the same day (SCC 35-2), but without demoulding oil revealed that the SCC 35 is intrinsically shear thickening. As a result, a special test campaign has been set up in order to investigate the influence of demoulding oil on the rheological properties. The specific mix proportions and fresh concrete results can be found in Appendix B.

The production of this series of SCC occurred according to section 3.2.1 and the testing procedure is described in section 3.3.4. Figures 4.21 and 4.22 show the effect of small (0.25 – 1 ‰, by vol. of concrete, SCC 48-8 and SCC 48-8a) and large additions (7.5 – 22.5 ‰, by vol., SCC 48-6 and SCC 48-6a) of demoulding oil in concrete. The small additions, lower than 1 ‰ do not seem to influence the rheological behaviour significantly, but larger additions cause the shear thickening to decrease and even disappear and cause the yield stress to increase. Figure 4.23 shows the influence of a 2.5 ‰ addition of demoulding oil on a reference mix with SP-2 (SCC 48-7) and the extremely shear thickening mix (SCC 42-2). As can be seen, even for the extremely shear thickening mix, all shear thickening disappears by adding 2.5 ‰ of demoulding oil.

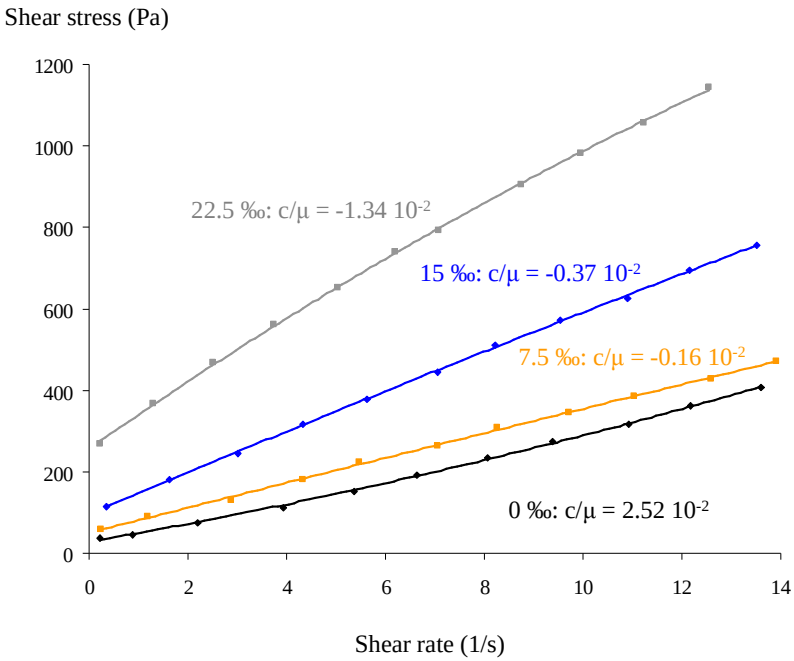

Figure 4.22: Large additions of oil cause the yield stress to increase and shear thickening to decrease and even disappear. Results of SCC 48-6 and SCC 48-6a.

The cause for this very special behaviour is currently unknown. It can be due to a decrease of the hydrodynamic forces which act between the cement particles during flow, or due to an increase in repulsive forces between the cement particles themselves, or maybe a combination of these effects. The question still remains open and maybe some specialist can clear the current clouds, covering this specific behaviour.

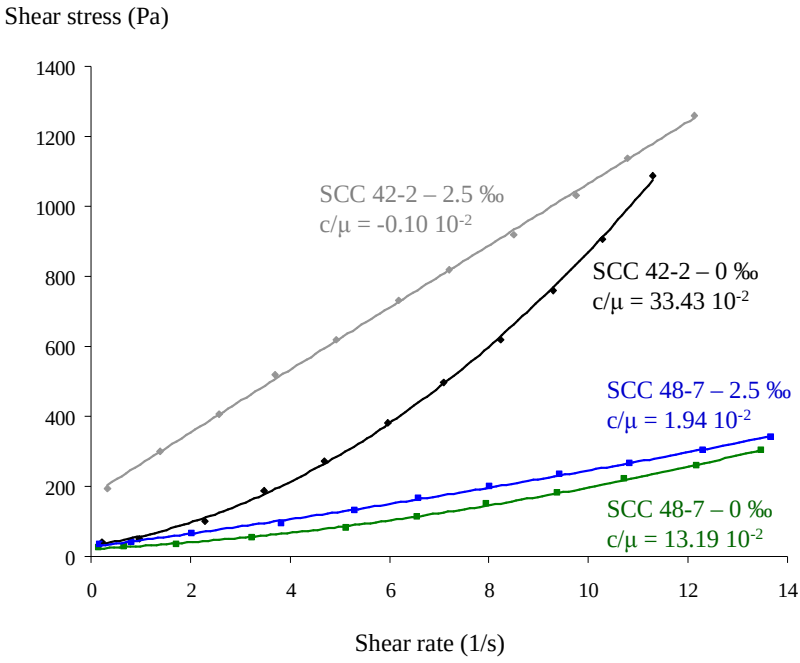

Figure 4.23: The addition of 2.5 ‰ of oil causes a drastic reduction in shear thickening, both for the reference mix (SCC 48-7), as for an extremely shear thickening mix (SCC 42-2).

5.5 Probable cause of shear thickening in SCC

As a conclusion of the above mentioned effects, the more probable cause of shear thickening in cement based materials is the formation of clusters. As has been shown, shear thickening is already observed in self-compacting pastes, in which grain inertia appears to have a insufficient influence. Increasing volume fraction, by decreasing w/p-ratio in SCC, increases the intensity of shear thickening, but does not affect the critical shear stress, which is in accordance to the cluster theory. Increasing SP-dosage increases the amount of particles susceptible for shear thickening, due to a larger degree of dispersion achieved. The addition of coarse aggregates on the other hand causes a decrease in shear thickening behaviour, due to the destruction of clusters by the coarse aggregates flowing nearby, which contain a non-negligible amount of inertia. The physical background of the influence of demoulding oil must still be investigated.

On the other hand, it should be kept in mind that under certain circumstances, grain inertia can become important and this effect should also be considered when studying shear thickening behaviour of cement paste and concrete. According to the grain inertia theory, even traditional concrete or cement paste should show shear thickening behaviour, when sheared at a (very) high shear rate.
What about the modified Bingham model? Does it provide any additional physical meaning? According to the above mentioned results, it does not. During the research campaign, no exponent n of Herschel-Bulkley larger than 2 has been observed, although this should be theoretically possible. As a result, the modified Bingham model still remains valid to fit the flow curve, but it does not add any extra physical meaning. On the other hand, it still defines that the viscosity at zero shear rate is not equal to 0, and the advantage to derive an extended version of the Poiseuille equation (chapter 6) is still valid.

5.6 Why is shear thickening not often (or often not) reported?

The number of publications reporting non-linear behaviour of fresh concrete is very limited [4.8-4.11][4.47-4.49]. In most cases, as it is for traditional concrete for example, there is no non-linear behaviour to report. As a result, in the course of history, a kind of "Bingham-culture" has been established and is generally accepted [4.1-4.5]. Reporting non-linear behaviour is consequently something revolutionary, subjected to a lot of criticism and disbelief. During the last years, shear thickening is gradually being proved to be a physical characteristic of the material and not a measurement artefact or dreaming image of the authors. On the other hand, shear thickening still encounters, justly, the necessary criticism.
In order to answer the question why shear thickening is not often (or often not) reported, it is not only a cultural issue, but it can be it is not observed at all, even when it is intrinsically present in the material. For example, for the SCC 63 tested in this project, containing silica fume (fig. 4.19): it is not known whether or when this SCC will shear thicken. The only conclusion which can be drawn from figure 4.19 is that it does not show shear thickening for the range of shear rates or shear stresses applied. This can be the main argument, apart from the disbelief, why shear thickening is not so often reported. As many researchers conduct rheometer experiments at low shear rates, because in the planned application of their concrete only low shear rates are applied, it can be that the highest stress measured in the rheometer is lower than the critical shear stress. As a result, no shear thickening is observed nor reported. Or it can be that only one or two of the data points at the highest shear stresses show some shear thickening, while the other data points do not. In these cases, these deviating points will be omitted by the arguments of non-equilibrium or measurement errors. As a result, shear thickening is possibly observed, but not reported, due to an insufficient amount of data. Only in case quite high shear rates are applied, like in this research project, a sufficient amount of consistent data is collected in order to conclude that the observed shear thickening is in fact a material property. On the other hand, increasing shear rates in a rheometer is not evident. More or larger measurement artefacts can occur and the results can become invalid. Increasing shear rates up to 50 s^{-1}, at least for concrete, is still a

large challenge in concrete rheometry, although these shear rates are applied on the material during mixing and possibly during pumping. Any researcher dealing with large shear rates in concrete, and also needing rheological characterisation, should be very careful when choosing the shear rate in the rheometer. Too high shear rates can create material inhomogeneity, while measuring at too low shear rates can hide some (unwanted and unfavourable) effects.

6 Summary

In the first section of this chapter, three models to describe the rheological behaviour of fresh concrete, in steady state conditions, are discussed. For non-linear (shear thickening) behaviour, the modified Bingham model is preferred to the Herschel-Bulkley model.

The difference, from a rheological point of view, between traditional concrete and self-compacting concrete consists of a lower yield stress and a higher plastic viscosity for SCC. In some cases, shear thickening behaviour in case of SCC can be observed.

The third section of this chapter describes the concrete compositions, mixing procedures and testing procedures. For the concretes tested with the Tattersall Mk-II rheometer, as the same mixing procedure has been applied in all cases, mixing is assumed to have no significant influence on the rheological properties.

In section four, a short overview of the parameters influencing yield stress and plastic viscosity is given, based on results in literature. Our experimental data does not deviate significantly from the results in literature, except the observation of shear thickening behaviour.

Shear thickening behaviour of self-compacting concrete is described in detail, as it is important in processes involving high shear rates, like mixing and pumping. It is shown that the shear thickening behaviour is not a measurement artefact due to thixotropy, particle migration and the occurring of plug flow, nor it is a rheometer mistake. It is proven that it is a real characteristic of self-compacting concrete.

Based on the results of cement pastes and concrete, several parameters influencing shear thickening, namely the w/p-ratio, slump flow and superplasticizer content, the type of fillers, the coarse aggregates and the addition of demoulding oil, are described. From these results, it is concluded that the formation of clusters is a more probable cause for shear thickening than grain inertia, in this case.

The reason why shear thickening is not so often reported is that, first, there must be shear thickening behaviour, which is mostly not the case, except for SCC, and secondly, the applied shear stresses or shear rates must be sufficiently high to observe clearly the shear thickening behaviour. In most cases, the applied shear rates in concrete rheometers remain quite low. Increasing shear rate in the rheometer increases the danger of more or more pronounced measurement artefacts.

7 References

[4.1] Tattersall G.H., Banfill P.F.G., "The rheology of fresh concrete," Pitman, London (1983).

[4.2] Tattersall G.H., "The rationale of a two-point workability test," Mag. Conc. Res. **25** (1973) 169-172.

[4.3] Tattersall G.H., Bloomer S.J., "Further development of the two-point test for workability and extension of its range," Mag. Conc. Res. **31** (1979), 202-210.

[4.4] Wallevik O.H., Gjørv O.E., "Modification of the two-point workability apparatus," Mag. Conc. Res. **42** (1990), 135-142.

[4.5] Domone P.L.J., Yongmo X., Banfill P.F.G., "Developments of the two-point workability test for high-performance concrete," Mag. Conc. Res. **51** (1999), 171-179.

[4.6] Bingham E.C., "An investigation of the laws of plastic flow," U.S. Bur. Stand. Bull. **13** (1916), 309-353.

[4.7] Herschel W.H., Bulkley R., "Konsistenzmessungen von Gummi-Benzol-Lösungen," Kolloid Z. **39** (1926), 291-300.

[4.8] de Larrard F., Ferraris C.F., Sedran T., "Fresh concrete: A Herschel-Bulkley material," Mat. Struct. **31** (1998), 494-498.

[4.9] Cyr M., Legrand C., Mouret M., "Study of the shear thickening effect of superplasticizers on the rheological behaviour of cement pastes containing or not mineral additives," Cem. Conc. Res. **30** (2000), 1477-1483.

[4.10] Heirman G., Vandewalle L., Van Gemert D., Wallevik O., Cauberg N., "Contribution to the solution of the Couette inverse problem for Herschel-Bulkley fluids by means of the integration method," Proc. of the 2nd Int. Symp. on Advances in Concrete through Science and Engineering, Québec-City (2006).

[4.11] Heirman G., Vandewalle L., Van Gemert D., "An analytical solution of the Couette inverse problem for shear thickening SCC in a wide-gap concentric cylinder rheometer," J. non-Newt. Fluid Mech. **150** (2008), 93-103.

[4.12] Yahia A., Khayat K.H., "Analytical models for estimating yield stress of high-performance pseudoplastic grout," Cem. Conc. Res. **31** (2001), 731-738.

[4.13] Geiker M.R., Wallevik O.H., "Rheology of cement based materials," DTU-RILEM Doctoral course, Lyngby (2007).

[4.14] Wallevik O.H., "Rheology – a scientific approach to develop self-compacting concrete," Proc. of the 3rd Int. RILEM Symp. on SCC, Reykjavik (2003), 23-31.

[4.15] De Schutter G., Bartos P., Domone P., Gibbs J., "Self-Compacting Concrete," Whittles Publishing, Caithness (2008), 296pp.

[4.16] Okamura H., Ozawa K., "Mix design for Self-Compacting Concrete," Concrete library of JSCE **25** (1995), 107-120.

[4.17] Khayat K.H., "Viscosity-enhancing admixtures for cement-based materials – an overview," Cem. Conc. Comp. **20** (1998), 171-188.

[4.18] Feys D., Heirman G., De Schutter G., Verhoeven R., Vandewalle L., Van Gemert D., "Comparison of two concrete rheometers for shear thickening behaviour of SCC," Proc. of the 5th Int. RILEM Symp. on SCC, Ghent (2007), 365-370.

[4.19] Chopin D., de Larrard F., Cazacliu B., "Why do HPC and SCC require a longer mixing time ?" Cem. Conc. Res. **34** (2004), 2237-2243.

[4.20] Flatt R.J., Houst Y.F., "A simplified view on chemical effects perturbing the action of superplasticizers," Cem. Conc. Res. **31** (2001), 1169-1176.

[4.21] Wallevik O.H., Geiker M.R., "State of the art report, chapter 4, testing rheological properties," Final report of RILEM TC RFC-committee, in press.

[4.22] Williams D.A., Saak A.W., Jennings H.M., "The influence of mixing on the rheology of fresh cement pastes," Cem. Conc. Res. **29** (1999), 1491-1496.

[4.23] Geiker M.R., Ekstrand J.P., Hansen R., "Effect of mixing on properties of SCC," Proc. of the 5th Int. RILEM Symp. on SCC, Ghent (2007), 231-238.

[4.24] Wallevik O.H., "Why is SCC different from country to country?", Proc. of the 4th Int. RILEM Symp. on SCC and the 2nd North-American Conf. on the design and use of Self-Consolidating Concrete, Chicago (2005).

[4.25] Wallevik O.H., "Rheological properties of Mortar and Concrete, including measurements and differences of SCC in several countries," Lecture notes of the RILEM-DTU course on the rheology of cement based materials, Lyngby (2003).

[4.26] Wallevik O.H., Nielsson I., "Self-Compacting Concrete – A rheological approach", Proc. of the Int. Workshop on SCC, Kochi (1998), 136-159.
[4.27] Carlswärd J., Emborg M., Utsi S., Öberg P., "Effect of constituents on the workability and rheology of self-compacting concrete," Proc. of the 3rd Int. RILEM Symp. on SCC, Reykjavik (2003), 143-153.
[4.28] Vikan H., Justnes H., "Influence of silica fume on rheology of cement paste," Proc. of the 3rd Int. RILEM Symp. on SCC, Reykjavik (2003), 190-201.
[4.29] Struble L.J., Jiang Q., "Effects or air entrainment on rheology," ACI Mat. J. **101:6** (2004), 448-456.
[4.30] Yahia A., Tanimura M., Shimoyama Y., "Rheological properties of highly flowable mortar containing limestone filler – effect of powder content and W/C ratio," Cem. Conc. Res. **35** (2005), 532-539.
[4.31] Billberg P., "Influence of filler characteristics on SCC rheology and early hydration," Proc. of the 2nd Int. RILEM Symp. on SCC, Tokyo (2001), 285-294.
[4.32] Sheinn A.M.M., Ho D.W.S., Tam C.T., "Effect of particle shape on paste rheology of SCC," Proc. of the 3rd Int. RILEM Symp. on SCC, Reykjavik (2003), 232-239.
[4.33] Brameshuber W., Uebachs S., "The influence of the temperature on the rheological properties of self-compacting concrete," Proc. of the 3rd Int. RILEM Symp. on SCC, Reykjavik (2003), 174-183.
[4.34] Geiker M.R., Brandl M., Thrane L.N., Bager D.H., Wallevik O.H., "The effect of measuring procedure on the apparent rheological properties of self-compacting concrete," Cem. Conc. Res. **32** (2002), 1791-1795.
[4.35] Geiker M.R., "On the combined effect of measuring procedure and coagulation rate on apparent rheological properties," Proc. of the 3rd Int. RILEM Symp. on SCC, Reykjavik (2003), 35-40.
[4.36] Wallevik J.E., "Rheology of particle suspensions, Fresh concrete, mortar and cement paste with various types of lignosulphonates," Ph-D dissertation, The Norwegian University of Science and Technology, Trondheim (2003).
[4.37] Ovarlez G., Bertrand F., Rodts S., "Local determination of the constitutive law of a dense suspension of non-colloidal particles through MRI," J. Rheol. **50** (2006), 259-292.
[4.38] Mewis J., Internal communication.
[4.39] Magarotto R., Moro S., Internal communication.
[4.40] Bossis G., Brady J.F., "The rheology of Brownian suspensions," J. Chem. Phys. **91:3** (1989), 1866-1874.
[4.41] Bagnold R.A., "Experiments on a gravity-free dispersion of large solid spheres in a Newtonian fluid under shear," Proc. Roy. Soc. **225A** (1954), 49-63.
[4.42] Artelt C., Garcia E., "Impact of superplasticizer concentration and of ultra-fine particles on the rheological behaviour of dense mortar suspensions," Cem. Conc. Res. **38** (2008), 633-642.
[4.43] Macosko C.W., "Rheology Principle, measurements and applications," Wiley-VCH, New-York (1994).
[4.44] Maranzano B.J., Wagner N.J., "The effects of interparticle interactions and particle size on reversible shear thickening: Hard-sphere colloidal dispersions" J.Rheol. **45:5** (2001), 1205-1222.
[4.45] Maranzano B.J., Wagner N.J., "The effect of particle size on reversible shear thickening of concentrated colloidal dispersions," J. Chem. Phys. **114** (2001), 10514-10527.
[4.46] Krishnamurthy L.-N., Wagner N.J., Mewis J., "Shear thickening in polymer stabilized colloidal dispersions," J. Rheol. **49:6** (2005), 1347-1360.
[4.47] Feys D., Verhoeven R., De Schutter G., "Evaluation of time-independent rheological models applicable to fresh Self Compacting Concrete," Appl Rheol **17:5** (2007), 56244.
[4.48] Feys D., Verhoeven R., De Schutter G., "Fresh self compacting concrete: a shear thickening material," Cem. Conc. Res. **38** (2008), 920-929.
[4.49] Feys D., Verhoeven R., De Schutter G., "Why is fresh self-compacting concrete shear thickening?" Cem. Conc. Res., article in press.

CHAPTER 5:

CONCRETE RHEOLOGY: TIME DEPENDENT BEHAVIOUR

As mentioned in the previous chapter, performing rheological measurements on concrete is not a straightforward task. The size of the aggregates, the presence of a yield stress, the danger of segregation and the contribution of friction to the rheological properties can cause large complications. For all cement based materials (cement paste, mortar and concrete), the measured rheological properties vary in time [5.1]. In this chapter, the time dependent behaviour of fresh concrete will be discussed. In a first part, thixotropy, structural breakdown and loss of workability will be defined and described. In case of thixotropy and structural breakdown, no direct measurements have been performed in this research project. Consequently, the thixotropic models with their results and the description of the effects of structural breakdown are based on literature. For the loss of workability, measurements have been performed, which are in good agreement with [5.2]. In the last part of this chapter, the influence of thixotropy (and structural breakdown) on the measurements will be discussed briefly.

1 Origin and distinction

Thixotropy, structural breakdown and loss of workability are three different effects which can be distinguished easily in theory, but not in practice. Thixotropy is defined as a reversible build-up and breakdown of internal structure due to flocculation or coagulation of cement particles, for which the influence of the inter-particle forces is still significant [5.3]. It is stated by J.E. Wallevik that cement particles with a size up to 40 μm are influenced by inter-particle forces [5.4]. It is suspected that all cement particles smaller than 40 μm can undergo thixotropic behaviour. Thixotropy is caused by "physical" connections between cement particles, called junctions in the Hattori-Izumi theory [5.5-5.6].
Structural breakdown has been observed by Tattersall [5.1][5.7-5.8] by keeping the rotational velocity constant in a concentric cylinder rheometer. The resulting torque response of the cement paste showed a more or less exponential decrease with time. This behaviour has been named structural breakdown, but in fact, it includes both

the breakdown due to thixotropy and the (real) structural breakdown defined below. One can say that the structural breakdown defined by Tattersall, is structural breakdown in the "broad sense", while the real structural breakdown, without thixotropy can be called structural breakdown in the narrow sense. This last structural breakdown, in its narrow sense, is considered to be the breaking of existing "chemical" linkages between cement particles [5.1][5.4], most probably formed during the first hydration peak, although further chemical linkages (due to hydration) can also be formed at later ages. In contrast to the thixotropic behaviour, the chemical linkages do, in general, not build-up so fast. As a result, during the observation time, only the breakdown is seen, and not the build-up process. Also in contrast to the thixotropic behaviour, structural breakdown can occur for all sizes of the cement particles.

Loss of workability is the formation of permanent connections, due to coagulation or chemical reactions [5.9-5.10], between cement particles, which cannot be broken for a certain amount of work applied. Increasing the amount of work in a cement paste or concrete will consequently decrease the loss of workability and increase the thixotropy and structural breakdown.

During the dormant period, after water addition, the chemical reaction between the cement and the water proceeds slowly. In this process, the original klinker materials transform (partly) into hydration products, causing the hydration products to grow [5.9]. During this growth, cement particles approach to each other, connect and form a gel-like structure. Finally, setting starts, caused by a combination of connections, and the cement paste becomes as hard as rock. In case superplasticizers are added to the cement paste in order to decrease the number of connections during and after mixing, the growth of the outer hydration products reduces the efficiency of the superplasticizer [5.10]. Some superplasticizer manufacturers overcome this problem by modifying their polymer products in order to increase the time frame during which the concrete keeps sufficient workability.

Due to the physical or chemical connections, whether they are reversible or not, the size of the agglomerates increases, and water is entrapped between the particles in these agglomerates [5.11-5.12]. This results in an increase in both yield stress and viscosity. Decreasing the internal structure due to shearing, inducing thixotropic and structural breakdown, will decrease the particle size and release the entrapped water, leading to a decrease in yield stress and viscosity, up to a certain shear rate. At higher shear rates, other effects, like cluster formations, grain inertia, or a significantly increasing water demand can become significant.

In [5.4], J.E. Wallevik made a distinction between size 3 (< 40 μm) and size 4 (> 40 μm) cement particles. Size 3 particles are still influenced by the inter-particles forces, and contribute to the thixotropic behaviour, structural breakdown and loss of workability. Size 4 particles are too large and due to inertia, they are not influenced by the inter-particle forces. The chemical "linkages" formed between the cement particles occur independently of their size, meaning that both size 3 and 4 particle-connections can undergo structural breakdown. A distinction between thixotropy, structural breakdown and loss of workability is shown in figure 5.1.

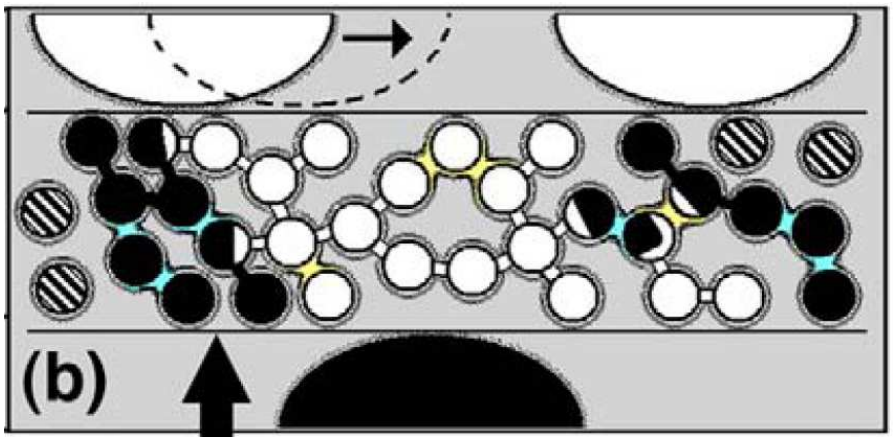

Figure 5.1: Representation of time dependent connections. The white connections represent reversible thixotropic coagulations. The yellow connections form the reversible chemical linkages, while the black and blue connections are irreversible (loss of workability), due to coagulation and hydration respectively. Figure from J.E. Wallevik [5.4].

2 Thixotropy

This part will give an overview of the most common models used to describe the thixotropic behaviour of cement based materials.

2.1 Microstructural models

2.1.1 Original Hattori-Izumi theory

The original theory by Hattori and Izumi [5.5-5.6] states that the shear viscosity η_{HI} is dependent on the total amount of reversible "junctions" or connections between particles (eq. 5.1).

$$\eta_{HI} = B_3 \cdot J_t^{2/3} \tag{5.1}$$

where: η_{HI} *= shear viscosity (Pa s)*
B_3 *= friction coefficient (N s)*
J_t *= number of reversible junctions per unit of volume (m^{-3})*

In order to define J_t, the total number of primary particles (n_3) per unit of volume must be known. This number represents the total number of particles per volume which can undergo reversible coagulation and which are in a completely dispersed state. When J_t is defined as the total number of reversible junctions, then the total number of particles (n_t) equals the total number of primary particles n_3 minus J_t, assuming that no permanent connections are present and that the connections do not form closed networks. When n_t reaches the value of 1, the suspension is in a fully coagulated state.
The Hattori-Izumi theory also assumes that the number of connections only increases when the shear rate equals zero, and only decreases during shear. The decrease in the total number of particles, due to coagulation, is described by means of the coagulation rate constant H (eq. 5.2).

$$-\frac{dn_t}{dt} = \frac{H \cdot n_t^2}{n_3} \tag{5.2}$$

where: H *= coagulation rate constant (1/s)*

Combining build-up during rest, expressed by H, and breakdown during shear, the total number of junctions after a certain amount of time equals:

$$J_t = n_3 \cdot U_3 = \frac{n_3 \cdot \left(U_0 \cdot \left(\dot{\gamma} \cdot H \cdot t^2 + 1\right) + H \cdot t\right)}{\left(H \cdot t + 1\right) \cdot \left(\dot{\gamma} \cdot t + 1\right)} \tag{5.3}$$

where: $J_0 = n_3 U_0$ *refers to the initial state (at t = 0)*

U_0,U_3 = coagulation state at the beginning and end respectively (0 = fully dispersed, 1 = fully coagulated) (-)

Permanent junctions between particles, which are denoted as J_t^p, causing loss of workability, are not incorporated in the Hattori-Izumi theory, but they have a similar effect on the shear viscosity.

2.1.2 Modified Hattori-Izumi theory

In his Ph-D dissertation [5.3][5.13], J.E. Wallevik suggested three modifications to the original Hattori-Izumi theory in order to describe the thixotropic behaviour of cement based materials.

A Fading memory

Instead of assuming a constant coagulation rate H and a constant shear rate, Wallevik suggested to apply fading memory equations instead. In this way, the material can remember the previous actions it had undergone, with decreasing importance with increasing elapsed time. This modification incorporates two more variables m_a and m_b which define how much the coagulation state should remember the past shear and coagulation respectively. The functions H • t and dγ/dt • t are replaced by the memory modules Θ and Γ (eq. 5.4-5.6).

$$U_3 = \frac{J_t}{n_3} = \frac{U_0 \cdot (\Gamma \cdot \Theta + 1) + \Theta}{(\Theta + 1) \cdot (\Gamma + 1)} \tag{5.4}$$

$$\Gamma(geo,t) = \int_0^t e^{-(t-t')/m_a} \cdot \dot{\gamma}(geo,t') \cdot dt' \tag{5.5}$$

$$\Theta(geo,t) = \int_0^t e^{-(t-t')/m_b} \cdot H(geo,t',\dot{\gamma}) \cdot dt' \tag{5.6}$$

where: *Γ = memory module for shear (-)*
Θ = memory module for coagulation (-)
the index "geo" indicates the dependency of a parameter on the rheometer geometry.
m_a, m_b = parameters indicating how much the past should be remembered (s)
t = current time in the experiment (s)
t' = time varying between the initial time and the current time, over which the integration must be taken (s)

B Incorporation of yield stress

As cement based materials have a yield stress, the Hattori-Izumi theory has been modified in order to determine the increase or decrease in yield stress and plastic viscosity due to thixotropic variations. This is expressed in equations 5.7 to 5.9:

$$\eta = B + \frac{\sqrt{C_y}}{\dot{\gamma}} \tag{5.7}$$

$$B = \mu + \left(a_1 \cdot B_3 \cdot {n_3}^{2/3}\right) \cdot {U_3}^{2/3} = \mu + \mu'' \tag{5.8}$$

$$C_y = \tau_0 + \left(a_2 \cdot B_3 \cdot {n_3}^{2/3}\right) \cdot {U_3}^{2/3} = \tau_0 + \tau_0'' \tag{5.9}$$

where: η *= total shear viscosity (Pa s)*
μ *= plastic viscosity in case no reversible connections are present (Pa s)*
τ_0 *= yield stress in case no reversible connections are present (Pa)*
μ'', τ_0'' *= thixotropic counterparts of plastic viscosity and yield stress (Pa s and Pa respectively)*
a_1, a_2 *= parameters (-)*

Note that any loss of workability, which is caused by the permanent junctions between the particles must be incorporated in μ and τ_0 themselves. An increase in loss of workability will consequently be reflected by an increase in these two parameters and not in their thixotropic counterparts.

C Coagulation Rate

As a last modification, Wallevik proposed a change in the coagulation rate function. The coagulation rate H, defined in the original Hattori-Izumi theory, only reflects the increase in the number of junctions due to Brownian motion. As it has also been shown in equations 2.16 and 2.17 from chapter 2, describing general thixotropic behaviour, coagulation can also be induced by a certain shear rate, lower than the critical shear rate. On the other hand, for shear rates above the critical shear rate, breakdown becomes dominant. As a result, the coagulation rate H has been defined as a function of the applied shear rate relative to the critical shear rate.

2.1.3 Particle aggregation modelling

The particle aggregation modelling does not take into account the number of reversible junctions, but it models the consequences of increases or decreases in the size of particle aggregations. Thus, when particles in a suspension do aggregate, they form larger elements in the suspension and entrap water in their voids. As a result, the effective volume fraction increases, causing the apparent viscosity of the suspension to be larger, compared to the fully dispersed state. Chougnet et al. have applied this theory successfully to describe variations in yield stress and apparent viscosity during the dormant period for a cement paste and for a thixotropic silica suspension [5.14].
Based on the experiments, some parameters have been fitted but as this model has not been applied frequently, no database of parameters is available and experiments are still needed to determine the model parameters.

2.2 Static yield stress

In most cases, the influence of thixotropy on the viscosity has been neglected in practice. Furthermore, the development of the yield stress is much more important, especially when studying the decrease in formwork pressure [5.15], the disadvantages of multi-layer casting [5.16-5.17] and even during rheological measurements.
Based on the general thixotropic model described in chapter 2, the Coussot model (eq. 5.10-5.11) [5.18] already incorporates some simplifications but still describes thixotropic behaviour quite accurately. Roussel has developed an even more simple thixotropic model for cement pastes and fluid concretes (eq. 5.12-5.13) [5.16][5.19].

$$\tau = \eta_0 \cdot \left(1 + \lambda^n\right) \cdot \dot{\gamma} \tag{5.10}$$

$$\frac{d\lambda}{dt} = \frac{1}{\theta} - \alpha \cdot \lambda \cdot \dot{\gamma} \tag{5.11}$$

$$\tau = \left(1 + \lambda_0 \cdot e^{-\alpha \cdot \dot{\gamma} \cdot t}\right) \cdot \tau_0 + \mu_p \cdot \dot{\gamma} \tag{5.12}$$

$$\tau = \tau_0 + A_{thix} \cdot t \tag{5.13}$$

Where: τ = *shear stress (Pa)*
η_0 = *apparent viscosity at fully dispersed state (Pa s)*
λ = *structural state (0 = fully dispersed, ∞ = fully coagulated) (-)*
$d\gamma/dt$ = *shear rate (1/s)*
θ = *characteristic parameter for structuration (s)*
α = *characteristic parameter for destructuration (-)*
λ_0 = *initial structural state (-)*
τ_0 = *yield stress at fully dispersed state (Pa)*
μ_p = *plastic viscosity of cement paste or concrete (Pa s)*
t = *time (s)*
A_{thix} = *characteristic time for structuration of cement paste or concrete (Pa/s)*

Equation 5.12 describes the shear stress evolution (decrease) during flow, assuming that the plastic viscosity is not influenced by thixotropy. Equation 5.13 describes the build-up of (yield) stress during rest. The parameter A_{thix}, which is a material parameter, is a constant, resulting in a linear increase of the static yield stress with time, which has also been observed by Billberg (fig. 5.2) [5.15-5.16][5.20]. During the first one or two hours of age, the increase of dynamic yield stress can be neglected relatively to the static yield stress [5.21]. The procedure of static yield stress measurements has been described in chapter 3.

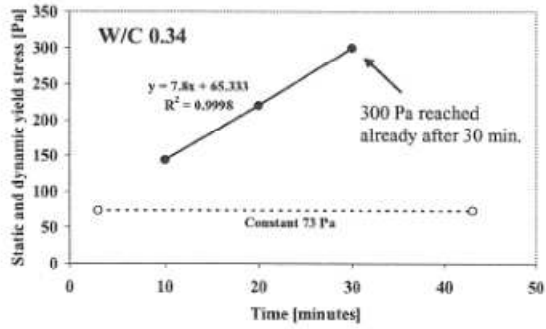
W/C 0.34
y = 7.8x + 65.333
R² = 0.9998
300 Pa reached
already after 30 min.
Constant 73 Pa
Static and dynamic yield stress [Pa]
Time [minutes]

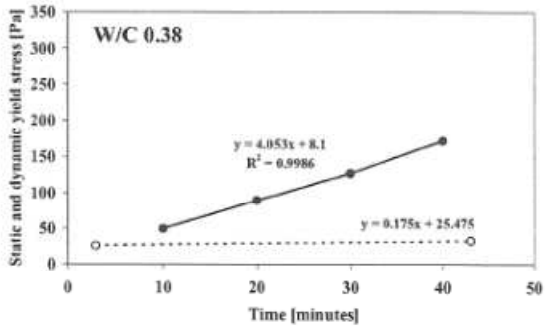
W/C 0.38
y = 4.053x + 8.1
R² = 0.9986
y = 0.175x + 25.475
Static and dynamic yield stress [Pa]
Time [minutes]

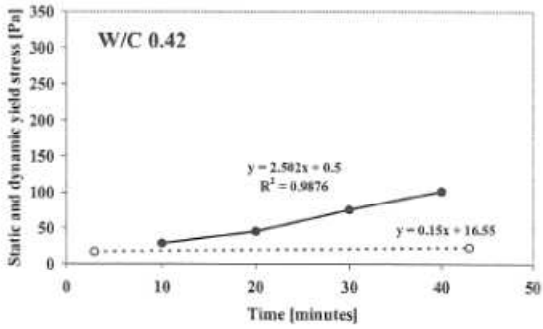
W/C 0.42
y = 2.502x + 0.5
R² = 0.9876
y = 0.15x + 16.55
Static and dynamic yield stress [Pa]
Time [minutes]

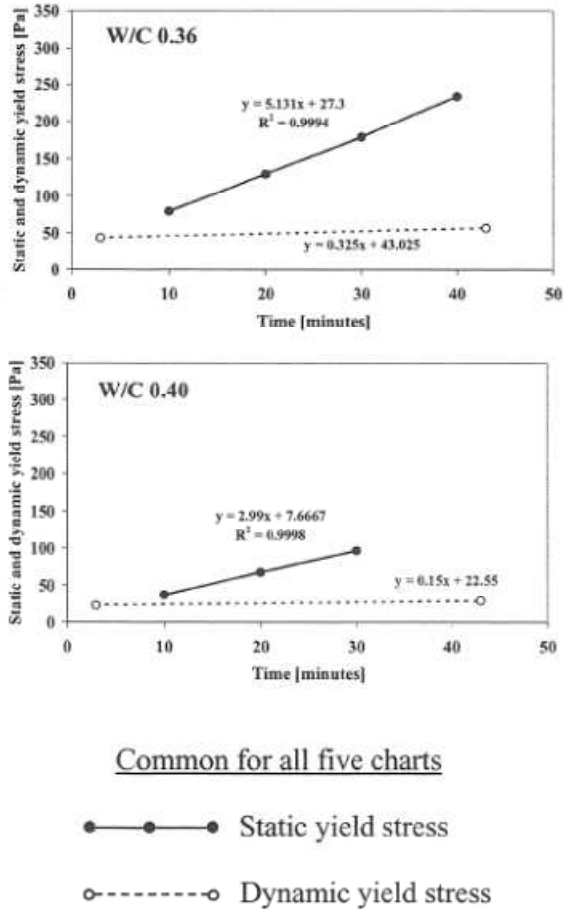

Figure 5.2: Linear increase of static yield stress during rest for cement pastes with different w/c-ratios, proving the validity of equation 5.13. Figure from P. Billberg [5.15].

The increase in static yield stress in fluid concretes is caused by the cement paste. Similarly as for the dynamic yield stress, the presence of aggregates increases the value of the static yield stress according to equation 2.12 of chapter 2 [5.22-5.23], but only in cases where friction between aggregates can be neglected. As a result, in order to study the thixotropic properties of a fluid concrete, it is sufficient to know the thixotropic properties of the corresponding cement paste.

In order to incorporate loss of workability in this model, the values of τ_0 and μ_p themselves must be changed in equations 5.12 and 5.13.

In their study, Jarny et al. [5.24] found that the timescales during which thixotropy and loss of workability influence the measurements are different. For relatively short times (10 - 100 s), thixotropy dominates the transient behaviour, but for longer time scales (1000 s), the influence of loss of workability is no longer negligible.

2.3 Sudden changes in shear rate

In chapter 3, it has been described that the thixotropic properties can be quantified by means of sudden increases (or decreases) in shear rate. By measuring the difference between the maximum (or minimum) value and the equilibrium value, and by the time needed to achieve this equilibrium, thixotropy can be very well understood. In their research dealing with the decrease in formwork pressures, Khayat and co-workers have developed a similar method to investigate the thixotropic properties [5.26-5.30]. Figure 5.3 shows schematically the testing procedure.

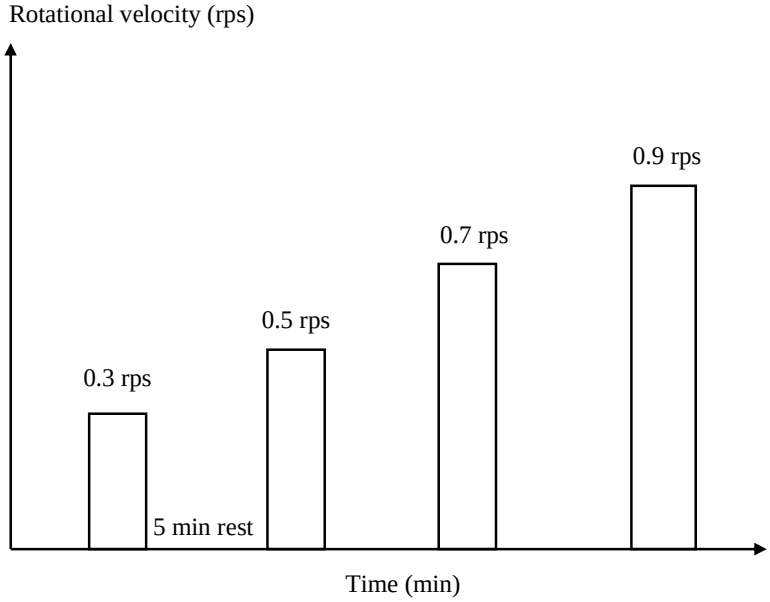

Figure 5.3: Principle of the testing procedure applied to obtain the results in figure 5.4. Each rotational velocity is maintained during 2.5 minutes, followed by a resting period of 5 minutes. Figure after J.J. Assaad and K.H. Khayat [5.29].

After 5 minutes of rest each time, the concrete is sheared at a certain constant rotational velocity, in increasing order. The rotational velocity in the rheometer is maintained during 2.5 minutes and the maximum, initial torque and the equilibrium torque are retained. Connecting the maximum torque points and the equilibrium points delivers two curves, as can be seen in figure 5.4. The area between the two curves is called the breakdown area (A_b) and has been found to relate very well with the decay in formwork pressure due to thixotropy [5.28-5.30].
On the other hand, the value of A_b is dependent on the measuring procedure: the time of rest, the differences between the rotational velocities applied and the registering speed and accuracy of the torque sensor. A physical meaning for the A_b value is not available, but with this parameter, the evolution of formwork pressures, and hence thixotropy, has been determined very well.

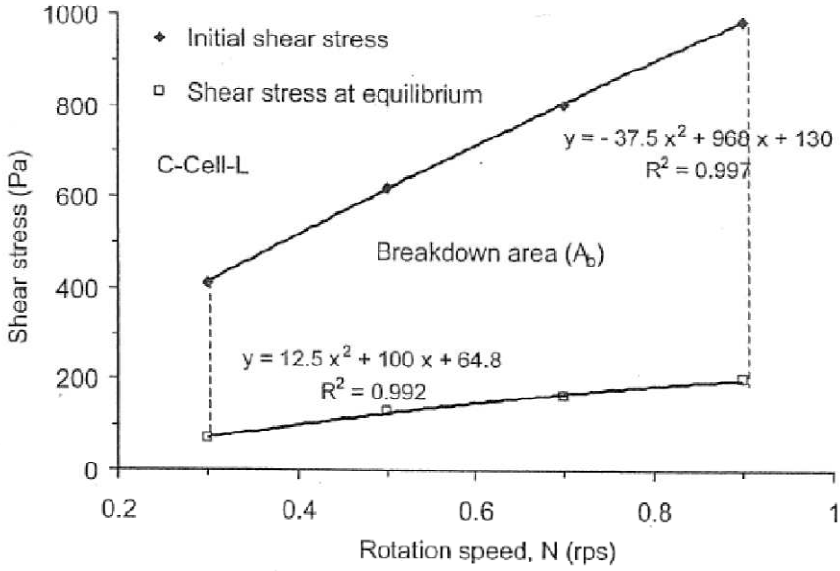

Figure 5.4: Determination of the breakdown area A_b between the up-curve (full dots), formed by connecting the maximum torque responses at each rotational velocity, and the equilibrium curve (open dots), formed by connection all equilibrium torque data. Figure from J.J. Assaad and K.H. Khayat [5.29].

2.4 Loop curves

The most applied thixotropic measurement procedure is the determination of a loop curve [5.15][5.31-5.34]. After a period of rest, the shear rate is increased gradually up to a certain maximal value and decreased again (fig. 5.5). The area between the two curves, also called A_b (Pa/s) in most cases, is a parameter related to the thixotropic behaviour. Although this procedure is frequently applied, it is not really suitable for comparative purposes between laboratories. The value does not only depend on the maximal shear rate applied, the resting time and the rheometer device, it is also dependent on the rate of increase and decrease in shear rate, the accuracy of fitting the curves (especially the up-curve) in order to calculate the area between the curves and the accuracy of data registration. Nevertheless, this methodology has been applied by many researchers [5.15][5.31-5.34] when studying the thixotropic behaviour of self-compacting concrete.

A similar procedure has been applied in the Center for Advanced Cement-Based Materials of the Northwestern University in the USA, although when calculating the area, the down curve has been chosen to be the initial down curve at an age of 12 minutes, for each test performed [5.31]. In this way, a combination of the influence of thixotropy and loss of workability is obtained each time.

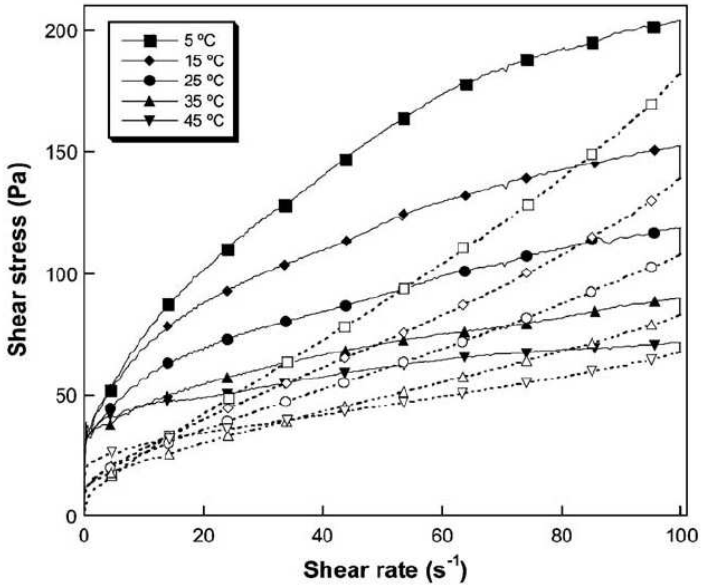

Figure 5.5: Example of loop curves, determined on cement pastes at different temperatures. Figure after V. Fernandes-Altable and I. Casanova [5.32]

2.5 Discussion

Four types of rheological models have been described in the previous sections, each having their advantages and disadvantages. From the point of view of simplicity, the loop curve method is the most favourable, while the microstructural models are seriously complicated and have a lot of parameters that need to be fitted by experiments and calculations or simulations. On the other hand, the microstructural models are currently the only models describing the influence of thixotropy on the viscosity of cement based materials. In case of the loop curves, the single parameter A_b does not provide the ability to make a distinction between the influence of thixotropy on yield stress and viscosity and for the static yield stress model, it has been assumed that the influence of thixotropy on viscosity is of minor importance. The A_b-value determined by the sudden changes in shear rate is also dependent on a lot of parameters and difficult to interpret physically, but it has been proven it can be applied to describe some physical phenomena.
In my opinion, the model which forms the best compromise between the physics and practice, is the static yield stress model, but investigations should be carried out in order to find out what the influence of the structural parameter λ on the viscosity is. In fact, the effect of λ should be similar to the effect on the yield stress, according to the theory of Wallevik (eq. 5.8-5.9). This should result in a simple extension of the current model.
For the sake of clarity during the next part of this thesis, it should be highlighted that for each shear rate, larger than the critical shear rate (see chapter 2), there exists an

equilibrium value of the structure parameter (U_3 or λ), which decreases with increasing shear rate (fig. 5.6). As a result, with increasing shear rate, the equilibrium values of yield stress and viscosity decrease and the material becomes more liquid.

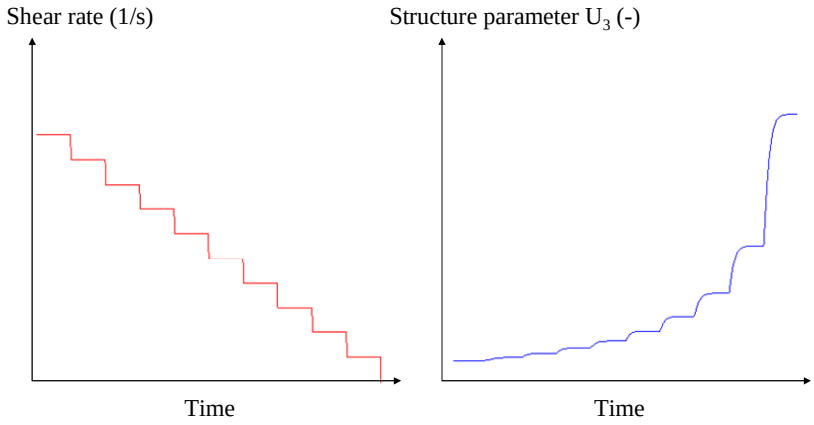

Figure 5.6: Example of evolution of structure parameter (blue, right) with decreasing shear rate (red, left), according to the modified Hattori-Izumi theory.

Currently, the precise relationship between the equilibrium value of the structure parameter and the shear rate is still unknown for cement based materials, but according to the Coussot model (eq. 5.10-5.11) [5.18], the equilibrium structure parameter at a certain shear rate should scale with the inverse of the shear rate. For the modified Hattori-Izumi theory, no relationship between the equilibrium U_3 and the shear rate has been found and the static yield stress model of Roussel does not take this effect into account.

3 Structural breakdown

3.1 Theory

3.1.1 Structural breakdown in the broad sense

As described in the first section of this chapter, the structural breakdown in the broad sense is a combination of the thixotropic breakdown and the breaking of chemical linkages. This effect has been measured by Tattersall [5.1][5.7-5.8], by keeping the rotational velocity in a concentric cylinder rheometer constant, and measuring the torque decay with time. Tattersall obtained an exponential decrease of the torque with time (for cement pastes), expressed in equation 5.14. The factor B in this equation is dependent on the rotational velocity, the work needed in order to break one linkage and the number of linkages (eq. 5.15).

$$T = T_E + (T_0 - T_E) \cdot e^{(-B \cdot t)} \tag{5.14}$$

$$B = \frac{2 \cdot \pi \cdot K}{n_0 \cdot \psi} \cdot \omega \cdot (\omega - \omega_1) \tag{5.15}$$

where: T = *torque at time t (Nm)*
T_E = *torque at equilibrium (Nm), in principle at t =* ∞
T_0 = *initial torque value (Nm)*
B = *structural breakdown parameter (1/s)*
t = *time (s)*
K = *material constant (Pa s)*
n_0 = *number of linkages at the start of the experiment (*m^{-3}*)*
ψ = *work needed to break one linkage (Nm)*
ω = *rotational velocity in the rheometer (rev/s)*
ω_1 = *material constant (rev/s)*

Based on equation 5.14, the relationship between $\ln(T-T_E)$ with time should be linear in a semi logarithmic diagram, with a slope equal to –B. Under a certain set of circumstances, this is true, but bi-linear curves, defining two different values of B, have also been observed. The results of this study can be found in [5.1] and [5.35-5.36].

3.1.2 Structural breakdown in the narrow sense

As mentioned in the first section of this chapter, the distinction between thixotropy and the real structural breakdown is very difficult to establish in practice, as it can only be seen when the material is allowed to show build-up. Structural breakdown in its narrow sense is the consequence of the breaking of chemical “linkages” under shear, which have been formed during the hydration process of the concrete or cement paste [5.1][5.4]. As a result, structural breakdown will cause a decrease in internal structure and consequently a decrease in yield stress and viscosity, similar to

thixotropic breakdown. On the other hand, the build-up is not as fast as for thixotropy and it can be that the build-up due to hydration is not reversible, leading to loss of workability.
In a recent paper, Wallevik has combined the thixotropic behaviour and structural breakdown in a numerical model of 19 parameters in order to simulate the results of rheometer tests much more accurately [5.4]. Structural breakdown has been taken into account in the variations in yield stress and plastic viscosity by adding an additional term in equations 5.8 and 5.9, similar as the thixotropic terms. The results of the simulations in [5.4] are astonishing, but the model appears to be inapplicable to any practical situation.

3.2 Consequences

When shearing concrete or cement paste at rather high shear rates, not only thixotropy will decrease the rheological parameters, but also structural breakdown. In order to distinguish between the two effects, thixotropic build-up should be awaited at a certain shear rate, and the resulting increase in shear stress is due to thixotropy. In practice, the distinction is not so clear, and as a consequence, the occurring effects are suspected to be the result of only thixotropy or structural breakdown. As a result, structural breakdown enhances the effect of decreasing the structural state with increasing shear rate (fig. 5.6), but with decreasing shear rate, the structural state is not influenced in the same way.
In the remaining part of this thesis, especially in chapter 9, it is not certain whether thixotropy is occurring and if it does occur, its magnitude cannot be determined. In this case, the name structural breakdown refers to both the breaking of the chemical linkages and the breaking of the coagulations due to thixotropy, reflecting structural breakdown in its broad sense.

4 Loss of workability

4.1 Testing procedure

Measurements in order to investigate the loss of workability have been performed with the Tattersall Mk-II rheometer on the main part of the 59 SCC mixes for explicit rheometer testing. The mixing was performed according to the procedure described in section 3.2.1 of chapter 4. The initial test results, which have been used for the analyses performed in chapter 4, have been determined at an age of 15 minutes (15 minutes after water addition). Depending on the workability retention, the SCC has undergone additional measurements at 30, 60, 90, 120 or 150 minutes of age. A full list of the measurements performed can be found in Appendix B.

The concrete has not been re-mixed before each measurement. In this way, thixotropy has an influence on the results of slump flow and V-funnel flow time. The concrete in the rheometer on the other hand, has undergone a pre-shearing period before each test in order to eliminate thixotropy. In this way, the reference state of the concrete in the rheometer has been defined by the maximal shear rate occurring in the rheometer [5.16]. When the initial measurement of the concrete has not been performed at an age of 15 minutes, or if the concrete did not show a sufficient structural breakdown (both due to the breaking of thixotropic and chemical connections) during the pre-shearing at an age of 15 minutes, the results have not been incorporated in this analysis. In this way, only rheometer results determined at the same time and with the same reference state are compared.

4.2 Evolution in time of different parameters

The values of yield stress, viscosity at a shear rate of 5/s, shear thickening (c/μ), slump flow and V-funnel flow time at a certain time are divided by the corresponding value obtained at 15 minutes of age. In this way, the relative parameters can be plotted as a function of time (t - 15 min) (fig. 5.7). Examining the obtained results delivers the following general relationships (eq. 5.16-5.19):

$$\frac{\tau_{0,t}}{\tau_{0,15}} = e^{(A_{YS}\cdot(t-15))} \tag{5.16}$$

$$\frac{\mu_{5,t}}{\mu_{5,15}} = 1 + A_{visc}\cdot(t-15) \tag{5.17}$$

$$\frac{SF_t}{SF_{15}} = e^{(-A_{SF}\cdot(t-15))} \tag{5.18}$$

$$\frac{VF_t}{VF_{15}} = e^{(A_{VF}\cdot(t-15))} \tag{5.19}$$

where: *t = concrete age at which the parameter has been determined (min)*
Indices "t" and "15" indicate the value of the parameter at time "t" or the initial value (at t = 15 min)
τ_0 = yield stress (Pa)
μ_5 = tangential viscosity at a shear rate of 5/s (Pa s)
SF = slump flow (mm)
VF = V-funnel flow time (s)
A_x = characteristic value for parameter x (1/s)

Equations 5.16 and 5.17 show the relative increase in yield stress (exponentially) and viscosity (linearly) with time, purely due to loss of workability, which is in great accordance with the results obtained by Petit et al. [5.2]. Shear thickening is found to have no significant variations within the time frames measured. The values of A_{YS} or A_{visc} are constants for each concrete and determine how fast the yield stress and viscosity increase with time. Equations 5.18 and 5.19 show the evolution of slump flow and V-funnel flow time with time, but as mentioned previously, thixotropy has not been eliminated from these parts of the concrete. As a result, the time variation is a combined effect of loss of workability and thixotropy. Furthermore, equation 5.18 is only valid for SCC with SP 1, while for concrete with SP 2, no uniform relationship has been observed. Most concretes with SP 2 showed a slight increase in slump flow until 60 minutes of age, followed by a sharp decrease around 90 or 120 minutes of age.

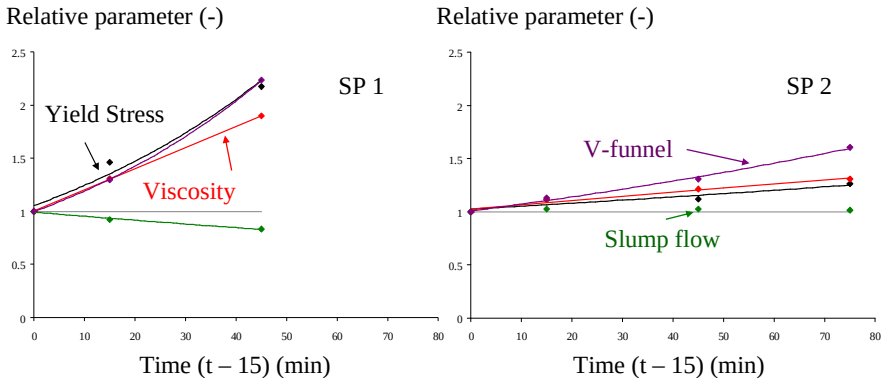

Figure 5.7: Time evolution of yield stress (black) and viscosity (red) due to loss of workability; and slump flow (green) and V-funnel flow time (purple) due to a combination of thixotropy and loss of workability, for the reference mix made with SP 1 (left) which has a short workability retention and the reference mix made with SP 2 (right) which has a longer workability retention.

The following discussion will only focus on the evolution of yield stress and viscosity, as only in these parameters the pure loss of workability is reflected.

4.3 Influencing parameters

4.3.1 SCC with SP 2 (long workability retention)

Analysis has indicated that both A_{YS} and A_{visc} decrease with increasing sp/c content. This means that yield stress and viscosity increase slower with increasing sp/c content. The effect of the w/c-ratio is similar, but less intense. A significant influence of temperature (which has not been controlled during the tests, but only measured) has not been found, which is in contradiction with the results of Petit et al. [5.2][5.37-5.38].

4.3.2 SCC with SP 1 (short workability retention)

The results for SCC with SP 1 are less straightforward to analyse. These results show a larger scatter and the good relationships obtained for SCC with SP 2 have not been observed. Instead, increasing temperature has been found to increase A_{YS} and A_{visc}, and also increases in w/c-ratio tend to increase the values of A_{YS} and A_{visc}. The influence of sp/c is not easy to determine and even shows the opposite as for SP 2. It can be that the lower correlation of the relationships for SCC with SP 1 is due to a certain loss of workability between the addition of the SP and the initial test. In this way, the reference measurements are not real references, while for SP 2, not much variation between the initial values of the SCC and the initial measurements are assumed.
On the other hand, A_{YS} and A_{visc} appear to be linearly related, for both SP, indicating that changing a certain parameter in the composition influences the time evolution of yield stress and viscosity in the same way.

5 Influence of thixotropy on rheological measurements

5.1 Pre-shearing or pre-mixing

As mentioned in the previous chapter when dealing with measurement artefacts, thixotropy can cause apparent shear thickening in concrete [5.25][5.39-5.40]. When at the highest shear rates during the rheological measurements the internal structure is still breaking down and consequently, it is not in equilibrium, an overestimation of the shear stresses at these shear rates is obtained (fig. 5.8). As a result, it is important to bring the concrete in its "reference state", which corresponds to the highest shear rates the concrete undergoes during testing. Mostly, the reference state can be imposed by mixing the concrete in the mixer before each measurement. A second method, when only the rheological properties (and perhaps their evolution in time) are needed, is by imposing the largest shear rate at which the concrete will be tested during a sufficiently long time in order to obtain the equilibrium structure corresponding to this specific shear rate.

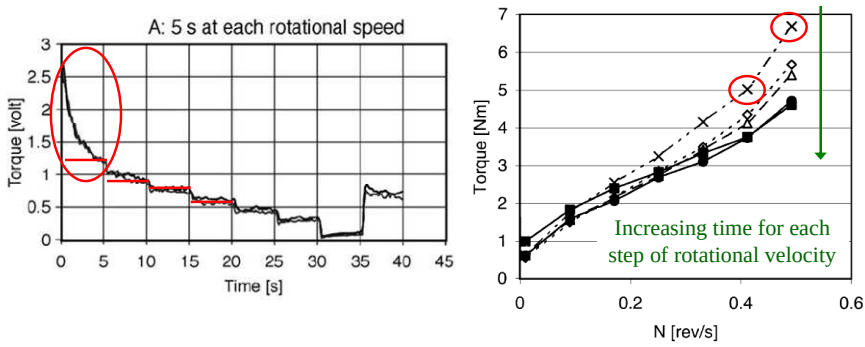

Figure 5.8: When at the highest rotational velocities the equilibrium structure has not been reached, the flow curve can apparently become shear thickening. A sufficiently long pre-shearing period or a sufficiently long time step at each rotational velocity (green arrow) will eliminate this measurement artefact, indicated with the red circles. Figure from M.R. Geiker et al. [5.39].

A typical time needed to pre-shear the concrete varies between 30 and 60 seconds, which is in accordance with the theory of Jarny et al. [5.24] saying that the timescale of the transient, thixotropic behaviour is of the order between 10 and 100 seconds. On the other hand, measurements must be performed relatively fast, in order to avoid any influence of the loss of workability during the measurements.

5.2 Flow bifurcation

For thixotropic materials, recent studies have shown that the flow in a rheometer is not occurring as predicted by the standard yield stress models. In several papers [5.18][5.24][5.41-5.43], Coussot and co-workers have shown that there exists a

"critical shear rate" under which the material does not flow homogeneously, which has been visualized by means of MRI-measurements in a wide-gap Couette rheometer. If an apparent shear rate lower than the critical shear rate is imposed, the material will divide itself into an unsheared part and a part being sheared at the critical shear rate. Decreasing the apparent (imposed) shear rate will decrease the thickness of the sheared zone. The velocity profile, measured by MRI in a large gap Couette geometry shows a discontinuous variation, which is shown in figure 5.9.

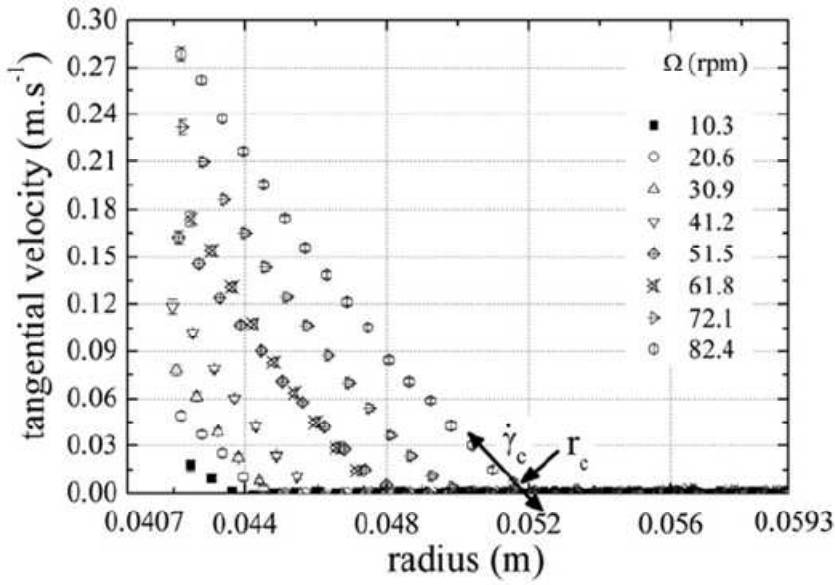

Figure 5.9: MRI-velocity measurements in a large gap Couette geometry, showing clearly the discontinuous variations in velocity and the critical shear rate. Figure from S. Jarny et al. [5.24].

Explaining this effect in detail would be beyond the scope of this thesis, but the background is hidden in the Coussot model (eq. 5.10-5.11). For a given shear stress, depending on the initial (local) value of the structure parameter, the structure parameter λ will evolve to its equilibrium value or to infinite, which indicates flow stoppage. In a wide gap rheometer, the shear stress varies with the inverse of the radius squared, resulting in a zone which will continue flowing with a shear rate equal to or larger than the critical shear rate, and a zone which will stop flowing in time, due to the increase in the structure parameter.
As cement based materials are thixotropic, this effect can have its consequences on the measured values of yield stress and viscosity of these materials. On the other hand, as it is a transient phenomenon, it is quite difficult to determine the effect without MRI tools.

5.3 What is the real rheological curve?

As the equilibrium structure (U_3 or λ) depends on the shear rate, it can be questioned what the real rheological curve of a thixotropic material is. In figure 5.10, the black lines represent the rheological curves with constant structure [5.44]. These curves must be determined faster than the time during which any change due to thixotropy takes place in the material. This is the current method of determining the rheological properties of a cement based material. The structure is imposed by pre-shearing or mixing and should be maintained during the entire measurement. This last part, namely maintaining the imposed structure, is not always easy to achieve. When lowering the shear rate in the rheometer, the cement paste or concrete has the tendency to rebuild the internal structure, and the larger the difference between the imposed structure and the equilibrium structure at these lower shear rates, the faster the rebuild.

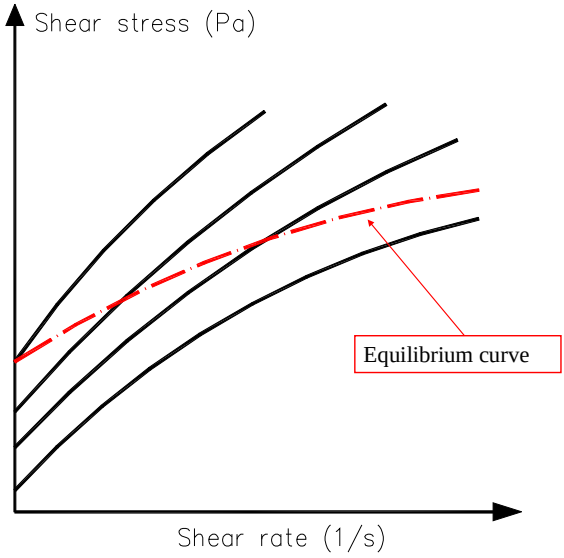

Figure 5.10: The black lines represent the flow curves of a thixotropic material with a constant structure, while the red line forms the equilibrium curve. Figure after D.C.-H. Cheng [5.44].

On the other hand, the red curve in figure 5.10 represents the equilibrium curve, connecting each data point of which the rheological properties have been determined in equilibrium [5.44]. This kind of measurement can also be performed on concrete, by decreasing the shear rate stepwise and waiting for equilibrium at each step. It can also be achieved by stepwise increasing the shear rate from zero and waiting for equilibrium due to structural breakdown (again, structural breakdown is in this case the combined effect of the real structural breakdown and the thixotropic

breakdown). The disadvantage of this method is that it is very time consuming, and possibly, loss of workability can start to influence the results. Moreover, the current rheometers are not equipped with a procedure to perform this type of measurements. As can be seen, both methods have their shortcomings and the 'real' rheological curve depends on definitions and agreements. For cement based materials, the real rheological curve is defined as the one which is obtained at the reference structural state [5.16], although discussions may arise on what the reference state is. It should correspond with the practical application of the cement paste or concrete, although in some cases, this is not easy to achieve. This leads us back to the discussion at the end of chapter 3, dealing with the range of shear rates which should be imposed on the material.

6 Summary

In this chapter, the time dependent rheological behaviour, being thixotropy, structural breakdown and loss of workability of cement based materials has been described.

Thixotropy can be described by means of several models. The microstructural models, like the modified Hattori-Izumi theory, relate the internal structure (number of reversible junctions or the size of the agglomerates) to the variations in yield stress and viscosity. Although these models are very close to the physical reality, practical applications are restricted due to the high number of parameters which must be determined through experiments and numerical calculations.

A more simplified model, developed by Roussel, describes the evolution of static yield stress during rest and during shear. For this model, only 2 parameters need to be determined, of which A_{thix}, which corresponds to the rate of increase of the static yield stress due to build-up is the most important one. This model has been applied in order to predict the influence of thixotropy on multi-layer casting.

The procedure with sudden changes in the shear rate, applied by Khayat and co-workers, is dependent on a lot of measuring parameters, but it is applicable to practical situations.

The most easy way to determine the thixotropic properties is by calculating the breakdown area (A_b) between the up- and down-curves in a loop experiment. On the other hand, the real physical meaning of A_b is not known and the results are very sensitive to the way of execution of the test.

Structural breakdown is very difficult to distinguish from thixotropy, and has approximately the same consequences as thixotropic breakdown. The only difference is that the broken linkages due to structural breakdown do not build-up fast. Consequently, structural breakdown has been defined in two different ways. In its broad sense, it incorporates thixotropic breakdown and the torque (or shear stress) shows an exponential decay at constant rotational velocity (or shear rate). In its narrow sense, it is more difficult to describe, and similar equations as for thixotropic breakdown have been suggested.

The influence of loss of workability of several SCC mixes on the rheological properties has been determined experimentally. Within the time frame measured, yield stress appears to increase exponentially, the viscosity increases linearly and the shear thickening remains approximately constant. An attempt has been made to determine the influence of the concrete composition on the rate of increase of the rheological properties.

In the last part of this chapter, it has been shown that insufficient understanding of thixotropy and structural breakdown can lead to wrong experimental results. Furthermore, the time dependent behaviour of cement based materials complicates the execution of rheological measurements significantly.

7 References

[5.1] Tattersall G.H., Banfill P.F.G., "The rheology of fresh concrete," Pitman, London (1983).

[5.2] Petit J.-Y., Wirquin E., Vanhove Y., Khayat K., "Yield stress and viscosity equations for mortars and self-consolidating concrete," Cem. Conc. Res. **37** (2007), 655-670.

[5.3] Wallevik J.E., "Rheology of particle suspensions, Fresh concrete, mortar and cement paste with various types of lignosulphonates," Ph-D dissertation, The Norwegian University of Science and Technology, Trondheim (2003).

[5.4] Wallevik J.E., "Rheological properties of cement paste: Thixotropic behavior and structural breakdown," Cem. Conc. Res. **39** (2009), 14-29.

[5.5] Hattori K., "Electrokinetics and rheological behaviour of cement suspensions," Department of Civil Engineering, Chuo University, Tokyo.

[5.6] Hattori K., Izumi K., "A new viscosity equation for non-newtonian suspensions and its application," in "Rheology of Fresh Cement and Concrete," Proc. of the Int. Conf. organized by the British Society of Rheology, Liverpool (1990).

[5.7] Tattersall G.H., "Structural breakdown of cement paste at constant rate of shear," Nature **175** (1955), 166.

[5.8] Tattersall G.H., "The rheology of Portland cement paste," British Journal of Applied Physics **6** (1955), 165-167.

[5.9] Neville A.M., Brooks J.J., "Concrete technology," Logman scientific and technical, Harlow (1987).

[5.10] Flatt R.J., Houst Y.F., "A simplified view on the chemical effects perturbing the action of superplasticizers," Cem. Conc. Res. **31** (2001), 1169-1176.

[5.11] Mewis J., "Thixotropy – a general review," J. non-Newt. Fluid Mech. **6** (1979), 1-20.

[5.12] Barnes H.A., "Thixotropy – a review," J. non-Newt. Fluid Mech. **70** (1997), 1-33.

[5.13] Wallevik J.E., "Computational rheology thixotropic explorations of cement pastes; an introduction," Proc. of the 3rd Int. Symp. on SCC, Reykjavik (2003), 41-48.

[5.14] Chougnet A., Palermo T., Audibert A., Moan M., "Rheological behaviour of cement and silica suspensions: Particle aggregation modelling," Cem. Conc. Res. **38** (2008), 1297-1301.

[5.15] Billberg P., "Form pressure generated by self-compacting concrete – Influence of thixotropy and structural behaviour at rest," Ph-D dissertation, School of Architecture and Built Environment, Stockholm (2006).

[5.16] Roussel N., "A thixotropy model for fresh fluid concretes: Theory, validation and applications," Cem. Conc. Res. **36** (2006), 1797-1806.

[5.17] Roussel N., "Rheology of fresh concrete: from measurements to predictions of casting processes," Mat. Struct. **40** (2007), 1001-1012.

[5.18] Roussel N., Le Roy R., Coussot P., "Thixotropy modelling at local and macroscopic scales," J. non-Newt. Fluid Mech. **117** (2004), 85-95.

[5.19] Roussel N., "Steady and transient flow behaviour of fresh cement pastes," Cem. Conc. Res. **35** (2005), 1656-1664.

[5.20] Billberg P., Österberg T., "Thixotropy of self-compacting concrete," Proc. of the 2nd Int. Symp. on SCC, Tokyo (2001), 99-108.

[5.21] Roussel N., Ovarlez G., "A physical model for the prediction of lateral stress exerted by self-compacting concrete on formworks," Proc. of the 2nd Int. Symp. on Advances in Concrete through science and Engineering, Québec-City (2006).

[5.22] Mahaut F., Chateau X., Coussot P., Ovarlez G., "Yield stress and elastic modulus of suspensions of noncolloidal particles in yield stress fluids, " J. Rheol. **52** (2008), 287-313.

[5.23] Mahaut F., Mokéddem S., Chateau X., Roussel N., Ovarlez G., "Effect of coarse particle volume fraction on the yield stress and thixotropy of cementitious materials," Cem. Conc. Res. **38** (2008), 1276-1285.

[5.24] Jarny S., Roussel N., Le Roy R., Coussot P., "Modelling thixotropic behavior of fresh cement pastes from MRI measurements, " Cem. Conc. Res. **38** (2008), 616-623.

[5.25] Geiker M.R., Wallevik O.H., "Rheology of cement based materials," DTU-RILEM Doctoral course, Lyngby (2007).

[5.26] Khayat K.H., Saric-Coric M., Liotta F., "Influence of thixotropy on Stability Characteristics of Cement Grout and Concrete," ACI – Mat. J. **99:3** (2002), 234-241.

[5.27] Assaad J., Khayat K.H., "Assessment of Thixotropy of Self-Consolidating Concrete and Concrete-Equivalent-Mortar – Effect of Binder Composition and Content," ACI – Mat. J. **101:5** (2004), 400-408.

[5.28] Assaad J., Khayat K.H., "Formwork Pressure of Self-Consolidating Concrete made with Various Binder Types and Contents," ACI – Mat. J. **102:4** (2005), 215-223.

[5.29] Assaad J.J., Khayat K.H., "Effect of Viscosity-Enhancing Admixtures on Formwork Pressure and Thixotropy of Self-Consolidating Concrete," ACI - Mat. J. **103:4** (2006), 280-287.

[5.30] Khayat K.H., Assaad J.J., "Use of Thixotropy-Enhancing Agent to Reduce Formwork Pressure exerted by Self-Consolidating Concrete," ACI – Mat. J., **105:1** (2008), 88-96.

[5.31] Ferron R.D., Gregori A., Sun Z., Shah S.P., "Rheological Method to Evaluate Structural Buildup in Self-Consolidating Concrete Cement Pastes," ACI – Mat. J. **104:3** (2007), 242-250.

[5.32] Fernàndez-Altable V., Casanova I., "Influence of mixing sequence and superplasticiser dosage on the rheological response of cement pastes at different temperatures," Cem. Conc. Res. **36** (2006), 1222-1230.

[5.33] Koehler E.P., Keller L., Gardner N.J., "Field measurements of SCC rheology and formwork pressures," Proc. of the 5th Int. RILEM Symp. on Self-Compacting Concrete, Ghent (2007), 411-416.

[5.34] Oesterheld S., Müller F.V., Wallevik O.H., "The influence of workability loss and thixotropy on formwork pressure in self-compacting concrete containing stabilizers," Proc. of the 3rd North-American Conf. on Self-Consolidating Concrete, Chicago (2008).

[5.35] Dimond C.R., "The rheology of cement pastes," Ph-D dissertation, University of Sheffield, Sheffield (1975).

[5.36] Tattersall G.H., Dimond C.R., "Hydraulic cement pastes: their structure and properties," Proc. of a conference held at the university of Sheffield, Publication 15.121, Slough, Cement and Concrete Association (1976), 118-133.

[5.37] Petit J.-Y., Khayat K.H., Wirquin E., "Coupled effect of time and temperature on variations of yield value of highly flowable mortar," Cem. Conc. Res. **36** (2006), 832-841.

[5.38] Petit J.-Y., Wirquin E., Duthoit B., "Influence of temperature on yield value of highly flowable micromortars made with sulfonate-based superplasticizers," Cem. Conc. Res. **35** (2005), 256-266.

[5.39] Geiker M.R., Brandl M., Thrane L.N., Bager D.H., Wallevik O.H., "The effect of measuring procedure on the apparent rheological properties of self-compacting concrete," Cem. Conc. Res. **32** (2002), 1791-1795.

[5.40] Geiker M., "On the combined effect of measuring procedure and coagulation rate on apparent rheological properties," Proc. of the 3rd Int. Symp. on SCC, Reykjavik (2003), 35-40.

[5.41] Jarny S., Roussel N., Rodts S., Bertrand F., Le Roy R., Coussot P., "Rheological behavior of cement pastes from MRI velocimetry," Cem. Conc. Res. **35** (2005), 1873-1881.

[5.42] Coussot P., Ragouilliaux A., Ovarlez G., Herzhaft B., "Transition from a simple yield stress fluid to a thixotropic material," Proc. of the XVth Int. Congress on Rheology, Monterey (2008), 713-715.

[5.43] Ragouilliaux A., Herzhaft B., Ovarlez G., Coussot P., "Aging and yielding of colloidal suspensions by MRI velocimetry," Proc. of the XVth Int. Congress on Rheology, Monterey (2008), 1033-1035.

[5.44] Cheng D.C.-H., "Hysteresis Loop Experiments and the Determination of Thixotropic Properties," Nature **216** (1967), 1099-1100.

PART II:

PRESSURE DRIVEN CONCRETE FLOW

CHAPTER 6:

THE POISEUILLE FORMULA FOR LAMINAR FLOW

In this chapter, the link between rheology on one side and hydraulics on the other side will be discussed. This specific chapter is a purely theoretical one, where in a first part, the Poiseuille formula for laminar flow will be "re-derived", starting from the universal shear stress distribution law. In a second part, the Poiseuille formula for Newtonian liquids will be extended for materials like fresh concrete. The practical applications of the obtained extended versions will be given in chapters 7 and 9, dealing with gravitational flow tests and full scale pumping tests with SCC. The advantage of these extended versions is that the pressure loss can be predicted based on the values of discharge, the rheological properties and the geometry of the pipe. The Weissenberg-Rabinowitsch correction [6.1], presented in chapter 3 (eq. 3.11) when discussing capillary rheometers, works in the opposite way, meaning that the rheological properties are obtained from the values of pressure loss, discharge and the capillary geometry. This correction does not provide the exact solution for shear thickening yield stress materials, like fresh SCC, as will be discussed in chapter 7.

1 The Poiseuille formula for Newtonian liquids

1.1 Conditions of use

The original Poiseuille formula for laminar flow can only be applied if the following conditions are fulfilled [6.1-6.4]:

- The flow is fully developed and isothermal
- The liquid is incompressible and homogeneous
- The flow is one-dimensional, with no radial or tangential flow component
- The flow must be steady and in laminar conditions
- No slippage at the wall is allowed
- The liquid must be Newtonian

1.2 Derivation of the original Poiseuille formula

In this section, the Poiseuille formula will be derived, starting from a known wall shear stress and known rheological properties (viscosity). The information in this section is quite trivial, but it serves as a guideline for the next section, when deriving extended versions of this formula for non-Newtonian liquids.
When a certain pressure loss over a certain length is known, the shear stress at the wall can be calculated according to equations 6.1 and 6.2, which express an equilibrium of forces in case of cylindrical pipes. Note that equations 6.1 and 6.2 are also valid for non-Newtonian materials.

$$\Delta p_{tot} \cdot \pi \cdot R^2 = 2 \cdot \pi \cdot \tau_w \cdot R \cdot L \tag{6.1}$$

$$\tau_w = \frac{\Delta p_{tot}}{L} \cdot \frac{R}{2} = \Delta p \cdot \frac{R}{2} \tag{6.2}$$

where: Δp_{tot} *= total pressure loss over the length L of the pipe (Pa)*
R *= radius of the pipe (m)*
τ_w *= shear stress at the wall (Pa)*
L *= length of the section (m) (over which the total pressure loss is measured)*
Δp *= pressure loss per unit of length (Pa/m)*

As mentioned in chapter 3, when dealing with the capillary rheometers, the evolution of shear stress inside a circular pipe varies linearly from zero in the centre to the maximal value (wall shear stress) near the wall (eq. 6.3) [6.1]. This law is a so called universal law, meaning it is independent of the rheological properties of the material.

$$\tau_r = \tau_w \cdot \frac{r}{R} \tag{6.3}$$

where: τ_r *= shear stress at a distance r from the centre of the pipe (Pa)*
r *= radial parameter, varying between 0 in the centre to R at the wall (m)*

Incorporating the Newtonian rheological model (eq. 6.4) into equation 6.3 delivers the shear rate at a distance r from the centre (eq. 6.5).

$$\tau = \eta \cdot \dot{\gamma} \tag{6.4}$$

$$\dot{\gamma}_r = \frac{\tau_w}{\eta} \cdot \frac{r}{R} \tag{6.5}$$

where: η *= viscosity of the material (Pa s)*
$d\gamma/dt$ *= shear rate (1/s)*

$(d\gamma/dt)_r$ = shear rate at position r (1/s)

Integrating equation 6.5 to "-r", with as integration constant the velocity at the wall, being zero according to the no-slip condition, delivers the velocity as a function of the radius (eq. 6.6), as it is assumed that there is no radial nor tangential flow component:

$$v_r = \frac{1}{2} \cdot \frac{\tau_w}{\eta} \left(\frac{R^2 - r^2}{R} \right) \tag{6.6}$$

where: *v_r = velocity at position r (m/s)*

Integrating the velocity distribution over the area of the pipe delivers the discharge or flow rate Q (eq. 6.7), and when substituting the wall shear stress by means of equation 6.2, the Poiseuille formula for laminar flow of Newtonian liquids in cylindrical pipes is obtained (eq. 6.8).

$$Q = \frac{1}{4} \cdot \frac{\pi \cdot \tau_w \cdot R^3}{\eta} \tag{6.7}$$

$$Q = \frac{1}{8} \cdot \frac{\pi \cdot \Delta p \cdot R^4}{\eta} = \frac{1}{128} \cdot \frac{\pi \cdot \Delta p_{tot} \cdot D^4}{\eta \cdot L} \tag{6.8}$$

where: *Q = discharge (m³/s)*

As a result, the Poiseuille formula states that the total pressure loss is linearly dependent on the discharge, the length of the pipe and the viscosity, and it is inversely dependent on the diameter to the power of 4. Generally, the Poiseuille formula is written as Δp_{tot} being a function of Q, but as this explicit writing is not straightforward in the next section, the equation is kept in the form presented in eq. 6.8.

2 Extended Poiseuille formulae for non-Newtonian liquids

2.1 Non-Newtonian rheological models

As the purpose of this chapter is to define an extended version of the Poiseuille formula for fresh concrete, the three models applicable for concrete, discussed in chapter 4, which are the Bingham model (eq. 6.9) [6.5], Herschel-Bulkley (eq. 6.10) [6.6] and the modified Bingham model (eq. 6.11) [6.7-6.8], will be applied.

$$\tau_B = \tau_{0,B} + \mu_{p,B} \cdot \dot{\gamma}_B \tag{6.9}$$

$$\tau_{HB} = \tau_{0,HB} + K_{HB} \cdot \dot{\gamma}_{HB}^{\,n_{HB}} \tag{6.10}$$

$$\tau_{MB} = \tau_{0,MB} + \mu_{MB} \cdot \dot{\gamma}_{MB} + c_{MB} \cdot \dot{\gamma}_{MB}^{\,2} \tag{6.11}$$

where: the indices B, HB, MB indicate the Bingham, Herschel-Bulkley or modified Bingham parameters.

2.2 Shear rate as a function of the radial parameter

As the shear stress distribution is a universal law, independent of the rheological properties, the shear rate at a certain distance r from the centre of the pipe can be calculated by incorporating equations 6.9, 6.10 or 6.11 into equation 6.3:

$$\dot{\gamma}_{r,B} = \frac{\tau_w \cdot \frac{r}{R} - \tau_{0,B}}{\mu_{p,B}}, \text{ for } r > r_{plug}, \text{ otherwise } 0 \tag{6.12}$$

$$\dot{\gamma}_{r,HB} = \left(\frac{\tau_w \cdot \frac{r}{R} - \tau_{0,HB}}{K_{HB}} \right)^{\frac{1}{n_{HB}}}, \text{ for } r > r_{plug}, \text{ otherwise } 0 \tag{6.13}$$

$$\dot{\gamma}_{r,MB} = \frac{-\mu_{MB} + \sqrt{\mu_{MB}^{\,2} + 4 \cdot c_{MB} \cdot \tau_w \cdot \frac{r}{R} - 4 \cdot c_{MB} \cdot \tau_{0,MB}}}{2 \cdot c_{MB}}, \text{ for } r > r_{plug},$$

$$\text{otherwise } 0 \tag{6.14}$$

$$r_{plug} = \frac{\tau_0}{\tau_w} \cdot R \tag{6.15}$$

Equation 6.15 defines the radius at which the material is divided in a unsheared and a sheared part. The unsheared part is also called the plug, and is well known in case

of pumping [6.9]. Note that the "Herschel-Bulkley" shear rate at the plug radius shows an inclination equal to infinity, for $n_{HB} > 1$.
The evolution of the shear rate across the pipe is shown in figure 6.1, for a yield stress = 20 Pa, all viscosity parameters = 10 Pa s, the flow index n = 1.2, c = 0.5, the wall shear stress = 100 Pa and the pipe radius being 0.1 m.

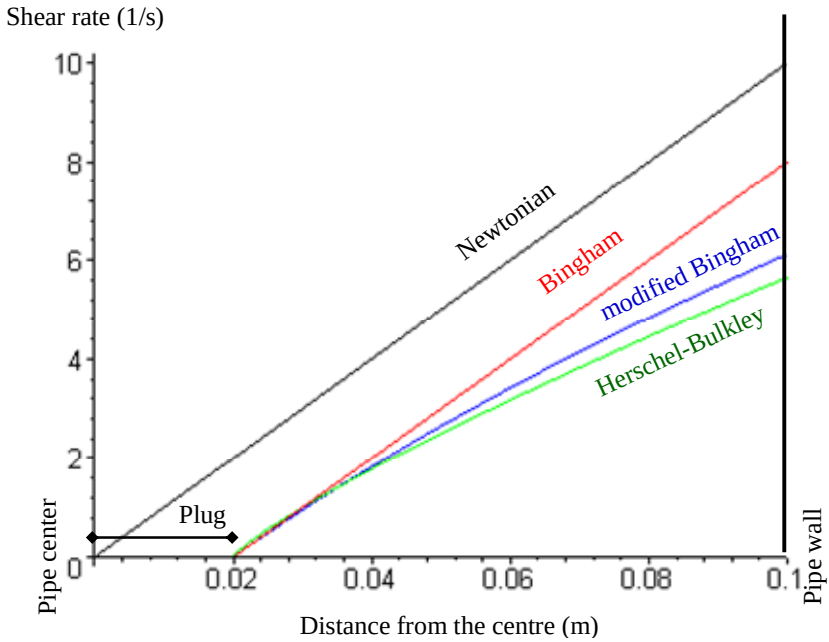

Figure 6.1: Evolution of shear rate across the pipe for a Newtonian (black), a Bingham (red), a Herschel-Bulkley (green) and a modified Bingham material (blue). Note that for all yield stress materials, a zone with zero shear rate exists, causing plug flow.

2.3 Velocity as a function of the radial parameter

The same procedure as for Newtonian liquids must be applied: the velocity distribution has been obtained by integrating the shear rate equations to –r, and imposing zero velocity at the wall.

$$v_{r,B} = \frac{1}{2} \cdot (r - R) \cdot \frac{\tau_w \cdot R + \tau_w \cdot r - 2 \cdot \tau_{0,B} \cdot R}{\mu_{p,B} \cdot R}, \text{ for } r > r_{plug}$$

$$v_{r,B} = \frac{1}{2} \cdot R \cdot \frac{(\tau_{0,B} - \tau_w)^2}{\mu_{p,B} \cdot \tau_w}, \text{ otherwise} \qquad (6.16)$$

$$v_{r,HB} = -\frac{R \cdot K_{HB} \cdot n_{HB}}{\tau_w \cdot (1+n_{HB})} \cdot \left(\left(\frac{\tau_w \cdot r - \tau_{0,HB} \cdot R}{R \cdot K_{HB}} \right)^{\left(\frac{1+n_{HB}}{n_{HB}}\right)} - \left(\frac{\tau_w - \tau_{0,HB}}{K_{HB}} \right)^{\left(\frac{1+n_{HB}}{n_{HB}}\right)} \right),$$

for $r > r_{plug}$

$$v_{r,HB} = \frac{R \cdot K_{HB} \cdot n_{HB}}{\tau_w \cdot (1+n_{HB})} \cdot \left(\frac{\tau_w - \tau_{0,HB}}{K_{HB}} \right)^{\left(\frac{1+n_{HB}}{n_{HB}}\right)}, \text{ otherwise} \quad (6.17)$$

$$v_{r,MB} = -\frac{1}{12 \cdot {c_{MB}}^2 \cdot \tau_w} \begin{pmatrix} 6 \cdot \mu_{MB} \cdot c_{MB} \cdot \tau_w \cdot (R-r) + (X-W) \cdot {\mu_{MB}}^2 \cdot R \\ +4 \cdot X \cdot c_{MB} \cdot (\tau_w \cdot r - \tau_{0,MB} \cdot R) \\ +4 \cdot W \cdot c_{MB} \cdot R \cdot (\tau_{0,MB} - \tau_w) \end{pmatrix},$$

for $r > r_{plug}$

$$v_{r,MB} = -\frac{R}{12 \cdot {c_{MB}}^2 \cdot \tau_w} \begin{pmatrix} 6 \cdot \mu_{MB} \cdot c_{MB} \cdot (\tau_w - \tau_{0,MB}) + {\mu_{MB}}^3 - W \cdot {\mu_{MB}}^2 \\ +4 \cdot W \cdot c_{MB} \cdot (\tau_{0,MB} - \tau_w) \end{pmatrix},$$

otherwise (6.18)

with

$$X = \sqrt{\frac{{\mu_{MB}}^2 \cdot R + 4 \cdot c_{MB} \cdot \tau_w \cdot r - 4 \cdot c_{MB} \cdot \tau_{0,MB} \cdot R}{R}} \quad (6.19)$$

$$W = \sqrt{{\mu_{MB}}^2 + 4 \cdot c_{MB} \cdot \tau_w - 4 \cdot c_{MB} \cdot \tau_{0,MB}} \quad (6.20)$$

Equations 6.16 and 6.18 are visualized in figure 6.2, with equal values for all parameters as the results shown in figure 6.1. As can be seen, the velocity is constant in the plug for the yield stress materials (Bingham and modified Bingham). Due to the shear thickening, the average velocity and also the discharge, which will be shown in the next section, are lower for the modified Bingham model, compared to the result for the Bingham model. Note that equation 6.17, derived in case of Herschel-Bulkley, is giving some problems due to the infinite inclination of the shear rate function near the plug radius.

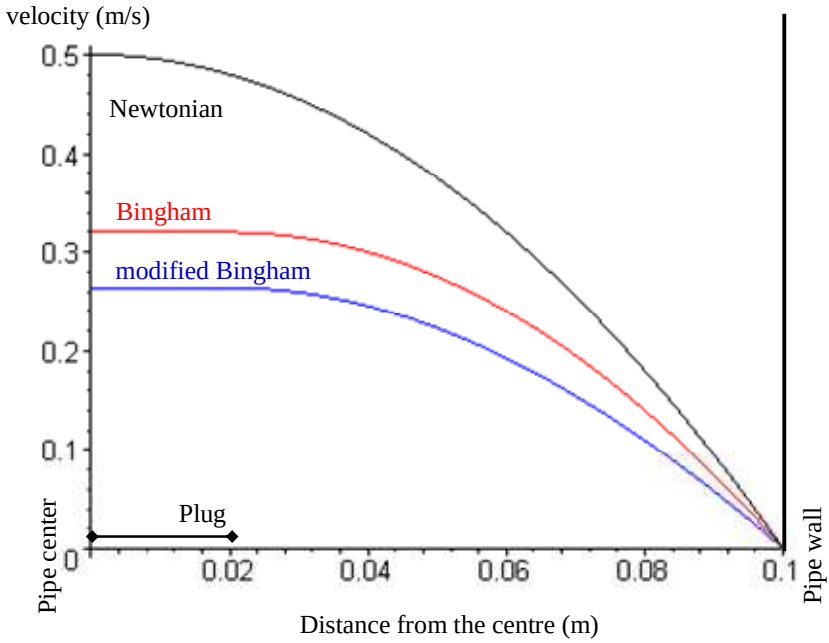

Figure 6.2: Velocity profile for a Newtonian (black), a Bingham (red) and a modified Bingham material (blue). Note that in the plug, the velocity is constant.

2.4 Determination of discharge

The discharge is calculated as the integral of the velocity distribution to the pipe area. Equations 6.21 and 6.22 give the relationship between discharge and pressure loss (or wall shear stress), for a Bingham and modified Bingham material respectively. The calculation of an analytical solution in case of a Herschel-Bulkley material is found to be impossible, but it can be approximated numerically. As mentioned in chapter 4, this is the third disadvantage of applying the Herschel-Bulkley equation to fresh concrete.

$$Q_B = \frac{3 \cdot R^4 \cdot \Delta p_{tot}{}^4 + 16 \cdot \tau_{0,B}{}^4 \cdot L^4 - 8 \cdot \tau_{0,B} \cdot L \cdot R^3 \cdot \Delta p_{tot}{}^3}{24 \cdot \Delta p_{tot}{}^3 \cdot L \cdot \mu_{p,B}} \qquad (6.21)$$

$$Q_{MB} = \frac{\pi R^3}{840 {c_{MB}}^4 {\tau_w}^3} \begin{pmatrix} -{\mu_{MB}}^7 + W{\mu_{MB}}^6 + 140\mu_{MB}{c_{MB}}^3\left({\tau_{0,MB}}^3 - {\tau_w}^3\right) \\ -2W{\mu_{MB}}^4 c_{MB}\left(\tau_w + 6\tau_{0,MB}\right) + 14{\mu_{MB}}^5 c_{MB}\tau_{0,MB} \\ -70{\tau_{0,MB}}^2{c_{MB}}^2{\mu_{MB}}^3 - 8W{c_{MB}}^3\tau_w\tau_{0,MB}\left(3\tau_w + 4\tau_{0,MB}\right) \\ +2W{\mu_{MB}}^2{c_{MB}}^2\left(3{\tau_w}^2 + 24{\tau_{0,MB}}^2 + 8\tau_w\tau_{0,MB}\right) \\ +120W{c_{MB}}^3{\tau_w}^3 - 64W{c_{MB}}^3{\tau_{0,MB}}^3 \end{pmatrix} \tag{6.22}$$

Equation 6.21 is known as the Buckingham-Reiner equation for the flow of Bingham fluids [6.10-6.12]. As can be seen, incorporating an extra term in order to include shear thickening behaviour causes the complexity of the newly found formula to increase significantly [6.13]. Dimensional analysis of equation 6.22 indicates that all terms between the brackets have a dimension of Pa^7s^7. The term before the brackets has a dimension of $m^3Pa^{-7}s^{-8}$. As a result, the dimension of the total right hand side is m^3/s, which is the proper dimension for a discharge.
Explicit functions of Δp as a function of Q, which would be very useful in practice, are not straightforward in case of Bingham and modified Bingham liquids.
For the shear rate distributions shown in fig. 6.1 and the velocity profiles of fig 6.2, the discharges equal 7.85 l/s, 5.76 l/s and 4.64 l/s for the Newtonian, Bingham and modified Bingham liquid respectively.

3 Summary

In this chapter, the derivation of the original Poiseuille formula for Newtonian liquids in laminar pipe flow has served as a guideline to obtain similar equations for concrete. In case the fresh concrete behaves as a Bingham material, the Buckingham-Reiner equation is obtained, while for SCC described by means of the modified Bingham equation, the resulting relationship between discharge and wall shear stress (pressure loss) is much more complicated. For Herschel-Bulkley materials, no analytical solution is available.

4 References

[6.1] Macosko C.W., "Rheology Principle, measurements and applications," Wiley-VCH, New-York (1994).

[6.2] Hagen G., "Ueber die Bewegung des Wassers in engen cylindrischen Rohren," Poggendorfs Ann. Phys. Chem. **46** (1839): 423-442.

[6.3] Poiseuille J.L.M., "Recherches expérimentales sur le mouvement des liquides dans les tubes de très-petits diameters," CR Acad. Sci. Paris. **11** (1840); 961-967, 1041-1049.

[6.4] Poiseuille J.L.M., "Recherches expérimentales sur le mouvement des liquides dans les tubes de très-petits diameters," CR Acad. Sci. Paris. **12** (1841), 112-115.

[6.5] Bingham E.C., "An investigation of the laws of plastic flow," U.S. Bur. Stand. Bull. **13** (1916), 309-353.

[6.6] Herschel W.H., Bulkley R., "Konsistenzmessungen von Gummi-Benzol-Lösungen," Kolloid Z. **39** (1926), 291-300.

[6.7] Yahia A., Khayat K.H., "Analytical models for estimating yield stress of high-performance pseudoplastic grout," Cem. Conc. Res. **31** (2001), 731-738.

[6.8] Feys D., Verhoeven R., De Schutter G., "Fresh self compacting concrete: a shear thickening material," Cem. Conc. Res. **38** (2008), 920-929.

[6.9] Kaplan D., "Pumping of concretes," Ph-D dissertation (in French), Laboratoire Central des Ponts et Chausées, Paris (2001).

[6.10] Buckingham E., "On plastic flow through capillary tubes." Proc. Am. Soc. Testing Mat. **21** (1921), 1154–1161.

[6.11] Skelland A.H.P., "Non-Newtonian Flow and Heat transfer," John Wiley & Sons, Inc., New York (1967).

[6.12] Brown N.P., Heywood N.I., "Slurry Handling, Design of Solid-Liquid Systems," Elsevier Applied Science, London (1991).

[6.13] Calie B., "Pumping of Self-Compacting Concrete under pressure," Master-thesis (in Dutch), Ghent-University, Ghent (2007).

CHAPTER 7:

GRAVITATIONAL FLOW TESTS

As an intermediate step between the rheological characterisation of SCC, as described in chapters 4 and 5, and the full scale pumping tests of chapters 8 and 9, a simple test setup has been worked out in order to verify the validity of the extended Poiseuille formula, derived in chapter 6. The gravitational flow tests have served as a kind of prediction tool for the design of the pumping circuits. In the first part of this chapter, the test setup and data treatment are described. The second part shows the testing procedure and the composition of the SCC-mixes, while in the third part, the results are given. In the fourth section, the results will be discussed and the extended Poiseuille formula will be applied. In the last section, the conditions of use of the Poiseuille formula will be verified.

1 Test setup

1.1 Principle

The principle of the gravitational flow tests is based on the design of a capillary rheometer [7.1]. Upstream of the capillary, there is a reservoir containing the material to be tested, on which a certain pressure can be executed. Downstream of the capillary, there is in most cases a free exit. The pressure loss over the capillary is the upstream, applied pressure, while the discharge must be measured.

1.2 Gravitational flow test setup

1.2.1 Upstream reservoir

The upstream reservoir of the gravitational flow tests is a vertical PVC-tube, with an inner diameter of 30 cm and a height of 2.3 m. At the bottom of this reservoir, a special connection system is installed in order to attach (and remove) the pipes easily. This system is equipped with a valve, which must be opened and closed manually (fig. 7.1).

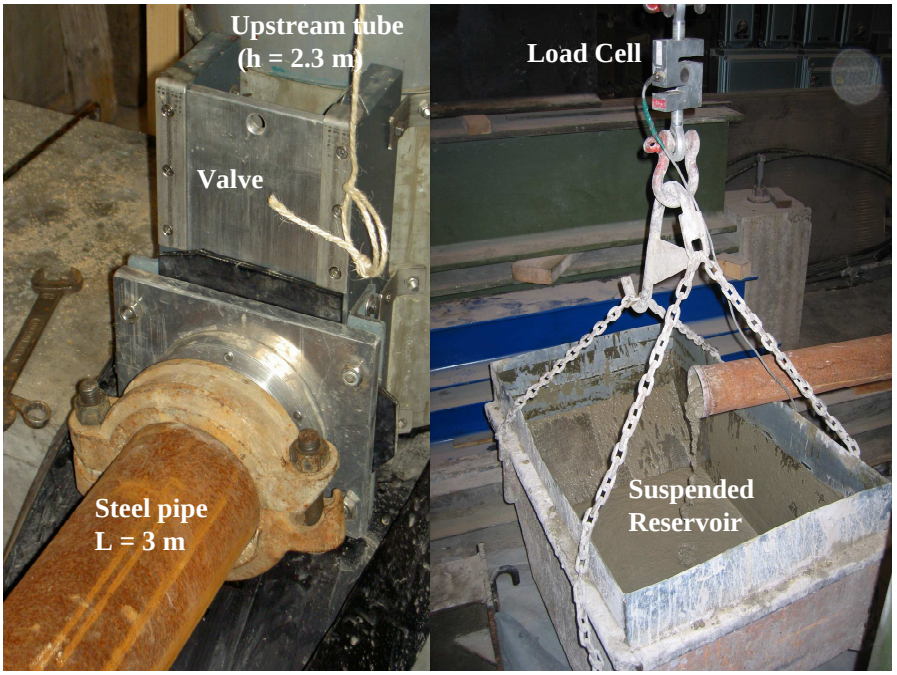

Figure 7.1: Left: the upstream reservoir, the valve (currently open) and the connection to the pipe. Right: The downstream reservoir equipped with a load cell.

1.2.2 Capillary

The capillary exists of steel pipes, with an inner diameter of 106 mm. The pipes have been treated in advance of the tests by means of pumping a sand-water solution in order to decrease the wall roughness. The roughness itself has not been measured, but literature indicates that the roughness of steel pipes is between 10 and 1000 µm [7.2]. Note that, in case of laminar flow, the roughness is of no importance [7.3].
The steel pipes are available in sections of 3 m. By connecting several pipes together, longer capillaries can be created. At both ends of each pipe, special attachment rings are foreseen. A special rubber seal keeps the connection "cement-paste-tight" and a steel clamp holds the two pipes together (fig. 7.2). For the gravitational flow tests, the total length of the connected pipes was between 3 and 12 m, while for the pumping tests described in chapters 8 and 9, longer circuits have been built in the same way.

Figure 7.2: Connection between two pipes, with a rubber seal to assure cement paste tightness and a clamp.

1.2.3 Downstream

Downstream of the capillary is a free exit, under which a reservoir is hanging. This reservoir collects the concrete flowing out of the pipe, and once the flow has stopped, the concrete is placed very easily in the upstream reservoir again (fig. 7.1).

1.3 Measurements

1.3.1 Pressure

The upstream pressure, to which the total pressure loss over the capillary is assumed to be equal, is determined by the height of the concrete in the reservoir at any time because no other force than gravity is applied. As the diameter of the reservoir is three times larger than the diameter of the pipe, the pressure loss per unit length in the upstream reservoir is 81 times smaller than in the pipe. As a result, this pressure loss during flow can be neglected. When density is known, the upstream pressure, and consequently the total pressure loss can be easily calculated (eq. 7.1):

$$p(t) = \rho_c \cdot g \cdot h_c(t) \tag{7.1}$$

where: $p(t)$ = *upstream pressure at time t (Pa)*
ρ_c = *density of the concrete (kg/m³)*
g = *gravitational acceleration (m/s²)*
$h_c(t)$ = *height of the concrete in the upstream reservoir at time t (m)*

As can be seen in equation 7.1, measuring the height of the concrete in the reservoir is sufficient to know the pressure. The height is measured by means of monitoring the displacement of a device, which is floating on top of the concrete in the reservoir (fig. 7.3-7.4).
Note that the initial height of concrete and the floating device has been calibrated before each test, while the calibration of the zero value has been executed before the first filling of the reservoir.

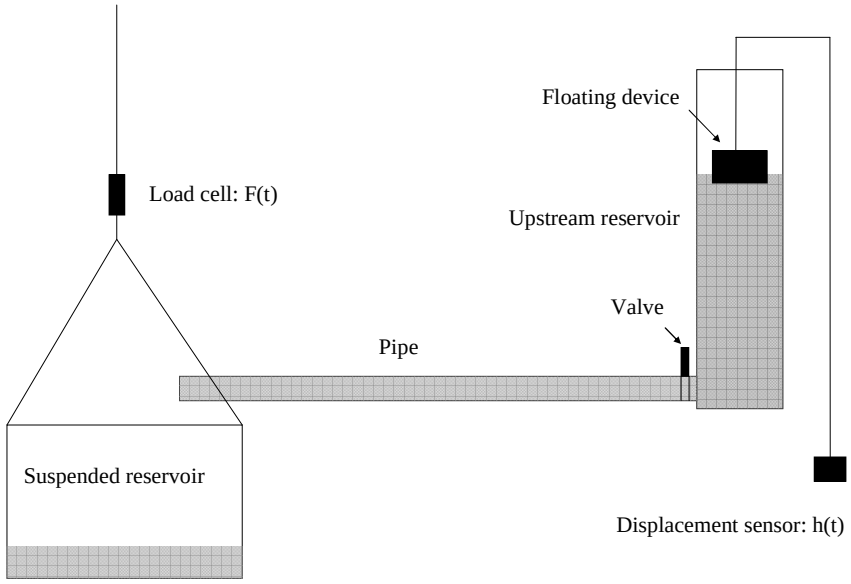

Figure 7.3: Overview of the test setup with upstream the floating device, following the height of the concrete and downstream the load cell to which the suspended reservoir is attached.

Figure 7.4: Detailed picture of the floating device.

1.3.2 Discharge

The discharge has been measured by means of the rate of change of the volume of concrete flowing out of the pipe. The downstream reservoir is suspended to a rolling bridge in the laboratory, and the connection between the reservoir and the rolling bridge is equipped with a load cell (fig. 7.1), capable of measuring forces up to 20 kN. By means of equations 7.2 and 7.3, the discharge can be easily calculated by means of the time evolution of the force executed by the downstream reservoir on the load cell.

$$V(t) = \frac{F(t) - F_0}{\rho_c \cdot g} \tag{7.2}$$

$$Q(t) = \frac{dV(t)}{dt} \tag{7.3}$$

where: *V(t) = volume of concrete in the reservoir at time t (m^3)*
F(t) = force executed by the reservoir and the concrete at time t (N)
F_0 = force executed by the empty reservoir (N)
Q(t) = discharge at time t (m^3/s)

Note that the constant F_0 in equation 7.2 is only added in order to be fully correct. It does not influence the calculation of the discharge.
Both the height of the concrete in the upstream reservoir, as the force executed by the downstream reservoir are measured with the same data acquisition system, at a rate of two measurements per second.

2 Testing procedure

The testing procedure for all 15 SCC mixes used was as follows:

- Mixing concrete, if necessary in two batches
- Determination of slump flow, density and sieve stability
- Sampling for the rheometer
- Preparation of the gravitational flow test
- First gravitational flow test + rheometer test at an age of 30 minutes
- Repetition of these tests each 30 minutes
- Cleaning

In the coming sections, each of these steps will be discussed in more detail.

2.1 Concretes tested

In total, 15 SCC mixes have been tested, of which the full table of compositions is given in Appendix C. The nomenclature of the concretes is as follows: flow-xm-y-zzmin, where "x" stands for the length of the pipe, "y" denotes the number of the mix tested at this length and "zz" indicates the age of the concrete. In the table in Appendix C, the corresponding numbers of the mixes (SCC 48, 52, …) refer to the numbering of chapter 4 and Appendix B. The composition of the main types of SCC used during the testing program is given in table 7.1.

	SCC 48	SCC 52	SCC 36
Gravel 8/16 (kg/m³)	434	459	434
Gravel 2/8 (kg/m³)	263	278	263
Sand 0/4 (kg/m³)	853	901	853
CEM I 52.5 N (kg/m³)	360	300	360
Limestone filler (kg/m³)	240	200	240
Water (l/m³)	165	165	165
SP-type	SP 2	SP 2	SP 1
W/P	0.275	0.330	0.275
Tested at	3, 6, 9, 12 m	6, 9, 12 m	3, 6 m

Table 7.1: Composition of main mixes and corresponding lengths of the pipes at which these concretes have been tested.

2.2 Mixing

The mixing procedure is equal to the mixing procedure applied in section 3.2.1 of chapter 4, but a different mixer has been applied. The largest concrete mixer in the Magnel Laboratory has a capacity of 200 l, but the mixing is less intense. As a result, a larger amount of SP is needed in case of SCC in the large mixer, compared to similar SCC produced in the small mixer. For the flow tests with a single 3 m pipe, one mix of 200 l is sufficient to execute the tests. For tests with longer pipes, more concrete is needed. Consequently, the SCC mix has been prepared in two

separate batches of 125 l each, in case of a pipe length of 6 or 9 m, or 137.5 l each in case the pipe is 12 m long.
Although both parts of the mixes contained equal amounts of all constituent materials, differences between the first and second batch occur due to the initial state of the mixer. When starting the first batch, the mixer is only pre-wetted, but between the two batches, no cleaning has been performed in order to keep the time difference as small as possible. As a result, the surface of the mixer is covered with cement paste, resulting in a larger amount of cement paste in the second SCC batch. This effect has been counteracted during the later stages of this research, by reducing the amount of SP added to the second batch.
The reference time is taken as the time at which the water is added to the second batch. As a result, the first batch is slightly older, with an average value of 7 minutes.

2.3 Determination of fresh concrete properties

In case two batches have been produced, the slump flow of the concrete of both batches has been determined, together with the density and sieve stability of a common sample of both batches. For the tests with the 3 m pipe, only one slump flow value has been determined, together with the density and sieve stability. The obtained test results can be found in Appendix C. Note that these tests have only been executed once on the SCC and that no rheometer test has been performed in this stage yet.

2.4 Sampling for the rheometer

Once the fresh concrete properties have been determined, the concrete is transported to the main hall of the laboratory, where the gravitational flow test setup is installed. Before inserting the concrete inside the test setup, the reservoir of the Tattersall Mk-II rheometer is filled with SCC. This concrete remains in the rheometer during the full testing period.

2.5 Preparation of the gravitational flow test

The concrete is placed in the upstream reservoir, with the valve between this reservoir and the pipes being open. Due to gravity, the concrete fills the pipes. As the pipes have not been prepared in any way, the cement paste attaches to the pipe walls and gradually, the relative amount of coarse aggregates increases. As a result, due to a frictional contribution to the flow resistance, the concrete slows down and possibly stops. In case of a stoppage, which can be interpreted as a blocking [7.4] (see chapter 8), its location is determined, the connection between the pipes is opened and the aggregates are removed.
Finally, a front of aggregates flows out of the last pipe (fig. 7.5). This inhomogeneous part of the concrete is removed (ca. 10 l), and once a homogeneous SCC flows out, the valve is closed. The test setup is now ready for the first measurement. During this preparation stage, no measurements have been executed.

Figure 7.5: Front of aggregates during preparation of the test.

2.6 First gravitational flow test

At a concrete age of 30 minutes, relative to the water adding time during the production of the last batch, the valve is opened again and the concrete starts flowing out of the pipe. Gradually, the upstream reservoir empties and the downstream reservoir fills up. Once the flow has stopped, the valve is closed and the concrete in the downstream reservoir is placed in the upstream reservoir again. In this way, the SCC is re-used for several tests.
Shortly after the start of the gravitational flow test, the rheological properties of the SCC have been determined with the Tattersall Mk-II rheometer in the same way as described in chapter 4.

2.7 Repetition of the gravitational flow tests

At concrete ages of 60, 90, 120, … minutes, the tests have been repeated, as long as the workability of the concrete remained sufficient to ensure a proper cleaning. The procedure is equal as in section 2.6. Between two gravitational flow tests, there is no intermediate cleaning or emptying and refilling of the test setup. The final situation of a certain test serves as the initial state for the next one.

2.8 Cleaning

Once the decision has been taken to stop the test series, the concrete is removed and the test setup is cleaned with water. After cleaning, the setup is rebuilt and ready for the next concrete to be produced. In this way, the initial conditions, except for the choice of the length of the pipe, are equal for all concretes tested.

3 Results

Before any results are given, two problems must be handled, namely the discontinuous flow and the peak in the Q(t)-curve.

3.1 Discontinuous flow

During the execution of a flow test, the outflow changes from a continuous to a discontinuous flow. In case of a discontinuous flow, the concrete drops out of the pipe (fig. 7.6), causing discrete increases in the volume in the downstream reservoir. This discontinuous flow at the end of the pipe is a typical phenomenon for yield stress liquids, but the flow inside the pipes is suspected to occur continuously, based on the continuous decrease in upstream pressure observed.

Figure 7.6: Discontinuous flow of SCC into the suspended reservoir, causing sudden increases in the volume.

As a result, difficulties arise when determining the discharge by means of equation 7.3. With the obtained discrete, sudden increases in the volume, the discharge shows several peak values, while at other times the values equal zero. This effect has been counteracted by fitting a mathematical curve onto the results of the volume variation with time. After careful considerations and several test results, curves of the form presented in equation 7.4 have been fitted to all results of all concretes [7.5]:

$$V(t) = (a \cdot \tanh(b \cdot t) + c \cdot \tanh^2(d \cdot t)) \cdot e^{(-f \cdot t)}) + g \cdot (1 - e^{(-K \cdot t^3)}) \cdot (1 - e^{(-h \cdot t)}) \quad (7.4)$$

where: *V(t) = volume at time t (m³)*
t = time (s)
a, b, c, d, f, g, h, K = parameters that need to be fitted

Equation 7.4 has two parts. The first part consists of a tanh-function and a tanh²-function, in order to describe the initial part of the test. This part has a decreasing importance with time, expressed by the exponential time-function. The second part represents an S-shaped curve, of which the final, horizontal part is the most important. This second part has an increasing importance with time (fig. 7.7). Note that this equation is only a tool to facilitate the data treatment, but there is no explicit physical meaning for any of the parameters.

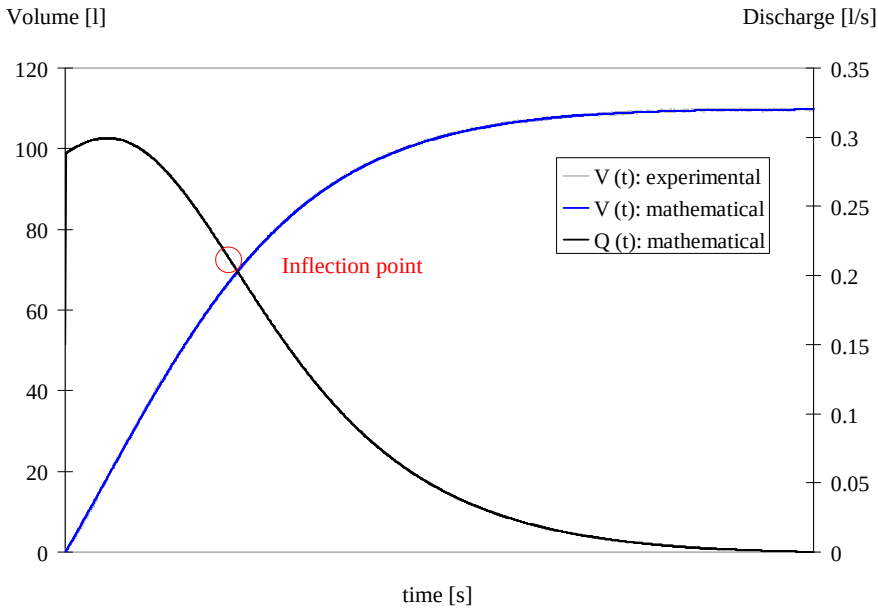

Figure 7.7: Mathematical approximation of V(t). Peak and inflection point in Q(t)-curve.

Once the eight parameters of equation 7.4 have been determined, the time derivative of this equation can be calculated, giving the variation of discharge with time.

3.2 Peak in Q(t)

Due to the presence of the tanh²-term in equation 7.4, the Q(t)-curve shows a peak (fig. 7.7). As the upstream pressure is monotonically decreasing with time, there

seems no external cause of this phenomenon which is related to the test setup. One cause could be the thixotropic properties of the concrete. Between the placement of the concrete in the test setup and the first test, or between two consecutive tests, the concrete is stationary for a few minutes and it has the chance to build up some internal structure [7.6-7.7].
In literature, it has been described that the static yield stress of a certain thixotropic material at rest is influenced by the stress applied during the "liquid-solid" transition [7.8]. It is not certain whether the concrete has undergone a liquid-solid transition, but if it does, the stress applied during this transition equals the yield stress. In this condition, the static yield stress is higher and the thixotropic nature of the material is more pronounced.
From a practical point of view, the data influenced by thixotropy is not taken into account for the analyses. Thixotropy is estimated to be eliminated at the inflection point of the Q(t) curve (fig. 7.7). At this point, the flow is no longer accelerating relative to the pressure evolution. This inflection point is easily determined as the time at which the second derivative of the Q(t)-curve, or the 3rd derivative of the V(t)-curve (eq. 7.4) equals zero.

3.3 Results

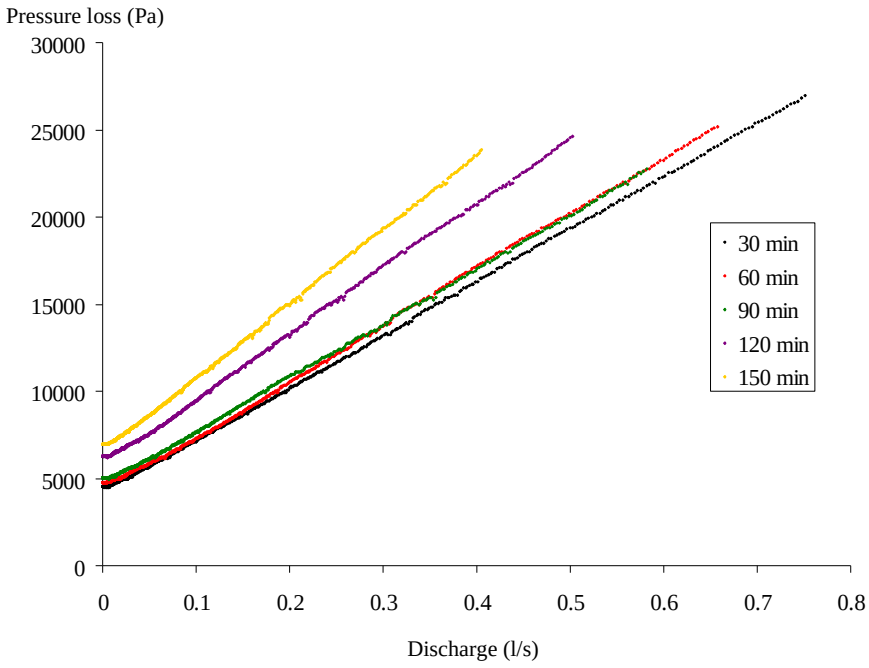

Figure 7.8: Pressure loss – discharge curve for flow-3m-3 (SCC 48).

The pressure loss – discharge curve for the test flow-3m-3, made with SCC 48, tested at 5 different ages is shown in figure 7.8, while the results for flow-12m-2 (SCC 52) are given in figure 7.9. The other test results can be found in Appendix C. Note that in figures 7.8 and 7.9 the pressure loss is expressed as the total pressure loss over the length of the pipe. In some of the next figures, the pressure loss can be expressed as the pressure loss per unit of length.

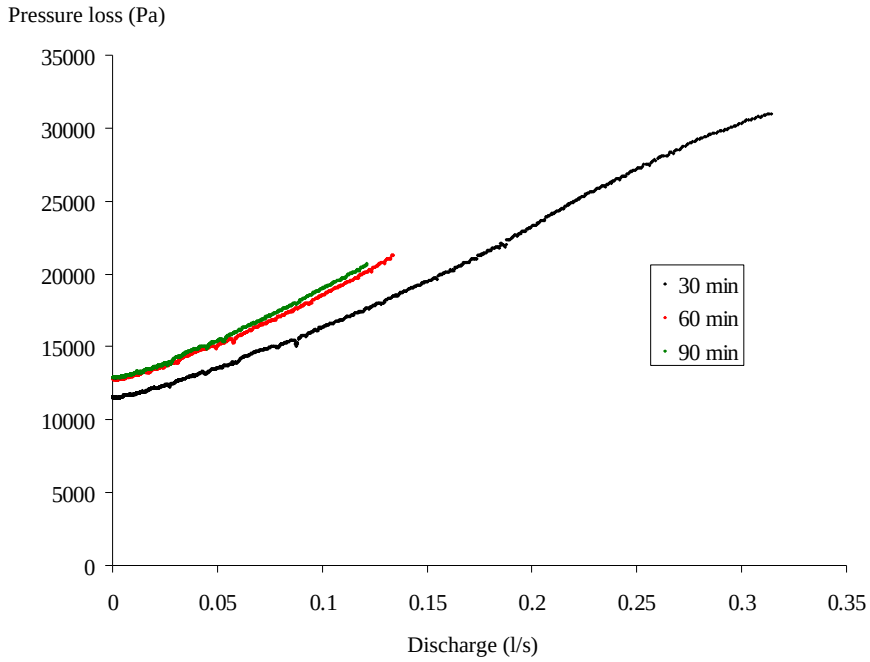

Figure 7.9: Pressure loss – discharge curve for flow-12m-2 (SCC 52).

3.4 Principle of comparison with rheometer data

Before starting the discussion and the actual comparison with the rheometer data, it is worth mentioning that there are two possibilities to compare the data. The first possibility consists of incorporating the rheological data of the concrete and the pipe geometry into the corresponding extended Poiseuille formula. In this way, theoretical and experimental pressure loss – discharge curves are compared.
A second possibility is to regard the gravitational flow test setup as a capillary rheometer [7.1] and to apply the corresponding transformation formulae (see chapter 3). In this way, the data of two different rheometers are compared. As already mentioned before, this second procedure does not deliver 100% accurate measurements, because the last term of equation 3.11, the so-called Weissenberg-Rabinowitch correction [7.1], is not easily determined in case of a shear thickening yield stress material due to its complex shape in a ln(Q) – ln(p) diagram.

As a result, the data of the gravitational flow tests have only been compared with the Tattersall Mk-II rheometer data by means of the extended Poiseuille formula.

4 Discussion

4.1 Length of the pipe

As can be seen in Appendix C, only two SCC (SCC 48 and SCC 52) have been produced for the tests with pipe lengths of 9 and 12 m. For the tests with a 6 m pipe, similar concretes have been produced (flow-6m-1 and flow-6m-5). The analysis will be discussed based on the results of SCC 48. The results for SCC 52 are similar, but less clear. The test results for the 3 m pipes will be discussed separately in section 4.5.

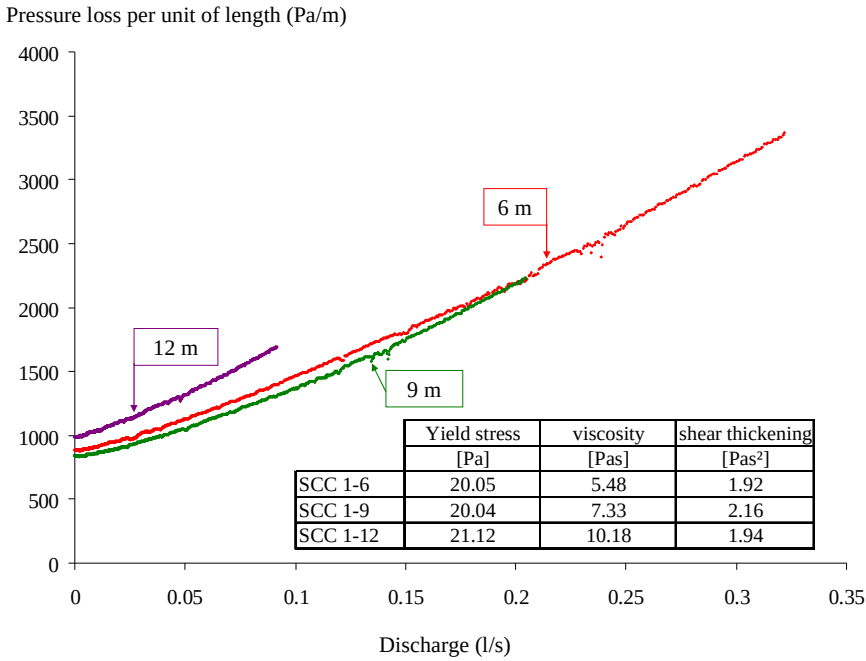

	Yield stress [Pa]	viscosity [Pas]	shear thickening [Pas²]
SCC 1-6	20.05	5.48	1.92
SCC 1-9	20.04	7.33	2.16
SCC 1-12	21.12	10.18	1.94

Figure 7.10: The pressure loss per m of pipe as a function of discharge shows very similar results for the 6 and 9 m test and slightly higher results for the 12 m test. The rheological properties of the applied concretes are shown in the table.

The table in figure 7.10 shows the rheological data of SCC 48, at an age of 60 minutes, for the tests executed at 6, 9 and 12 m. As can be seen, the SCC for the 6 m pipe and the one for the 9 m test have quite similar rheological values (especially at the lower shear rates), while the SCC for the 12 m test shows slightly higher flow resistance. When expressing the pressure loss per unit of length (1 m in this case), it can be clearly seen in figure 7.10 that the pressure loss – discharge curves for the 6 and 9 m test accord quite well. The 12 m curve is slightly higher, due to the higher rheological properties (see next section). As a result, the total pressure loss is linearly dependent on the length of the pipe, which is trivial in

hydraulics [7.3], but worth mentioning in case of concrete. This will be further discussed in chapter 9.

4.2 Rheological properties

Figure 7.11 shows the rheometer data for the SCC applied for flow-6m-5. This SCC has kept its workability quite a long time (more than 210 minutes) and a clear increase in yield stress and viscosity is visible. Note that, due to technical reasons, the test at 60 minutes has not been performed with this SCC. In figure 7.12, the corresponding hydraulic curves (pressure loss – discharge) for this concrete are shown, and apart from the result obtained at 30 minutes of age, the evolution is very similar as for the rheometer data.

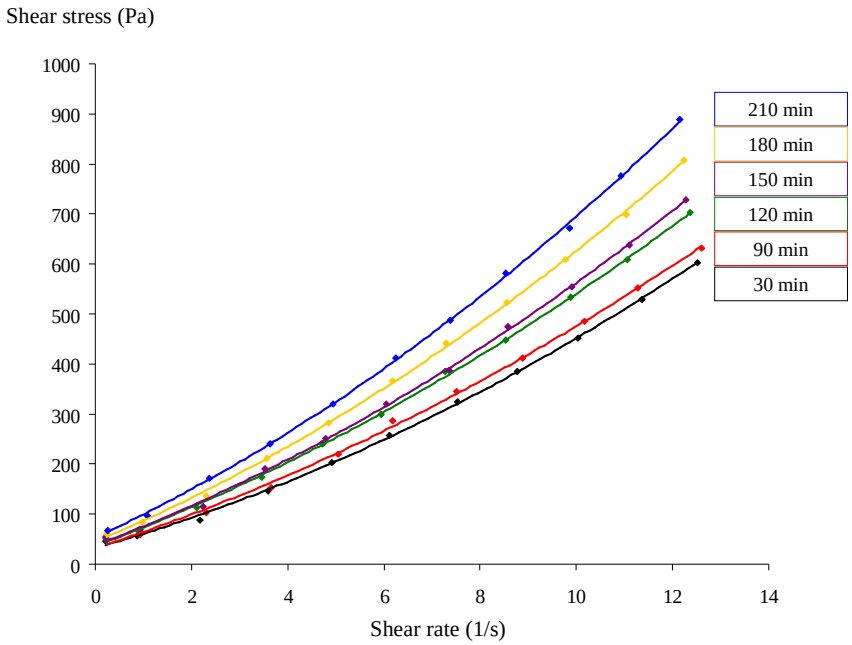

Figure 7.11: Evolution of rheological properties of SCC 52, tested in flow-6m-5.

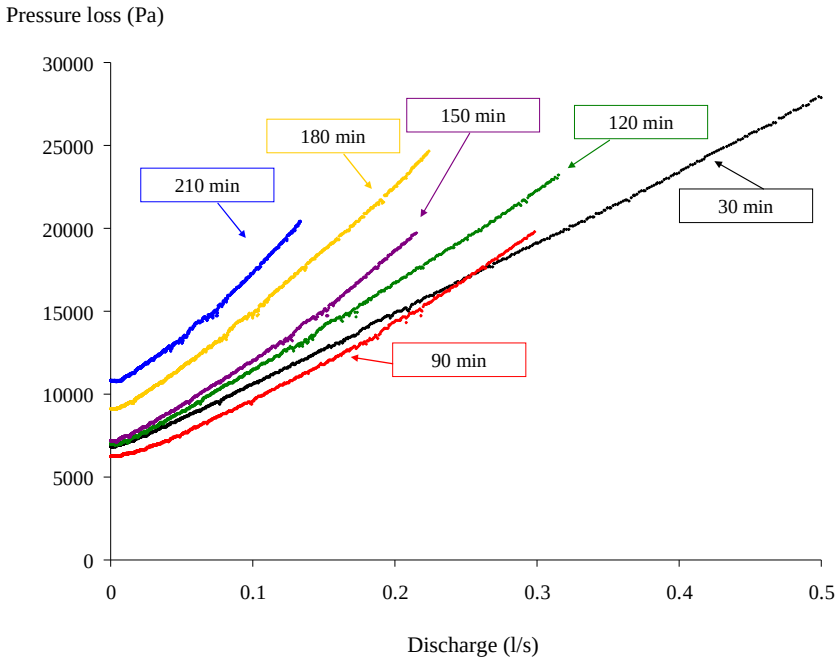

Figure 7.12: Evolution of total pressure loss as a function of discharge with time of SCC 52, tested in flow-6m-5.

The SCC applied for flow-6m-2, 3 and 4 are the only SCC with SP 1 while the other SCC have been produced with SP 2 (see chapter 4 and 5 for the distinction). As a result, SCC 36, applied for the flow-6m-4 test has a large(r) loss of workability. This loss of workability is also reflected in figure 7.13, showing a larger increase in the hydraulics curves, compared to the previous concrete.
This analysis has shown that the evolution with time of the pressure loss – discharge curves is similar as the evolution of the rheological properties, showing that the hydraulic curves are linearly influenced by the rheological properties.

4.3 Discharge

As can be seen in the previous sections, the pressure loss – discharge curves do not show linear behaviour. From hydraulics, it is known that a linear relationship between pressure loss and discharge stands for a laminar regime, while in the case of turbulence, pressure loss relates to the discharge to the power 1.7 – 2 [7.3]. On the other hand, as SCC is a shear thickening material, non-linearity can be induced by the rheological properties. As it has been mentioned in chapter 4, the shear thickening in SCC is not very intense and quadratic behaviour is seldomly exceeded [7.9]. The relation between pressure loss and discharge is also never larger than quadratic. As a result, the non-linearity is induced by the SCC itself and the flow occurs in laminar regime.

Unfortunately, the tests with the extremely shear thickening mixes did not work out as they should have and a more extensive verification is missing.

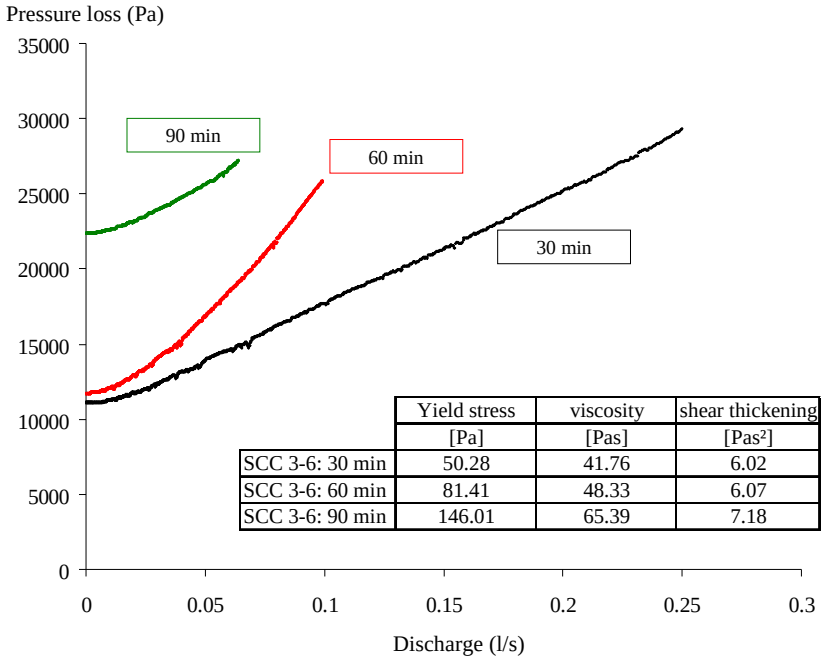

	Yield stress [Pa]	viscosity [Pas]	shear thickening [Pas²]
SCC 3-6: 30 min	50.28	41.76	6.02
SCC 3-6: 60 min	81.41	48.33	6.07
SCC 3-6: 90 min	146.01	65.39	7.18

Figure 7.13: SCC 36 (flow-6m-4) shows a fast increase in rheological properties (see table), which is reflected in a more rapid increase of total pressure loss as a function of discharge.

4.4 Application of the extended Poiseuille formula

The results in the previous section indicate that applying the extended Poiseuille formula can be justified. This formula has been applied on the results of flow-9m-2-30min, flow-12m-1-60min and flow-12m-2-90min, shown in figures 7.14, 7.15 and 7.16 respectively. These figures indicate the quite good agreement between the obtained experimental pressure loss – discharge relationships and the theoretical curve, based on the corresponding rheological data and the pipe geometry. Except for the concretes tested with a 3 m pipe, the agreement of the other results is similar. No tests in order to examine the influence of the diameter on the pressure losses have been performed, due to the large technical complications. On the other hand, such tests would be very useful in order to determine possible slippage.

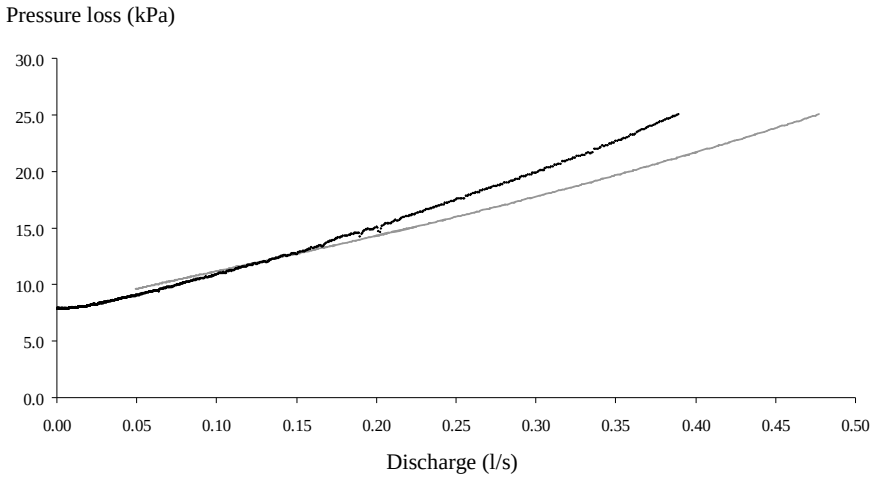

Figure 7.14: Comparison of experimental results (black) with the extended Poiseuille formula (grey) for flow-9m-2-30min.

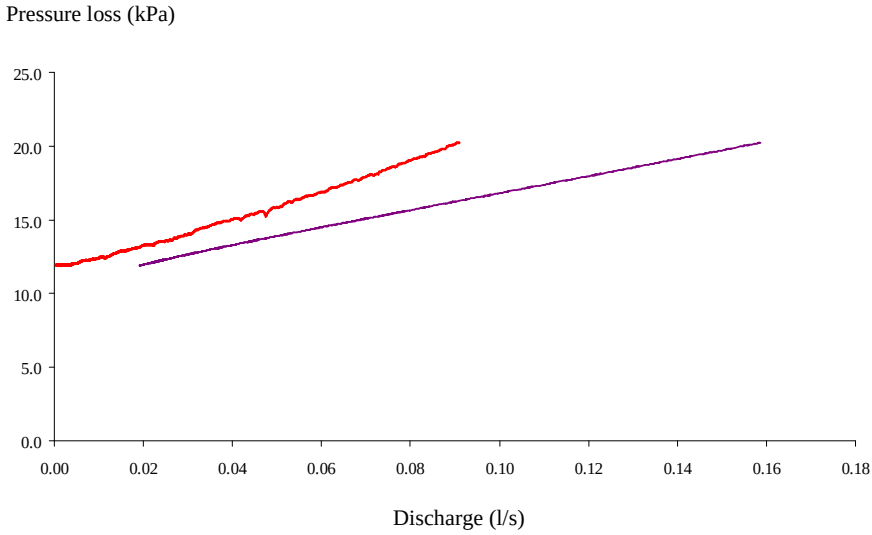

Figure 7.15: Comparison of experimental results (red) with the extended Poiseuille formula (purple) for flow-12m-1-60min.

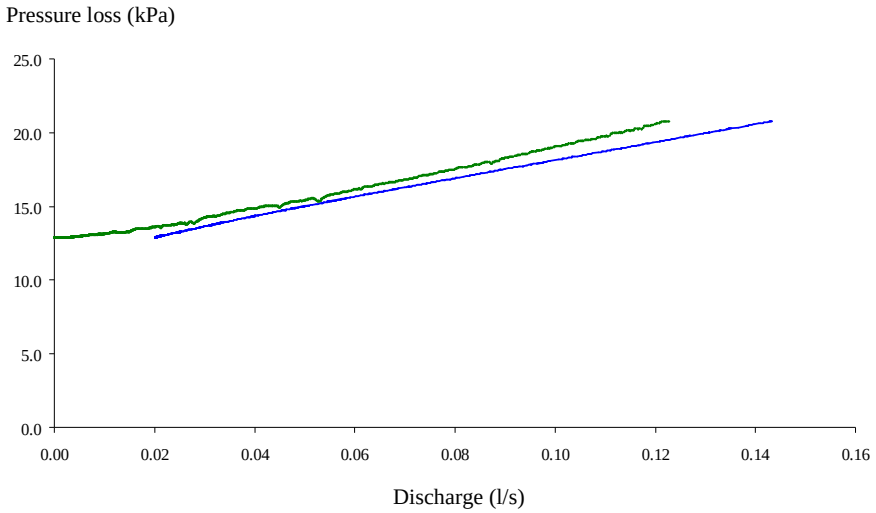

Figure 7.16: Comparison of experimental results (green) with the extended Poiseuille formula (blue) for flow-12m-2-90min.

4.5 Special pressure losses

In case of the flow of a material in a straight section, without any changes in geometry, the pressure losses are dominated by the flow resistance of the material. On the other hand, if the streamlines need to change direction, additional (special) pressure losses are induced [7.3][7.10-7.12]. In this specific test setup, special pressure losses are mainly induced at the entrance of the pipe. The flow needs to change direction (from vertical to horizontal), it needs to contract (reduction of the diameter with a factor 3) and the velocity increases. When expressing the total pressure loss as in equation 7.5, it can be seen that the special pressure losses gain importance when the length L decreases.

$$\Delta p_{tot} = \Delta p \cdot L + \Delta p_{sp} \tag{7.5}$$

where: Δp_{tot} *= total pressure loss (Pa)*
Δp *= pressure loss per unit of length, in case of a straight pipe (Pa/m)*
L *= length of the straight pipe (m)*
Δp_{sp} *= special pressure losses (Pa)*

The results obtained with the 3 m pipe do not only deviate from the obtained experimental results with longer pipes, but also the extended Poiseuille formula does not provide as good agreements as in the case of longer pipes. As a result, it can be estimated that the special (entrance) pressure losses are no longer negligible in case of short pipes, but from a length of 6 m on, the influence of these special pressure losses becomes less significant.

The analysis also indicates that applying the extended Poiseuille formula to the results of flow-3m-1, 2 and 3 delivers better agreements in the first two cases and the worst agreement in the third case. In the third case, the SCC was more fluid than in the other cases, which results in a lower pressure loss per unit of length and a larger importance of the special pressure losses. As a result, it can be concluded that the special pressure losses are important in case of tests with short pipes and relatively fluid SCC.

4.6 Differences between batches

As mentioned in section 2.2, for tests with a pipe length of more than 3 m, the total SCC amount has been produced in two different batches, resulting in some differences in the composition and the fresh properties like slump flow. The concrete in the rheometer is taken from the common batch and remains unchanged during the full testing procedure. The two batches themselves do not mix up well in the transporting reservoir and some differences can be obtained, which can be clearly seen in figure 7.13.
In this figure, it can be seen that the rheological properties are gradually increasing, while the experimental hydraulics curves show a “yield pressure” which is almost equal for the first and for the second test. The results of the first test are mainly determined by the fresh concrete properties of the first batch, while during the second test, it is mainly concrete of the second batch which is flowing through the pipes. At later times, the SCC is suspected to mix up better and the results are more straightforward, as can also be seen in figures 7.11 and 7.12.
As a result, the difference between the two batches can explain some apparently illogical results.

4.7 Segregating concrete

The SCC prepared for the flow tests flow-6m-2 and 3 was not successful and showed significant segregation. Although the concrete is not good, a test has been attempted in order to verify the flow behaviour of segregating concrete. As can be seen, test results have not been included as the concretes showed significant blocking at the bottom of the upstream reservoir during the preparation. Consequently, testing segregating concrete was not a good idea.

4.8 Tests with traditional concrete?

One could wonder whether this test setup can also be used in case of traditional concrete. No explicit tests have been performed, but using traditional concrete would complicate the execution significantly. At the end of the test flow-6m-4-90min, the flow of SCC stopped at the moment the upstream reservoir was still half full. Due to loss of workability, this SCC showed a large increase in yield stress (fig. 7.13), resulting in this high stoppage height. In case of traditional concrete, the yield stress is already high, causing this test setup to be less convenient. On the other hand, if an

external additional pressure can be applied on the concrete in the upstream reservoir, the possibilities of this setup can be extended.

5 Verification of the extended Poiseuille formula

In this section, the conditions to apply the Poiseuille formula, as mentioned in chapter 6, will be verified:

- The flow is fully developed and isothermal: Due to the low discharges, no heating of the concrete occurs, so the isothermal aspect is confirmed. On the other hand, due to the free exit, the flow is not fully developed at the end of the pipe, but this effect can be neglected when the pipe is sufficiently long.
- The liquid must be incompressible: SCC is composed of solid and liquid materials only. However, concrete in general has a small air content of approximately 1.5 to 2 %, distributed in a large amount of small air bubbles (with an average diameter around 0.5 mm), representing the compressible part. The compressibility is assumed to be negligible in this case.
- No radial or tangential flow component is allowed: This is assumed to be fulfilled, but no verification tool really exists.
- The flow should be steady: This means that no variations in time can occur, although, the time-variations in this test setup are slow, especially compared to the registering speed of 2 measurements per second. The tests are conducted in quasi steady state.
- There is no slip at the walls: This is the most difficult condition to verify. Until now, no test procedure or equipment is available to determine the velocity profile during the flow of concrete. During these particular tests, due to the low pressures applied and the high stability of the SCC, no separation of water/cement paste near the pipe walls is expected. The good agreement between the experimental data and the calculated results indicates that there is no significant slippage near the walls. On the other hand, if the SCC has a tendency to segregate, special attention should be paid to this condition.
- The material is homogeneous: This is another condition which can be doubted. Near the wall, the concentration of aggregates decreases, resulting in a more fluid material at this location. For this specific setup, the incorporation of this effect in the extended Poiseuille formula is not needed, but as will be shown in chapter 9, this additional correction can already improve the predictions for pumping pressures significantly.
- The flow is occurring in laminar conditions: This has been proven in section 4.3, where it has been shown that the non-linearity in the pressure loss – discharge curve is only due to the shear thickening of the SCC and not due to turbulence.

6 Summary

The gravitational flow tests have been executed as an intermediate step between the rheological characterization of SCC and the execution of full scale pumping tests. The test setup consists of a vertical upstream reservoir with a height of 2.3 m, a number of steel pipes with an inner diameter of 106 mm through which the SCC must flow and a downstream, suspended reservoir, collecting the SCC. Pressure loss and discharge are calculated from the measurements of the height of the concrete and the variation of the force executed by the downstream reservoir on the load cell respectively.

After elimination of thixotropy, it can be clearly seen that the total pressure loss is linearly dependent on the length of the pipe, the rheological properties of the concrete and the discharge. As a result, the extended Poiseuille formula predicts the pressure loss – discharge curves quite well. For short pipes and relatively fluid concretes, the obtained results deviate from the experiments with longer pipes and the prediction of the extended Poiseuille formula is not as good. This can be due to the relative importance of the special (entrance) losses, which are no longer negligible.

By applying the extended Poiseuille formula, it has been shown that the flow occurs in laminar regime and that no significant wall slip occurs. The question still remains whether at the high discharges during pumping (20 l/s instead of 1 l/s), the same conclusions are still valid.

7 References

[7.1] Macosko C.W., "Rheology Principle, measurements and applications," Wiley-VCH, New-York (1994).

[7.2] Thijsse J., "Formulae for the friction head loss along conduit walls under turbulent flow", 3rd IAHR congress, Grenoble (1949), 1-11.

[7.3] Fox J.A., "An introduction to engineering fluid mechanics," The MacMillan Press, London (1974).

[7.4] Kaplan D., "Pumping of concretes," Ph-D dissertation (in French), Laboratoire Central des Ponts et Chausées, Paris (2001).

[7.5] Calie B., "Pumping of Self-Compacting Concrete under pressure," Master-thesis (in Dutch), Ghent-University, Ghent (2007).

[7.6] Wallevik J.E., "Rheology of particle suspensions, Fresh concrete, mortar and cement paste with various types of lignosulphonates," Ph-D dissertation, The Norwegian University of Science and Technology, Trondheim (2003).

[7.7] Roussel N., "A thixotropy model for fresh fluid concretes: Theory, validation and applications," Cem. Conc. Res. **36** (2006), 1797-1806.

[7.8] Ovarlez G., Chateau X., "Influence of shear stress applied during flow stoppage and rest period on the mechanical properties of thixotropic suspensions," Phys. Rev. E. **77** (2008), 061403.

[7.9] Feys D., Verhoeven R., De Schutter G., "Evaluation of time-independent rheological models applicable to fresh Self Compacting Concrete," Appl. Rheol. **17:5** (2007), 56244.

[7.10] Fester V., Chhiba M., Kotze R., Haldenwang R., Slatter P., "Measurements of velocity profiles of slurries in complex geometries," Proc. of the XIVth Int. Conf. on Transport and Sedimentation of Solid Particles, St.-Petersburg (2008), 93-103.

[7.11] Fester V.G., Kazadi D.M., Mbiya B.M., Slatter P.T., "Loss coefficients for flow of Newtonian and non-Newtonian fluids through diaphragm valves," Chem. Eng. Res. Des. **85** (2007), 1314-1324.

[7.12] Edwards M.F., Jadallah M.S.M., Smith R., "Head losses in pipe fittings at low Reynolds numbers," Chem. Eng. Res. Des., **63** (1985), 43-50.

CHAPTER 8:

PUMPING TESTS: TEST SETUP AND PROCEDURES

This chapter describes the setup for the 7 days of full scale pumping executed at the Magnel Laboratory for Concrete Research. The pump, pipes and circuits and the measurement systems will be described in the first section. The second part contains the composition and properties of the concrete mixes used. In the third section, the different testing procedures will be given. The last sections describe some general considerations like blocking and cleaning and the safety during pumping. This chapter does not contain any specific results, except for the discharge calibration procedure. In the next chapter, the results obtained with the different procedures will be given and discussed.

1 Test setup

1.1 Concrete pump

The concrete pump used is a truck-mounted piston pump [8.1-8.3], rented from a private company. For the seven days during which all pumping tests have been executed, the same pump has been applied. The pump itself is a Schwing concrete pump P 2023, provided with a placing boom KVH 24-4H (fig. 8.1). As the placing boom has not been applied during the tests, further details are not incorporated in this description. The pump can achieve a maximal pressure (on the concrete) of 95 bar, or a maximal discharge of 150 m³/h, which corresponds to 41.5 l/s. Both the maximal concrete pressure and the maximal discharge cannot be achieved simultaneously. The pump contains two hydraulic cylinders having 230 mm in diameter and 2000 mm of stroke length. As a result, if a 100% filling is assumed, each cylinder contains 83.1 l of concrete.
The pumping system is automatically generated by the pump itself. Alternately, one cylinder pulls concrete from the reservoir of the pump, while the other cylinder pushes the concrete inside the pipes. When the cylinders are full and empty respectively, a special valve switches the connection between the pipe system and

the cylinders. Consequently, the cylinders swap jobs, meaning that the first cylinder pushes the concrete in the pipes and the second cylinder pulls concrete from the reservoir. This process is repeated until the pumping is stopped. As a result, during the pushing of the cylinder, the discharge is approximately constant, but during the switch, a sudden decrease and increase in both discharge and pressure are recorded (see section 3.3).
The valve which makes the connection between the pipe system and the cylinders of the pump is the “Schwing rock valve”, which is depicted in figure 8.2. This powerful valve changes very suddenly and must turn inside the concrete reservoir, crushing aggregates if necessary.

Figure 8.1: Truck mounted concrete pump

The concrete reservoir of this specific pump can contain maximally 0.75 m³ of concrete (fig. 8.3). A concrete volume of at least 200 or 250 l is needed in order to submerge the cylinders completely. If this is not fulfilled, air pockets will be pulled in the cylinders and will be pushed inside the pipes. Furthermore, if the amount of concrete is low in the reservoir, the concrete splashes out during the change of the rock valve, leading to a messy environment.

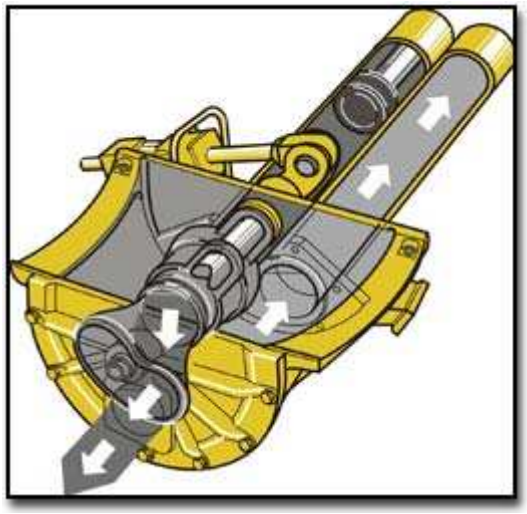

Figure 8.2: Principle of the Schwing rock valve (from www.schwing.de)

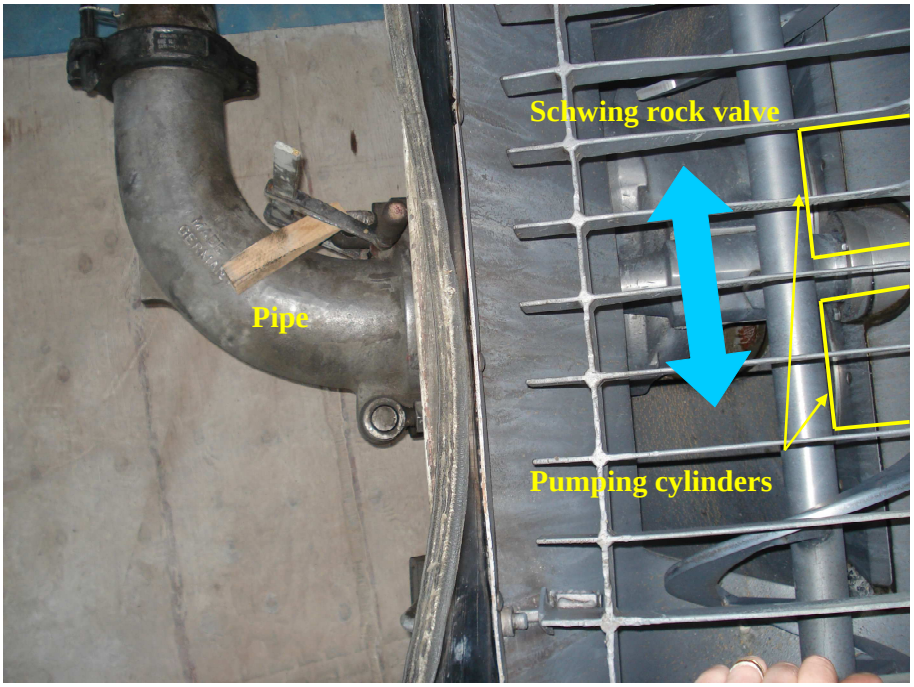

Figure 8.3: Top view inside the concrete reservoir, showing the rock valve and the entrance of the two pumping cylinders. The cylinder at the top of this picture is connected with the pipes.

The operator of the pump, who has also been hired from the company for these tests, has a remote control, with which he can move the placing boom, start and stop the pump, and control the discharge. The discharge of the pump can be changed in 10 steps from the minimal value, which is around 4-5 l/s, to the maximal output of around 40 l/s. For safety reasons, we have decided not to increase discharge over 20 l/s (step 5), except once. As discharge is (more or less) controlled, the applied pressure is variable, depending on the properties of the concrete and the geometry of the pipes.

1.2 Pipes and circuits

1.2.1 Pipes

The pipes used for the pumping tests are steel pipes, with an inner diameter of 106 mm, a wall thickness of 3 mm and a length of 1 or 3 m (fig. 8.4). The pipe at the exit of the pump has a larger diameter and as a result, a reduction to the 106 mm inner diameter has been applied immediately after the exit of the pump. Curves of 90° with a curving radius of 17 cm measured on the centre line of the curve, were also available (fig. 8.4). These pipes are the same as the ones applied for the gravitational flow tests (see chapter 7). One flexible rubber hose, with an inner diameter of around 106 mm and with a length of 4 m was available (fig. 8.4). The connections between the pipes have been equipped with the same rubber seals and clamps as described in chapter 7.

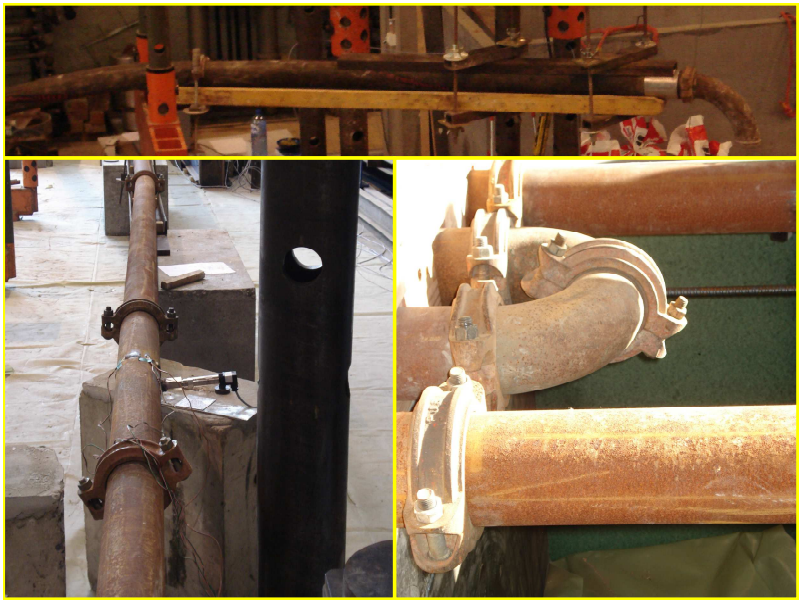

Figure 8.4: Top: flexible hose. Bottom left: Straight pipes of 1 and 3 m. Bottom right: Combination of 2 curves, making a 180° turn.

1.2.2 Sampling reservoir

In order to be able to take samples, the downstream reservoir used for the gravitational flow tests, was suspended to the rolling bridge at the end of the circuit (see fig. 8.7). In order to take a sample, a certain amount of concrete is pumped in the reservoir, which then is moved aside from the setup, where the buckets and the wheelbarrow can be easily filled by means of the valve at the bottom of this reservoir.

1.2.3 Short circuit

With the available pipes, a short loop circuit of 25 m of length has been built. This circuit has been used for five of the seven days of pumping.
After the exit of the pump and the reduction pipe, a 90° curve has been installed, followed by a straight horizontal section of 12 m. After this straight section, the concrete is returned to the pump by a 180° turn, made by two curves and a 1 m pipe in between. The circuit continues with an inclined straight part of 9 m, followed by the
4 m flexible hose. At the end of this hose, a 90° curve is attached, in order to point the concrete flow down, inside the sampling reservoir. During most of the tests executed, the valve at the bottom of the sampling reservoir is open and the concrete falls back inside the reservoir of the pump. In this way, with a restricted amount of concrete of 1.25 to 1.5 m³, tests have been executed during several hours. A schematic overview of the setup, a picture of the circuit and the position of the sampling reservoir are shown in figures 8.5 to 8.7.

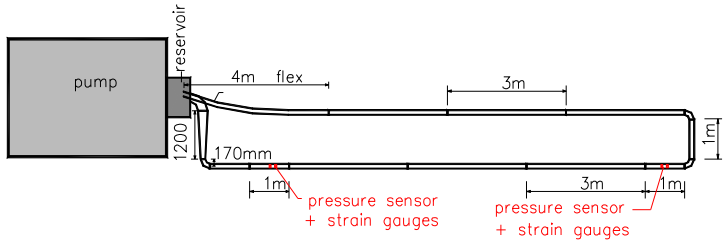

Figure 8.5: Design of the short circuit of 25 m.

Figure 8.6: Short circuit (25 m).

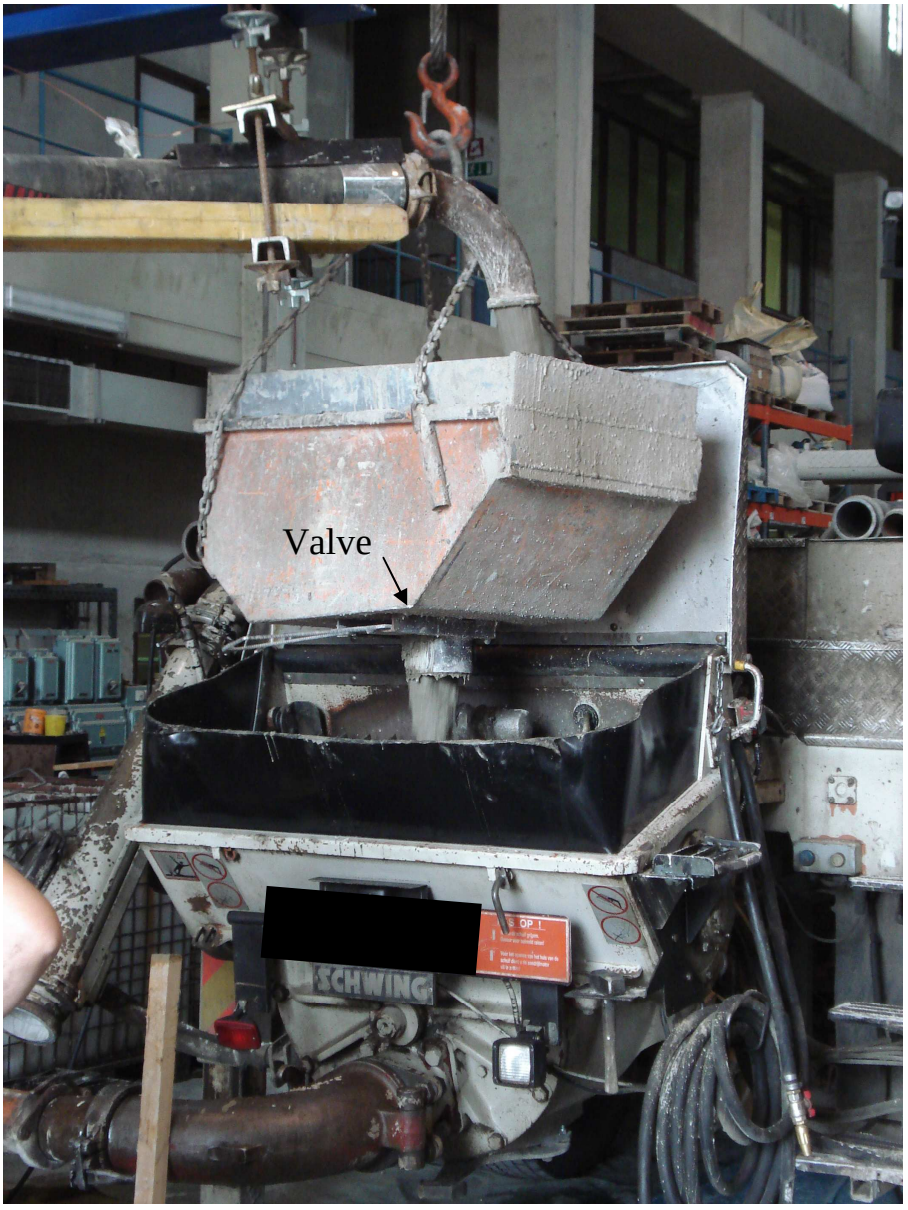

Figure 8.7: Position of sampling reservoir at the end of the circuit. During pumping, the valve is in most cases open, allowing the concrete to flow back inside the reservoir of the pump.

1.2.4 Long circuits

For the last two days, the circuit has been extended up to a maximal length of 105 m. Figures 8.8 and 8.9 give a schematic overview of the long circuits, while figures

8.10 and 8.11 show the 105 m circuit from the rear and front side of the laboratory respectively. At the end of the circuit, the concrete falls through the sampling reservoir in the reservoir of the pump.
As can be seen in figures 8.8 and 8.9, two different circuits have been built, in which not only the placement of the measurement equipment has changed, but the second circuit is also 24 m shorter than the first one. This has been done in order to decrease the total pressure in the circuit and in an attempt to avoid blocking.

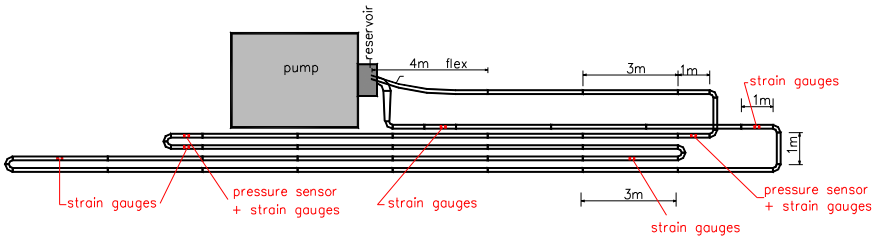

Figure 8.8: Design of the 105 m long circuit and position of the measurement sections.

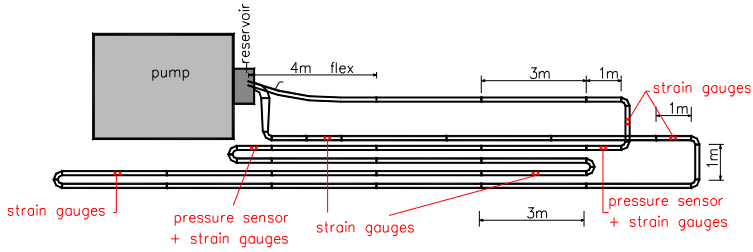

Figure 8.9: Design of the 81 m long circuit and position of the measurement sections.

Figure 8.10: Long circuit (105 m), seen from the rear side of the laboratory.

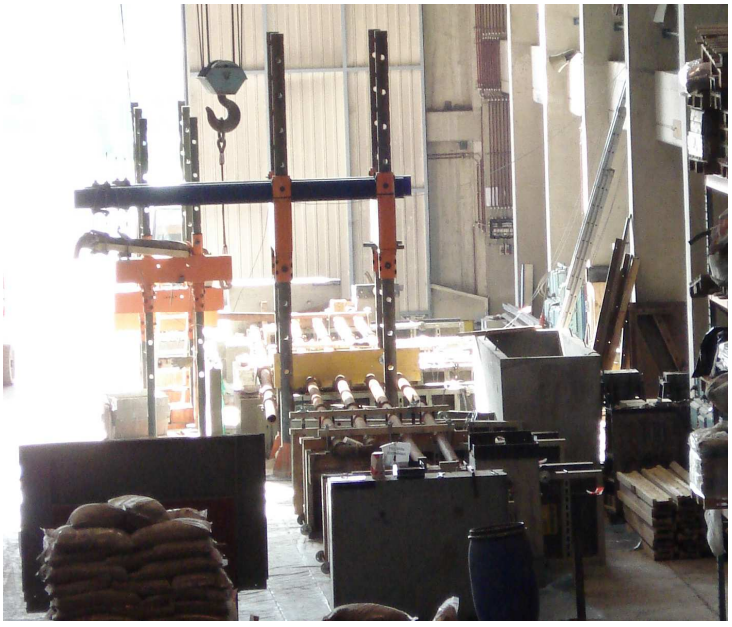

Figure 8.11: Long circuit (105 m), seen from the front side of the laboratory. Note that the pump and the sampling reservoir are not yet installed.

1.3 Measurement systems

1.3.1 Pressure losses

The most essential elements to measure are the pressure and the pressure losses. In the short circuit, the pressure losses have been measured in the straight horizontal part. Two specially equipped pressure sensors have been installed at a distance of 10 m from each other and the pressure loss per unit of length can be easily calculated. The pressure sensors are regular pressure transducers, equipped with an oil chamber and a sealed membrane. In this way, solid materials are (suspected to be) prevented to enter the oil chamber or block the membrane. The maximal capacity of the pressure sensors is 35 bar, with a safety margin of an additional 35 bar. Although these sensors are manufactured for heavy duty measurements, one of the sensors was broken at the start of the first pumping test with the long circuit.
During the second day of testing (17/04/2007), the downstream pressure sensor has been installed after the first 90° curve in order to examine the influence of the curves on the pressure losses.
At the same position of each pressure sensor, three strain gauges have been glued on the exterior pipe walls, in order to measure the deformation of the pipes (fig. 8.12). As the pipes are relatively thin, the deformation can clearly be measured and it relates to the applied pressure [8.1][8.4]. These strain gauges functioned as a kind of back-up in case something happens with the pressure sensors, reproducing pressure values, based on a calibration executed when the sensors were working. From our experience, we would like to say that this back-up has proven to be very useful.
As the strain gauges have proven to be useful, five more pipes have been equipped with each three strain gauges. These measuring units have been used in the long circuit, in order to measure the pressure losses in different sections. As can be seen in figures 8.8 and 8.9, the pressure losses in three straight sections, and one section with a bend have been measured.
The calibration of the strain gauges was not based on the results of the last day of testing on the short circuit, due to the uncertainty of the linear evolution of pressure loss with the length of the pipe (see chapter 9) [8.1]. Instead, at the last blockings in the long circuits, which occurred near the end of the circuit, the pressure is supposed to be equal in every part of the circuit as there is no flow. The calibration has been performed based on these blockings. On the other hand, some of the individual strain gauges showed very strange results, which can be caused by the additional deformation due to the pressure shocks and additional motion of the circuit. As a result, after careful considerations, some strain gauges have not been used in order to calculate the pressure losses. As one of the main consequences, the measured strains in the first section, closest to the pump, are seriously doubted and no results of this section, although this is the most useful one, have been incorporated in the analysis.

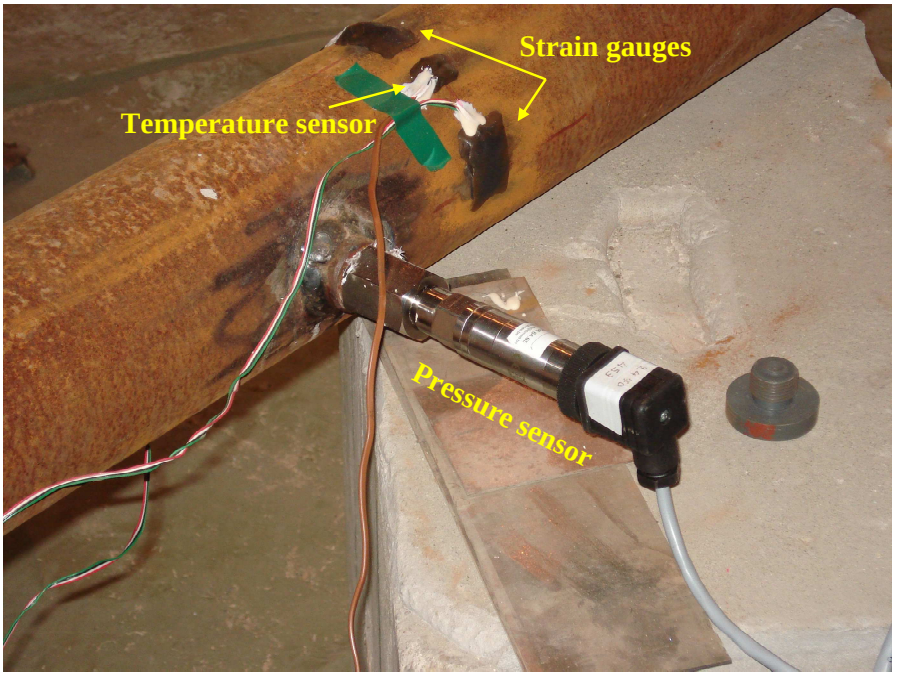

Figure 8.12: Pressure sensor, strain gauges (of which one is at the rear side of the pipe) and the temperature sensor. The strain gauges and temperature sensor are protected to any hazards by a kind of rubber cover.

Furthermore, the pressure loss at flow stoppage was never equal to zero and it showed quite strange and illogical variations in time. As a result, during the analysis of the results, the pressure loss at flow stoppage has been "re-zeroed" and the calculation of the pressure loss during the test was based on the zero values before and after the test, if available. In fact, the pressure loss at flow stoppage should not equal zero due to the yield stress of the material [8.5-8.6], but the illogical order of pressure losses made us decide to induce this procedure and the consequent error.
During the tests, the results produced by the pressure sensors and strain gauges are measured with one (or a combined set of two) data acquisition system(s) at a rate of 10 measurements per second. Although this fast measuring rate, which is the fastest for the system used, has created some enormous files, we are able to monitor the pressure change during the switch of the rock valve. Between two switches of this valve, the pressure reaches an equilibrium value (fig. 8.13). The data in the files have been analysed manually in order to eliminate the non-equilibrium pressure values.

1.3.2 Discharge

The second parameter needed is the discharge. Although we did not have an electromagnetic discharge meter [8.1], an effective but indirect discharge measurement procedure has been worked out.
As a first idea, volumetric discharge measurements would have been carried out during the tests. This means that the sampling reservoir should be closed during pumping and the weight increase should be measured by the load cell to which the reservoir is attached. During the first measurement, this procedure has been applied, but not with the hoped success. The valve is not closed easily during the flow of concrete (it takes around 10 seconds), and consequently, the reopening of the valve was too late, leading to a first complete mess in the lab due to the overflow of the reservoir. As a result, this procedure has been eliminated during the measurements, but it will be discussed again in section 3.3, dealing with the discharge calibration.

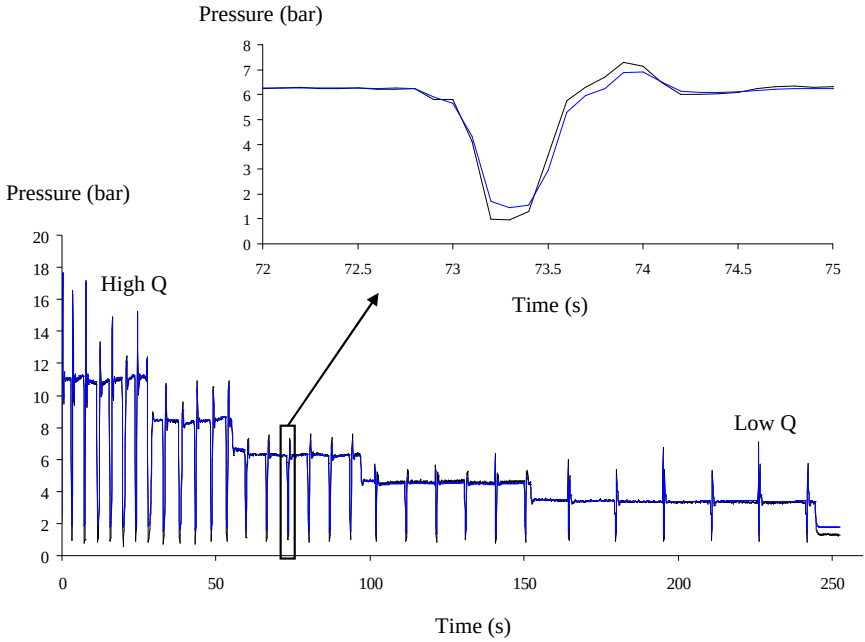

Figure 8.13: Upstream pressure evolution as a function of time, resulting from a stepwise decreasing discharge, measured with the pressure sensor (black) and the calibrated strain gauges (blue). The upper figure shows a detailed pressure evolution during a switch of the pumping valve.

Consequently, an easier measurement has been performed. Figure 8.13 shows the evolution of the upstream pressure with time during an experiment with a stepwise decreasing discharge. As can be seen, especially in the enlarged part, the pressure decreases to a certain minimum value, and increases back to the equilibrium value in

a time span of around one second. Each time a minimum is passed, the amount of one full cylinder is pumped inside the pipes. Assuming a 100% filling ratio of the cylinders, one can easily calculate the discharge from the time needed for a certain amount of strokes to be pumped. Similar as for the pressure measurements, this specific procedure, based on the output file, is a back-up for the measurements which have been performed with a stopwatch on site. The procedure with the stopwatch is very similar as the one with the output file. The time needed for a certain amount of strokes, which can be clearly heard, is measured.

1.3.3 Temperature

Temperature has been monitored at each pressure measurement location by means of a temperature sensor at the exterior wall of the pipe (fig. 8.12). Because of friction, both the pipe walls and the concrete are heated [8.7] and tests have been stopped earlier than planned when the concrete has reached 32-35°C.

2 Pumped concretes

2.1 Delivery

Due to the large amount of concrete (1.5 m³ and 3.25 m³ for the short and long circuits respectively), the concrete has been delivered to the laboratory by a ready mix company. In most cases, the concrete was delivered in the lab 45 minutes after the water adding time in the mixing plant. This delivery time includes production and transport. For the morning deliveries, due to traffic problems, the delivery time has been extended up to 1 h and even 1.5 hours. The concrete has been delivered in a regular concrete mixer with a maximal capacity of 5 m³. During the insertion of the concrete in the circuit, the first 250 l (or 500 l in case of the long circuit) of material (water + cement + aggregates + concrete) were removed. The reservoir of the pump was filled completely and the mixer has left the laboratory shortly afterwards.

2.2 Concrete compositions

During the seven days of testing, 19 concrete mixes have been used for pumping. 18 of these mixes were self-compacting, of which 3 were commercial products of the plant and 15 mixes were designed by the lab. Two of the mixes were segregating when arriving, due to heavy rainfall, but the pumping continued. The only traditional concrete was also designed by the production plant.

The production plant had the same suppliers for the cement, the limestone filler (limestone filler 2: see chapter 4), and the superplasticizer (SP 2). The grading curves of the used sand and rounded aggregates were similar to the products in the lab. On the other hand, the aggregates are not dry, as in the lab, and the moisture content has been taken into account during the production in the plant.

When investigating the mixtures in table 8.1, one can see that there is not much variation in the compositions, except for the plant mixes. This is due to the large variability in SP-demand between similar mixes. The only parameters changed in this part of the research are, apart from the SP-content which we did not have under control, the powder amount, and consequently the w/p and w/c-ratio (SCC LM-4, LM-9 and LM-11). Mixes SCC LM-15 and LM-17, which have been designed by the production plant, are similar mixes, with a different amount of SP (although the final amount of SP in mix SCC LM-17 is currently still unknown).

The mixes SCC LM-9 and 10 showed a very low segregation resistance, due to the heavy rain showers during transport. The results of these two concretes are analysed qualitatively, while a quantitative analysis is not really useful.

The nomenclature of the mixes as shown in table 8.1 will be used in the remaining part of this chapter and in chapter 9.

	6/03/2007			17/04/2007		
	OBC 1	LM 1	LM 2	LM 3	LM 4	LM 5
Amount (m³)	1.5	1.25	1.25	1.5	1.25	1.25
Composition (kg/m³)						
Gravel 8/16		434	434	434	459	434
Gravel 3/8		263	263	263	278	263
Sand 0/5		853	853	853	901	853
CEM I 52.5 N		360	360	360	300	360
Limestone filler 2		239	239	239	200	239
Water		165	165	165	165	165
SP 2		11	11	15.22	12.16	20.95
P-amount (kg/m³)	640	599	599	599	500	599
W/C-ratio (-)	0.551	0.458	0.458	0.458	0.550	0.458
W/P-ratio (-)	0.314	0.275	0.275	0.275	0.330	0.275
SP/C-ratio (%)	1.98	4.60	4.60	6.37	6.08	8.77
Slump flow at plant (mm)				690	710	710
Remarks	Plant-Mix					

	5/06/2007			18/09/2007		
	LM 6	LM 7	LM 8	TC 1	LM 9	LM 10
Amount (m³)	1.5	1.25	1.25	1.55	1.25	1.25
Composition (kg/m³)						
Gravel 8/16	434	434	434		410	434
Gravel 3/8	263	263	263		248	263
Sand 0/5	853	853	853		805	853
CEM I 52.5 N	360	360	360		400	360
Limestone filler 2	239	239	239		300	239
Water	165	165	165		165	165
SP 2	13.33	12.69	14.44		18.15	11
P-amount (kg/m³)	599	599	599	328	700	599
W/C-ratio (-)	0.458	0.458	0.458	0.538	0.413	0.458
W/P-ratio (-)	0.275	0.275	0.275	0.521	0.236	0.275
SP/C-ratio (%)	5.58	5.31	6.04	1.31	6.05	4.60
Slump flow at plant (mm)	720	650	680		700	650
Remarks				Plant-Mix	Segregating due to	
				contains FA	heavy rainfall	

	4/12/2007			12/02/2008		6/05/2008	
	LM 11	LM 12	LM 13	LM 14	LM 15	LM 16	LM 17
Amount (m³)	1.5	1.5	1.5	3.25	3.25	3.25	3.25
Composition (kg/m³)							
Gravel 8/16	410	434	434	434		434	
Gravel 3/8	248	263	263	263		263	
Sand 0/5	805	853	853	853		853	
CEM I 52.5 N	400	360	360	360		360	
Limestone filler 2	300	239	239	239		239	
Water	165	165	165	160		165	
SP 2	?	?	?	21.9		?	
P-amount (kg/m³)	700	599	599	599	581	599	581
W/C-ratio (-)	0.413	0.458	0.458	0.444	0.452	0.458	0.452
W/P-ratio (-)	0.236	0.275	0.275	0.267	0.324	0.275	0.324
SP/C-ratio (%)	?	?	?	9.16	2.47	?	?
Slump flow at plant (mm)	*700*	*675*	*700*	640	650	*700*	*700*
Remarks	target SF	target SF	target SF		Plant-Mix	target SF	Plant-Mix
							target SF

Table 8.1: Concrete compositions for the 19 concretes pumped.

3 Testing procedures

3.1 Regular pumping tests

All concretes from SCC LM-1 to 11, SCC LM-13, SCC OBC-1 and TC-1 have undergone several regular pumping tests, called “pumping cycles”. This testing procedure consists of pumping the concrete at the five lowest available discharges, in descending order, maintaining each discharge during 5 full strokes in order to have an accurate pressure and discharge measurement. A typical result of such a test can be seen in figure 8.13, where the upstream pressure is plotted as a function of time. In the beginning, the pressure is high and the vertical spikes are close to each other, indicating a high discharge. At the end, the opposite is seen and the discharge is consequently low. The discharge is measured over the 5 full strokes, while the pressure loss is calculated from the average pressure difference between the upstream and downstream sensors, taken during these five strokes and when the pressure is in equilibrium.
The first pumping cycle is normally executed at a concrete age of 60 minutes, unless traffic jams did not allow this. This test has been repeated each 30 minutes, in order to investigate the evolution in time. Between two pumping cycles, the concrete was at rest, or was subjected to other types of tests.
Before each test, a sample of concrete is taken in order to investigate the fresh properties, by means of the Tattersall Mk-II rheometer [8.8] and standard tests on SCC. Not all standard tests have been performed, some tests have been omitted when getting more experienced (like the L-box), while other tests have been included more frequently (density, air content and sieve stability). Normally, the fresh properties have been determined each two pumping cycles. All results of the rheometer and the standard tests on fresh SCC can be found in Appendix D.

3.2 Special thixotropy tests

As the main aim of the regular pumping tests was to investigate the influence of the rheological properties of the concrete on the pumping (pressures), the aim of the special thixotropy tests is mainly the opposite: testing the influence of pumping on the rheological properties. The name “special thixotropy test” has been chosen during the experiments, because it was assumed that only thixotropy was influencing the obtained results. As will be shown in chapter 9, this is not the case, but the name has been kept for reasons of simplicity.
This testing procedure has been executed on concretes SCC LM-12 and SCC LM-14 to 17. The test for SCC LM-12 has been executed on the short circuit, while the results for the other concretes have been obtained in the long circuits.
The basic principle of the test is shown in figure 8.14. The procedure consists of three parts which are repeated each time with a higher maximum discharge. The first part is maintaining the discharge until the pressure loss reaches the equilibrium value. This part can take, certainly in the case of low discharges, more than 10 minutes. The second part is a discharge calibration (see next section) and sampling of the concrete. The sampled concrete is each time tested in the rheometer

and subjected to a slump flow, V-funnel, sieve stability, density and air content measurement. The third part is stepwise decreasing the discharge to the lowest value, similar as a pumping cycle, but not exceeding the discharge from the first part. At discharge step 1, there is consequently no down-curve. After the determination of the down-curve, the discharge is increased by one step and all parts are repeated. This procedure, as it takes somewhat more than one hour, has only been applied once to each concrete, except for SCC LM-15.

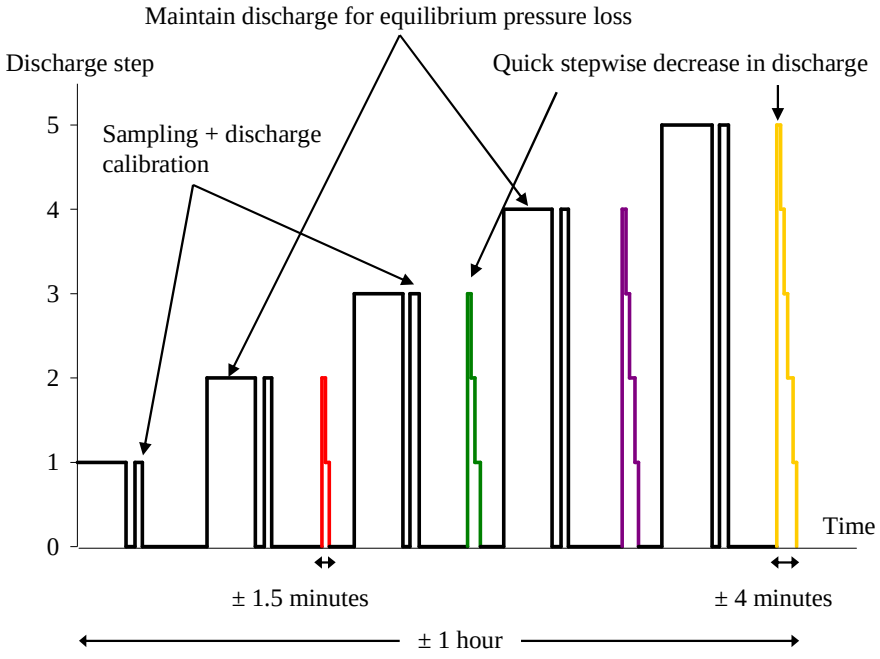

Figure 8.14: Principle of the testing procedure for special thixotropy tests.

This procedure, as described in figure 8.14 has been fully applied to the concrete SCC LM-17. For the other concretes, a variation on the procedure has been applied. For SCC LM-12, the intermediate down-curves have not been executed, only the down-curve starting from discharge step 5 (the orange-yellow curve in fig. 8.14). For SCC LM-14, due to too large pressures, the discharge has not been increased over step 4. For SCC LM-16, the same applies as for SCC LM-14, but the procedure has been repeated three times at step 3. SCC LM-15 has undergone the procedure twice, with a 30 minute rest in between. During the first test, the discharge was not increased over step 4, but during the second test, step 5 has been reached.

3.3 Discharge calibration

When taking a sample, the valve at the bottom of the sampling reservoir is closed. As the reservoir is attached to the rolling bridge with a load cell in between, the weight variation of the reservoir can be measured, also at a rate of 10 measurements per second. When pumping one full stroke inside the reservoir, the corresponding time can be measured, both with the stopwatch as afterwards in the output file. With known density, the volume variation with time can be calculated, and discharge is consequently known.
The volumetric discharge measurements fit very well with the obtained results with the stopwatch and the output file, even with the assumption of 100% filling of the cylinders (fig. 8.15). On the other hand, it is mentioned in literature that the cylinders do not fill 100% [8.1], and as a result, a clarification is needed.

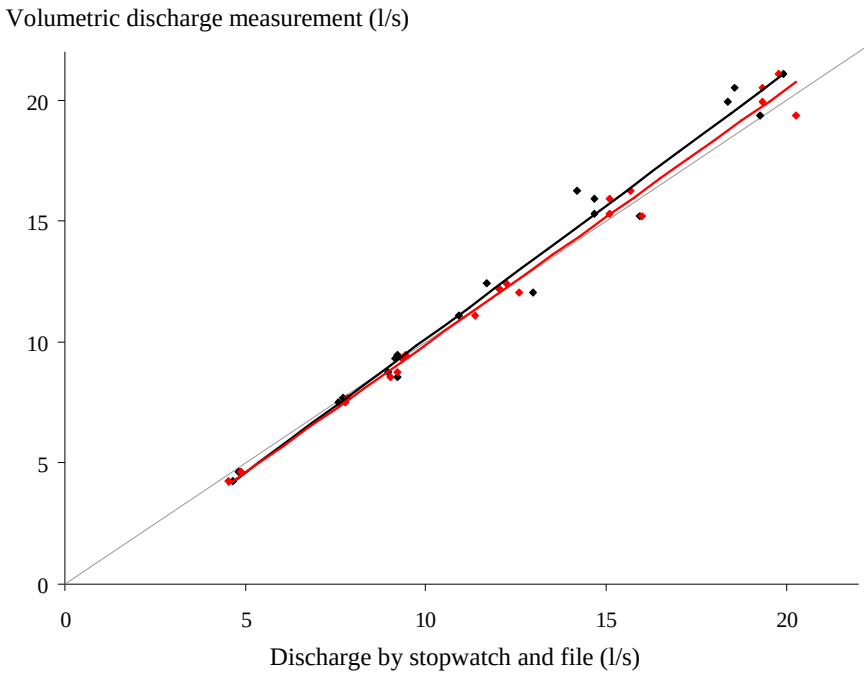

Figure 8.15: Comparison of volumetric discharge measurement (with reservoir and load cell) with the discharge, measured by the stopwatch (black) and the file (red), indicates a very good agreement (grey line is 1-to-1 relationship), assuming 100% filling of the cylinders. Data from SCC LM-11, 12 and 13.

The physics behind this remarkably good agreement can be explained by means of the schematic representation of figure 8.16 [8.1]. The red curve represents (approximately) the real discharge during the pumping. For the determination of the discharge with the reservoir and the load cell, only the data in equilibrium, represented by the horizontal red line, have been used. For the other methods, with

the stopwatch and the output file, the discharge is assumed to be constant during the full measuring period, corresponding to the blue line. As can be seen, the assumed discharge and the real discharge differ.

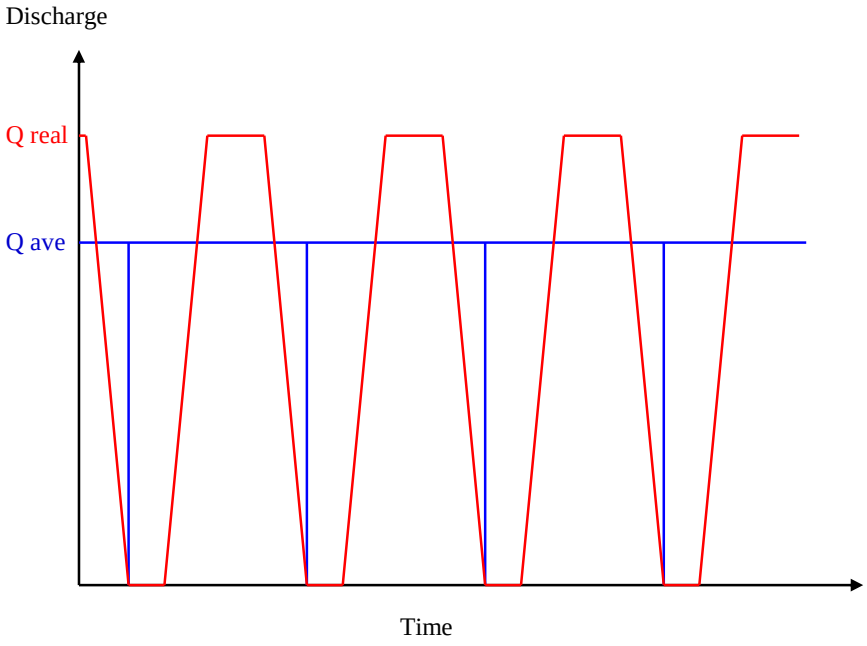

Figure 8.16: Real discharge (red curve) and the assumed discharge (blue curve) for the measurements with the stopwatch and the output file. Note that the volumetric discharge has been determined by only taking the data in equilibrium (red) into account.

$$Q_{real,eq} = k_{fill} \cdot k_{nconst} \cdot Q_{ave} \qquad (8.1)$$

where: $Q_{real,\,eq}$ *= the occurring discharge during equilibrium (m³/s)*
Q_{ave} *= the average discharge measured by means of the stopwatch (m³/s)*
k_{fill} *= correction factor (< 1), for the non-perfect filling of the cylinders (-)*
k_{nconst} *= correction factor (> 1), due to the assumption of a constant discharge during the measurements, while it is not (-)*

From equation 8.1, the two correction factors (k) need to be determined in order to know the real discharge, at equilibrium, which is the discharge during which the pressure losses are measured. Due to a lucky coincidence, the two correction factors appear to compensate each other, allowing us to use the measured discharge as the correct discharge value.

In fact, we should be able to calculate the filling ratio of the cylinders, but as the variation of discharge during the switch of the valve is complicated, this calculation has not been performed.

3.4 Segregation tests

This test procedure has been applied in order to investigate dynamic segregation of the SCC during the flow in the pipes, causing so-called slippage layers [8.1][8.4][8.9-8.10]. The principle of the test is shown in figures 8.17 and 8.18. The test setup consist of a wooden box, with a sharp metal blade at one edge, which is put in the concrete outflow. The distance between the sharp blade and the inner part of the pipe, called "x" (fig. 8.17) is varied from 5 over 3, 2 and 1 to 0.5 cm.

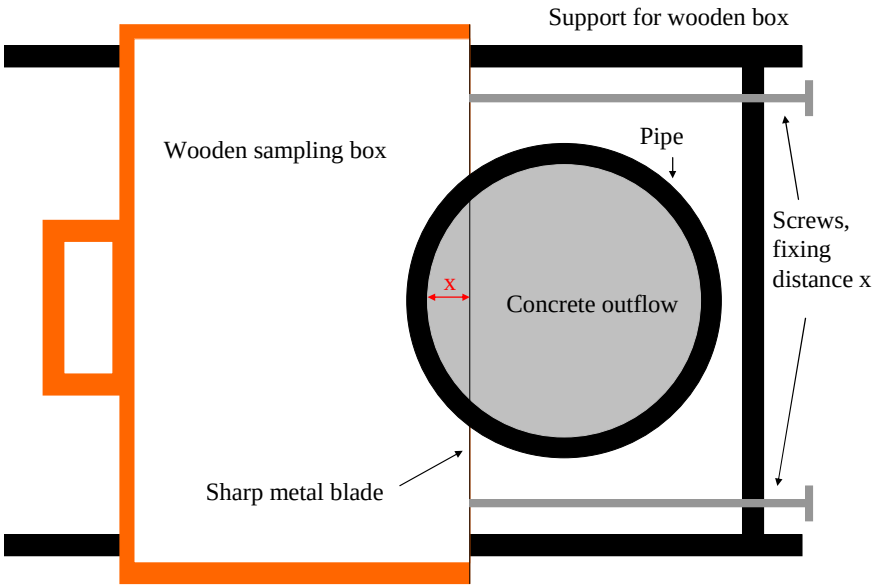

Figure 8.17: Principle of the sampling for the segregation tests (top view).

Due to the sharp metal blade, the flow is split into a main part, which flows in the reservoir of the pump, and a part which is collected in the wooden box. The position of the steel blade is a critical point during the tests. As the box is situated at the end of the circuit, it is very close to the last (downward) bend. The blade is put parallel to the flow direction of the concrete just before the bend. This specific position has been chosen in order to eliminate as much as possible the inertia effects on the coarse aggregates, probably caused by the bend.
From the concrete in the wooden box, a sample of 2-3 kg is taken, weighted, and washed on the sieve of 2 mm. The aggregates remaining on the sieve, larger than 2 mm, are collected and dried in an oven at 105°C. From the collected aggregates, at

the different distances x, the grain size distribution is determined and compared to the theoretical values. The ratio of the collected aggregates to the total concrete mass (measured) is calculated.

Figure 8.18: Execution of the segregation test (side view). The wooden box is being pushed in the concrete flow.

This test has been executed on SCC LM-3 to 10 and on the TC, but as will be explained in chapter 9, the results are inconclusive. As a result, this specific test has not been repeated during later pumping tests. The execution of these tests occurred between two pumping cycles.

3.5 Temperature test

On SCC LM-3, a temperature test has been executed. This test consisted of continuously pumping this SCC, at 11-12 l/s (step 3) and monitoring the temperature evolution. This test has been executed between the two last pumping cycles for SCC 3, but as it caused significant stiffening of the concrete, due to a temperature of 34°C, at an age of 230 minutes, the last cycle has not been performed, and the temperature test has no longer been executed. On the other hand, temperature evolution has been monitored simultaneously with each pumping test. As a result, the influence of pumping on the temperature can be easily derived and this special test is in fact not needed.

4 Blocking

Blocking is surely the most dangerous condition during pumping, and it causes a large amount of problems. Kaplan discussed in his thesis [8.1], in detail for traditional concretes, four different causes of blocking. Blocking during pumping operations appears really seldom, and is in most cases due to an error in pipe configuration or concrete composition. Blocking during restart is also extensively discussed by Kaplan, in which he argues that this type of blocking is caused by segregation, although this could also be caused by thixotropy, in case of rapidly rebuilding concretes. A third type of blocking can occur during cleaning with water. For a much more detailed discussion on blocking, we refer to the thesis of Kaplan [8.1].

The main part of the blockings occurs during start-up. In this case, the amount of fine materials in the concrete decreases with increasing pumping distance and as a result, a group of coarse aggregates moves ahead of the bulk concrete. In this way, if we recall chapter 2, the maximum volume fraction decreases, while the effective volume fraction increases. This leads to a significant increase in apparent viscosity, and combined with an increased importance of friction caused by the coarse aggregates, the flow is finally stopped.

The decrease in fine materials during start-up is caused by two phenomena: attachment to the wall, in order to eliminate the roughness of the pipes, and filling of the interior of the rubber seals. Furthermore, due to inertia, the coarse aggregates move ahead of the bulk concrete at the end of a stroke [8.1].

This decrease in fine materials can be prevented by pumping a water-cement mixture in front of the concrete before start-up [8.1-8.2]. As a result, pumping in an inclined upward pipe is the most advantageous. For horizontal pipes, the cement-water mixture spreads in the whole circuit, only covering the lower part of the pipes. Opening the pipes in order to remove a blocking results in the loss of a main part of this mixture. An inclined, downward pipe is the worst case for start-up. Due to gravity, the coarse aggregates fall down and collect at the end of the downward section.

In our experimental program, blocking never occurred in the short circuit, but it did occur in the long circuits. Especially when the first concrete of the day was pumped inside the long circuit, 4-5 blockings occurred when trying to fill the circuit. For the second concrete, only 1 or 2 blockings were observed. Between the two concretes, the pipes are cleaned by means of a sponge and air pressure (see next section), but the circuit has not been de-assembled and cleaned with water. In this way, the walls are still partly covered with a (dry) layer and the rubber seals are still full.

Blocking only occurred at the exit of a bend or in the flexible hose. This is in accordance to the description of Kaplan and Crepas [8.1-8.2]. These results indicate that a very complex flow pattern is occurring inside the bends and reductions. As a result, reducing the length of the long circuit did only reduce the applied pressure, not the number of blockings.

Figure 8.19 shows a plot of pressure as a function of time, when inserting SCC LM-16, where long periods of rest are visible, due to the removal of the blockings. Increasing pressure can also be noticed, due to the increasing length of the filled pipes, and consequently, the increasing pressure losses. The most striking parts in

figures 8.19 and 8.20 are the peaks in the figures. These peaks establish in a few seconds, during which full blocking and flow stoppage occurs. The pressure recorded during blocking is 55-60 bar, which is 1.5 times higher than the maximal pressure recorded during flow. Note that the pump was operating at its lowest capacity (step 1) at that moment. Increasing the capacity can possibly break up the blocking, but can also increase the blocking pressure.

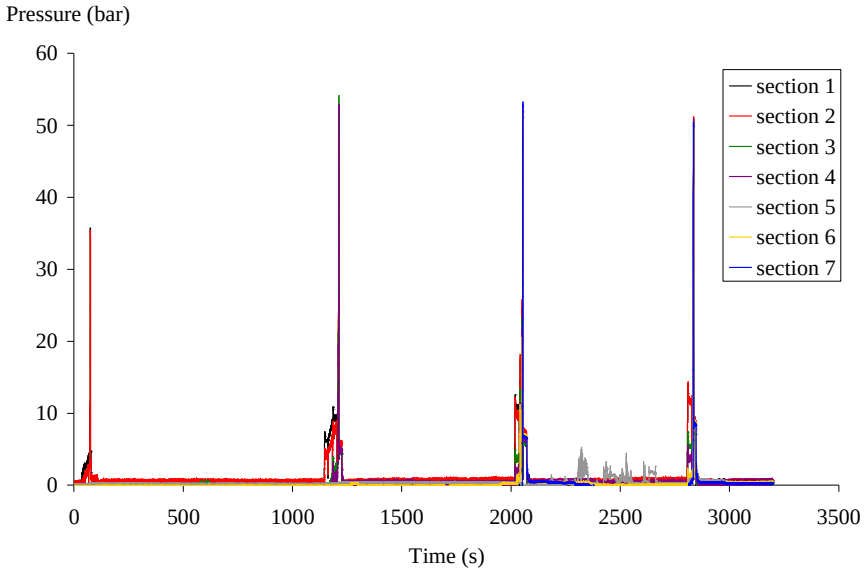

Figure 8.19: Blocking during the insertion of SCC LM-16 causes very high pressure peaks.

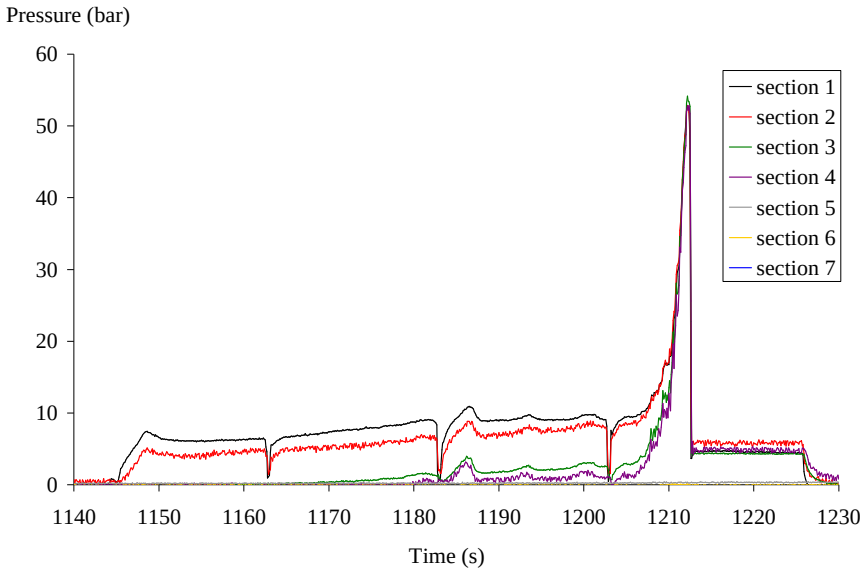

Figure 8.20: Detail of the second blocking of fig. 8.19, illustrating the gradual increase in pressure as more concrete is pumped inside the circuit, and the sudden pressure rise due to blocking. Note that the concrete did not reach sections 5, 6 and 7 in this case.

5 Cleaning

Cleaning has been performed by means of a sponge ball, driven by air pressure [8.1-8.2]. The small circuit has been cleaned in one step, pushing all concrete in a reservoir at the end of the circuit. The long circuit has been interrupted at 3 or 4 different locations, not only to restrict the amount of concrete flowing out at the end of the circuit (the long circuit contains 1 m^3 of concrete itself), but also to reduce the air pressure and ease the cleaning.

Cleaning by air pressure is mostly applied on site and is a quite spectacular procedure. As the amount of concrete in the pipes decreases when the sponge moves further in the pipes, the total flow resistance decreases and the sponge accelerates. Normally, when the sponge is near 2/3 of the circuit, the air pressure is removed. Still, at the end, the sponge has maximal velocity and is "shot" inside the capturing reservoir. No specific "sponge-catcher", as described in the thesis of Kaplan, was available [8.1].

The reservoir of the pump and the cylinders have been cleaned thoroughly with water after the last test of each concrete delivery. All pipes of the circuits and the rubber seals have only been cleaned with water at the end of a testing day. Between two concrete deliveries, only cleaning with the sponge ball has been performed. As a result, the rubber seals are still full of material, possibly causing less blocking when inserting the second concrete inside the long circuit.

On site, when only using the pump and the placing boom, a possible procedure of cleaning consists of pulling the concrete back inside the pump, after the concrete has been pumped out of the reservoir as much as possible, if necessary, back inside the concrete mixer. When performing this reverse pumping operation, a sponge is put at the end of the placing boom and is pulled inside the reservoir. The concrete pulled back in the reservoir is deposited on the site. When this procedure is not possible, due to too stiff concrete or too long pipes, the same procedure as during our tests applies.

Kaplan has mentioned a safer procedure for cleaning longer pipe systems, namely pushing the concrete by water [8.1-8.2]. From a safety point of view, this procedure is much better, but the cleaning water is still contaminated with cement and can, officially, not be deposited in nature. During cleaning with water, blocking can also occur due to the non-perfect seal between the water and the concrete.

6 Safety

Pumping of concrete can be a dangerous practice. Even if the concrete is well designed to be pumped, most problems arise during the insertion in the pipes. As has been shown in the section dealing with blocking, the pressure shoots up to a certain very high value, which the whole circuit must stand. Breaking of the weakest link can cause many problems, like cleaning of a few m^3 of concrete, or even worse, someone getting hit by a flying object.

Considering on site pumping, when the concrete blocks in the placing boom, it can be that, possibly due to an increase in pumping pressure or by reversing concrete flow [8.2], the blocking gets dissolved. In case of a sudden de-blocking, the boom can swing significantly, and if someone standing on top of the formwork is holding the end of the boom at that time, he can be thrown of the formwork, possibly with very severe consequences. As a result, the insertion of the concrete in the pipes should be done in a restricted area, where nobody is present. Secondly, when blocking occurs, the pressure should not be increased in order to handle the problem, but the blocking should be properly removed. Although this is very time consuming, it enhances the safety on site significantly. A proper preparation of the cement-paste before pumping is of crucial importance.

The cleaning procedure by means of air pressure is also not very safe. Our personal experience has indicated that the sponge is indeed spectacularly shot out of the pipes. The operator of the pump has shared his experience on on-site cleaning. One time, there was a misunderstanding and the air pressure was not removed on time. Three people sitting on a wheel-barrow in order to hold the sponge, were thrown of. The worst experience he told us, was of a colleague of him, a well build man, who was going to stop the sponge by a wooden plate which he was holding with his knee. This man was moved 6 m far and 3 m high (this might be a little exaggerated by our operator), having a shattered knee and leg, a broken arm and a few broken ribs.

As can be seen, pumping concrete is a dangerous job, where people put their lifes in hands of the operator. Common sense and a good understanding of the possible consequences are seriously advised !

7 Summary

In this chapter, the concrete piston pump, the steel pipes and the short and long circuits have been described. The pressure losses are measured by means of two pressure sensors and pipes equipped with strain gauges. Discharge is measured by registering the time needed for a certain amount of strokes. Although the filling ratio of the pumping cylinders is not equal to 100%, the discharge measurement procedure has been proven to work very well, without any corrections, in order to measure the discharge at constant pressure.

In total 18 different self-compacting and 1 traditional concrete mixtures have been pumped.

Two different procedures have been applied. The regular procedure is a short stepwise decrease of the discharge from 20 l/s to 5 l/s, which has been repeated each 30 minutes. The special thixotropy procedure has been applied on 5 different concretes and consisted of increasing discharge by 1 step, maintaining it until equilibrium, sampling and discharge calibration and quickly decreasing discharge stepwise.

In between the regular tests, a special dynamic segregation testing procedure has been performed on 9 different concretes, including the TC.

Temperature is monitored continuously, although one test has been specifically performed in order to investigate the influence of pumping on temperature.

Blocking and cleaning have been briefly described, indicating the possible safety hazards. A fundamental understanding of what can happen and a good common sense are advised during pumping operations with concrete.

8 References

[8.1] Kaplan D., "Pumping of concretes," Ph-D dissertation (in French), Laboratoire Central des Ponts et Chausées, Paris (2001).

[8.2] Crepas R.A., "Pumping concrete, techniques and applications, 3rd edition," Crepas and Associates, Inc., Elmhurst (1997).

[8.3] Guptill N.R. et al. (ACI-Comm 304), "Placing concrete by pumping methods," American Concrete Institute, Farmington Hills (1998).

[8.4] Kaplan D., de Larrard F., Sedran T., "Design of Concrete Pumping Circuit," ACI Mat. J. **102:2** (2005), 110-117.

[8.5] Ovarlez G., Chateau X., "Influence of shear stress applied during flow stoppage and rest period on the mechanical properties of thixotropic suspensions," Phys. Rev. E. **77** (2008), 061403.

[8.6] Ovarlez G., Chateau X., Roussel N., "Influence of the shear stress applied during flow stoppage and rest on the mechanical properties of thixotropic suspensions," Proc. of the XVth Int. Cong. on Rheology, Monterey (2008), 1042-1044.

[8.7] Beitzel H., Beitzel M., "Pump application for self-compacting concrete under extreme conditions," Proc. of the 3rd North-American conf. on the design and use of self-consolidating concrete, Chicago (2008).

[8.8] Tattersall G.H., Banfill P.F.G., "The rheology of fresh concrete," Pitman, London (1983).

[8.9] Haist M., Mechtcherine V., Beitzel H., Müller H.S., "Retrofitting of building structures using pumpable self-compacting lightweight concrete," Proc. of the 3rd Int. RILEM Conf. on Self-Compacting Concrete, Reykjavik (2003), 776-785.

[8.10] Kaplan D., Sedran T., de Larrard F., Vachon M., Marchese G., "Forecasting pumping parameters," Proc. of the 2nd Int. RILEM Conf. on Self-Compacting Concrete, Tokyo (2001), 575-584.

CHAPTER 9:

PUMPING TESTS: RESULTS AND DISCUSSION

In this chapter, the results of the full scale pumping tests will be discussed. The test setup, measurement systems and testing procedures have been described in the previous chapter. All results of the pumping tests can be found in Appendix D. This chapter contains, after the introduction, two main parts. The first part describes the influence of the rheological properties of SCC on pumping, while in the second part, the opposite, namely the influence of pumping on rheology, is discussed. Combining these two parts reflects the full title of this thesis: interactions between rheological properties and pumping of SCC. Before the summary, a rough prediction tool for the pumping pressures and a brief advise for pumping SCC in practice will be given.
Before going into any discussion, it is very important to know that the results obtained in this thesis are only valid for the considered concrete mixes and the used pipe configurations. In other cases, different results can be (and have been) obtained, for example by D. Kaplan [9.1]. The experiments described in this thesis have revealed some insights into pumping of self-compacting concrete, but many aspects still need to be explored in the future.

1 Introduction

Pumping of normal concrete has been studied in literature both from a purely scientific point of view, as with a practical perspective. From the practical side, advise is given dealing with pump types, length and diameter of the conveying line, concrete composition, … [9.2-9.3].
From the scientific approach, Kaplan has summarized the available literature dealing with pumping of concrete [9.1]. He stated that an important element during the flow of concrete in pipes is the behaviour near the wall. The wall friction τ_f, which has the unit of a stress (Pa), can be dominated by several phenomena, and the resulting outcome is each time different. In the coming sections, the influence of several types of behaviour will be briefly discussed, based on several results available in the literature.

1.1 Different behaviour laws for the wall friction

1.1.1 Wall friction is constant

This is the most easy situation, in which the friction stress is independent of the applied pressure and the flow velocity. As a result, the pressure losses are determined only by the geometry of the conveying line and the rheological properties of the material [9.1][9.4]. This type of flow behaviour is based on the no-slip assumption and as a result, the extended versions of the Poiseuille formula are valid, at least if the rheological properties of the material remain constant in the pipe. In case a lubrication layer, which is a layer with lower rheological properties, is formed near the wall, discharge is increased for a certain pressure loss. In this case, as slippage does not occur, the extended Poiseuille formulae can be modified once more which will be discussed in section 2.2.1 of this chapter.

1.1.2 Wall friction is dependent on the flow velocity

In this case, the no-slip condition for the Poiseuille formula is no longer fulfilled, and the total velocity can be divided into two components, one due to shearing and one due to slippage [9.1][9.5-9.6]. In this situation, it is assumed that the wall friction is still independent of the pressure. The pressure losses per unit of length still remain constant over the length of the pipe and, in case of a horizontal circuit and laminar conditions, the total pressure decreases linearly with the length of the pipe.

1.1.3 Wall friction is dependent on the local pressure

Instead of a liquid behaviour, as it is the case in the two sections described above, the interaction between the concrete and the wall is more solid-solid like. As a result, Coulombs friction law is valid, stating that the force needed to displace a certain solid material over another solid material is dependent on the applied normal force and the friction coefficient between these two materials. As a result, the pressure losses do not longer evolve linearly with the length of the pipe, but a decreasing exponential curve is obtained [9.6-9.7]. This can be very disadvantageous in case of long conveying lines.
This type of behaviour is typical for the so-called unsaturated concretes, which means that for this type of concretes, the water can migrate internally to other zones, decreasing the magnitude of stress transfer in the liquid and increasing the solid-solid, frictional behaviour [9.6-9.7]. In case of saturated concretes, the water does not migrate sufficiently and the behaviour at the wall remains liquid-like [9.6]. The difference between pumping saturated and unsaturated concretes is significant. Browne and Bamforth [9.6] have calculated the maximal distance a certain concrete can be pumped under a certain set of conditions. In case the concrete was saturated, the maximal distance was 250 m. In case of unsaturated concrete, the maximal pumping distance was 1.1 m! This means that if in that pipe system, a section of 1.1 m of saturated concrete becomes unsaturated, the whole system gets blocked.

1.1.4 Wall friction is dependent both on the pressure and the flow velocity

This is a combination of the two above mentioned effects, but it is very difficult to calculate. Currently, this situation has only been reported once [9.8].

1.2 What in case of self-compacting concrete?

Recalling chapter 1, the three basic properties of SCC are the flowing ability, the passing ability and the stability. In order to achieve these properties, the amount of coarse aggregates is reduced, and very special attention is paid to segregation and bleeding. As a result, the transformation from saturated concrete to unsaturated concrete is not likely to occur, and the amount of possible friction between the aggregates and the wall is reduced, which decreases the probability of the wall friction to be dependent on the pressure. Consequently, for self-compacting concrete, it is assumed that the wall friction is constant or only dependent on the flow velocity, and that the pressure shows a linear evolution with the length of the pipe, at least in case the rheological properties remain constant over the length of the pipe (see section 3.4.3). Currently, it is not clear whether slip is occurring or not, but this will be discussed in sections 2.2.3 and 2.2.4.
It would be wrong to exclude the unsaturated condition in case of SCC, because during start-up, blocking occurred, which is the result of water migration relative to the movement of the aggregates. But as after start-up, during the execution of the tests, no further blockings have been observed, not in the short nor in the long circuits, it is assumed that the wall friction is not dependent on the pressure during the tests.

2 Influence of rheology on pumping

2.1 Straight sections

As described in chapter 8, the pressure loss is measured between two fixed points in the circuit, when the pressure is at equilibrium between two switches of the valve of the pump. The pressure difference is divided by the distance between the sensors in order to obtain a pressure loss per unit of length. As shown in chapters 6 and 7 and in the case of saturated concretes, the total pressure loss is supposed to relate linearly with the length of the pipe, but this will be further discussed in section 3.4.3. For the short circuit, only one measurement section has been installed. For the long circuits, the pressure losses have been measured in three straight sections. Unfortunately, for only two of these sections the results are available. Mostly, the results of the last section have been applied in the analyses.

The results given hereafter are mainly based on the results of the regular pumping tests, as described in section 3.1 of chapter 8. For SCC LM-3, 4 and 5, the downstream pressure sensor has been installed behind the first bend, resulting in the incorporation of the losses in a bend in the measured pressure losses. As there is no straight-section reference for these concretes, the results have been omitted in the main part of the analysis, but they agree qualitatively with the other results. The influence of a bend on the pressure losses will be briefly discussed in section 2.4.

A few minutes before each pumping cycle during the regular pumping tests, a sample of concrete is taken. From this sample, the rheological properties have always been determined with the Tattersall Mk-II rheometer [9.9-9.10]. The rheological properties are modelled by means of the modified Bingham model (chapter 4) or with the Bingham model if no shear thickening has been observed.

The volume of the concrete sampled for the rheometer is around 12.5 l. The total amount of concrete being pumped during the regular pumping tests is around 1.25 m³. As a result, the sampled amount of concrete is 1% of the total volume of concrete, and it can be doubted whether this sample is fully representative. In some cases, the sample appeared to be too stiff, in other cases it was too fluid. In the tables of Appendix D, the doubtful samples have been marked. If the concrete is too fluid, the Tattersall rheometer is no longer able to produce reliable results (see chapter 3). In these cases, the rheometer results are better not applied in the analyses and in some cases, like SCC LM-9, cycle 1, the transformation procedure does not deliver any results. For all measurements, the torque value at equilibrium during pre-shearing at the maximal rotational velocity is also given as a flow resistance parameter. Unfortunately, no reproducibility tests have been performed with the rheometer during the pumping tests.

As will be shown in section 3.1 of this chapter, the pumping pressures are dependent on the number of times the concrete has been pumped. As a result, only the obtained results which are considered to be in equilibrium, have been taken into account.

2.1.1 Traditional versus self-compacting concrete

Figure 9.1 shows the pressure loss – discharge curves for the 6 pumping cycles which have been performed on SCC LM-8, while figure 9.2 shows the two cycles for the traditional concrete.

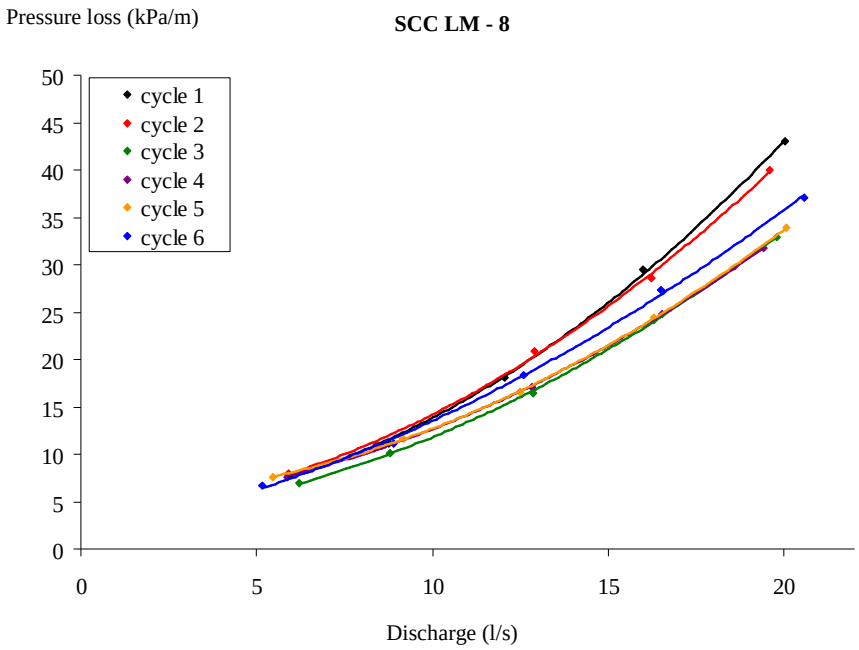

Figure 9.1: Pressure loss – discharge curve for SCC LM-8. Note that, for this concrete, the equilibrium is achieved in cycles 3, 4 and 5.

A first striking difference between the curves of the self-compacting and the traditional concrete is that the SCC-curves show non-linearity, while for the traditional concrete, the curves are straight. This is in accordance with the findings of chapters 6 and 7, when dealing with the extended Poiseuille formula and the gravitational flow tests: a non-linear rheological behaviour is translated in a non-linear pressure loss – discharge curve. As can be seen in Appendix D, for all SCC pumped in the short circuit, the curves are (sometimes only slightly) non-linear. On the other hand, for some SCC, like SCC LM-2 and 3, no shear thickening has been observed in the rheometer. Could it be that due to the high shear rates in the pipes (see next section), the critical shear stress for shear thickening (see chapter 2 and 4) is only exceeded in the pipes and not in the rheometer? This might be an explanation, but no certainty exists.

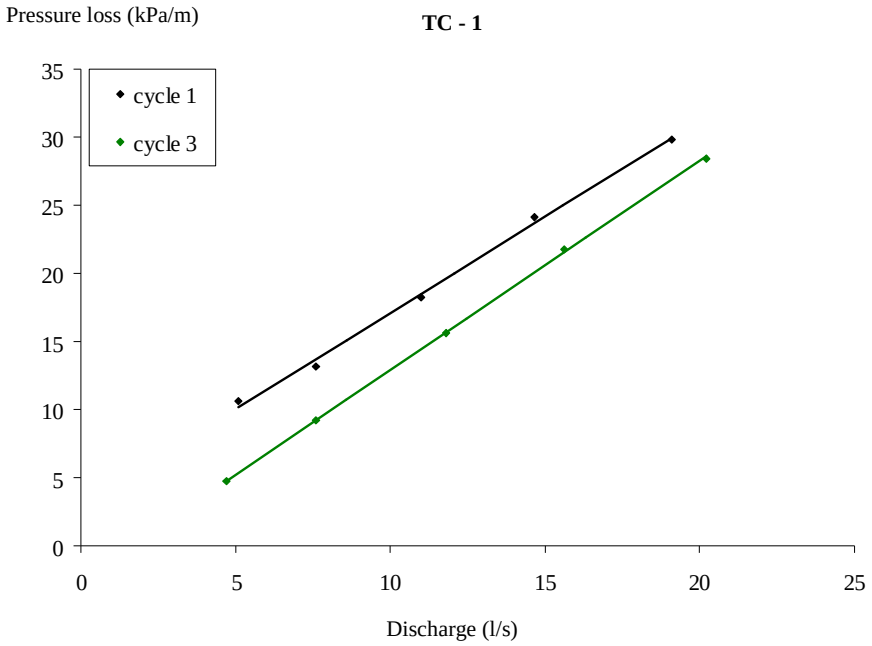

Figure 9.2: Pressure loss – discharge curve for TC-1.

For the curves of SCC LM-14 to 17, although it can be seen in the data points, no non-linear relationships have been visualised, due to the different testing procedure and due to the lower amount of data points available. The result of these concretes will be discussed in section 3 of this chapter.

2.1.2 Influence of rheological parameters

In order to investigate the influence of the rheological parameters on the pressure losses, 17 results have been retained, after elimination of the non-equilibrium cycles (numbers 1 and 2 of each concrete), the segregating concretes (SCC LM-9 and 10), and the doubtful rheometer results. Figure 9.3 shows the correlation between the pressure losses at each discharge with the tangential viscosity determined at a shear rate of 10/s, while figure 9.4 compares the pressure losses with the yield stress.
As can be seen in figures 9.3 and 9.4, the pressure losses relate very well to the tangential viscosity, determined at a shear rate of 10/s (consequently incorporating shear thickening), and also to a certain extent with the yield stress. Especially at the high discharges, the correlation between pressure loss and viscosity is remarkably high. At lower discharges, this correlation decreases and at the lowest discharge (discharge 1), the correlation between pressure loss and yield stress is even higher.

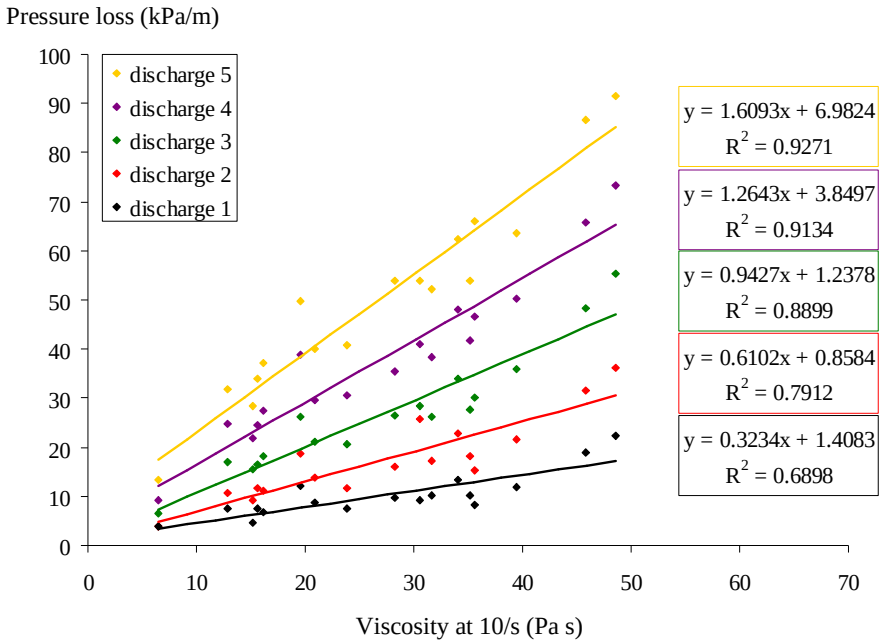

Figure 9.3: Pressure loss per unit length is remarkably well correlated with the tangential viscosity at a shear rate of 10/s, especially for the higher discharges.

On the other hand, yield stress and viscosity are not independent from each other. As can be seen in the tables of Appendix D, SCC with a low viscosity mostly also have a low yield stress. Analysis of the results in figures 9.3 and 9.4 has indicated that the pressure loss is more sensitive to a variation in viscosity than to an equivalent variation in yield stress. The above mentioned variations in viscosity and yield stress are determined by one standard deviation from the median value of the results in figures 9.3 and 9.4, excluding the highest and lowest data points. At the highest discharge (step 5), an increase in viscosity with one standard deviation causes an increase in pressure loss which is twice as high as the resulting increase in pressure loss caused by an increase in yield stress with one standard deviation. The special thixotropy tests from section 3 indicate also a larger dependency of the pressure losses on the viscosity, compared to the yield stress.

The influence of the viscosity has been eliminated from the pressure loss data by calculating the difference between the viscosity of a certain concrete and the reference viscosity, and the calculation of the change in pressure loss corresponding to this difference in viscosity, according to the linear correlations obtained in fig. 9.3. As a result, the influence of viscosity is eliminated from the pressure loss data and in this case, the relationship between yield stress and pressure loss also disappears, indicating that yield stress and viscosity are indeed related.

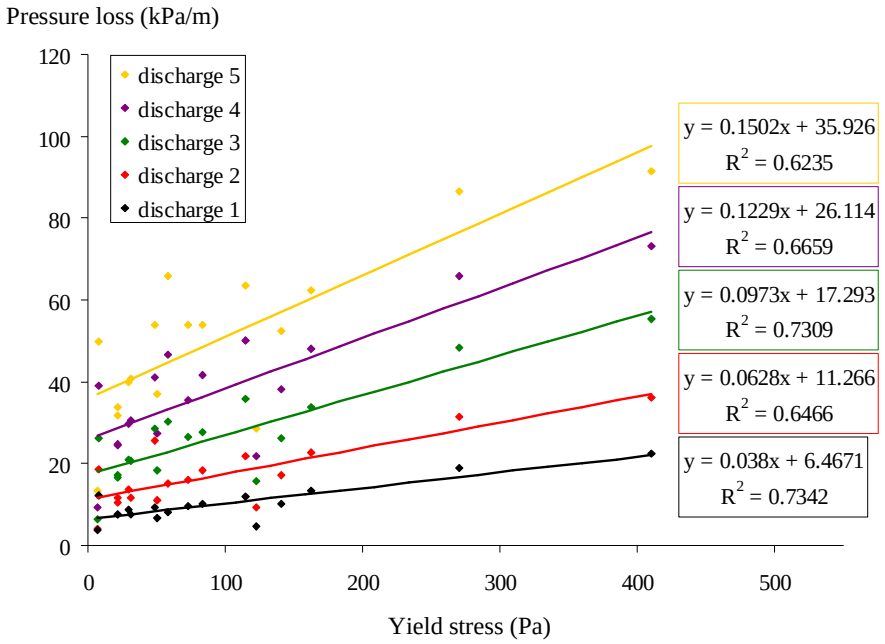

Figure 9.4: Pressure loss related to yield stress.

In figure 9.3, the tangential viscosity at 10/s is chosen. Further analysis has indicated that, for each discharge step separately, there is an optimal shear rate at which the tangential viscosity should be determined in order to find the best correlation between the tangential viscosity and the pressure loss. This shear rate varies between 12/s and 15/s for all discharges, improving the correlations in figure 9.3 with 1 % or 2 %. As a result, not only the viscosity is an important parameter, but also the possible shear thickening in the SCC influences the pressure losses.
Figure 9.5 compares the results of the TC with SCC LM–7, which has a slightly higher viscosity. As a result, especially at the higher discharges, a larger pressure loss is observed. When comparing figures 9.1 and 9.2, similar pressure losses for SCC LM–8 and the TC are observed. These concretes have similar values for the viscosity.
In chapter 4, it has been shown that SCC with silica fume has a much lower viscosity and does not show shear thickening in the shear rate range measured. This type of concrete has not been pumped, but the pressure losses are expected to be much lower than in case of SCC with limestone filler. Pumping SCC with silica fume would mean a large advantage, but the local price of silica fume is much too high in order to incorporate it in standard SCC. Furthermore, it should be mentioned that the frame available to optimize the rheological properties for pumping is really small due to the restrictions imposed by the needed workability during casting and by the final properties of the concrete needed, like strength and durability.

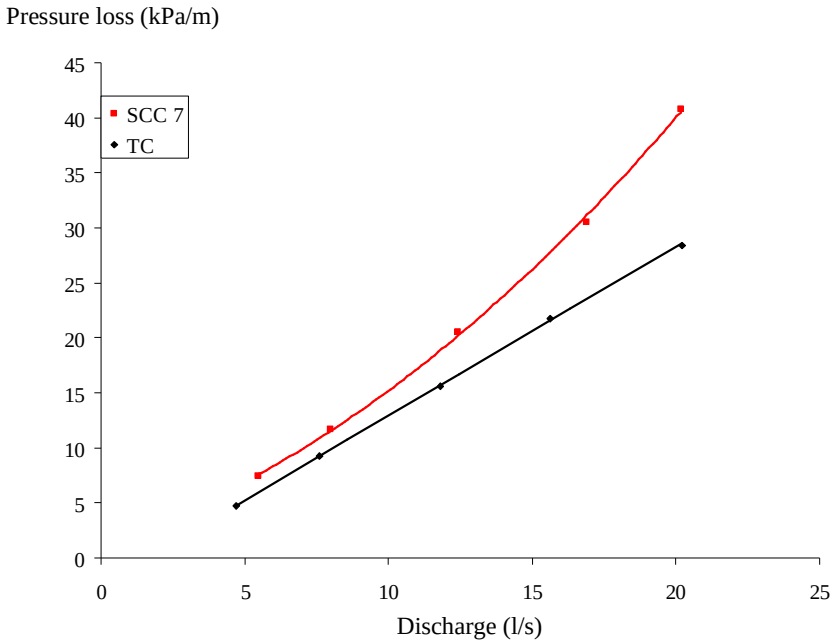

Figure 9.5: The pressure loss of SCC LM–7 (red) is higher than the pressure loss of the traditional concrete (black), especially at the high discharges, due to the larger viscosity of the SCC.

Also in chapter 4, it has been mentioned that adding a relatively small amount of oil reduces the shear thickening behaviour significantly. Should oil be added to SCC which will be pumped? If only pumping is concerned, maybe yes, it will reduce the pumping pressures certainly at high discharges, but as the influence of oil on other properties, like strength and durability, is not fully understood, it should not (yet?) be added on purpose. During the full scale pumping tests, it has been observed that the oil sprayed in the reservoir of the pump partly mixes with the pumped concrete.

2.1.3 Compared to literature

Kaplan proposed in his thesis a bi-linear model for the pressure loss – discharge curves (fig. 9.6) [9.1]. The inflection point is the separation between pure plug flow (part 1), during which all shear rate is concentrated in a small zone with lower rheological properties near the pipe wall, and the part in which shearing of the concrete causes an additional contribution to the discharge (part 2).
This bi-linear relationship has not been observed during any of our pumping tests. The results of our tests are considered to be all in the second part of the curve of figure 9.6. The reason for this can be easily explained with the values of the yield stress. In chapter 6, it has been mentioned that the yield stress influences the plug radius. The smaller the yield stress, the smaller the plug radius. In our case (pumping

SCC and a TC with a rather low yield stress), the plug radius is suspected to be small, and the homogeneous part of the concrete, which is the part not influenced by any effect mentioned in section 2.2, is partly subjected to shear. In the thesis of Kaplan, the yield stresses of the (traditional) concretes were much higher, resulting in a larger plug radius. As a result, the obtained results and conclusions for SCC are only valid in case the yield stress of the concrete is lower than (approximately) 0.5 times the wall shear stress. In case the yield stress increases over 0.5 times the wall shear stress, the yield stress starts to have a significant influence, because the amount of concrete being sheared will decrease.

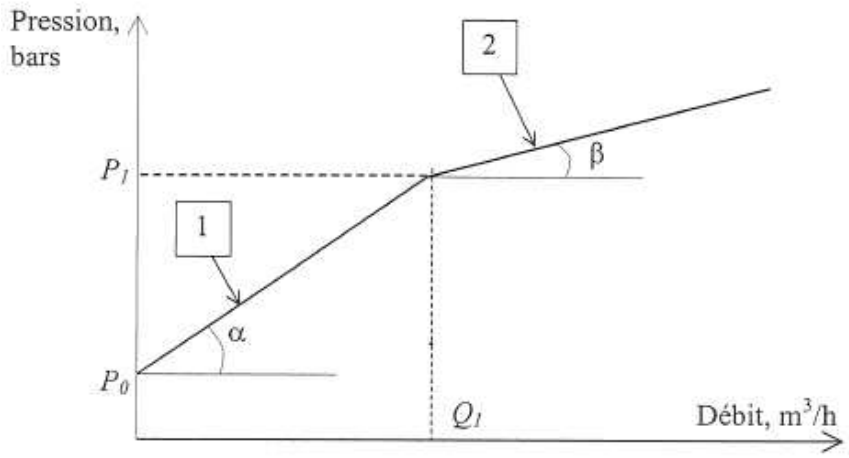

Figure 9.6: Bi-linear relationship between pressure (pression) and discharge (débit), proposed by Kaplan. Figure from D. Kaplan [9.1].

2.2 Theoretical predictions based on rheological properties

Similar as for the gravitational flow tests, the extended Poiseuille formula has been applied in order to compare any theoretical predictions, based on the rheometer data, with the obtained experimental results. In case the concrete did not show any shear thickening, the Buckingham-Reiner equation has been applied (chapter 6) [9.11], in case of shear thickening, both the Buckingham-Reiner (based on the approximated Bingham relationship) and the extended Poiseuille formula for shear thickening materials have been applied.

When applying the Buckingham-Reiner equation, the pressure losses are overestimated with a factor between 2 and 5.5. In case of the extended Poiseuille formula for shear thickening, the overestimation was between a factor 4 and 10.5. Although comparison of different rheometers has shown that not always the same results are obtained [9.12-9.13] and it can be questioned which rheometer delivers the best results, a factor 5 or 10 is too large to be attributed to erroneous rheometer results only. Furthermore, the comparison between the rheometer values and the gravitational flow tests has shown rather good agreements (chapter 7).

Considering the conditions of application of the Poiseuille formula, (at least) two of these can be doubted to be fulfilled. It has been argued by Kaplan that there is a contribution of slippage to the total velocity [9.1] or that a lubrication layer can be formed near the wall. As a result, both the conditions of homogeneity and no-slip can be questioned. Investigating more in detail the different phenomena influencing the concrete properties, three different causes have been found:

- Geometrical wall effect
- Structural breakdown
- Dynamic segregation

The influence of these effects will be discussed in the following sections.

2.2.1 Geometrical wall effect

The aggregates in the concrete cannot penetrate the rigid wall formed by the pipe. As a result, the concentration of aggregates decreases when approaching the pipe wall, creating a kind of lubrication layer. It is assumed that this effect has no longer an influence at a distance equal to half of the maximal aggregate size ($d_{max}/2$) from the wall. It has been shown in literature that the rheological properties of cement paste are smaller than these of mortar and concrete [9.14]. Consequently, it can be argued that the rheological properties are not constant, but they vary along the cross section of the pipe. A new, further extension of the Poiseuille formula has been developed, assuming constant yield stress, viscosity and shear thickening in the main part of the pipe, and linearly decreasing yield stress and viscosity from a distance $d_{max}/2$ from the wall to the wall itself. The values at the wall are assumed to be the properties of the cement paste, but as no measurements on the corresponding cement paste have been performed, these values are assumed to be 1/100 of the concrete values (fig. 9.7), which is based on other measurements with SCC and SCC-paste and literature results [9.14-9.15]. For the shear thickening, a linearization of the evolution of intensity of shear thickening with the maximal aggregate size, according to figure 4.20 (chapter 4), is applied (fig. 9.7). This procedure induces a partly increase in shear thickening when approaching the wall.

Figure 9.7 shows on the left side the assumed evolution of the yield stress and the plastic viscosity in case the concrete can be described by means of the Bingham model. On the right side, the evolution of yield stress and the parameter c of the modified Bingham model is shown. Note that the variation of the viscosity term μ is not displayed, as it shows a similar evolution as the yield stress and similar to the plastic viscosity of the Bingham model.

The rheological properties measured in the rheometer are average values because slippage and the geometrical wall effect are prevented. For each rheological parameter (yield stress, viscosity, shear thickening), varying with the distance from the centre of the pipe, the average is calculated over the whole cross section. These averages correspond to the measured (average) values in the rheometer. As a result, at least for the yield stress and the viscosity, the local values are higher near the centre of the pipe, compared to the average values in the rheometer (fig. 9.7).

Figure 9.8 shows the corresponding shear rates and velocity profiles in case of the Bingham and modified Bingham model. Especially in case of the Bingham model, a large increase in velocity can be observed close to the pipe wall, which appears to be

similar to the effect of a slippage layer [9.1]. As a result, total discharge is increased for equal pressure losses. In case of the modified Bingham model, a similar phenomenon can be observed, although the effect is less pronounced. This is attributed to the large importance of the shear thickening in the vicinity of the pipe wall.

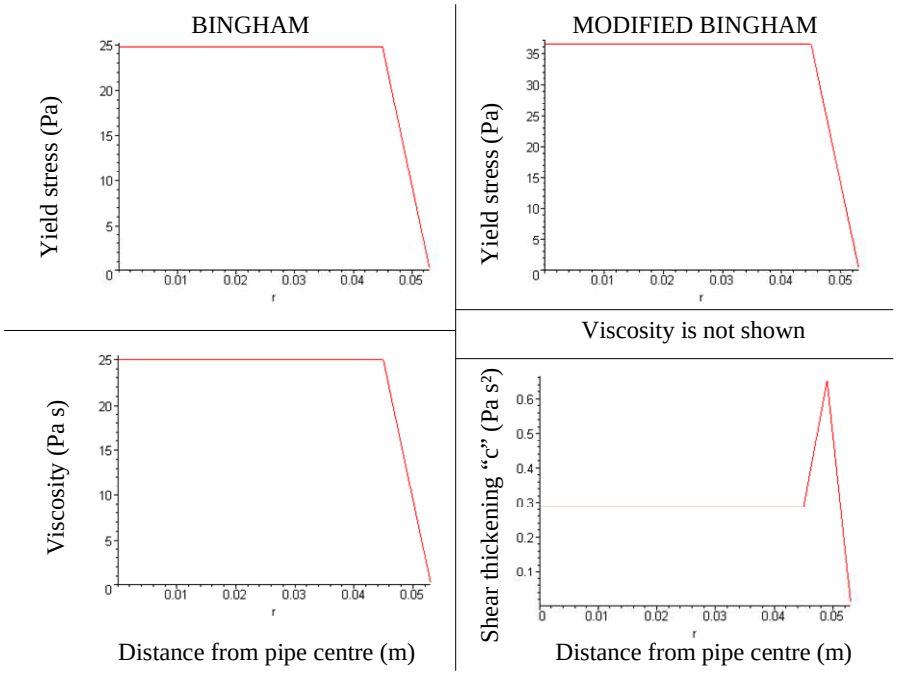

Figure 9.7: Yield stress and viscosity evolution across the pipe in case of a Bingham model (left; τ_0 = 21.25 Pa; μ_p = 21.42 Pas) and yield stress and shear thickening coefficient "c" for the modified Bingham model (right; τ_0 = 31.22 Pa; μ = 16.73 Pas; c = 0.367 Pas²). Both results are based on the properties of SCC LM-7, cycle 3, with a pressure loss of 20.571 kPa/m (discharge 3). Note that for the modified Bingham model, the viscosity evolution, which evolves similarly to the yield stress, is not shown.

Applying this new model delivers a ratio of predicted to measured pressure losses between 0.6 and 2 in case of the Bingham model, and 2 to 9 for the shear thickening materials. The reduction of predicted pressure losses in case of shear thickening materials is not large, due to the significant importance of the shear thickening near the pipe wall.

On the other hand, as shown in figure 9.9, the prediction ratio (predicted / measured pressure loss) depends on the discharge. In case of the Bingham model, increasing discharge results in a decrease in prediction ratio, while the opposite is observed when applying the modified Bingham model. As a result, it can be concluded that the applied intensity of shear thickening is too large, but as the Bingham calculations show the opposite (and the results are not close to plug flow), there must be at least

some effect causing apparent shear thickening behaviour. As shear thickening is probably overestimated in the rheometer, the increase in velocity near the pipe wall may be larger in reality (compared to the predictions) when applying the modified Bingham model.

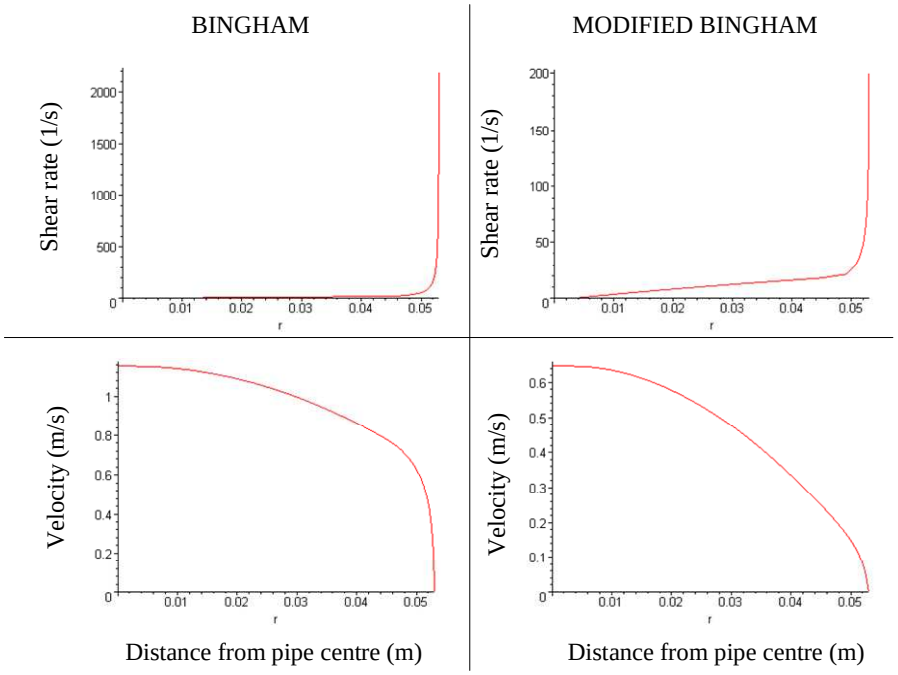

Figure 9.8: Shear rate and velocity across the pipe. A large increase in velocity is observed near the wall (similar as for a slippage layer), especially in case of the Bingham model. For the modified Bingham model, the effect is less pronounced due to the large (maybe overestimated) influence of shear thickening near the wall.

Applying this new extension of the Poiseuille formula, based on the measured rheological properties and the assumed evolution across the pipe improves the prediction ratio. On the other hand, this model, with its shortcomings, will never be able to give the correct velocity profile. First of all, the input data are based on a measurement with a rheometer on a small sample of concrete, which induces an error. By comparing the results from the pumping tests with the results from the Tattersall rheometer, we are comparing the values of two different rheometers. As shown in chapter 3, two different rheometers deliver different rheological properties, creating a second error in the calculations. Furthermore, when calculating the maximal shear rates for homogeneous concrete, based on the obtained wall shear stress values and without the incorporation of the geometrical wall effect, values between 35/s and 45/s are obtained. This is a factor 2 to 3 larger than the maximal shear rate (assumed) in the rheometer. Extrapolating rheometer data is a very

dangerous practice, with large risks for new errors. This is probably the reason why the shear thickening behaviour in the pipes does not appear to be as intense as in the rheometer. Increasing the rotational velocity in the rheometer, in order to reduce this problem, is also not easy to perform. As a result, there is a discrepancy in the applied shear rate ranges. The assumption of the linear evolution of the rheological properties near the wall is probably not correct neither. The packing density and maximum packing density should be calculated across the pipe, and according to the Krieger-Dougherty equation [9.16], and the equivalent equation for the yield stress (see chapter 2) [9.17], a more correct evolution of yield stress and viscosity can be determined. On the other hand, the shear rate and velocity calculations get much more complicated when deviating from the linear evolution of the rheological properties across the pipe. In addition, the evolution of shear thickening with decreasing aggregate content should be studied much more in detail in order to apply it in the model. As a last shortcoming, the assumption of the cement paste values (being 1/100 of the concrete values for yield stress and viscosity) near the wall can be mentioned, although this is the easiest one to solve. By extracting the cement paste from the pumped concrete, one can determine its rheological properties with a standard plate-plate rheometer, when available.

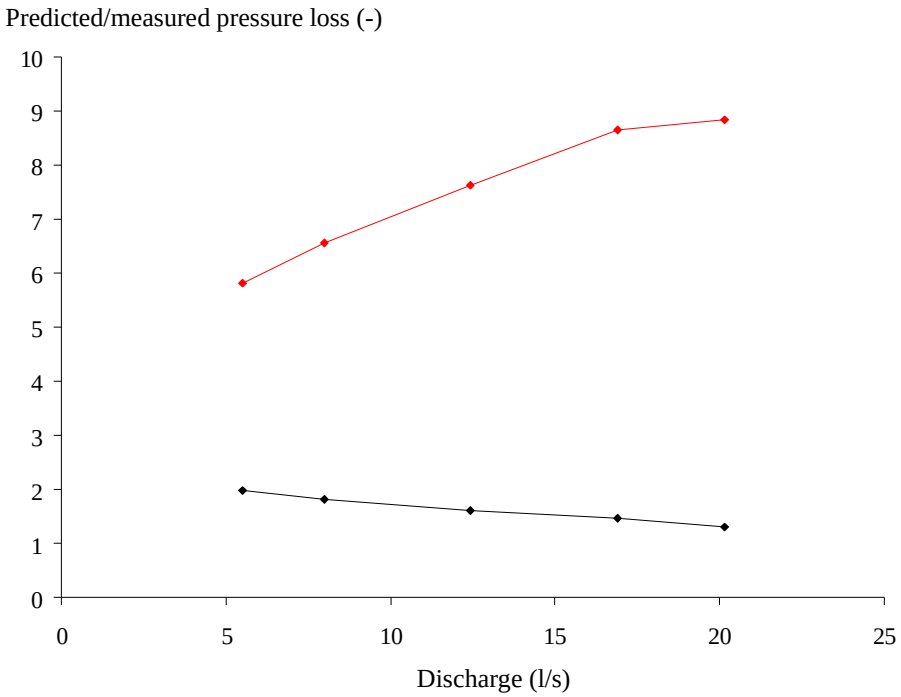

Figure 9.9: Prediction ratio for SCC LM–7 (cycle 3), based on the Bingham model (black line) and the modified Bingham model (red line) as a function of discharge.

In his thesis, Kaplan did not incorporate the geometrical wall effect into his calculations [9.1]. Instead, he assumed that a layer of mortar with thickness "e" was formed, with constant rheological properties, which related very well with the results of his pumping tests, performed in part 1 of the curve of figure 9.6. The thickness e of the layer was defined by the maximal distance the coarse aggregates can move to reach maximal packing in the centre of the pipe. No specific results of this layer thickness are mentioned, due to the complexity of the calculations.
The pumping results of Kaplan have been performed on a 148 m circuit, built with steel pipes of 125 mm inner diameter. Rheological testing has been performed with the BTRheom, and a modified version, called a tribometer, to measure the friction between mortar and a smooth wall.
The application of the Buckingham-Reiner equation with the geometrical wall effect on some of the results of Kaplan deliver an overprediction of the pressure losses with a factor 2 to 8. This appears to be much larger than our own results, but when considering that the BTRheom delivers results for yield stress and viscosity which are approximately twice as high as the Tattersall rheometer [9.12-9.13], this prediction factor reduces from 1 (almost perfect) to 4. Although the results are similar, there is a large difference between the concretes of Kaplan and our concretes. When defining pure plug flow as the situation where the shear rate is concentrated in the boundary layer (defined by $d_{max}/2$) and the shear rate equals zero in the bulk concrete, plug flow has only been observed twice in our case. A first time when pumping SCC LM-3 for 15 minutes at a constant discharge, the yield stress increased up to 400 Pa, and "sausages" were flowing out of the pipe. A second time, this effect has been seen in the calculations at the lowest discharge with the TC. For the concretes of Kaplan, the situation is completely opposite. Pure plug flow is only not present at the highest discharges for some concretes, after correction of the rheometer values, and for the first SCC (BAP 1) [9.1].
From these results, it can be concluded that the geometrical wall effect, a physical phenomenon which certainly occurs, increases discharge significantly at equal pressure losses. On the other hand, calculating the specific velocity profile and resulting discharge, based on the measured rheological properties is very sensitive to the sampling, rheometer accuracy and the assumptions made in the model. Isolating the two other effects (structural breakdown and dynamic segregation) by incorporating the geometrical wall effect in the calculations is currently impossible.

2.2.2 Structural breakdown

As shear stress varies linearly from zero in the centre to the maximal value at the wall, shear rate follows a similar pattern [9.11]. The values of the shear rate near the wall can even be significantly increased due to the geometrical wall effect (fig. 9.8). When discussing structural breakdown (thixotropy) in chapter 5, it has been mentioned that for each shear rate, an equilibrium structure exists and that the rheological properties decrease with decreasing structure (and increasing shear rate) [9.9][9.14][9.18]. If it is assumed that the concrete (or cement paste) flows in layers, and no mixing occurs between the layers (which is logical in case of pure plug flow), the layers near the wall have lower rheological properties than the layers in

the centre. As the shear stresses are higher near the wall, a lower viscosity causes a larger shear rate and a larger velocity gradient.
It has been mentioned by the technical staff, when performing the segregation tests (see next section), that the concrete extracted near the wall appeared to be more fluid than the regular samples. This might be an indication of this structural breakdown, but as long as no specific measurements are performed, this effect is not certain to occur.
In addition, this theory is based on the assumption that the layers do not mix, which can be justified in straight sections, but which can be doubted in curves. Furthermore, the quantification of this effect is not straightforward. The influence of thixotropy (or only structural breakdown) on the viscosity, as this is the most important factor, should be known in detail, although no measurement systems and procedures are currently available.

2.2.3 Dynamic segregation

If with the two previously mentioned effects, in the hypothetical situation these can be calculated correctly, it is not possible to perfectly predict the pressure losses, the effect of dynamic segregation can be considered. Kaplan has assumed in his thesis that this effect dominates the main part of the measurements [9.1]. The aggregates are believed to move to the centre of the pipe until maximum packing density is achieved.
In case of the pumped SCC, the accuracy and certainty of the measured values is too low in order to confirm or exclude dynamic segregation. On the other hand, as the velocity profile of SCC is different compared to the traditional concretes of Kaplan, different results dealing with dynamic segregation may be expected. Note that by dynamic segregation, a displacement of the (coarse) aggregates away from the wall, additional to the geometrical wall effect, is meant.
By means of the following paragraphs, a discussion can be opened for arguments in favour and against dynamic segregation. In case of pure plug flow, for high yield stress concretes, dynamic segregation is necessary in order to make the concrete flow. In this way, a lubrication layer is formed near the wall and the contribution of solid friction at the wall is reduced. Secondly, as shown in chapter 3, a concentration profile has been observed in a wide gap concentric cylinder rheometer, independent of the rotational velocity. As a result, this concentration profile can also be expected during the flow of concrete in pipes.
On the other hand, dynamic segregation needs to be developed over a certain length of the circuit, and as the viscosity of SCC is higher than the viscosity of TC, dynamic segregation, if present, can be slowed down. Changes in the direction of the streamlines, like in case of reductions and bends, can reduce the thickness of the formed lubrication layer, increasing the local pressure losses. Furthermore, the largest difference between the flow of TC and SCC in pipes is that, if the SCC is well designed, the plug radius is quite small and a part of the SCC itself undergoes shearing, especially at high velocities. As a result, if the concentration of coarse aggregates would increase significantly near the centre of the pipe, the shearing would reduce this concentration by pushing the aggregates back to the outside region. In chapter 4, the particle Reynolds number has been determined for

aggregates suspended in mortar, and it has been shown that inertia forces are not negligible for the coarse aggregates. The shear rate at the boundary of the lubrication layer, assumed to be at a distance $d_{max}/2$ from the wall, is between 10/s and 40/s, which corresponds quite well to the conditions described in chapter 4. Consequently, when the concentration of coarse aggregates increases near the centre, and due to the shear rate (velocity gradient) present, inertia causes two coarse particles to change flow direction when passing close to each other. As the centre of the pipe shows a higher concentration, particles can have a larger tendency to move to the pipe wall, until other interaction forces prevent any further approach and the particles are again forced to move to the centre. In this way, a kind of zig-zag movement of the particles is assumed, but in average, dynamic segregation should be reduced. Remind that this is only a possible theory, which must be confirmed or rejected by means of observations. In case it is confirmed, the magnitude of this movement should be investigated, in order to know whether it has a significant influence on dynamic segregation. The reason why this has not been observed in traditional concrete, is that the plug radius is quite large and as the particles move at a uniform velocity, no inertia forces (relative to each other) are present.
It is thought that dynamic segregation is not as significantly present in case of SCC, compared to the case of traditional concrete, based on the above stated theories. Further investigations are needed for verification.

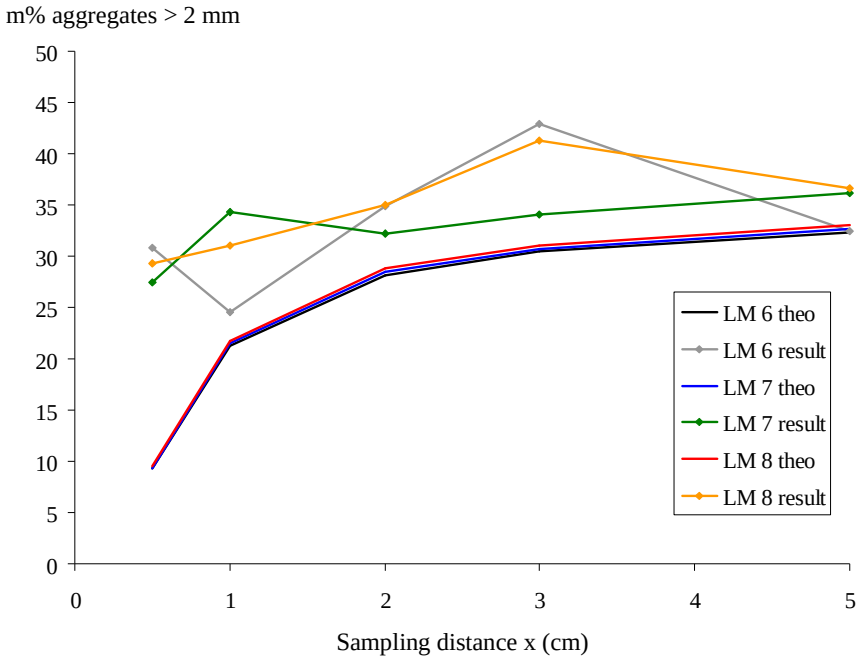

Figure 9.10: Mass-% of aggregates larger than 2 mm measured during the segregation tests on SCC LM-6, 7 and 8. The full lines indicate the theoretical amount (theo), based on the grain size distribution and the geometrical wall effect.

Nevertheless, tests have been performed in order to verify whether dynamic segregation occurs. This procedure consisted of collecting a part of the concrete flowing out of the pipe, in a wooden box with a sharp metal edge at a certain distance x from the inner pipe wall. The collected concrete is moved away from the pumping site and is treated according to section 3.4 of chapter 8. As mentioned in the previous section, our technical staff had problems when taking samples from the wooden box, in order to wash out all materials smaller than 2 mm. The concrete in this wooden box appeared to be more fluid than the regular samples, taken with the suspended reservoir for the rheometer tests and the standard tests, and it showed in some cases a large tendency to segregate. The first samples (LM-3, 4 and 5) were taken by pouring a certain mass (between 2 and 3 kg) of the concrete from the wooden box on the sieves. If the concrete segregates, the amount of aggregates is underestimated. This problem has been solved with the other concretes, by using a shovel to take 2-3 kg of concrete from the box, but still, sampling is not easy and induces large errors.

Figure 9.10 shows the results for segregation tests on SCC LM-6, 7 and 8, expressing the amount of aggregates as % of mass compared to the mass of the total sample, both experimental and theoretical, dependent on the distance x from the inner pipe wall. The theoretical curves have been calculated based on the grain size distribution of the delivered concrete, incorporating the geometrical wall effect. As can be seen, the amount of coarse aggregates should decrease with decreasing distance x. For the concretes in figure 9.10, the samples have been taken by shovel from the wooden box. It can be seen that the experimental amount of aggregates is larger than the theoretical one, which is in fact impossible besides the effect of the sampling errors.

The samples of SCC LM-3, 4 and 5 have been taken by pouring concrete from the wooden box. This resulted in a significantly lower amount of coarse aggregates, as shown in figure 9.11 for SCC LM-5. It is uncertain whether the experimental, lower amount of aggregates is due to dynamic segregation or due to the sampling error. For TC-1, sampled with the shovel, the results appear to agree very well with the theoretical values, except at the smallest sampling distance. As a result, it can be concluded that, if no sampling errors are involved, the geometrical wall effect, and only this, has been measured for TC-1. Consequently, there should be no dynamic segregation for TC-1.

Unfortunately, as already mentioned, the sampling method of the concrete from the wooden box induces too large variations in the obtained results. Consequently, the test results are regarded to be inconclusive, nor proving or denying the existence of dynamic segregation. Although the testing procedure was originally very promising, this method is too coarse for the fine results which needed to be obtained.

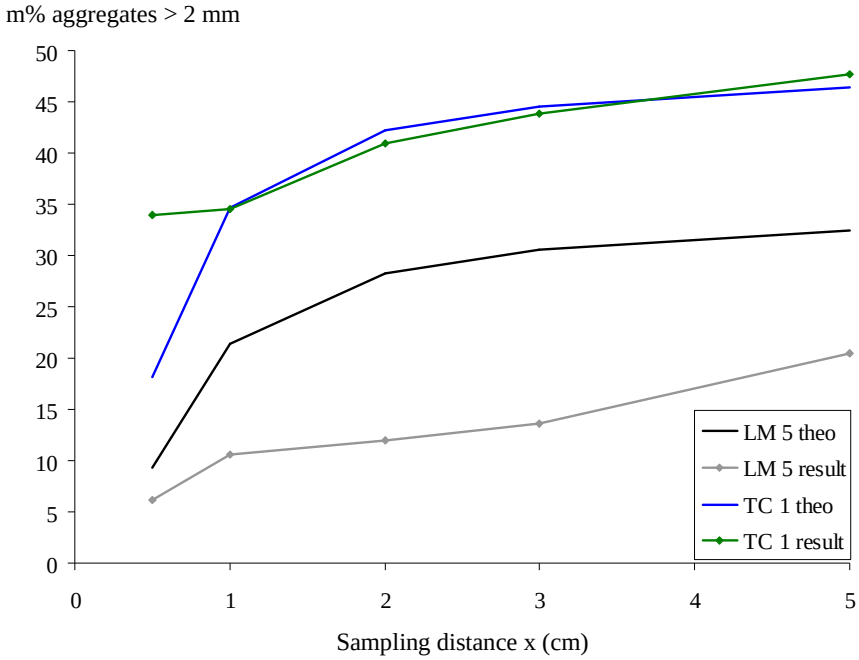

Figure 9.11: Results of segregation tests for SCC LM-5 and TC-1.

2.2.4 Combination of effects

The geometrical wall effect is certain to occur, although the quantification of its influence is not really easy. Structural breakdown should further reduce the pressure loss at a certain discharge, although this effect is very difficult to measure. No evidence has been found whether dynamic segregation does or does not exist. As a result, no decisions can be taken and the natural mechanisms reducing pressure during pumping of concrete are not fully understood yet.

As a result, the velocity profile can be described as follows: in the centre, there is a uniform velocity due to the plug. Near the wall, a large velocity gradient should be present due to a lubrication layer, formed by the geometrical wall effect and possibly dynamic segregation, and influenced by structural breakdown. In between, a smaller velocity gradient is present. The velocity profile should have a form similar to the profiles shown in figure 9.8. Note that, as SCC has been experienced as a quite sticky material, no real slippage is assumed. When recalling the introduction of this chapter, the wall friction is assumed to be independent of the flow velocity and the pressure, and that in fact, if the rheological properties of the material at all distances from the centre are perfectly known, the pressure loss – discharge curves should be very well predicted by means of modifications to the extended versions of the Poiseuille formula.

The best way to determine these effects is by directly measuring the velocity profile in the concrete. These measurements should be done accurately, certainly in the

vicinity of the wall, and fast, within 4 seconds, due to the pumping system. Currently, no such equipment is available at a reasonable price.

2.2.5 Comparison to the gravitational flow tests

The extended version of the Poiseuille formula for shear thickening materials, as derived in chapter 6, predicts the pressure loss – discharge curves of the gravitational flow tests of chapter 7 very well, without the incorporation of the geometrical wall effect. Incorporating the geometrical wall effect underestimates the occurring pressure losses with a factor 2. Unfortunately, there is currently no explanation for this inconsistency between the results of the gravitational flow tests and the pumping tests. Although, one argument could be that the SCC for the gravitational flow tests was quite fluid, and that the rheometer might have overestimated shear thickening and underestimated the viscosity. As the shear rates in the gravitational flow tests were really low, shear thickening did not play a significant role, which possibly explains this discrepancy. A second argument can be that this error can be due to the special pressure losses at the entrance of the pipe, which can be much larger than estimated. But no certainty exists and further research is needed.

2.3 Theoretical predictions based on the friction factor

In hydraulics, the pressure loss and discharge (squared) are expressed by means of non-dimensional units (eq. 9.1) [9.19]. The relationship between these parameters is expressed by the friction factor λ. In high turbulent regime, λ is a constant, while in laminar regime, it equals 64/Re (Re = Reynolds number).

$$\frac{\Delta p_{tot}}{L \cdot \rho \cdot g} = \lambda \cdot \frac{Q^2}{4 \cdot \pi^2 \cdot g \cdot R^5} \tag{9.1}$$

where: Δp_{tot} *= total pressure loss (Pa)*
L *= length (m)*
ρ *= density (kg/m³)*
λ *= friction factor (-)*
Q *= discharge (m³/s)*
R *= radius of the pipe (m)*

Based on the results of the pumping tests, the friction factor has been calculated for a large series of pumping cycles. As a first observation, the friction factor relates to the inverse of the discharge, confirming the laminar regime, as the Reynolds number contains a linear term in the discharge. Further attempts in order to relate λ or λQ to any other parameter, did not result in the expected correlations. Even only selecting the 17 concretes of figure 9.3 and relating λQ to the tangential viscosity at 10/s did not deliver the same, good correlations. In figure 9.3, the relationships are approximately independent of the discharge, while the friction factor, or even λQ are not completely independent of Q, which is probably due to the non-linear

relationship between pressure loss and discharge. As a result, as currently the parameters influencing the friction factor are not determined, any predictions based on this theory are very difficult to establish. Furthermore, as will be shown in the next section, the parameters influencing pressure losses in bends are also not fully known yet, making a prediction of pressure losses, with reasonable accuracy, in a random circuit very difficult.

2.4 Pressure losses in bends

The obtained results so far are only valid for straight sections. In literature, some information can be found dealing with pressure losses in curved sections, but the results are not consistent. Kaplan mentions that the bends in his circuit do not cause any additional pressure losses [9.1], while others state that for traditional concrete, a 90° bend is equivalent to 3 m of straight pipes [9.2].

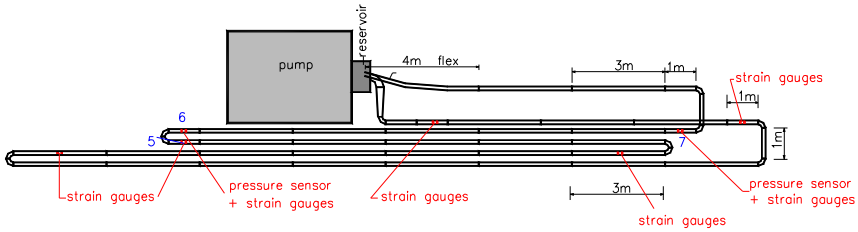

Figure 9.12: SCC LM-14 and 15 have been pumped in the 105 m circuit, containing a measurement section with a 180° bend (5 to 7) and a straight measurement section (6 to 7).

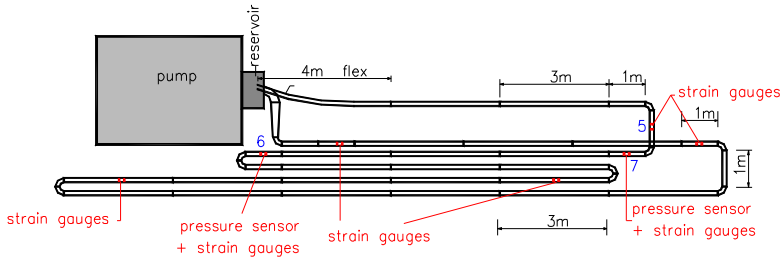

Figure 9.13: SCC LM-16 and 17 have been pumped in the 81 m circuit, containing a measurement section with a 90° bend (6 to 5) and a straight measurement section (6 to 7).

In this project, an attempt has been made to study the pressure losses in bends, but as the results are already very complicated in straight sections, no detailed analysis has been performed for the bends. For SCC LM-3, 4 and 5, the measurement section contained one 90° bend, but as there are no reference measurements in the straight section for these concretes, the specific pressure loss over this bend cannot be determined. On the other hand, for the concretes tested in the long circuits, namely SCC LM-14 to 17, one of the measurement sections contained a 180° (SCC LM-14

and 15) or 90° bend (SCC LM-16 and 17). The R/D-ratio of these bends, which is the ratio of the radius of the bend to the diameter of the pipe, equals 1.6, indicating that the bends are very sharp.
As can be seen in figures 9.12 and 9.13, the straight measurement section (6 to 7) is always completely incorporated in the measurement section with the bend (5 to 7 or 6 to 5). From the measurements in the straight section, the pressure loss per unit of length can be calculated. From the total pressure loss measured in the section with a bend, the pressure loss over all straight pipes, which are approximately 1 m longer than the measurement section 6-7, is subtracted. The remaining pressure loss is divided by the pressure loss per unit length of a straight pipe, and divided by the length on the centre line of the bend in order to obtain an amplification factor. This amplification factor indicates how many meters of straight pipes correspond with one meter of this bend. In order to know the total pressure loss over a certain bend, the amplification factor should be multiplied with the pressure loss per unit of length in a straight pipe and the distance on the centre line of the bend.
Figure 9.14 shows the amplification factor for the 90° bend, for SCC LM-17. The results of SCC LM-16 are similar. Figure 9.15 shows the amplification factor of a 180° bend, for SCC LM-15.

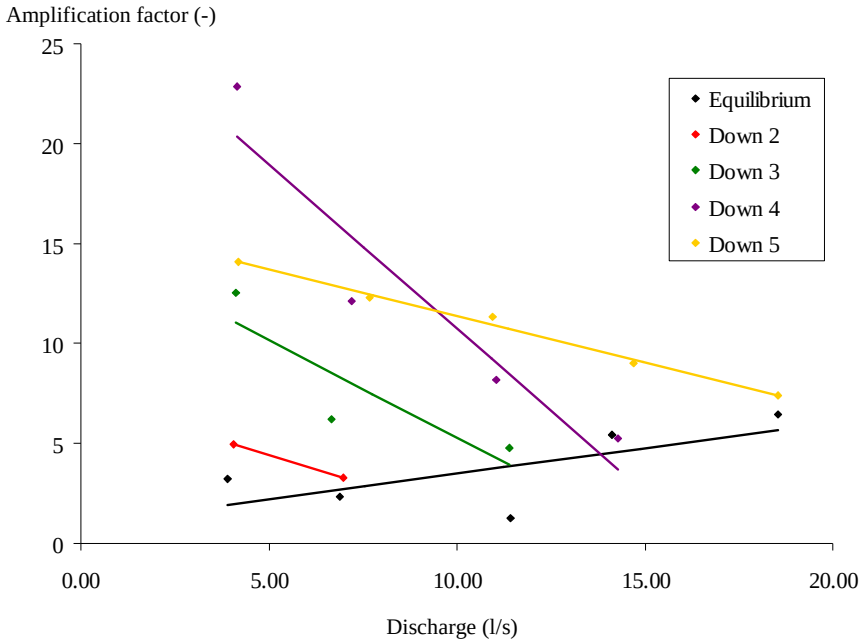

Figure 9.14: Amplification factor for the 90° bend for SCC LM-17.

As can be seen in figures 9.14 and 9.15, the test results are separated, depending on the step in the "special thixotropy tests" (see chapter 8). From figure 9.14, it can be concluded that at lower discharges, the relative importance of a 90° bend is larger

than at high discharges, which can be seen by the coloured lines. The black line connects all equilibrium points and indicates that the relative importance of the bend increases with increasing fluidity (decreasing viscosity, see next section). Figure 9.15 confirms in some way the first observation: a larger importance of the 180° bend at low discharges, but the influence of structural breakdown appears to be opposite to the results of the 90° bend. The amplification factor of a 90° curve was between 2.3 and 22.9. The amplification factor of a 180° bend varied between 6.5 and 21.7. When replacing a 90° bend by a 3 m straight pipe, as stated in [9.2], the amplification factor would be equal to 11 in our case.

As can be seen, a bend certainly causes a higher pressure loss than a straight section, but further investigation is definitely needed in order to be able to quantify this effect. It is mentioned in literature that the pressure losses over a bend increase with decreasing ratio of bend radius to pipe diameter, and that a 180° curve cannot be regarded as a combination of 2 successive 90° bends. When decreasing the viscosity, the relative pressure loss over a bend is thought to increase, due to a decrease in pressure losses in straight sections, and a larger importance of inertia forces compared to viscous forces. The reason why this is not seen in figure 9.15 is currently unclear and must be investigated.

Note that these results are only valid for the studied pipe configurations and concretes. There is no guarantee that the same values (and maybe the same trends) will be obtained in other cases. Furthermore, the accuracy of these results is quite low and further investigation is needed for these very complicated flow problems.

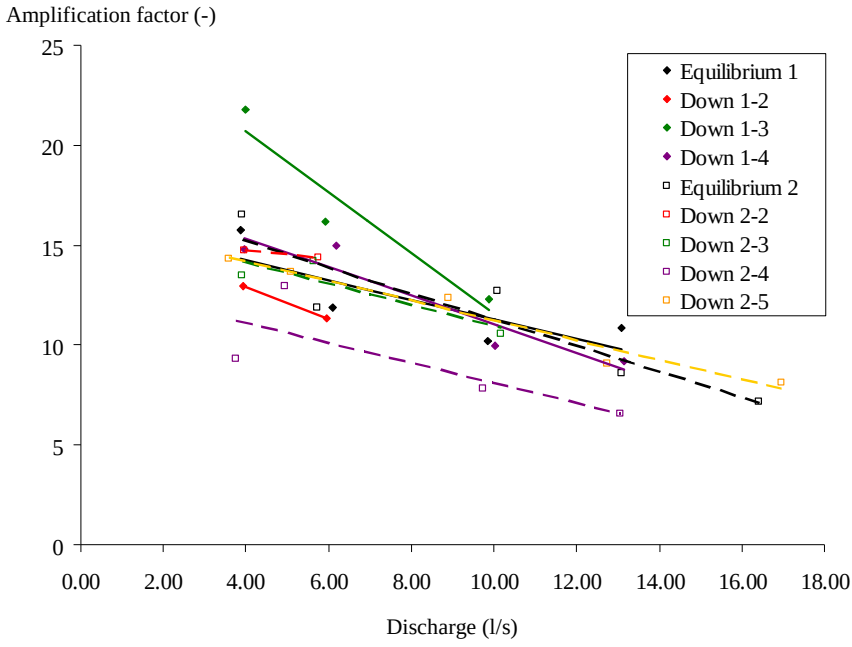

Figure 9.15: Amplification factor for the 180° bend for SCC LM-15.

3 Influence of pumping on rheology

3.1 Introduction

As already mentioned in section 2.1, dealing with the pressure losses in straight sections, and as shown in figure 9.1, the pressure loss – discharge curves change with time, and not really according to what is expected (loss of workability). Figure 9.16 is a reprint of figure 9.1, but the pressure losses are expressed as a function of time, for each discharge step.

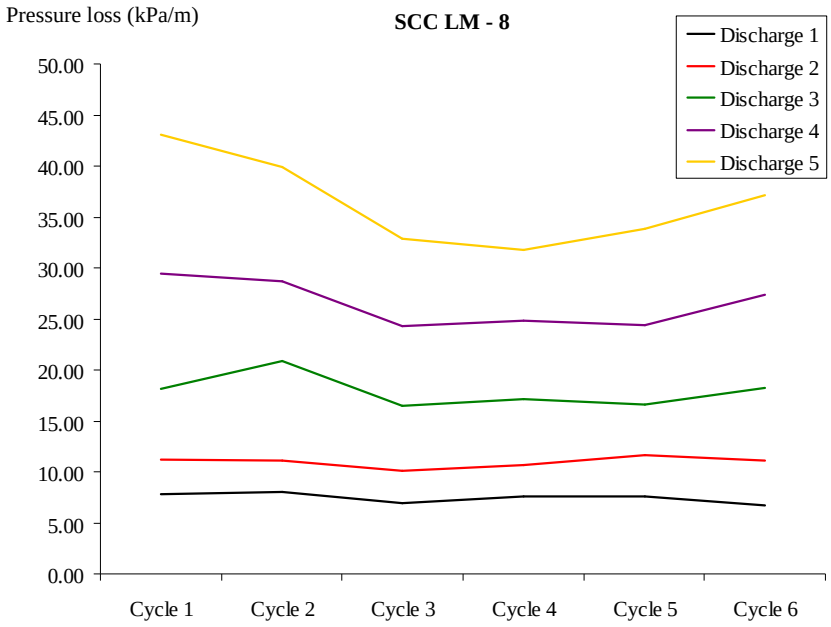

Figure 9.16: Time evolution of pressure losses per discharge, showing a decrease in the beginning and a possible increase at the end, especially at high discharges.

Depending on the concrete composition, a decrease in pressure loss, during 2 or 3 cycles is observed at the high discharges. At higher ages, a possible increase in pressure loss can be seen. When comparing the rheometer results of the pumped and the non-pumped samples of SCC LM-10 and 11, one can see that the torque at equilibrium during pre-shearing (Torque at max. vel. in the tables of Appendix D) is continuously increasing in case of the non-pumped concrete, while it first decreases and finally increases in case of the pumped concrete. Due to sampling and measurement errors, especially with SCC LM-10, the rheometer measurements can not provide full proof whether these changes in flow resistance are really occurring, but they form a good indication that pumping does something with the concrete.

Furthermore, for all concretes subjected to the regular pumping tests, similar patterns as in figure 9.16 have been obtained (see Appendix D). Especially the decreasing pressure losses at the high discharges during the first cycles are intriguing and have led to the development of the "special thixotropy tests", as described in chapter 8, figure 8.14. By means of the results of these special thixotropy tests, the two effects which appear to have the largest influence on the concrete properties during pumping will be discussed separately in the next sections.

3.2 Structural breakdown

The evolution of pressure losses at the high discharges shows a decrease during the first pumping cycles, as shown in figure 9.16. As a first idea, this effect was attributed to thixotropy. As a result, special thixotropy tests have been executed on five different concretes. Instead of stepwise decreasing the discharge, it is increased, in much longer steps. Figure 9.17 shows a typical result of a special thixotropy test, performed on SCC LM-17, where the pressure losses were measured in the last straight section.

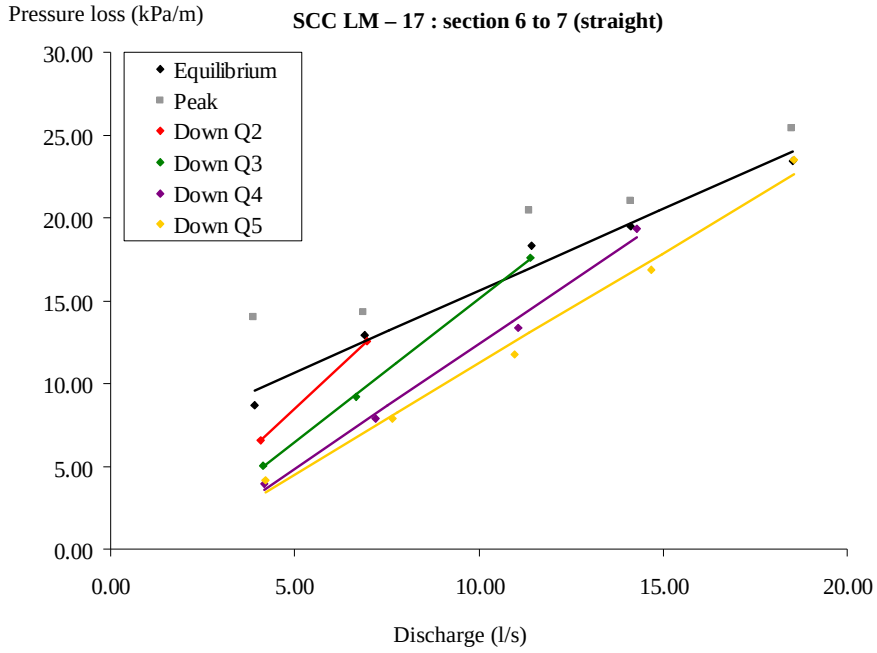

Figure 9.17: Pressure loss – discharge curves for SCC LM-17, subjected to a "special thixotropy test." The colours match with the colours of figure 8.14 (chapter 8).

Figure 9.18 has been taken from chapter 3, showing the response of a thixotropic material to a sudden change in shear rate [9.20]. When determining the black points from figure 9.17, each time, equilibrium is awaited (EQ in figure 9.18), while for the

coloured curves, the rebuild has been prevented by the rapidly decreasing discharge (Down in figure 9.18). In this way, the pressure loss at a certain discharge is lower when a higher discharge has been applied before.

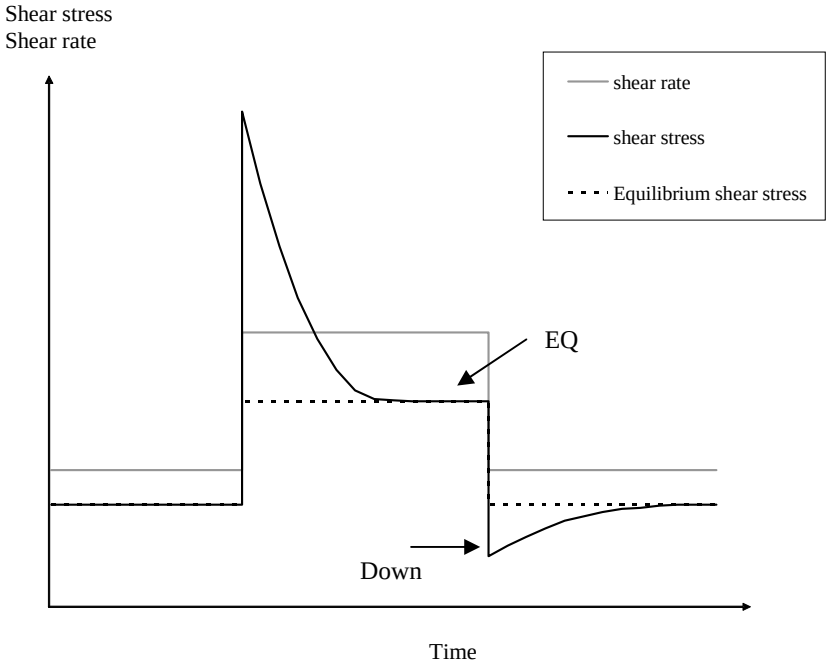

Figure 9.18: Response of a non-thixotropic (dashed line) and a thixotropic (full black line) material to a sudden increase and decrease in shear rate (grey full line).

On the other hand, it can be doubted whether this effect is really thixotropy. SCC LM-15 has undergone the special thixotropy test twice, with a resting period of 30 minutes in between. When comparing the results of the last down-curve of the first test (Down 1-4), with the results of the second test, no increase or further decrease in pressure loss has been observed (fig. 9.19). Apparently, the concrete does not rebuild during the 30 minutes of rest. This can be due to the very slow rebuilding of the concrete, or it can be that the observed effect is non-reversible, and then by definition, it is not thixotropy [9.20-9.21], but only (or mainly) structural breakdown. For the sake of simplicity, this effect will be called structural breakdown, although it is most probably a combined effect of a decrease in thixotropic internal structure and the pure structural breakdown, defined as the breaking of chemical linkages [9.9][9.22]. This term corresponds to the “structural breakdown in its broad sense”, as defined in chapter 5.

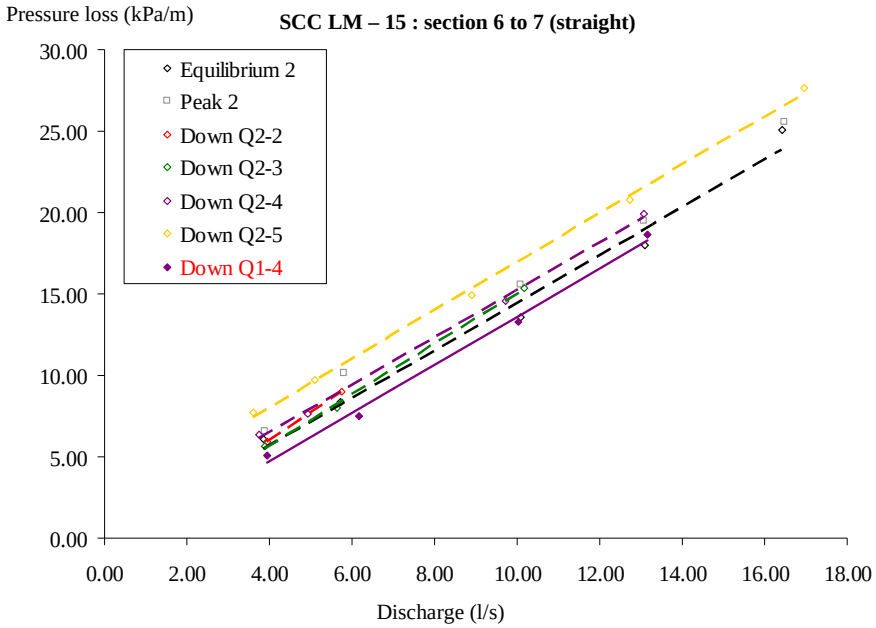

Figure 9.19: Pressure loss – discharge curves for the second special thixotropy test on SCC LM-15. The full purple dots and the full line represent the last down-curve of the first test.

Structural breakdown influences the rheological properties in one single way: yield stress and viscosity are decreased, the more the internal structure decreases. As the pressure losses are mainly dependent on the viscosity of the concrete, a decrease in pressure loss is translated in a decrease in viscosity. On the other hand, yield stress should also decrease, but in some cases, the opposite has been found.

3.3 Air content and air voids distribution

3.3.1 Determination of air content and air voids distribution

After reaching equilibrium at each discharge, a sample of the concrete has been taken. This sample has undergone several tests, of which one was the determination of the air content (of the fresh concrete) by means of the pressure method. The air content shows a continuous increase in most cases, as can be seen in table 9.1 for SCC LM-15 and in Appendix D.
After the pumping tests, four cores of each of the last pumped concretes (SCC LM-14 to 17) have been drilled and polished. The surface of the cores has been coloured in black, and the voids have been filled with barium-sulfate, which is a white powder, causing a large contrast between the voids and the black surface (fig. 9.20). Each of these samples has been subjected to an air void analysis test four times. The air void analyser measures the number and the length of white parts on predefined

(virtual) lines on the sample, and by means of the software, an air voids distribution is calculated. More information on the air void analyser can be found in [9.23-9.25].

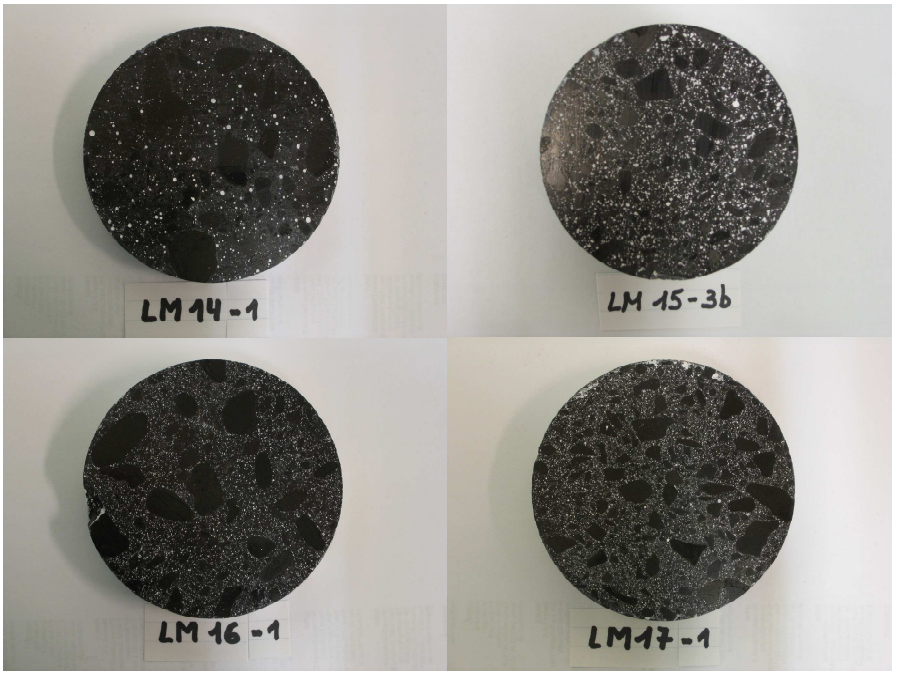

Figure 9.20: Prepared samples for the air void analyser.

As the software of the air void analyser does not provide detailed information for air bubbles larger than 500 µm, a second measurement on all samples has been performed by means of image analysis. Both methods are complementary to each other, and a detailed air void distribution can be determined, as can be seen in figure 9.21. The d_{50} equals 490, 370, 190 and 130 µm for SCC LM-14 to 17 respectively. The air void distribution of non-pumped concretes, similar to SCC LM-15 and 16 has also been determined. The d_{50} of the non-pumped concretes was around 600 and 450 µm, respectively. The total air content of the pumped concretes was 2.8, 9.5, 6.4 and 9.3%, obtained for the hardened samples of SCC LM-14 to 17 and 2.4 and 2.0% for the non-pumped concretes LM-15 and 16, clearly indicating, except for SCC LM-14, the increase in air content due to pumping.
The air voids of SCC LM-15 deserve special attention. The air bubbles in this concrete are less spherical than in the others (it might be difficult to see this in figure 9.20). It is suspected that the original air bubbles are even smaller than in the other concretes, because this concrete has been pumped during a longer time. During cleaning, these bubbles may have formed some kind of agglomerates, resulting in apparently larger air bubbles.

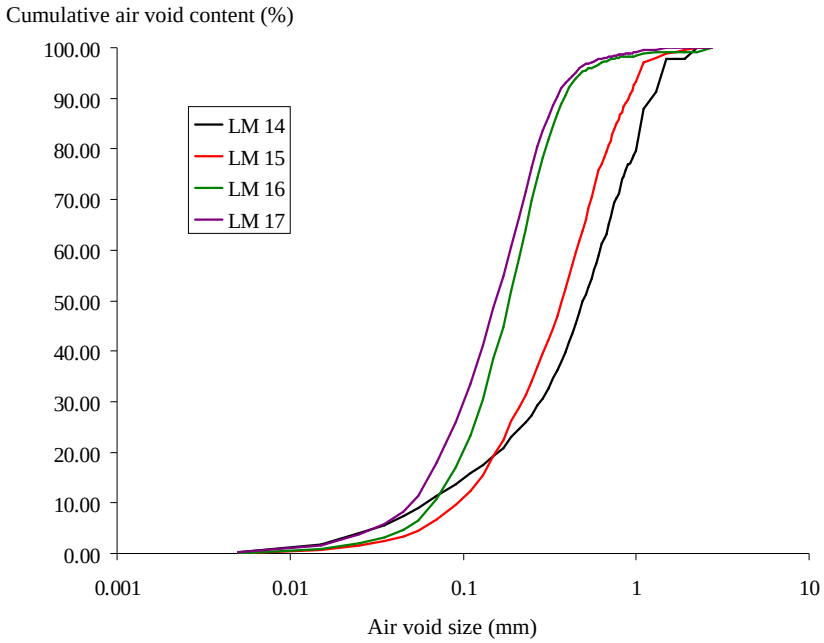

Figure 9.21: Cumulative air void distribution of the pumped concretes.

3.3.2 Possible causes

The cause of the increase in air content during pumping has not been found, but some theories can be assumed. First at all, it has been discussed in chapter 8 that the filling ratio of the pumping cylinders is not equal to 100%. The remaining part is probably air, which is pushed in the pipes and mixes up with the concrete, although no proof is available for this phenomenon. Secondly, the concrete falls back inside the reservoir from a certain height. This process includes air bubbles inside the concrete in the reservoir.

3.3.3 Influence on rheological properties

The influence of air bubbles in liquids has been briefly discussed in chapter 2 when introducing foams. In this part, the capillary number has been defined, which is the ratio of the shearing forces on the air bubbles to the surface tension forces [9.26]. At low capillary numbers, the bubbles remain spherical and the flow resistance increases. At high capillary numbers, the bubbles deform in the flow field and the flow resistance decreases. The larger the amount of bubbles, the larger the influence. For self-compacting concrete, the yield stress is determined at low shear stresses and the bubbles are expected to remain spherical. When determining the viscosity, the bubbles are deformed due to the high shear stresses. As a result, a significant increase in (small) air bubbles causes an increase in yield stress and a decrease in viscosity. For concretes SCC LM-15 to 17, the amount of air bubbles in the cement

paste varies between 16 and 23%, indicating a large importance of the air bubbles on the rheological behaviour [9.27]. Furthermore, as the concrete (or cement paste) is subjected to high shear rates in the pipes, the larger bubbles break up into smaller pieces, causing a decrease in the average bubble size and consequently enhancing the increase in yield stress. As the bubbles are quite small and the yield stress increases, the bubbles do not escape any longer.
Increasing air content probably decreases shear thickening behaviour, as this compressible part of the cement paste can absorb some extra stress, independently whether cluster formation or momentum transfer cause shear thickening. In the rheometer, shear thickening has been found to decrease, disappear and even become shear thinning, but this can be due to the change from high to low Ca-number in the shear rate range of the rheometer. For Ca-numbers around 1, the effects are still unknown. As a result, the effect of increasing air content is expected to decrease the shear thickening, but the results do not provide a full proof.

3.4 Combination of structural breakdown and air content

3.4.1 Influence on viscosity

Both the structural breakdown and the increase in air content cause a decrease in viscosity, which is confirmed in three ways: the pressure losses decrease, the measured viscosity (or torque at maximal velocity) in the rheometer decreases, as long as the results are reliable, and the V-funnel flow time decreases (see table 9.1 for SCC LM-15 and Appendix D for all concretes). As a result, the decrease in pressure losses in fig. 9.17 is probably a combination of structural breakdown and increasing air content.
In case of SCC LM-16, the part of the special thixotropy test at discharge 3 has been repeated three times. From the results in Appendix D, it can be concluded by combining all phenomena that the viscosity of the concrete decreased, only due to an increase in air content.

3.4.2 Influence on yield stress

On the other hand, structural breakdown and an increase in air content have opposite effects on the yield stress of the concrete. In this case, the evolution of yield stress (and slump flow), depends on which effect dominates. In case structural breakdown dominates the effect of the air content, the yield stress should decrease. Combining a decrease in yield stress and a decrease in viscosity can lead to a loss of stability of the SCC. This effect has been observed in case of SCC LM-17, where the slump flow did not significantly increase, but it did not decrease neither. In this case, the yield stress is suspected to remain constant, but due to the decreasing viscosity, the sieve (un)stability values increase from 10.5 to 18.5%, expressing an increase in segregation. Similar, but less pronounced results have been obtained with SCC LM-12, pumped in the short circuit.
In the other case, when the effect of the air content dominates the structural breakdown, the yield stress should increase and the slump flow must decrease. This has been observed for both SCC LM-15 and 16, especially at the higher discharges

(see table 9.1 for SCC LM-15 and Appendix D). As a result, as yield stress increases, it can be that the designed slump flow for a proper filling of the formwork is no longer achieved due to pumping.

	LM-15				
	Q0 start	Q1-1	Q1-2	Q1-3	Q1-4
Production	11u30				
Time	**12:42**	**13:05**	**13:17**	**13:27**	**13:38**
Tests on fresh SCC					
Slump flow (mm)	675	645	625	660	570
V-Funnel (s)	5.1	5.4	4.2	3.8	3.4
L-box (-)	0.83	-	-	-	-
Density (kg/m³)	2388	2319	2275	2278	2238
Sieve Stability (%)	1.6	4.2	7.0	6.6	4.0
Air content (%)	2.1	2.1	2.4	3.2	4.2
Rheometer tests					
Yield stress (Pa)	27.4	45.8	25.3	61.6	40.6
Viscosity at 0/s (Pa s)	25.3	27.6	20.0	25.1	9.8
shear thickening (c/visco)	0.010	0.005	0.000	0.000	0.000
Viscosity at 5/s (Pa s)	27.8	28.9	20.0	25.1	9.8
Torque at max. velocity (Nm)	2.89	3.11	2.08	2.34	1.18
Max Torque: thixo (Nm)	3.10	3.26	2.17	2.51	1.25

	LM-15					
	Q2-1	Q2-2	Q2-3	Q2-4	Q2-5	Q0 end
Production	11u30					
Time	**14:21**	**14:28**	**14:39**	**14:52**	**15:02**	**15:11**
Tests on fresh SCC						
Slump flow (mm)	525	543	505	498	445	548
V-Funnel (s)	3.5	3.1	3.3	3.5	3.7	7.9
L-box (-)	-	-	-	-	-	0.60
Density (kg/m³)	2283	2260	2228	2250	2225	2338
Sieve Stability (%)	3.36	4.5	1.9	0.8	0.3	1.2
Air content (%)	3.7	3.9	4.6	5.0	6.2	2.3
Rheometer tests						
Yield stress (Pa)	46.1	50.6	87.5	73.0	88.8	48.3
Viscosity at 0/s (Pa s)	10.1	11.0	14.9	8.1	7.0	26.9
shear thickening (c/visco)	0.000	0.000	0.000	0.000	0.000	0.010
Viscosity at 5/s (Pa s)	10.1	11.0	14.9	8.1	7.0	29.5
Torque at max. velocity (Nm)	1.24	1.39	2.02	1.24	1.23	3.34
Max Torque: thixo (Nm)	1.36	1.52	2.16	1.30	1.32	4.84

Table 9.1: Fresh concrete results for SCC LM-15, tested during the first special thixotropy test (upper part) and the second test (lower part), indicating the increase in air content, decrease in V-funnel flow time and viscosity, and increase in yield stress and decrease in slump flow. The results in grey are doubted to be representative.

A criterion to determine which effect dominates is currently unavailable, although from the restricted number of results, it appears that more fluid concretes show a larger tendency to segregate, while less fluid concretes tend to lose even more

fluidity. However, both the effects of the air content and the structural breakdown appear to become more significant with increasing discharge (or to be more correct: with increasing velocity). Further investigation should prove this statement. In case this is true, pumping velocities should be decreased in order to keep the final fresh properties of the concrete close to the designed, original values.
For SCC LM-12 and 17 on the one hand, and SCC LM-15 and 16 on the other hand, a main part of the results has been explained. Remains SCC LM-14 which does not follow the proposed theories completely. Although SCC LM-14 obeys mainly the structural breakdown theory, which can be seen in the decrease in viscosity, the partly increase in sieve (un)stability and the small variations in slump flow, assuming that the results for Q4 are influenced by ageing (see section 3.6), it does not show a significant increase in air content. This can be due to the large amount of SP in the concrete, due to the low water amount, which increases the surface tension of air bubbles in cement paste. In this case, the bubbles have less tendency to deform and to break up and they escape more easily nearby a free surface. The average air bubble size of the pumped SCC LM-14 is also much larger than for the other samples, supporting this theory. Still, it is not certain whether this theory explains the real physics of this phenomenon. Further investigation is needed.

3.4.3 Consequences

As mentioned previously, due to high speed pumping, the fresh properties of self-compacting concrete can evolve in two completely opposite directions. Or the SCC can segregate as the viscosity decreases and the yield stress does not significantly increase, or the SCC can lose a part of its filling ability, possibly causing problems of filling (complex) formworks entirely.
Due to an increase in air content, which, hopefully, on site will not be as significant as in our case as the concrete is only pumped once, and the decrease in air bubbles size, air bubbles do not escape as easily as before pumping, which can lead to blowholes on the surface of the concrete. Note that any vibration in SCC is prohibited as it can cause segregation. An increase in air content probably decreases the compressive strength and durability, although in this case, no significant decrease in compressive strength due to pumping has been observed.
When considering only structural breakdown, concrete pumped on site will only achieve an equilibrium pressure loss in straight sections, at a certain distance from the pump, if the pipe is sufficiently long, as travelling distance is related to time. As a result, the pressure evolution before this equilibrium distance is no longer a linear function of the pipe length, but the pressure loss per unit of length is decreasing when moving further away from the pump. An attempt has been made to measure this effect in the long pumping circuits, by incorporating different measurement sections on different locations in the circuit, but no sufficiently accurate results have been obtained.
As a last general consequence, it can be questioned what the influence of the structural breakdown and possibly the increase in air content is on the cancelling of formwork pressures due to thixotropy (rebuild), in case there is an influence…
Specifically for the regular pumping tests, it is assumed that the decrease in pressure losses at high discharges is due to structural breakdown during the first two cycles,

as the discharge has not been applied during a sufficiently long time in one cycle. As a result, the concrete is in a kind of equilibrium from the third or fourth cycle on, until other effects (like loss of workability,…) take over and cause an apparent increase in the pressure losses.

3.5 Temperature

3.5.1 Temperature test

In order to investigate the influence of pumping on the temperature of the concrete, one special test has been performed. The test consisted of continuously pumping SCC LM-3 at a discharge of around 12 l/s. The temperature evolution with time and influence of temperature on the total pressure loss are given in figure 9.22. As can be seen, temperature increases linearly as a function of time, at a rate of 0.44 °C/min in this case. Corresponding to the temperature increase, the total pressure loss, including the loss over the 90° bend increases with temperature. The large scatter in the pressure losses is probably due to the measuring ratio of 1 measurement per 10 seconds, instead of 10 measurements per second, causing no possibility to eliminate lower pressure losses due to the change in the valve of the pump.

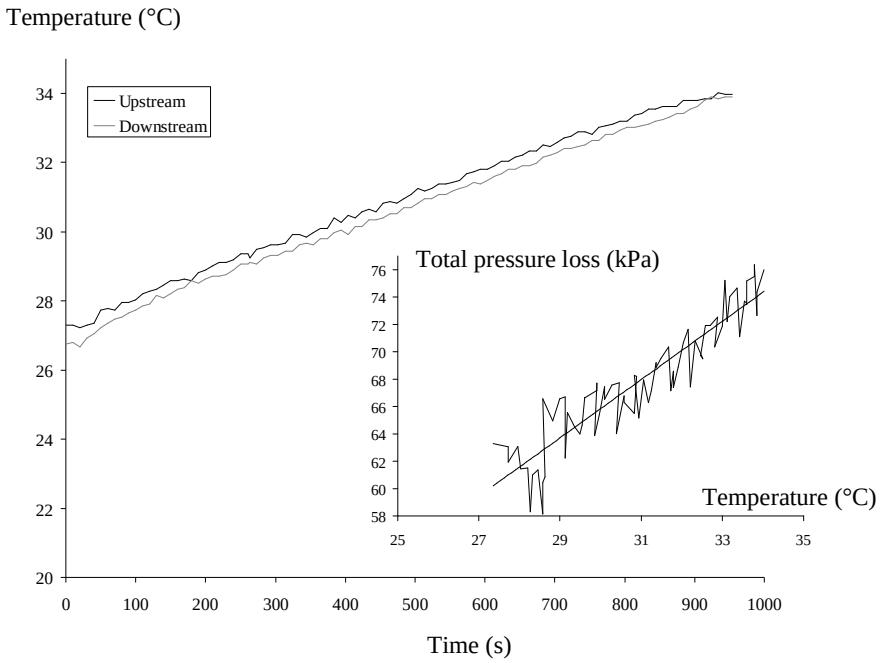

Figure 9.22: Temperature evolution with time, and pressure loss as a function of temperature, for SCC LM-3, pumped during 15 minutes at 12 l/s.

Note that this test has been executed at a concrete age of 210 minutes. As a result, the increase in viscosity, causing the increase in pressure loss can also be the consequence of ageing/loss of workability and is most probably not only due to the temperature increase. Also the yield stress of this concrete increased significantly, due to temperature and ageing. As a result, by the end of the test, pure plug flow has been observed.

3.5.2 Temperature evolution during regular tests

For all pumping tests, temperature has been monitored continuously. At each discharge, the temperature increase per unit of time has been determined separately. This temperature increase (dT/dt) is linearly related to the pressure loss per unit of length for each concrete, causing a faster increase in temperature at higher pressure losses (fig. 9.23). At low discharges, and low pressure losses, the temperature increase can be equal to zero, or even be negative, probably due to the lower ambient temperature.

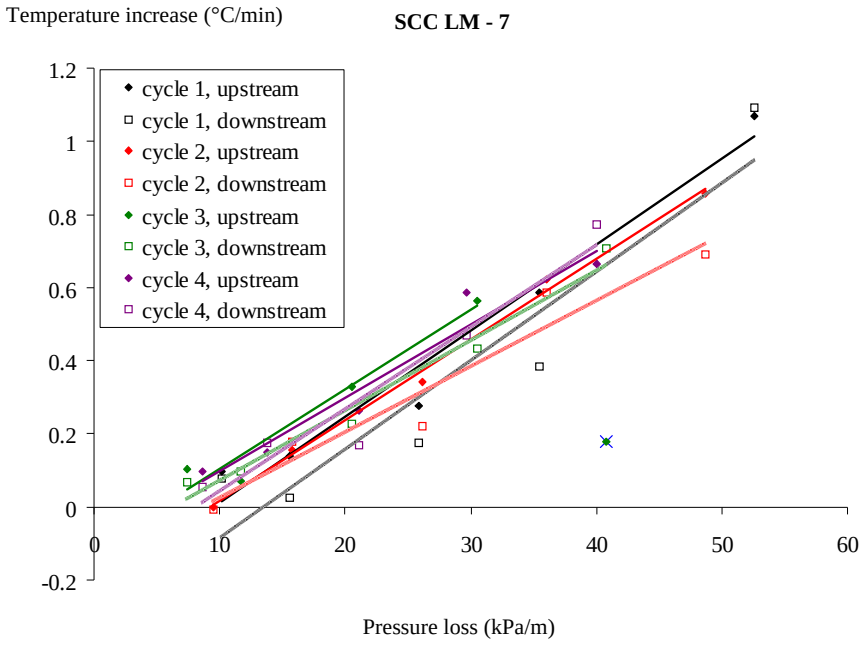

Figure 9.23: Temperature increase, measured both at the upstream and downstream pressure sensor, as a function of pressure loss for SCC LM-7, showing that the relationship is not significantly dependent on time.

From figure 9.23, it can be seen that time does not significantly influence the temperature increase at a certain pressure loss. Comparing the curves of the different cycles, which have been performed with a 30 minute time interval, indicates that all

curves have approximately the same inclination, and the same intercept with the vertical axis. As a result, the relationship between temperature increase per unit of time and the pressure loss per unit of length appears to be a constant material property. Note that temperature between the cycles does not decrease [9.28]. As a result, the obtained temperature at the end of a certain cycle is the starting temperature for the next cycle. The starting temperature of 27°C in figure 9.22 is the consequence of the four pumping cycles SCC LM-3 has undergone before the temperature test.
On the other hand, the increase of pressure loss with increasing temperature, as shown in figure 9.22, has not been observed for any other concrete. This can be partly due to the high age of SCC LM-3 (fig. 9.22), or it can be that the effect of temperature on the pressure losses is not as significant as structural breakdown and the increase in air content and as a result, it can be hidden by the other effects. The influence of loss of workability (possibly induced by the high temperature) will be discussed in the next section.
Analysis has revealed some trends influencing the temperature increase. Concrete containing more aggregates, like SCC LM-4 and TC-1 show a larger temperature increase for a certain pressure loss than concretes produced with less aggregates (like SCC LM-11). Segregating concretes (SCC LM-9 and 10) show apparently also a larger increase in temperature. On the other hand, no clear relationships between the temperature increase and any other parameter, besides pressure loss, have been found. Two very similar concretes, like SCC LM-5 and 6, show completely different behaviour. According to the theory of thermodynamics, the rate of increase in temperature should be related to the heat capacity of the pumped concretes, but as this parameter has not been measured, no results can be reported. All results of the temperature increase as a function of pressure loss can be found in Appendix D.

3.6 Loss of workability

Referring back to figure 9.16, the decrease in pressure loss at the higher discharges has been explained to be the consequence of structural breakdown and increasing air content, but the cause of the increase in pressure loss between cycles 5 and 6 is still unknown. As this is only occurring at high ages of the concrete, from 3 – 3.5 hours on, possibly enhanced by the high temperature [9.29], loss of workability is becoming important, especially for SCC LM-3, 8 and 14. Unfortunately, due to the very difficult sampling of the non-pumped concrete, which was in most cases not representative for the concrete applied in the pump, and the lack of more time, staff and testing equipment, the loss of workability of the non-pumped concrete has not been followed. On the other hand, this would be extremely difficult, as the temperature conditions need to be kept at the same level as in the pipes, and thixotropy (rebuild) must be eliminated before performing each standard test (see chapter 5). As a result, there is no proof that loss of workability is causing the increase in pressure losses between cycles 5 and 6 for SCC LM-8 and the increase in V-funnel flow time and viscosity for SCC LM-14, test Q4.

4 Advise for practitioners

4.1 Prediction of total pumping pressure needed

4.1.1 Theory

The total pressure needed to pump concrete in a certain circuit over a certain distance can be divided into three different parts: the normal pressure losses in straight sections, the special pressure losses in bends and reductions and the difference in height that needs to be overcome (multiplied by the density and the gravitational acceleration).
For the normal pressure losses, as shown in section 2.2.1, the Buckingham-Reiner equation (eq. 6.21) with incorporation of the geometrical wall effect can be used, as this formula delivers a ratio of the predicted pressure losses to the experimental pressure losses between 0.6 and 2. Note that the prediction ratio is in most cases larger than 1. As a result, shear thickening is neglected and the SCC can be approached as a Bingham liquid. Note that in case of severe shear thickening (which hopefully will not occur in practice) and very low yield stress concretes, this approach might lead to erroneous estimations. Also keep in mind that in case the rheological properties are measured with a different rheometer than the Tattersall Mk-II rheometer (or the Contec Viscometer), the yield stress and plastic viscosity must be corrected.
With the input of the rheological properties, the geometry of the pipe and the maximum aggregate size, the discharge corresponding to a certain pressure loss can be calculated. By means of trial and error, the pressure loss (per unit of length) at the designed discharge can be obtained. This pressure loss per unit of length should be multiplied with the length of the pipe in order to obtain the total pressure needed to pump the concrete in the straight, horizontal part of the conveying line. In case pipes with different diameters are used, the calculation should be executed for each diameter separately and the total pressure is the sum of the total pressures obtained for each diameter.
Special pressure losses occur especially in the bends and the reductions present in the circuit. As in this research project, no reductions have been investigated and the determination of the influence of a bend on the pressure losses is very inaccurate, a more extended literature review is advised. Also keep in mind that the obtained amplification factors for the bends are only valid for this specific configuration (R/D) and concrete. All special pressure losses must be added in order to know the total special pressure loss.
The static pressure can be very simply calculated as ρgh, where ρ is the density, g is the gravitational acceleration and h is the height difference between the beginning and end of the circuit. Other height differences, like when pumping over a house, do not matter, when pumping is going on, except during start-up!
Note that this calculation is only valid in regime conditions. During the insertion of the concrete, much higher pressures can be needed and possibly blocking can occur.
This prediction tool provides the ability to know the order of magnitude of the pressure needed, but it does not predict the correct value due to the large

uncertainties of the known phenomena and due to the currently unknown properties. Application with care is advised and an experimental verification will provide a larger certainty.

4.1.2 Example

Consider the situation shown in figure 9.24. A concrete pump is stationed in a factory and a formwork of 8 m high must be filled from the top. The conveying line consists of a horizontal part of 9 m long, an inclined part of 50 m long and another horizontal part of 1 m. The diameter of the pipe is 106 mm. In the circuit, three 90° bends with a R/D-ratio of 1.6 are installed and no reductions are present.

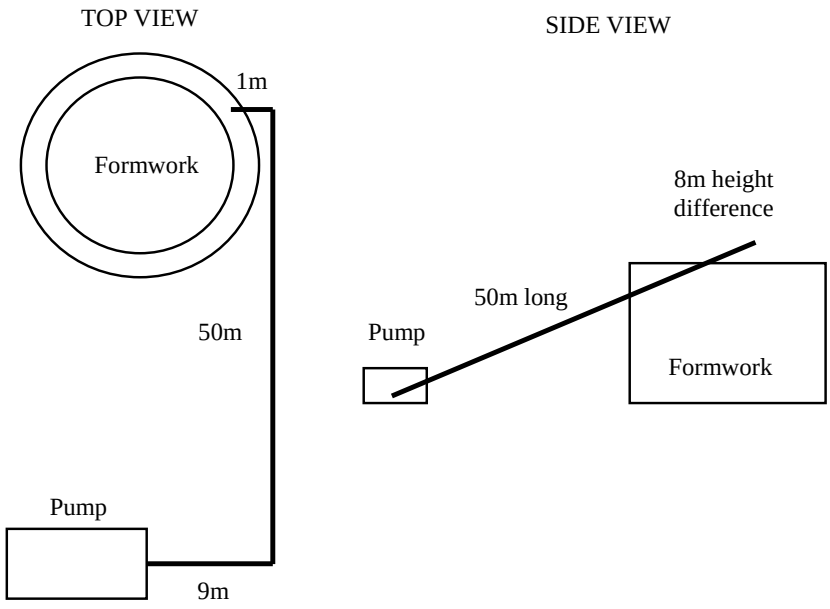

Figure 9.24: Example of pumping circuit. The total length of straight sections is 60 m, the total height difference is 8 m, the pipe diameter is 106 mm and three 90° bends with a R/D-ratio of 1.6 are installed.

The rheological properties have been determined with the Tattersall Mk-II rheometer resulting in a yield stress of 50 Pa and a plastic viscosity of 20 Pas. Some shear thickening is present, but it can be neglected. The maximal aggregate size of the SCC is 16 mm and the density equals 2350 kg/m³.
The planned discharges are 7 l/s and 15 l/s.
The pressure losses per unit of length in the straight sections have been calculated with the Buckingham-Reiner equation, incorporating the geometrical wall effect, and they are equal to 18.0 kPa/m for 7 l/s and 37.5 kPa/m for 15 l/s. The total

pressure loss in the straight section equals 1080 kPa and 2250 kPa for the 7 l/s and 15 l/s case respectively.
The special pressure losses over one 90° bend with R/D = 1.6 are estimated by means of figure 9.14. The amplification factors are 7.25 for both discharges, based on the averages for the obtained results at each discharge. As the length on the centreline of this 90° curve is 0.267 m, a total pressure loss of 18•7.25•0.267 = 34.8 kPa and 37.5•7.25•0.267 = 72.6 kPa has been obtained in the respective cases. The total pressure losses over all bends equal 104.4 kPa for the 7 l/s and 217.8 kPa for the 15 l/s case.
The additional pressure needed to overcome the height difference equals 8•2350•9.81 = 184 kPa.
The total pressure needed is 1368.4 kPa or 13.7 bar in case of a discharge of 7 l/s and 2651.8 kPa or 26.5 bar is case of 15 l/s. These pressure values correspond more or less with the range of pressures observed during the full scale pumping tests in the lab.

4.2 Practical situations

During the full scale pumping tests performed in the lab, the concretes have undergone the pumping process a series of time. For SCC LM-17, in the 81 m circuit, it is assumed that all concrete has passed through the pump 8 times. As a result, the observed effects are much more significant compared to on-site pumping, where the concrete only passes the pump once. Consequently, the results obtained in this project, like the large reductions in V-funnel flow time and slump flow, will probably not be obtained in practice, in this magnitude. These effects are expected to occur, but at a smaller scale.
Focussing on the theory of structural breakdown, this effect is expected to increase with increasing discharge and decreasing pipe diameter, both causing a larger shear rate and velocity in the concrete. In practice, mostly larger pipes are applied, and structural breakdown probably decreases. On the other hand, discharge can be (much) higher, increasing the effect. In case the pipe is long enough, the equilibrium structure can be achieved in the pipes and the concrete will be more fluid. Shorter circuits will induce a lower increase in fluidity.
As the causes of the air content are not precisely known, it is more difficult to predict what is going to happen in practice. Most probably, pipe diameter will not significantly influence the air content, but air bubbles size can be decreased with the application of smaller pipes, because more large bubbles can break into smaller elements. Increasing discharge or velocity on the other hand, probably causes a larger increase in air content. As a result, also for the air content, the effect increases with increasing discharge/ velocity.
As a conclusion, low velocities are advised when pumping self-compacting concrete, and on-site monitoring, like sampling and comparing of the pumped and non-pumped concrete should give an indication whether one of the effects is significantly visible. Remember that the concrete properties can evolve in two different directions, it can become more fluid or it can become more stiff. As simple test methods, a slump flow test and a sieve stability test are advised to be performed

on site (although sieve stability is not really straightforward on site, and another test indicating segregation sufficiently accurately can be applied). A decrease in slump flow indicates the importance of the air content, while an increase in sieve (un)stability, combined with a more or less constant or increasing slump flow, reveals the dominance of structural breakdown. In case of increasing air content, the SCC can be made a little bit more fluid, while in the other case, it should be made a little bit more stiff. But keep in mind that these conclusions are only based on a very small amount of tests, and that more investigation, possibly on site, must be executed in order to have more certainty!
Any results of pumping on site can be reported to the Magnel Laboratory in order to increase the knowledge in this field.

5 Summary

The results from the regular pumping tests indicate that for self-compacting concrete, the pressure loss – discharge curves show non-linear behaviour, while for the traditional concrete, linearity has been observed. When investigating the pressure loss at a certain discharge, the viscosity of the concrete, possibly modified by the shear thickening, is the most determining factor, with increasing importance with increasing velocity. As in general, SCC has a higher viscosity than TC, SCC will cause higher pressure losses. The flow has been found to occur in laminar conditions, but a direct relationship between the pressure losses or friction factor with any other parameter has not been found yet. In contrast to the concretes studied by Kaplan, apart from a few measurements, no pure plug flow has been observed in this research project.

When applying the Buckingham-Reiner equation or the extended Poiseuille formula for shear thickening materials derived in chapter 6, the pressure losses are significantly overestimated. This can be due to three different effects, reducing the viscosity of the material in the vicinity of the wall: the geometrical wall effect, structural breakdown and possibly dynamic segregation. An attempt has been made to incorporate the geometrical wall effect into the extended Poiseuille formula, but no proof can be found whether only this phenomenon causes the reduction in the pressure losses. The main disadvantages or shortcomings of this method are the extrapolation of the rheometer results and the assumption of the linear evolution of the yield stress and the viscosity over the boundary layer. On the other hand, the comparison of the predictions with the experiments shows that an effect inducing some kind of shear thickening must be present, but extrapolating the rheometer results leads to an overestimation of the shear thickening at higher shear rates. Segregation tests, in order to measure dynamic segregation, are found to be inconclusive, due to the sampling difficulties. As a result, there is no proof whether dynamic segregation does or does not occur.

By means of the special thixotropy tests, it has been found that the pressure loss at a certain discharge is lower if a higher discharge has been applied before. This effect has two causes: structural breakdown and an increase in air content. Structural breakdown causes the yield stress and the viscosity to decrease, while increasing the air content results in an increase in yield stress and a decrease in viscosity. Both effects are occurring simultaneously for each concrete, but one effect can dominate the other. If structural breakdown dominates the effect of the air content, the concrete can show a larger tendency to segregate. In the opposite case, when the effects of the air content dominate the structural breakdown, the slump flow decreases and the designed filling ability of SCC can be reduced. Based on a very restricted amount of results, we have the impression that the more fluid concretes show a larger tendency to segregate and that the less fluid concretes become stiffer, due to pumping. These effects appear to have an increasing importance with increasing velocity, although further investigation is needed.

Temperature has been found to increase during pumping, and this increase increases linearly with increasing pressure losses. On the other hand, no clear relationship has been found between the temperature increase and any other properties of the pumped concretes.

As advise for practical situations, it is recommended to reduce the pumping velocities, and to examine the difference between the pumped and non-pumped concrete. When a difference is noticed, it is always possible to slightly adapt the concrete mix design or pumping conditions.

6 References

[9.1] Kaplan D., "Pumping of concretes," Ph-D dissertation (in French), Laboratoire Central des Ponts et Chausées, Paris (2001).

[9.2] Crepas R.A., "Pumping concrete, techniques and applications, 3rd edition," Crepas and Associates, Inc., Elmhurst (1997).

[9.3] Guptill N.R. et al. (ACI-Comm 304), "Placing concrete by pumping methods," American Concrete Institute, Farmington Hills (1998).

[9.4] Sakuta M., Kasanu I., Yamane S., Sakamoto A., "Pumpability of fresh concrete," Takenaka Technical Research Laboratory, Tokyo (1989).

[9.5] Morinaga M., "Pumpability of concrete and pumping pressure in pipelines," Proc. of the RILEM Seminar on Fresh Concrete: Important properties and their measurement, Leeds (1973), 1-39.

[9.6] Browne R.D., Bamforth P.B., "Tests to establish concrete pumpability," ACI-Journal **74** (1977), 193-203.

[9.7] Ede A.N., "The resistance of concrete pumped through pipelines," Mag. Conc. Res. **9** (1957), 129-140.

[9.8] Tanigawa Y., Mori H., Noda Y., "Theoretical study on pumping of fresh concrete," Transaction of concrete Institute of Japan **13** (1991).

[9.9] Tattersall G.H., Banfill P.F.G., "The rheology of fresh concrete," Pitman, London (1983).

[9.10] Feys D., Verhoeven R., De Schutter G., "Evaluation of time-independent rheological models applicable to fresh Self Compacting Concrete," Appl. Rheol. **17:5** (2007), 56244.

[9.11] Macosko C.W., "Rheology Principle, measurements and applications," Wiley-VCH, New-York (1994).

[9.12] Ferraris C.F., Brower L.E., Banfill P., Beaupré D., Chapdelaine F., de Larrard F., Domone P., Nachbaur L., Sedran T., Wallevik O., Wallevik J.E., "Comparison of concrete rheometers: International tests at LCPC (Nantes, France) in October, 2000," NIST report 6819, Gaithersburg (2001).

[9.13] Ferraris C.F., Brower L.E., Beaupré D., Chapdelaine F., Domone P., Koehler E., Shen L., Sonebi M., Struble L., Tepke D., Wallevik O., Wallevik J.E., "Comparison of concrete rheometers: International tests at MB (Cleveland OH, USA) in May, 2003," NIST report 7154, Gaithersburg (2004).

[9.14] Wallevik J.E., "Rheology of particle suspensions, Fresh concrete, mortar and cement paste with various types of lignosulphonates," Ph-D dissertation, The Norwegian University of Science and Technology, Trondheim (2003).

[9.15] Geiker M.R., Wallevik O.H., "Rheology of cement based materials," DTU-RILEM Doctoral course, Lyngby (2007).

[9.16] Krieger I.M., "Rheology of monodisperse lattices," Adv. Coll. Interface Sc. **3:2** (1972), 111-136.

[9.17] Mahaut F., Chateau X., Coussot P., Ovarlez G., "Yield stress and elastic modulus of suspensions of noncolloidal particles in yield stress fluids, " J. Rheol. **52** (2008), 287-313.

[9.18] Roussel N., Le Roy R., Coussot P., "Thixotropy modelling at local and macroscopic scales," J. non-Newt. Fluid Mech. **117** (2004), 85-95.

[9.19] Fox J.A., "An introduction to engineering fluid mechanics," The MacMillan Press, London (1974).

[9.20] Mewis J., Wagner N.J., "Thixotropy," Adv. Colloidal Interface Sci., article in press.

[9.21] Barnes H.A., "Thixotropy - a review," J. Non-Newt. Fluid Mech. **70** (1997), 1-33.

[9.22] Wallevik J.E., "Rheological properties of cement paste: Thixotropic behavior and structural breakdown," Cem. Conc. Res. **39** (2009), 14-29.

[9.23] Roberts L.R., Scheiner P., "Microprocessor-based Linear Traverse Apparatus for Air-Void Distribution Analysis," Proc. of the 3th ICMA, Texas (1981), 211-227.

[9.24] Boel V., "Microstructure of self-compacting concrete in relation to gas permeability and durability aspects," Ph-D dissertation (in Dutch), Ghent University, Ghent (2006).

[9.25] Jakobsen U.H., Pade C., Thaulow N., Brown D., Sahu S., Magnusson O., De Buck S., De Schutter G., "Automated air void analysis of hardened concrete – a Round Robin study", Cem. Conc. Res., **36** (2006), 1444-1452.

[9.26] Rust A.C., Manga M., "Effect of bubble deformation on the viscosity of dilute suspensions," J. Non-Newt. Fluid Mech. **104** (2002), 53-63.

[9.27] Feys D., Roussel N., Verhoeven R., De Schutter G., "Influence of air content on the steady state rheological properties of fresh self-compacting concrete, without air entraining agents," Proc. of the 2nd Int. Symp. on Self-Consolidating Concrete, Beijing (2009).
[9.28] Calie B., "Pumping of Self-Compacting Concrete under pressure," Master-thesis (in Dutch), Ghent-University, Ghent (2007).
[9.29] Petit J.-Y., Wirquin E., Duthoit B., "Influence of temperature on yield value of highly flowable micromortars made with sulfonate-based superplasticizers," Cem. Conc. Res. **35** (2005), 256-266.

CHAPTER 10:

CONCLUSIONS

It is time to summarize the findings obtained during 4 years of research. This chapter contains the main results and conclusions of this research (section 1), but it also poses a lot of question marks, "to-do's" for the future (section 2). Finally, the research goals from chapter 1 are reflected, looking for an answer to the question: "Did we succeed?" (section 3).

1 Conclusions of this research project

1.1 Concrete rheometry

In this research project, different equipments were used in order to obtain, in one or another way, the rheological properties of (self-compacting) concrete. In fact, five different setups have been used: the Contec Viscometer 5 and the Tattersall Mk-II rheometer, as "real" concrete rheometers, a parallel-plate rheometer for cement paste and two different kinds of "capillary rheometers". As a first conclusion, we can say that the rheological properties of a certain SCC are still unknown, but we have been able to determine rheological properties, depending on the equipment applied. Comparing the obtained rheological properties from different apparatuses reveals that there are a lot of differences and difficulties and the real rheological properties of concrete are currently unknown.

1.2 Rheological properties in steady state

1.2.1 Yield stress and viscosity

It has been found that the variation of yield stress and viscosity induced by changes in the constituent materials of self-compacting concrete, obtained in steady state conditions, do not deviate significantly from the results reported in literature. Of course, as concrete (and especially SCC) is different from country to country, a different range of values of the Bingham parameters has been obtained. On the other hand, it has been experienced that duplicating a certain SCC mix is not

straightforward, and that the properties of SCC in its fresh state are very sensitive to any (small) variation in the composition.

1.2.2 Shear thickening

In contrast to the results for yield stress and viscosity, a rather new phenomenon has been proven to occur in case of SCC, sheared at high shear rates in a concrete rheometer, namely shear thickening. It has been shown that the obtained shear thickening is not a measurement artefact due to thixotropic (or structural) breakdown, it is not due to particle migration during the tests, plug flow has been eliminated and it has been observed in three (in fact: in five) different rheometers.
For several reasons, the modified Bingham model has been preferred to the Herschel-Bulkley equation in order to describe rheological properties of self-compacting concrete. The intensity of shear thickening is indicated by the parameter c/μ.
When analysing the shear thickening behaviour, two different parameters have been focussed on: the intensity of shear thickening and the critical shear stress for the onset of shear thickening. Experiments have shown that a decrease in w/p-ratio increases the intensity of shear thickening but does not affect the critical shear stress. Increasing the slump flow (possibly by increasing SP-content) increases the intensity and decreases the critical shear stress. When changing the filler, the most striking result has been obtained for silica fume: there was no shear thickening, but it is expected that the applied (low) shear stress did not exceed the critical shear stress. Shear thickening is intrinsically present in the self-compacting cement paste, and the addition of coarse aggregates, somewhat surprisingly, reduces the intensity. Adding oil reduces shear thickening due to a currently unknown reason.
Investigating the cause of shear thickening has revealed two possible phenomena: cluster formation and grain inertia. In the results obtained, it is more likely that cluster formation is the main cause of shear thickening. On the other hand, grain inertia should not be neglected, as it cannot be fully excluded.
As an answer to the question why shear thickening has not often been reported, it can be stated that the maximal shear stress during the tests executed in other institutes is too low in order to observe and investigate shear thickening. As in this research project, the shear rates in the final application (pumping) are very high, the shear rate range during the rheological characterization has been extended.
For the shear thickening behaviour itself, it can be concluded that in cases of slow flow of concrete, like during standard testing, and the flow inside the formwork, shear thickening can be neglected, but for fast flows, occurring during mixing and pumping, it can cause unwanted and very dangerous consequences and it should not be forgotten.

1.3 Time dependent rheological properties

1.3.1 Experimental determination of loss of workability

Three different phenomena influence the time dependent properties of fresh concrete: thixotropy, structural breakdown and loss of workability. Only loss of

workability has been examined experimentally with the Tattersall Mk-II rheometer. It has been found that the yield stress increases exponentially and that the viscosity (at a shear rate of 5/s) increases linearly with time. The shear thickening remains approximately constant. The obtained results for the time variation of slump flow and V-funnel are also influenced by thixotropy and cannot be analysed in the same way.
A clear distinction between the workability retention of the two different superplasticizers used has been observed. For each type of SP, an attempt has been made to find a correlation between the loss of workability and the constituent elements of the SCC. For the SP with the long workability retention, nice relationships have been obtained, while for the SP with the short workability retention, much more scatter in the data has been observed.

1.3.2 Consequences of time dependent behaviour

The main consequence of the time dependent behaviour of the rheological properties of fresh SCC is that it complicates the execution and interpretation of measurements significantly. Incomplete understanding of the possible consequences of these phenomena can lead to large mistakes in the obtained rheological behaviour.
As a second consequence, the real rheological curve (for a certain rheometer) depends on the definition of 'real'. Should equilibrium be awaited at each step of constant shear rate, or should the internal structure of the concrete be set at a certain reference state, corresponding to the minimal structure or maximal shear rate applied? Depending on the answer to this question, different rheological curves can be obtained, which are in fact all correct. In this research project, a reference state has been induced for all rheometer measurements.

1.4 The extended Poiseuille formula for laminar flow

1.4.1 Derivation

An extended version of the Poiseuille formula for laminar flow has been derived based on the universal shear stress distribution in a cylindrical pipe and the rheological properties of the material. In case the material obeys the Bingham law, the Buckingham-Reiner equation has been obtained, while the incorporation of shear thickening increases the complexity of the formula significanty. Note that the obtained formula is analytically correct, as no assumptions and approximations have been made.

1.4.2 Application to slow flow

This extended version of the Poiseuille formula has been verified by means of gravitational flow tests, in which SCC flows from an upstream to a downstream reservoir through a pipe with a certain length. The driving force in order to make the concrete flow is gravity and the maximal discharge is around 1 l/s.
The results indicate that for long pipes, the total pressure loss relates linearly with the length of the pipe, the rheological properties of the material and the discharge.

As the theoretical prediction by means of the extended Poiseuille formula and the experimental results agree well, it can be concluded that the flow occurs in laminar conditions and no significant wall slip is present.
For short pipes and rather fluid concretes, the special (entrance) pressure loss causes a deviation between the theory and the experiments.
On the other hand, when incorporating the geometrical wall effect, which certainly occurs during the flow of concrete in pipes, into the extended Poiseuille formula, the predicted pressure losses are underestimated. The causes are currently still unknown.

1.4.3 Application to fast flow

Full scale pumping tests with a maximal discharge of 20 l/s have indicated that the extended versions of the Poiseuille formula overestimate the pressure losses significantly. Three possible causes which can decrease the pressure loss at constant discharge have been discussed: the geometrical wall effect, structural breakdown and dynamic segregation. Unfortunately, the accuracy of sampling and measurements was insufficient in order to confirm or decline a certain phenomenon.
The velocity profile of SCC flowing through a cylindrical pipe is assumed to contain a small plug with uniform velocity in the centre, a large velocity gradient in the vicinity of the wall and a smaller velocity gradient in between. Direct measurements of the velocity profile should reveal the real physics of concrete flowing through a pipe.

1.5 Influence of rheology on pumping

1.5.1 Straight sections

For self-compacting concrete flowing in straight horizontal pipes, it has been found that the pressure losses are mainly influenced by the viscosity and the shear thickening of the concrete. The yield stress is not as important as the viscosity, and as a result, as the viscosity of SCC is in general higher than the viscosity of traditional concrete, pumping SCC at a certain discharge will cause higher pressure losses when compared to pumping TC at this discharge.
The results have also revealed that the shear thickening which has been estimated in the rheometer is larger than the “shear thickening” observed during pipe flow. This can be the result of the different shear rate ranges applied in both testing procedures.
The above mentioned correlation between the pressure losses and the viscosity will decrease with increasing ratio of yield stress / wall shear stress, as the plug radius increases and the amount of sheared material decreases. As a result, for high yield stress concretes or mortars, the yield stress will have a significant influence on the pressure losses.

1.5.2 Bends

The pressure losses in bends are in case of SCC (much) larger than the pressure losses in straight sections. Increasing the discharge and increasing the viscosity leads

to a lower amplification factor for a bend, although the number of results should be increased in order to verify the stated relationships.

1.5.3 Prediction of total pressure?

When considering the concrete as a Bingham material, neglecting shear thickening, the Buckingham-Reiner equation can be applied. Incorporating the geometrical wall effect in this equation leads to a prediction of the pressure losses which are a factor 1 to 2 higher than the experimental pressure losses. Based on the restricted amount of results for the bends, one can predict the order of magnitude of the pressure needed in a certain pipe geometry and for a certain SCC, but no precise predictions can be made. Careful application of the prediction tool is advised and experimental verification must reveal the real pressures needed. Note that the needed pressure is only determined in regime conditions and that larger pressures can occur during start-up.

1.6 Influence of pumping on rheology

Two effects have the most significant influence on the rheological properties of SCC flowing through pipes: structural breakdown and increasing air content. Both effects cause a decrease in viscosity, which results in a lower pressure loss at a certain velocity, if a higher velocity has been applied before.
On the other hand, structural breakdown and the increase in air content act in an opposite way on the yield stress. If structural breakdown dominates the effects of the increase in air content, the yield stress decreases and segregation can be provoked. If the effect of the increase in air content dominates structural breakdown, the yield stress increases and the designed filling ability can be lost. From the few experimental results obtained, more fluid SCC tends to segregate and less fluid SCC tends to stiffen more. Both effects are also thought to have an increasing influence with increasing velocity (gradient) in the pipes.

1.7 Advise in practice

In order to reduce the risks of segregation or improper filling of the formwork due to the changes in rheological properties of SCC during pumping, and in order to reduce the pumping pressures, it is advised to pump SCC at low velocities. As a result, decreasing the discharge and/or increasing the pipe diameter will reduce energy consumption and the risks for a low quality product.
For verification purposes, it is advised to take a sample of the SCC before and after pumping and compare the slump flow and sieve stability values. If the slump flow remains approximately constant and the segregation resistance decreases due to pumping, the SCC delivered should be made a little stiffer. If the slump flow decreases, a slightly more fluid SCC should be delivered.
In case of self-compacting concrete, the regime condition is the most safe situation during pumping, as it is not likely, when common sense is used, that a hazardous situation will occur. On the other hand, start-up and cleaning are much more dangerous practices. During start-up, blocking can occur, leading to a sudden

increase in total pressure, which can result in the breaking of a certain part in the conveying line or excessive movements of the placing boom. During cleaning with air pressure, the sponge ball has a large velocity and can become a dangerous projectile. Not only common sense is advised in these cases, but the people on the building site should have a substantial knowledge of the phenomena which can occur during these processes, in order to minimize injuries and casualties.

2 Further research

2.1 Rheology in general

Self-compacting concrete is different from country to country, from region to region, due to variations in the available constituent elements. As SCC is quite sensitive to variations in any part of its composition, the research on the rheological properties of SCC should not be stopped. The link between the rheological properties and the composition of the concrete should be investigated, in order to reveal the real physics in concrete and in order to be able to control the quality and sustainability of the fresh concrete better.

2.2 Comparison of rheometers

Many different types of rheometers are available on the market, but it is not known which rheometer delivers the best results. They all have advantages and disadvantages and it is difficult to select the appropriate rheometer. Furthermore, they all deliver different results for the rheological properties of a certain concrete, making it impossible to determine which one delivers the correct results. Comparative studies on different concrete rheometers should be continued, not only with concrete, but also with other fluids, in order to distinguish between intrinsic differences and concrete related differences. Note that these comparative researches can also include “capillary rheometers” for concrete (see section 2.7).

2.3 Shear thickening

Shear thickening has been proven to be a real material characteristic of self-compacting concrete. In this research, some of the influencing parameters have been determined, but still, many other parameters need to be investigated. For example, further investigations should reveal whether shear thickening is dependent on the surface area of the fine materials, possibly related to the surface covered by superplasticizers. Also the type of cement, after elimination of the possible influence of surface area, can be investigated.

In fact, shear thickening is intrinsically present in the cement paste, and a main part of the research can be focussed on cement pastes. In this way, only small samples are needed and the effect of particle migration is less probable to occur. As a result, higher shear rates can be applied.

The main cause of shear thickening still needs to be determined, and probably, as in the limit every type of concrete must shear thicken at high shear stresses, the cause of shear thickening can depend on several conditions.

As has been shown in chapter 4, the addition of coarse aggregates in mortar reduces the shear thickening behaviour. Both the specific causes of this phenomenon still need to be investigated, and the change of shear thickening with increasing content of coarse aggregates must be determined much more accurately.

In future research, shear thickening must not be forgotten in situations where high shear rates are likely to occur, as it can cause a much larger shear stress at a certain shear rate, compared to a prediction by means of the Bingham model.

2.4 Thixotropy and structural breakdown

Thixotropy and structural breakdown are probably the most difficult parameters to understand and investigate, and the measurements must be executed really very carefully. Currently, the knowledge of thixotropy and structural breakdown is increasing, but a fundamental understanding of the phenomenon is needed in order to be able to control it. Furthermore, as has been already mentioned, thixotropy and structural breakdown influence the value of the viscosity, but in contrast to the yield stress, not many investigations have been performed in order to determine the magnitude of increase or decrease in viscosity due to thixotropy and structural breakdown. Does viscosity relate to the internal structure equally, similarly or differently as the yield stress? Can a parameter A_{thix}' be determined for the increase in viscosity due to rebuild? And what is the exact relationship between the structure parameter and the applied shear rate or shear rate difference? And concerning the results in this thesis: what is the influence of thixotropy and structural breakdown on the shear thickening behaviour?
As can be seen, the field of thixotropy and structural breakdown still needs more exploration, but one of the main questions is how we can relate these complex theories to practical situations, like pumping for example.

2.5 Influence of air on the properties of concrete

The influence of air bubbles on the rheological properties of concrete, has been explained qualitatively in order to interpret the pumping results, but a quantitative model would be useful. What is the exact evolution of yield stress, viscosity and shear thickening with increasing air content and variations in air bubbles size, keeping in mind that no air-entraining agents can be applied as the surfactants in these agents modify significantly the surface tension of the air bubbles in the cement paste.
Secondly, air bubbles will probably have an influence on the hardened concrete properties. It should be investigated to which level the strength, durability, creep and shrinkage are not significantly negatively influenced. These results can be important in case the concrete has been or must be pumped.

2.6 Influence of oil additions on the properties of concrete

It has been mentioned that adding (the applied type of) demoulding oil decreases shear thickening and increases the yield stress of SCC. The specific causes are currently unknown, but as oil is used a lot in practice, it would be useful to know what the specific influence is, and as a possible outcome, demoulding oil can be used as a “rheology modifier”, advantageous for pumping of SCC.

On the other hand, adding oil in order to modify the rheological properties should not be done on purpose before the influence on the hardened properties is known. If this outcome appears to be negative, special care is needed in any situation where demoulding oil is used.

2.7 Development of a capillary rheometer for concrete

In this research project, a prototype of a capillary rheometer for concrete (the gravitational flow test setup) has been developed. It can be discussed whether the walls of the pipes should be smooth or whether some tools should be provided in order to prevent wall slip or the formation of lubrication layers.
The gravitational flow test described is only a very rough tool, and it needs many modifications in order to provide high quality information of the rheological properties of SCC, or maybe better: of the flow resistance of SCC in pipes. As primary modifications, the following steps are advised:

- Reducing the entrance pressure losses. In the current setup, the flow must contract and change direction in a very abrupt way, which can lead to high special pressure losses, influencing the results.
- Application of different pipe diameters. When the flow of the same concrete is studied in different pipe diameters, which has not been done in this research project, the possibility exists of investigating wall slip or lubrication layers in the concrete. The principle is similar as for the traditional capillary rheometers (chapter 3).
- Some tool should be provided in order to bring the concrete in a reference state before the test. In this research, the elimination of thixotropy resulted in a loss of almost half of the data. If this can be avoided, much more valuable information can be retrieved from this test setup.
- In order to accelerate the flow, or to be able to investigate concrete with a rather high yield stress, the upstream pressure should be increased. This can be done by increasing the height of the upstream reservoir, but this also increases the amount of concrete needed. When the amount of concrete needs to be kept constant, pressure can be added by means of air or by means of a hydraulic jack.

As can be seen, the test setup is far from perfect and a large amount of improvements are needed, but it is expected to have great possibilities, as it is a kind of measuring tool for concrete flowing through pipes, without the need of a pump.

2.8 The flow of concrete in pipes

By means of the above mentioned capillary rheometer, or by means of pumping, the flow of concrete in pipes must be investigated much more in detail, because the real physics of the flow process are still unrevealed.

2.8.1 Lubrication layers

As mentioned in chapter 9, wall slip is assumed not to occur in case of SCC, as it is a quite sticky material, but the velocity gradient near the wall is larger than when the concrete is considered to be homogeneous, indicating the existence of a lubrication layer. The geometrical wall effect has been discussed and a first attempt to model this effect has been proposed. By means of further research, this effect should be studied much more in detail, but as long as concrete rheometers deliver different results, it will never be certain whether only the geometrical wall effect causes the lubrication layer.
In order to investigate the lubrication layers more in detail, an accurate sampling and measuring system can be developed, capable of measuring the rheological properties of the concrete at any position in the pipe. Other solutions are also available as will be discussed in sections 2.8.3 and 2.8.4 of this chapter.

2.8.2 Difference between SCC and TC

When comparing the results of D. Kaplan on traditional concrete and our results on SCC, a significant difference can be noticed. The plug radius in case of TC is almost equal to the pipe radius and the (traditional) concrete is forced to create a lubrication layer in order to flow. In case of SCC, this lubrication layer also exists, but probably its importance is less significant. Furthermore, the plug radius in case of SCC is much smaller and a part of the SCC is sheared in the pipes.
These two types of concrete show different behaviour, which is probably related to the plug radius or yield stress of the concrete. In order to understand the phenomena in detail, the whole range of yield stresses between SCC and TC can be investigated. In this way, a kind of transition may be observed, which should increase the understanding of the flow of concrete in pipes.

2.8.3 Modification of the pumping test setup

The main shortcoming of the applied pumping circuits is the constant diameter of the pipes. It would be better to install different measuring sections with different pipe diameters. As a first idea, five straight horizontal measurement sections of 9 to 12 m long can be installed. Suppose three different pipe diameters are available: small, medium and large, then the circuit should be as follows: small – medium – large – medium – small. In this way, if the first part with the small pipes is sufficiently long, the main part of structural breakdown has occurred in this section. The results of the first and last section, and the results of the second and fourth section can be compared in order to verify the further occurring of structural breakdown. The results of section three to five can be compared in order to investigate the lubrication layers.
In this situation, at least 10 pressure sensors will be needed, which increases the costs significantly. From our experience, strain gauges deliver useful results, but these are not sufficiently accurate for some of the precise measurements that need to be performed. Strain gauges can be applied in the neighbourhood of the pressure sensor, acting as a back-up tool. With this number of pressure sensors, a more detailed investigation of the pressure losses over bends and in reductions can be

executed, as the flow of concrete in bends and reductions is still not fully understood yet.

2.8.4 Direct measurements of velocity profile

One of the most useful improvements which can be made for understanding the flow of concrete in pipes, is the direct measurement of the velocity profile. The tools are currently available, for example MRI, but the costs are still too elevated in order to be applied on concrete.

2.9 Influence of pumping on the rheological properties

Based on a small range of experiments, it has been found that SCC can segregate due to pumping, or it can lose a part of its filling ability. The causes are assumed to be structural breakdown, an increase in air content and a decrease in air bubbles size. Further investigation should confirm hopefully the assumed causes, and maybe the boundary between "increasing danger for segregation" and "loss of filling ability" can be determined. As a result, more experiments in the laboratory are needed, but a (very) large contribution from the concrete industry can significantly help the understanding of the occurring phenomena.
These phenomena should be taken into account when dealing with the filling of formworks and in fact when dealing with the full casting process. In this way, the gap in the research between the rheological characterisation of SCC and the casting in formworks is closed.

2.10 Filling of formworks

As mentioned in the first chapter, this research project is the start of a range of different projects to understand the full casting process. With the obtained results for pumping, a theoretical, experimental and numerical investigation on the filling of formworks can be started. It should be kept in mind that self-compacting concrete is currently the only type of concrete which allows casting from the bottom. This procedure will speed up the casting process and increase the casting height (especially in precast plants). Further investigation must reveal the advantages and disadvantages of this specific filling process.

3 Are the research goals met?

The original goals of this research project have been described in section 2.2 of chapter 1. Three main subjects have been defined: the study of the rheological properties of SCC and the study of the flow of SCC in the pipes.
Concerning the study of the rheological properties of SCC, which has to serve as an input for the investigation of pumping, it can be said that the goal is partly achieved. We are able to measure the rheological properties in steady state and control the possible errors which can occur during the measurement. The variation in the properties can be qualitatively predicted when a certain variation in one of the constituent elements has been applied, but a quantitative prediction tool has not been achieved. Similar conclusions can be drawn for the time dependent properties: a good understanding of the phenomena has been achieved, but predictions and calculations are not available. As a result, the rheological properties of the SCC must be measured anytime.
The investigation of the flow of SCC in pipes has shown large improvements in the understanding of the process, but the flow of concrete in pipes still has some secrets which need to be revealed. In case of pumping SCC, the same principle applies as for the rheological measurements. A qualitative knowledge of what is occurring has been obtained, but it is currently impossible to describe it by means of mathematical models. Consequently, also for the flow of SCC in pipes, the different parameters need to be measured and an accurate prediction is not available.

APPENDICES

APPENDIX A:

CALIBRATION OF THE TATTERSALL MK-II RHEOMETER

1 Applied materials and reference rheometer

Both a very viscous oil (poly-iso-butene) and "white" honey have been applied as reference materials. The oil is a Newtonian liquid and the honey is, to be exact, shear-thinning. On the other hand, for the shear rate range at which the tests are performed, the honey can be classified as a Bingham material with an apparent yield stress. Both materials have been tested in the Tattersall Mk-II rheometer at different temperatures. As a result, different values of the viscosity (and the yield stress) have been obtained per material. Once the tests on the Tattersall Mk-II rheometer have been performed, a small sample has been taken to a cone and plate rheometer, where the rheological properties have been determined at the same set of temperatures. The rheological properties of the oil have been determined at three different temperatures by executing at each temperature three tests with each rheometer. For the honey, four different temperatures have been applied, with three tests per temperature in the cone and plate geometry and five tests per temperature in the Tattersall Mk-II rheometer.

2 Results for oil

In figure A.1, the average of the results at each temperature for the oil, measured with the cone and plate rheometer, clearly indicate Newtonian behaviour and the dependency of viscosity on temperature.
In the Tattersall Mk-II rheometer, the oil does not show Newtonian behaviour. At high rotational velocities, it can be seen that the relationship between torque and rotational velocity is linear. At low rotational velocities and low torque values, the linear behaviour is not obtained. This is suspected to be due to the flow of oil between the blades of the inner cylinder. As rotational velocity or torque increases, the flow between the inner and outer cylinder superposes with the flow between the blades. Based on these measurements, a zone of non-linearity has been defined by the relationship $T = 1 - N/55$ (fig. A.2).

Omitting the data points in the zone of non-linearity, and extrapolating the linear relationship of the remaining data points of the tests at the three different temperatures causes the lines to coincide in one point. If the flow between the blades would be prevented, this point should be the origin of the T – N curve. The data in the zone of non-linearity obey a power-law relationship $T = A \bullet N^{2.55}$.

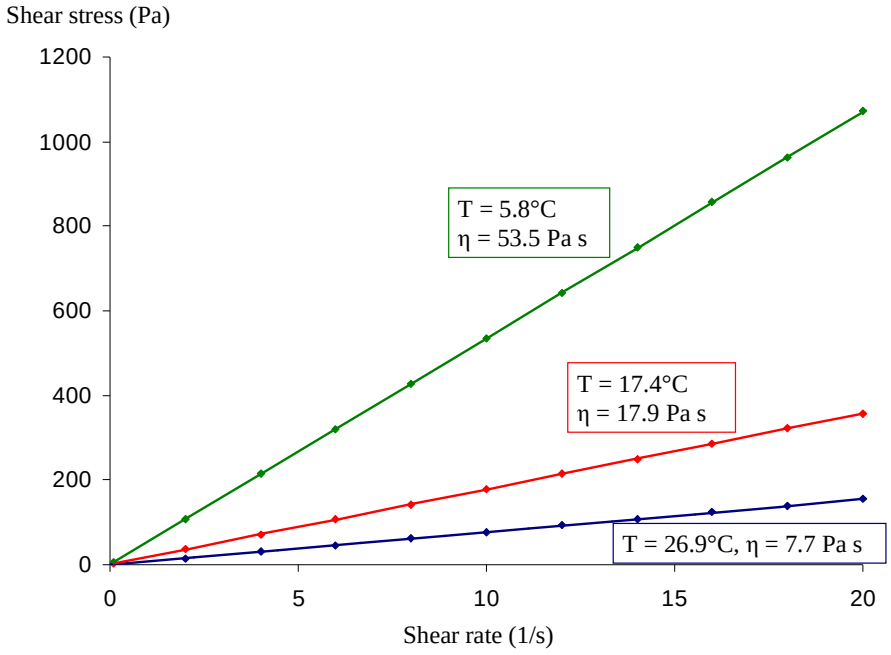

Figure A.1: Newtonian behaviour of the oil, at different temperatures, determined with the cone and plate rheometer.

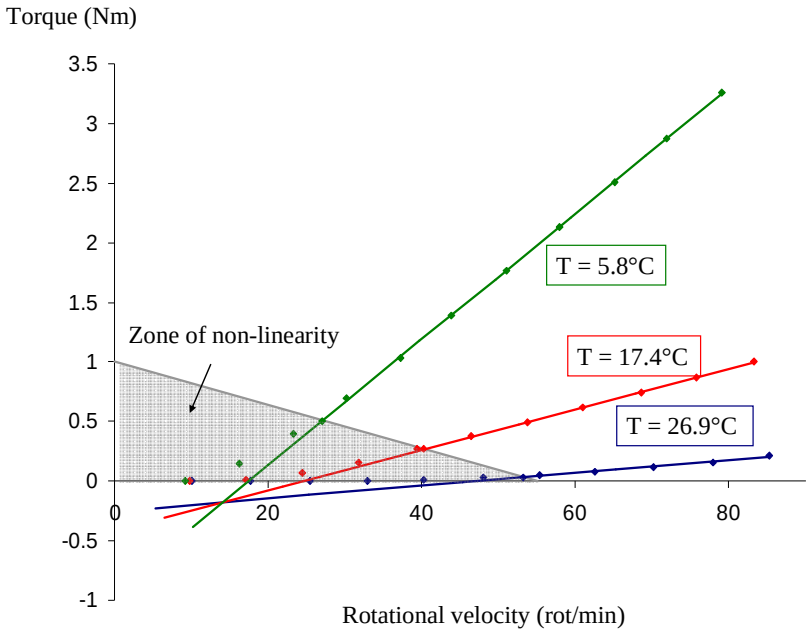

Figure A.2: Torque as a function of rotational velocity for the oil measured in the Tattersall Mk-II rheometer. Definition of the zone of non-linearity.

3 Results for honey

Figure A.3 shows the results for the honey tested at four different temperatures in the cone and plate rheometer. It can be seen that both yield stress and viscosity increase with decreasing temperature.
In the Tattersall Mk-II rheometer, the data outside the zone of non-linearity show a linear relationship, but the extrapolated lines do not coincide in one point, due to the presence of a yield stress (fig. A.4). For each curve at a certain temperature, obtained for honey, a corresponding Newtonian curve, with equal inclination is calculated. The "yield torque" is defined as the difference in torque value between the obtained curve and the corresponding Newtonian curve with equal inclination.

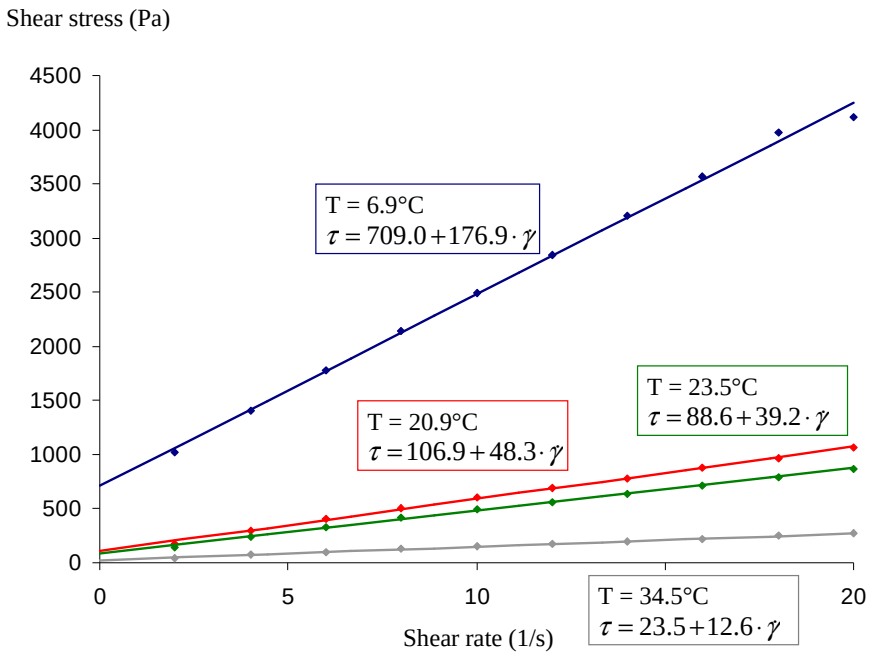

Figure A.3: Determination of yield stress and plastic viscosity of honey by means of the cone and plate rheometer.

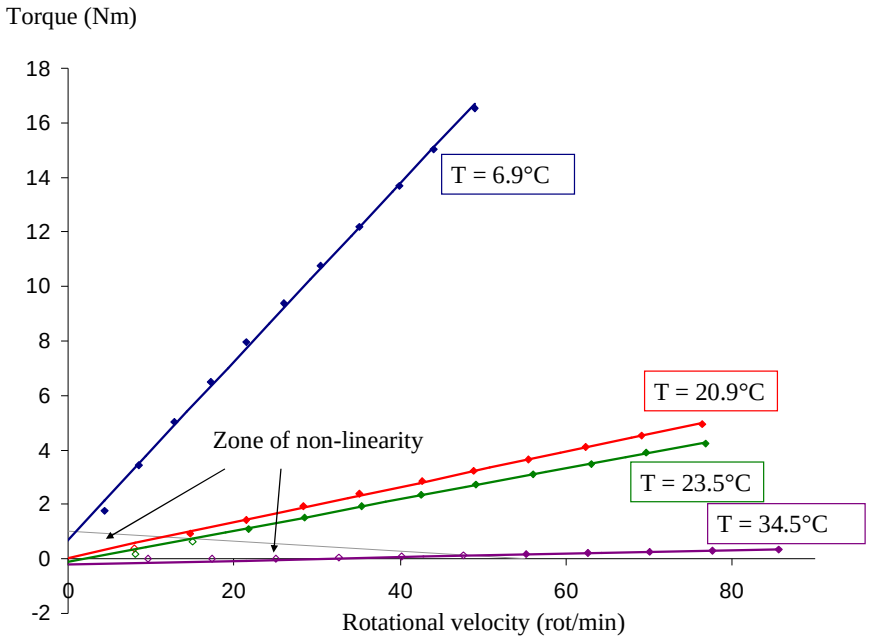

Figure A.4: Torque as a function of rotational velocity for honey obtained with the Tattersall Mk-II rheometer at different temperatures.

4 Transformation of data for Bingham materials

In order to transform data points expressed in torque and rotational velocity into shear stress and shear rate, the following steps (fig. A.5) must be applied in case of a Bingham material, which can be recognized by the linear relationship between torque and rotational velocity in a T - N diagram outside the zone of non-linearity (fig. A.5a).

1 The yield torque is calculated following the procedure mentioned in part 3 of this section (fig. A.5b).

2 The intersection of the extrapolated line outside the zone of non-linearity with the edge of this zone is calculated, corresponding to a value N_i. Inside the zone of non-linearity, a curve of the form $T = T_0' + A \bullet N^{2.55}$ is fitted to the data points. On the extrapolated line from outside the zone of non-linearity, the N-value, corresponding to T_0' is defined as N_a (fig. A.5c-d).

3 All data points outside the zone of non-linearity are corrected by a horizontal translation towards the origin over a distance N_a. The new N-values are described by $N' = N - N_a$ (fig. A.5e).

4 All data points inside the zone of non-linearity are corrected as follows: $N' = (N_i - N_a) \bullet (N/N_i)^{2.55}$. As a result, all corrected data points inside the zone of non-linearity are situated on the extrapolated line of the data points outside this zone, in a T – N' diagram (fig. A.5f). Logically, applying step 3 or step 4 on the data point which is on the intersection of the T – N diagram with the edge of the zone of non-linearity results in the same value for N'.

5 A new value for T_0 in the T – N' diagram is obtained. The new line must be shifted vertically in order to match T_0 with the yield torque obtained in step 1 (fig. A.5g).

When applying the above procedure, the influence of the zone of non-linearity has been eliminated. The new data can be compared to the results from the cone and plate rheometer and the calibration constants can be derived. The torque (in Nm) must be multiplied with 124.37 in order to obtain the shear stress (Pa). The rotational velocity (in rot/min) is multiplied with 0.1931 in order to obtain the shear rate (s^{-1}) (fig. A.5h).

Note that, due to insufficient accuracy, the data obtained for the honey at the highest temperature have been omitted in order to calculate the calibration constants.

Problems can arise when not sufficient data points are available in order to determine the power-law relationship in the zone of non-linearity. If only 1 data point is available, the second data point is chosen to be the intersection of the extrapolated curve from outside the zone with the edge of the zone. If no data points are in the zone of non-linearity, but there is an intersection, the intersection point is the only data point available, and the A-value is chosen based on a linear correlation between the inclination of the extrapolated line and other obtained A-values.

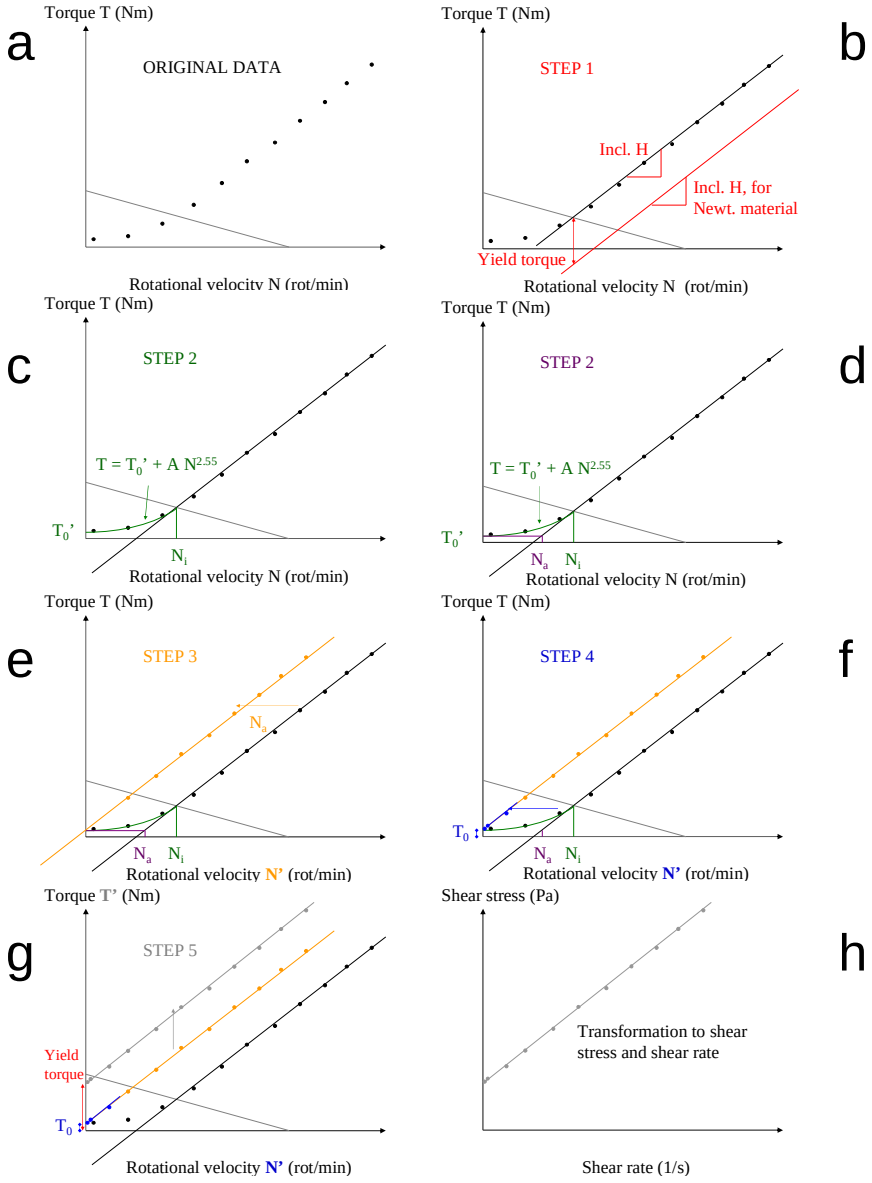

Figure A.5: Different steps in transformation of T – N data into a shear stress – shear rate relationship.

5 Transformation for non-Bingham materials

When the relationship between T and N outside the zone of non-linearity is not linear, difficulties arise to determine the extrapolated curve. Two additional steps are included in the transformation procedure in order to overcome this problem. From the raw T – N data, the best fitting straight line through the five data points at the lowest N-values is determined. Although this induces a new error, in most cases, this procedure seems reasonable, except in cases where the data show a clear curvature, especially in case of very fluid concrete when a few data points show a near zero torque value. In this case, some points are omitted to obtain a straight line, in order to fit the data nicely, which is illustrated in figure A.6. In order to determine N_a, the corresponding N-value with T_0' is determined by means of the straight line defined above.

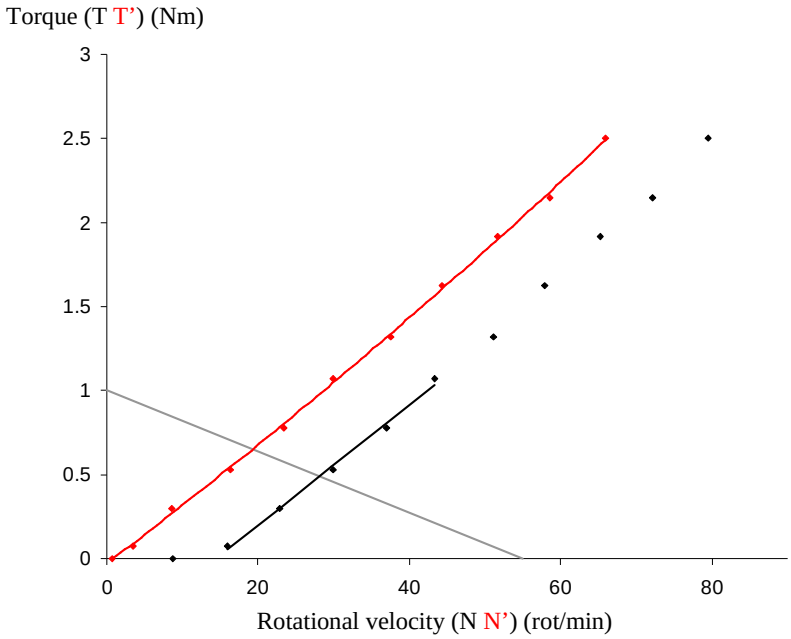

Figure A.6: Transformation of data (black = original, red = obtained results after step 4) for a non-Bingham material.

APPENDIX B:

TEST RESULTS OF RHEOLOGICAL MEASUREMENTS

1 Introduction

This part of the appendix will give the composition of all concretes tested, described in chapters 4 and 5. When an asterix (*) is written next to the value of the amount of SP, it means that the total amount has not been added in one time. The units are expressed in kg/m³ of concrete, except for the SP-content which is in l/m³. The values of the standard tests as slump flow, T50, V-funnel, L-box and sieve stability are also given, if the test has been executed. Note that segregation has mostly been examined visually, with three possible outcomes: No, Slightly and Yes. The concretes marked in red have not been retained for the main analyses for shear thickening (chapter 4) and loss of workability (chapter 5), due to segregation, a delay in the first test (yellow mark) or due to application of different filler materials. The concretes with different filler materials have been analysed separately.

2 Rheological tests performed with the Tattersall Mk-II rheometer at the Magnel Laboratory

Mix number	SCC 1 test	SCC 2	SCC 3
Date	12/04/2005	15/04/2005	15/04/2005
Sand 0/4	853	853	853
Gravel 2/8		263	
Gravel 8/16	698	453	
Crushed Aggr. 7/14			698
CEM I 52,5 N	360	360	360
Limestone filler 1	240	240	240
water	165	165	165
SP 1	3.2	4.7*	3

Mix number	SCC 1 test				SCC 2			SCC 3			
Date	12/04/2005				15/04/2005			15/04/2005			
Age (min)	15	30	60	90	15	30	60	15	30	60	90
Slump Flow (mm)	957.5	900	867.5	690	690	637.5	575	725	605	587.5	560
T 50 (s)											
V-funnel (s)	12.4	9.9	27.4		13.9	18.0	31.0	13.9	14.9	25.5	31.9
L-box-ratio (-)	0.98	0.78	0.84		0.78	0.72	0.58	0.66	0.54	0.60	0.37
Segr? / Sieve stab	Yes				No	No	No	No	No	No	No
Yield stress (Pa)	53.9	67.1	78.9	118.0	129.9	189.9	282.7	85.6	123.9	165.6	229.8
Viscosity at 0 sr (Pas)	9.52	19.1	21.7	36.3	59.6	75.7	81.2	28.7	44.6	42.0	69.1
c (Pa s²)	2.88	2.71	3.26	0.46	3.02	4.20	8.92	1.60	2.07	2.13	0.66

Mix number	SCC 4	SCC 5	SCC 16	SCC 5-2	SCC 1-2	SCC 6	SCC 7	SCC 8	SCC 9	SCC 10
Date	19/04/2005	19/04/2005	26/04/2005	26/04/2005	28/04/2005	20/05/2005	20/05/2005	24/05/2005	24/05/2005	27/05/2005
Sand 0/4	853	853	853	853	853	853	853	853	853	853
Gravel 2/8						263		263		263
Gravel 8/16		698	698	698	698	453	698	453	698	453
Crushed Aggr. 2/7	268									
Crushed Aggr. 7/14	411									
CEM I 52,5 N	360	300	360	300	360	300	400	400	450	450
Limestone filler 1	240	300	240	300	240	300	200	200	150	150
water	170	170	170	165	165	165	165	165	165	165
SP 1	3.5*	2.8	2.5*	3.5*	2.8*	3.1	2.5	3.66*	3.8*	3.4*
Welan Gum (total added)							4 g			

Mix number	SCC 11	SCC 32
Date	27/05/2005	10/06/2005
Sand 0/4	853	853
Gravel 2/8		263
Gravel 8/16	698	434
CEM I 52,5 N		360
CEM I 52,5 R HES	360	
Limestone filler 1	240	
Quartzite filler		240
water	165	175
SP 1	3.04*	2.88*
Welan Gum		2 g

Mix number	SCC 4					SCC 5		SCC 16		
Date	19/04/2005					19/04/2005		26/04/2005		
Age (min)	15	30	60	90	120	15	30	15	30	60
Slump Flow (mm)	860	800	682.5	682.5	645	970	725	675	585	525
T 50 (s)	2.2	2.1	3.3	5.0	7.3	1.2	4.8	1.5	4.2	6.1
V-funnel (s)	9.6	19.4	16.0	18.0	29.0	5.8	15.6	7.7	9.3	11.7
L-box-ratio (-)	0.93	1.00	0.93	0.81	0.82	0.99	1.00	0.75	0.76	0.57
Segr? / Sieve stab	No	No	No	No	No	Yes	Yes	No	No	No
Yield stress (Pa)	42.8	45.2	52.9	56.3	67.9	34.3	35.5	60.9	78.4	120.4
Viscosity at 0 sr (Pas)	6.65	11.5	14.6	21.1	22.3	0	2.22	21.8	26.1	27.5
c (Pa s²)	1.68	1.33	1.49	1.11	1.33	1.38	1.32	0.89	1.05	0.73
Mix number	SCC 5-2			SCC 1-2				SCC 6		
Date	26/04/2005			28/04/2005				20/05/2005		
Age (min)	25	30	60	15	30	60	90	30	60	90
Slump Flow (mm)	580		500	715	645	590	565	710	595	590
T 50 (s)	4.2		5.5	2.3	2.2	2.5	10.2	2.1	2.7	3.1
V-funnel (s)	13.4		21.1	8.5	11.4	17.0	19.7	7.7	10.5	11.7
L-box-ratio (-)	0.60		0.48	0.80	0.75	0.58	0.48	0.88	0.64	0.54
Segr? / Sieve stab	No		No	No	No	No	No	No	No	No
Yield stress (Pa)	124.7	151.5	245.3	115.4	127.5	191.4	247.1	75.9	115.9	180.2
Viscosity at 0 sr (Pas)	41.4	43.9	58.0	41.5	47.0	56.1	75.5	25.4	34.6	43.8
c (Pa s²)	0.65	1.28	2.24	0.77	0.74	2.59	0.92	1.12	1.41	2.06
Mix number	SCC 7				SCC 8			SCC 9		
Date	20/05/2005				24/05/2005			24/05/2005		
Age (min)	25	40	60	90	25	60	90	20	30	60
Slump Flow (mm)	740	635	642.5	540	650	505	445	575	515	467.5
T 50 (s)	2.6	6.1	5.3	19.4	1.5	17.7		2.5	5.0	
V-funnel (s)	8.2	9.8	12.7	18.8	13.4	17.6	20.3	14.0	15.5	24.3
L-box-ratio (-)	0.92	0.88	0.77	0.68	0.68	0.43	0.28	0.61	0.58	0.31
Segr? / Sieve stab	No	No	No	No	No	No	No	No	No	No
Yield stress (Pa)	71.7		101.7	136.6	127.3	244.7	357.7	153.2	222.5	312.6
Viscosity at 0 sr (Pas)	23.0		47.2	41.9	43.9	64.6	85.1	47.3	43.0	78.1
c (Pa s²)	0.82		-0.41	0.57	1.61	2.89	3.51	1.16	3.81	3.16
Mix number	SCC 10				SCC 11				SCC 32	
Date	27/05/2005				27/05/2005				10/06/2005	
Age (min)	15	30	60	90	15	30	60	90	25	60
Slump Flow (mm)	595	565	520	470	652.5	615	545	545	532.5	415
T 50 (s)	4.6	6.1	10.2		1.8	2.9	8.4	4.5	3.4	
V-funnel (s)	13.8	14.7	23.3	25.0	9.1	12.0	26.7	28.6	14.2	25.6
L-box-ratio (-)	0.68	0.54	0.40	0.15	0.77	0.73	0.60	0.42	0.42	0.00
Segr? / Sieve stab	No	No	No	No	No	No	No	No	No	No
Yield stress (Pa)	133.2	176.2	268.6	349.4	77.5	92.0	133.1	154.4	241.5	472.2
Viscosity at 0 sr (Pas)	46.5	50.0	60.9	73.1	26.8	29.0	34.3	46.3	75.5	117.3
c (Pa s²)	2.15	3.71	5.38	5.69	1.34	1.84	2.71	2.60	1.04	1.50

Mix number	SCC 33	SCC 35	SCC 35-2	SCC 36	SCC 36-2	SCC 37	SCC 38	SCC 39	SCC 40	SCC 41
Date	10/06/2005	17/06/2005	17/06/2005	24/06/2005	24/06/2005	1/07/2005	1/07/2005	15/07/2005	10/06/2005	5/08/2005
Sand 0/4	853	853	853	853	853	853	853	853	853	901
Gravel 2/8		263	263	263	263	263	263	263	263	278
Gravel 8/16	698	434	434	434	434	434	434	434	434	459
CEM I 52,5 N	360	360	360	360	360	300	400	250	450	300
Limestone filler 1		240	240	240	240	300	200	350	150	200
Quartzite filler	240									
water	170	170	170	165	165	165	165	165	165	165
SP 1	2.48*	2.88*	2.6	3.4	3.2	2.7*	3.4	2.66*	3.4	2.5
Welan Gum				1.5 g						1 g

Mix number	SCC 42	SCC 43
Date	5/08/2005	12/08/2005
Sand 0/4	805	947
Gravel 2/8	248	292
Gravel 8/16	410	483
CEM I 52,5 N	400	250
Limestone filler 1	300	150
water	165	165
SP 1	3.74*	1.8

Mix number	SCC 33			SCC 35			SCC 35-2			
Date	10/06/2005			17/06/2005			17/06/2005			
				With demoulding oil						
Age (min)	15	30	60	30	60	90	15	30	60	90
Slump Flow (mm)	570	490	415	585	500	477.5	675	615	485	482.5
T 50 (s)	4.0			2.7			2.5	2.2		
V-funnel (s)	11.8	16.3	23.5	7.3	9.2	11.0	9.7	9.8	14.6	21.9
L-box-ratio (-)	0.41	0.45	0.23	0.59	0.43	0.36	0.76	0.63	0.51	0.32
Segr? / Sieve stab	No	No	No	No	No	No	No	No	No	No
Yield stress (Pa)		360.4	622.3	100.3	209.6	379.5	81.4	130.2	202.4	312.1
Viscosity at 0 sr (Pas)		93.9	152.3	30.1	47.7	64.0	23.5	32.2	41.4	59.4
c (Pa s²)		5.26	5.80	-0.08	-0.09	0.37	2.43	3.50	4.55	5.40

Mix number	SCC 36				SCC 36-2				SCC 37			
Date	24/06/5002				24/06/2005				1/07/2005			
Age (min)	15	30	60	90	15	30	60	90	15	30	60	90
Slump Flow (mm)	775	660	577.5	535	922.5	772.5	655	615	710	585	540	460
T 50 (s)	3.5	6.4	12.2		1.7	3.7	7.2	7.0	3.0	5.4	7.3	
V-funnel (s)	11.9	13.7	19.4	34.5	7.6	11.0	15.8	21.0	9.6	12.0	18.4	29.4
L-box-ratio (-)	0.90	0.83	0.74	0.62	1.00	0.81	0.78	0.59	0.86	0.78	0.53	0.20
Segr? / Sieve stab	No	No	No	No	Slightly	No	No	No	No	No	No	No
Yield stress (Pa)		68.3	118.5	173.0	24.7	34.8	36.5	106.0	49.6	88.5	180.6	510.9
Viscosity at 0 sr (Pas)		21.8	24.1	34.8	1.54	8.64	16.1	17.3	22.9	31.7	38.2	39.4
c (Pa s²)		3.82	6.02	7.15	3.72	4.05	4.27	6.28	2.40	2.98	4.95	9.27

Mix number	SCC 38				SCC 39			SCC 40	
Date	1/07/2005				15/07/2005			15/07/2005	
Age (min)	15	30	60	90	15	30	60	15	30
Slump Flow (mm)	842.5	680	627.5	602.5	635	560	445	835	480
T 50 (s)	3.8	4.1	9.8	20.3	4.6	4.4		4.1	
V-funnel (s)	10.6	14.4	25.4	24.7	9.4	10.3	12.6	15.3	34.4
L-box-ratio (-)	0.93	0.90	0.80	0.64	0.67	0.59	0.00	0.78	0.39
Segr? / Sieve stab	No	No	No	No	No	No	No	No	No
Yield stress (Pa)	21.2	27.1	41.6	65.3	47.4	93.2	255.3	47.0	180.46
Viscosity at 0 sr (Pas)	2.29	8.34	13.9	16.8	23.5	34.0	4.2	16.4	44.6
c (Pa s²)	4.04	4.37	5.01	6.01	1.39	1.65	2.69	7.37	9.60

Mix number	SCC 41				SCC 42			SCC 43		
Date	5/08/2005				5/08/2005			12/08/2005		
Age (min)	15	30	60	90	15	30	60	15	30	90
Slump Flow (mm)	750	675	530	470	655	525		637.5	435	360
T 50 (s)	2.8	3.3	9.2		3.9	10.3		2.3		
V-funnel (s)	8.8	9.1	12.7	19.2	19.2	28.5		6.4	10.2	15.2
L-box-ratio (-)	0.99	0.79	0.65	0.30	0.64	0.50		0.41	0.15	0.00
Segr? / Sieve stab	No	No	No	No	No	No		No	No	No
Yield stress (Pa)	43.2	81.6	126.3	182.0	124.4	242.2	496.6	83.6	122.0	165.6
Viscosity at 0 sr (Pas)	31.9	60.5	51.7	61.5	0.95	2.16	19.8	33.7	35.2	39.9
c (Pa s²)	0.98	0.21	2.32	1.83	17.7	25.8	42.0	0.10	0.69	0.21

Mix number	SCC 45	SCC 36-3	SCC 46	SCC 47	SCC 48	SCC 48-2	SCC 48-3	SCC 48-4	SCC 50	SCC 51
Date	12/08/2005	2/09/2005	2/09/2005	2/09/2005	23/09/2005	23/09/2005	30/09/2005	30/09/2005	7/10/2005	7/10/2005
Sand 0/4	853	853	901	805	853	853	853	853	853	853
Gravel 2/8	263	263	278	248	263	263	263	263	263	263
Gravel 8/16	434	434	459	410	434	434	434	434	434	434
CEM I 52,5 N		360	300	400	360	360	360	360	360	360
CEM I 52.5 CE HSR LA	360									
Limestone filler 1	240	240	200	300	240	240	240	240	240	240
water	165	165	137.5	192.5	165	165	165	165	160	160
SP 1	2.6	3	3.32*	2.8*	3.4					
SP 2					9*	9*	10	10	13*	18*
Welan Gum		1 g								

Mix number	SCC 52
Date	14/10/2005
Sand 0/4	901
Gravel 2/8	278
Gravel 8/16	459
CEM I 52,5 N	300
Limestone filler 1	200
water	160
SP 2	7

Mix number	SCC 45				SCC 36-3			SCC 46		
Date	12/08/2005				2/09/2005			2/09/2005		
Age (min)	15	30	60	90	15	30	60	15	30	60
Slump Flow (mm)	755	560	555	520	640	510	465	805	582.5	410
T 50 (s)	1.9	6.5	6.2	10.2	1.5	8.5		2.9	13.2	
V-funnel (s)	14.7	15.8	21.1	25.8	16.2	15.3	32.3	16,4	25.8	74.7
L-box-ratio (-)	0.79	0.69	0.67	0.61	0.62	0.55	0.00	0.97	0.61	0.08
Segr? / Sieve stab	No	No	No	No	No	No	No	Slightly	No	No
Yield stress (Pa)	68.1	122.4	156.2	208.0	114.3	157.0	347.9	147.3	217.3	385.7
Viscosity at 0 sr (Pas)	22.3	25.0	48.7	41.9	56.9	53.4	79.3	69.7	102.4	111.4
c (Pa s²)	7.11	10.2	10.3	13.5	3.62	5.02	6.08	6.21	7.06	15.8

Mix number	SCC 47			SCC 48			SCC 48-2		
Date	9/09/2005			23/09/2005			23/09/2005		
Age (min)	15	30	60	20	40	60	15	30	60	90
Slump Flow (mm)	615	530	447.5	520	475	445	602.5	575	510	535
T 50 (s)		3.8		3.0			4.7	5.0	8.0	8.2
V-funnel (s)	6.5	8.8	14.6	9.8	9.9	10.9	10.5	10.5	14.7	15.3
L-box-ratio (-)	0.62	0.54	0.27	0.51	0.44	0.30	0.74	0.77	0.72	0.64
Segr? / Sieve stab	No	No	No	No	No	No	No	No	No	No
Yield stress (Pa)	34.1	78.9	152.6	93.7	118.3	139.3	62.6	69.3	80.2	123.0
Viscosity at 0 sr (Pas)	16.7	18.6	40.7	38.6	41.3	44.4	33.9	40.9	43.6	39.0
c (Pa s²)	0.71	0.99	1.02	0.15	0.58	0.79	1.78	2.06	2.62	5.05

Mix number	SCC 48-3				SCC 48-4				SCC 50			
Date	30/09/2005				30/09/2005				7/10/2005			
Age (min)	20	60	90	120	15	30	60	90	15	30	60	100
Slump Flow (mm)	600	617.5	627.5	580	630	647.5	645	640	655	627.5	652.5	617.5
T 50 (s)	3.2	2.8	2.4	4.2	2.6	3.5	4.0	5.2	3.6	5.1	6.5	5.9
V-funnel (s)	10.6	11.2	13.6	20.6	11.5	13.0	15.0	18.5	11.3	11.8	13.1	18.9
L-box-ratio (-)	0.77	0.70	0.74	0.67	0.78	0.82	0.84	0.75	0.88	0.89	0.81	0.85
Segr? / Sieve stab	No	No	No	No	No	No	No	No	No	No	No	No
Yield stress (Pa)		82.1	105.4	141.2	69.1	77.2	77.5	87.2	51.3	53.5	56.6	75.3
Viscosity at 0 sr (Pas)		43.0	46.2	48.3	33.6	39.5	43.6	45.9	38.0	40.4	41.7	45.0
c (Pa s²)		2.16	3.33	4.51	4.34	4.67	4.98	5.49	3.01	4.04	4.31	5.93

Mix number	SCC 51				SCC 52				
Date	7/10/2005				14/10/2005				
Age (min)	15	30	60	90	15	30	60	90	120
Slump Flow (mm)	660	625	665	665	665	595	590	592.5	545
T 50 (s)	3.7	6.2	3.5	5.5	2.3	3.7	3.4	4.6	7.9
V-funnel (s)	16.0	16.9	18.0	23.1	8.0	9.2	11.5	13.6	18.3
L-box-ratio (-)	0.85	0.86	0.84	0.77	0.86	0.81	0.77	0.72	0.63
Segr? / Sieve stab	No	No	No	No	No	No	No	No	No
Yield stress (Pa)	79.8	77.7	85.1	102.6	57.6	65.4	71.9	79.6	92.8
Viscosity at 0 sr (Pas)	24.1	28.5	24.6	36.3	40.7	43.9	50.2	51.3	59.3
c (Pa s²)	10.4	11.2	14.4	14.9	1.21	1.85	1.82	1.77	1.90

Mix number	SCC 53	SCC 54	SCC 55	SCC 56	SCC 48-5	SCC 57	SCC 59	SCC 58	TC 1
Date	14/10/2005	10/11/2005	10/11/2005	17/11/2005	9/12/2005	9/12/2005	20/12/2005	20/12/2005	17/11/2005
Sand 0/4	901	805	853	853	853	853	853	853	640
Gravel 2/8	278	248	263	263	263	263	263	263	462
Gravel 8/16	459	410	434	434	434	434	434	434	763
CEM I 52,5 N	300	400	400	300	360	360	360	360	360
Limestone filler 1	200	300	200	300	240	240			
Silica Fume								117	
Fly ash							178		
Water	133.33	186.5	165	165	165	165	165	165	165
SP 2	16.4*	7.67*	13.5*	9*	13*				
SP 3						7.5	6*	10*	

Mix number	SCC 53				SCC 54			
Date	14/10/2005				10/11/2005			
Age (min)	20	30	60	90	15	30	60	90
Slump Flow (mm)	745	715	700	667.5	645	572.5	585	545
T 50 (s)	2.9	4.0	7.9	10.3	1.8	2.5	3.5	4.3
V-funnel (s)	11.9	14.7	23.7	31.9	7.2	9.3	14.9	16.0
L-box-ratio (-)	0.95	0.95	0.87	0.86	0.75	0.75	0.70	0.61
Segr? / Sieve stab	No	No	No	No	No	No	No	No
Yield stress (Pa)	117.2	126.8	154.6	145.8	42.9	47.5	58.8	88.1
Viscosity at 0 sr (Pas)	59.1	70.2	78.1	72.6	24.7	24.4	34.6	37.4
c (Pa s²)	3.38	3.77	4.88	6.49	2.19	2.81	3.01	4.94

Mix number	SCC 55					SCC 56					
Date	10/11/2005					17/11/2005					
Age (min)	15	30	60	90	120	15	30	60	90	120	150
Slump Flow (mm)	665	670	650	625	632.5	747.5	810	730	692.5	685	690
T 50 (s)	1.8	2.4	2.9	5.5	3.7	2.1		2.8	4.2	4.8	2.5
V-funnel (s)	10.5	10.5	11.8	15.7	22.6	8.8	10.0	12.5	13.7	18.3	22.6
L-box-ratio (-)	0.91	0.87	0.85	0.90	0.85	0.98	0.99	0.97	0.97	0.92	0.85
Segr? / Sieve stab	No	No	No	No	No	No	No	No	No	No	No
Yield stress (Pa)	78.3	39.3	44.6	53.5	64.7	28.3	29.7	31.8	35.8	48.9	56.8
Viscosity at 0 sr (Pas)	16.0	28.5	34.3	29.8	38.6	14.9	21.7	24.3	22.6	32.9	39.5
c (Pa s²)	2.51	2.32	2.59	4.19	4.59	3.06	2.92	3.39	4.40	5.12	6.54

Mix number	SCC 48-5					SCC 57				
Date	9/12/2005					9/12/2005				
Age (min)	15	30	60	90	120	15	30	60	90	
Slump Flow (mm)	627.5	602.5	610	595	572.5	667.5	665	682.5	595	
T 50 (s)	2.6	3.0	3.6	5.7	4.9	3.1	3.1	3.7	7.4	
V-funnel (s)		10.8	12.9	11.7	17.7	8.2	12.9	15.9	16.4	
L-box-ratio (-)		0.72	0.81	0.78	0.80	0.84	0.90	0.84	0.92	
Segr? / Sieve stab	No	No	No	No	No	No	No	No	No	
Yield stress (Pa)		60.7	65.0	72.1	94.5	61.0	73.2	85.1	101.7	
Viscosity at 0 sr (Pas)		36.1	39.1	39.0	47.8	19.6	32.7	43.0	42.4	
c (Pa s²)		1.29	1.60	1.96	2.38	5.44	4.98	4.89	5.59	

Mix number	SCC 59				SCC 58			TC 1		
Date	20/12/2005				20/12/2005			17/11/2005		
Age (min)	15	30	60	90	15	30	60	15	30	60
Slump Flow (mm)	650	595	565	600	547.5	520	480			
T 50 (s)	2.3	3.1	5.0	3.6						
V-funnel (s)	8.3	7.4	8.0	10.2	3.8	4.8	4.9			
L-box-ratio (-)	0.77	0.77	0.73	0.68	0.62	0.54	0.45			
Segr? / Sieve stab	No	No	No	No	No	No	No			
Yield stress (Pa)	76.0	103.7	131.0	153.4	60.9	69.8	81.0	890.3	921.1	884.5
Viscosity at 0 sr (Pas)	40.3	51.4	60.7	68.4	11.8	13.2	15.3	26.3	18.5	19.4
c (Pa s²)	0.75	0.91	1.00	0.96	-0.08	-0.02	-0.05			

Mix number	TC 2	TC 3	SCC 60	SCC 61	SCC 62	SCC 63	SCC 60-2	SCC 60-3	SCC 60-4	SCC 61-2
Date	2/12/2005	2/12/2005	30/03/2006	30/03/2006	31/03/2006	31/03/2006	26/04/2006	26/04/2006	26/04/2006	28/04/2006
Sand 0/4	640	640	853	853	853	853	853	853	853	853
Gravel 2/8	462	462	263	263	263	263	263	263	263	263
Gravel 8/16	763	763	434	434	434	434	434	434	434	434
CEM I 52,5 N	360	360	360	360	360	360	360	360	360	360
Limestone filler 1			240				240	240	240	
Limestone filler 2				239						239
Silica Fume						150				
Fly ash					183					
Water	198	216	165	165	165	165	165	165	165	165
SP 2			14.55*	11.82*	13.64*	30.91*	14.55*	17.27*	20*	16.36*

Mix number	SCC 61-3	SCC 61-4	SCC 62-2	SCC 62-3	SCC 62-4	SCC 67
Date	28/04/2006	28/04/2006	5/05/2006	5/05/2006	5/05/2006	10/08/2007
Sand 0/4	853	853	853	853	853	853
Gravel 2/8	263	263	263	263	263	263
Gravel 8/16	434	434	434	434	434	434
CEM I 52,5 N	360	360	360	360	360	360
Limestone filler 2	239	239				
Fly ash			183	183	183	
Kaolinite Clay						218
Water	165	165	165	165	165	165
SP 2	13.64*	5.45*	12.73*	15.45*	9.09*	90.9*

Mix number	TC 2			TC 3			SCC 60				
Date	2/12/2005			2/12/2005			30/03/2006				
Age (min)	15	30	60	15	30	60	15	30	60	90	120
Slump Flow (mm)							640	662.5	642.5	620	635
T 50 (s)											
V-funnel (s)							11.2	13.5	13.1	17.6	18.5
L-box-ratio (-)							0.81	0.78	0.78	0.79	
Segr? / Sieve stab							8.88%	No	No	No	No
Yield stress (Pa)	111.9	135.7	173.0	50.1	62.0	68.6	70.5	60.2	56.6	72.0	85.7
Viscosity at 0 sr (Pas)	16.3	17.0	15.5	10.4	10.3	11.7	26.6	32.2	45.6	39.8	40.5
c (Pa s²)							2.43	2.81	2.23	3.03	3.73

Mix number	SCC 61				SCC 62				SCC 63			
Date	30/03/2006				31/03/2006				31/03/2006			
Age (min)	15	30	60	90	15	30	60	90	15	30	60	90
Slump Flow (mm)	612.5	615	595	670	715	692.5	732.5	737.5	622.5	605	595	585
T 50 (s)												
V-funnel (s)	9.3	9.0	13.3	16.0	6.4	7.0	9.1	10.0	4.0	5.3	7.2	8.0
L-box-ratio (-)	0.75	0.73	0.80	0.78	0.85	0.89	0.93	0.94	0.71	0.80	0.71	0.76
Segr? / Sieve stab	5.37%	No	No	No	9.20%	No	No	No	9.31%	No	No	No
Yield stress (Pa)	41.6		43.9	51.5	47.2	48.7	49.0	54.1	36.8	31.7	38.9	38.1
Viscosity at 0 sr (Pas)	27.3		27.9	29.1	32.7	34.8	38.8	38.6	9.16	10.0	10.7	11.5
c (Pa s²)	0.86		1.53	1.99	1.31	1.55	1.37	1.72	-0.05	0.07	0.14	0.20

Mix number	SCC 60-2		SCC 60-3		SCC 60-4		SCC 61-2		SCC 61-3		SCC 61-4	
Date	26/04/2006		26/04/2006		26/04/2006		28/04/2006		28/04/2006		28/04/2006	
Age (min)	15	30	15	30	15	30	15	30	15	30	15	30
Slump Flow (mm)	610	655	730	730	895	842.5	797.5	802.5	710	685	300	265
T 50 (s)												slump = 17
V-funnel (s)	10.8	12.9	9.6	11.9	10.1	11.4	6.1	8.1	6.8	7.8	27.4	
L-box-ratio (-)	0.79	0.85	0.93	0.91	0.94	1.01	1.00	0.97	0.87	0.95		
Segr? / Sieve stab	8.82%	No	10.12%	No	17.18%	No	22.73%	Slightly	12.45%	No	0.00%	No
Yield stress (Pa)	40.9	41.6	23.0	21.4	1.69	0.49	18.5	18.4	25.1	25.2	501.9	
Viscosity at 0 sr (Pas)	29.5	34.1	10.8	9.99	0.30	1.97	0.49	0.26	11.5	11.7	89.2	
c (Pa s²)	2.28	2.31	2.28	2.39	1.96	1.89	1.28	1.34	1.22	1.55	-0.08	

Mix number	SCC 62-2		SCC 62-3		SCC 62-4		SCC 67				
Date	5/05/2006		6/05/2006		7/05/2006		10/08/2007				
Age (min)	15	30	15	30	15	30	15	30	60	90	120
Slump Flow (mm)	617.5	635	765	737.5	460	480	685	622.25	605	565	515
T 50 (s)											
V-funnel (s)	6.9	7.1	7.1	8.0	8.4	10.3	6.1	8.0	9.6	11.5	13.1
L-box-ratio (-)	0.85	0.80	1.00	0.98			0.73	0.71	0.53	0.54	0.61
Segr? / Sieve stab	6.94%	No	15.39%	No	No	No	No	No	No	No	No
Yield stress (Pa)	46.5	48.2	26.8	24.4	170.0	162.5	22.8	22.6	23.0	23.2	22.8
Viscosity at 0 sr (Pas)	36.5	35.3	18.3	18.2	63.6	65.4	5.06	6.75	8.66	5.38	7.04
c (Pa s²)	1.14	1.56	1.47	1.61	0.92	0.93	0.47	0.51	0.36	0.66	0.49

3 Tests performed at BBRI with ConTec viscometer 5

The following tables will give the values for the standard tests on SCC and the rheometer values for the concretes tested. The rheological values have been obtained after transformation by means of the Reiner-Riwlin equations for Herschel-Bulkley materials. For the last test series, performed on 29/04/2005, no raw data were available.

Mix number	SCC 1-2	SCC 2-2	SCC 3-2	SCC 4-2	SCC 5	SCC 6	SCC 7	SCC 8	SCC 9	SCC 10
Date	18/02/2005	18/02/2005	18/02/2005	18/02/2005	18/02/2005	18/02/2005	25/02/2005	25/02/2005	25/02/2005	25/02/2005
sand 0/5	853	853	853	853	853	853	853	853	853	853
gravel 2/8		263				263		263		263
gravel 8/16	698	453			698	453	698	453	698	453
crushed aggr 2/7				206						
crushed aggr 7/10			349	206						
crushed aggr 10/14			349	206						
CEM I 52,5 N	360	360	360	360	300	300	400	400	450	450
Limestone filler 1	240	240	240	240	300	300	200	200	150	150
water	166.6	166.6	166.6	166.6	166.6	166.6	166.6	166.6	166.6	166.6
SP 1	2.75	2.83	3.83*	3.83	2.75	2.83	2.75	2.83	2.92	3.58*

Mix number	SCC 1-3	SCC 15	SCC 16	SCC 17	SCC 1-4	SCC 11	SCC 13	SCC 14	SCC 18
Date	25/02/2005	25/02/2005	25/02/2005	25/02/2005	22/03/2005	22/03/2005	22/03/2005	22/03/2005	22/03/2005
sand 0/4					853	853	923	782	853
sand 0/5	853	853	853	853					
gravel 8/16	698	698	698	698	698	698	755	640	698
CEM I 52,5 N	360	360	360	360	360		300	400	360
CEM I 52,5						360			
Limestone filler 1	240	240	240	240	240	240	200	300	240
water	166.6	156.6	171.6	176.6	166.6	166.6	166.6	166.6	166.6
SP 1	2.75	2.75	2.75	2.75	2.83	3	3.33	4.67*	3.17
Welan Gum (total added)							3,6 g*		2,4 g

Mix number	SCC 1-2	SCC 2-2		SCC 3-2	SCC 4-2		SCC 5		SCC 6		SCC 7	
Date	18/02/05	18/02/2005		18/02/05	18/02/2005		18/02/2005		18/02/2005		25/02/2005	
Age (min)	15	15	30	15	15	30	15	30	15	30	15	30
Slump Flow (mm)	680	780	687.5	595	905	840	760	770	907.5	752.5	515	510
T 50 (s)											3.17	4.39
V-funnel (s)	9.25	8.8	10.23	12.17	9.74	22.34	7.8	10.22	6.98	9.51	13.85	14.9
L-box-ratio (-)	0.74	0.84	0.71	0.40	1.00	0.97	0.89	0.84	1.00	0.94	0.35	0.34
Segr? / Sieve stab	No	No	No	No	Slighlty	Slightly	No	No	Slighlty	No	No	No
Yield stress (Pa)	22.0	19.9	18.7			7.9	16.2	18.8	10.1	9.3	45.8	85.9
K (Pa s^n)	14.6	11.4	16.3			8.7	10.4	14.4	5.9	9.5	33.9	50.0
n (-)	1.35	1.44	1.31			1.46	1.44	1.36	1.52	1.38	1.15	1.07

Mix number	SCC 8		SCC 9		SCC 10		SCC 1-3		SCC 15	SCC 16	
Date	25/02/2005		25/02/2005		25/02/2005		25/02/2005		25/02/05	25/02/2005	
Age (min)	15	30	15	30	15	30	15	30	45	15	15	30
Slump Flow (mm)	545	482.5	480	410	670	575	630	555		-	520	467.5
T 50 (s)	3.4	-	-	-	2.31	3.46	2.42	2.1		-	2.74	-
V-funnel (s)	12.9	16.06	14.44	17.38	10.45	13.51	11.73	15.73		-	10.78	12.94
L-box-ratio (-)	0.48	0.34	0.10	0.02	0.77	0.65	-	0.55		-	0.38	0.27
Segr? / Sieve stab	No	No	No	No	No	No	No	No		No	No	No
Yield stress (Pa)	51.1	91.0	61.5	123.6	21.4	28.1			50.0	330.9	52.8	97.7
K (Pa s^n)	39.4	59.4	69.0	100.2	20.7	28.9			25.8	25.8	22.1	35.7
n (-)	1.16	1.08	0.95	0.86	1.30	1.21			1.24	1.24	1.21	1.10

Mix number	SCC 17		SCC 1-4		SCC 11		SCC 13		SCC 14		SCC 18	
Date	25/02/2005		22/03/2005		22/03/2005		22/03/2005		22/03/2005		22/03/2005	
Age (min)	15	30	15	30	15	30	15	30	15	30	15	30
Slump Flow (mm)	880	780	590	515.6	680	605	915	890	810	725	662.5	590
T 50 (s)	0.73	1.77	3.78	4.36	1.82	4.01	0	1.44	1.9	3.23	2.85	5.21
V-funnel (s)	4.76	7.8	14.1	15.24	10.35	13.01	6.59	7.56	11.04	15	12.98	22.31
L-box-ratio (-)	0.94	0.71	0.64	0.61	0.79	0.70	0.94	0.94	0.94	0.94	0.75	
Segr? / Sieve stab	No	No	No	No	No	No	Yes	Yes	No	No	No	No
Yield stress (Pa)		8.5		53.8	25.7	31.4	7.0	4.6	14.5	13.2	21.2	32.7
K (Pa s^n)		5.1		29.6	9.4	12.1	10.6	11.0	3.4	6.6	18.8	21.9
n (-)		1.39		1.21	1.42	1.40	1.25	1.16	1.81	1.68	1.37	1.31

Mix number	SCC 19	SCC 20	SCC 12	SCC 19-2	SCC 21	SCC 22	SCC 23	SCC 24	SCC 25	SCC 26
Date	22/03/2005	22/03/2005	25/03/2005	25/03/2005	25/03/2005	25/03/2005	25/03/2005	25/03/2005	25/03/2005	25/03/2005
sand 0/4	853	853	853	853	853	853	853	853	853	853
gravel 2/8		263								
gravel 8/16	698	453	698	698			698	698	698	698
crushed aggr 2/7						268				
crushed aggr 7/14					698	411				
CEM I 52,5 N	360	360		360	360	360	300	400	450	360
CEM III A 42,5 LA			360							
Limestone filler 1	240	240	240	240	240	240	300	200	150	240
water	176.6	176.6	166.6	176.6	176.6	176.6	176.6	176.6	176.6	166.6
SP 1			3							
SP 2	10.83*	11.67*		10.83	11.67*	12.5*	11.67	15*	20.42*	17.5*
Welan Gum (total added)		3,6 g	4 g				2,4 g			

Mix number	SCC 26-2	SCC 30	SCC 31	SCC 32	SCC 33
Date	29/04/2005	29/04/2005	29/04/2005	29/04/2005	29/04/2005
sand 0/4	853	853	853	853	853
gravel 2/8				263	
gravel 8/16	698	698	698	453	698
CEM I 52,5 N	360		360	360	360
CEM III A 42,5 LA		360			
Limestone filler 1	240	240			
Quartzite filler			240	240	240
water	166.6	166.6	166.6	176.6	171.6
SP 1			3.92*	2.83*	3.17
SP 2	15	15*			
Welan Gum (total added)		2,4 g			

Mix number	SCC 19		SCC 20		SCC 12		SCC 19-2		SCC 21		SCC 22	
Date	22/03/2005		22/03/2005		25/03/2005		25/03/2005		25/03/2005		25/03/2005	
Age (min)	15	30	15	30	15	30	15	30	15	30	15	30
Slump Flow (mm)	595	620	630	670	852.5	815	667.5	622	600	570	650	610
T 50 (s)	1.82	1.16	1.43	1.92	1.68	2.56	1.02	1.84	1.59	4.02	1.9	2.07
V-funnel (s)	5.97	6.58	6.19	7.2	7.34	10.89	5.88	7.36	7.32	9.24	6.3	7.77
L-box-ratio (-)	0.66	0.76	0.71	0.73	0.99	0.93	0.64	0.70	0.60	0.64	0.70	0.73
Segr? / Sieve stab	No	No	No	No	No	No	No	No	No	No	No	No
Yield stress (Pa)	26.4	24.4	27.5	25.6	13.1	15.7		28.5	35.5	25.9	24.8	21.5
K (Pa s^n)	17.9	19.9	14.0	12.0	9.5	10.0		16.0	17.9	20.9	15.4	14.4
n (-)	1.05	1.00	1.17	1.22	1.44	1.45		1.20	1.19	1.14	1.18	1.19
Mix number	SCC 23		SCC 24		SCC 25		SCC 26		SCC 26-2		SCC 30	SCC 31
Date	25/03/2005		25/03/2005		25/03/2005		25/03/2005		29/04/2005		29/04/05	29/04/05
Age (min)	15	30	15	30	15	30	15	30	15	30	15	15
Slump Flow (mm)	755	735	600	595	610	561	655	675	680	645	905	769.5
T 50 (s)	1.53	2.29	1.27	1.81	1.69	2.99	1.88	3.87	0.83	1.97		3.09
V-funnel (s)	5.69	6.37	5.87	7.42	6.59	6.86	6.41	7.53	7.36	9.61	7.53	14.33
L-box-ratio (-)	0.92	0.98	0.63	0.64	0.65	0.72	0.80	0.89	0.76	0.74	0.95	0.75
Segr? / Sieve stab	Yes	Yes	No	No	No	No	No	No	No	No	No	No
Yield stress (Pa)	14.3	11.1	24.9	25.0	33.1	33.3	22.3	16.2				
K (Pa s^n)	10.2	8.7	15.2	12.4	16.4	13.3	13.9	14.2				
n (-)	1.31	1.33	1.08	1.16	1.03	1.12	1.28	1.26				

Mix number	SCC 32		SCC 33	
Date	29/04/2005		29/04/2005	
Age (min)	15	30	15	30
Slump Flow (mm)	650	510	710	632.5
T 50 (s)	2.83	8.1	2.69	1.9
V-funnel (s)	11.41	12.82	13.09	14.54
L-box-ratio (-)	0.49	0.45	0.75	0.65
Segr? / Sieve stab	No	No	No	No

4 Comparative tests between Tattersall Mk-II and ConTec Viscometer 5, executed at KULeuven

Mix number	SCC 1	SCC 2	SCC 3	SCC 4
Date	5/02/2007	5/02/2007	6/02/2007	6/02/2007
sand 0/5	853	853	805	805
gravel 2/16	697	697	658	658
CEM I 52,5 N	360		400	
CEM I 52.5 R HES		360		400
Limestone filler 1	240		300	
Limestone filler 2		240		300
water	165	165	165	165

Mix number	SCC 1					SCC 2		
Date	5/02/2007					5/02/2007		
SP 1 (kg/m³)								
SP 2 (kg/m³)	14	17	19	21	23	12	14	14
Slump Flow (mm)	387.5	572.5	622.5	705	750	650	905	830
Tattersall Mk-II								
Yield stress (Pa)	245.8	106.9	67.5	56.3	47.7	36.1	21.9	42.6
K (Pa s^n)	64.8	42.4	30.6	27.8	24.4	10.0	3.7	16.1
n (-)	1.11	1.15	1.21	1.24	1.24	1.67	1.88	1.54
ConTec Viscometer 5								
Yield stress (Pa)	172.5	84.9	41.1	43.0	36.1	35.4	21.0	22.1
K (Pa s^n)	81.5	37.4	34.4	26.0	28.0	16.2	16.2	14.2
n (-)	1.03	1.21	1.16	1.24	1.22	1.47	1.45	1.50
Mix number	SCC 3					SCC 4		
Date	6/02/2007					6/02/2007		
SP 1 (kg/m³)						4	5	
SP 2 (kg/m³)	22	26	29	32	37			
Slump Flow (mm)	375	540	625	670	772.5	652.5	915	
Tattersall Mk-II								
Yield stress (Pa)	296.1	156.7	96.7	65.3	37.7	217.0	35.4	43.0
K (Pa s^n)	47.8	53.3	42.3	29.7	17.0	36.1	12.8	15.2
n (-)	1.28	1.20	1.21	1.27	1.34	1.81	1.84	1.77
ConTec Viscometer 5								
Yield stress (Pa)	210.4	96.2	69.9	41.1	24.8		55.2	59.3
K (Pa s^n)	73.6	45.4	31.6	44.6	31.5		18.6	27.0
n (-)	1.20	1.27	1.32	1.15	1.18		1.77	1.58

5 Tests in order to investigate the influence of coarse aggregates, performed with ConTec viscometer 5 at KULeuven

Mix number	SCC 1	SCC 2	SCC 3
Date	7/04/2008	7/04/2008	7/04/2008
sand 0/5	853	853	805
CEM I 52,5 N	360	360	400
Limestone filler 1	240	240	300
water	165	165	165
SP 1	3.6	3.4	4.9

Mix number	SCC 1				SCC 2				SCC 3			
Date	7/04/2008				7/04/2008				7/04/2008			
z max (mm)	2	8	12	16	2	8	12	16	2	8	12	16
Gravel 2/8 (kg/m³)		263	263	263		263	263	263		248	248	248
Gravel 8/12 (kg/m³)			290.4	290.4			288.4	288.4			277.1	277.1
Gravel 12/16 (kg/m³)				163.4				165.6				131.2
Slump flow (mm)				870				780				680
V-funnel (s)				9.1				11.7				23.1
Sieve stability (%)				11.0				10.0				3.0
Density (kg/m³)				2378				2381				2341
Air content (%)				0.8				1.4				2.8
ConTec Viscometer 5												
Yield stress (Pa)	4.3	7.0	10.8	13.5	8.8	10.4	17.5	18.3	22.1	28.9	46.3	72.2
K (Pa s^n)	2.6	4.7	13.4	18.9	3.8	6.2	14.3	24.4	3.3	5.4	19.6	39.8
n (-)	1.45	1.46	1.35	1.30	1.41	1.41	1.36	1.25	1.99	1.96	1.69	1.48

6 Tests in order to investigate the influence of demoulding oil, performed with the Tattersall Mk-II at the Magnel Laboratory

Mix number	SCC 48-6	SCC 48-6a	SCC 48-7	SCC 42-2	SCC 48-8	SCC 48-8a
Date	26/04/2007	26/04/2007	25/05/2007	25/05/2007	22/06/2007	22/06/2007
Sand 0/4	853	853	853	805	853	853
Gravel 2/8	263	263	263	248	263	263
Gravel 8/16	434	434	434	410	434	434
CEM I 52,5 N	360	360	360	400	360	360
Limestone filler 1	240	240	240	300	240	240
water	165	165	165	165	165	165
SP 1				5.82		
SP 2	25.45	25.45	26.36		25.45	25.45

Mix number	SCC 48-6		SCC 48-6a		SCC 48-7		SCC 42-2		SCC 48-8		SCC 48-8a	
Date	26/04/2007		26/04/2007		25/05/2007		25/05/2007		22/06/2007		22/06/2007	
Amount of oil (‰)	0	15	7.5	22.5		2.5		2.5		1	0.25	0.5
Slump flow (mm)	655		645		705		765		715		710	
V-funnel (s)	7.83	7.16	6.4	8.88	6.55	6.54	15.64	11.33	7.63	6.2	6.77	5.82
Sieve stability (%)	12.44%	5.40%	10.59%	3.49%	-	-	-	-	-	-	-	-
Yield stress (Pa)	28.3	96.5	50.1	257.6	21.1	27.3	31.7	174.1	22.5	24.1	21.1	21.5
Visco at 0 sr (Pa s)	20.8	51.4	30.9	84.3	7.6	18.2	19.3	90.1	14.7	15.8	8.9	8.2
c (Pa s^2)	0.53	-0.19	-0.05	-1.13	1.00	0.35	6.46	-0.09	1.13	0.63	1.03	0.98

7 Tests on cement pastes

This part of the appendix contains the compositions of the tests executed on traditional and self-compacting cement pastes. The tests have been performed in a parallel rotating plates rheometer. No other workability tests have been executed on the cement pastes. The measurements on the first traditional cement paste failed due to excessive slippage in the rheometer.

Mix number	TCP 1	SCCP 1	SCCP 2	SCCP 3	SCCP 4	TCP 2
CEM I 52,5 N	973	973	973	985	973	1216
Limestone filler 1				739		
Limestone filler 2	646	646	646		646	
Water	446	446	446	406	446	608
SP 1		10.8	10	13.3	9	

APPENDIX C:

GRAVITATIONAL FLOW TESTS

1 Introduction

This appendix contains the concrete compositions and the results of the slump flow tests, density measurements and sieve stability experiments. Also, for each concrete age, the rheometer results and the (total) pressure loss – discharge curves are given. Remind that the nomenclature of the concrete mixes is as follows: "flow x m – y – zz min", where x indicates the length of the pipe, y gives the number of the mix tested at this length and zz stands for the age of the concrete, referred to the water addition of the second (or only) batch. For each concrete mix, the corresponding number as given in Appendix B is mentioned.

2 Concrete compositions

Test	flow 3m - 1	flow 3m - 2	flow 3m - 3	flow 3m - 4	flow 3m - 5	flow 3m - 6	flow 6m - 1	flow 6m - 2	flow 6m - 3	flow 6m - 4
Amount	**200 l**	**200 l**	**200 l**	**200 l**	**200 l**	**200 l**	**2 x 125 l**	**2 x 125 l**	**2 x 125 l**	**2 x 125 l**
SCC number	**48**	**48-2**	**48-3**	**61**	**63**	**64**	**48**	**42**	**42-2**	**36**
Date	**4/09/2006**	**4/09/2006**	**10/10/2006**	**10/10/2006**	**20/10/2006**	**20/10/2006**	**17/11/2006**	**17/11/2006**	**24/11/2006**	**24/11/2006**
sand 0/4	853	853	853	853	853	853	853	805	805	853
gravel 2/8	263	263	263	263	263	263	263	248	248	263
gravel 8/16	434	434	434	434	434	434	434	410	410	434
CEM I 52,5 N	360	360	360	360	360	360	360	400	400	360
limestone filler 1	240	240	240			150	240	300	300	240
limestone filler 2				239						
silica fume					150					
water	165	165	165	165	165	180	165	165	165	165
SP 1 (batch 1)						?		1	0.7	0.36
SP 1 (batch 2)								0.8	0.65	0.4
SP 2 (batch 1)	3.25	3.5	3.5	3	6.75		2.75			
SP 2 (batch 2)							2.75			

Test	flow 6m - 5	flow 9m - 1	flow 9m - 2	flow 12m - 1	flow 12m - 2
Amount	**2 x 125 l**	**2 x 125 l**	**2 x 125 l**	**2 x 137.5 l**	**2 x 137.5 l**
SCC number	**52**	**48**	**52**	**48**	**52**
Date	**8/12/2006**	**15/12/2006**	**15/12/2006**	**12/01/2007**	**12/01/2007**
sand 0/4	901	853	901	853	901
gravel 2/8	278	263	278	263	278
gravel 8/16	459	434	459	434	459
CEM I 52,5 N	300	360	300	360	300
limestone filler 1	200	240	200	240	200
water	165	165	165	165	165
SP 1 (batch 1)					
SP 1 (batch 2)					
SP 2 (batch 1)	1.5	3	1.6	3.3	1.76
SP 2 (batch 2)	1.5	2.75	1.6	3.025	1.76

3 Fresh concrete test results

Test	flow 3m - 1	flow 3m - 2	flow 3m - 3	flow 3m - 4	flow 3m - 5	flow 3m - 6	flow 6m - 1	flow 6m - 2	flow 6m - 3	flow 6m - 4
Amount	200 l	200 l	200 l	200 l	200 l	200 l	2 x 125 l	2 x 125 l	2 x 125 l	2 x 125 l
SCC number	48	48-2	48-3	61	63	64	48	42	42-2	36
Date	4/09/2006	4/09/2006	10/10/2006	10/10/2006	20/10/2006	20/10/2006	17/11/2006	17/11/2006	24/11/2006	24/11/2006
slump flow (batch 1) (mm)	602.5	632.5	755	622.5	595	792.5	640	-	942	587.5
slump flow (batch 2) (mm)	-	-	-	-	-	-	725	-	872.5	775
density (kg/m³)	2362.5	2368.75	2358.75	2381.25	2275	2356.25	2368.75	-	2393.75	2381.25
sieve stability (%)	8.8	9.1	15.3	10.3	9.7	11.2	16.3	-	53.9	16.2

Test	flow 6m - 5	flow 9m - 1	flow 9m - 2	flow 12m - 1	flow 12m - 2
Amount	2 x 125 l	2 x 125 l	2 x 125 l	2 x 137.5 l	2 x 137.5 l
SCC number	52	48	52	48	52
Date	8/12/2006	15/12/2006	15/12/2006	12/01/2007	12/01/2007
slump flow (batch 1) (mm)	600	705	675	692.5	680
slump flow (batch 2) (mm)	660	670	655	645	695
density (kg/m³)	2368.75	2368.75	2375	2375	2365.625
sieve stability (%)	4.2	16.2	8.8	15.6	5.7

4 Rheometer results

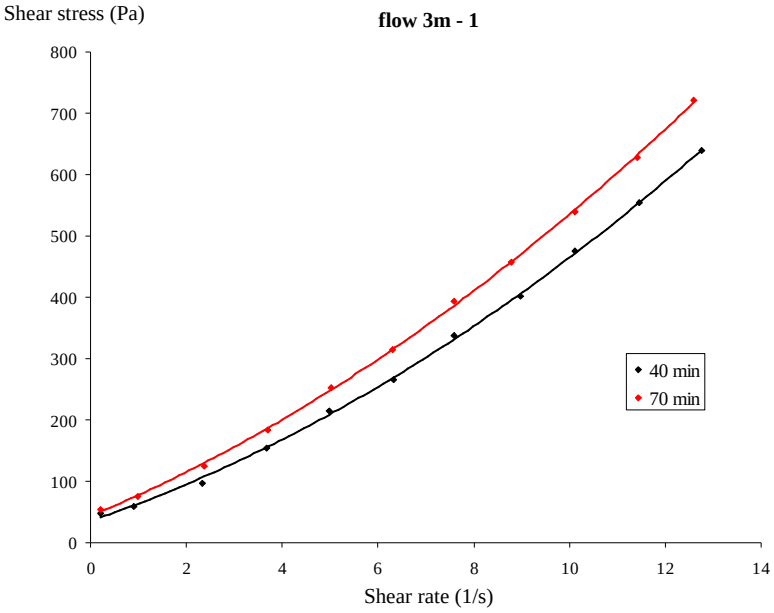

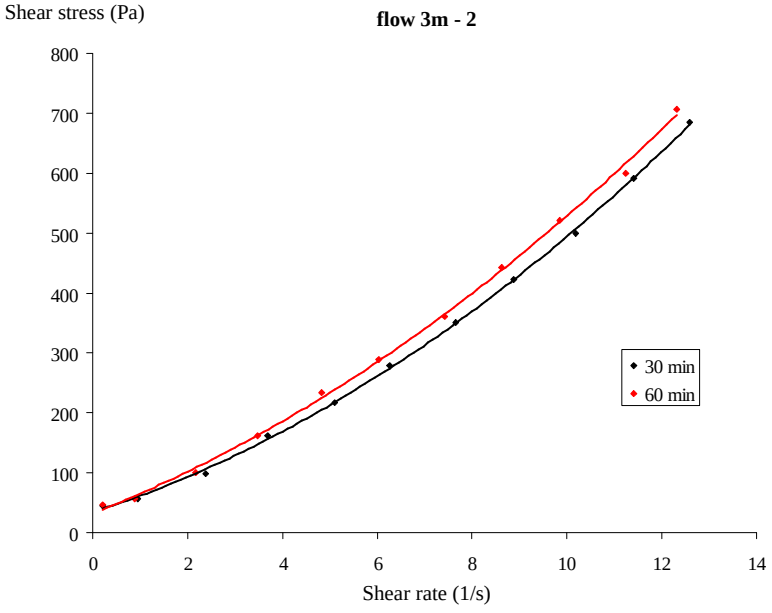

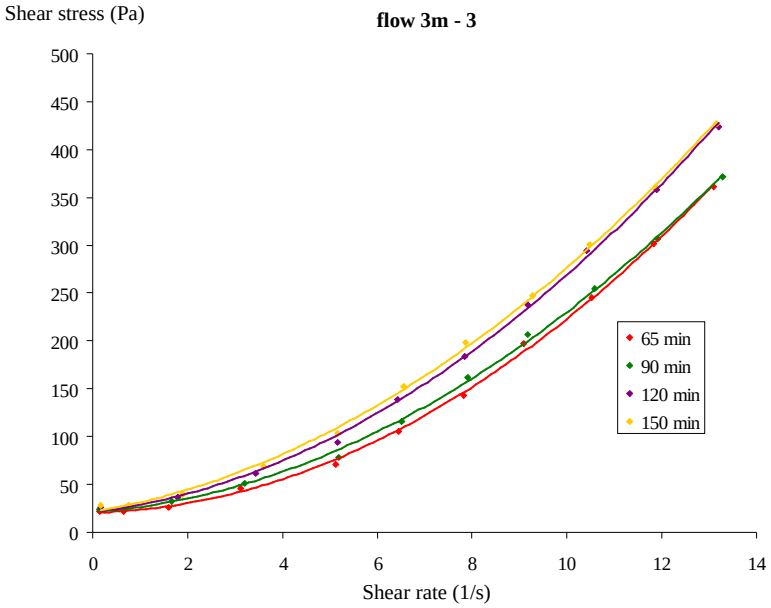
Shear stress (Pa)
flow 3m - 3
500
450
400
350
300
250
200
150
100
50
0
0
2
4
6
8
10
12
14
Shear rate (1/s)
65 min
90 min
120 min
150 min

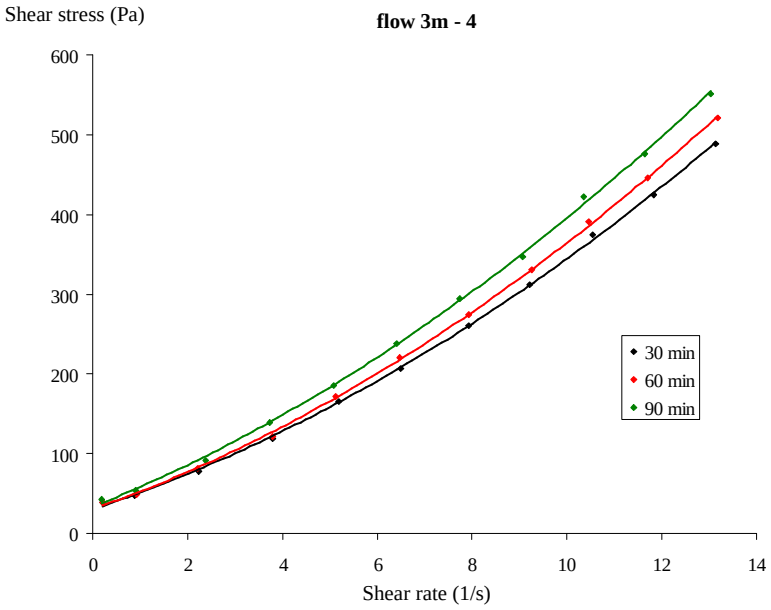
Shear stress (Pa)
flow 3m - 4
600
500
400
300
200
100
0
0
2
4
6
8
10
12
14
Shear rate (1/s)
30 min
60 min
90 min

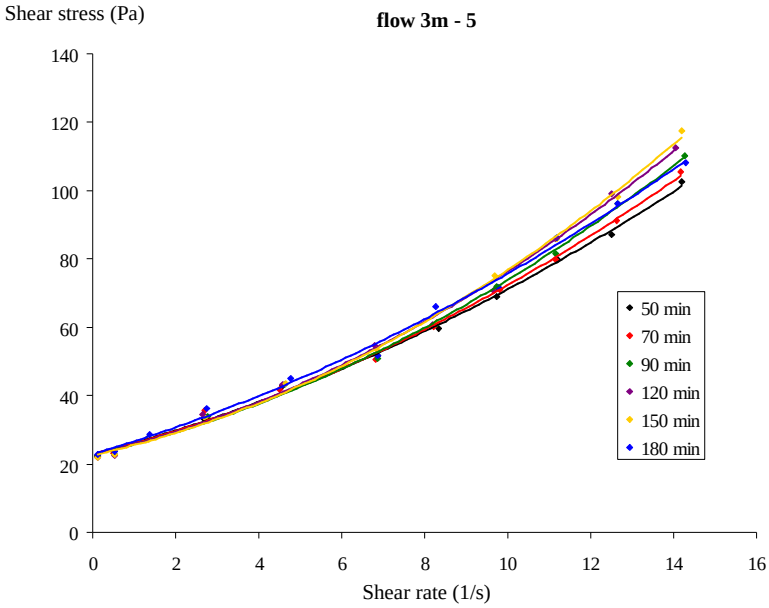
Shear stress (Pa)
flow 3m - 5
140
120
100
80
60
40
20
0
0
2
4
6
8
10
12
14
16
Shear rate (1/s)
50 min
70 min
90 min
120 min
150 min
180 min

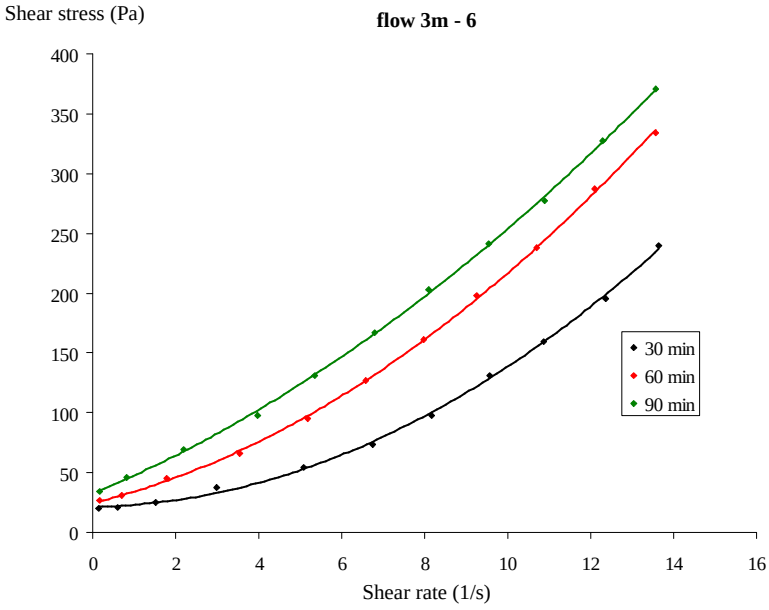
Shear stress (Pa)
flow 3m - 6
400
350
300
250
200
150
100
50
0
0
2
4
6
8
10
12
14
16
Shear rate (1/s)
30 min
60 min
90 min

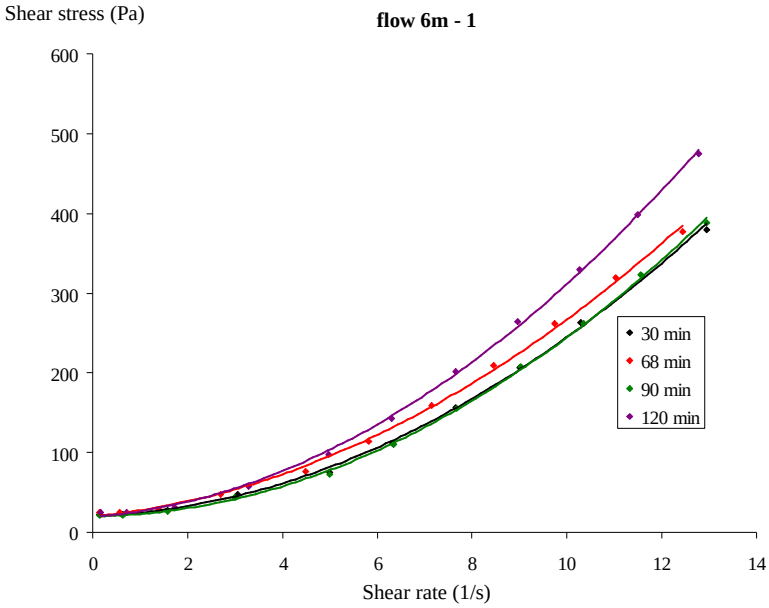
Shear stress (Pa)
flow 6m - 1
600
500
400
300
200
100
0
0
2
4
6
8
10
12
14
Shear rate (1/s)
30 min
68 min
90 min
120 min

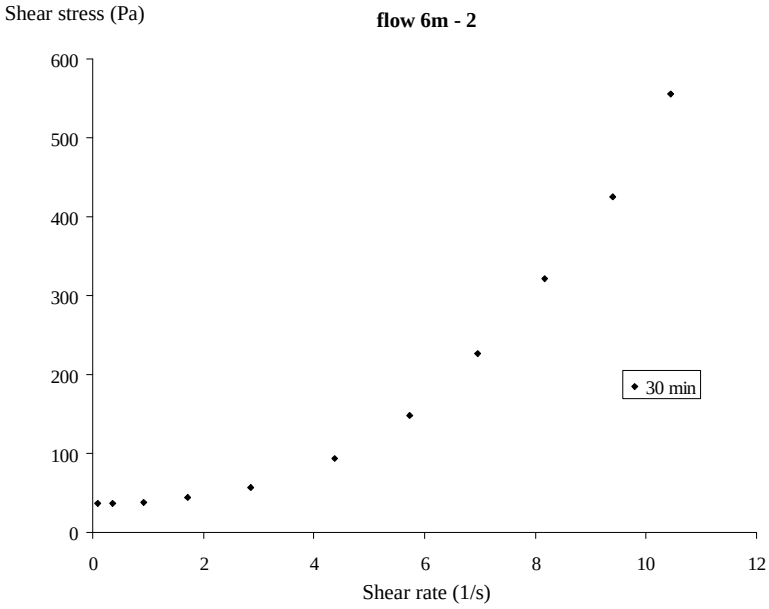
Shear stress (Pa)
flow 6m - 2
600
500
400
300
200
100
0
0
2
4
6
8
10
12
Shear rate (1/s)
30 min

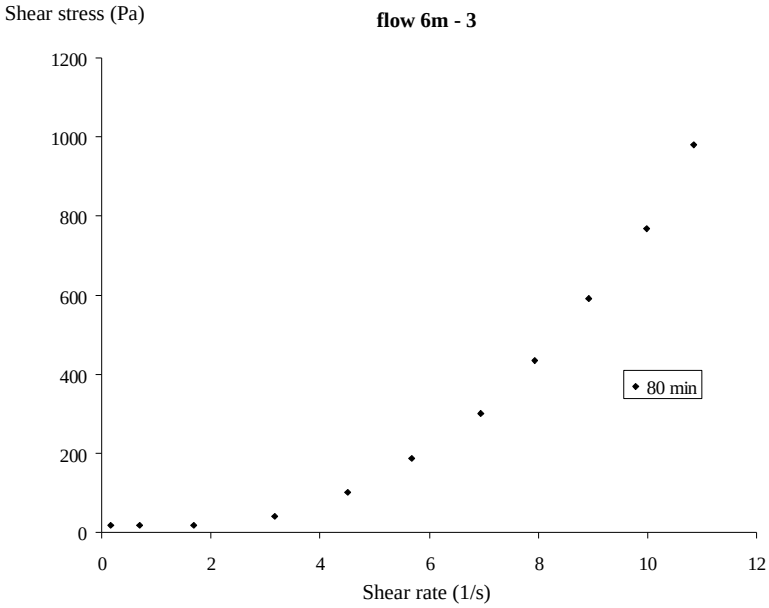
Shear stress (Pa)
flow 6m - 3
1200
1000
800
600
400
200
0
0
2
4
6
8
10
12
Shear rate (1/s)
80 min

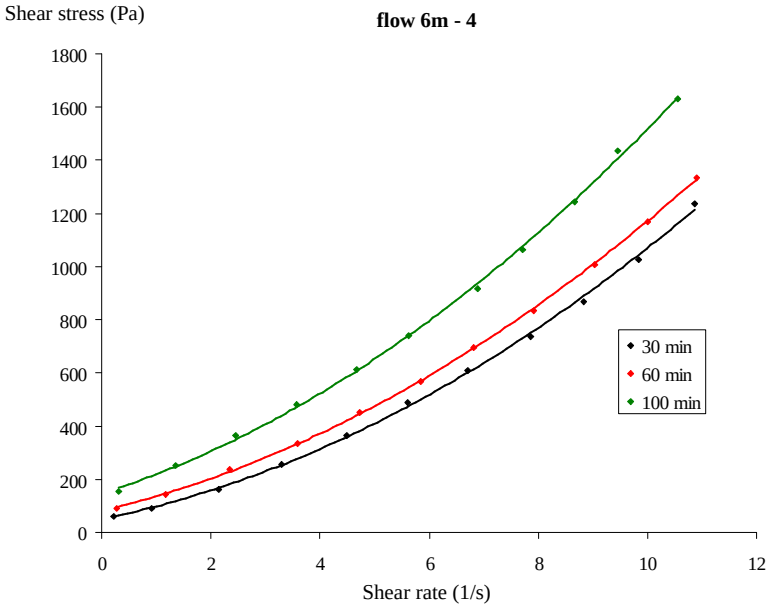
Shear stress (Pa)
flow 6m - 4
1800
1600
1400
1200
1000
800
600
400
200
0
0
2
4
6
8
10
12
Shear rate (1/s)
30 min
60 min
100 min

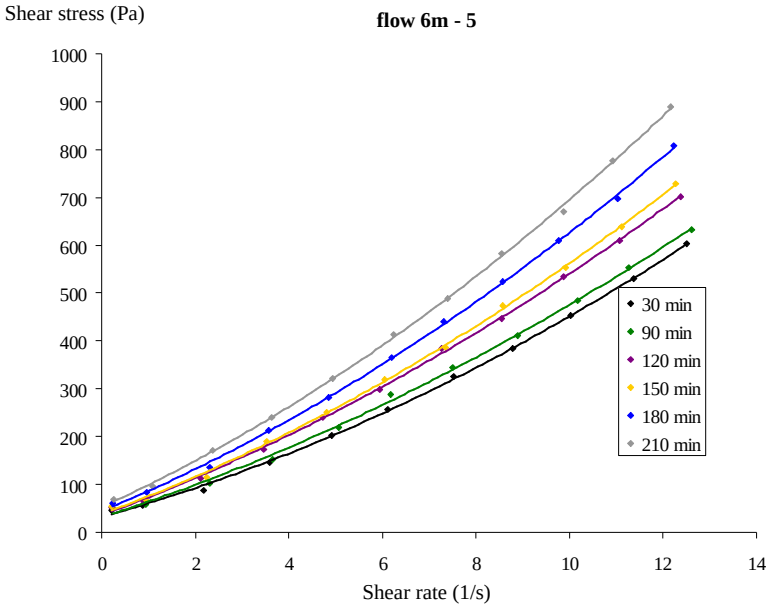
Shear stress (Pa)
flow 6m - 5
1000
900
800
700
600
500
400
300
200
100
0
0
2
4
6
8
10
12
14
Shear rate (1/s)
30 min
90 min
120 min
150 min
180 min
210 min

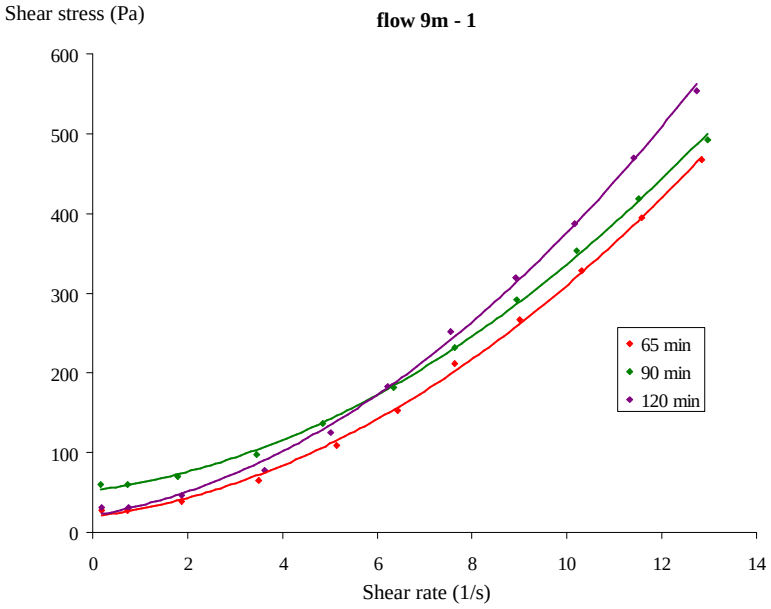
Shear stress (Pa)
flow 9m - 1
600
500
400
300
200
100
0
0
2
4
6
8
10
12
14
Shear rate (1/s)
65 min
90 min
120 min

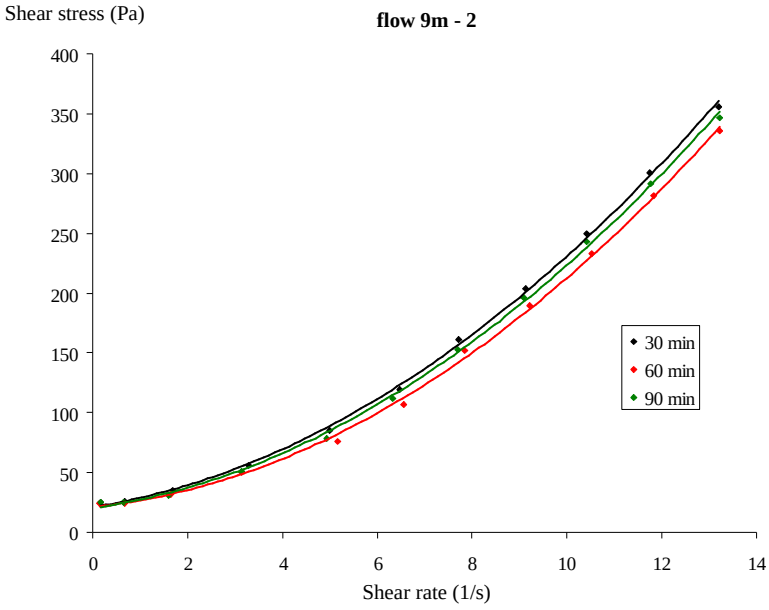
Shear stress (Pa)
flow 9m - 2
400
350
300
250
200
150
100
50
0
0
2
4
6
8
10
12
14
Shear rate (1/s)
30 min
60 min
90 min

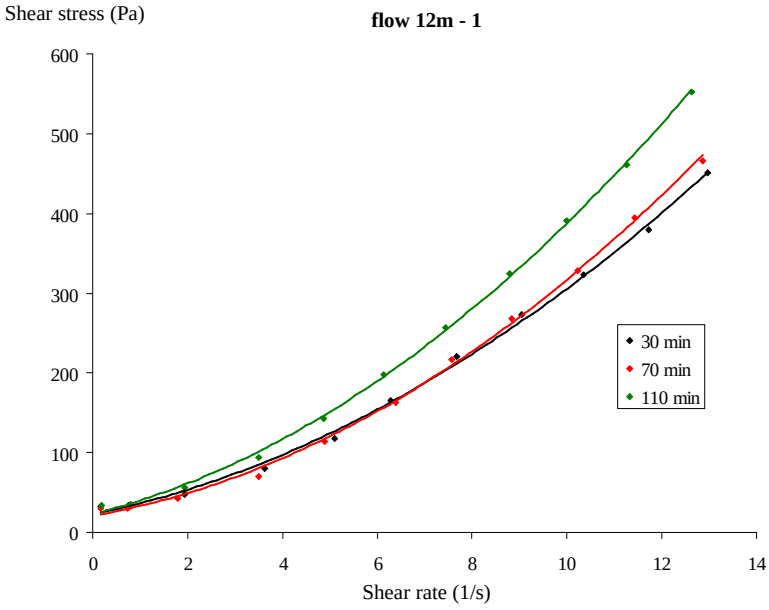
Shear stress (Pa)
flow 12m - 1
600
500
400
300
200
100
0
0
2
4
6
8
10
12
14
Shear rate (1/s)
30 min
70 min
110 min

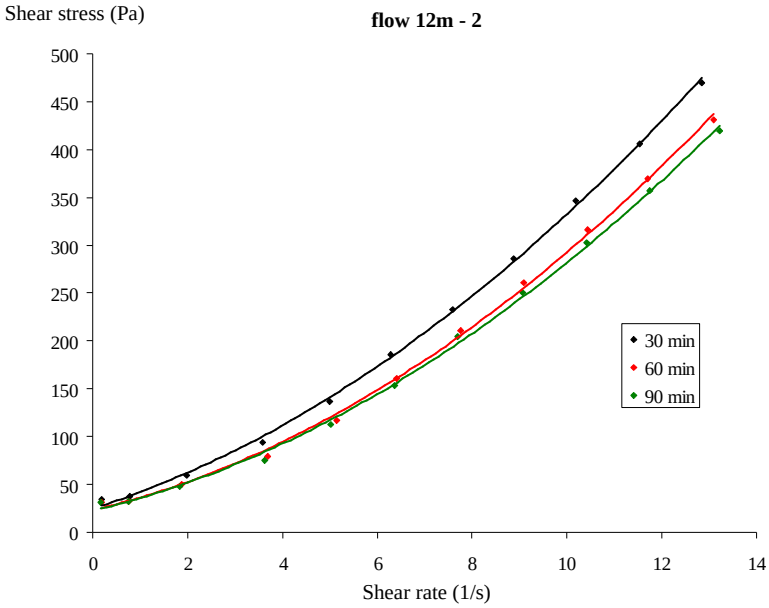
Shear stress (Pa)
flow 12m - 2
500
450
400
350
300
250
200
150
100
50
0
0
2
4
6
8
10
12
14
Shear rate (1/s)
30 min
60 min
90 min

5 Flow test results

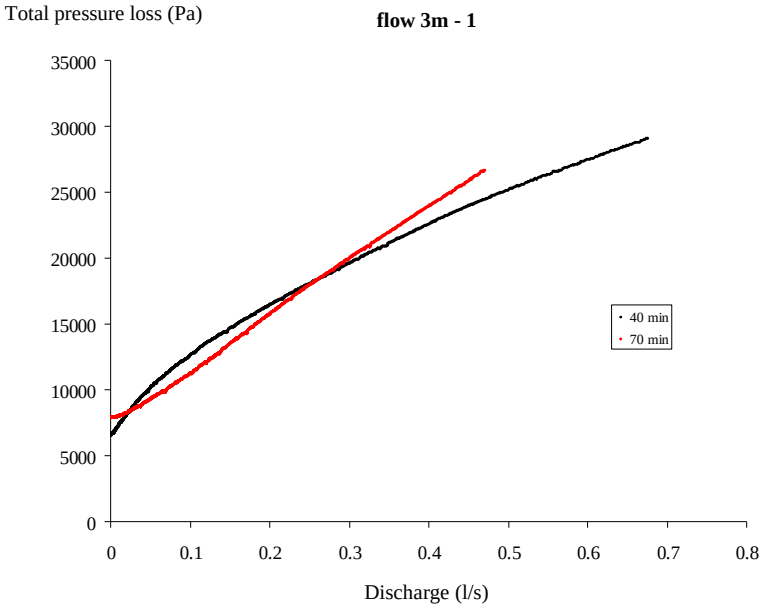

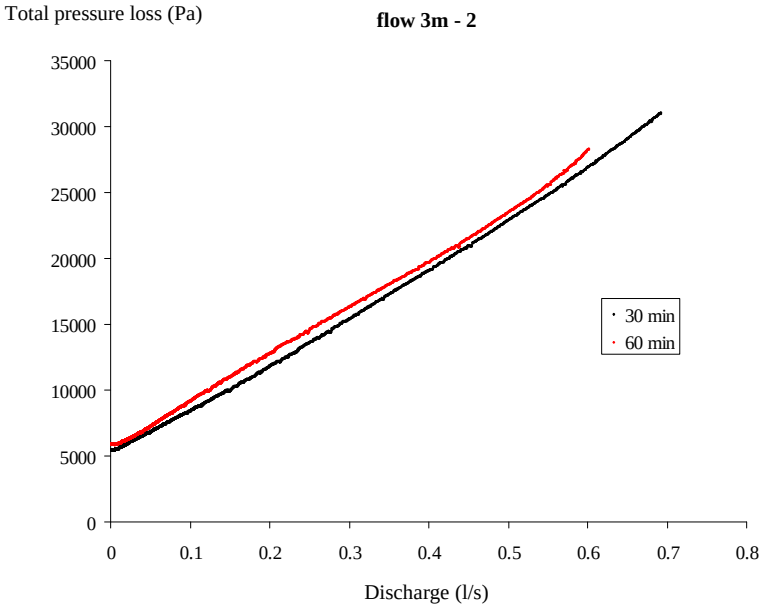

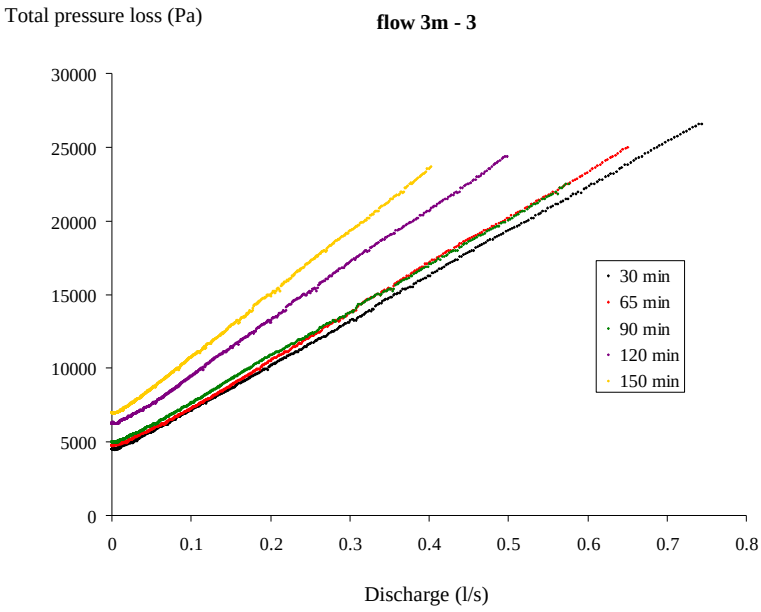
Total pressure loss (Pa)
flow 3m - 3
30000
25000
20000
15000
10000
5000
0
0
0.1
0.2
0.3
0.4
0.5
0.6
0.7
0.8
30 min
65 min
90 min
120 min
150 min
Discharge (l/s)

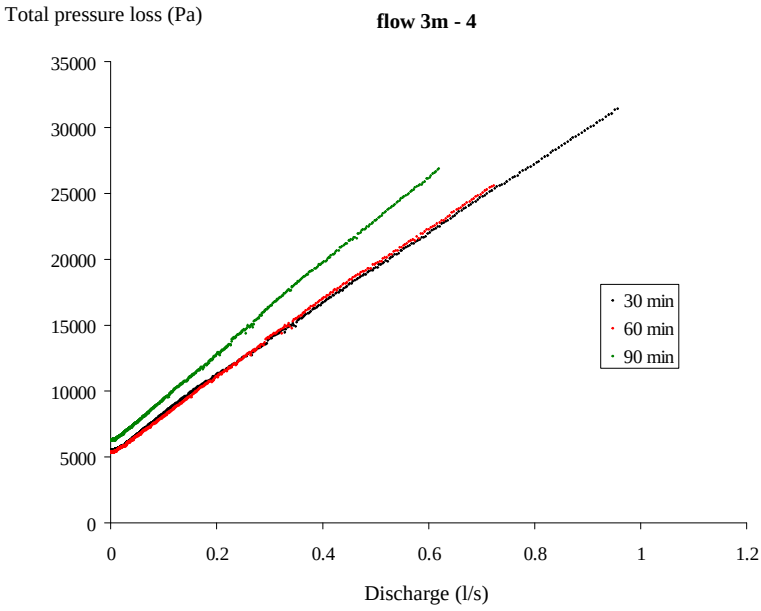
Total pressure loss (Pa)
flow 3m - 4
35000
30000
25000
20000
15000
10000
5000
0
0
0.2
0.4
0.6
0.8
1
1.2
30 min
60 min
90 min
Discharge (l/s)

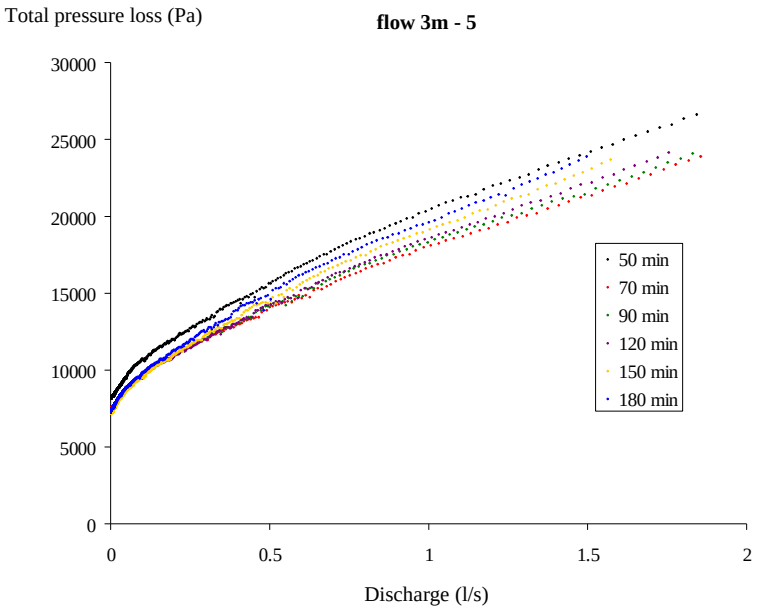
Total pressure loss (Pa)
flow 3m - 5
30000
25000
20000
15000
10000
5000
0
0
0.5
1
1.5
2
Discharge (l/s)
50 min
70 min
90 min
120 min
150 min
180 min

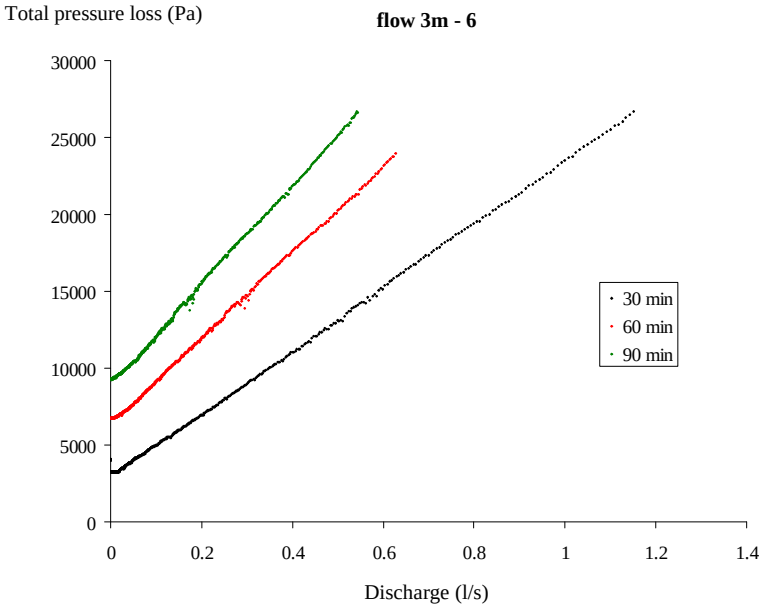
Total pressure loss (Pa)
flow 3m - 6
30000
25000
20000
15000
10000
5000
0
0
0.2
0.4
0.6
0.8
1
1.2
1.4
Discharge (l/s)
30 min
60 min
90 min

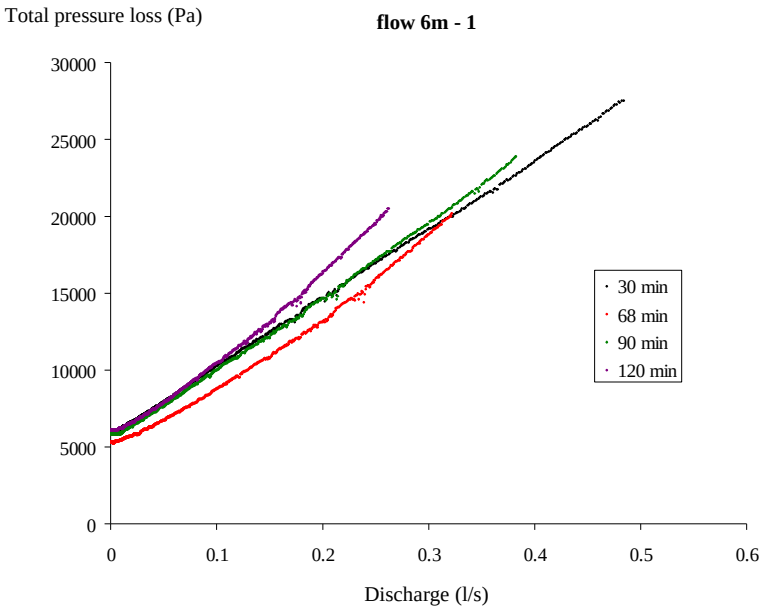
Total pressure loss (Pa)
flow 6m - 1
30000
25000
20000
15000
10000
5000
0
0
0.1
0.2
0.3
0.4
0.5
0.6
Discharge (l/s)
30 min
68 min
90 min
120 min

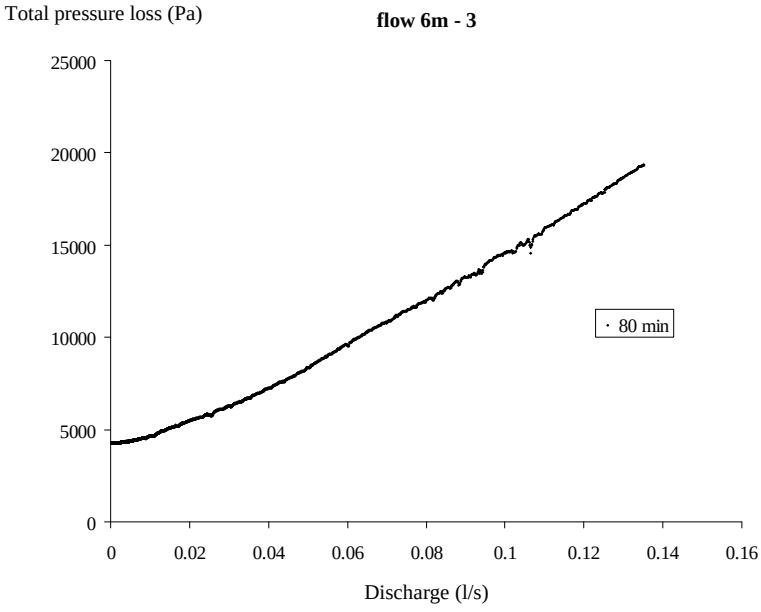
Total pressure loss (Pa)
flow 6m - 3
25000
20000
15000
10000
5000
0
0
0.02
0.04
0.06
0.08
0.1
0.12
0.14
0.16
Discharge (l/s)
80 min

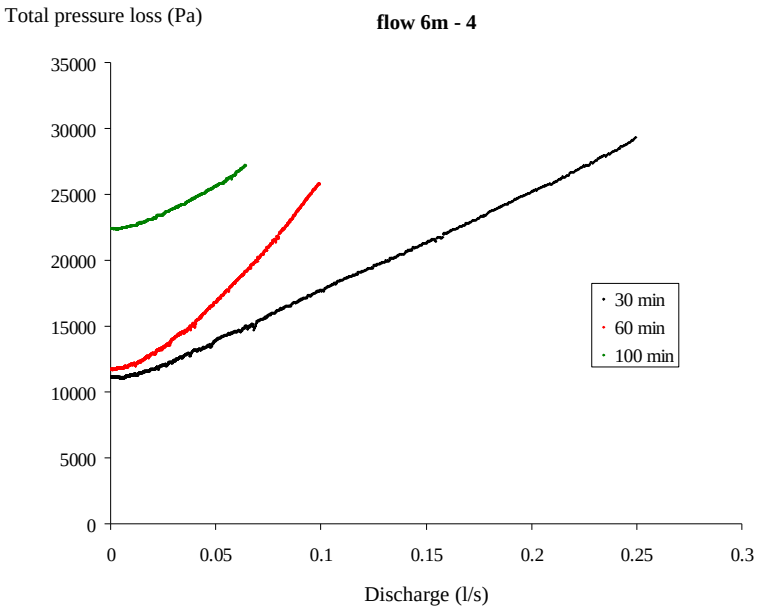
Total pressure loss (Pa)
flow 6m - 4
35000
30000
25000
20000
15000
10000
5000
0
0
0.05
0.1
0.15
0.2
0.25
0.3
Discharge (l/s)
30 min
60 min
100 min

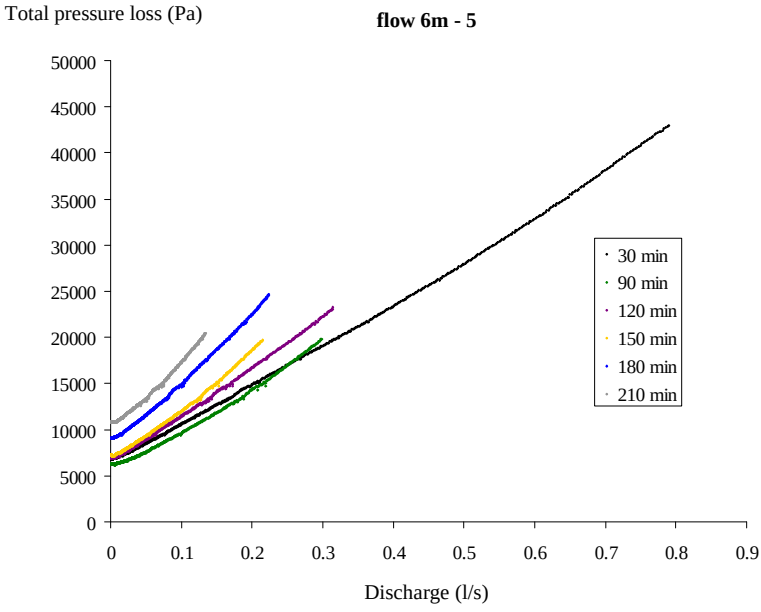
Total pressure loss (Pa)
flow 6m - 5
50000
45000
40000
35000
30000
25000
20000
15000
10000
5000
0
0
0.1
0.2
0.3
0.4
0.5
0.6
0.7
0.8
0.9
Discharge (l/s)
30 min
90 min
120 min
150 min
180 min
210 min

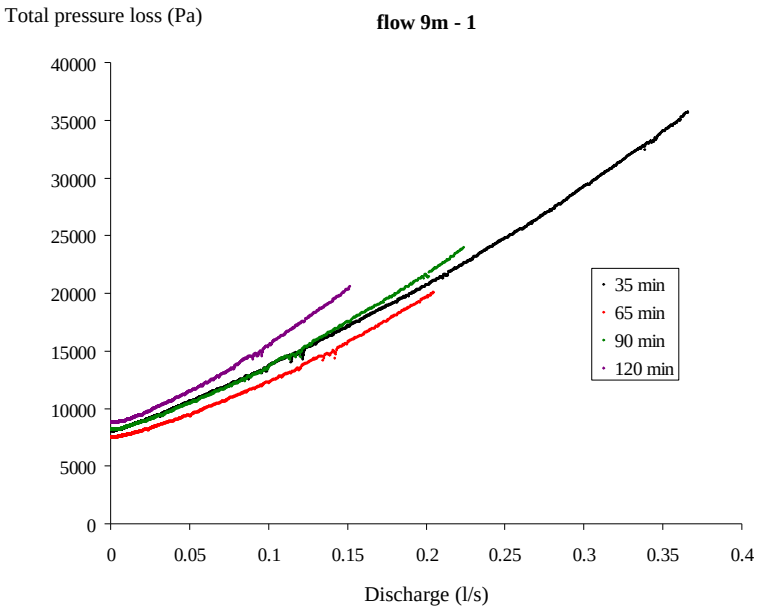
Total pressure loss (Pa)
flow 9m - 1
40000
35000
30000
25000
20000
15000
10000
5000
0
0
0.05
0.1
0.15
0.2
0.25
0.3
0.35
0.4
Discharge (l/s)
35 min
65 min
90 min
120 min

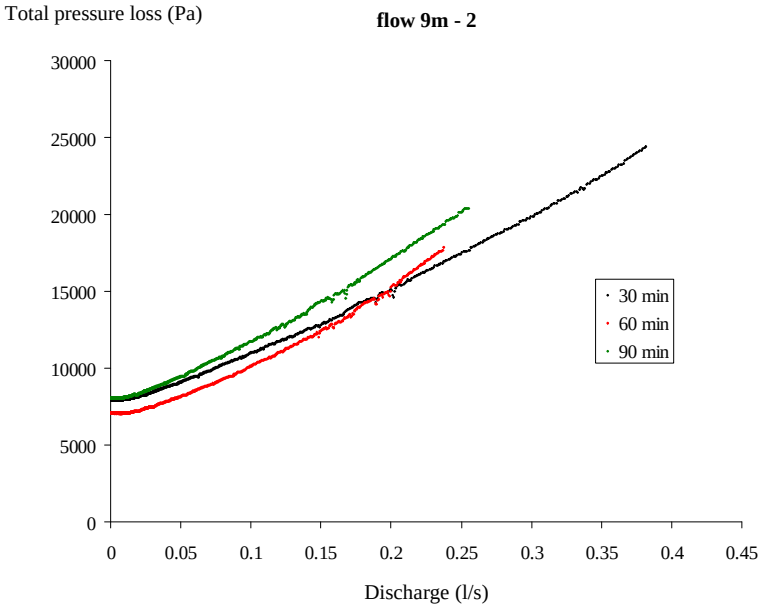
Total pressure loss (Pa)
flow 9m - 2
30000
25000
20000
15000
10000
5000
0
0
0.05
0.1
0.15
0.2
0.25
0.3
0.35
0.4
0.45
Discharge (l/s)
30 min
60 min
90 min

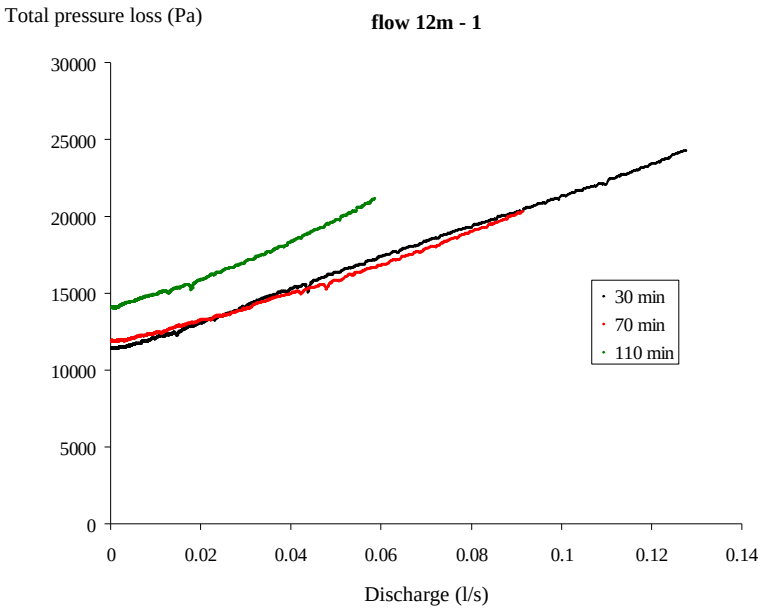
Total pressure loss (Pa)
flow 12m - 1
30000
25000
20000
15000
10000
5000
0
0
0.02
0.04
0.06
0.08
0.1
0.12
0.14
Discharge (l/s)
30 min
70 min
110 min

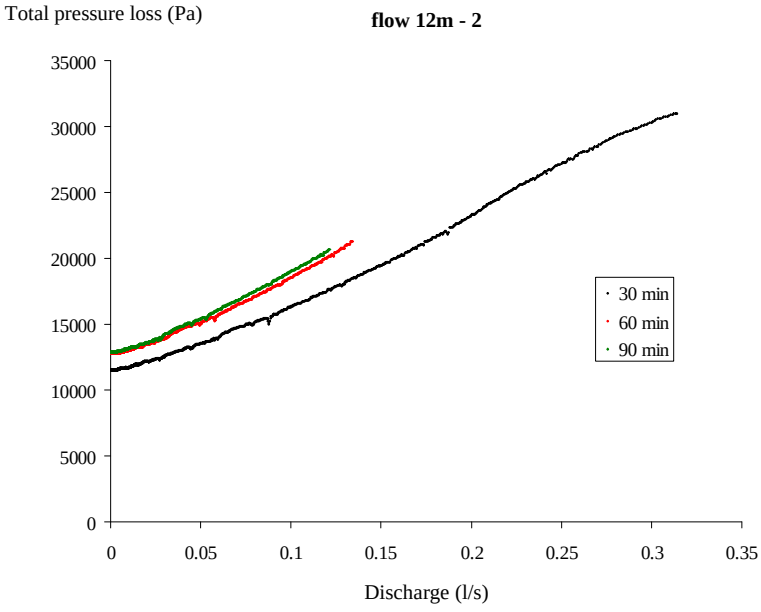
Total pressure loss (Pa)
flow 12m - 2
35000
30000
25000
20000
15000
10000
5000
0
0
0.05
0.1
0.15
0.2
0.25
0.3
0.35
Discharge (l/s)
30 min
60 min
90 min

APPENDIX D:

PUMPING TESTS

1 Introduction

This appendix contains all information of each concrete which has been pumped, discussed in chapters 8 and 9. For each concrete, the composition and initial slump flow at the plant are given in table 8.1 of chapter 8. In the tables in this appendix, the results of the tests on fresh concrete, like slump flow, V-funnel, density, air content and sieve stability, will be given. The results of the rheometer tests are also given, both in fundamental rheological units and also the maximal observed torque and the torque in equilibrium during pre-shearing. The maximal torque corresponds to a certain level of thixotropy, the second torque value is a parameter related to the flow resistance. If the concrete is too fluid, the Tattersall Mk-II rheometer fails to deliver good results (see chapter 3). In this case, the rheometer results will be put in *italic*, in case I think they are not really reliable. If a "-" is mentioned, this means that the results are not possible to be transformed, due to too low accuracy and problems in the transformation procedure.

For each concrete pumped in the short circuit, except SCC LM-12, the pressure loss per unit of length at different discharges is given, for each cycle. Also four graphs are given for these concretes: a pressure loss – discharge relationship at each cycle; a time evolution of the pressure loss for each discharge, the rheometer results, if available, and the relationship between temperature increase (°C/min) and the pressure loss.

For SCC LM-12, three figures are given: the pressure loss – discharge for both the equilibrium situation and the down-curve, the rheometer results and the temperature evolution. For SCC LM-14, the pressure loss – discharge curves are given for two straight measurement sections, together with the rheometer data and the temperature evolution. SCC LM-15 has been subjected to the "special thixotropy test" twice. The first figures display pressure loss – discharge curves for the first and second test, followed by the rheometer data and temperature curves. For SCC LM-16 and 17, similar curves as for SCC LM-14 are given, but temperature data are not available. For SCC LM-17, the rheometer data did not deliver good results.

As mentioned in chapter 9, sampling is not straightforward. Sometimes, a bucket of aggregates can be obtained and next time, it can be a bucket of cement paste. If the

sample is doubted to be representative for the concrete, the background of the corresponding column in the table is put in grey.
For some concretes, a non-pumped sample has been kept aside in order to evaluate the influence of time on the properties. Unfortunately, sampling from a concrete mixer is also not straightforward and the sample does in most cases not represent the concrete properties. As a result, only a qualitative comparison can be executed.
If necessary, some comments are added.

2 Results

2.1 SCC OBC-1

	SCC-OBC-1			
	Cycle 1	**Cycle 2**	**Cycle 3**	**Cycle 4**
Concrete Age (min)	**95**	**125**	**150**	**195**
Tests on fresh SCC				
Slump flow (mm)	737.5		727.5	615
V-Funnel (s)	4.9		2.0	2.5
L-box (-)	0.95		0.89	0.68
Density (kg/m³)	2244			
Sieve Stability (%)	6.74			
Air Content (%)	4.4			
Rheometer tests				
Yield stress (Pa)	*1.6*	11.6	-	20.0
Viscosity at 0/s (Pa s)	*7.5*	1.3	-	3.4
shear thickening (c/mu)	*0.064*	0.131	-	0.047
Viscosity at 5/s (Pa s)	*12.3*	3.0	-	5.0
Torque at max. vel (Nm)	1.17	0.20	0.26	0.60
Max. torque (thixo)(Nm)	1.42	0.26	0.33	0.66

Pressure loss (kPa/m)				
Discharge 1	5.86	6.99	6.88	7.49
Discharge 2	11.75	9.76	11.44	11.72
Discharge 3	22.29	19.70	18.74	20.06
Discharge 4	32.99	28.36	27.70	25.85
Discharge 5		35.08	34.79	35.42

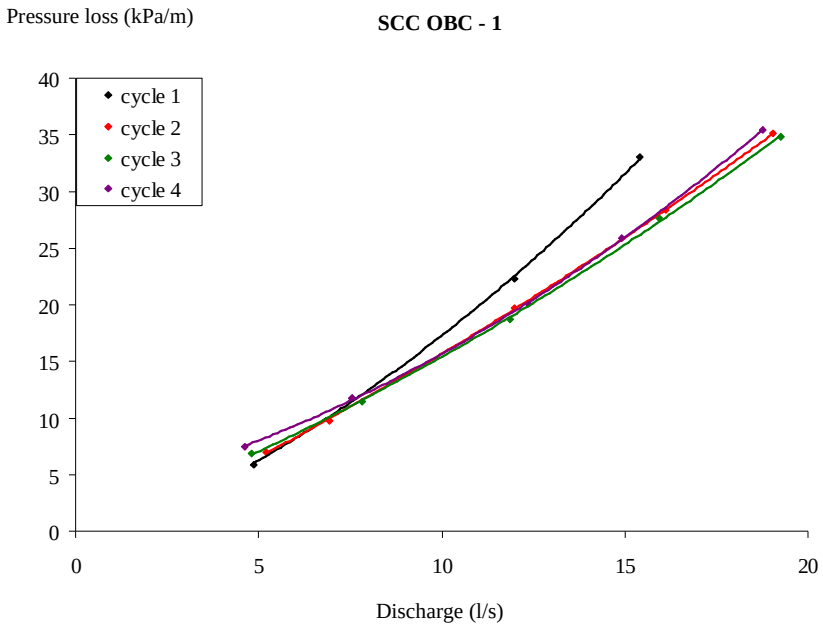
Pressure loss (kPa/m)
SCC OBC - 1
cycle 1
cycle 2
cycle 3
cycle 4
40
35
30
25
20
15
10
5
0
0
5
10
15
20
Discharge (l/s)

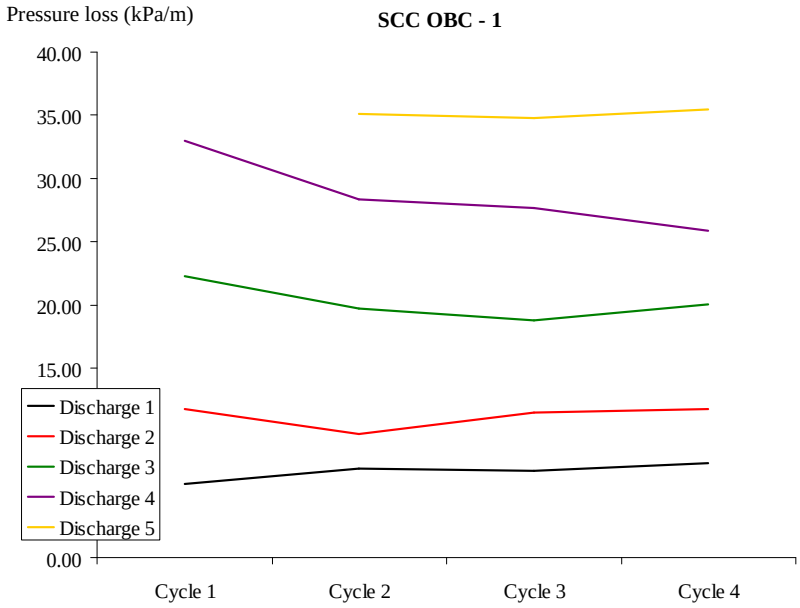
Pressure loss (kPa/m)
SCC OBC - 1
40.00
35.00
30.00
25.00
20.00
15.00
0.00
Discharge 1
Discharge 2
Discharge 3
Discharge 4
Discharge 5
Cycle 1
Cycle 2
Cycle 3
Cycle 4

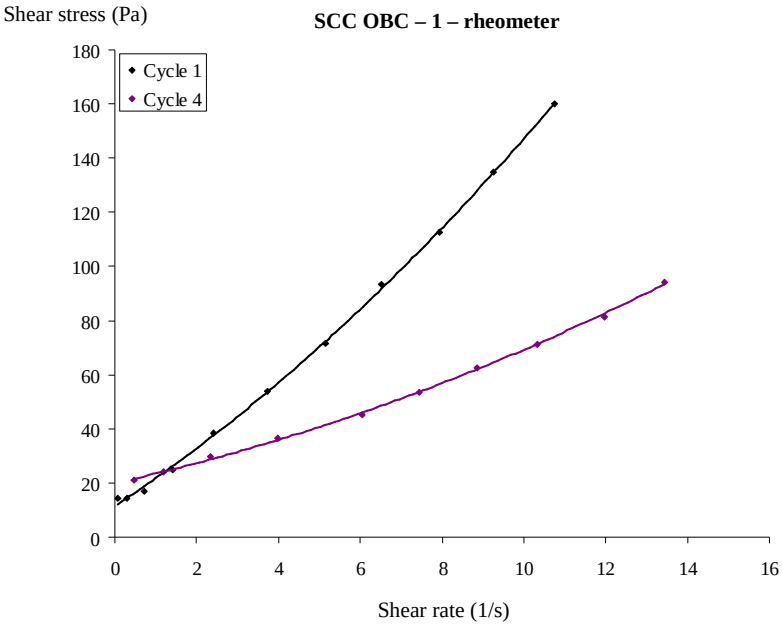
Shear stress (Pa)
SCC OBC – 1 – rheometer
Cycle 1
Cycle 4
180
160
140
120
100
80
60
40
20
0
0
2
4
6
8
10
12
14
16
Shear rate (1/s)

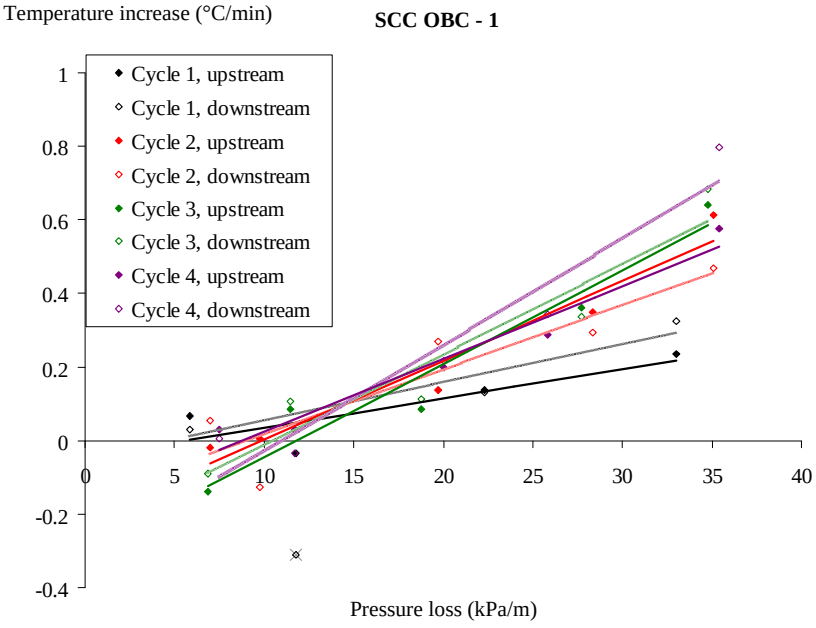
Temperature increase (°C/min)
SCC OBC - 1
Cycle 1, upstream
Cycle 1, downstream
Cycle 2, upstream
Cycle 2, downstream
Cycle 3, upstream
Cycle 3, downstream
Cycle 4, upstream
Cycle 4, downstream
1
0.8
0.6
0.4
0.2
0
-0.2
-0.4
0
5
10
15
20
25
30
35
40
Pressure loss (kPa/m)

2.2 SCC LM-1

	SCC-LM-1		
	Cycle 1	**Cycle 2**	**Cycle 3**
Concrete Age (min)	**67**	**90**	**127**
Tests on fresh SCC			
Slump flow (mm)	637.5		710
V-Funnel (s)	11.1		5.3
L-box (-)	0.72		0.9
Density (kg/m³)	2394		
Sieve Stability (%)	3.45		
Air Content (%)	1.3		
Rheometer tests			
Yield stress (Pa)	81.7	18.3	49.0
Viscosity at 0/s (Pa s)	52.3	4.6	24.7
shear thickening (c/mu)	0.014	0.072	0.012
Viscosity at 5/s (Pa s)	59.5	7.9	27.7
Torque at max. vel (Nm)	6.18	0.89	3.14
Max. torque (thixo)(Nm)	8.33	1.37	4.01

Pressure loss (kPa/m)			
Discharge 1	11.69	9.40	9.24
Discharge 2	20.49	16.78	15.68
Discharge 3	36.16	29.88	28.48
Discharge 4	53.57	44.22	40.97
Discharge 5	79.76	60.03	53.87

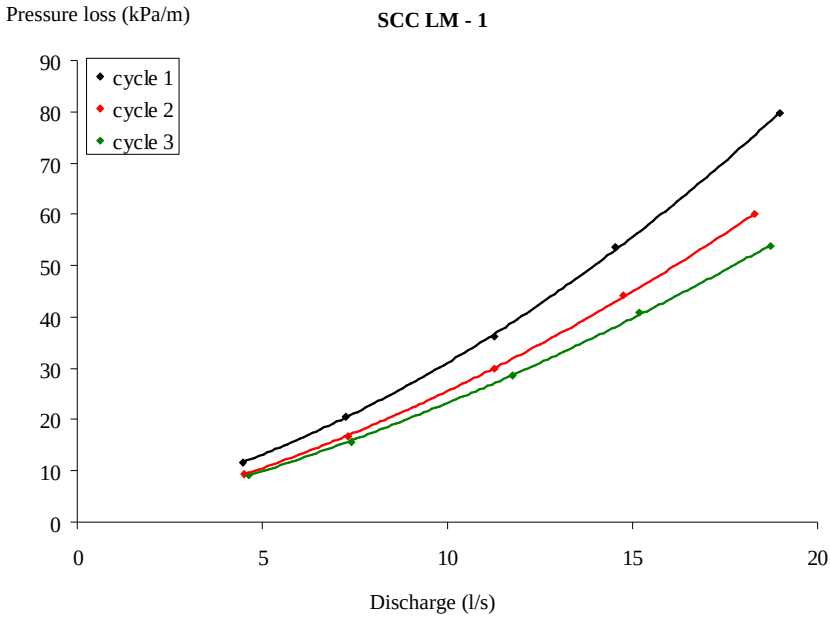
Pressure loss (kPa/m)
SCC LM - 1
cycle 1
cycle 2
cycle 3
90
80
70
60
50
40
30
20
10
0
0
5
10
15
20
Discharge (l/s)

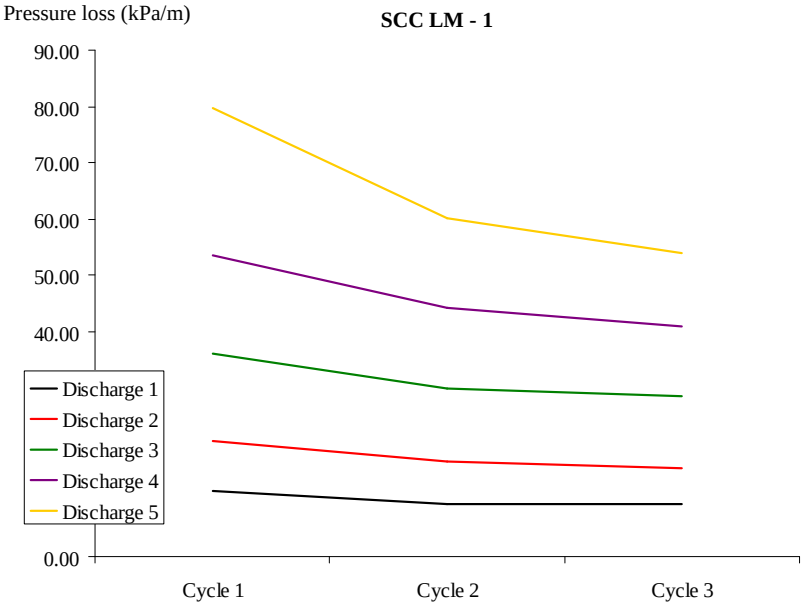
Pressure loss (kPa/m)
SCC LM - 1
90.00
80.00
70.00
60.00
50.00
40.00
0.00
Discharge 1
Discharge 2
Discharge 3
Discharge 4
Discharge 5
Cycle 1
Cycle 2
Cycle 3

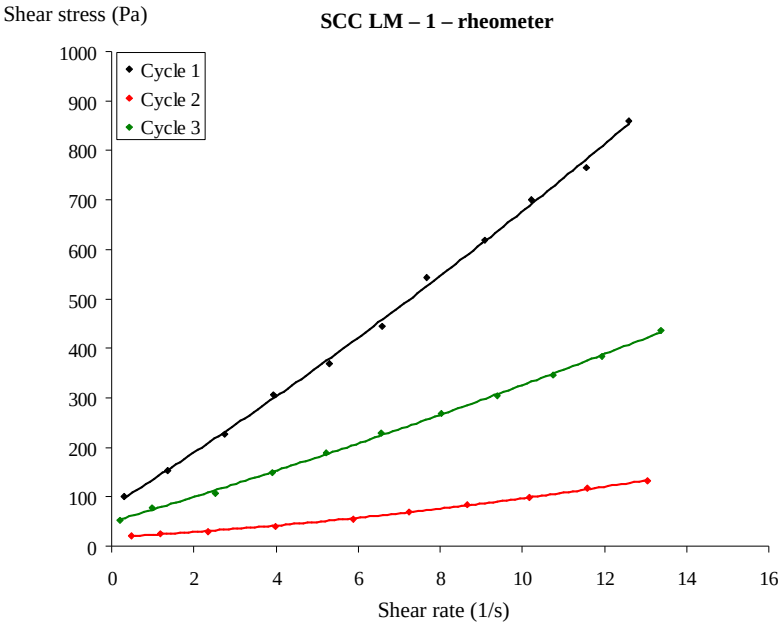
Shear stress (Pa)
SCC LM – 1 – rheometer
Cycle 1
Cycle 2
Cycle 3
1000
900
800
700
600
500
400
300
200
100
0
0
2
4
6
8
10
12
14
16
Shear rate (1/s)

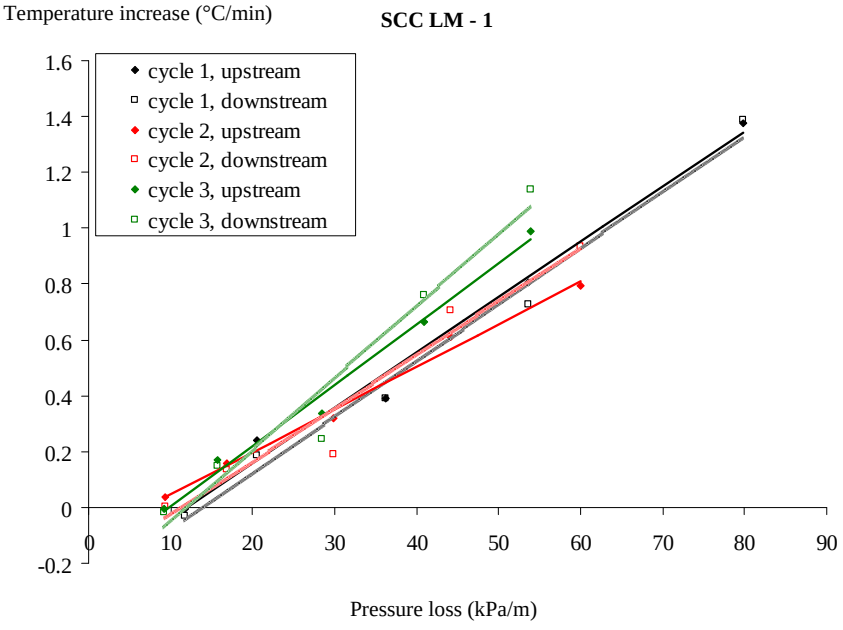
Temperature increase (°C/min)
SCC LM - 1
cycle 1, upstream
cycle 1, downstream
cycle 2, upstream
cycle 2, downstream
cycle 3, upstream
cycle 3, downstream
1.6
1.4
1.2
1
0.8
0.6
0.4
0.2
0
-0.2
0
10
20
30
40
50
60
70
80
90
Pressure loss (kPa/m)

2.3 SCC LM-2

	SCC-LM-2				
	Cycle 1	**Cycle 2**	**Cycle 3**	**Cycle 4**	**Cycle 5**
Concrete Age (min)	**71**	**90**	**125**	**150**	**180**
Tests on fresh SCC					
Slump flow (mm)	720		660		522.5
V-Funnel (s)	7.1		4.5		4.9
L-box (-)	0.86		0.72		0.53
Density (kg/m³)	2338				
Sieve Stability (%)	10.86				
Air Content (%)	2.55				
Rheometer tests					
Yield stress (Pa)	156.9	118.7	114.4	36.6	162.5
Viscosity at 0/s (Pa s)	76.3	61.4	39.5	14.8	34.1
shear thickening (c/mu)	0.000	0.014	0.000	0	0
Viscosity at 5/s (Pa s)	76.3	69.7	39.5	14.8	34.1
Torque at max. vel (Nm)	7.73	7.23	4.59	1.68	4.36
Max. torque (thixo)(Nm)	10.50	8.89	4.80	2.32	4.87

Pressure loss (kPa/m)					
Discharge 1	13.98	12.34	11.81	12.22	13.27
Discharge 2	26.21	19.16	21.73	18.65	22.65
Discharge 3	50.74	33.48	35.88	31.57	33.92
Discharge 4	74.80	52.04	50.19	42.57	48.12
Discharge 5	102.59	73.31	63.45	57.67	62.44

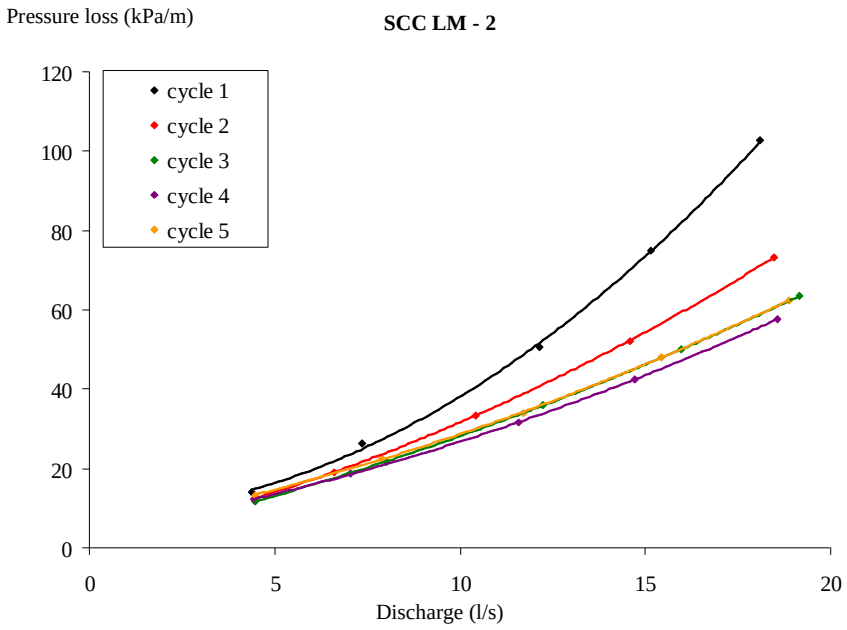
Pressure loss (kPa/m)
SCC LM - 2
cycle 1
cycle 2
cycle 3
cycle 4
cycle 5
120
100
80
60
40
20
0
0
5
10
15
20
Discharge (l/s)

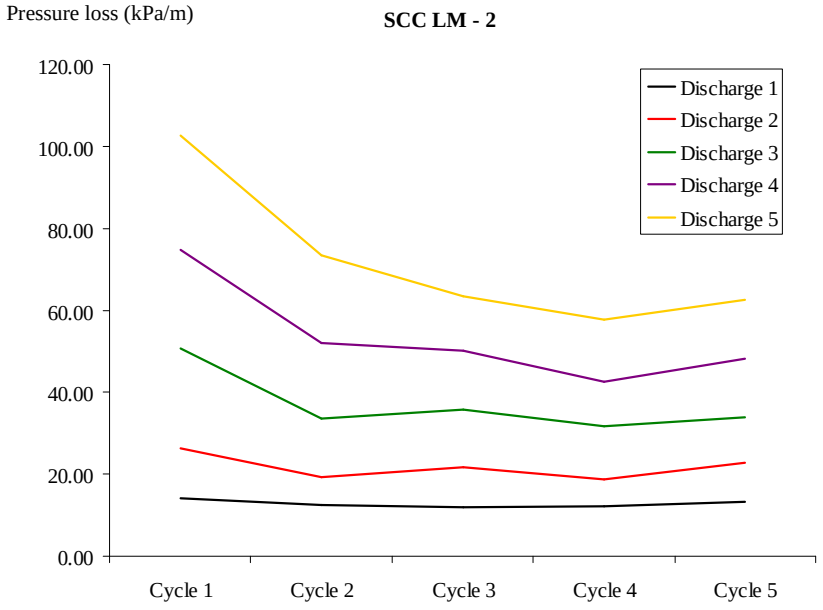
Pressure loss (kPa/m)
SCC LM - 2
Discharge 1
Discharge 2
Discharge 3
Discharge 4
Discharge 5
120.00
100.00
80.00
60.00
40.00
20.00
0.00
Cycle 1
Cycle 2
Cycle 3
Cycle 4
Cycle 5

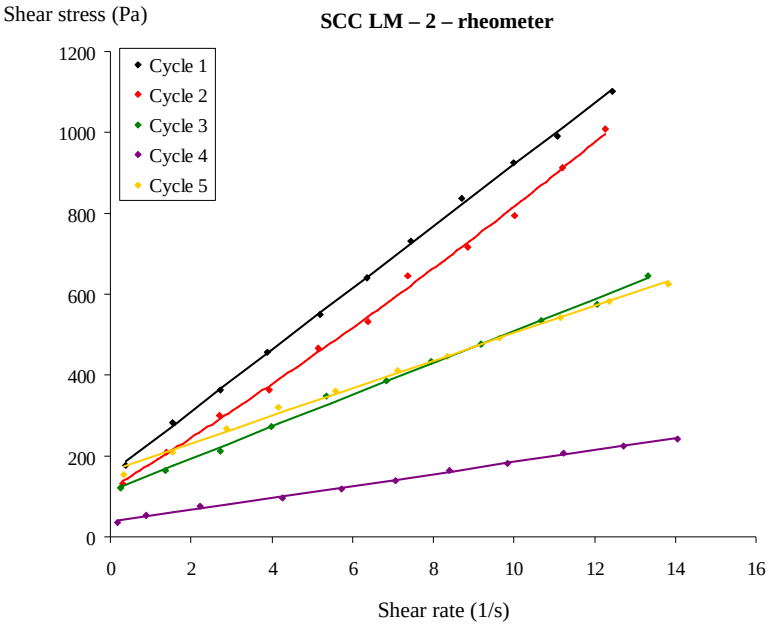
Shear stress (Pa)
SCC LM – 2 – rheometer
Cycle 1
Cycle 2
Cycle 3
Cycle 4
Cycle 5
1200
1000
800
600
400
200
0
0
2
4
6
8
10
12
14
16
Shear rate (1/s)

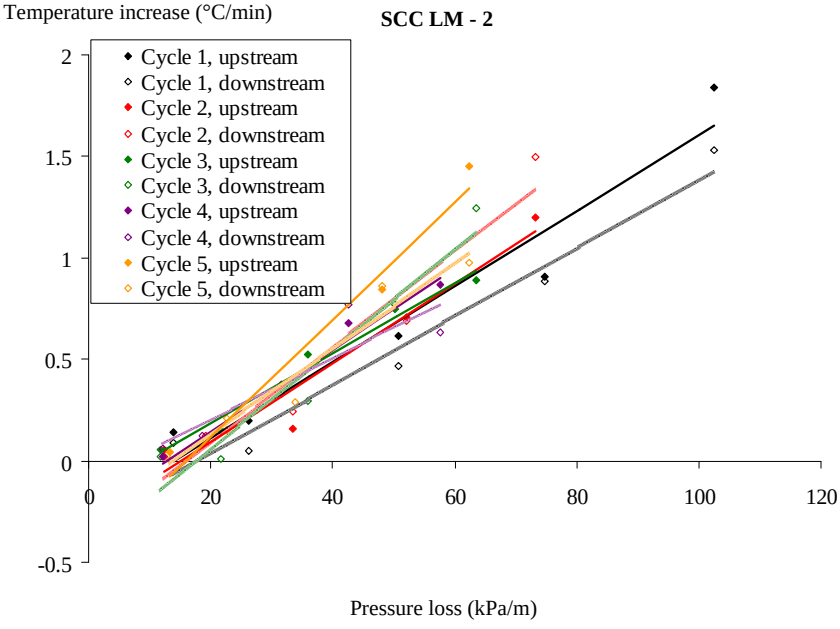
Temperature increase (°C/min)
SCC LM - 2
Cycle 1, upstream
Cycle 1, downstream
Cycle 2, upstream
Cycle 2, downstream
Cycle 3, upstream
Cycle 3, downstream
Cycle 4, upstream
Cycle 4, downstream
Cycle 5, upstream
Cycle 5, downstream
2
1.5
1
0.5
0
-0.5
0
20
40
60
80
100
120
Pressure loss (kPa/m)

2.4 SCC LM-3

	SCC-LM-3					
	Cycle 1	**Cycle 2**	**Cycle 3**	**Cycle 4**	**Cycle 5**	**Cycle 6**
Concrete Age (min)	**105**	**145**	**170**	**195**	**Cancelled**	**230**
Tests on fresh SCC						
Slump flow (mm)	775		470			110 (slump)
V-Funnel (s)	5.4		5.3			16.9
L-box (-)	0.97		0.32			-
Density (kg/m³)	2381					
Sieve Stability (%)	11.1					0.0
Air Content (%)	1.3					
Rheometer tests						
Yield stress (Pa)	65.7	106.7	270.1	410.1		531.3
Viscosity at 0/s (Pa s)	29.7	38.2	45.8	48.6		26.2
shear thickening (c/mu)	0.022	0.000	0.000	0.000		0.000
Viscosity at 5/s (Pa s)	36.2	38.2	45.8	48.6		26.2
Torque at max. vel (Nm)	4.27	4.38	6.14	7.12		6.27
Max. torque (thixo)(Nm)	5.06	6.06	8.45	9.28		20.18

Pressure loss (kPa/m)						
Discharge 1	19.99	18.69	18.94	22.38		
Discharge 2	39.25	31.43	31.54	36.20		
Discharge 3	63.73	52.13	48.41	55.32		
Discharge 4	108.32	73.35	65.68	73.19		
Discharge 5	145.06	96.08	86.64	91.52		

Remark: The pressure losses have been measured over an 11 m straight section and a short curve of 90°. The curve has been considered as a straight pipe with a length equal to 0.267 m.

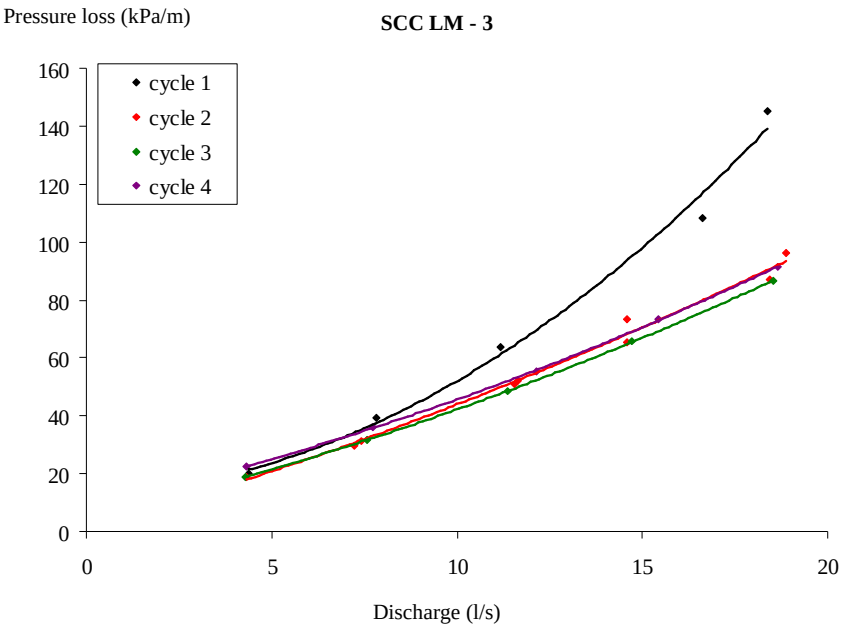
Pressure loss (kPa/m)
SCC LM - 3
cycle 1
cycle 2
cycle 3
cycle 4
160
140
120
100
80
60
40
20
0
0
5
10
15
20
Discharge (l/s)

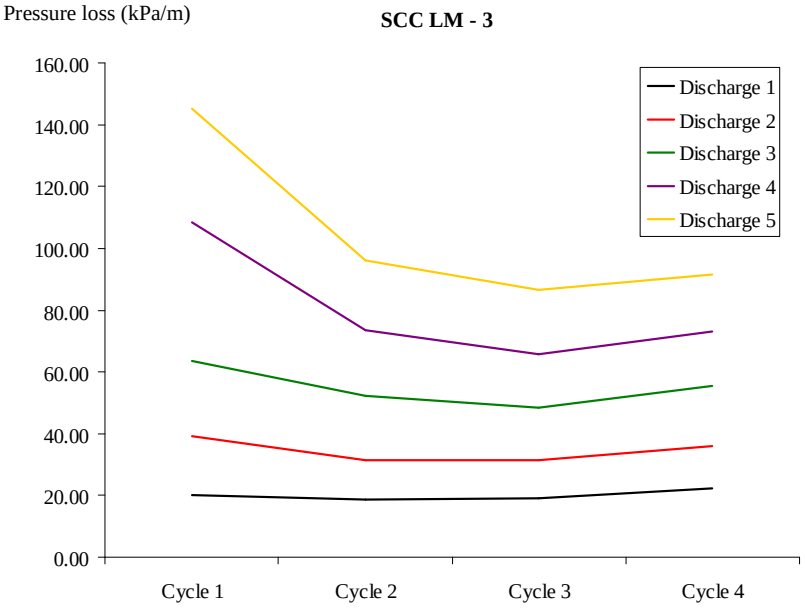
Pressure loss (kPa/m)
SCC LM - 3
Discharge 1
Discharge 2
Discharge 3
Discharge 4
Discharge 5
160.00
140.00
120.00
100.00
80.00
60.00
40.00
20.00
0.00
Cycle 1
Cycle 2
Cycle 3
Cycle 4

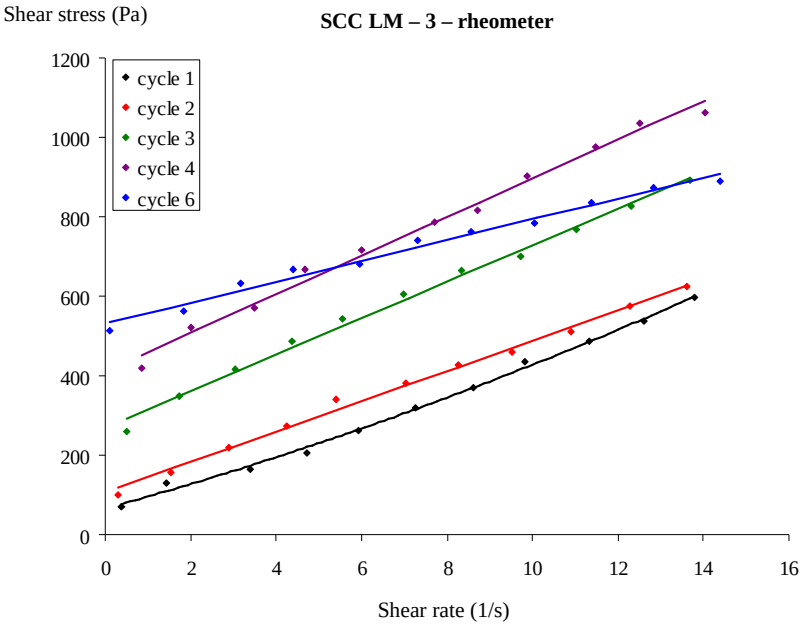
Shear stress (Pa)
SCC LM – 3 – rheometer
cycle 1
cycle 2
cycle 3
cycle 4
cycle 6
1200
1000
800
600
400
200
0
0
2
4
6
8
10
12
14
16
Shear rate (1/s)

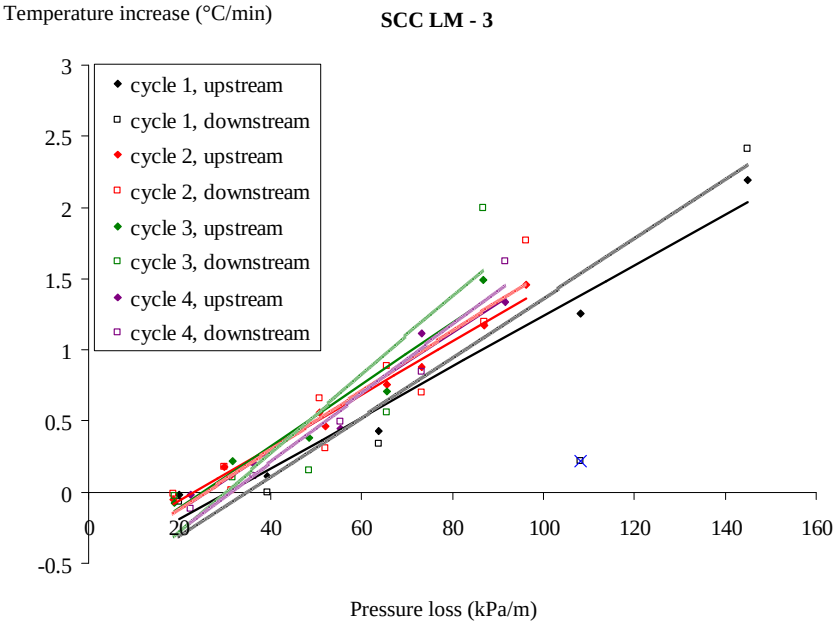
Temperature increase (°C/min)
SCC LM - 3
cycle 1, upstream
cycle 1, downstream
cycle 2, upstream
cycle 2, downstream
cycle 3, upstream
cycle 3, downstream
cycle 4, upstream
cycle 4, downstream
3
2.5
2
1.5
1
0.5
0
-0.5
0
20
40
60
80
100
120
140
160
Pressure loss (kPa/m)

2.5 SCC LM-4

	SCC-LM-4			
	Cycle 1	**Cycle 2**	**Cycle 3**	**Cycle 4**
Concrete Age (min)	**60**	**90**	**115**	**145**
Tests on fresh SCC				
Slump flow (mm)	780		700	645
V-Funnel (s)	2.6		3.2	4.1
L-box (-)	1.00		0.97	0.80
Density (kg/m³)	2338			
Sieve Stability (%)	14.3			5.7
Air Content (%)	1.8			
Yield stress (Pa)	120.0	83.0	30.4	140.6
Viscosity at 0/s (Pa s)	39.0	35.2	14.1	31.6
shear thickening (c/mu)	0.005	0.000	0.024	0.000
Viscosity at 5/s (Pa s)	41.1	35.2	17.5	31.6
Torque at max. vel (Nm)	5.01	4.10	2.08	3.96
Max. torque (thixo)(Nm)	9.62	5.09	2.71	4.76

Pressure loss (kPa/m)				
Discharge 1	9.63	10.06	10.57	10.13
Discharge 2	18.80	18.32	18.98	17.19
Discharge 3	31.76	27.71	29.90	26.33
Discharge 4	43.75	41.72	39.52	38.25
Discharge 5	56.84	53.86	53.67	52.30

Remark: The pressure losses have been measured over an 11 m straight section and a short curve of 90°. The curve has been considered as a straight pipe with a length equal to 0.267 m.

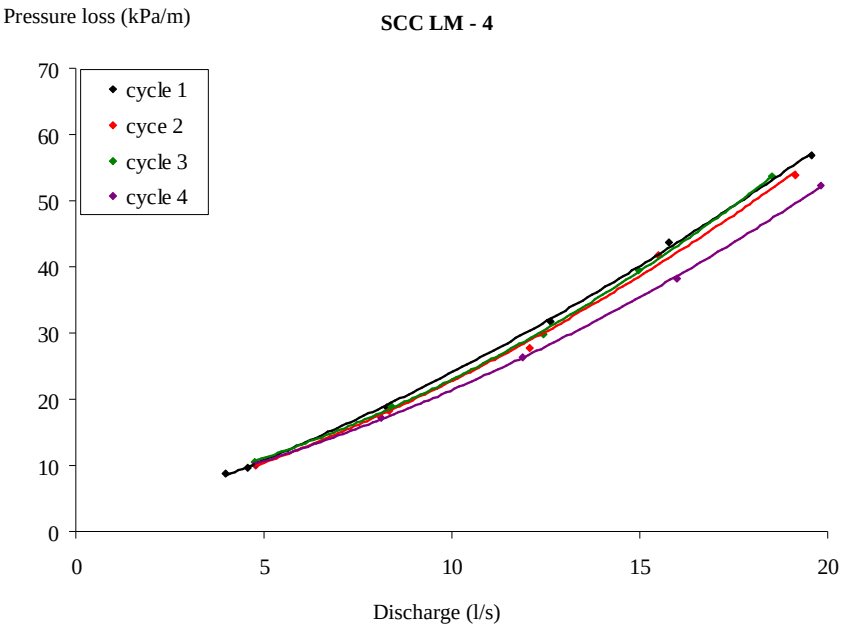
Pressure loss (kPa/m)
SCC LM - 4
cycle 1
cyce 2
cycle 3
cycle 4
70
60
50
40
30
20
10
0
0
5
10
15
20
Discharge (l/s)

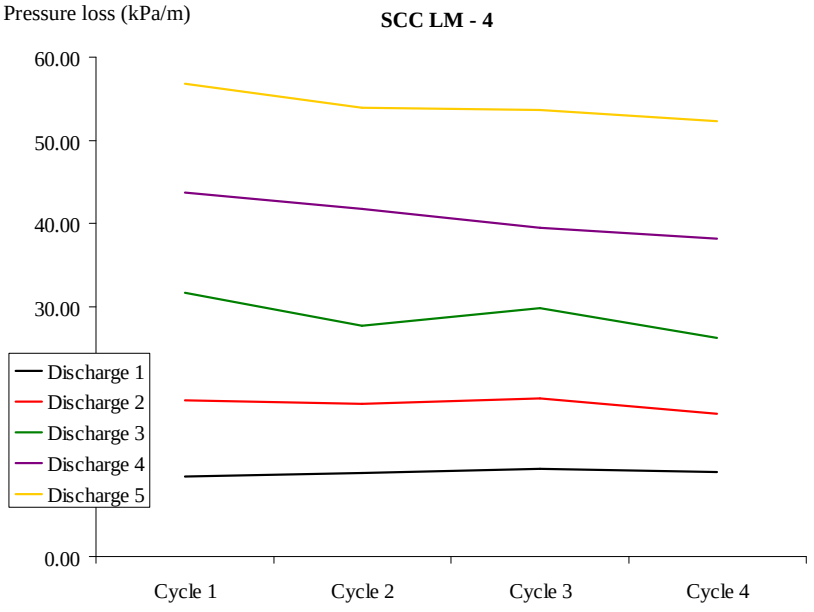
Pressure loss (kPa/m)
SCC LM - 4
60.00
50.00
40.00
30.00
0.00
Discharge 1
Discharge 2
Discharge 3
Discharge 4
Discharge 5
Cycle 1
Cycle 2
Cycle 3
Cycle 4

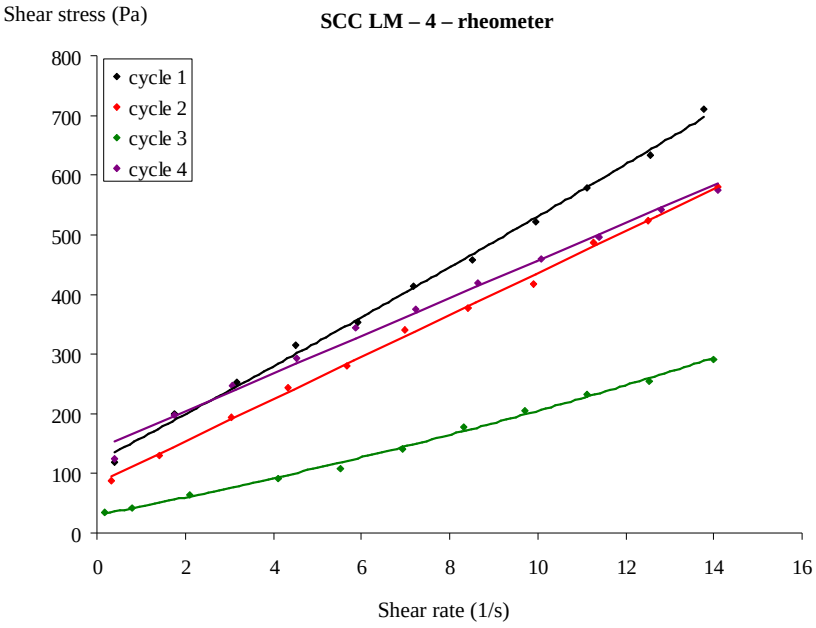
Shear stress (Pa)
SCC LM – 4 – rheometer
cycle 1
cycle 2
cycle 3
cycle 4
800
700
600
500
400
300
200
100
0
0
2
4
6
8
10
12
14
16
Shear rate (1/s)

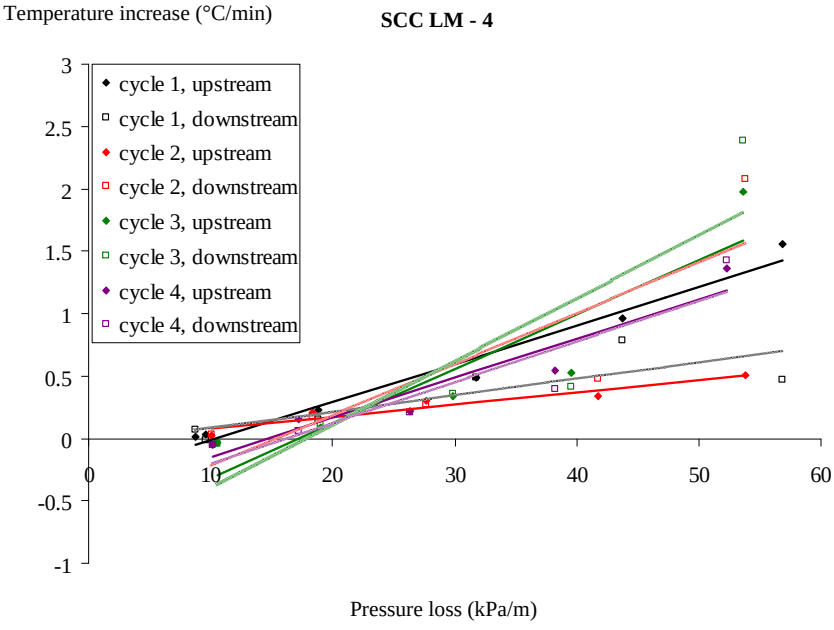
Temperature increase (°C/min)
SCC LM - 4
cycle 1, upstream
cycle 1, downstream
cycle 2, upstream
cycle 2, downstream
cycle 3, upstream
cycle 3, downstream
cycle 4, upstream
cycle 4, downstream
3
2.5
2
1.5
1
0.5
0
-0.5
-1
0
10
20
30
40
50
60
Pressure loss (kPa/m)

2.6 SCC LM-5

	SCC-LM-5		
	Cycle 1	**Cycle 2**	**Cycle 3**
Concrete Age (min)	**50**	**80**	**105**
Tests on fresh SCC			
Slump flow (mm)	740		660
V-Funnel (s)	5.3		4.3
L-box (-)	0.91		0.75
Density (kg/m³)	2388		
Sieve Stability (%)	9.1		10.9
Air Content (%)	1.9		
Rheometer tests			
Yield stress (Pa)	60.9	58.2	73.4
Viscosity at 0/s (Pa s)	36.1	30.7	28.2
shear thickening (c/mu)	0.017	0.008	0.000
Viscosity at 5/s (Pa s)	42.4	33.2	28.2
Torque at max. vel (Nm)	4.81	3.83	3.26
Max. torque (thixo)(Nm)	5.78	4.47	3.98

Pressure loss (kPa/m)			
Discharge 1	9.45	8.34	9.63
Discharge 2	21.32	16.15	16.10
Discharge 3	36.49	30.21	26.45
Discharge 4	55.76	46.46	35.51
Discharge 5	83.96	65.92	53.94

Remarks: The pressure losses have been measured over an 11 m straight section and a short curve of 90°. The curve has been considered as a straight pipe with a length equal to 0.267 m.
Before pouring the concrete in the pump, the reservoir of the pump has not been sprayed with oil.

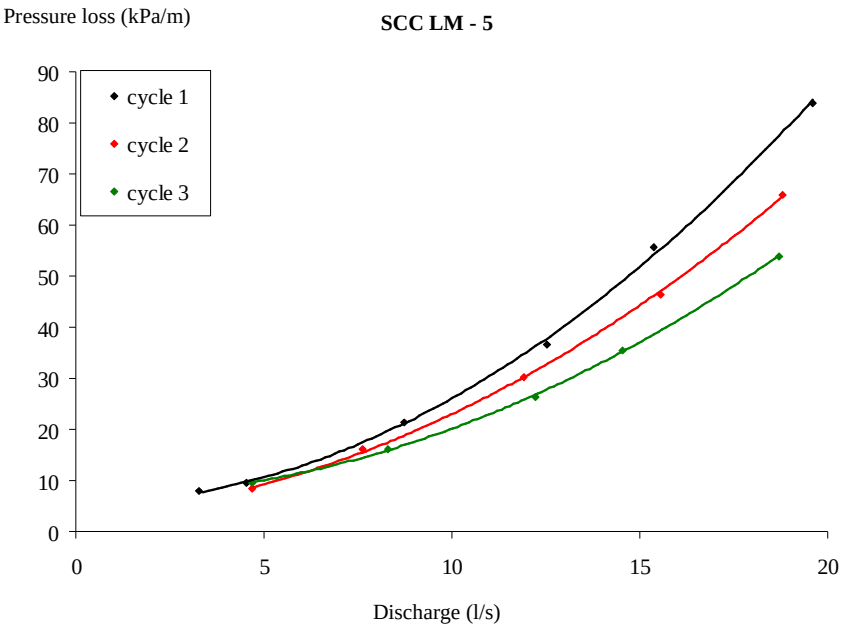
Pressure loss (kPa/m)
SCC LM - 5
cycle 1
cycle 2
cycle 3
90
80
70
60
50
40
30
20
10
0
0
5
10
15
20
Discharge (l/s)

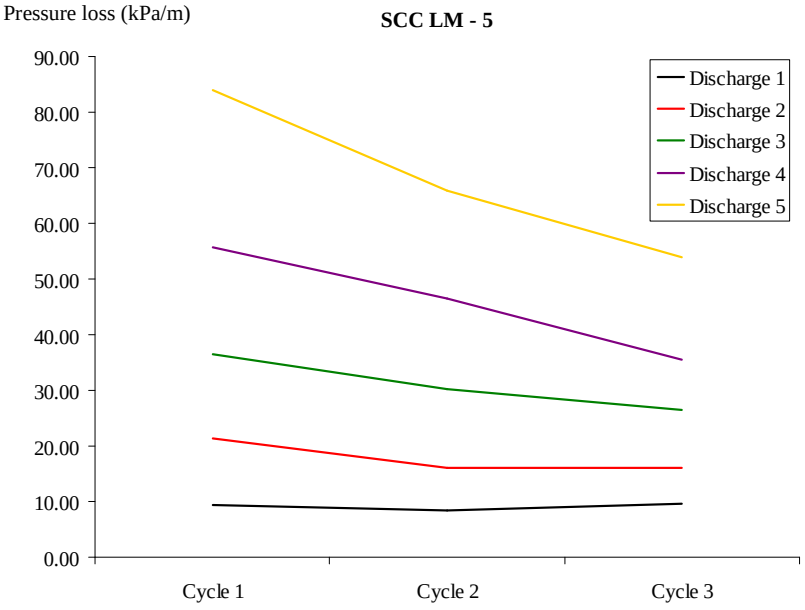
Pressure loss (kPa/m)
SCC LM - 5
Discharge 1
Discharge 2
Discharge 3
Discharge 4
Discharge 5
90.00
80.00
70.00
60.00
50.00
40.00
30.00
20.00
10.00
0.00
Cycle 1
Cycle 2
Cycle 3

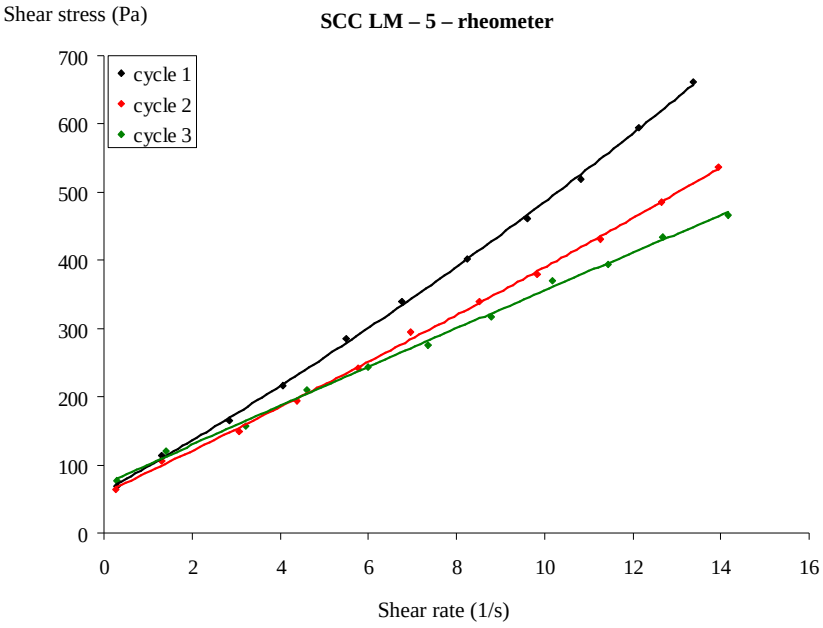
Shear stress (Pa)
SCC LM – 5 – rheometer
cycle 1
cycle 2
cycle 3
700
600
500
400
300
200
100
0
0
2
4
6
8
10
12
14
16
Shear rate (1/s)

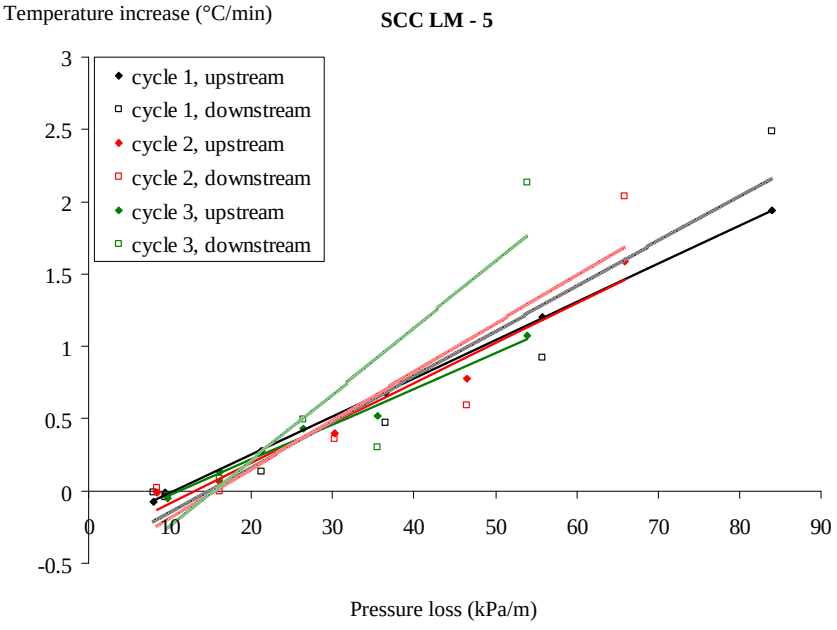
Temperature increase (°C/min)
SCC LM - 5
cycle 1, upstream
cycle 1, downstream
cycle 2, upstream
cycle 2, downstream
cycle 3, upstream
cycle 3, downstream
3
2.5
2
1.5
1
0.5
0
-0.5
0
10
20
30
40
50
60
70
80
90
Pressure loss (kPa/m)

2.7 SCC LM-6

	SCC-LM-6		
	Cycle 1	**Cycle 2**	**Cycle 3**
Concrete Age (min)	**75**	**105**	**135**
Tests on fresh SCC			
Slump flow (mm)	735		687.5
V-Funnel (s)	5.6		3.4
L-box (-)	0.99		1
Vol. Mass (kg/m³)	2398		
Sieve Stability (%)	11.1		14.2
Air Content (%)	-		
Rheometer tests			
Yield stress (Pa)	*10.8*	*0.1*	*8.0*
Viscosity at 0/s (Pa s)	*17.9*	*15.0*	*9.4*
shear thickening (c/mu)	*0.042*	*0.031*	*0.054*
Viscosity at 5/s (Pa s)	*25.5*	*19.7*	*14.5*
Torque at max. vel (Nm)	2.85	2.01	1.62
Max. torque (thixo)(Nm)	3.63	2.81	2.26

Pressure loss (kPa/m)			
Discharge 1	11.17	9.31	12.20
Discharge 2	17.05	14.05	18.58
Discharge 3	28.02	21.39	29.16
Discharge 4	38.94	32.28	38.93
Discharge 5	53.54	41.78	49.68

Remark: Before pouring the concrete in the pump, the reservoir of the pump has not been sprayed with oil.

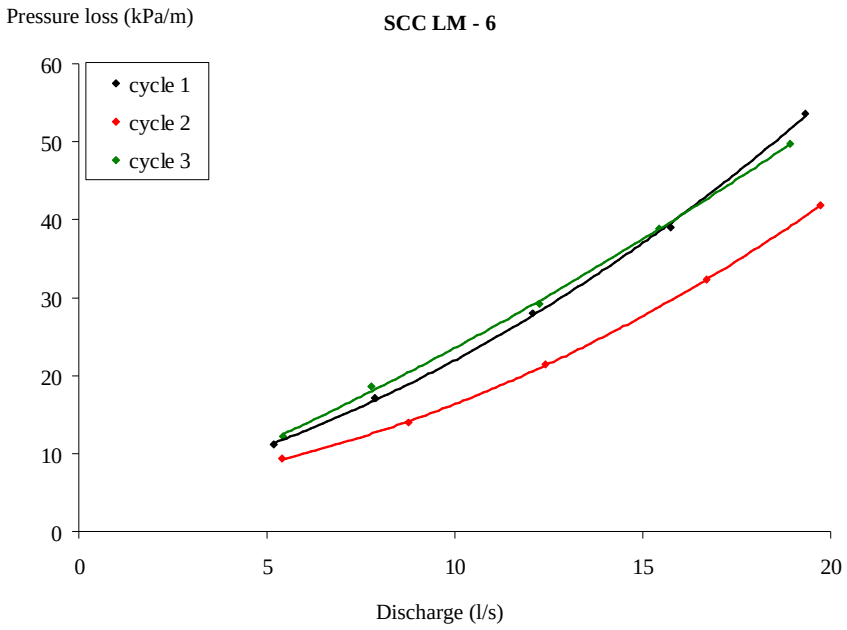
Pressure loss (kPa/m)
SCC LM - 6
cycle 1
cycle 2
cycle 3
60
50
40
30
20
10
0
0
5
10
15
20
Discharge (l/s)

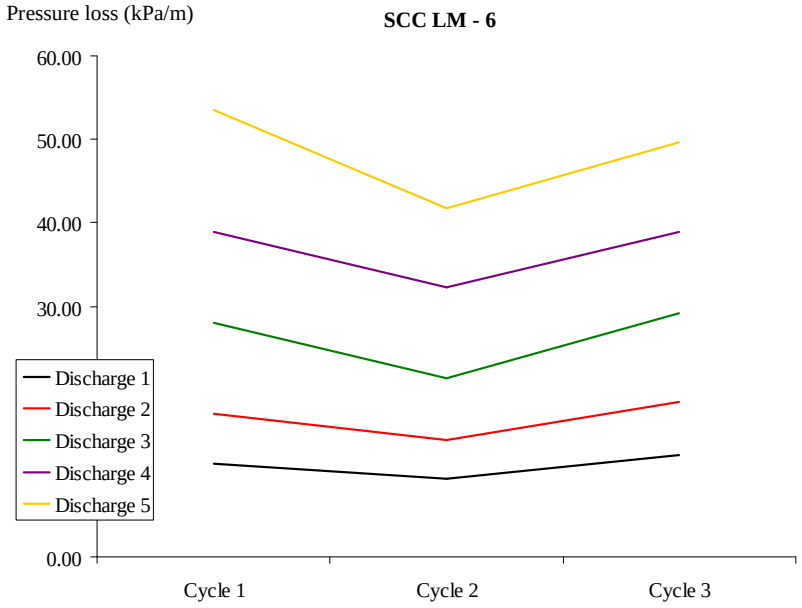
Pressure loss (kPa/m)
SCC LM - 6
60.00
50.00
40.00
30.00
0.00
Discharge 1
Discharge 2
Discharge 3
Discharge 4
Discharge 5
Cycle 1
Cycle 2
Cycle 3

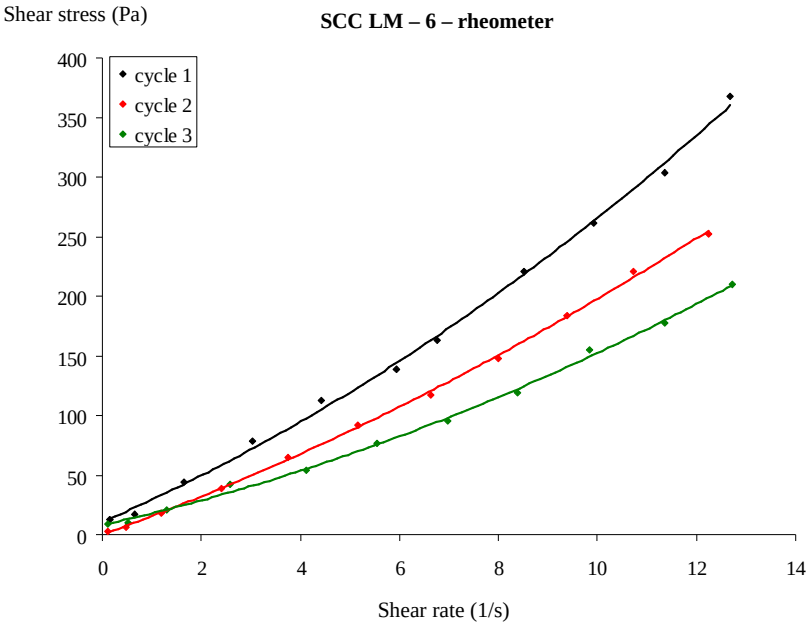
Shear stress (Pa)
SCC LM – 6 – rheometer
cycle 1
cycle 2
cycle 3
400
350
300
250
200
150
100
50
0
0
2
4
6
8
10
12
14
Shear rate (1/s)

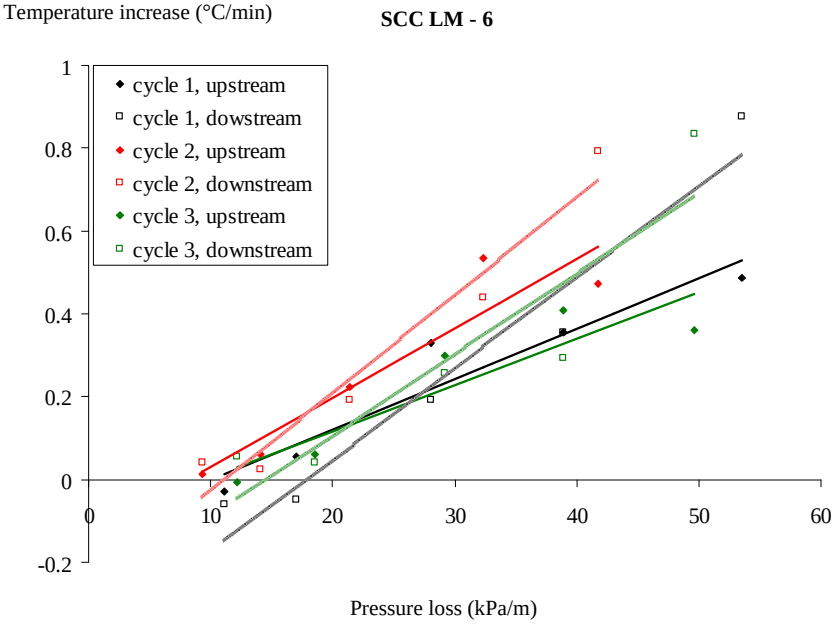
Temperature increase (°C/min)
SCC LM - 6
cycle 1, upstream
cycle 1, dowstream
cycle 2, upstream
cycle 2, downstream
cycle 3, upstream
cycle 3, downstream
1
0.8
0.6
0.4
0.2
0
-0.2
0
10
20
30
40
50
60
Pressure loss (kPa/m)

2.8 SCC LM-7

	SCC-LM-7			
	Cycle 1	**Cycle 2**	**Cycle 3**	**Cycle 4**
Concrete Age (min)	**60**	**90**	**120**	**150**
Tests on fresh SCC				
Slump flow (mm)	770		695	710
V-Funnel (s)	4.6		3.0	3.5
L-box (-)	0.98		0.91	0.93
Density (kg/m^3)	2375			
Sieve Stability (%)	10.2			9.4
Air Content (%)	1.8			
Rheometer tests				
Yield stress (Pa)	39.7	18.4	31.2	29.4
Viscosity at 0/s (Pa s)	25.1	17.2	16.4	14.7
shear thickening (c/mu)	0.018	0.031	0.023	0.021
Viscosity at 5/s (Pa s)	29.5	22.6	20.1	17.8
Torque at max. vel (Nm)	3.43	2.56	2.40	2.10
Max. torque (thixo)(Nm)	4.10	2.87	3.11	2.41

Pressure loss (kPa/m)				
Discharge 1	10.20	9.51	7.45	8.67
Discharge 2	15.61	15.79	11.66	13.79
Discharge 3	25.86	26.14	20.57	21.09
Discharge 4	35.51	36.02	30.49	29.66
Discharge 5	52.54	48.71	40.76	39.98

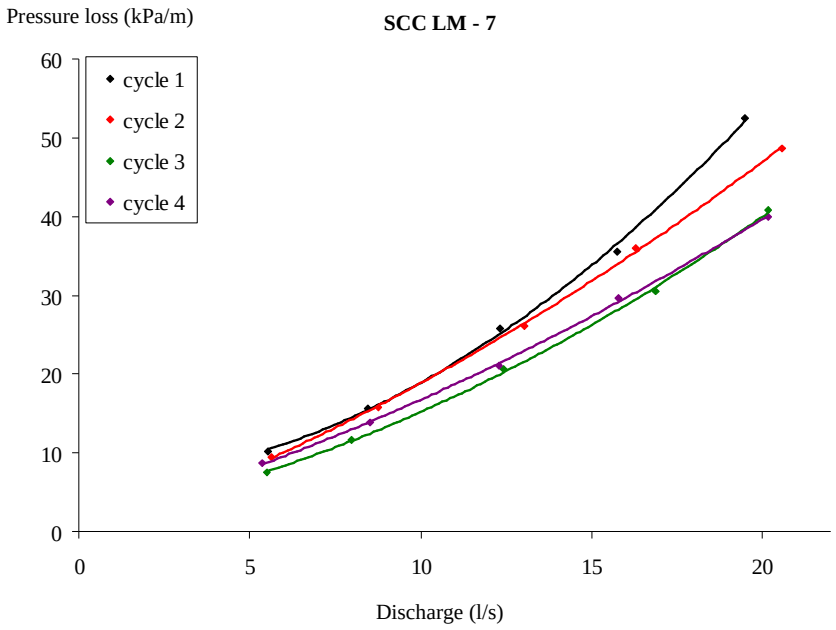
Pressure loss (kPa/m)
SCC LM - 7
cycle 1
cycle 2
cycle 3
cycle 4
60
50
40
30
20
10
0
0
5
10
15
20
Discharge (l/s)

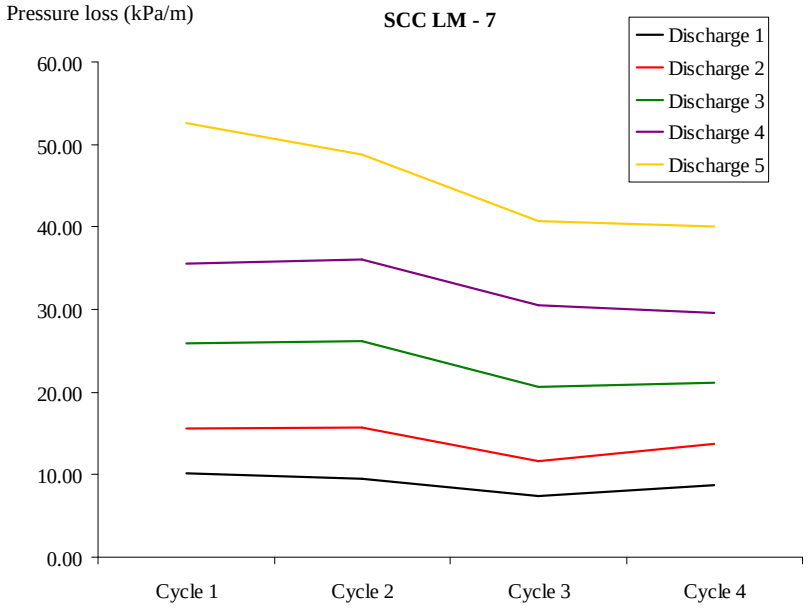
Pressure loss (kPa/m)
SCC LM - 7
Discharge 1
Discharge 2
Discharge 3
Discharge 4
Discharge 5
60.00
50.00
40.00
30.00
20.00
10.00
0.00
Cycle 1
Cycle 2
Cycle 3
Cycle 4

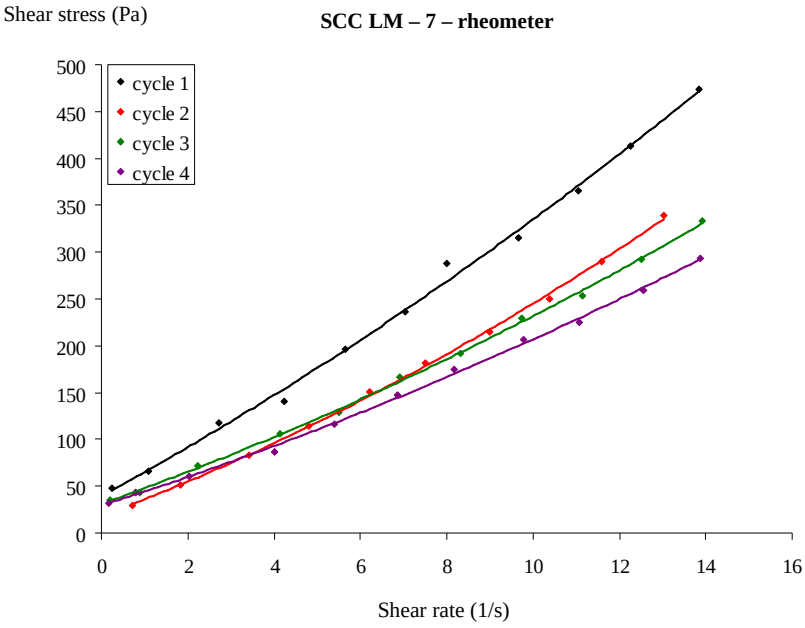
Shear stress (Pa)
SCC LM – 7 – rheometer
cycle 1
cycle 2
cycle 3
cycle 4
500
450
400
350
300
250
200
150
100
50
0
0
2
4
6
8
10
12
14
16
Shear rate (1/s)

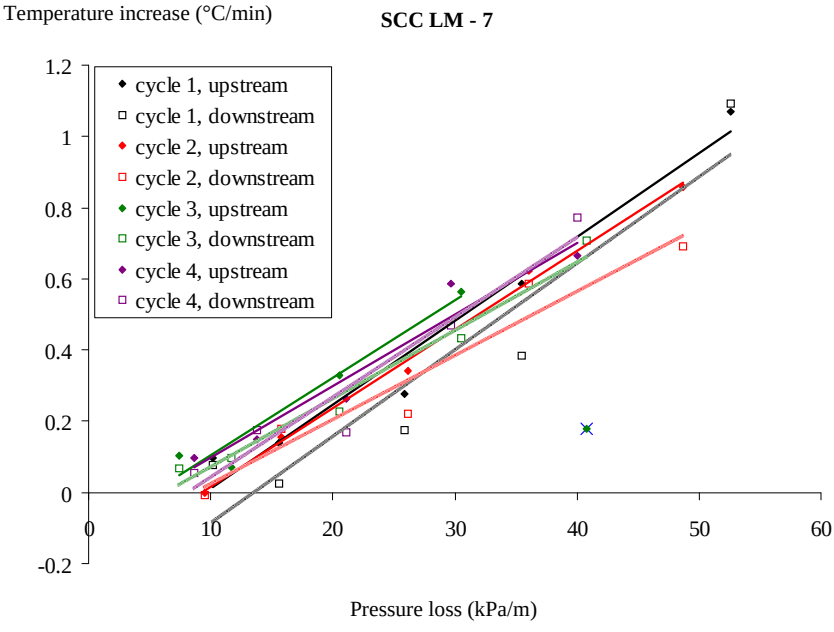
Temperature increase (°C/min)
SCC LM - 7
cycle 1, upstream
cycle 1, downstream
cycle 2, upstream
cycle 2, downstream
cycle 3, upstream
cycle 3, downstream
cycle 4, upstream
cycle 4, downstream
1.2
1
0.8
0.6
0.4
0.2
0
-0.2
0
10
20
30
40
50
60
Pressure loss (kPa/m)

2.9 SCC LM-8

	SCC-LM-8					
	Cycle 1	**Cycle 2**	**Cycle 3**	**Cycle 4**	**Cycle 5**	**Cycle 6**
Concrete Age (min)	**60**	**90**	**120**	**150**	**180**	**210**
Tests on fresh SCC						
Slump flow (mm)	790		740		692.5	570
V-Funnel (s)	2.8		3.4		3.1	3.5
L-box (-)	1.00		1.02		0.83	0.65
Density (kg/m³)	2350					
Sieve Stability (%)	24.4					8.0
Air Content (%)	1.1					
Rheometer tests						
Yield stress (Pa)	29.8	*10.1*	19.3	*21.8*	21.4	50.0
Viscosity at 0/s (Pa s)	15.6	*12.6*	19.4	*3.5*	9.4	16.2
shear thickening (c/mu)	0.056	*0.029*	0.024	*0.134*	0.033	0.000
Viscosity at 5/s (Pa s)	24.3	*16.3*	24.1	*8.2*	12.5	16.2
Torque at max. vel (Nm)	3.08	1.74	2.76	1.17	1.50	1.92
Max. torque (thixo)(Nm)	3.80	2.02	3.81	1.54	1.67	2.14

Pressure loss (kPa/m)						
Discharge 1	7.84	8.02	6.91	7.59	7.63	6.74
Discharge 2	11.20	11.06	10.13	10.64	11.65	11.13
Discharge 3	18.11	20.88	16.51	17.09	16.55	18.30
Discharge 4	29.47	28.64	24.23	24.83	24.42	27.36
Discharge 5	43.03	39.94	32.89	31.81	33.87	37.11

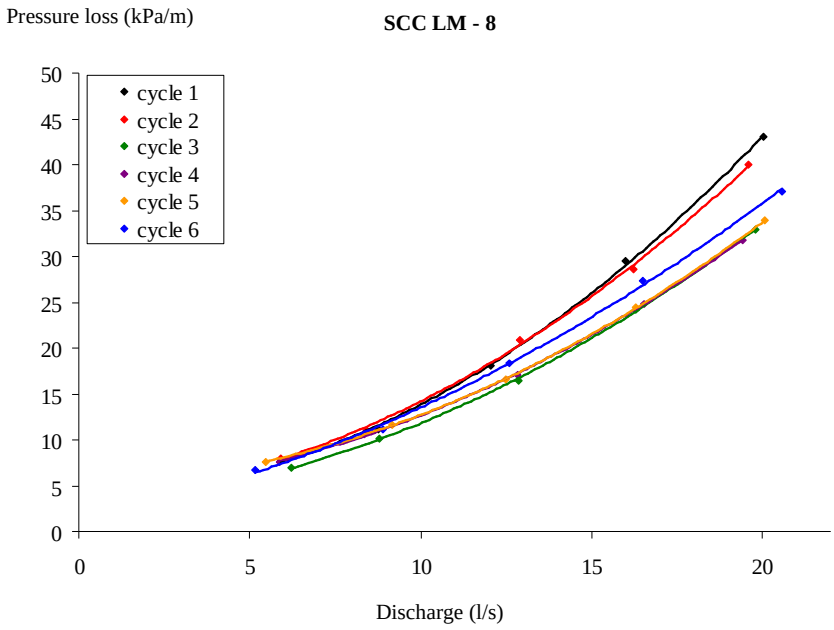
Pressure loss (kPa/m)
SCC LM - 8
cycle 1
cycle 2
cycle 3
cycle 4
cycle 5
cycle 6
50
45
40
35
30
25
20
15
10
5
0
0
5
10
15
20
Discharge (l/s)

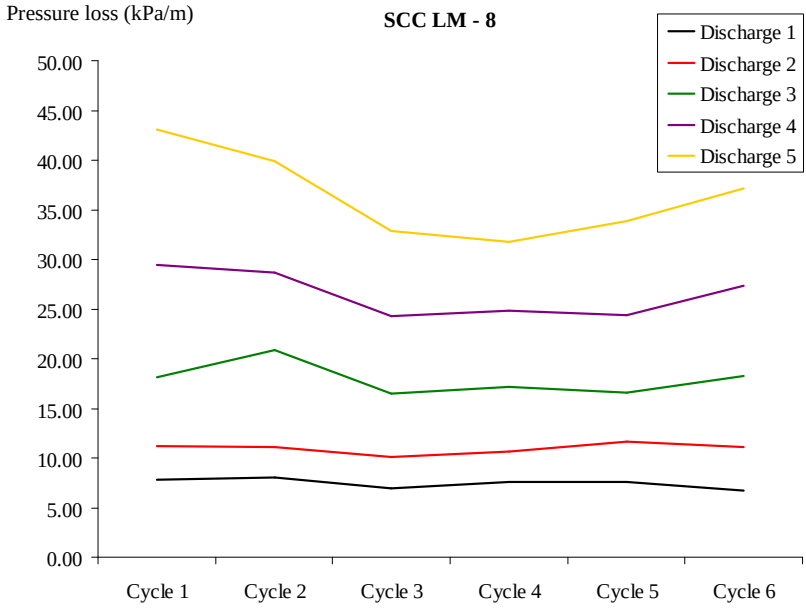
Pressure loss (kPa/m)
SCC LM - 8
Discharge 1
Discharge 2
Discharge 3
Discharge 4
Discharge 5
50.00
45.00
40.00
35.00
30.00
25.00
20.00
15.00
10.00
5.00
0.00
Cycle 1
Cycle 2
Cycle 3
Cycle 4
Cycle 5
Cycle 6

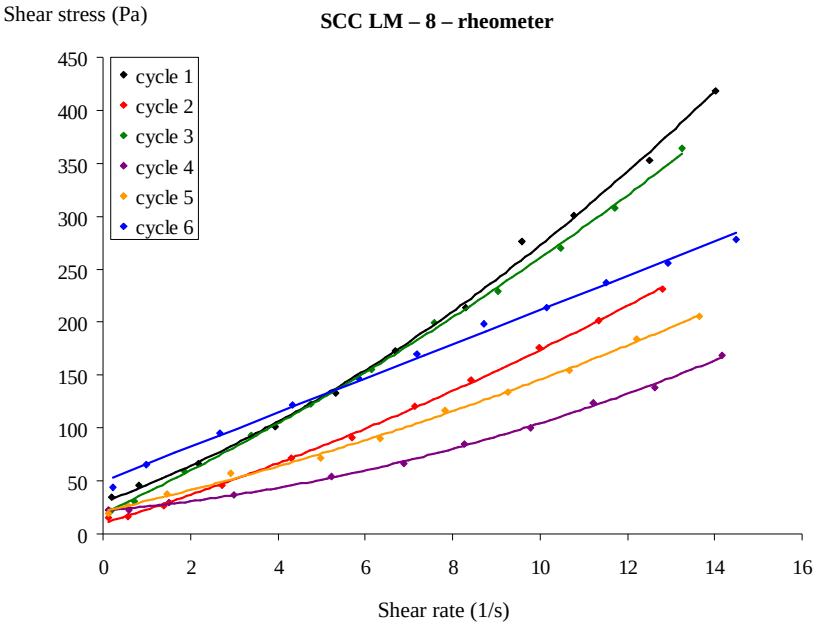
Shear stress (Pa)
SCC LM – 8 – rheometer
cycle 1
cycle 2
cycle 3
cycle 4
cycle 5
cycle 6
450
400
350
300
250
200
150
100
50
0
0
2
4
6
8
10
12
14
16
Shear rate (1/s)

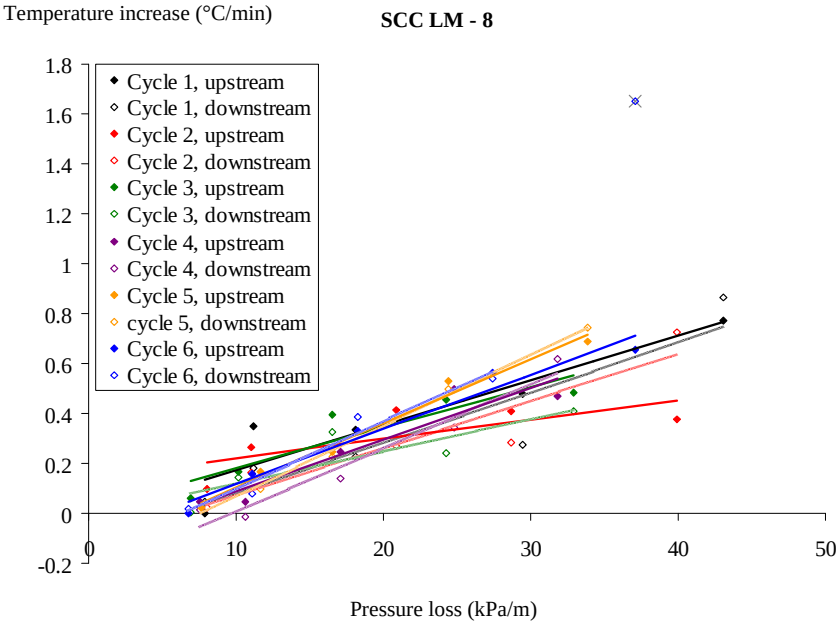
Temperature increase (°C/min)
SCC LM - 8
Cycle 1, upstream
Cycle 1, downstream
Cycle 2, upstream
Cycle 2, downstream
Cycle 3, upstream
Cycle 3, downstream
Cycle 4, upstream
Cycle 4, downstream
Cycle 5, upstream
cycle 5, downstream
Cycle 6, upstream
Cycle 6, downstream
1.8
1.6
1.4
1.2
1
0.8
0.6
0.4
0.2
0
-0.2
0
10
20
30
40
50
Pressure loss (kPa/m)

2.10 TC-1

	TC-OBC-1		
	Cycle 1	**Cycle 3**	**Cycle 3**
Concrete Age (min)	**120**	**165**	**165**
	no pump	**no pump**	**pump**
Tests on fresh concrete			
Slump (mm)	190		240
Flow table (mm)	645		775
Walz (-)	1.011		1.003
Density (kg/m³)	2263		2350
Air Content (%)			5.2
Rheometer tests			
Yield stress (Pa)	310.0	329.1	122.7
Viscosity at 0/s (Pa s)	32.6	34.4	15.2
shear thickening (c/mu)			
Viscosity at 5/s (Pa s)	32.6	34.4	15.2
Torque at max. vel (Nm)	5.11	5.50	2.26
Max. torque (thixo)(Nm)	7.78	11.90	2.73

Pressure loss (kPa/m)	**pump**		**pump**
Discharge 1	10.59		4.70
Discharge 2	13.12		9.22
Discharge 3	18.27		15.64
Discharge 4	24.09		21.79
Discharge 5	29.79		28.39

Remarks: The columns with “pump” and “no pump” indicate whether the concrete has been pumped or not. For cycle 1, the rheometer test and tests on fresh concrete have been executed on non-pumped concrete, as it is always the case for the regular tests.
Cycle 2 has been cancelled due to a lack of time. Instead, cycle 3 has been performed 45 minutes after cycle 1.

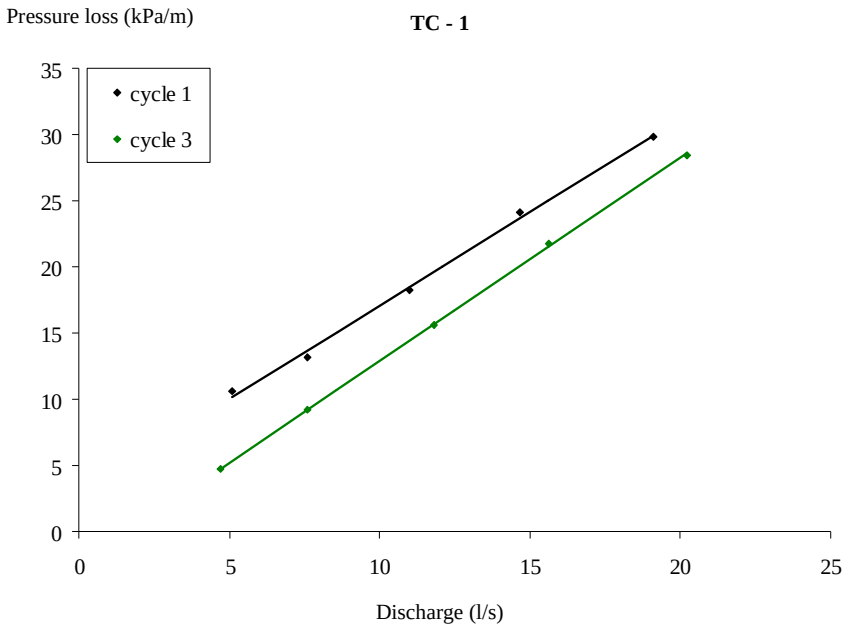
Pressure loss (kPa/m)
TC - 1
cycle 1
cycle 3
35
30
25
20
15
10
5
0
0
5
10
15
20
25
Discharge (l/s)

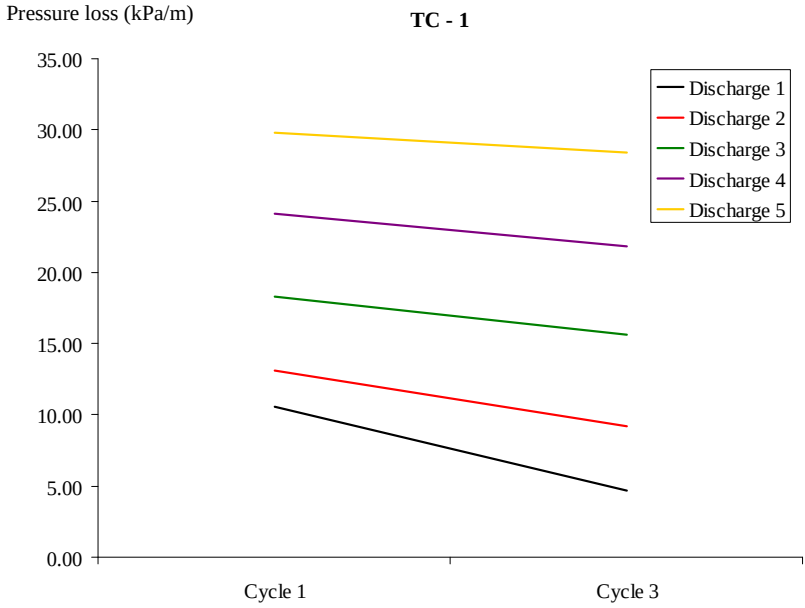
Pressure loss (kPa/m)
TC - 1
Discharge 1
Discharge 2
Discharge 3
Discharge 4
Discharge 5
35.00
30.00
25.00
20.00
15.00
10.00
5.00
0.00
Cycle 1
Cycle 3

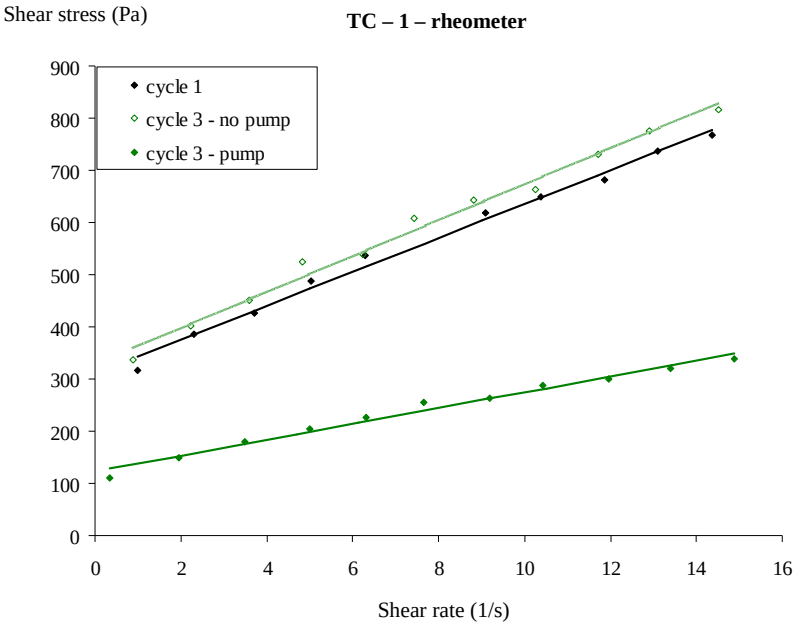
Shear stress (Pa)
TC – 1 – rheometer
cycle 1
cycle 3 - no pump
cycle 3 - pump
900
800
700
600
500
400
300
200
100
0
0
2
4
6
8
10
12
14
16
Shear rate (1/s)

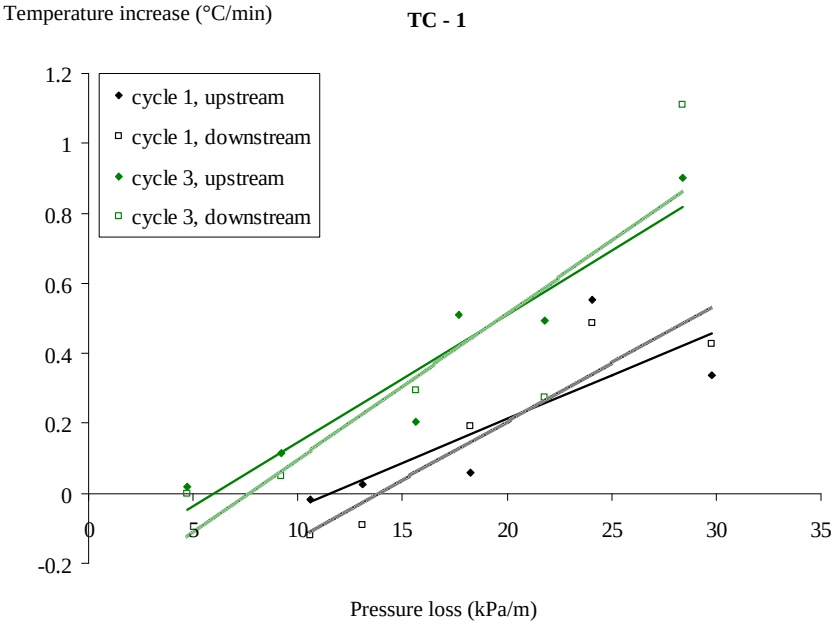
Temperature increase (°C/min)
TC - 1
cycle 1, upstream
cycle 1, downstream
cycle 3, upstream
cycle 3, downstream
1.2
1
0.8
0.6
0.4
0.2
0
-0.2
0
5
10
15
20
25
30
35
Pressure loss (kPa/m)

2.11 SCC LM-9

	SCC-LM-9			
	Cycle 1	**Cycle 1**	**Cycle 3**	**Cycle 3**
Concrete Age (min)	**60**	**60**	**105**	**105**
	no pump	**pump**	**no pump**	**pump**
Tests on fresh SCC				
Slump flow (mm)	940			795
V-Funnel (s)	2.3			3.5
L-box (-)	1.02			0.99
Density (kg/m³)	2375			2363
Sieve Stability (%)	31.9			19.1
Air Content (%)	1			
Rheometer tests				
Yield stress (Pa)	-	-	*10.5*	*11.9*
Viscosity at 0/s (Pa s)	-	-	*5.1*	*0.6*
shear thickening (c/mu)	-	-	*0.027*	*0.484*
Viscosity at 5/s (Pa s)	-	-	*6.5*	*3.6*
Torque at max. vel (Nm)	0.33	*0.01*	0.32	0.29
Max. torque (thixo)(Nm)	0.43	*0.01*	0.50	0.49

Pressure loss (kPa/m)				
Discharge 1		3.83		7.70
Discharge 2		4.67		9.45
Discharge 3		10.15		14.64
Discharge 4		20.32		18.72
Discharge 5		34.81		25.61

Remarks: Severely segregating SCC.
The columns with “pump” and “no pump” indicate whether the concrete has been pumped or not. For cycle 1, the rheometer test and tests on fresh concrete have been executed on non-pumped concrete, as it is always the case for the regular tests.
Cycle 2 has been cancelled due to a lack of time. Instead, cycle 3 has been performed 45 minutes after cycle 1.

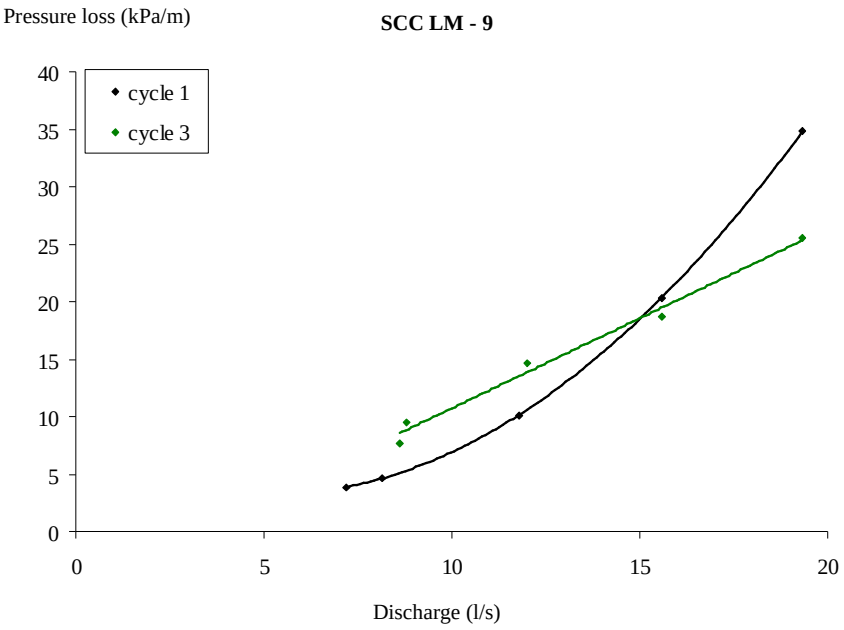
Pressure loss (kPa/m)
SCC LM - 9
cycle 1
cycle 3
40
35
30
25
20
15
10
5
0
0
5
10
15
20
Discharge (l/s)

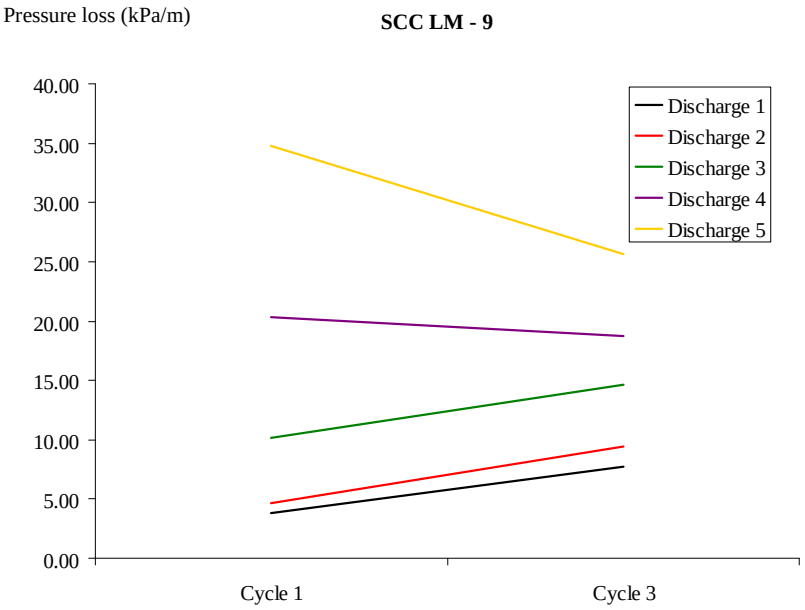
Pressure loss (kPa/m)
SCC LM - 9
Discharge 1
Discharge 2
Discharge 3
Discharge 4
Discharge 5
40.00
35.00
30.00
25.00
20.00
15.00
10.00
5.00
0.00
Cycle 1
Cycle 3

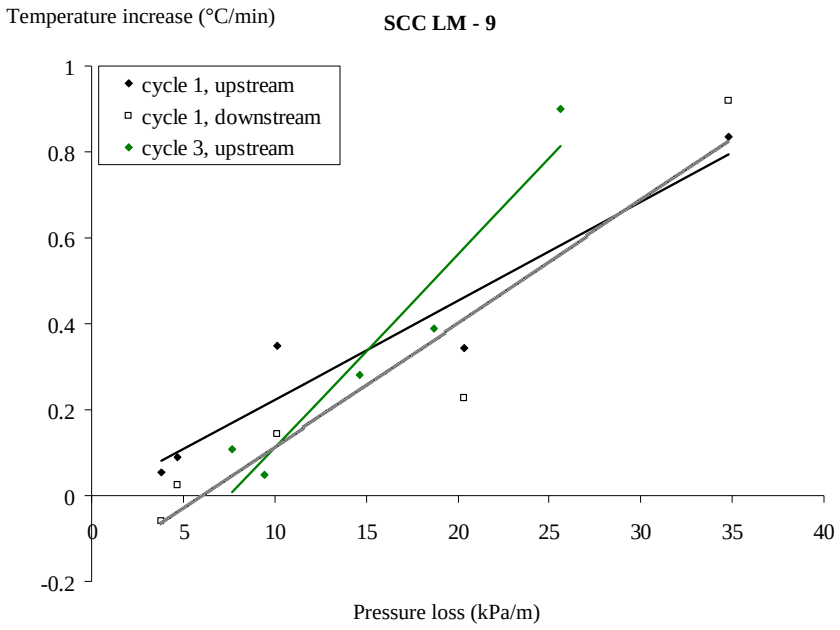
Temperature increase (°C/min)
SCC LM - 9
cycle 1, upstream
cycle 1, downstream
cycle 3, upstream
1
0.8
0.6
0.4
0.2
0
-0.2
0
5
10
15
20
25
30
35
40
Pressure loss (kPa/m)

2.12 SCC LM-10

	SCC-LM-10							
	Cycle 1	**Cycle 2**	**Cycle 3**	**Cycle 4**	**Cycle 5**	**Cycle 6**	**Cycle 7**	**Cycle 8**
Concrete Age (min)	**60**	**90**	**120**	**150**	**180**	**210**	**240**	**270**
Tests on fresh SCC	**pumped concrete**							
Slump flow (mm)	740		830		765		685	
V-Funnel (s)	4.2		2.5		2.5		2.5	
L-box (-)	0.96		0.97		0.93		0.81	
Density (kg/m³)	2350		2375		2331		2281	
Sieve Stability (%)	16.7						23.6	
Air Content (%)	0.5						3.5	
Rheometer tests	**pumped concrete**							
Torque at max. vel (Nm)	0.84	0.52	0.40	0.31	0.42	0.41	0.47	0.65
Max. torque (thixo)(Nm)	1.16	0.80	0.71	0.40	0.51	0.48	0.54	0.76
Rheometer tests	**not pumped concrete**							
Torque at max. vel (Nm)	0.37	0.45	0.56	0.79	0.97	1.18	1.50	1.94
Max. torque (thixo)(Nm)	0.42	0.66	0.77	1.36	1.44	1.85	2.03	2.57

Pressure loss (kPa/m)								
Discharge 1	3.44	1.17	1.17	4.01	3.25	2.61	2.34	1.24
Discharge 2	5.20	1.60	1.80	4.10	3.44	2.99	2.73	1.31
Discharge 3	10.82	4.87	3.94	6.22	7.08	7.60	7.72	9.00
Discharge 4	17.80	9.61	9.07	10.98	11.04	11.62	14.57	15.08
Discharge 5	29.62	17.82	14.82	18.67	17.88	19.72	20.89	21.97

Remark: SCC segregating at arrival. Rheometer tests are impossible to be interpreted.

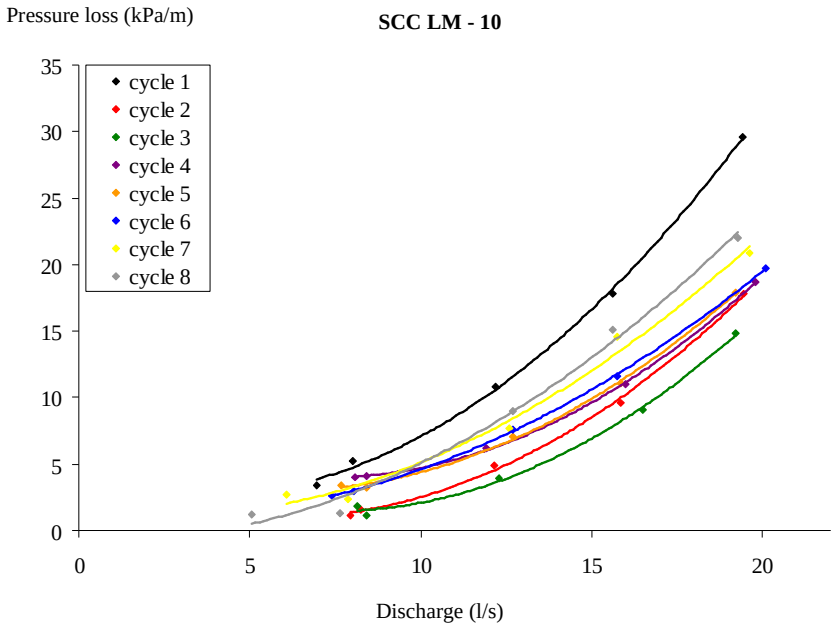
Pressure loss (kPa/m)
SCC LM - 10
cycle 1
cycle 2
cycle 3
cycle 4
cycle 5
cycle 6
cycle 7
cycle 8
35
30
25
20
15
10
5
0
0
5
10
15
20
Discharge (l/s)

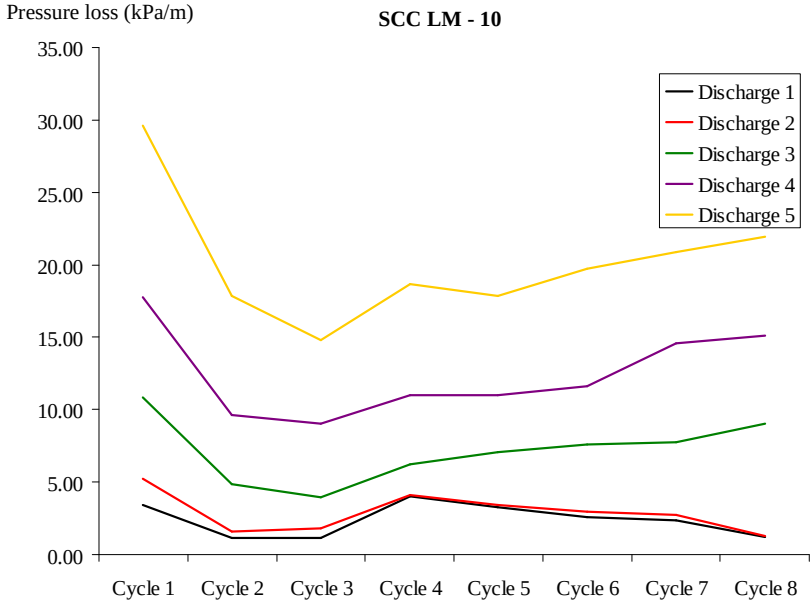
Pressure loss (kPa/m)
SCC LM - 10
Discharge 1
Discharge 2
Discharge 3
Discharge 4
Discharge 5
35.00
30.00
25.00
20.00
15.00
10.00
5.00
0.00
Cycle 1
Cycle 2
Cycle 3
Cycle 4
Cycle 5
Cycle 6
Cycle 7
Cycle 8

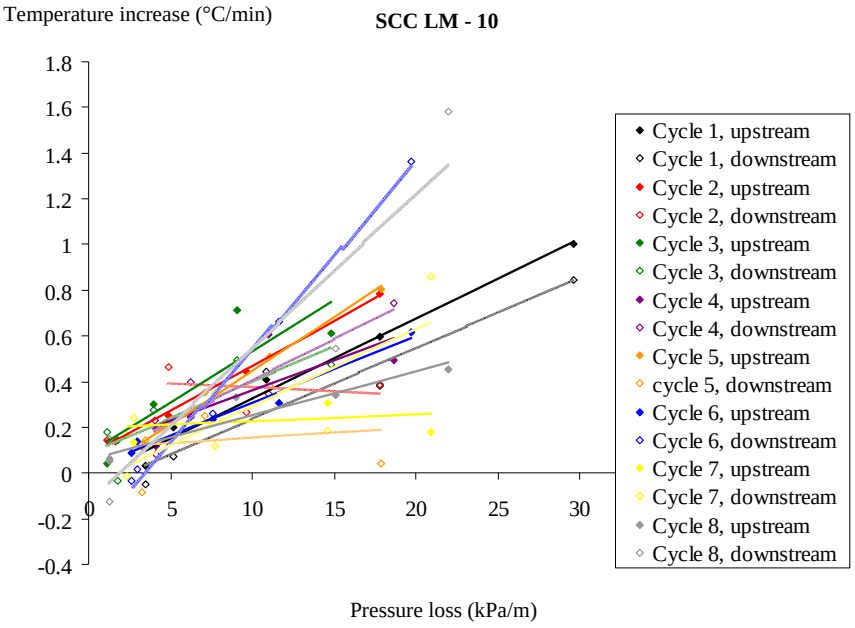
Temperature increase (°C/min)
SCC LM - 10
1.8
1.6
1.4
1.2
1
0.8
0.6
0.4
0.2
0
-0.2
-0.4
0
5
10
15
20
25
30
Pressure loss (kPa/m)
Cycle 1, upstream
Cycle 1, downstream
Cycle 2, upstream
Cycle 2, downstream
Cycle 3, upstream
Cycle 3, downstream
Cycle 4, upstream
Cycle 4, downstream
Cycle 5, upstream
cycle 5, downstream
Cycle 6, upstream
Cycle 6, downstream
Cycle 7, upstream
Cycle 7, downstream
Cycle 8, upstream
Cycle 8, downstream

2.13 SCC LM-11

	SCC-LM-11			
	Cycle 1-1	**Cycle 2**	**Cycle 3**	**Cycle 4**
Tests on fresh SCC	**pumped concrete**			
Slump flow (mm)	465		660	665
V-Funnel (s)	12.1		3.1	3.1
L-box (-)	0.31		0.8	0.74
Density (kg/m³)	2325		2294	2250
Sieve Stability (%)	1.3		20.2	9.7
Air Content (%)	2.7		4	4.9
Rheometer tests	**pumped concrete**			
Yield stress (Pa)	55.7	9.3	22.3	10.9
Viscosity at 0/s (Pa s)	25.5	11.0	14.6	5.1
shear thickening (c/mu)	0.003	0.004	0.000	0.020
Viscosity at 5/s (Pa s)	26.3	11.4	14.6	6.1
Torque at max. vel (Nm)	2.94	1.13	1.60	0.62
Max. torque (thixo)(Nm)	3.89	1.64	1.73	0.68
Rheometer tests	**not pumped concrete**			
Yield stress (Pa)	*2.5*	*4.6*	*11.2*	*10.9*
Viscosity at 0/s (Pa s)	*6.5*	*5.5*	*8.2*	*9.2*
shear thickening (c/mu)	*0.045*	*0.085*	*0.073*	*0.079*
Viscosity at 5/s (Pa s)	*9.4*	*10.2*	*14.2*	*16.5*
Torque at max. vel (Nm)	0.84	1.00	1.54	1.80
Max. torque (thixo)(Nm)	0.92	1.21	2.23	2.58

Pressure loss (kPa/m)				
Discharge 1	17.89	9.87	7.94	
Discharge 2	27.90	16.62	14.50	
Discharge 3	47.03	27.58	25.41	
Discharge 4	70.30	38.13	35.40	
Discharge 5	96.15	53.76	49.57	

Remarks: The “not-pumped” sample in the rheometer is not representative for the concrete. Only a qualitative comparison can be made.
Cycle 1 consists of three curves: Down from 5 to 1, up from 1 to 5 and down from 5 to 1 again. In the table, only the pressure losses of the first down-curve are given. The other curves are shown in the pressure loss – discharge figure.

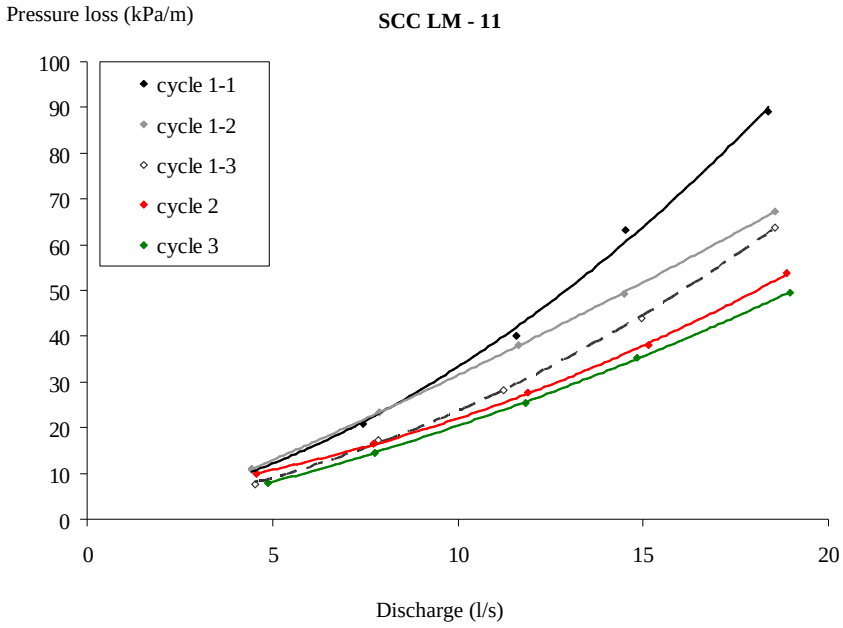
Pressure loss (kPa/m)
SCC LM - 11
cycle 1-1
cycle 1-2
cycle 1-3
cycle 2
cycle 3
100
90
80
70
60
50
40
30
20
10
0
0
5
10
15
20
Discharge (l/s)

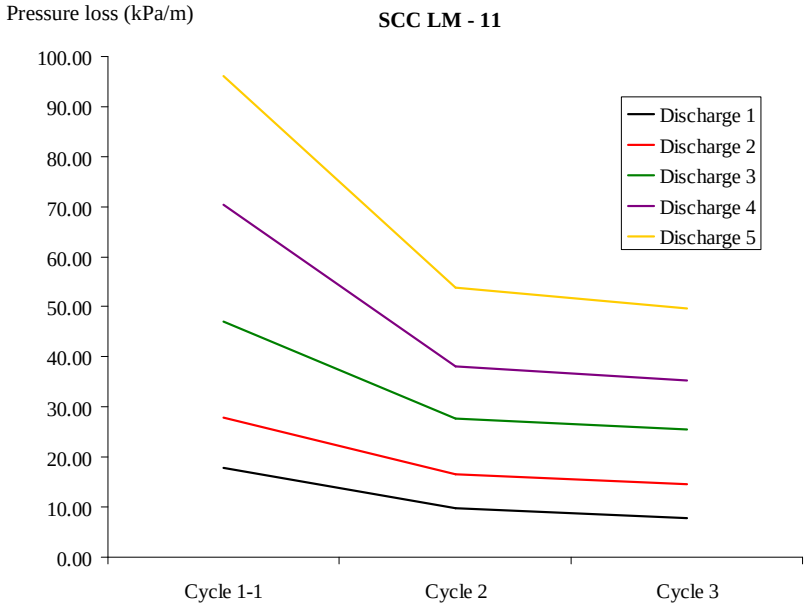
Pressure loss (kPa/m)
SCC LM - 11
Discharge 1
Discharge 2
Discharge 3
Discharge 4
Discharge 5
100.00
90.00
80.00
70.00
60.00
50.00
40.00
30.00
20.00
10.00
0.00
Cycle 1-1
Cycle 2
Cycle 3

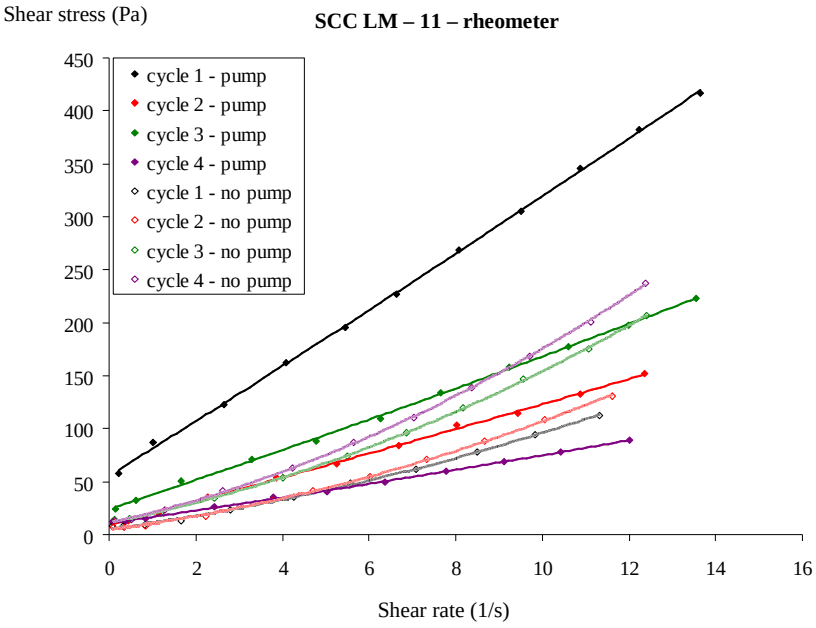
Shear stress (Pa)
SCC LM – 11 – rheometer
cycle 1 - pump
cycle 2 - pump
cycle 3 - pump
cycle 4 - pump
cycle 1 - no pump
cycle 2 - no pump
cycle 3 - no pump
cycle 4 - no pump
450
400
350
300
250
200
150
100
50
0
0
2
4
6
8
10
12
14
16
Shear rate (1/s)

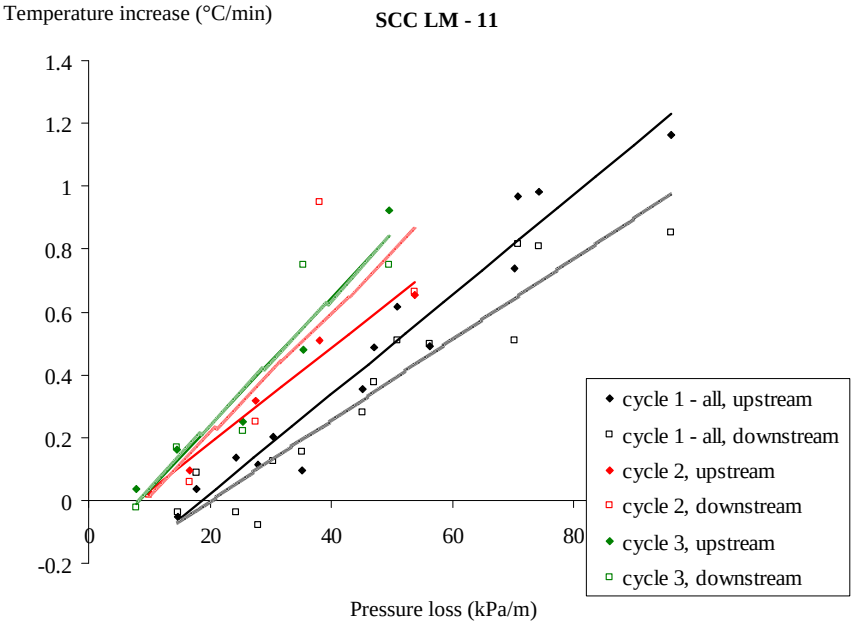
Temperature increase (°C/min)
SCC LM - 11
1.4
1.2
1
0.8
0.6
0.4
0.2
0
-0.2
0
20
40
60
80
cycle 1 - all, upstream
cycle 1 - all, downstream
cycle 2, upstream
cycle 2, downstream
cycle 3, upstream
cycle 3, downstream
Pressure loss (kPa/m)

2.14 SCC LM-13

	SCC-LM-13		
	Cycle 1	**Cycle 2**	**Cycle 3**
Tests on fresh SCC			
Slump flow (mm)	820	865	750
V-Funnel (s)	2.0	1.9	2.0
L-box (-)	1.00	1.06	1.00
Density (kg/m³)	2375	2281	2325
Sieve Stability (%)	14.2	9.2	11.5
Air Content (%)	0.9	1.9	2.3
Rheometer tests			
Yield stress (Pa)	*4.6*	-	*6.7*
Viscosity at 0/s (Pa s)	*9.5*	-	*2.3*
shear thickening (c/mu)	*0.025*	-	*0.091*
Viscosity at 5/s (Pa s)	*11.9*	-	*4.4*
Torque at max. vel (Nm)	1.18	0.21	0.33
Max. torque (thixo)(Nm)	1.27	0.22	0.42

Pressure loss (kPa/m)			
Discharge 1	8.42	5.52	3.86
Discharge 2	9.06	5.69	3.95
Discharge 3	13.61	8.25	6.53
Discharge 4	18.82	12.46	9.32
Discharge 5	26.34	16.74	13.33
Discharge 6		21.99	18.33

Remarks: The SCC is segregating in the rheometer, making measurements and interpretations very difficult.
Cycle 1 consists of three curves: Down from 5 to 1, up from 1 to 5 and down from 5 to 1 again. In the table, only the pressure losses of the first down-curve are given. The other curves are shown in the pressure loss – discharge figure.

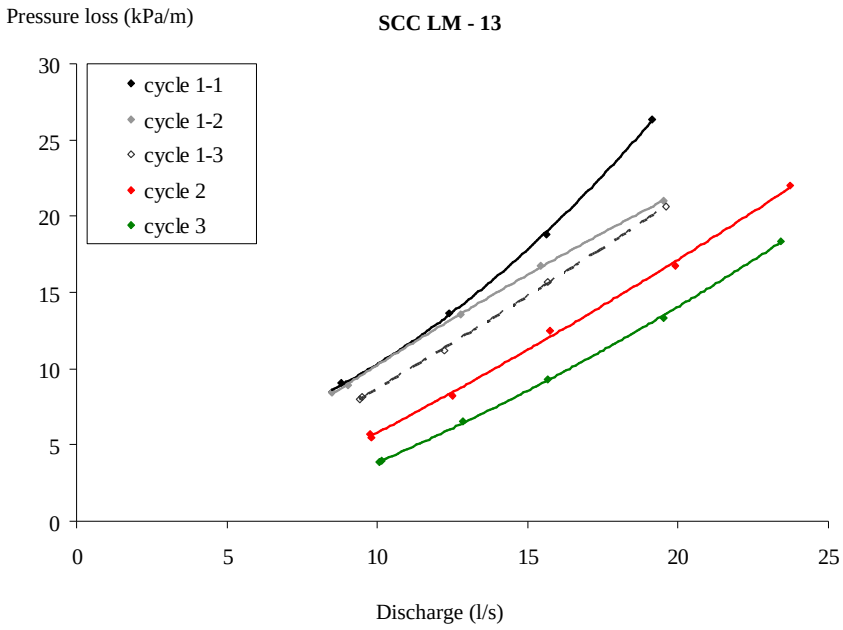
Pressure loss (kPa/m)
SCC LM - 13
cycle 1-1
cycle 1-2
cycle 1-3
cycle 2
cycle 3
30
25
20
15
10
5
0
0
5
10
15
20
25
Discharge (l/s)

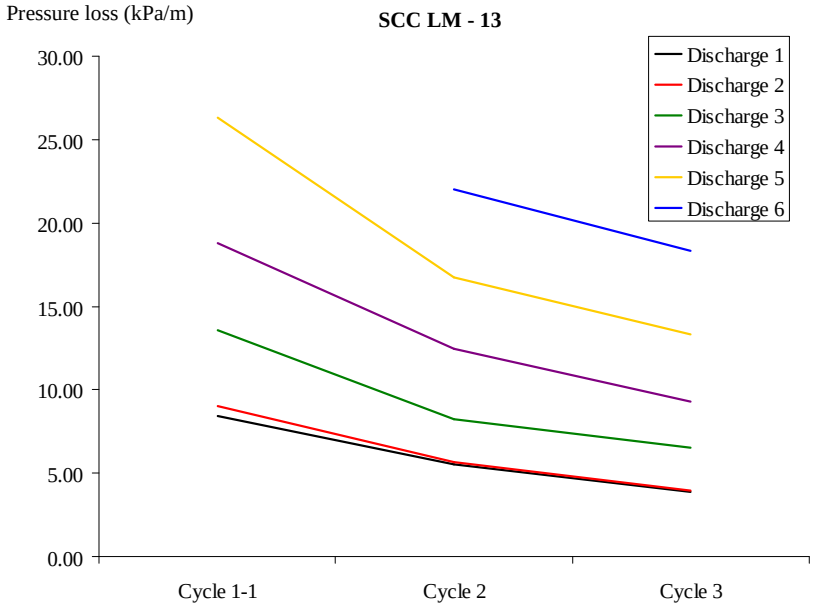
Pressure loss (kPa/m)
SCC LM - 13
Discharge 1
Discharge 2
Discharge 3
Discharge 4
Discharge 5
Discharge 6
30.00
25.00
20.00
15.00
10.00
5.00
0.00
Cycle 1-1
Cycle 2
Cycle 3

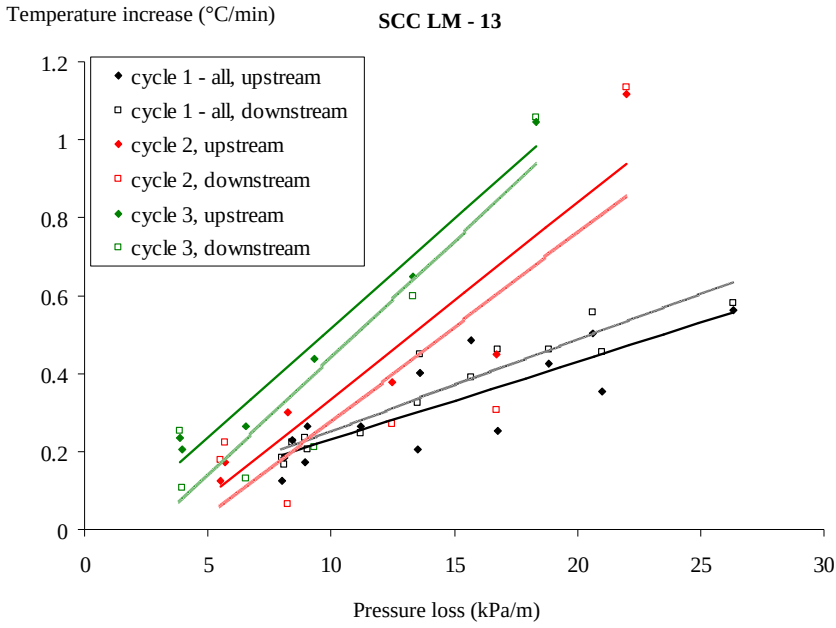
Temperature increase (°C/min)
SCC LM - 13
cycle 1 - all, upstream
cycle 1 - all, downstream
cycle 2, upstream
cycle 2, downstream
cycle 3, upstream
cycle 3, downstream
1.2
1
0.8
0.6
0.4
0.2
0
0
5
10
15
20
25
30
Pressure loss (kPa/m)

2.15 SCC LM-12

	LM-12					
	Q0 before	**Q1**	**Q2**	**Q3**	**Q4**	**Q5**
Tests on fresh SCC						
Slump flow (mm)	775	735	725	755	735	645
V-Funnel (s)	2.76	3.16	3.07	2.34	2.23	2.09
L-box (-)	0.90					0.83
Density (kg/m³)	2325	2331	2331	2331	2306	2325
Sieve Stability (%)	8.2	12.3	8.1	12.3	12.9	9.4
Air content (%)	2.1	2.4	2.7	2.8	2.8	3.2
Rheometer tests						
Yield stress (Pa)	*0.4*	5.0	14.6	8.9	*7.3*	11.6
Viscosity at 0/s (Pa s)	*6.1*	11.7	9.4	10.6	*4.8*	6.4
shear thickening (c/visco)	*0.028*	0.000	0.000	0.000	*0.000*	0.000
Viscosity at 5/s (Pa s)	*7.8*	11.7	9.4	10.6	*4.8*	6.4
Torque at max. velocity (Nm)	0.66	1.11	1.46	1.04	0.4	0.62
Max Torque: thixo (Nm)	0.73	1.25	1.55	1.21	0.45	0.67

Remark: SCC subjected to special thixotropy-test. The samples are taken, according to the scheme in chapter 8, after reaching equilibrium at discharge "x", indicated by the number Qx. Test Q0 indicates that the concrete has not been pumped.

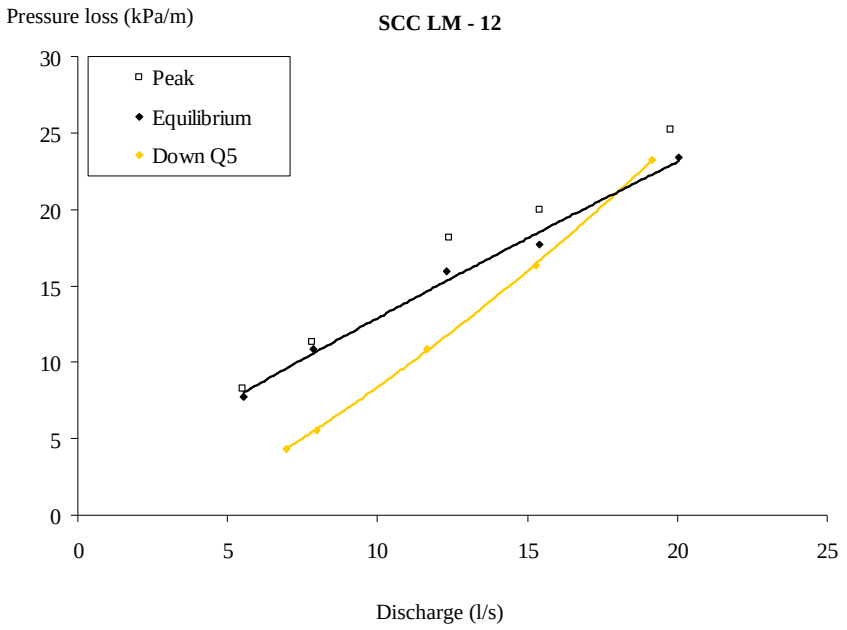

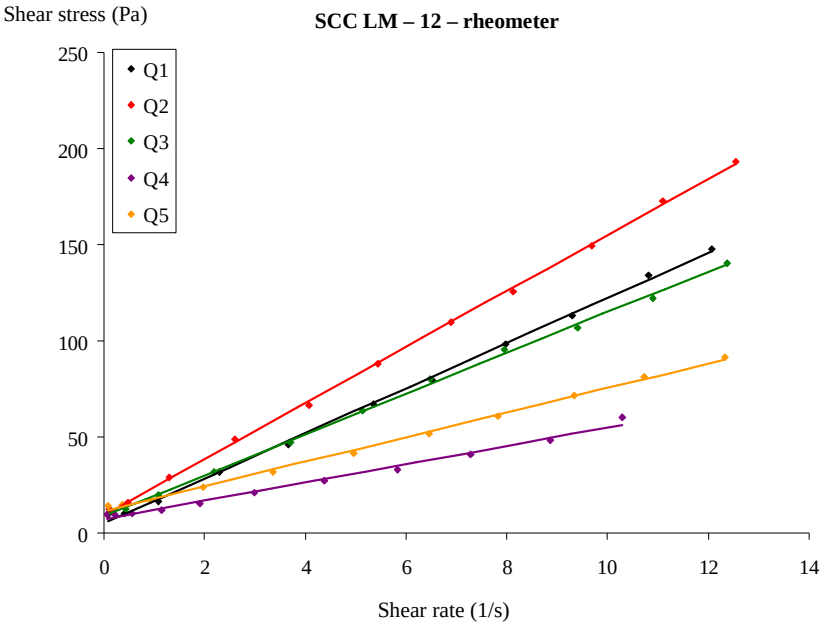
Shear stress (Pa)
SCC LM – 12 – rheometer
Q1
Q2
Q3
Q4
Q5
250
200
150
100
50
0
0
2
4
6
8
10
12
14
Shear rate (1/s)

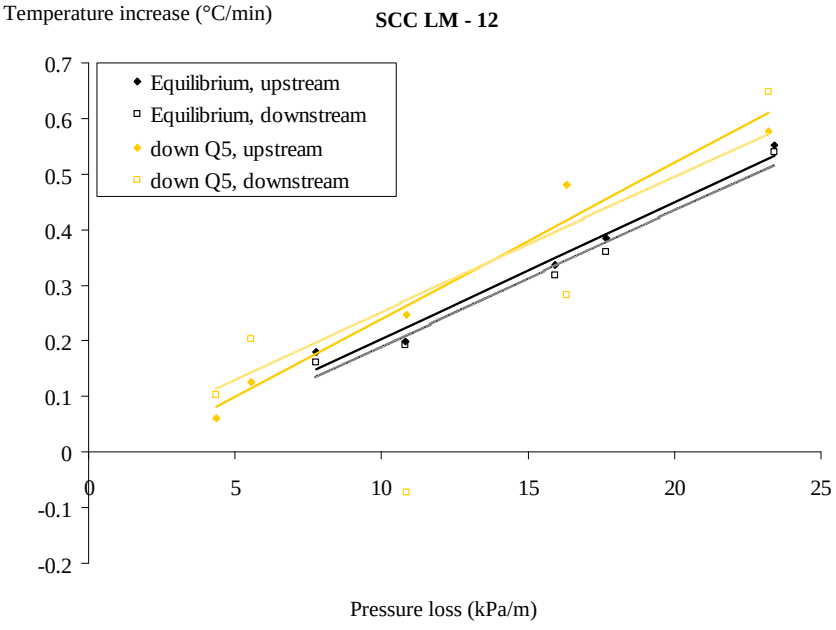
Temperature increase (°C/min)
SCC LM - 12
Equilibrium, upstream
Equilibrium, downstream
down Q5, upstream
down Q5, downstream
0.7
0.6
0.5
0.4
0.3
0.2
0.1
0
-0.1
-0.2
0
5
10
15
20
25
Pressure loss (kPa/m)

2.16 SCC LM-14

	LM-14					
	Q0 start	**Q1**	**Q2**	**Q3**	**Q4**	**Q0 end**
Production	**7:00**					
Time	**8:18**	**9:34**	**9:43**	**10:05**	**10:33**	**10:40**
Tests on fresh SCC						
Slump flow (mm)	730	818	758	745	658	695
V-Funnel (s)	8.3	5.2	6.1	3.7	5.8	8.2
L-box (-)	0.92	-	-	-	-	0.77
Density (kg/m³)	2381	2344	2345	2369	2388	2363
Sieve Stability (%)	6.9	10.9	11.0	14.2	7.5	3.7
Air content (%)	1.4	1.6	1.8	1.6	1.5	1.3
Rheometer tests						
Yield stress (Pa)	49.2	19.2	47.3	19.8	70.2	79.8
Viscosity at 0/s (Pa s)	48.1	29.1	33.7	21.9	28.3	51.7
shear thickening (c/visco)	0.011	0.013	0.015	0.010	0.017	0.011
Viscosity at 5/s (Pa s)	53.3	32.8	38.7	24.0	33.2	57.4
Torque at max. velocity (Nm)	5.34	3.43	4.08	2.5	3.87	5.95
Max Torque: thixo (Nm)	7.41	4.05	4.4	2.78	5.48	7.14

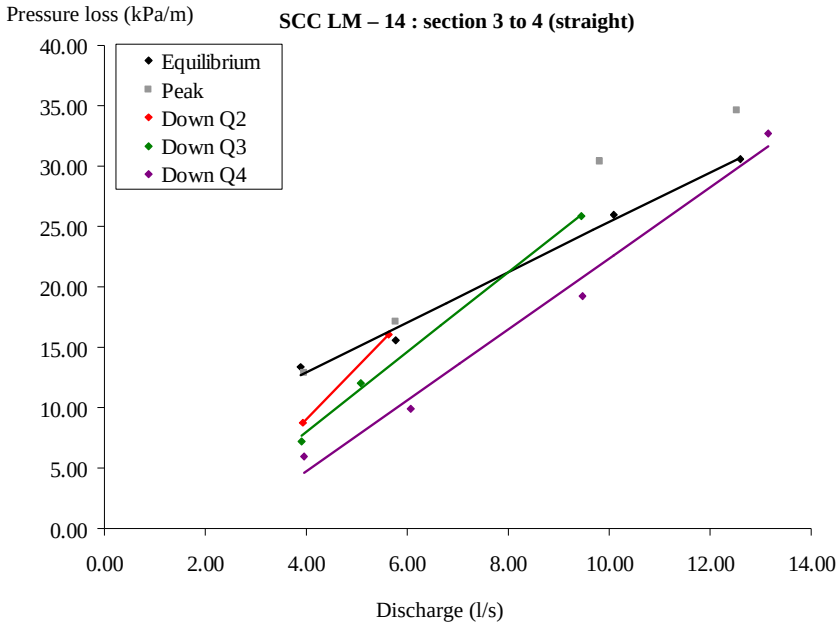
Pressure loss (kPa/m)
SCC LM – 14 : section 3 to 4 (straight)
Equilibrium
Peak
Down Q2
Down Q3
Down Q4
40.00
35.00
30.00
25.00
20.00
15.00
10.00
5.00
0.00
0.00
2.00
4.00
6.00
8.00
10.00
12.00
14.00
Discharge (l/s)

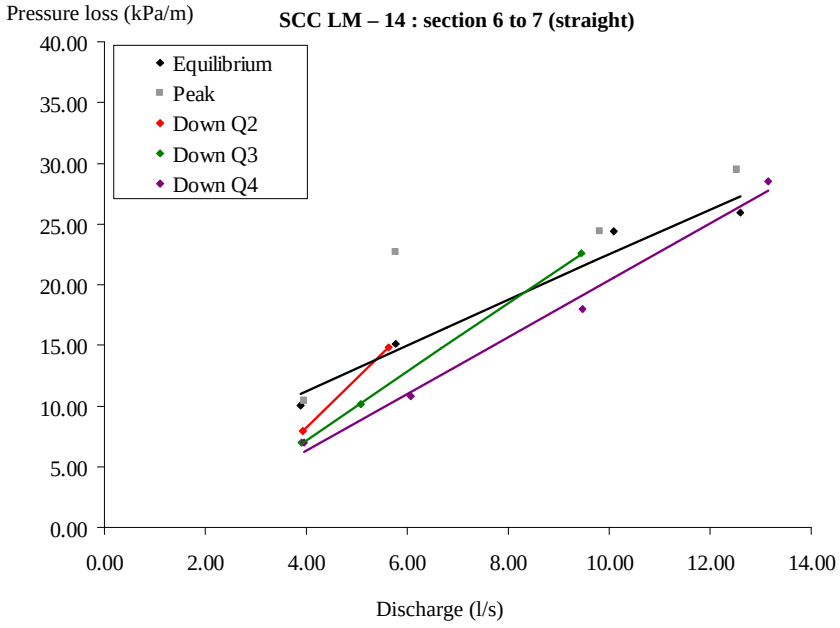
Pressure loss (kPa/m)
SCC LM – 14 : section 6 to 7 (straight)
Equilibrium
Peak
Down Q2
Down Q3
Down Q4
40.00
35.00
30.00
25.00
20.00
15.00
10.00
5.00
0.00
0.00
2.00
4.00
6.00
8.00
10.00
12.00
14.00
Discharge (l/s)

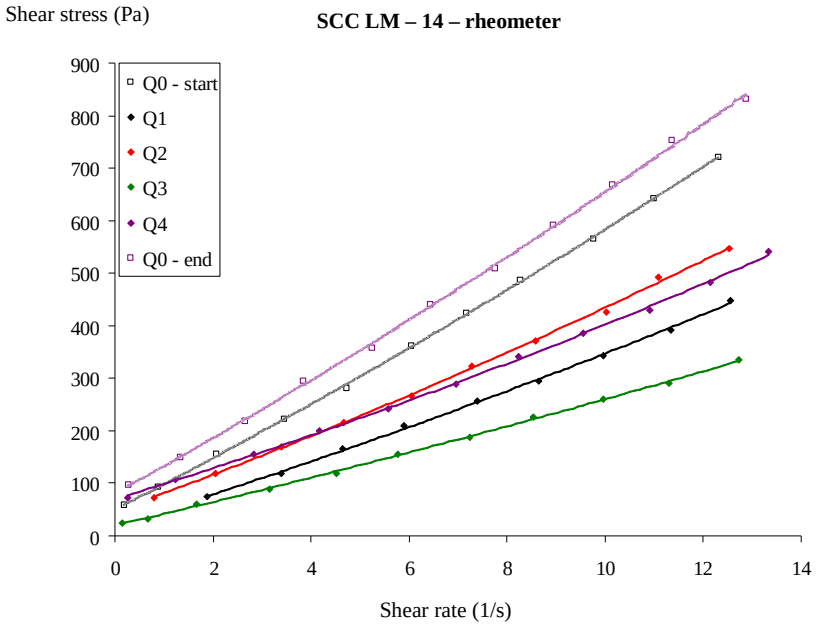
Shear stress (Pa)
SCC LM – 14 – rheometer
Q0 - start
Q1
Q2
Q3
Q4
Q0 - end
900
800
700
600
500
400
300
200
100
0
0
2
4
6
8
10
12
14
Shear rate (1/s)

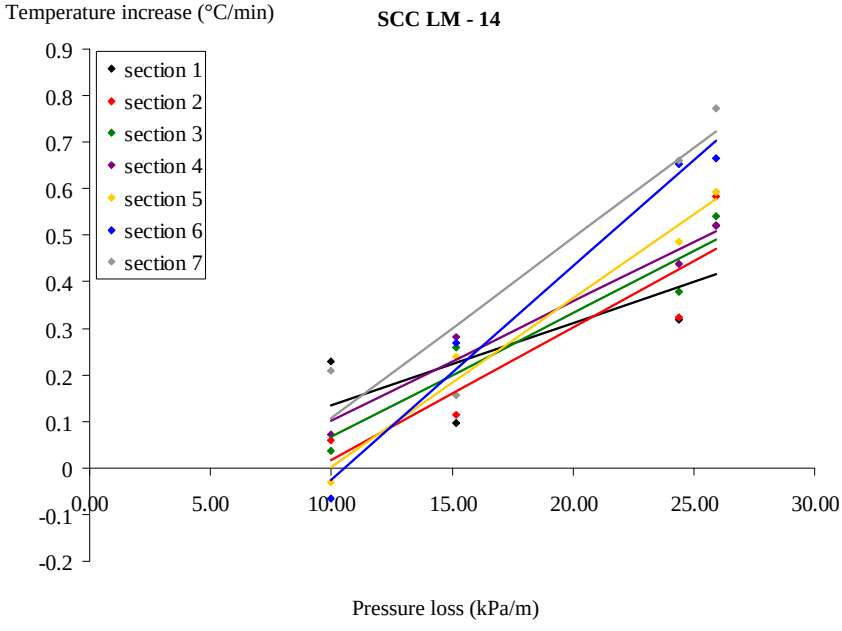
Temperature increase (°C/min)
SCC LM - 14
section 1
section 2
section 3
section 4
section 5
section 6
section 7
0.9
0.8
0.7
0.6
0.5
0.4
0.3
0.2
0.1
0
-0.1
-0.2
0.00
5.00
10.00
15.00
20.00
25.00
30.00
Pressure loss (kPa/m)

2.17 SCC LM-15

	LM-15				
	Q0 start	**Q1-1**	**Q1-2**	**Q1-3**	**Q1-4**
Production	**11:30**				
Time	**12:42**	**13:05**	**13:17**	**13:27**	**13:38**
Tests on fresh SCC					
Slump flow (mm)	675	645	625	660	570
V-Funnel (s)	5.1	5.4	4.2	3.8	3.4
L-box (-)	0.83	-	-	-	-
Density (kg/m³)	2388	2319	2275	2278	2238
Sieve Stability (%)	1.6	4.2	7.0	6.6	4.0
Air content (%)	2.1	2.1	2.4	3.2	4.2
Rheometer tests					
Yield stress (Pa)	27.4	45.8	25.3	61.6	40.6
Viscosity at 0/s (Pa s)	25.3	27.6	20.0	25.1	9.8
shear thickening (c/visco)	0.010	0.005	0.000	0.000	0.000
Viscosity at 5/s (Pa s)	27.8	28.9	20.0	25.1	9.8
Torque at max. velocity (Nm)	2.89	3.11	2.08	2.34	1.18
Max Torque: thixo (Nm)	3.10	3.26	2.17	2.51	1.25

	LM-15					
	Q2-1	**Q2-2**	**Q2-3**	**Q2-4**	**Q2-5**	**Q0 end**
Production	**11:30**					
Time	**14:21**	**14:28**	**14:39**	**14:52**	**15:02**	**15:11**
Tests on fresh SCC						
Slump flow (mm)	525	543	505	498	445	548
V-Funnel (s)	3.5	3.1	3.3	3.5	3.7	7.9
L-box (-)	-	-	-	-	-	0.60
Density (kg/m³)	2283	2260	2228	2250	2225	2338
Sieve Stability (%)	3.36	4.5	1.9	0.8	0.3	1.2
Air content (%)	3.7	3.9	4.6	5.0	6.2	2.3
Rheometer tests						
Yield stress (Pa)	46.1	50.6	87.5	73.0	88.8	48.3
Viscosity at 0/s (Pa s)	10.1	11.0	14.9	8.1	7.0	26.9
shear thickening (c/visco)	0.000	0.000	0.000	0.000	0.000	0.010
Viscosity at 5/s (Pa s)	10.1	11.0	14.9	8.1	7.0	29.5
Torque at max. velocity (Nm)	1.24	1.39	2.02	1.24	1.23	3.34
Max Torque: thixo (Nm)	1.36	1.52	2.16	1.30	1.32	4.84

Remark: This concrete has been subjected to the thixotropy test twice. The “1” or “2” after the Q indicates the first or second test. The last number indicates the maximal discharge applied.

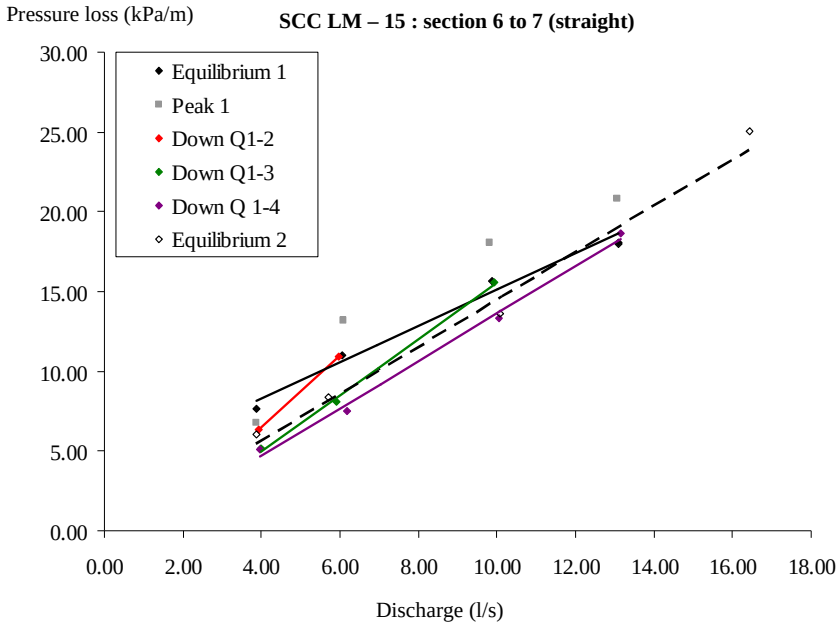
Pressure loss (kPa/m)
SCC LM – 15 : section 6 to 7 (straight)
Equilibrium 1
Peak 1
Down Q1-2
Down Q1-3
Down Q 1-4
Equilibrium 2
30.00
25.00
20.00
15.00
10.00
5.00
0.00
0.00
2.00
4.00
6.00
8.00
10.00
12.00
14.00
16.00
18.00
Discharge (l/s)

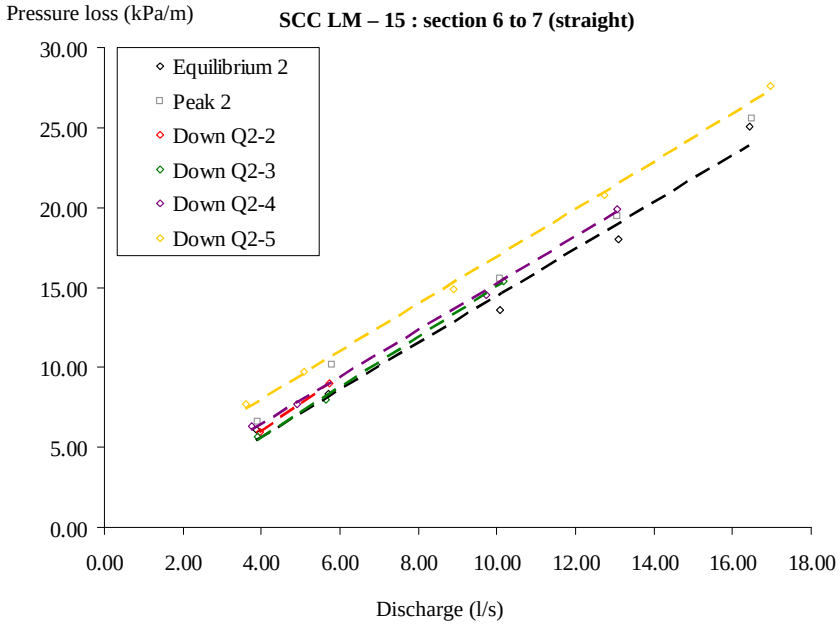
Pressure loss (kPa/m)
SCC LM – 15 : section 6 to 7 (straight)
Equilibrium 2
Peak 2
Down Q2-2
Down Q2-3
Down Q2-4
Down Q2-5
30.00
25.00
20.00
15.00
10.00
5.00
0.00
0.00
2.00
4.00
6.00
8.00
10.00
12.00
14.00
16.00
18.00
Discharge (l/s)

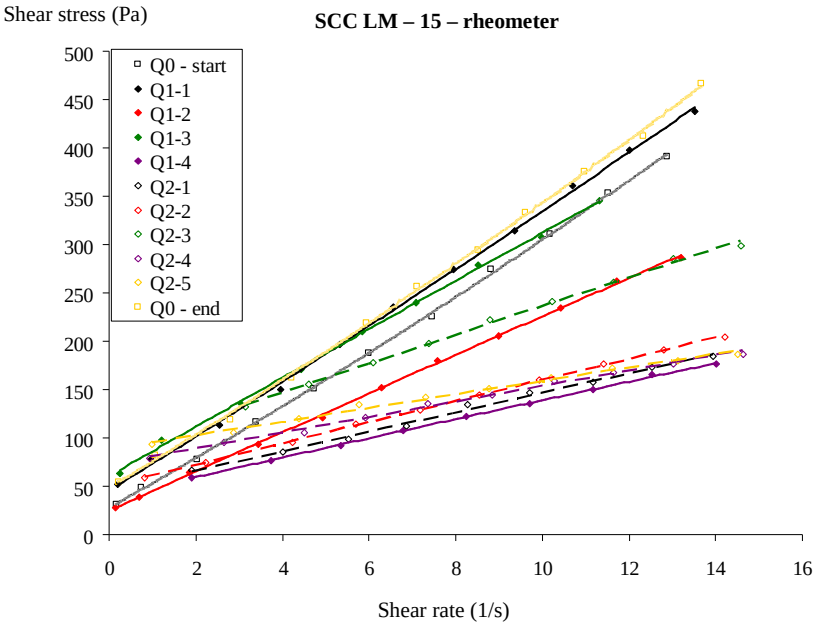
Shear stress (Pa)
SCC LM – 15 – rheometer
Q0 - start
Q1-1
Q1-2
Q1-3
Q1-4
Q2-1
Q2-2
Q2-3
Q2-4
Q2-5
Q0 - end
500
450
400
350
300
250
200
150
100
50
0
0
2
4
6
8
10
12
14
16
Shear rate (1/s)

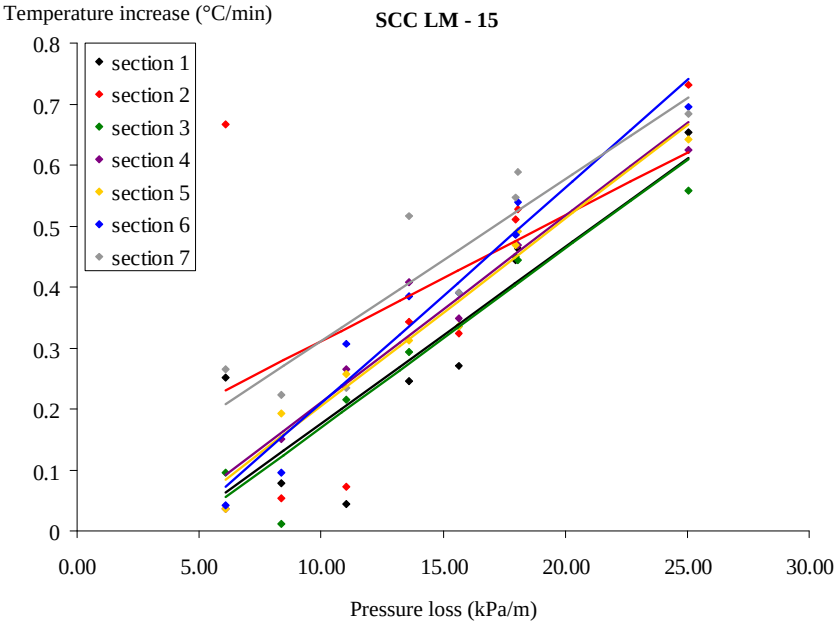
Temperature increase (°C/min)
SCC LM - 15
section 1
section 2
section 3
section 4
section 5
section 6
section 7
0.8
0.7
0.6
0.5
0.4
0.3
0.2
0.1
0
0.00
5.00
10.00
15.00
20.00
25.00
30.00
Pressure loss (kPa/m)

2.18 SCC LM-16

	LM 16							
	Q0 start	**Q 1**	**Q 2**	**Q 3**	**Q 3 bis**	**Q 3 ter**	**Q 4**	**Q0 end**
Production				8:20				
Time	**10:37**	**10:55**	**11:05**	**11:17**	**11:30**	**11:43**	**11:53**	**12:00**
Tests on fresh SCC								
Slump flow (mm)	770	670	675	655	585	620	535	670
V-Funnel (s)	5.2	5.2	4.0	4.8	3.7	3.8	3.9	5.6
L-box (-)	0.95							0.85
Density (kg/m³)	2350	2363	2359	2375	2375	2350	2275	2394
Sieve Stability (%)	10	8.7	12.7	6.9	6.8	7.8	5.7	6.2
Air content (%)	0.8	1.1	1	1.4	1.3	2.2	3.9	0.3
Rheometer tests								
Yield stress (Pa)	*0.6*	33.1	31.7	25.7	31.7	33.0	34.4	12.5
Viscosity at 0/s (Pa s)	*6.5*	20.3	19.5	10.3	12.1	12.0	9.8	20.8
shear thickening (c/visco)	*0.095*	0.018	0.000	0.017	0.010	0.000	0.000	0.000
Viscosity at 5/s (Pa s)	*12.7*	23.9	19.5	12.0	13.3	12.0	9.8	20.8
Torque at max. velocity (Nm)	*1.16*	2.86	2.15	1.39	1.59	1.36	1.15	2.15
Max Torque: thixo (Nm)	*1.62*	3.66	2.49	1.84	1.95	1.97	2.27	4.94

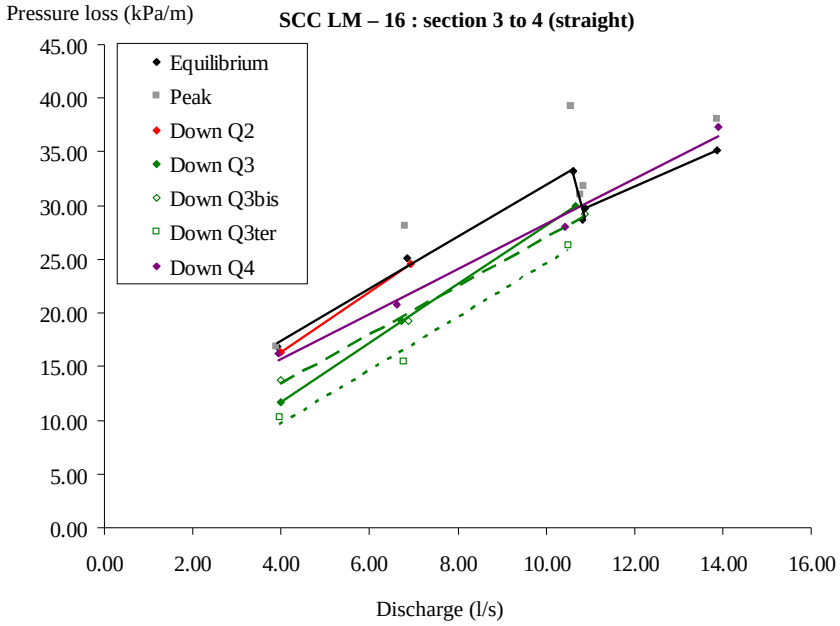

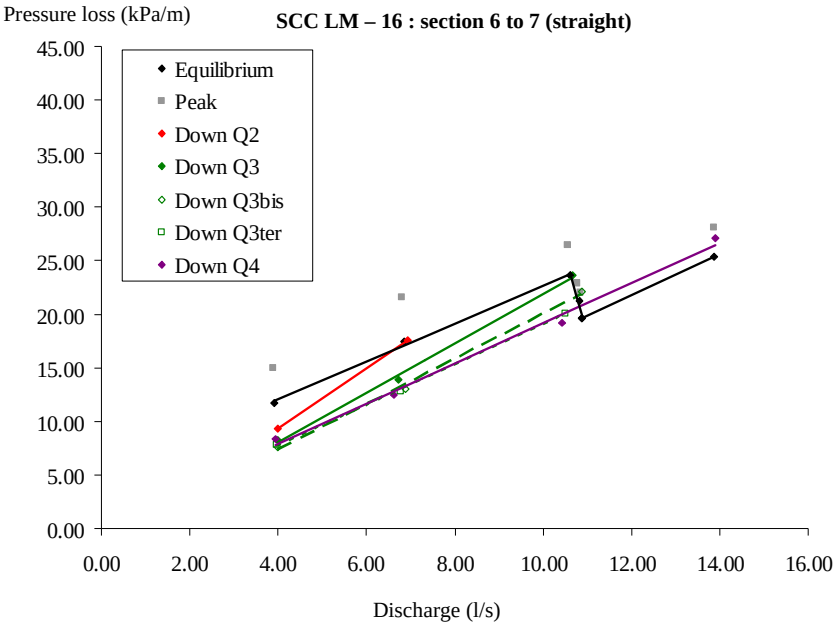
Pressure loss (kPa/m)
SCC LM – 16 : section 6 to 7 (straight)
Equilibrium
Peak
Down Q2
Down Q3
Down Q3bis
Down Q3ter
Down Q4
45.00
40.00
35.00
30.00
25.00
20.00
15.00
10.00
5.00
0.00
0.00
2.00
4.00
6.00
8.00
10.00
12.00
14.00
16.00
Discharge (l/s)

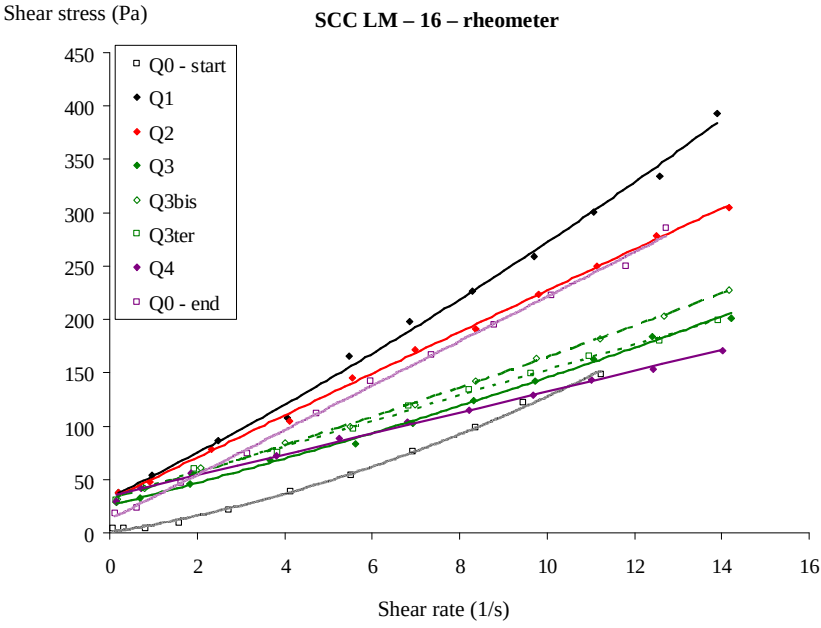
Shear stress (Pa)
SCC LM – 16 – rheometer
Q0 - start
Q1
Q2
Q3
Q3bis
Q3ter
Q4
Q0 - end
450
400
350
300
250
200
150
100
50
0
0
2
4
6
8
10
12
14
16
Shear rate (1/s)

2.19 SCC LM-17

	LM 17						
	Q0 start	**Q1**	**Q2**	**Q3**	**Q4**	**Q5**	**Q0 end**
Production	**13:00**						
Time	**14:09**	**14:18**	**14:28**	**14:39**	**14:48**	**14:59**	**15:07**
Tests on fresh SCC							
Slump flow (mm)	905	785	780	750	765	750	775
V-Funnel (s)	3.1	3.4	3.1	2.7	2.4	2.2	3.8
L-box (-)	1						1.01
Density (kg/m³)	2300	2313	2281	2250	2250	2238	2363
Sieve Stability (%)	6.5	10.5	-	11.7	15.6	18.5	7.8
Air content (%)	0.2	1.4	1.9	3.1	3.9	4.9	0.2
Rheometer tests							
Yield stress (Pa)	-	*13.3*	*1.0*	*12.7*	*8.4*	*14.2*	
Viscosity at 0/s (Pa s)	-	*4.4*	*3.7*	*0.4*	*1.5*	*0.8*	
shear thickening (c/visco)	-	*0.161*	*0.114*	*1.000*	*0.159*	*0.188*	
Viscosity at 5/s (Pa s)	-	*11.5*	*7.9*	*4.5*	*3.9*	*2.3*	
Torque at max. velocity (Nm)	0.62	1.24	0.62	0.34	0.23	0.15	
Max Torque: thixo (Nm)	0.74	1.57	0.81	0.5	0.31	0.3	

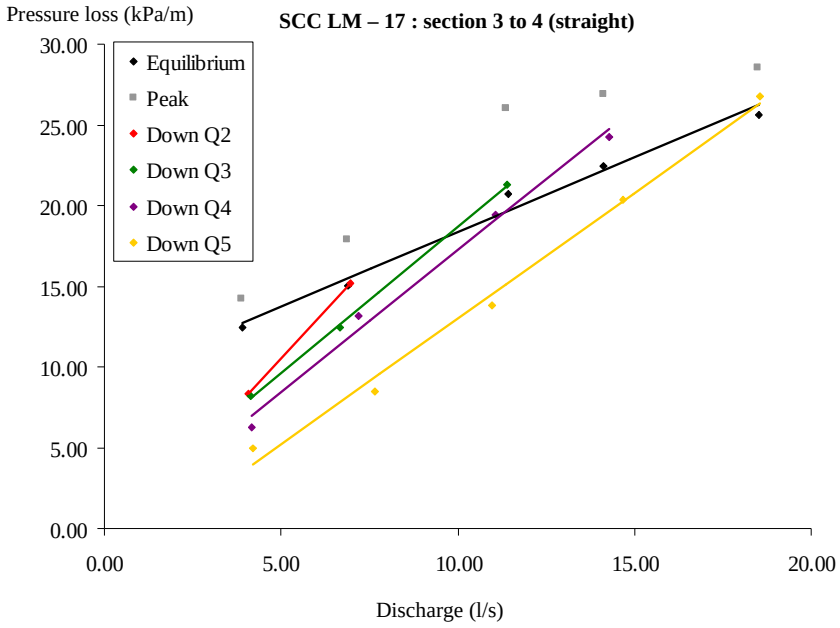
Pressure loss (kPa/m)
SCC LM – 17 : section 3 to 4 (straight)
Equilibrium
Peak
Down Q2
Down Q3
Down Q4
Down Q5
30.00
25.00
20.00
15.00
10.00
5.00
0.00
0.00
5.00
10.00
15.00
20.00
Discharge (l/s)

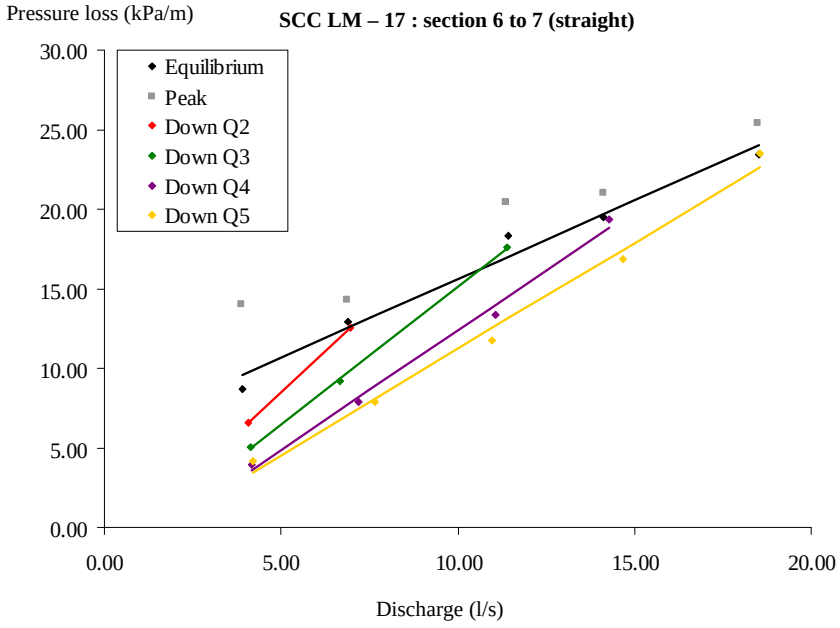
Pressure loss (kPa/m)
SCC LM – 17 : section 6 to 7 (straight)
Equilibrium
Peak
Down Q2
Down Q3
Down Q4
Down Q5
30.00
25.00
20.00
15.00
10.00
5.00
0.00
0.00
5.00
10.00
15.00
20.00
Discharge (l/s)